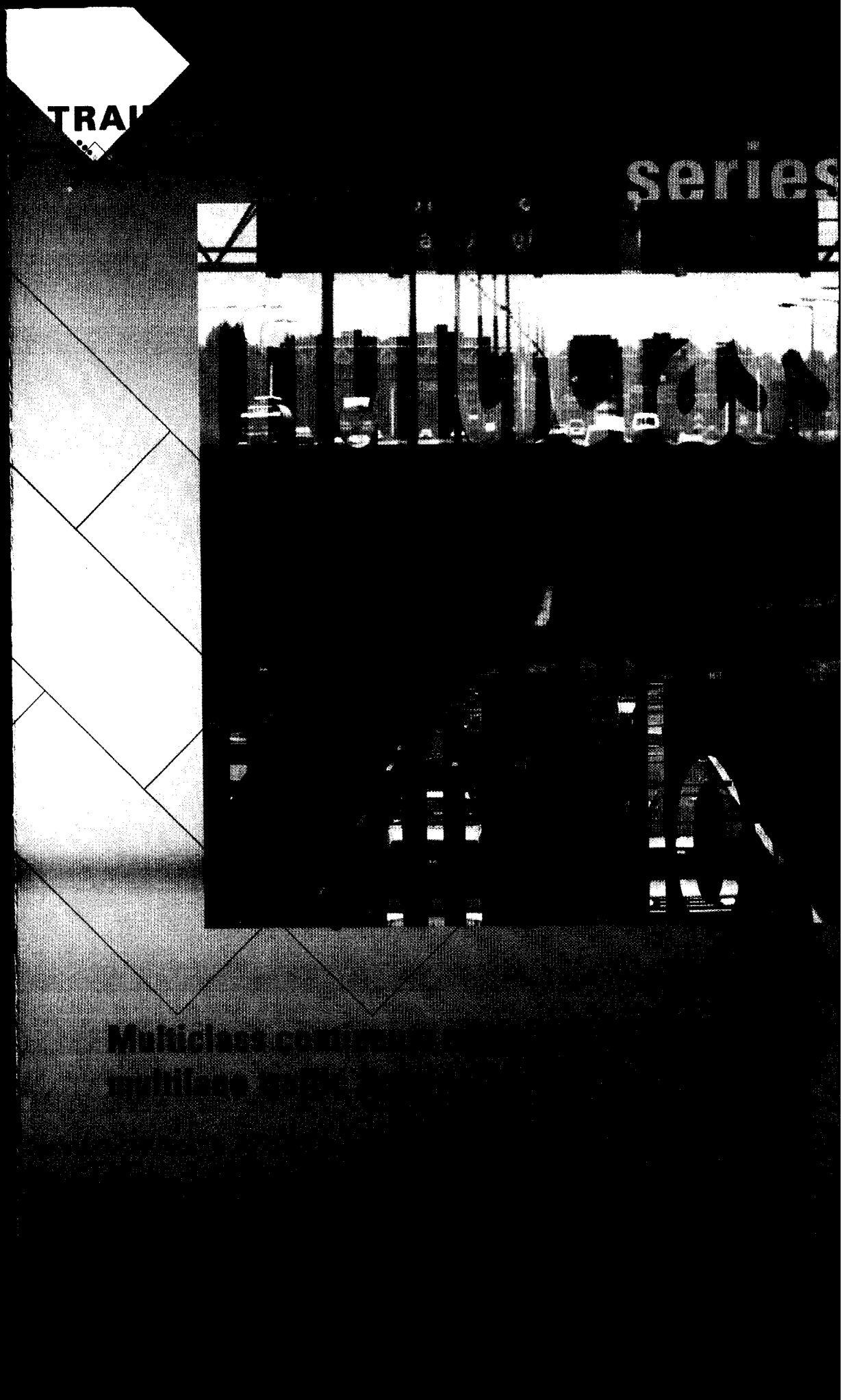
TRA
series

Multiclass Continuum Modelling of Multilane Traffic Flow

Serge Paul Hoogendoorn

Delft University Press, 1999

This thesis is the result of the Ph.D. study performed from 1995 to 1999 at the Delft University of Technology, Faculty of Civil Engineering and Geosciences, Transportation and Traffic Engineering section

Published and distributed by:

Delft University Press
P.O. Box 98
2600 MG Delft
The Netherlands
Telephone: +31 15 2783254
Telefax: +31 15 2781661
E-mail: DUP@DUP.TUDelft.NL

ISBN 90-407-1931-4

Printed in the Netherlands

Multiclass Continuum Modelling of Multilane Traffic Flow

Proefschrift

ter verkrijging van de graad van doctor
aan de Technische Universiteit Delft,
op gezag van de Rector Magnificus prof. ir. K.F. Wakker,
in het openbaar te verdedigen ten overstaan van een commissie,
door het College voor Promoties aangewezen,

op maandag 20 september 1999 te 10:30 uur

door

Serge Paul HOOGENDOORN

wiskundig ingenieur
geboren te Rotterdam

Dit proefschrift is goedgekeurd door de promotor:
Prof. dr. ir. P.H.L. Bovy

Samenstelling promotiecommissie:

Rector Magnificus,	voorzitter
Prof. dr. ir. P.H.L. Bovy,	Technische Universiteit Delft, promotor
Prof. dr. M. Ben-Akiva,	Massachusetts Institute of Technology, USA
Prof. dr. ir. M.F.A.M. van Maarseveen,	Universiteit Twente
Prof. Dr.-Ing. M. Papageorgiou,	Technical University of Crete, Greece
Prof. dr. ir. J.H. van Schuppen,	Centrum voor Wiskunde en Informatica, Amsterdam
Prof. dr. ir. G.S. Stelling,	Technische Universiteit Delft

Everything should be made as simple as possible, but not simpler

Albert Einstein

PREFACE

Since Lighthill and Whitham proposed their kinematic traffic flow model five decades ago, the mathematical description of traffic flow operations has been a lively subject of research and debate for traffic engineers. This has resulted in a broad scope of flow models describing traffic flow operations. These models describe the traffic stream either from the viewpoint of the individual driver under the influence of vehicles in his proximity (*microscopic* models), or from the viewpoint of the collective vehicular flow (*macroscopic* models). In addition to the controversy between these microscopic and macroscopic modelling streams, several researchers have joined the debate on the macroscopic modelling approach most suitable for a correct description of traffic flow. Moreover, recent theoretical and empirical findings of Boris Kerner and co-workers resulted in increased public attention for the subject of macroscopic flow modelling. Also, due to improving mathematical techniques and increased computational capacity to solve large-scale control problems, applications of realistic flow models in model based control approaches have become feasible.

In this dissertation, we develop, analyse, and operationalise a macroscopic traffic flow model describing the multiclass traffic flow operations on multilane roadway facilities. The results described in this thesis are the main research findings carried as part of the project 'Dynamic Lane Usage'. The project has been supported by the Beek-committee of the Delft University of Technology. The performed research is part of the Research Programme Traffic Flow and Control of the Netherlands TRAIL Research School. Within the framework of this programme, several interdependent projects are or have been carried out. Among these are research regarding roadway capacity, travel time functions for multiple user-class dynamic assignment models, and automation of motorway traffic flow. The project contributes to the TUD-DIOC Programme FTAM (Freight Transport Automation and Multimodality) – project 3, especially with respect to the modelling of automated truck-lanes on motorways.

Several years of dedicated research and hard work form the foundation of this thesis. During these years, several people reached out a helping hand. I am indebted to each from whom I have learned and who have contributed in many ways to this dissertation.

I especially wish to acknowledge the crucial contributions of Professor Piet H.L. Bovy, supporting my research with admirable enthusiasm. He has been one of the main driving forces behind the work presented in this thesis. I would also like to express my gratitude to Professor Henk van Zuylen, providing additional material and perspectives on the topic of gas-kinetic flow modelling. I am also grateful to Nanne van der Zijpp for spending time to provide valuable comments, which helped improve the quality of the material presented in this thesis. I would also like to acknowledge the Dutch Ministry of Transport, Public Works and Water management for providing the data used in this thesis. In addition, I would like to express my gratitude towards all members of the promotion committee, taking the time to read this dissertation thesis and to provide very useful comments.

Finally, my love and deepest appreciation to my wife Sascha, whom I admire for her strength and support during very tumultuous times in our lives. Without realising it, she made this dissertation possible.

CONTENTS

LIST OF FREQUENTLY USED SYMBOLS

Independent variables (chapter 3)			Section
$\mathbf{x}$	:	location $\mathbf{x} \in \mathbb{R}^n$ (m)	3.1
t	:	time instant $t \in \mathbb{R}$ (s)	3.1
$\mathbf{v}^0$	:	general *continuous* attribute-set $\mathbf{v}^0 = \{v_i^0\}$ with $v_i^0 \in \mathbb{R}$	3.3/6
$\mathbf{a}$	:	general *discrete* attribute-set $\mathbf{a} = \{a_i\}$ with $a_i \in \mathbb{N}$	3.6
$\mathbf{v}$	:	velocity $\mathbf{v} \in \mathbb{R}^n$ (m/s)	3.2
v^0	:	desired velocity $v^0 \in \mathbb{R}$ (m/s)	3.3
u	:	user-class $u \in \mathbf{U} \subset \mathbb{N}$	3.7
j	:	roadway lane $j \in \mathbf{J} \subset \mathbb{N}$	3.7
M	:	number of lanes	3.7
c	:	driving-state $c \in \mathbf{C} \subset \mathbb{N}$	3.7

Generalised* mesoscopic variables (chapter 3)			Section
$\lambda_{\mathbf{a}}(\mathbf{x},t;n)$	:	traffic intensity for n-vehicle platoons at $(\mathbf{x},t)$ (veh/s)	3.2/3/6
$\kappa_{\mathbf{a}}(\mathbf{x},t;n)$	:	traffic concentration for n-vehicle platoons at $(\mathbf{x},t)$ (veh/m^n)	3.2/3/6
$g_{\mathbf{a}}(\mathbf{x},\mathbf{v},\mathbf{v}^0,t)$	:	joint probability density function at $(\mathbf{x},t)$	3.2/6
$\rho_{\mathbf{a}}(\mathbf{x},\mathbf{v},\mathbf{v}^0,t)$	:	phase-space traffic density at $(\mathbf{x},t)$ (veh/m^n)	3.4/6
$\mu_{\mathbf{a}}(\mathbf{x},\mathbf{v},\mathbf{v}^0,t)$	:	phase-space traffic momentum at $(\mathbf{x},t)$ (veh/s)	3.4/6
$\varepsilon_{\mathbf{a}}(\mathbf{x},\mathbf{v},\mathbf{v}^0,t)$	:	phase-space traffic energy at $(\mathbf{x},t)$ $(veh\ m^n/s^2)$	3.4/6
$\tau_{\mathbf{a}}(v,v^0\|x,t)$	:	expected acceleration time of vehicle with (v,v^0) at (x,t) (s)	4.4

* The mesoscopic traffic flow variables are generalised with respect to velocity $\mathbf{v}$, continuous attributes $\mathbf{w}$, and discrete attributes $\mathbf{a}$ respectively.

Generalised gas-kinetic relations (chapter 4)		Section
$\pi_{\mathbf{a}}^{\mathbf{a}'}(\mathbf{v}', \mathbf{v}_0' \mid \mathbf{v}, \mathbf{v}^0; \alpha)$	: event-driven transition probability from $(\mathbf{v},\mathbf{v}^0;\mathbf{a})$ to $(\mathbf{v}',\mathbf{v}_0';\mathbf{a}')$ for event-driven process α	4.5
$\phi_{\mathbf{a}}^{\mathbf{a}'}(\mathbf{v}', \mathbf{v}_0' \mid \mathbf{v}, \mathbf{v}^0; \beta)$	: condition-driven transition probability from $(\mathbf{a},\mathbf{v}^0)$ to $(\mathbf{a}',\mathbf{v}_0')$ for condition-driven process β	4.5
$\Pi_{\mathbf{a}}(\mathbf{x}, \mathbf{v}, \mathbf{v}^0, t; \alpha)$	: event-rate of vehicles specified by $(\mathbf{v},\mathbf{v}^0;\mathbf{a})$ of event-driven process α	4.5

Class-specific and lane-specific gas-kinetic relations (chapter 4/5)		Section
$p_{(u,j,c)}^{(u,j',c')}(v, v^0)$	: immediate lane-changing probability from lane j to j', yielding transition from state c to c'	4.6
$\Delta_{(u,j,c)}^{(u,j',c')}(v, v^0)$	: spontaneous ($c = 1$) and postponed ($c = 2$) overtaking rates from lane j to lane j', yielding transition from c to c' (*veh/s*)	4.6
$\tilde{\Psi}_{(u,j)}(v)$	: event-independent interaction rate of vehicle with velocity v with slower vehicles of class u on lane j (1/*s*)	4.6
$\delta_j(x,t)$	: vehicle spacing correction factor on lane j at (x,t)	4.6
$\Xi_{(u,j)}$	: interaction rate of vehicle with velocity v with slower vehicles of class u on lane j (1/*s*)	4.6

Generalised conservative variables (chapter 6)		Section
$N_{\mathbf{a}}^{\mathbf{k}}(\mathbf{x},t)$	: **k**-th order generalised conservative moment at $(\mathbf{x},t)$	int. II
$r_{\mathbf{a}}(x,t)$	: density at (x,t) (*veh/m*)	3.5/6
$m_{\mathbf{a}}(x,t)$	: momentum at (x,t) (*veh/s*)	3.5/6
$e_{\mathbf{a}}(x,t)$	: energy at (x,t) (*veh* m/s^2)	3.5/6
$J_{\mathbf{a}}(x,t)$	: flux of velocity variance at (x,t) (*veh* m^2/s^3)	3.5/6
$H_{\mathbf{a}}(x,t)$	: stagnation traffic enthalpy at (x,t) (m^2/s^2)	3.5/6
$\theta_{\mathbf{a}}(x,t)$	: fraction of constrained vehicles at (x,t)	3.5/6
$m_{\mathbf{a}}^{e}(x,t)$	: equilibrium momentum at (x,t) (*veh/s*)	6.4
$e_{\mathbf{a}}^{e}(x,t)$	: equilibrium energy at (x,t) (*veh* m/s^2)	6.4
$m_{\mathbf{a}}^{a}(x,t)$	: acceleration momentum at (x,t) (*veh/s*)	6.4
$e_{\mathbf{a}}^{a}(x,t)$	: acceleration energy at (x,t) (*veh* m/s^2)	6.4
$\mathrm{T}_{\mathbf{a}}(x,t)$	: generalised acceleration time at (x,t) (*s*)	6.3
$\mathcal{I}_{\mathbf{a}}^{k}(\mathbf{x},t)$	: *k*-th order moment-decreasing interaction-rate	6.2
$\mathcal{X}_{\mathbf{a}}^{k}(\mathbf{x},t)$	: *k*-th order moment-increasing interaction-rate	6.2
$\mathcal{R}_{\mathbf{a}}^{k}(\mathbf{x},t)$	: *k*-th order interaction-rate	6.2

Generalised primitive/characteristic variables (chapter 7)			Section
$M_a^k(\mathbf{x},t)$	:	**k**-th order primitive moment at (**x**,*t*)	int. II
$V_a(x,t)$	:	expected velocity at (x,t) (m/s)	3.5/6
$\Theta_a(x,t)$	:	velocity variance at (x,t) (m^2/s^2)	3.5/6
$P_a(x,t)$	:	traffic pressure at (x,t) $(veh\ m/s^2)$	3.5/6
$\Gamma_a(x,t)$	:	velocity skewness at (x,t) (m^3/s^3)	3.5/6
$V_a^e(x,t)$	:	equilibrium velocity at (x,t) (m/s)	7.3
$\Theta_a^e(x,t)$	:	equilibrium velocity variance at (x,t) (m^2/s^2)	7.3
$V_a^a(x,t)$	:	acceleration velocity at (x,t) (m/s)	7.3
$C_a(x,t)$	:	covariance velocity and acceleration velocity (m^2/s^2)	3.5/6
$z_a^{(i)}(x,t)$	:	*i*-th characteristic variable	7.4
$c_a(x,t)$	:	local sound velocity (m/s)	7.4
C_a^0	:	path-line	7.4
$C_a^{\pm}$	:	Mach-lines	7.4

Behavioural parameters			Section
τ_u^0	:	acceleration time of *platoon-leader* of class *u* (s)	4.4
L_a	:	average length of vehicles (m)	2.2
$l_a(v)$	:	space effectively occupied by vehicle (m)	4.6
d_a^{min}	:	minimal distance headway (m)	2.2
T_a	:	average reaction time (s)	2.2
F_a	:	speed-risk factor (s^2/m)	2.2
H_a	:	gross time headway (s)	2.2
h_a	:	net time headway (s)	8.3
D_a	:	gross distance headway (m)	2.2
η_a	:	traffic viscosity coefficient	6.7
κ_a	:	kinematic coefficient	6.7

Numerical solution approach (chapter 9)			Section
Δx	:	spatial discretisation step (m)	9.2
Δt	:	temporal discretisation step (s)	9.2
i	:	space-step index	9.2
k	:	time-step index	9.2
x_i	:	location $i\Delta x$ (m)	9.2
t_k	:	time-instant $k\Delta t$ (s)	9.2
$\mathbf{w}_a(x,t)$	:	vector of conservative variables (r_a,m_a,e_a)	9.1
$\mathbf{f}_a^C(\mathbf{w}_a)$	:	conservative flux-vector	9.1
$\mathbf{f}_a^D(\mathbf{w}_a)$	:	diffusive flux-vector	9.1
$\mathbf{q}_a$	:	conservative source-term	9.1
$\mathbf{A}_a(\mathbf{w}_a)$	:	conservative flux-Jacobian	9.1
$\mathbf{h}_i$	:	numerical conservative flux at x_i	9.2
$\mathbf{f}^{\pm}$	:	conservative flux contributions (conservative flux-splitting)	9.3
$\mathbf{A}^{\pm}$	:	non-conservative flux contributions (non-conservative flux-splitting)	9.3
$\lambda_i^{\pm}$	:	i-th eigenvalue of $\mathbf{A}^{\pm}$	9.3

Operators			Section
$\otimes\mathbf{x}$	:	diag(x_1,…,x_n) (diagolisation operator)	3.8
$\oplus\mathbf{A}$	:	$\mathbf{A}\cdot(1,\ldots,1)^T$ (summation of matrix columns)	4.5
$\langle f(\mathbf{w})\rangle_a$	:	$\int f(\mathbf{w})g_a(\mathbf{w})d\mathbf{w}$ (*mean operator* with respect to probability density function $g_a(\mathbf{w})$)	9.2
$[f(\mathbf{w})]_a$	:	$\int f(\mathbf{w})\rho_a(\mathbf{w})d\mathbf{w}$ (*aggregation operator* with respect to generalised Phase-Space Density $\rho_a(\mathbf{w})$)	9.2

1 INTRODUCTION

The control task of heterogeneous traffic flow on motorways is characterised by the highly complex interplay of multiple control measures, multiple target groups (types of road users), multiple objectives (efficiency, safety, etc.), and the large differences in behaviour between user-classes. In order to improve the traffic conditions on motorways given the highly complex interplay of the multiple control instruments, gaining a clear insight into the response behaviour of the heterogeneously composed traffic flow to traffic control strategies is of dominant importance. Such insights may reveal control strategies yielding the desired traffic behaviour and may significantly improve the efficiency of the transportation facility.

The aforementioned high complexity of the control task requires a model-based approach. In this respect, current traffic continuum flow theory is deficient in the sense that it does not deal adequately with heterogeneously composed traffic on multilane motorways. In order to cope with the complex traffic control task, first a suitable traffic control theory is required that can deal with the multiplicity of control objectives and target groups, while for its application a much more elaborate theory of motorway traffic flow operations is necessary.

In this dissertation thesis, we propose such a new continuum traffic flow model describing the operations of multilane heterogeneous traffic. To this end, a new traffic flow theory is established. This theory is different from current continuum traffic flow theories in that it describes heterogeneously composed traffic as a collection of *platoons* moving along stochastic trajectories on the multilane infrastructural facility, rather than describing traffic by independently moving vehicular particles. This approach enables the description of the correlation between the vehicles necessary for a correct description of vehicular interaction.

Using this approach, *gas-kinetic traffic flow models* are developed that describe the dynamics of the so-called *Multiclass Multilane Phase-space density* for free-flowing and platooning vehicles, governed by convection, acceleration, deceleration, and various types of lane-

changing. This is achieved by establishing a generic gas-kinetic model describing the motion of traffic entities in the n-dimensional space. This generic model is specified for platoon-based multilane multiclass traffic flow. The resulting model contributes to current gas-kinetic flow modelling in a number of ways. First, it presents a generalisation of these models with respect to general driver attributes, such as user-class, traversed roadway lane, and driver's state. Secondly, an improved interaction term is presented, remedying the unrealistic vehicular chaos assumption. Thirdly, an improved acceleration term is proposed describing acceleration towards the desired velocity of the platoon leader. Finally, finite vehicular spacing requirements are taken into account.

The *macroscopic* flow equations derived from the gas-kinetic equations describe the dynamics of the conservative flow variables density, momentum and energy for the distinguished classes and lanes. Similar to the generalised gas-kinetic equations, the model contributes to macroscopic traffic flow modelling in a number of respects. For one, it generalises traditional macroscopic flow models with respect to distinguishing various attributes. Secondly, it presents dynamic equations cast in *conservative variables*. By recasting the conservative model in its primitive form describing the dynamics of density, velocity, and velocity variance, the generalised model can be compared with other higher-order flow models. This reveals the incorrectness in the usual interpretation of the terms of the latter models. The macroscopic model is also formulated in its characteristic form using the so-called *characteristic variables* or *Riemann variables*. These reveal the way in which small perturbations in the flow are transported in the multiclass traffic stream. Insight into the motion of these disturbances is essential for mathematical analysis of the traffic flow model. The macroscopic model formulation naturally yields expressions for the multiclass multilane equilibrium conditions (equilibrium velocity and velocity variance, and the distribution of vehicles across roadway lanes). These relationships show the *asymmetric interactions* between fast classes and slow classes.

This thesis also contributes to the field of numerical solution techniques for higher-order macroscopic traffic flow models. Both generic solution approaches, as well as dedicated solution approaches for the multilane case are proposed. These approaches are based on both the conservative (adaptation of the Van Leer flux-vector splitting scheme) and the characteristic model formulations (adaptation of the approximate Riemann solver).

To calibrate class-specific model parameters and relationships, a new data smoothing technique is proposed, based on low-pass filtering of consecutive real-life traffic observations. This technique enables specifying all relevant model parameters and relationships.

Finally, the resulting operational model is tested for plausibility and applicability. In this context, we have observed that the discrete MLMC model remedies the criticisms of anisotropy, unaffected slow vehicles, and invariant driver's personality. Moreover, the model describes the hysteresis effect observed in real-life traffic operations, and the seemingly spontaneous occurrence of jams. With respect to the latter, the distinction of classes and lanes reveals causes for congestion that aggregate macroscopic models cannot reproduce (e.g. mixing of classes). Moreover, we show the applicability of the discrete MLMC model for class and lane specific traffic management assessment and control purposes.

In the remainder of this introduction, we will discuss in detail motivations, objectives, approaches, and results of the research.

1.1 Research motivation

It is well known that Dynamic Traffic Management (DTM) can provide efficient tools to remedy negative side effects of congestion. Aim of Dynamic Traffic Management on motorway networks is to make optimal use of currently available infrastructural facilities and roadway space and to improve the quality of travel by providing information to road-users. To this end, a number of traffic control options, such as ramp-metering, dynamic route information, incident management, and speed homogenising control, have been proposed and implemented in practice while a number of new types of traffic control are currently under development. Examples of such contemporary class-specific traffic control measures are the dynamic assignment of specific roadway lanes to specific user-classes, introduction of pay-lanes, introduction of various levels of driver support (e.g. Adaptive Cruise Control, lateral control), and provision of on-board information to equipped vehicles.

1.1.1 User-class and lane distinction

A large number of these contemporary and future traffic control options recognise the importance of distinguishing user-classes. These user-classes can be categorised according to the following criteria:

1. *Vehicle type characteristics.* Different types of vehicles may reflect differences in for instance maximum velocity, acceleration and deceleration capabilities, and safe minimum distance to leading vehicle. Examples of vehicle-types are trucks, busses, person-cars, vans, and motorbikes.
2. *Driver characteristics.* Differences in driving characteristics reflect differences in among other things brisk and careful driving. That is, drivers maintaining different minimum distances with respect to the leading vehicle, different desired velocities, different anticipatory behaviour, different reaction times, etc. These differences may result from differences in experience, route familiarity, and levels of risk-acceptance.
3. *Traveller-type characteristics.* User-classes can be identified by the purpose of travel, e.g. commuters, business-related, freight, recreational.
4. *Socio-economic characteristics.* Socio-economic differences are reflected by for instance value-of-time, and income. This categorisation enables differentiating between socially or economically important user-classes, such as police-cars, ambulances, High Occupancy Vehicles (HOV's), and goods vehicles.
5. *Level of route-information.* Vehicles are equipped with on-board systems providing route information at various levels.
6. *Level of driver-support.* Automated systems are introduced, which provide various levels of support to the driving task. Lateral and longitudinal driving control systems can be distinguished.
7. *Driving direction.* E.g. contra-flow traffic.
8. *Travel destination.* The destination of a road-user on the motorway yields differences with respect to among other things lane-choice.

In addition to the relevance for traffic control options distinguishing user-classes, we envisage that the accuracy in description of traffic flow will benefit from class distinction. This is

motivated by the observed large differences between the identified user-classes, with respect to for instance vehicle lengths, reaction times, acceleration capabilities, desired speeds, and gap-acceptance behaviour. Similar arguments hold for the distinction of motorway lanes, in that several control measures are applied to the different lanes of the motorway differently (e.g. dynamic speed-limits), *and* because of observed differences in the traffic operations on the different motorway lanes.

1.1.2 Model-based control approaches

The traffic control task of traffic flow on motorways is characterised by the highly complex interplay of multiple control objectives, multiple control measures, multiple user-groups, and large differences in behaviour of these user-classes. To handle this complexity, a model-based approach is required. That is, operational models are needed to conditionally predict the state of multilane heterogeneous traffic flow, given specific control configurations.

Several model approaches have been proposed in the past. These can be classified as microscopic, mesoscopic, or macroscopic. Microscopic flow models describe the dynamics of each individual vehicle as a function of the positions and velocities of the neighbouring vehicles. Macroscopic models do not consider dynamics of individual vehicles, but the dynamics of aggregate flow quantities (e.g. instance density and velocity). Mesoscopic models combine the computational efficiency of macroscopic flow models with the opportunity to derive properties that refer to individual vehicles, by moving the latter according to dynamic laws that are usually governed by macroscopic equations. We will refer to models describing vehicular flow as a continuous medium as *continuum models*.

Although, in principle, microscopic models are very well suited to deal with multiple lanes and multiple user-classes, for our purpose of theory development and control application they have a number of drawbacks. For instance, in contrast to analytical models, they do not allow the analytical derivation of theoretical results. Additionally, because of the high demand on computer hardware, their application in real-time control is prohibitive. Finally, both from the viewpoint of the foreseen model application, as well as having the strong belief that the highly non-linear and chaos-like behaviour of traffic flow requires a continuum modelling approach to accurately reproduce *macroscopic* quantities of traffic flow, such as queue-length and capacities, we envisage that a macroscopic flow approach is needed. However, current continuum traffic flow theory is deficient in the sense that it does not deal adequately with heterogeneously composed traffic on multilane motorways.

Thus, to adequately deal with the complex control task, a suitable traffic control theory able to handle the multiplicity of control objectives and user-classes is needed. On the other hand, a more refined macroscopic traffic flow theory, able to deal adequately with heterogeneous traffic flow is necessary. Moreover, we expect that the modelling accuracy of the current macroscopic traffic flow models can be improved significantly by distinguishing several user-classes with their specific flow characteristics and parameters.

1.2 Framework of research and research objectives

The research presented in this thesis is part of the project 'Dynamic Lane Usage'. Within the context of this project, we aim to develop a control theory for the automated generation of

dynamic lane allocation control policies. Lane allocation to specific user groups is an important control option in dynamic traffic management. It is envisaged that by dynamically allocating freeway lanes to either socially or economically important user-classes a more efficient and policy effective use of the existing infrastructure can be accomplished.

The main research objectives of the project 'Dynamic Lane Usage' are:

- Development of a model describing heterogeneous traffic flow operations and lane choice behaviour on motorways.
- Development of an automated controller generating dynamic lane allocation control actions.

In this respect, a set of valuable mathematical tools is provided by model based optimal control theory. As the name suggests, control laws are determined that optimise motorway traffic operations forecasted by the prediction model. To this end, we need to predict both user-class specific *traffic demands,* given operational dynamic lane allocation configurations (e.g. right lane designated for trucks and high-occupancy vehicles only while left and middle lanes designated for other vehicles), as well as traffic operations given these predicted demands. Based on the latter predictions, the optimal controller determines control laws optimising an *objective function*, reflecting the goals and the constraints of traffic managers.

The objective of the dissertation research is twofold, namely to develop:

- Valid models suitable for multiclass control purposes on multilane traffic corridors.
- Suitable generic theories on which to base these models.

To operationalise such models, numerical solution approaches are to be developed, analysed and compared. We emphasise that in the case of complex non-linear multi-variable traffic flow models, specification of such numerical schemes is not self-evident. The models need to be calibrated and validated, while being aimed at real-life situations on motorway networks.

1.3 Research approach

In the approach taken in the dissertation research, we distinguish the approach to model derivation, the approach to mathematical and numerical solutions, and the data analysis and model calibration approach (see Figure 1-1). Let us briefly outline the different approaches.

1.3.1 Multiclass platoon-based Multilane traffic flow description

To enable the derivation of traffic flow models delineating the dynamics of multilane heterogeneous traffic flow, a platoon-based traffic flow theory is needed. Considering traffic flow as a collection of platoons enables the correct description of the interdependencies of vehicles of the different user-classes, and the consequent acceleration and interaction processes. This cannot be achieved by considering traffic as a collection of independent moving particles (cf. Prigogine and Herman (1971), Paveri-Fontana (1975), Helbing (1996)).

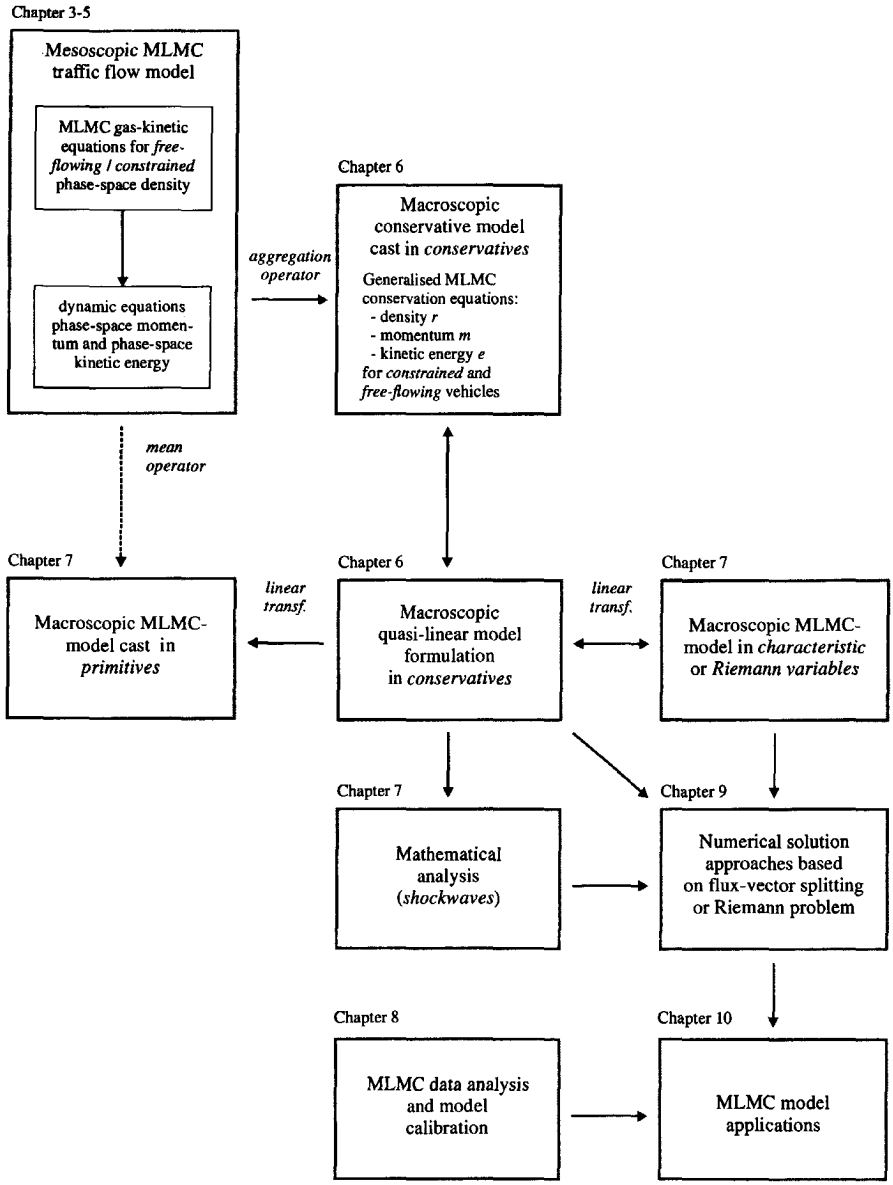

Figure 1-1: Overview of model derivation, mathematical and numerical analysis approaches.

In addition, to enable a correct transition from microscopic principles to a macroscopic description of traffic flow, a *probabilistic* approach is necessary. Such an approach describes trajectories of vehicles or platoons as realisations of random processes. The transformation from the microscopic platoon-based probabilistic description of traffic to macroscopic dynamics equations can be performed by identifying an intermediate mesoscopic model form,

that is well-known in statistical physics. This so-called gas-kinetic model uses the concept of the generalised Phase-Space Density (PSD) (see chapter 3).

1.3.2 Model derivation approach (chapters 4,5 and 6)

The gas-kinetic equations describe the dynamics of the generalised PSD in the *n*-dimensional space that are governed by processes of different natures, namely *continuum* processes (such as inflow and outflow of vehicles, smooth acceleration), and *non-continuum* processes. The latter processes yield non-smooth changes in the attribute-set, either caused by an event experienced by a vehicle, or a vehicle changing its state. These generalised gas-kinetic equations can subsequently be specified for the attribute set consisting of user-class, lane, and state. This is achieved by distinguishing different continuum and non-continuum processes, such as acceleration towards the desired velocity, deceleration caused by vehicle interactions, immediate lane-changing to either of the adjacent lanes, postponed lane changing, spontaneous lane-changing, and state-transitions from the constrained status to the free-flowing status. By quantification of these processes, the dynamics of the constrained and free-flowing MLMC-PSD can be established.

Since the resulting equations describe the dynamics of contributions by vehicles driving at a distinct velocities and desired velocities to respectively density, momentum, and energy, dynamic equations of these so-called *conservative variables* can be determined by aggregation of the gas-kinetic equations with respect to velocities and desired velocities.

1.3.3 Model transformations and approach to mathematical analysis (chapter 7)

The model presented in this thesis is cast in the *class-specific and lane-specific conservative variables* density, momentum, and energy. This so-called conservative formulation enables a clear interpretation of the MLMC traffic dynamics from the viewpoint of the *collective* longitudinal and lateral flows of specific classes on the different lanes. Moreover, this formulation yields a simplified model derivation, and the adequacy to correctly compute numerical solutions to the MLMC model using flux-vector splitting schemes.

Macroscopic flow models proposed during the long history of macroscopic modelling research are generally cast using the so-called *primitive traffic variables density, velocity,* and (sometimes) *velocity variance*, which can be considered to describe the *expected motion of the average driver.* It is widely accepted that the different terms present in the primitive formulation can be interpreted from the driver's viewpoint. Consequently, to show the similarities and differences with other macroscopic flow models (e.g. Lighthill and Whitham (1955), Payne (1971), Papageorgiou (1991), Lyrintzis *et al.* (1994), Liu *et al.* (1998), Kerner and Konhäuser (1995), Kerner *et al.* (1996), Helbing (1996)), the model is recast using the so-called *primitive* variables. The primitive formulation reveals whether the interpretation of model terms from the driver's viewpoint proposed for aggregate-lane aggregate-class models is applicable.

To analyse the way disturbances are transported in heterogeneous traffic flow, we can apply a similar transformation approach to determine the so-called *characteristic* model form.

1.3.4 Data analysis and model calibration approach (chapter 8)

To calibrate and validate the developed multilane multiclass traffic flow model, local measurements of individual vehicles on a two-lane motorway in the Netherlands are used. Since temporal aggregation (aggregation of measurements into periods of equal length) potentially yields statistically inaccurate averages, we develop a data aggregation approach based on identifying successive periods with equal numbers of observations.

During the empirical data study, we have observed that determining the velocity variance by calculating the sample velocity variance yields unrealistically high values of the velocity variance, caused by transitions in the traffic operations in a sample period. To remedy this, a new filtering approach is developed. This dynamic filter is based on application of a low-pass filter to the individual velocity measurements, distinguished with respect to class and roadway lane. By doing so, a correct dynamic estimation of the mean velocity can be determined. Considering the fluctuations of the measured velocities of the individual vehicles to the mean velocity, the velocity variance can also be correctly established using the filter-approach. Additionally, a second method is proposed to determine correct estimates of the velocity variance. Both methods yield similar estimation results.

1.3.5 Approach to numerical analysis (chapter 9)

As with other recently developed traffic flow models, numerical treatment of the developed MLMC traffic flow model is complex. To numerically solve higher-order flow models, such as the multilane multiclass model developed in this thesis, two new approaches are considered. Since the basic phenomena are of convective nature, the so-called characteristics of the system and their properties play an essential role in mathematical description and in many numerical discretisation schemes. The numerical approach must involve physical properties described by the model, and behave differently for different traffic conditions, by considering the direction in which disturbances are transported in the heterogeneous flow.

To this end, we will employ the characteristic form, since this form enables the mathematical analysis of among other things shock waves and discontinuities by showing how traffic density, traffic velocity and traffic pressure are transported in the vehicular flow. Using the characteristic formulation will enable application of so-called Godunov-type numerical approximation schemes. Other approaches are based on direct application of the conservative formulation of the model, by splitting of the so-called conservative flux.

1.4 Relevance of the research results

The relevance of the research reported in this thesis can be categorised according to the theoretical and scientific achievements and the practical relevance of the presented results. Let us briefly consider both.

Theoretical and scientific relevance

The developed theory will provide a genuine extension and generalisation of traditional macroscopic traffic flow theory. That is, earlier homogeneous aggregate-lane models are generalised to suit modelling heterogeneous traffic flow, incorporating interactions between road-

way lanes. We will show the merits of continuum traffic flow models as a means to describe and analyse traffic flow operations. We envisage that the developed flow model will provide insight into both interactions between distinct user-classes and the nature of the control problem at hand, given complex (network-) configurations and traffic control instruments. Consequently, a better understanding of the response of heterogeneous traffic flows to multiple control measures is acquired.

Practical relevance

The research resulted in improved models for operational traffic control. Moreover, the distinction between lanes and user-classes will enable new and superior control strategies. This potentially yields a more efficient utilisation of both the scarcely available infrastructure and the available traffic control instruments, by incorporation of the model developed in this dissertation in model-based control approaches.

1.5 Summary of main results

The research reported in this thesis contributes to both the gas-kinetic and macroscopic traffic flow theory. Additionally, improved numerical schemes for general higher-order traffic flow models have been established. Finally, new approaches to MLMC data analysis were developed, yielding new insights and calibration of the parameters and relations of the developed model. In this section, we present an overview of the main results.

1.5.1 Platoon-based traffic flow theory in the n-dimensional space

In this thesis, we propose a platoon-based description of traffic rather than describing traffic as a collection of single 'independent' particles. The approach is probabilistic in that trajectories of platoons are realisations of stochastic processes. Using this description, the traffic flow is represented by the moments of the distributions describing the location of the vehicles in the platoons. In other words, we define the traffic density by the *expected number of vehicles* per unit roadway length. We prove that the relation 'flow = density × velocity' holds for the platoon-based description of traffic as well.

The platoons are described by specifying the *generalised Phase-Space Density* (abbreviated as PSD), describing the expected number of vehicles having a specific attribute-set in a infinitesimal volume in the n-dimensional space. This attribute set is characterised by for instance lane, user-class, velocity, desired velocity, and state of vehicles.

Using the generalised PSD, the concepts of *conservative macroscopic variables* (traffic density, traffic momentum, traffic energy), *primitive macroscopic variables* (traffic density, velocity, velocity variance), and *characteristic variables* are defined.

1.5.2 Generic gas-kinetic model for n-dimensional flows

In this thesis, we derive generic equations mesoscopically describing the motion of traffic entities in n dimensions, for instance vehicles on a multilane roadway, or pedestrians moving in a two-dimensional space. These *generic gas-kinetic equations* depict how the generalised PSD changes due to so-called *continuum* and *non-continuum* processes. Convection, accel-

eration, and smooth adaptation of continuous attributes (e.g. desired velocities, and acceleration times) are continuum processes causing smooth changes in the generalised PSD. Non-continuum processes have been divided in *event-driven* and *condition-driven* processes. In this respect, event-driven processes reflect dynamic changes in the generalised PSD caused by for example interactions between traffic entities (for instance, a fast vehicle catching up with a slow vehicle, two pedestrians meeting each other head-on). Condition-driven processes cause changes in the generalised PSD caused by the state of the traffic entities (for instance, constrained vehicles leaving the platoon).

1.5.3 Gas-kinetic MLMC traffic flow model

The state-specific MLMC-PSD is a special case of the generalised PSD. Its dynamics are described by the MLMC gas-kinetic equations, determined from the generic gas-kinetic equations by specifying the continuum processes and the non-continuum processes to suit the description of MLMC traffic flow. We have determined that the dynamics of the MLMC-PSD are governed by dynamic processes, such as relaxation to the user-class specific desired velocity, interactions with other vehicles, and lane-changing caused by these interaction events or by preference for a specific lane. The interactions are *asymmetric* in that faster classes are more influenced by other vehicles than slower classes. To enable a realistic description of these processes, specific gas-kinetic equations for both unconstrained drivers as well as platooning drivers are determined from the generic gas-kinetic model. We show that the derived model is a MLMC-generalisation of traditional gas-kinetic equations, and constitutes one of the first theoretical developments in the field of mesoscopic flow models distinguishing both roadway lanes as well as user-classes.

It is shown that the *collision equations* used to describe the expected number of interactions per unit time used in other gas-kinetic models (e.g. Prigogine and Herman (1971), Paveri-Fontana (1975), Helbing (1996)) overestimate the number of interactions by assuming that vehicles move independently in the traffic flow (*vehicular chaos assumption*). We show that by considering the flow as a collection of platoons the correlation between vehicles is described realistically. To further improve the vehicle interaction term, spacing requirements of vehicles are considered, yielding an *increase* in the number of vehicular interactions.

The platoon-based description of traffic also enables the derivation of an improved acceleration term. This term reflects that on the one hand *platoon-leading* vehicles accelerate towards their own desired velocity, while on the other hand *platooning* vehicles accelerate towards the desired velocity of the platoon-leaders. The latter remedies the unrealistic assumptions that platooning vehicles either accelerate towards their own desired velocity (Paveri-Fontana (1975)), or do not accelerate at all (Helbing (1997a)).

Principally, the gas-kinetic multiclass multilane flow model can be used to mesoscopically simulate heterogeneous traffic flow on multilane roadways. In addition, the model provides mathematical insight in for instance class-specific and lane-specific velocity distributions given the interactions between the vehicles in the flow. However, in this dissertation thesis the gas-kinetic model constitutes the foundation of a macroscopic traffic flow model.

1.5.4 Macroscopic MLMC traffic flow model

MLMC traffic flow model in conservatives.

The developed model describes the dynamics of the MLMC conservative flow variables density, momentum and energy, rather the than traditionally used primitive variables density, velocity and velocity variance. On the input-side, end users can specify both mean class-specific desired velocities, acceleration times, traffic viscosities, and kinematic coefficients, as well as parameters describing target-lane choice behaviour and gap acceptance behaviour that among other things yield immediate lane-changing probabilities, postponed lane-changing rates, and spontaneous lane-changing rates.

The density dynamics are described by generalised conservation-of-vehicle equations. Comparable relations hold for traffic momentum and traffic energy dynamics. However, momentum and energy also change due to drivers aiming to drive at their user-class dependent desired velocity on the one hand and interactions causing decelerations on the other hand.

By inspecting these mixed-state macroscopic MLMC equations, lane-specific and class-specific equilibrium relations for momentum and energy are identified. These relations quantify asymmetric user-class and lane interactions. The mixed-state model also provides insight into the density distribution on roadway lanes, which follows from the gas-kinetic-based modelling approach. At this point, let us emphasise that these equilibrium relations and the derived quantities (e.g. class-specific capacities) are *endogenous*, and follow from the gas-kinetic model derivation approach.

Alternative MLMC traffic flow model formulations.

The conservative macroscopic MLMC model is recast using so-called *primitive* and *characteristic* variables respectively. The primitive variables density, velocity, and velocity variance describe the mean behaviour of the drivers of a specific user-class on a lane. The primitive MLMC model enables interpretation of traffic flow dynamics from the drivers' viewpoint. For instance, the mean velocity changes due to drivers anticipating on changing velocity variances downstream. We conclude that this interpretation *is not valid* for multiclass traffic flow: the terms in the flow equations are a result of convective processes (vehicle particles flowing into an infinitesimal roadway cell) and should be considered as such.

The *characteristic* formulation enables mathematical analysis of the model behaviour. It shows how properties of the MLMC flow are transported in the (x,t)-domain along the *characteristics*. By considering that in case of constrained traffic operations properties of the traffic flow are only transported upstream, this characteristic formulation has lead to the derivation of a new indicator for congestion. Moreover, the characteristic formulation enables the analysis of shock waves in MLMC traffic flow.

Equilibrium relations.

The *equilibrium expressions* for the MLMC velocity and velocity variance (or momentum and energy) quantify the asymmetric user-class and lane interactions. They result from competitive *acceleration* and *deceleration* processes: on the one hand, vehicles accelerate towards their desired velocity, while on the other hand, vehicles that interact with slower vehi-

cles from the same or different user-classes – without being able to immediately overtake to an adjacent lane – decelerate.

The equilibrium lane-distribution is established by determining the balance between the inflows and outflows of the lanes. The resulting equilibrium relation is expressed as a function of the number of interacting and constrained vehicles that are able to change lanes, and of the number of vehicles changing to their preferred lane.

1.5.5 Numerical solution approaches

Two new approaches to numerically solve general higher-order flow models are established. The developed approaches are based on the *conservative* and the *characteristic* model formulation respectively. The first approach is based on appropriate splitting of the conservative flux into contributions of traffic conditions upstream and downstream. The second approach is based on the *Godunov-scheme*, which uses exact solutions of the Riemann problem for the MLMC model, that are determined by assuming that the flow is in equilibrium and the viscous effects can be neglected.

The proposed methods consider physical properties of the model. The schemes behave differently for different traffic conditions, thereby considering the direction in which information is transported in the flow. The approaches are *explicit*, yielding fast computational schemes. Moreover, based on the characteristic formulation, we establish the necessary boundary conditions for congested and non-congested traffic flow operations.

1.5.6 Data analysis and filtering techniques

In order to prepare empirical calibration and validation, new analysis techniques are developed applying a low-pass filter to the velocity measurements of individual vehicles. The filter yields the correct smoothing of the velocity, while preserving the structural dynamic fluctuations. That is, in transition periods between traffic states (e.g. free-flow, synchronised flow, traffic jams), the filtered velocity follows the flow dynamics effectively.

By analysis of traffic data of a two-lane motorway, empirical equilibrium relations present in the model formulation are determined. That is, empirical relations are obtained relating the velocity variance, the immediate lane-changing probability and the lane-changing rates on the one hand, and the effective density on the other hand.

1.5.7 Model applications

Finally, applications of the discretised model in a variety of test-case scenarios are performed and analysed. From the macroscopic simulation, we conclude that the model satisfies the fundamental issues raised by Daganzo (1995). Moreover, the model captures hysteresis effects observed in real-life traffic operations, and describes the spontaneous occurrence of phantom-jams. By considering results from macroscopic simulations, we show that the model is able to realistically describe the MLMC traffic operations on Dutch motorways. Additionally, several test-cases are analysed and discussed which are of practical relevance (truck-overtaking prohibition, variable speed-limit control), showing the application potential of the developed MLMC model.

2 STATE-OF-THE-ART OF VEHICULAR TRAFFIC FLOW MODELLING

Research on the subject of traffic flow modelling started some forty years ago, when Lighthill and Whitham (1955) presented a macroscopic modelling approach based on the analogy of vehicles in traffic flow with the dynamics of particles in a fluid. During the last five decades a variety of traffic flow models have been proposed, aiming to improve on the original effort of Lighthill and Whitham.

Traffic flow models can be categorised based on a number of criteria (level of detail, operationalisation, representation of the processes). We discuss several traffic flow models, based on the *level-of-detail* classification (i.e. (sub-) microscopic, mesoscopic, and macroscopic modelling approaches). Since this thesis will deal with gas-kinetic and macroscopic flow models, the main emphasis will be on these modelling approaches.

After introducing some important models, we motivate the level of modelling detail that has been chosen in this thesis, considering the foreseen model applications in multilane traffic control of heterogeneous traffic flow. Subsequently, we elaborate upon the macroscopic modelling controversy, which has been the cause for some debate during the last decade of flow modelling research.

2.1 Traffic flow modelling and simulation

Traffic operations on motorways can be improved by field research and field experiments of real-life traffic flow. However, apart from the scientific problem of reproducing such experiments, the problem of costs and safety play a role of dominant importance as well. Due to the complexity of the traffic flow system, analytical approaches may not always provide the de-

sired results. Therefore, traffic flow (simulation-) models designed to characterise the behaviour of the complex traffic flow system have become an essential tool in traffic flow analysis and experimentation. Depending on the type of model, the application area of these simulation tools is very broad, e.g.:

- Evaluation of alternative treatments in (dynamic) traffic management.
- Design and testing of new transportation facilities (e.g. geometric designs).
- Operational flow models serving as a sub-module in other tools (e.g. model-based traffic control and optimisation, and dynamic traffic assignment).
- Training of traffic managers.

The description of observed phenomena in traffic flow is not self-evident. General mathematical models aimed at describing this behaviour using mathematical equations include the following approaches (cf. Papageorgiou (1998)):

1. Purely *deductive* approaches whereby known accurate physical laws are applied.
2. Purely *inductive* approaches where available input/output data from real systems are used to fit generic mathematical structures (ARIMA models, polynomial approximations, neural networks).
3. *Intermediate* approaches, whereby first basic mathematical model-structures are developed, after which a specific structure is fitted using real data.

Papageorgiou (1998) convincingly argues that it is unlikely that any (macroscopic) traffic flow theory will reach the descriptive accuracy attained in other domains of science (e.g. Newtonian physics or thermodynamics). The author states that the only accurate physical law in traffic flow theory is the *conservation of vehicles equation*; all other model structures reflect either counter-intuitive idealisations or coarse approximations of empirical observations. Consequently, the challenge of traffic flow researchers is to look for useful theories of traffic flow that have sufficient descriptive power, where *sufficiency* depends on the application purpose of their theories.

In this chapter, we present some of the modelling achievements of five decades of traffic flow modelling research. To this end, the discussed traffic models are classified according to a variety of criteria. In this chapter, we employ a classification based on the following criteria:

- Scale of the independent variables (continuous, discrete, semi-discrete);
- Level of detail (submicroscopic, microscopic, mesoscopic, macroscopic);
- Representation of the processes (deterministic, stochastic);
- Operationalisation (analytical, simulation);
- Scale of application (networks, stretches, links, and intersections).

Other criteria are possible as well, but are not considered in this thesis. Table 2-1 presents an overview of some well-known models, based on the proposed criteria. This table is not exhaustive, but rather it provides some indication with respect to the traffic modelling efforts during the last five decades.

Table 2-1: Overview of traffic flow models.

MIXIC (Van Arem et al (1995))	+		+	+	d	s	s	ml
SIMONE (Minderhoud (1999))	+	+	+	+	d	s	s	ml, d
PELOPS (Ludmann (1998))	+		+	+	d	s	s	ml
safe-distance models (May (1990))	+				c	d	a	sl
stimulus-response models (Leutzbach (1988), May (1990))	+				c	d	a	sl
psycho-spacing models (Wiedemann (1974))	+	+	+		c	s	s	ml
FOSIM (Vermijs (1995))	+	+	+	+	d	s	s	ml, d
CA-models (Nagel (1996,1998), Brilon and Wu (1998), Wu and Brilon (1999), Esser *et al*. (1999))	+	+			d	s	s	n, u
Particle pedestrian model (Hoogendoorn and Bovy (2000))	+	+	+	+	d	s	s	o
INTEGRATION (Van Aerde (1994)).	+				d	d	s	n
headway distr. models (Hoogendoorn and Botma (1996a), Hoogendoorn and Bovy (1997e,f,1999c))			+	+	c	s	a	c
reduced gas-kinetic model (Prigogine and Herman (1971))	+				c	d	a	al
improved gas-kinetic model (Paveri-Fontana (1975))	+	+			c	d	a	al
multilane gas-kinetic model (Helbing (1997b))	+	+		+	c	d	a	ml, d
multiclass gas-kinetic model (Hoogendoorn (1997), Hoogendoorn and Bovy (1999a))	+	+		+	c	d	a	al
Cluster models (Botma (1978))	+	+			c	d	a	al
LWR model (Lighthill and Whitham (1955))	+				c	d	a	al
Payne-type models ((Payne (1979))	+				c	d	a	al
Helbing-type models (Helbing (1996))	+			+	c	d	a	al
Cell-Transmission Model (Daganzo (1994a,b,1999))	+				d	d	s	n
METANET (Kotsialos *et al*. (1998,1999))	+				d	d	s	n
Semi-discrete model (Smulders (1989))					sd	s	a	al, d
FREFLO (Payne (1971,1979))	+				d	d	s	n
MASTER (Helbing *et al*.(1999))	+				d	d	a	ml

DI: dimension (other than time / space): velocity v, desired velocity v^0, lateral position y (lanes), and other
SC: scale (continuous, discrete, and semi-discrete);
RE: process representation (deterministic, stochastic);
OP: operationalisation (analytical, simulation);
AR: area of application (cross-section, single lane stretches, multilane stretches, aggregate lane stretches, discontinuities, motorway network, urban network, and other).

2.1.1 Level of detail

Traffic models may be classified according to the *level of detail* with which they represent the traffic systems. This categorisation can be operationalised by considering the *distinguished traffic entities* and the *description level* of these entities in the respective flow models. We propose the following classification:

1. Submicroscopic simulation models (high detail description of the functioning of vehicles' sub-units and the interaction with their surroundings).
2. Microscopic simulation models (high detail description where individual entities are distinguished and traced).
3. Mesoscopic models (medium detail).
4. Macroscopic models (low detail).

A *microscopic simulation* model describes both the space-time behaviour of the systems' entities (i.e. vehicles and drivers) as well as their interactions at a high level of detail (individually). For instance, for each vehicle in the stream a lane-change is described as a detailed chain of drivers' decisions.

Similar to microscopic simulation models, the *submicroscopic* simulation models describe the characteristics of individual vehicles in the traffic stream. However, apart from a detailed description of driving behaviour, also *vehicle control behaviour* (e.g. changing gears, AICC operation, etc.) in correspondence to prevailing surrounding conditions is modelled in detail. Moreover, the functioning of specific parts (sub-units) of the vehicle is described.

A *mesoscopic model* does not distinguish nor trace individual vehicles, but specifies the *behaviour* of individuals, for instance in probabilistic terms. To this end, traffic is represented by (small) groups of traffic entities, and their activities and interactions are described at a low detail level. For instance, a lane-change manoeuvre might be represented for an individual vehicle as an instantaneous event, where the decision to perform a lane-change is based on e.g. relative lane densities, and speed differentials. Some mesoscopic models are derived in analogy to gas-kinetic theory. These so-called gas-kinetic models describe the dynamics of velocity distributions, and will play an essential role in this dissertation.

Macroscopic flow models describe traffic at a high level of aggregation as a flow without distinguishing its constituent parts. For instance, the traffic stream is represented in an aggregate manner using characteristics as flow-rate, density, and velocity. Individual vehicle manoeuvres, such as a lane-change, are usually not explicitly represented. A macroscopic model may assume that the traffic stream is properly allocated to the roadway lanes, and employ an approximation to this end. Macroscopic flow models can be classified according the *number* of partial differential equations that frequently underlie the model one the one hand, and their *order* on the other hand.

2.1.2 Scale of the independent variables

Since almost all traffic models describe dynamical systems, a natural classification is based upon the time-scale. We will distinguish two time scales, namely continuous and discrete. A *continuous* model describes how the traffic system's state changes continuously over time in response to continuous stimuli. *Discrete models* assume that state changes occur discontinuously over time at discrete time instants.

Besides time, also other independent variables can be described by either continuous or discrete variables (e.g. position, velocity, desired velocity). Mixed models have also been proposed. For instance, Smulders (1989) describes a flow model that is continuous in time and discrete with respect to position.

2.1.3 Representation of the processes

In this respect, we will distinguish *deterministic* and *stochastic* models. The former models have no random variables implying that all actors in the model are defined by exact relationships. Stochastic models incorporate processes that include random variates. For instance, a car-following model can be formulated as either a deterministic or a stochastic relationship by defining the driver's reaction time as a constant or as a random variable respectively.

2.1.4 *Operationalisation*

With respect to the operationalisation criterion, models can be operationalised either as analytical solutions of sets of equations, or as a simulation model. For a thorough contemplation on the uses and misuses of simulation in traffic, we refer to chapter 13 of May (1990).

2.1.5 *Scale of application*

The application scale indicates the area of application of the model. For instance, the model may describe the dynamics of its entities for a single roadway stretch, an entire traffic network, a corridor, a city, etc.

In the remainder of this chapter, we discuss the modelling approaches in more detail, based on the *level-of-detail* classification ((sub-) microscopic, mesoscopic and macroscopic). We will also provide some examples of models for each of these modelling types. Aim of the discussion is to provide some insight into mechanisms of different modelling approaches.

2.2 Submicroscopic and microscopic traffic flow modelling

2.2.1 *Car-following models*

During the 1960's, research efforts focussed on the so-called *follow the leader models*. These models are based on the supposed mechanisms describing the process of one vehicle following another. That is, the behaviour of each vehicle is modelled in relation to the vehicle ahead. In this section, we will discuss three types of car-following models, namely safe-distance models, stimulus-response models, and psycho-spacing models.

Safe-distance models

Safe-distance car-following models describe the dynamics of a single vehicle in relation to its predecessor. In this respect, a very simple model is Pipes rule (cf. Pipes (1953)): "*A good rule for following another vehicle at a safe distance is to allow yourself at least the length of a car between you and the vehicle ahead for every ten miles an hour (16.1km/hr) of speed at which you are travelling*". Using this driving-rule, we can determine the required *gross distance headway* D_n of vehicle n driving with velocity v with respect to vehicle $n-1$:

$$D_n(v) = L_n(1 + v/16.1) \tag{2.1}$$

where L_n denotes the length of vehicle n. In Pipes' model, the minimal safe distance increases linearly with the velocity v of the vehicle. Forbes (1958) proposed a slightly different approach. He assumed that the *minimal gross-time headway* $H_n(v)$ is equal to the class specific reaction time T (which equals the *minimum time gap*) and the time a vehicle requires to traverse a distance equal to its length L_n:

$$H_n(v) = T + L_n / v \tag{2.2}$$

The reaction time is defined by the difference between the instant that an obstacle appears to the instance that the vehicle begins to decelerate. Expression (2.2) leads to a minimal space that is equal to:

$$D_n(v) = H_n(v)v = vT + L_n \tag{2.3}$$

Both Pipes' theory and Forbes' theory were compared to field measurements. It was concluded that according to Pipes' theory, the minimum headways are slightly less at low and high velocities than observed in empirical data. However, considering the simplicity of the model, the agreement with real-life observations was amazingly close (cf. Pignataro (1973)). Obviously, Forbes' theory also showed very close agreement with the field data.

Leutzbach (1988) discusses a more refined model describing the spacing of constrained vehicles in the traffic flow. He states that the overall reaction time T consists of:

- *The perception time.* This equals the time needed by the driver to recognise that there is an obstacle.
- *The decision time.* That is, the time needed to make decision to decelerate.
- *The braking time.* The time needed to apply the brakes.

The braking distance is defined by the distance needed by a vehicle to come to a full stop, incorporating the reaction time of the driver, and the maximal deceleration. The latter is among other things a function of the weight of the friction with the road surface μ, and the acceleration due to gravity g.

The *total safety distance model* assumes that drivers consider braking distances large enough to permit them to brake to a stop without causing a rear-end collision with the preceding vehicles if the latter vehicles come to a stop *instantaneously*. The safe distance headway equals:

$$D_n(v) = L_n + Tv + v^2/(2\mu g) \tag{2.4}$$

Let us consider two successive vehicles with approximately equal braking distances. We assume that the spacing between the vehicles must suffice to avoid a collision when the first vehicle comes to a full stop (the so-called *reaction time distance model*). That is, if the first vehicle stops, the second vehicle only needs the distance it covers during the overall reaction time T with *unreduced speed*, yielding Forbes' model.

The model of Jepsen (1998) proposes that the gross-distance headway $D_n(v)$ effectively occupied by vehicle n driving with velocity v is a function of the vehicle's length L_n, a constant minimal distance between the vehicles d_{min}, the reaction time T and a speed risk factor F:

$$D_n(v) = (L_n + d_{min}) + v(T + vF) \tag{2.5}$$

Experienced drivers have a fairly precise knowledge of their reaction time T. For novice drivers, rules of thumb apply ("stay two seconds behind the vehicle ahead", "keep a distance of half your velocity to the vehicle ahead"). From field studies, it is found that the delay of an unexpected event to a remedial action is in the order of 0.6 to 1.5 seconds. The *speed-risk factor* F stems from the observation that experienced drivers do not only aim to prevent rear-end collisions. Rather, they also aim to minimise the potential damage or injuries of a collision, and are aware that in this respect their velocity is an important factor. This is modelled by assuming that drivers increase their *time* headway by some factor – the *speed-risk factor* – linear to v. Finally, the *minimal distance headway* d_{min} describes the minimal amount of spacing between motionless vehicles, which can be observed at jam density.

Note that this occupied space equals the gross distance headway only if the following vehicle is constrained. In the remainder of this thesis, this property is used. Otherwise, the car-following distance is larger than the safe distance needed. Dijker *et al.* (1997,1998) discuss some empirical findings on user-class specific car-following behaviour in congested traffic flow conditions. The model of Jepsen (1998) is used in section 4.6.4 and section 6.7 to account for the *finite-space requirements* of vehicles in the multilane traffic stream.

Stimulus-response car-following models

Drivers who follow try to conform to the behaviour of the preceding vehicle. This car-following process is based on the following principle:

$$response = sensitivity \times stimulus \tag{2.6}$$

The *response* is in general braking or acceleration of the following vehicle, delayed by an overall reaction time T. Consider vehicle n following vehicle $n-1$. Let $x_n(t)$ denote the position of vehicle n at instant t. A well known model specification is (Chandler *et al.* (1958)):

$$a_n(t+T) = \gamma(v_{n-1}(t) - v_n(t)) \tag{2.7}$$

where $v_n(t)$ and $a_n(t)$ denote the velocity and the acceleration respectively of vehicle n at t, and γ denotes the driver's sensitivity. Thus, the *stimulus* is defined by the velocity difference between the leading and the following vehicle. The following expression has been proposed for driver's *sensitivity* γ (Gazis *et al.* (1961)):

$$\gamma = c\frac{(v_n(t+T))^m}{(x_{n-1}(t) - x_n(t))^l} \tag{2.8}$$

Thus, the following vehicle adjusts its velocity $v_n(t)$ proportionally to the both the distance and speed differences with a delay equal to T. The extent to which this occurs depends on the values of c, l and m.

In combining (2.7) and (2.8), and subsequently integrating the resulting equation, relations between the velocity $v_n(t+T)$ and the distance headway $x_{n-1}(t)-x_n(t)$ can be determined. Assuming stationary traffic conditions, the following relation between the *equilibrium velocity* V^e and the *density* r results:

$$V^e(r) = V^0(1 - (r / r_{jam})^{l-1})^{1/(1-m)} \tag{2.9}$$

for $m \neq 1$ and $l \neq 1$. We refer to Leutzbach (1988) for a more general expression.

In the model of Gazis *et al.* (1961), behaviour of free-flowing drivers is modelled very unrealistically: when the distance headway is very large, drivers still react to velocity differences. Also, slow drivers are *dragged along* when following faster vehicles. When vehicle-types are distinguished, this modelling assumption implies that a slow truck following a fast person-car increases its velocity until it drives at the same velocity as the leading person-car. In addition, the traffic is assumed homogeneous. That is, all model parameters are equal for all user-classes and all lanes of the roadway.

Since lane-changing processes cannot be easily described, car following models have been mainly applied to single lane traffic (e.g. tunnels, cf. Newell (1961)) and traffic stability analysis (Herman *et al.* (1959), May (1990; chapter 6)). That is, using car-following models

the limits of local and asymptotic stability of the stream can be analysed. Montroll (1961) proposed applying a stochastic term to equation (2.7) representing the *acceleration noise*, describing the difference between actual acceleration and the 'ideal' acceleration. A different application is the use of a simple follow-the-leader rule to derive a second-order macroscopic flow model (Payne (1971)):

$$V(x(t+T),t+T) = V^e(r(x+D,t)) \tag{2.10}$$

where $x(t)$ denotes the location of the driver at instant t, $V(x,t)$ its velocity at x and t, V^e the equilibrium velocity as a function of the density r at $(x+D,t)$; T equals the reaction time and D equals the gross-distance headway with respect to the preceding vehicle. Equation (2.10) shows that drivers adapt their velocity to the equilibrium velocity, which is a function of the traffic density at $x+D$. The equilibrium velocity represents a trade-off between the desired velocity of a driver (i.e. the velocity the driver aims to attain when conditions are free-flow), and a reduction in the velocity due to worsening traffic conditions. In this thesis, we will present an expression of the latter reduction, based on the expected frequency at which a driver needs to reduce his velocity due to interactions with slower vehicles.

Psycho-spacing models

For $l \neq 0$, the car-following equations (2.7) and (2.8) presume that the following driver reacts, on the one hand, to very small changes in the relative velocity $v_n(t)-v_{n+1}(t)$, even when the distance headway is large. On the other hand, the model assumes that the response equals zero as the velocity differences disappear, even if the distance between the consecutive vehicles is very small or large. To remedy this problem insights from perceptual psychology have been used to show that drivers are subject to certain limits in their perception of the stimuli to which they respond (cf. Todosiev and Barbosa (1964)).

The basic behavioural rules of such so-called *psycho-spacing* models are:

- At large spacings, the following driver is not influenced by the magnitude of the velocity differences.
- At small spacings, some combinations of relative velocities and distance headways do not yield a response of the following driver, because the relative motion is too small.

Wiedemann (1974) developed the first psycho-spacing model. He distinguished *constrained* and *unconstrained driving* by considering *perception thresholds*. Moreover, *lane-changing* and *overtaking* are incorporated in his modelling approach. Psycho-spacing models are the foundation of a number of contemporary microscopic simulation models (section 2.2.2).

2.2.2 *Microscopic simulation models*

The availability of fast computers has resulted in an increasing interest in complex microsimulation models. These models distinguish and trace single cars and their drivers. The driver's behaviour is generally described by a large set of if-then rules (production-rule systems). From driver behaviour and vehicle characteristics, position, speed and acceleration of each car are recalculated for each time step.

A large number of microscopic simulation models have been developed. Some of these are *true* microscopic simulations, in the sense that they model the car-following behaviour and

the lane-changing behaviour of each individual vehicle in the traffic flow. Usually, the car-following behaviour is based on the *psycho-spacing* modelling paradigm. To describe the lane-changing behaviour, microscopic models generally distinguish the decision to perform a lane-change, the choice of a target lane, and the acceptance of the available gap on this target lane. We refer to appendix C for a more detailed description of these processes.

Examples of microscopic simulation models are AIMSUN2 (Barceló *et al.* (1998)), FOSIM (Vermijs (1995)), and the model of Wiedemann (1974).

2.2.3 *Submicroscopic simulation models*

In addition to describing the time-space behaviour of the individual entities in the traffic system, submicroscopic simulation models describe the functioning of specific parts and processes of vehicles and driving tasks. For instance, a submicroscopic simulation model describes the way in which a driver applies the brakes, considering among other things the driver's reaction time, the time needed to apply the brake, etc. These submicroscopic simulation models are very suited to model the impacts of driver support system on the vehicle dynamics and driving behaviour. For example, the submicroscopic model SIMONE (Minderhoud (1999)) describes the functioning and the driver's operation of an Intelligent Cruise Control (ICC) system, influenced by the direct surroundings of the vehicle.

Other examples of submicroscopic models are MIXIC (Van Arem (1995)) and PELOPS (Ludmann (1998)). For a review on microscopic and submicroscopic simulation models, we refer to Ludmann (1998) and Minderhoud (1999).

2.2.4 *Cellular automaton models*

A more recent addition to the development of microscopic traffic flow theory are the so-called *Cellular Automaton* (CA) or *particle hopping* models. CA-models describe the traffic system as a lattice of cells of equal size (typically 7.5*m*). A CA-model describes in a discrete way the movements of vehicles from cell to cell (cf. Nagel (1996,1998)). The size of the cells are chosen such that a vehicle driving with a velocity equal to one moves to the next downstream cell during one time step. The vehicle's velocity can only assume a limited number of discrete values ranging from zero to v_{max}.

The process can be split-up into three steps:

- *Acceleration*. Each vehicle with velocity smaller than its maximum velocity v_{max}, accelerates to a higher velocity, i.e. $v \leftarrow \min(v_{max}, v+1)$.
- *Deceleration*. If the velocity is smaller than the distance gap d to the preceding vehicle, then the vehicle will decelerate: $v \leftarrow \min(v,d)$.
- *Dawdling* ("*Trödeln*"). With given probability p_{max}, the velocity of a vehicle decreases spontaneously: $v \leftarrow \max(v-1,0)$.

Using this *minimal set* of driving rules, and the ability to apply parallel computing*, the CA-model is very fast, and can consequently be used both to simulate traffic operations on large-

* When one relaxes the *parallel update* requirement, we generally do not speak of Cellular Automata models. However, the term *particle hopping model* still applies (cf. Nagel (1998)).

scale motorway networks, as well as for traffic assignment and traffic forecasting purposes. The initial single-lane model of Nagel (1996) has been generalised to multilane multiclass traffic flow (cf. Nagel *et al.* (1998)). Due to the simplicity of computation, the CA-models are applicable to large traffic networks.

The classical CA car-following model is *space-oriented* and of a heuristic nature. Brilon and Wu (1998), and Wu and Brilon (1999) proposed an alternative multilane CA-model, using *time-oriented* car-following rules. This model describes drivers' behaviour more realistically, while retaining all positive features of the original CA-model.

CA-models aim to combine advantages of complex micro-simulation models, while remaining computationally efficient. However, the car-following rules of both the space-oriented and time-oriented CA-models lack intuitive appeal and their exact mechanisms are not easily interpretable from the driving-task perspective. Moreover, they are too crude to describe and study microscopic details of traffic flow, such as overtaking and merging, sufficiently accurate from the perspective of a single driver's characteristics.

Verification of CA-models on German and American motorways and urban traffic networks (cf. Brilon and Wu (1998), and Wu and Brilon (1999), Nagel *et al.* (1998a), Esser *et al.* (1999)) shows fairly realistic results on a macroscopic scale, especially in the case of urban networks.. For instance, CA-model reproduces the speed-flow relations reasonably accurate. However, like other microscopic simulation models, the CA-model does not provide insight by means of mathematical analysis and manipulation. Nagel (1998) describes the relation of CA-models with simple macroscopic continuum models.

2.2.5 Particle models

In closure of this section on microscopic and submicroscopic simulation models, we briefly consider the so-called *particle models*. Although these models distinguish and trace the individual vehicles, their behaviour is described by aggregate equations of motion, for instance a macroscopic traffic flow model. These particle models can be considered as a specific type of numerical solution approach (so-called *particle discretisation methods*; cf. Hockney and Eastwood (1988)), applied to mesoscopic or macroscopic continuum traffic flow models. An example of a particle model is INTEGRATION (Van Aerde (1994)). A recent development is described by Hoogendoorn and Bovy (2000), who derived a stochastic microscopic pedestrian simulation model based on gas-kinetic pedestrian flow equations.

2.3 Mesoscopic traffic flow models

Mesoscopic flow models describe traffic flow at a medium detail level. Vehicles and driver behaviour are not distinguished nor described individually, but rather in more aggregate-terms (e.g. using probability distribution functions). However, the behaviour rules are described at an individual level. For instance, a gas-kinetic model describes velocity distributions at specific locations and time instants. The dynamics of these distributions are generally governed by various processes (e.g. acceleration, interaction between vehicles, lane-changing), describing the individual driver's behaviour.

Three well know examples of mesoscopic flow models are the so-called *headway distribution* models, *cluster* models, and the *gas-kinetic continuum* models. Since the latter modelling

type will form the basis of the multiclass macroscopic model for multilane traffic flow developed in this thesis, we will discuss the gas-kinetic approach in more detail.

2.3.1 Headway distribution models

A *time-headway* is defined by the difference in passage times of two successive vehicles. In general, it is assumed that these time-headways are identically distributed independent random variates. Headway distribution models are *mesoscopic* in the sense that they describe the *distribution* of the headways of the individual vehicles, while neither explicitly considering nor tracing each vehicle separately.

Examples of headway distribution models are Cowan's M3 distribution model (cf. Cowan (1975)), Buckley's semi-Poisson model (Buckley (1968)), and the Generalised Queuing Model (cf. Branston (1976)). *Mixed headway distribution models* distinguish between *leading* and *following* vehicles. The time headways of leading drivers and following drivers are taken from different probability distributions.

Headway distribution models have been criticised since these models assume that all vehicles are essentially the same. That is, the probability distribution functions are independent of the traveller type, the vehicle type, the travel purpose, the level of drivers' guidance, etc. To remedy this, Hoogendoorn and Bovy (1998e,f) and Hoogendoorn and Bovy (1999c) developed a headway distribution model for respectively multiclass traffic flow and multiclass multilane traffic flow. Using a new estimation technique (cf. Hoogendoorn and Botma (1997)), they analyse multiclass traffic on both two-lane rural roads as well as two-lane motorways in the Netherlands. Furthermore, headway distribution models neglect the role of traffic dynamics.

2.3.2 Cluster models

Cluster models are characterised by the central role of *clusters* of vehicles. A cluster is a group of vehicles that share a specific property. Different aspects of clusters can be considered. Usually, the *size* of a cluster (the number of vehicles in a cluster) and the *velocity* of a cluster are of dominant importance. Generally, the size of a cluster is dynamic: clusters can grow and decay. The within cluster traffic conditions, e.g. the headways, velocity differences, etc., are usually *not* considered explicitly: clusters are *homogeneous* in this sense. Usually, clusters emerge because of restricted overtaking possibilities due to e.g. overtaking prohibitions, or interactions with other vehicles making overtaking impossible, or due to prevailing weather or ambient conditions (see Botma (1978)).

2.3.3 Gas-kinetic continuum models of Prigogine and Herman

Instead of describing the traffic dynamics of individual vehicles, gas-kinetic traffic flow models describe the dynamics of the velocity distribution functions of vehicles in the traffic flow. In this section, we recall the seminal models of Prigogine and Herman (cf. Prigogine (1961), Prigogine and Herman (1971), Anderson *et al.* (1972)), after which a few extensions to this model type are dealt with.

The gas-kinetic models describe the dynamics of the reduced *Phase-Space Density* (PSD) $\tilde{\rho}(x,v,t)$ *. The reduced PSD can be interpreted as follows: at instant t the expected number of vehicles present at an infinitesimal region $[x,x+dx)$ driving with a velocity $[v,v+dv)$ equals $\tilde{\rho}(x,v,t)dxdv$. The concept of the reduced PSD is borrowed from statistical physics, and can be considered as a *mesoscopic generalisation* of the macroscopic traffic density $r(x,t)$. The reduced PSD reflects the *velocity distribution function* of a single-vehicle. Prigogine and Herman (1971) also introduce the *two-vehicle distribution function* $\tilde{\varphi}(x,v,x',v',t)$, which can be interpreted as follows: $\tilde{\varphi}(x,v,x',v',t)dxdvdx'dv'$ describes the expected number of *vehicle pairs*, where the vehicles are respectively located at $[x,x+dx)$ and $[x',x'+dx')$ while driving at velocity $[v,v+dv)$ and $[v',v'+dv')$.

Prigogine and Herman assumed that dynamic changes of the reduced PSD are caused by the following processes:

- *Convection.* Vehicles with a velocity v flowing into or out of the roadway segment $[x,x+dx)$ cause changes in the reduced PSD $\tilde{\rho}(x,v,t)$.
- *Acceleration towards the desired velocity.* Vehicles not driving at their desired velocity will accelerate if possible.
- *Deceleration due to interaction between drivers.* A vehicle that interacts with a slower vehicle will need to reduce its velocity when it cannot immediately overtake.

Their deliberations yielded the following partial differential equation:

$$\partial_t\tilde{\rho} + v\partial_x\tilde{\rho} = (\partial_t\tilde{\rho})_{acc} + (\partial_t\tilde{\rho})_{int} \tag{2.11}$$

where we have used the shorthand notation $\partial_t\tilde{\rho} = \partial\tilde{\rho}/\partial t$, and where $(\partial_t\tilde{\rho})_{acc}$ reflects changes caused by acceleration towards the desired velocity and $(\partial_t\tilde{\rho})_{int}$ denote changes caused by interactions between vehicles.

Interaction process

Prigogine (1961) assumed that when an incoming fast moving car (velocity v) reaches a slow moving vehicle (velocity $w < v$), it either passes directly, or it slows down to the velocity w of the slow vehicle. The following assumptions are made:

- The *slow-down event* has a probability of $1-\pi$, while the *immediate overtaking event* has probability π. Overtaking does *not* affect the velocity v of the fast vehicle.
- The velocity w of the slow vehicle is unaffected by interaction events.
- The lengths of vehicles can be neglected.
- The fast vehicle slows-down instantaneously.
- Interactions affecting more than two vehicles are neglected.

Based on these assumptions, the interaction term equals the so-called *collision equation*:

* In the sequel the 'reducedness' will be explained.

$$(\partial_t \tilde{\rho})_{\text{int}} = (1-\pi)\int (w-v)\tilde{\varphi}(x,v,x,w,t)\mathrm{d}w \tag{2.12}$$

The assumption of *vehicular chaos* – vehicles are *uncorrelated* – implies:

$$\tilde{\varphi}(x,v,x',v',t) = \tilde{\rho}(x,v,t)\cdot\tilde{\rho}(x',v',t) \tag{2.13}$$

Thus, the collision equation (2.12) becomes:

$$(\partial_t \tilde{\rho})_{\text{int}} = (1-\pi)\tilde{\rho}(x,v,t)\int (w-v)\tilde{\rho}(x,w,t)\mathrm{d}w \tag{2.14}$$

Acceleration process

The acceleration process describes relaxation of drivers' speed towards a traffic-condition dependent equilibrium velocity. Prigogine (1971) proposed the following expression:

$$(\partial_t \tilde{\rho})_{\text{acc}} = -\partial_v(\tilde{\rho}\cdot(\tilde{V}^0(v\,|\,x,t)-v)/\tau) \tag{2.15}$$

where τ denotes the acceleration time and $\tilde{V}^0(v\,|\,x,t)$ is the *desired velocity* distribution.

Nelson (1995) and Nelson *et al.* (1997) improved the gas-kinetic models, by relaxing the assumption of Prigogine and Herman (1971) that speeds of slowing-down vehicles are *uncorrelated* with speeds of impeding vehicles. This is achieved by describing both slowing-down and speeding-up interactions by a quadratic Boltzmann term, based on suitable *mechanical* (driver-reaction) and vehicular *correlation* models, while neglecting passing interactions.

2.3.4 *Improved gas-kinetic model of Paveri-Fontana*

The interaction term has been criticised, mainly concerning the validity of the *vehicular chaos assumption*. It has been argued that the collision term "corresponds to an approximation in which correlation between nearby drivers is neglected", being only valid in situations where no vehicles are platooning (cf. Munjal and Pahl (1969)). Paveri-Fontana (1975) considers a hypothetical scenario where a free-flowing vehicle catches up with a slow moving queue. He considers two extreme cases:

1. The incoming vehicle passes the *whole* queue as if it were one vehicle.
2. It consecutively passes each single car in the queue *independently*.

Paveri-Fontana shows that the Prigogine and Herman formalism reflects the second case, while the real-life situation falls between these two extremes. Paveri-Fontana (1975) also shows that the term reflecting the acceleration process yields a desired velocity distribution that is dependent on the local number of vehicles. This is in contradiction to the well-accepted hypothesis that driver's personality is indifferent with respect to changing traffic conditions (the so-called *personality condition*; cf. Daganzo (1995)). To remedy this deficiency, Paveri-Fontana considers the *Phase-Space Density* (PSD) $\rho(x,v,v^0,t)$. The latter can be considered as a generalisation of the *reduced* Phase-Space-Density with an independent variable describing the desired velocity v^0. He proposed using equation (2.11) in which*:

* For convenience, we have dropped the dependence on (x,t) from notation.

$$(\partial_t \rho)_{acc} = -\partial_v(\rho \cdot (v^0 - v)/\tau) \tag{2.16}$$

and:

$$(\partial_t \rho)_{int} = -\rho(v,v^0)\int_{w<v}(1-\pi)\,|\,w-v\,|\,\tilde{\rho}(w)\mathrm{d}w + \tilde{\rho}(v)\int_{w>v}(1-\pi)\,|\,w-v\,|\,\rho(w,v^0)\mathrm{d}w \tag{2.17}$$

where the *reduced PSD* equals:

$$\tilde{\rho}(v) = \tilde{\rho}(x,v,t) \overset{def}{=} \int \rho(x,v,v^0,t)\mathrm{d}v^0 \tag{2.18}$$

2.3.5 *Gas-kinetic multiclass traffic flow modelling*

Hoogendoorn (1997) and Hoogendoorn and Bovy (1999a) developed gas-kinetic multiclass traffic flow models, describing the dynamics of the so-called Multiclass Phase-Space-Density (MUC-PSD) $\rho_u(x,v,v^0,t)$, where u indicates the user-class u from the set **U**, yielding:

$$\partial_t \rho_u + v\partial_x \rho_u = (\partial_t \rho_u)_{acc} + (\partial_t \rho_u)_{int} \tag{2.19}$$

where:

$$(\partial_t \rho_u)_{acc} = -\partial_v(\rho_u \cdot (v^0 - v)/\tau_u) \tag{2.20}$$

describes the acceleration process of vehicles of class u towards their desired velocity v^0, given the acceleration time τ_u, and where:

$$(\partial_t \rho_u)_{int} = -(1-\pi_u) \times \sum_{s\in \mathbf{U}}\left(\int\left(\int_{w<v}|\,w-v\,|\,\rho_u(v,v^0)\rho_s(w,w^0)\,\mathrm{d}\,w - \int_{w>v}|\,w-v\,|\,\rho_u(w,v^0)\rho_s(v,w^0)\,\mathrm{d}\,w\right)\mathrm{d}\,w^0\right) \tag{2.21}$$

describes dynamic influences of vehicular interactions of class u with vehicles from the same or other classes. The assumptions underlying the model of Hoogendoorn (1997) and Hoogendoorn and Bovy (1999) are equivalent to those of Prigogine (1961) (see section 2.3.3). Compared to the model of Paveri-Fontana (1975), distinction of user-classes results in an *asymmetric* slow-down process of fast vehicles, i.e. vehicles of relatively fast user-classes catch up with vehicles of slow user-classes more frequently than vice-versa.

2.3.6 *Gas-kinetic multilane equations of Helbing*

Helbing (1997a) presents a gas-kinetic model for multilane traffic flow operations. The approach is similar to the approach of Paveri-Fontana (1975), although lane-changing is explicitly considered. Let j denote the lane index. Then, let $\rho_j(x,v,v^0,t)$ denote the so-called multilane Phase-Space Density (ML-PSD) on lane j. Helbing proposes the following relation:

$$\partial_t \rho_j + v\partial_x \rho_j = (\partial_t \rho_j)_{acc} + (\partial_t \rho_j)_{int} + (\partial_t \rho_j)_{vc} + (\partial_t \rho_j)_{lc} + \nu_j^+ - \nu_j^- \tag{2.22}$$

In contrast to the model of Paveri-Fontana (1975) and Hoogendoorn (1997), the multilane model of Helbing considers three additional terms:

- The *velocity diffusion term* $(\partial_t \rho_j)_{vc}$, taking into account the individual fluctuations of the velocity due to imperfect driving.

- The *lane-changing term* $(\partial_t \rho_j)_{lc}$ modelling dynamic changes in the ML-PSD due to vehicles changing from and to lane j.
- The rate of vehicles entering and leaving the roadway $\nu_j^{\pm}$.

The interaction process is similar to the original model of Paveri-Fontana. Another multilane gas-kinetic model was proposed by Klar and Wegener (1998).

The gas-kinetic model derived in this thesis is a platoon-based multilane multiclass generalisation of the multiclass models of Hoogendoorn (1997), and Hoogendoorn and Bovy (1999a), and the multilane model of Helbing (1997a).

2.4 Continuum macroscopic traffic flow models

Macroscopic traffic flow models assume that the *aggregate* behaviour of drivers depends on the traffic conditions in the drivers' direct environments. That is, they deal with traffic flow in terms of aggregate variables. Usually, the models are derived from the analogy between vehicular flow and flow of continuous media (e.g. fluids or gasses), yielding flow models with a limited number of equations that are relatively easy to handle.

In this section, we discuss *continuum* macroscopic flow models. That is, we will consider models describing the dynamics of macroscopic variables (e.g. density, velocity, and flow) using partial differential equations. Since the model to be established in this thesis is a macroscopic model, the discussion will be elaborate.

The independent variables of a continuous macroscopic flow model are location x and time instant t. To introduce the dependent traffic flow variables, consider a small segment $[x,x+dx)$ of a roadway referred to as 'cell x'. Most macroscopic traffic flow models describe the dynamics of the density $r = r(x,t)$, the velocity $V = V(x,t)$, and the flow $m = m(x,t)$*. The density $r(x,t)$ describes the *expected number of vehicles* on the roadway segment $[x,x+dx)$ *per unit length* at instant t. The flow $m(x,t)$ equals the *expected number of vehicles* flowing past x during $[t,t+dt)$ per time unit. The velocity $V(x,t)$ equals the *expected velocity of vehicle* defined by the $m(x,t)/r(x,t)$. Some macroscopic traffic flow also contain partial differential equations of the *velocity variance* $\Theta = \Theta(x,t)$, or the *traffic pressure* $P = P(x,t) = r\Theta$.

In this section, we will discuss three types of continuum macroscopic models, namely:

1. Lighthill-Whitham-Richards models (dynamic equations of r).
2. Payne-type models (dynamic equations of r and V).
3. Helbing-type models (dynamic equations of r, V, and Θ).

2.4.1 *Conservation of vehicles*

Let us assume that the dependent traffic flow variables are differentiable functions of time and space. Then, the following relations hold exactly:

$$m = rV \tag{2.23}$$

* These traffic variables will be formally introduced in section 3.1 of this thesis

and the *conservation of vehicles equation*:

$$\partial_t r + \partial_x m = 0 \tag{2.24}$$

describing that the number of vehicles in cell x increases according to the balance of inflow at the boundaries x and $x+dx$ of the cell.

Equations (2.23) and (2.24) constitute a system of two independent equations and three unknown variables. Consequently, to get a complete description of traffic dynamics, a third independent model equation is needed. In the ensuing of this section, several model specifications are considered.

2.4.2 *Lighthill-Whitham-Richards (LWR) type models*

The most straightforward approach is to assume that the expected velocity V can be described as a function of the density r:

$$V(x,t) = V^e(r(x,t)) \tag{2.25}$$

The resulting non-linear first-order partial differential equation was introduced by Lighthill and Whitham (1955), and Richards (1956):

$$\partial_t r + \partial_x (rV^e(r)) = 0 \tag{2.26}$$

A drawback of the LWR-model is that it does not yield a unique continuous solution. In addition, the admissible *generalised solutions* are not unique (cf. Lebaque (1996)). Generalised solutions of the non-linear equation (2.24) can be determined by studying the so-called *characteristic curves* along which information from the initial traffic conditions are transported (see section 7.5). It can be shown that from each point on the line $t = 0$, a single characteristic curve originates. These curves $C = \{x(t),t\}$ are *straight lines*, defined by:

$$C = \{t \cdot a(r(x,0)),t\} \tag{2.27}$$

where $a(r) = \mathrm{d}(rV^e(r))/\mathrm{d}r$. When $\partial_x a(r(x,0)) < 0$, the characteristic curves intersect and a *shock wave* is formed (see section 7.6). The shock wave velocity can then be determined using the so-called *Rankine-Hugoniot conditions* (see Hirsch (1990a)), stating that the velocity V_c of the shock, multiplied by the jump in the density shock $[r] = r_2 - r_1$ of the two regions 1 and 2 separated by the shock, equals the jump in the local flow-rate $m_2 - m_1$:

$$V_c = \frac{[m]}{[r]} = \frac{m_2 - m_1}{r_2 - r_1} \tag{2.28}$$

Clearly the direction of the shock wave depends on the sign of $m_2 - m_1$ (outflow from the shock minus inflow of the shock)*.

The equations *do not yield continuous solutions*. Therefore, in practical applications, the *entropy* or (*vanishing*) *viscosity solutions* are determined (see Lebaque (1996)). These vanishing viscosity solutions are solutions of the partial differential equation (2.24) to which a sec-

* Note that since for a shock to occur we have $[r] > 0$, an *upstream moving shock* ($V_c < 0$) implies $m_2 < m_1$. Since this can only occur when upstream traffic conditions are *congested*, in the one-dimensional case an *upstream directed* characteristic implies *congested* traffic conditions. See also section 7.5.4.

ond order viscosity term $\delta\cdot(\partial_x{}^2 r_\delta)$ is added. The resulting solutions r_δ are approximate solutions of (2.24). The *vanishing* viscosity solution is defined by $r = \lim_{\delta\to 0} r_\delta$. It is observed that the viscosity solution is a unique generalised and physically feasible *solution* of eq. (2.24).

2.4.3 *Payne-type models*

Payne (1971) proposed the first continuum traffic flow model by a coupled system of two partial differential equations, that is, the system of equations (2.23) and (2.24) are extended by a partial differential equation describing the dynamics of the velocity V.

Payne's model is derived from a simple car-following rule (2.10). Application of Taylor's expansion rule to the left-hand-side and the right-hand-side of (2.10) yields:

$$V(x(t+T),t+T) \approx V(x,t) + T\cdot V(x,t)\partial_x V(x,t) + T\partial_t V(x,t) \tag{2.29}$$

and:

$$V^e(r(x+D,t)) \approx V^e(r(x,t)) + D\partial_x r(x,t)\frac{\mathrm{d}}{\mathrm{d}r}V^e(r(x,t)) \tag{2.30}$$

Since, the density equals $r = 1/D$, by substituting (2.29) and (2.30) into (2.10), we find:

$$\partial_t V + \overbrace{V\partial_x V}^{C} = \overbrace{(V^e(r)-V)/T}^{R} - \overbrace{(c_0^2/r)\partial_x r}^{A} \tag{2.31}$$

where $c_0{}^2 = \xi/T > 0$ is the anticipation constant, with $\xi = -\mathrm{d}V^e/\mathrm{d}r$ describing the decrease-rate in the equilibrium velocity with increasing density. Assuming a constant decrease-rate implies a linear relation between the density r and the equilibrium velocity $V^e(r)$.

Payne identified *convection*, *relaxation*, and *anticipation* terms:

- *Convection* (term C of (2.31)) describes changes in the mean velocity due to inflowing and outflowing vehicles.
- *Relaxation* (term R of (2.31)) describes the tendency of the traffic flow to relax to an equilibrium velocity.
- *Anticipation* (term A of (2.31)) describes the drivers' anticipation on spatially changing traffic conditions downstream.

In the following section, these processes are discussed in more detail. For an overview of other recent developments of Payne-type models, we refer to Liu *et al.* (1998).

Similar to the LWR-model, the state of the system at a point (x,t) can be determined by considering the characteristics emanating from the line $t = 0$ (see section 7.5). In contrast to the LWR-model, *two* characteristics (the so-called *Mach-lines*) emanate from each point $(x,0)$ which are not straight lines. Rather, these curves $C^{\pm} = \{x^{\pm}(s),s\}$ are defined by the following differential equations:

$$\mathrm{d}x^{\pm} = (V(x(t),t) \pm c_0)\mathrm{d}t \quad \text{with} \quad x(0) = x \quad \text{and} \quad V(x,0) = V_0(x) \tag{2.32}$$

From this result we can conclude that c_0 is comparable to the *local sonic velocity* for the propagation of disturbances in gasses. Moreover, since small perturbations are transported along these characteristics, the absence of a path-line (defined by $\mathrm{d}x = V(x(t),t)\mathrm{d}t$ (see sec-

tion 7.5)) yields that disturbances in the flow are not transported together with the vehicles. Clearly, this also holds for the LWR-model, which is a serious drawback of both modelling approaches. We refer to section 7.5 for a detailed description of characteristic curves in vehicular traffic flow.

General form of Payne-type model

A more general model form of equation (2.31) is given by:

$$\dot{V} = \partial_t V + \overbrace{V\partial_x V}^{C} = \overbrace{(V^e(r) - V)/T}^{R} - \overbrace{(1/r)\partial_x P + (\eta/r)\partial_x^2 V}^{A} \tag{2.33}$$

where P is the *traffic pressure* and η is the *kinematic traffic viscosity*. The total time derivative $\dot{V}$ describes the rate of velocity changes experienced by a moving observer who observes the traffic flow while moving along with the stream at the same velocity V. Note that for the Payne model (2.31), we have $P = r \cdot c_0^2$ and $\eta = 0$. By introducing traffic viscosity, *approximate smooth* solutions of Payne's model result. In addition, the numerical treatment of these higher order models is simplified (cf. Babcock (1982)).

From equation (2.33) we observe that the total time derivative is composed of a true time derivative $\partial_t V$ and a *convection term C*. The latter term describes changes in the velocity V due to inflowing vehicles with a different velocity. The *relaxation term R* describes the tendency of the traffic stream to adjusts its velocity to an equilibrium value $V^e(r)$.

Several authors (e.g. Payne (1971), Kerner and Konhäuser (1995), Kerner *et al.* (1996), Lyrintzis *et al.* (1994), and Liu *et al.* (1998)) argue that the traffic flow interpretation of the term A of equation (2.33) differs from the classical meaning of this term in kinetic theory of compressible media. These authors argue that term A describes drivers *anticipatory behaviour* on changing traffic conditions downstream, reflected by regions of spatially changing traffic pressure P and changing spatial acceleration $\partial_x V$.

When an observer moving along with the traffic observes a region of spatially increasing traffic pressure ($\partial_x P > 0$), the total time derivative $\dot{V}$ decreases, implying that the moving observer decelerates. The second order term $\eta(\partial_x^2 V)/r$ shows that in regions of spatial accelerations, i.e. $\partial_x^2 V > 0$, this *diffusion* term yields an increase in the velocity of the moving observer. That is, when the moving observer drives in a region of spatial acceleration, the driving will *go along with the other drivers*. Summarising, the pressure term $\partial_x P$ describes the local anticipation behaviour of drivers, whereas the diffusion term $\partial_x^2 V$ describes the higher-order tendencies of drivers. In opposition, Helbing (1996) argues that the second order term should be deprived of its classical meaning of viscosity; rather the diffusion term reflects changing drivers' states (brisk to careful driving).

In chapter 7 of this thesis, we show that the latter interpretation of the anticipation term recalled in the above paragraph is flawed. We show that the spatial derivative of the traffic pressure P must be interpreted in a similar way as the pressure term in equations describing the dynamics of a compressible continuous medium like a fluid or a gas. That is, it reflects the changes in the mean velocity of the cell caused by groups of vehicles having different velocities flowing into the cell.

With respect to the higher-order anticipation term, in the kinetic theory of fluids and gasses, this so-called *viscosity term* reflects changes due to the *friction* between particles in the medium as well as between particles and boundaries. When particles move away from other particles (*accelerate*), friction causes the following particle to be 'dragged along' with the accelerating particle. Thus, *viscosity* in vehicular flow is not essentially different from viscosity in viscous continuous media.

Let us finally remark that two *competing* processes are conveyed by the relaxation term R in equation (2.33). On the one hand an *active* process, conveying that drivers aim to traverse the motorway at their desired velocities. On the other hand, a *damping process*, conveying that drivers are slowed down due to interaction with other vehicles. Kerner *et al.* (1996) show that under specific circumstances, these competing processes result in the spontaneous occurrence of seemingly random traffic jams, so-called *phantom jams* that are also observed in real-life traffic flow (e.g. Kerner (1999)). Payne (1971) has shown that given certain circumstances, his model yields unstable behaviour. That is, in a certain density area the traffic model is *metastable*. In this region, small variations in the traffic density will yield regions of increasing traffic densities, leading to the occurrence of *start-stop* waves or localised traffic jams. This is a very important property of the Payne-type models.

Models of Philips, Kühne, and Kerner

Philips (1979) proposed to use a *density dependent relaxation time* $T = T(r)$. Moreover, he approximates the traffic pressure using $P(r) = r\Theta^e(r)$, with $\Theta^e(r) = \Theta^0(1-r/r_{jam})$. Note that the velocity variance equals zero when the density equals the *jam-density* r_{jam}.

Kühne (1991) and Kerner *et al.* (1996) choose $P = r \cdot c_0^2$ and $\eta = \eta_0$. That is, both the velocity variance and the traffic viscosity are constants. The assumption of a constant velocity variance is not realistic. Rather, in equilibrium, the velocity variance *decreases* with *increasing* traffic density, i.e. $d\Theta^e(r)/dr < 0$ (see Helbing (1997c)). Finally, improvements to both Payne's original modelling efforts as well as several numerical schemes to solve the resulting modelling equations are due to Lyrintzis *et al.* (1994) and Liu *et al.* (1998).

Non-local traffic model of Helbing

A recent contribution to the field of macroscopic flow models is given by Helbing *et al.* (1998). The authors propose a flow model based on gas-kinetic principles. The relationship for the equilibrium velocity follows from the acceleration of vehicles on the one hand, and the interaction of vehicles on the other hand. The latter process incorporates a non-local interaction term that reflects the anticipatory behaviour of drivers:

$$V^e = V^0 - T(1 - p(r'))r'\tilde{\Theta} \tag{2.34}$$

where V^0 is the expected desired velocity, $p(r')$ is the *immediate lane-changing probability*, and $\tilde{\Theta}$ is an *interaction term* reflecting the influence on the velocity of vehicular interactions. The prime indicates that the corresponding variable should be considered at the *interaction point* $x' = x + \gamma \cdot (1/r_{jam} + TV)$, with $\gamma \approx 1$. The authors claim that the non-local interaction term is very favourable for robust numerical approximation.

2.4.4 *Helbing-type models*

Helbing (1996) has extended the Payne-type models by introducing an additional partial differential equation for the velocity variance Θ. His macroscopic model is derived from gas-kinetic equations and consists of the conservation of vehicles equation (2.24), the velocity dynamics (2.33), and the following equation describing the dynamics of the variance Θ:

$$\partial_t \Theta + V\partial_x \Theta = -2(P/r)\partial_x V + 2(\Theta^e - \Theta)/T - (1/r)\partial_x J \qquad (2.35)$$

where the *flux of velocity variance* $J = J(x,t) = r(x,t)\Gamma(x,t)$ is defined by the product of the density and the skewness of the velocity distribution. Rather than being experimentally determined, the equilibrium velocity V^e and variance Θ^e are determined by considering the interaction process between vehicles in the stream. The resulting expressions are functions of the density r, the velocity V and the velocity variance Θ, namely:

$$V^e(r,V,\Theta) = V^0 - T(1-p(r))P \quad \text{and} \quad \Theta^e(r,V,\Theta) = C - T(1-p(r))J \qquad (2.36)$$

where $p(r)$ denotes the immediate overtaking probability while C is the *covariance* between the velocity and the desired velocity. The model equations are 'closed' by specifying expressions for p, C and J. Helbing (1996) also proposes techniques to incorporate the fact that vehicles occupy a non-vanishing amount of roadway space.

The way in which disturbances in the flow are transported can again be analysed by considering the characteristic curves (see section 7.5). Helbing-type models have *three characteristic curves* (one path-line and two Mach-lines), along which small perturbations propagate. This implies that small disturbances are transported both along with the (mean) traffic flow as well as in the upstream and downstream directions with respect to this mean flow.

2.5 Semi-discrete and discrete macroscopic flow models

In this section, we will discuss some discrete macroscopic traffic flow models. Frequently, these models are established by application of a finite difference scheme to the continuous model equations described in the previous section. If so, it is of dominant importance that the numerical solution approach preserves the essential characteristics of the underlying continuum model. Additionally, when solutions of the continuum model are *not unique*, which is the case for all first-order models, care should be taken that the physically feasible solution is approximated by the numerical solution technique.

Most of these solution approaches involve numerical approximation in the spatial direction (dividing the roadway into small segments $i = [i\Delta x,(i+1)\Delta x)$), the temporal direction (dividing the time axis into small periods $k = [k\Delta t,(k+1)\Delta t)$), or both. Applicability of solution approaches depends on the mathematical characteristics of the underlying system of equations (e.g. order of the equations, number of equations).

2.5.1 *Discrete Lighthill-Whitham-Richards model*

Determination of analytical solutions for the LWR-model is possible using the *method of characteristics* (section 7.5). Since application of this method can be cumbersome, several approaches have been used to determine numerical solutions to the LWR-model.

The *Cell-Transmission model* (Daganzo (1994a,b)) is a discrete flow model that uses carefully selected segment sizes, and a *piecewise linear* relation for $M^e(r) = rV^e(r)$. That is, given a time-step Δt, the lengths Δx of cells are chosen such that under free-flow conditions, all vehicles in cell i flow into the downstream cell i+1, i.e. $\Delta x = V^0 \cdot \Delta t$. The number of vehicles flowing out of segment i is bounded by the space left on segment i+1. Daganzo (1999) further improves the Cell-Transmission model.

Lebaque (1996) applied the *Godunov-scheme* to the LWR model. The author shows that the Cell-Transmission model is a special case of the general Godunov solution approach. The scheme has the nice interpretation that the *flow* out of the segment i is locally defined by the smallest of two quantities, namely the *local traffic demand* and *supply* (cf. Lebaque (1993)).

Multiclass multilane generalisations

Daganzo (1997a) presents a generalised theory to model motorways in the presence of two vehicle types and a subset of lanes reserved for one of the vehicle classes. It describes the case of a long homogeneous motorway, based on the Cell-Transmission model.

2.5.2 *Semi-discrete and discrete Payne-type models*

Semi-discrete Payne-model

By spatial discretisation, Smulders (1989) determines a macroscopic flow model based on the model of Payne (1971) that is continuous in time and discrete in the spatial direction. Furthermore, using the theory of *martingales* he introduces a stochastic component based on a counting process. The author approximates the flow m by a convex sum approximation of the average density r and velocity V of consecutive discrete segments i and i+1*:

$$\mathrm{d}r_i = (m_{i-1} - m_i)\mathrm{d}t / \Delta x + (\mathrm{d}\xi_{i-1} - \mathrm{d}\xi_i) / \Delta x \tag{2.37}$$

where the approximation of the outflow of segment i equals:

$$m_i = (\alpha r_i + (1-\alpha) r_{i+1})(\alpha V_i + (1-\alpha) V_{i+1}) \tag{2.38}$$

and where ξ_i reflects the stochastic departure process of vehicles from segment i. The velocity dynamics are given by:

$$\mathrm{d}r_i = \overbrace{\frac{1}{\Delta x} V_{i-1}(V_{i-1} - V_i)\mathrm{d}t}^{C} + \overbrace{\frac{V^e(r_i) - V_i}{T}\mathrm{d}t}^{R} - \overbrace{\frac{c_0^2}{\Delta x}\frac{r_{i+1} - r_i}{r_i + c}\mathrm{d}t}^{A} + \overbrace{\mathrm{d}w_i}^{N} \tag{2.39}$$

where $c > 0$ is a constant.

With respect to the conservation equation (2.37), this approximation yields the conservation of vehicles. However, unless $\alpha = 1$ vehicles may flow out of an empty downstream segment i, possibly yielding negative density values. Moreover, if the downstream segment is congested

* For the purpose of clarity of the equations, the influence of on- and off-ramps has been neglected. Moreover, we have assumed that the number of lanes is constant from segment to segment.

(i.e. $r_{i+1} = r_{jam}$, and $V_{i+1} = 0$), vehicles will still flow out of the upstream cell into the saturated downstream section.

The approximation of the velocity dynamics is heuristically established by considering the traffic flow interpretation of the respective processes. In illustration, since the term $-c_0^2(\partial r/\partial x)/r$ is assumed to reflect drivers' anticipatory behaviour, it is approximated using a *forward* discretisation scheme, yielding term A of eq. (2.39). We note that Smulders (1989) has modified the latter term. The modified term has been validated successfully using empirical data (see Smulders (1989) and Smulders (1996)).

Multiclass generalisation

Hoogendoorn and Bovy (1996b) establish a multiclass model, which can roughly be considered as a multiclass generalisation of the semi-discrete model of Smulders (1989). This *continuous-time discrete-space* flow model is a system of ordinary differential equations describing the rate of change in the average density $r_{u,i}(t)$ of user-class u on segment i due to inflowing and out-flowing vehicles:

$$\mathrm{d}r_{u,i} = (m_{u,i-1} - m_{u,i})/\Delta x \mathrm{d}t \tag{2.40}$$

where $m_{u,i}$ denotes the flow-rate of vehicles of class u at the exit of segment i.

The dynamics describing the change in average speed are based on the following traffic flow characteristics as given by the following relationship:

$$\mathrm{d}V_{u,i} = \frac{\xi_u}{\Delta x} V_{u,i-1}(V_{u,i-1} - V_{u,i})\mathrm{d}t + \frac{V_u^e(r_{*,i}) - V_{u,i}}{T_u}\mathrm{d}t - \frac{\mu_u}{T_u}(V_{*,i+1} - V_{i,u})\mathrm{d}t \tag{2.41}$$

where '*' indicates class-aggregation, and where ξ_u and μ_u are convection and anticipation constants respectively. The function V_u^e is the *equilibrium* or *fundamental* equation describing the *equilibrium velocity* as a function of among other things current density, user-class composition, and the dynamic lane configuration provided by the controller. Furthermore, the interaction between user classes following from the characteristics of driver-vehicle combinations assigned to each lane is modelled in this fundamental relationship.

Discrete Payne-type models

Examples of discrete Payne-type models are the models of Payne (1979), Van Maarseveen (1982), Papageorgiou *et al.* (1989), Kotsialos *et al.* (1998,1999), Lyrintzis *et al.* (1994), and Liu *et al.* (1998). In the latter two contributions, several numerical solution techniques applied in physics are applied to the different traffic flow models (see chapter 9). Another method is applied by Kerner and Konhäuser (1995). Here, the equations (2.24) and (2.33) are transformed using $W = \partial_x V$ into a *quasi-linear* system of partial differential equations and successively solved using a central difference approach (cf. Hirsch (1990a,b)). Let us remark that most of these schemes need the second-order viscosity term for numerical stability.

A different approach is used by Van Aerde (1994), who numerically approximates solutions of the continuum model by a *particle discretisation method* thereby constructing the 'microscopic' simulation model INTEGRATION (see section 2.2.5). This particle discretisation approach has been extensively applied in other fields of research, for instance in hydrodynamic

flow modelling and filtering. Recently, Hoogendoorn and Bovy (2000) applied a particle discretisation method to numerically solve a gas-kinetic pedestrian flow model, thereby establishing a two-dimensional stochastic microscopic pedestrian flow model.

A numerical solution procedure for Helbing's model is proposed in Helbing (1997a). The author suggests using an explicit two-step (*predictor-corrector*) *MacCormack* scheme. The stability of this scheme depends on the relative magnitude of the viscosity terms. Hoogendoorn and Bovy (1998a,d) propose an *upwind scheme* based on *splitting of the flux-vector.* Their approach is based on the conservative model formulations and forms the foundation of the numerical solution approach used in this thesis (cf. chapter 9). Hoogendoorn and Bovy (1998a) also propose a scheme based on the Godunov-approach. A similar approach is discussed in chapter 9 of this thesis. Both numerical solution approaches to a large extent use physical properties of the underlying partial differential equations.

2.6 Links between microscopic, mesoscopic and macroscopic models

Although being fundamentally different, relations between (sub-) microscopic, mesoscopic and macroscopic flow models are reported in the literature. Figure 2-1 provides an overview of these relations.

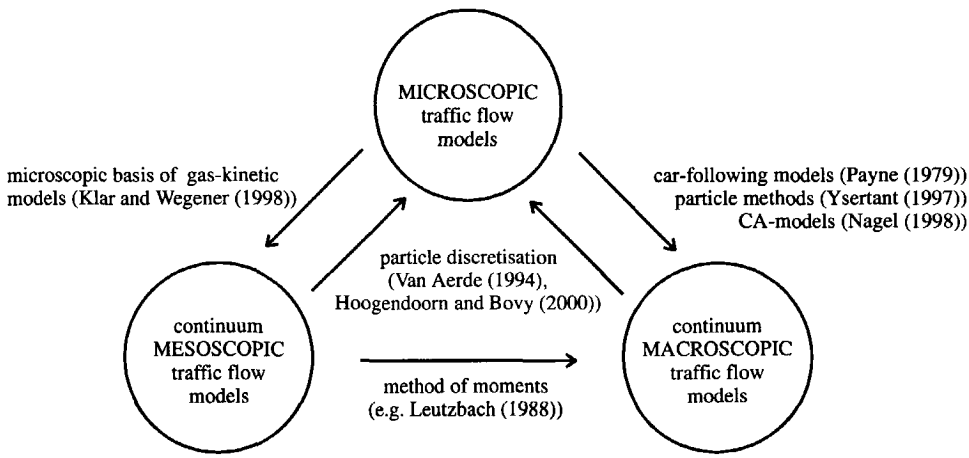

Figure 2-1: Relations between microscopic, mesoscopic, and macroscopic flow models.

Klar and Wegener (1998) describe a hierarchy of models: the authors present a simple microscopic flow model that is used to determine gas-kinetic flow equations. These are subsequently transformed into a macroscopic traffic flow model.

The derivation of the original Payne model can be considered as an example of 'degeneration' of microscopic flow model to a macroscopic flow model (see section 2.4.3). Application of the method of moments (e.g. Leutzbach (1988)) yields macroscopic equations from mesoscopic traffic flow models. Ysertant (1997) presents a particle method to derive macroscopic model equations for compressible fluids. Nagel (1998) shows the relation between CA-models and the simple wave model.

We have discussed derivation of microscopic models from macroscopic equations by Van Aerde (1984), using a particle discretisation method (section 2.2.5). Such methods have been applied to numerical approximation of dynamic models of flows in continuous media (Hockney and Eastwood (1988)). Application of particle discretisation methods to derive microscopic models from gas-kinetic equations has recently been reported by Hoogendoorn and Bovy (2000), who applied the method to gas-kinetic equations describing pedestrian flows.

2.7 Some remarks on the appropriate level-of-detail

When developing a model for the description of traffic flow, the appropriate 'level-of-detail' of the modelling approach (i.e. submicroscopic, microscopic, mesoscopic, macroscopic) must be considered. This section provides some viewpoints from the literature on this issue. Based on these viewpoints, we conclude that the correct level-of-detail that should be considered is largely dependent on the foreseen model application. The development and maintenance costs are of less importance. Although it has been suggested that macroscopic models should be used when the available model development time and resources are too limited for development of a microscopic model, we argue that in some occasions, macroscopic modelling approaches *provide better results* than modelling approaches with a higher level-of-detail. Additionally, we discuss potential to generalise approaches to distinguish classes and roadway lanes.

2.7.1 Chaotic-like behaviour of traffic flow

Several authors have observed the chaotic-like behaviour of the traffic system (cf. Bovy and Hoogendoorn (1998)). In other words, while dilute traffic is *stable*, in heavy traffic a small disturbance can be amplified and develop into a traffic jam. Empirical experiments performed by Forbes (1958), and Edie and Foote (1958,1960) have shown that a disturbance at the foot of an upgrade propagates from one vehicle to the next, while being amplified until at some point a vehicle came to a complete stop. This *instability effect* describes that once the density crosses some critical density, the traffic flow becomes rapidly more congested *without any obvious reasons*. More empirical evidence of this instability and start-stop wave formation can be found in among others Verweij (1985), Ferrari (1989), and Leutzbach (1991). Kerner and Rehborn (1997) and Kerner (1999) show empirically that local jams can persist for several hours, while maintaining their form and characteristic properties. In other words, the stable complex structure of a traffic jam can and does exist on motorways*. These findings show that traffic flow has some chaotic-like properties, implying that *microscopic disturbances* in the flow can result in the on-set of local traffic jams persisting for several hours.

Microscopic simulation models are founded on the assumption that the behaviour of each individual vehicle is a function of the traffic conditions in its direct environment. However, the (microscopic) behaviour of humans in real-life traffic – not in contrived "car-following experiments" – is hard to observe, measure and validate (cf. Daganzo (1994a)). Based on the observed chaotic-like behaviour of the collective traffic flow discussed in the previous para-

* Apart from the formation of stop-and-go waves and localised structures, Kerner and Rehborn (1997) describe a hysteric phase-transition from free-traffic to *synchronised flow* that mostly appears near on-ramps.

graph, this is unfortunate: the *microscopic details* of the simulation models have to be just right for the microscopic simulation to realistically describe and predict the stop-start waves in traffic flow. Thus, from a model calibration perspective, the large number of (sometimes unobservable) parameters play a compromising role.

Conversely, in macroscopic models, the number of parameters is relatively small and, more importantly, comparably easy to observe and measure. Calibration and validation of macroscopic models therefore requires less effort than the calibration of microscopic or mesoscopic models. Moreover, the macroscopic models are deemed to describe the macroscopic characteristics of the traffic flow more accurately.

In addition, microscopic simulation tools do not provide insight into the *macroscopic* mechanisms of traffic flow (e.g. shock wave behaviour). On the contrary, macroscopic models provide such insights by means of mathematical analysis and manipulation.

2.7.2 On-line model applicability

Since in a microscopic simulation model, each vehicle is described by its own equations of motion, computer-time and memory requirements grow proportionally to the number of simulated vehicles. Consequently, this type of modelling is most suitable for *off-line* traffic simulations, although with the emergence of fast and cheap microcomputers, this argument will gradually become of less importance. Nevertheless, macroscopic models are computationally less demanding, thereby allowing simulations of very large traffic networks.

More important is the fact that due to the very nature of microsimulation models, the absence of an equivocal relation between model input and output, renders these models unsuitable for direct application in model based control approaches. In other words, since optimal model-based control requires the availability of explicit input-output relations for fast (on-line) computation, microscopic simulation models are not easily applicable. In opposition, the solutions of macroscopic models are available in closed analytical form, and are excellently applicable for model-based traffic control approaches.

2.7.3 Model generalisability: user-class and lane distinction

Let us finally discuss the ability to generalise a model with respect to different user-classes and roadway lanes. In this respect, most microscopic simulation models are able to implement different user-classes such as person-cars, trucks, and vans. Moreover, most microscopic models describe the behaviour of these different vehicles on multilane facilities. Consequently, the generalisation with respect to user-classes and lanes in not an issue.

In the past, several researches have attempted to generalise both gas-kinetic models (cf. Helbing (1997b), Hoogendoorn (1997)) as well as macroscopic models (e.g. Daganzo (1997a), Hoogendoorn and Bovy (1996b), and Hoogendoorn (1997)) towards a multiclass and/or multilane traffic description. However, these models are either not operationalised, or lack the descriptive accuracy which we deem necessary. Let us emphasise that the generalisation is *not self-evident*, and requires detailed analysis before the asymmetric interaction processes between classes and lanes can be described correctly.

2.7.4 *Conclusions*

Microscopic simulation models are most suitable for *off-line* traffic simulations, for instance to perform detailed studies of geometric design and vehicle equipment (e.g. on-ramps, lane-merges, driver-support systems), or to gain insight into flow quantities that are difficult to determine empirically. However, their application in on-line traffic control is limited due to the large computation times and the absence of an explicit model input-output relation.

Gas-kinetic models have been criticised for having too many variables to be solved in real-time, hampering their application to among other things on-line traffic control. However, several researchers (e.g. Herman *et al* (1962), Prigogine and Herman (1971), Leutzbach (1990), Helbing (1996,1997,1998), Klar and Wegener (1998), and Hoogendoorn (1997), have used these gas-kinetic-type mesoscopic models for the derivation of their macroscopic models. This is typically done by application of the method of moments (e.g. Leutzbach (1988)). However, this derivation approach is quite cumbersome and complex. Hoogendoorn and Bovy (1998d) propose an alternative approach to derive the macroscopic flow equations from the gas-kinetic equations, by considering the *conservative* variables traffic density, traffic momentum, and traffic energy, rather than the traditionally used *primitive* variable density, velocity, and velocity variance (see section 6.3).

In retrospect, given the envisaged model application in a model based predictive controller on the one hand, and the chaotic-like behaviour of traffic flow on the other hand, a mesoscopic/macroscopic modelling approach is chosen in this thesis.

2.8 Macroscopic modelling stream controversy

Having opted for a *macroscopic* modelling approach, we need to pick a type of macroscopic model. The question which model type should be considered is not self-evident, given the ongoing debate between the LWR-model followers and the Payne-type model (and Helbing-model) followers. In this section we will discuss the main arguments presented by both streams to show the relative superiority of their respective modelling approaches. Let us remark that Lebaque and Lesort (1999) propose a methodology for theoretically comparing LWR-type models and Payne-type models. They propose a set of problems and situations that can be used as a test-case for model comparison. Although their approach has obvious limits, their work contributes to constitute an exhaustive model comparison framework.

2.8.1 *Critique on LWR-type models*

The simple continuum model has some shortcomings, given in the following list (see Liu *et al.* (1998) and Papageorgiou (1998)):

- *Steady-state speed-density relationship.* The LWR-models contain *stationary speed-density relations*, implying that the mean velocity adapts *instantaneously* to the traffic density rather than considering some delay. That is, the kinematic theory does not allow fluctuations around the equilibrium speed-density relationship.
- *Discontinuities in the density.* The kinematic wave-theory of Lighthill and Whitham shows shock wave formation by steeping velocity jumps to infinite sharp discontinuities in the density. In other words, it produces *discontinuous solutions* irrespective of

the smoothness of initial conditions, due to the dominating convective term in the non-linear partial differential equation (2.24). These are in contradiction with smooth shocks observed in real-life traffic that can be described by Payne-type models.

- *Regular start-stop waves.* The LWR-theory is not able to describe regular start-stop waves with amplitude-dependent oscillation times that are observed in real-life traffic (e.g. Verweij (1989).
- *Traffic hysteresis.* In real-life traffic flow, hysteresis phenomena have been observed (cf. Treiterer and Myers (1974)), showing that the average headways of vehicles approaching a jam are smaller than vehicles flowing out of a jam. These hysteresis phenomena are not described by the LWR models. Conversely, the Payne-type models are able to describe traffic hysteresis (see Zhang (1999)).
- *Localised structures and phantom-jams.* Similarly, the LWR-models are not able to predict the occurrence of localised structures and phantom-jams, i.e. the LWR-theory does not describe the amplification of small disturbances in heavy traffic.

2.8.2 *Critique on Payne-type models*

The most fundamental criticisms regarding the Payne-type models have been formulated in Daganzo (1995). The author's criticisms stem from the dissimilarity between vehicular flow and the flow of molecules in a fluid or a gas:

- *Anisotropy.* In opposition to fluid particles responding to both stimuli from upstream and downstream, a driver-vehicle combination is an anisotropic particle. In other words, a driver will primarily react to traffic conditions downstream. In opposition to vehicular flow, particles in a fluid or a gas 'react' to stimuli from all directions.
- *Unaffected slow-vehicles.* The speed of slow vehicles should be virtually unaffected by faster vehicles. Conversely, the slow particles in a fluidic flow or gas flow are affected by faster particles.
- *Personality.* Unlike particles in a fluid or gas, driver-vehicle combinations have their own personalities that remain largely unaffected by traffic conditions. For instance, drivers are aggressive or timid, or drivers aim to drive at their desired velocities.

Daganzo (1995) shows that existing Payne-type models can result in negative speeds at the tails of congested regions. This is caused by the second order dissipation term. However, Liu *et al.* (1998) unconvincingly argue that the violation of the anisotropy condition is a result of the pressure term. They state that by observing the *inviscid flow equations* (see also chapter 7 of this thesis) under congested conditions one characteristic curve moves *upstream*, while the other characteristic moves downstream (with a velocity which is larger than the average velocity of the flow). However, as is shown in chapter 7, these characteristics describe the upstream moving influence of congestion downstream, and the fact that some vehicles drive faster than others do. They *do not reflect physical movements of vehicles in traffic flow.* In other words, the fact that a characteristic curve is directed *upstream* does not imply that vehicles move in that direction. Neither is it necessary that all vehicles have the same velocity. In fact, as is shown in the remainder of this thesis, c_0^2 can be interpreted as the *variance* in the velocities of the different vehicles.

2.8.3 *Finite space requirements, velocity variance, and finite reaction and braking times*

In addition to Daganzo's criticism, Helbing (1996,1997) argues that three other conditions need to be fulfilled for a valid macroscopic traffic flow model:

- *Finite space requirements:* vehicles are modelled by infinitely small particles, i.e. the *finite space requirements of vehicles* are seldom incorporated. As a consequence, on some occasions, the traffic density temporarily becomes larger than the bumper-to-bumper jam density.
- *Consideration of the velocity variance.* Most macroscopic traffic flow models neglect the essential role of the velocity variance. Kühne (1984a,b) observed that the velocity variance is an indicator for the occurrence of traffic breakdown.
- *Finite braking times and reaction times*: most macroscopic flow models neglect the finite reaction and braking times of driver-vehicle units.

The model of Helbing (1996,1997a) considers each of these modelling issues.

2.9 Conclusions and implications for MLMC macroscopic modelling

Currently, neither mesoscopic nor macroscopic traffic flow models exist that can model multiple user-class traffic flow on multilane facilities, which can at the same time hold up against the issues presented in the previous section. Therefore, the need arises for a realistic macroscopic multiclass traffic flow model satisfying the mentioned issues. The remainder of this thesis describes the derivation, specification and application of such a macroscopic multiclass multilane model (see Figure 1-1).

Let us briefly outline the approach used to establish this model. First, we derive *special continuity equations* describing the dynamics of the *generalised Phase-space density*. The latter can be considered as a velocity-and-desired-velocity-specific density. Since the acceleration and lane-changing behaviour of free-flowing and car-following vehicles differ significantly, the MLMC-PSD is dis-aggregated into distinct contributions of platooning and free-flowing vehicles. By analysing heterogeneous traffic at this level of dis-aggregation, we are able to mathematically describe the various dynamical processes governing the dynamics of heterogeneous traffic flow. In other words, the mesoscopic modelling approach enables the description of individual processes, without needing to distinguish the individual entities in the flow (see section 2.3).

These deliberations yield generalised special continuity equations, describing conservation of vehicles in the so-called phase-space. Similar to the model of Paveri-Fontana (1975), these equations enable modelling drivers accelerating towards the class-specific desired velocity *and* drivers decelerating due to impeding vehicles from the same or other user-classes.

Aggregation of vehicles from equal classes driving at equal velocities but having different desired velocities transforms the special continuity equations into the so-called *reduced generalised special continuity equations*. These equations serve as an intermediate step between the *generalised* special continuity equations and the macroscopic model.

Subsequently, the method of moments is applied to the reduced generalised special continuity equations . This allows us to establish partial differential equations describing the dynamics

of the so-called conservative variables density, momentum, and energy. Due to the modelling approach, expressions for the equilibrium traffic momentum and equilibrium traffic energy result. These convey both acceleration processes towards the class-dependent mean desired velocity as well as deceleration processes due the within and between user-class interactions.

In chapter 7 the model is recast using both the *primitive variables* density, momentum and energy as well as the *Riemann variables*. These transformations allow more refined analysis of the macroscopic MUC equations and determination of reliable and accurate schemes for the numerical approximation of solutions to the macroscopic equations, which would not have been possible using the model in its original form.

2.10 Summary

This chapter provides an overview of the current state-of-the-art of vehicular traffic flow modelling in general. To provide a structured overview of these modelling achievements, the models have been classified according to level-of-detail (submicroscopic, microscopic, mesoscopic, macroscopic). Other criteria have been considered as well, namely scale of the independent variables (continuous, semi-discrete, discrete), representation of processes (deterministic, stochastic), operationalisation (analytical, simulation), and application area (e.g. links, stretches, networks).

Due to the purpose of this dissertation, we have emphasised mesoscopic and macroscopic continuum models. Moreover, in this chapter we have recalled some of the links between microscopic, mesoscopic and macroscopic models that have been reported in the literature.

Although, microscopic traffic flow models are principally well suited to accurately describe multiclass multilane traffic flow, several authors have pointed out the drawbacks of a microscopic approach in the context of the envisaged model applications (e.g. (on-line) impact assessment of traffic management applications and strategies on a macroscopic scale-level (capacity, queue-lengths)). Due to for instance the chaotic-like behaviour of traffic, and the need for on-line model applicability, we have decided that a macroscopic modelling approach would be most appropriate. However, suitable macroscopic multiclass multilane flow models correctly describing the interaction between vehicles from the respective classes and the roadway lanes are not yet available.

From the viewpoint of continuum flow modelling, *gas-kinetic models* are useful since these enable modelling processes of individual entities in the flow (e.g. acceleration, deceleration due to interaction, lane-changing), without describing the space-time behaviour of these individual entities. These gas-kinetic flow models have been successfully used as the foundation of macroscopic flow models. A similar method is deemed useful for the derivation of a macroscopic multiclass multilane flow model. However, the flawed acceleration terms (neglecting the correct acceleration behaviour of platooning vehicles) and interaction terms (neglecting the correlation between free-flowing and platooning vehicles and the finite-space requirements of the vehicles) need to be corrected.

The macroscopic models proposed during the last five decades of traffic flow modelling all are cast using the so-called *primitive variables* traffic density, velocity and (in some cases), the velocity variance. The resulting macroscopic equations have been interpreted from the viewpoint of the driver (relaxation, low-order anticipation, and high-order anticipation).

Another issue raised in the rich literature on macroscopic flow modelling is the appropriate number of dependent variables necessary for a correct description of traffic flow. In this chapter we have briefly considered the on-going debate among researchers adhering to the simple kinematic model on the one hand, and the Payne-type models on the other hand, by recalling the critiques of the respective streams. A third (and relatively new) model-type incorporates dynamic equations for the velocity variance as well. Due to the (theoretical) improvements of the latter model, we envisage that a generalisation of the latter model will yield a suitable macroscopic multilane multiclass flow model.

3 MULTICLASS MULTILANE PHASE-SPACE DENSITY

The backbone of the macroscopic multiple user-class traffic flow theory developed in this thesis is the lane-specific and class-specific Phase-Space Density (MLMC-PSD) for both unconstrained platoon-leaders as well as constrained vehicles. This concept is introduced in this chapter. That is, we present a generalisation of the original Phase-Space Density (PSD; cf. Paveri-Fontana (1975)) to both *discrete attributes* $\mathbf{a}$ (e.g. user-class u, roadway lane j, and the driver's state c), characterising specific groups of driver-vehicle combinations, as well as general *continuous attributes* $\mathbf{v}^0$ of characteristics of the vehicles (e.g. desired velocity v^0, acceleration time τ). Moreover, we will discuss the generalisation from the motion in a single dimension to two (or more) dimensions.

The PSD is a *mesoscopic generalisation* of the traditional macroscopic traffic density. That is, rather than just considering the expected number of vehicles per unit road-length at a specific location and a specific time-instant, contributions to the density from vehicles driving at a specific velocity while striving for a distinct desired velocity are considered separately.

Since the mesoscopic Phase-Space Density distinguishes vehicles driving at specific velocities having a specific desired velocity, expressions that are more accurate can be derived for the dynamics of the PSD than for macroscopic variables such as density and velocity. For instance, knowledge of velocity distributions enables establishing expressions for the *expected number of interactions* with slower vehicles (section 4.4). We can also describe modelling the acceleration-process towards the acceleration velocity (section 4.6).

Also with respect to *multiclass* traffic flow modelling, using the Phase-Space Density is beneficial. Especially the ability to accurately describe interaction processes between vehicles is of dominant importance to heterogeneous traffic flow modelling. For *lane-specific*

multiclass traffic flow the Phase-Space Density is equally invaluable. However, due to the observed differences in driving and lane-changing behaviour between *constrained* (or *platooning*) and *free-flowing* traffic on the one hand, and the need to describe the correlation between the vehicles in the stream sufficiently accurate, we will need to distinguish between contributions of the driver's states to the Phase-Space Density. This implies that we assume that traffic can be represented sufficiently accurate by a collection of platoons that are led by an *unconstrained* vehicle, and a *nonnegative* number of *constrained* followers.

We will also show how *macroscopic* traffic flow variables, such as density, velocity, velocity variance, momentum and energy, can be derived from the generalised Phase-Space Density using the mean operator $\langle\cdot\rangle$ and the aggregation operator $[\cdot]$ (Intermezzo I, page 55). Finally, aggregation with respect to attributes (e.g. user-classes or roadway lanes) is discussed. To this end, a new compact vector representation is proposed. We will show that using this representation, aggregation reduces to simple matrix multiplication.

3.1 Description of traffic flow using platoons

In this thesis we develop a continuum theory of multilane multiclass traffic flow. This section discusses some elementary notions and definitions from traffic flow theory that are relevant for understanding the issues raised in this dissertation. Using probability theory, we will introduce and define the concepts of intensity, concentration, density, flow-rate, and the instantaneous and local velocity distributions.

The objective of this section is to provide a theoretical foundation for the traffic flow description approach employed in this thesis. The main assumption is that the observed vehicle trajectories can be considered as realisations of random processes. This randomness follows on the one hand from the variations in the velocity of drivers, which we assume to be of a stochastic nature, and on the other hand from interactions with other drivers, whose trajectories are stochastic. Moreover, rather than assuming that the traffic flow can be adequately described by single vehicle units that are separated by a nonzero distance (cf. Leutzbach (1988)), we propose that the traffic flow advantageously can be modelled by a collection of n-vehicle platoons, with $n \geq 1$. Consequently, the definitions of local and instantaneous stream functions, as well as traffic intensity and concentration of Leutzbach (1998) are modified.

3.1.1 Vehicle trajectories

A traffic stream consists of several vehicles moving on the roadway. The movement of a vehicle can be represented by a *trajectory*, depicting the location $x(t)$ of a vehicle on the roadway at instant t. In other words, the trajectory of vehicle α is represented by the pair $(x_\alpha(t),t)$. From the trajectory of a vehicle α, its local velocity $v_\alpha = v_\alpha(x_\alpha(t),t)$ can be determined:

$$v_\alpha = \dot{x}_\alpha \tag{3.1}$$

We will assume that the velocity of a vehicle can be modelled as a random process $\underline{V}_\alpha(t)$. This assumption is justified by the observation that no drivers are able to maintain a constant velocity for any finite duration period. Rather, the velocity fluctuates over time and space. Therefore, the observed trajectory of a vehicle is an *instance* of this random process occur-

ring with a certain probability. That is, an observed trajectory $(x_\alpha(t),t)$ is a *realisation* of a random process $(\underline{X}_\alpha(t),t)$ (see Figure 3-1a). Alternatively, the trajectory of vehicle α can be defined by considering the time-instant $t_\alpha(x)$ at which vehicle α passes the observation location x. Thus, the observed trajectory can also be defined by a realisation of the random process $(x,\underline{T}_\alpha(x))$, which is equivalent to the random process $(\underline{X}_\alpha(t),t)$ (see Figure 3-1b).

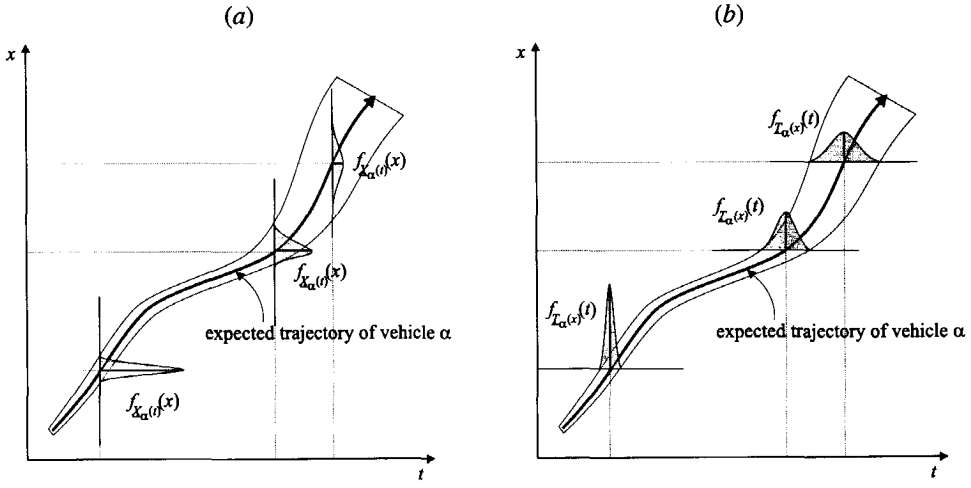

Figure 3-1: Probabilistic vehicle trajectories with respective probability density functions of the random variates $\underline{X}_\alpha(t)$ and $\underline{T}_\alpha(t)$.

3.1.2 Motivation for redefining intensity and concentration

In this subsection, we will define the notions of intensity, concentration, flow-rate, and density for a *platoon-based* traffic flow representation. The definitions presented in this section differ from the definitions given in the literature (cf. Leutzbach (1988), Daganzo (1997b)). We justify these proposed modifications by the conviction that traffic *cannot be adequately described* as a collection of infinitesimal particles which – to a large extent – operate *independently* of each other (*vehicular chaos*; cf. Prigogine and Herman (1971)). Instead, we argue that the location and velocity of different vehicles are dependent. This dependence can be captured sufficiently accurate for the purpose of macroscopic model development by describing the traffic flow as a collection of *platoons*.

We define a platoon as a set of n-vehicles, with $n \geq 1$, of which the vehicle heading the platoon is the *free-flowing* platoon leader, that moves independently of the other vehicles in the platoon, *and* a nonnegative number of *constrained* (*platooning*) followers, whose location and velocity is *entirely* determined by the platoon leader. Consequently, we assume that a platoon behaves as a solid block, in which no internal movements occur. Let us note that in this chapter we assume for convenience that the distance between the vehicles in a platoon is zero. However, chapters 4 and 6 this assumption is relieved by considering the *minimal safe distance* of vehicles in the traffic stream, which is a function of among other things the pla-

toon velocity and the reaction time of the drivers in the platoon. Consequently, we account for vehicular space requirements.

3.1.3 Traffic intensity and concentration

Let us consider a unidirectional M-lane roadway. Moreover, we assume that a traffic stream is observed at a fixed point x during interval $[t_0,t)$. The *local stream function* (cf. Leutzbach (1988)) or *cumulative flow function* (cf. Daganzo (1997b)) $\Phi(x,t)$ is defined by the *accumulated vehicle count* from the initial instant t_0 until instant t at the observation point x on all roadway lanes. That is, given the trajectories of vehicles α, $\Phi(x,t)$ is defined by:

$$\Phi(x,t) \stackrel{def}{=} \sum_{\alpha \in A} \chi_\alpha(x,t) \tag{3.2}$$

where the indicator *function* χ_α is defined by:

$$\chi_\alpha(x,t) = \chi_\alpha(x,t;t_0) \stackrel{def}{=} \begin{cases} 1, & t_0 \le \underline{T}_\alpha(x) < t \\ 0, & \underline{T}_\alpha(x) < t_0 \quad \text{or} \quad \underline{T}_\alpha(x) \ge t \end{cases} \tag{3.3}$$

That is, $\chi_\alpha(x,t)$ indicates whether vehicle α has passed observation location x in period $[t_0,t)$. $\Phi(x,t)$ represents a *non-decreasing, integer-valued stochastic process*. Using $\Phi(x,t)$, the *intensity* $\lambda(x,t;n)$ at location x and time instant t on lane j is defined by:

$$\lambda(x,t;n) \stackrel{def}{=} \lim_{\Delta t \to 0} \frac{1}{\Delta t} \Pr(\Phi(x,t+\Delta t) - \Phi(x,t) = n), \quad \text{for } n \ge 0 \tag{3.4}$$

where we implicitly assumed that the limit exists. In other words, the value $\lambda(x,t;n)\Delta t$ (i.e. the intensity multiplied by the period duration) equals *the probability that n vehicles pass the observation point x during the infinitesimal time period* $[t,t+\Delta t)$. The definition of intensity differs from the definition by Leutzbach (1988), in that we allow multiple vehicles – a *platoon* – to pass the observation point x during the infinitesimal time interval collectively. In opposition, Leutzbach assumes that vehicles pass an observation point one at a time, and consequently that the probability that more than one vehicle passes the observation point during the infinitesimal interval $[t,t+\Delta t)$ is zero.

The motivation for defining the intensity in this new way is that vehicles (and consequently *vehicle platoons*) are modelled as *infinitesimal particles*. When all vehicles are freely flowing, we may assume that there is always a finite amount of space between the vehicles on the roadway lanes. In this case, the probability that two vehicles pass the observation location during the infinitesimal period $[t,t+\Delta t)$ approaches zero as $\Delta t \to 0$. However, this is generally not true when *constrained traffic* is considered. That is, when a fast vehicle catches up with a slow vehicle, the vehicular particles 'collide'. Unless the fast vehicle is able to immediately overtake the slow vehicle, we assume that after the interaction, the vehicular particles continue their trip as a pair occupying the same location x at time instant t. Thus, the intensity $\lambda(x,t;n)\Delta t$ describes the probability that during the period $[t,t+\Delta t)$ a *n-vehicle platoon* passes the observation location.

Next, let us assume that the traffic stream is observed at instant t in the region $[x_0,x)$. The *instantaneous stream function* $\Psi(x,t)$ (cf. Leutzbach (1988)) is defined by the accumulated vehicle count at instant t for the interval $[0,x)$, where by definition, the x-axis is directed to the right, that is:

$$\Psi(x,t) \overset{def}{=} \sum_{\alpha \in A} \delta_\alpha(x,t) \tag{3.5}$$

where the indicator function δ_α is defined by:

$$\delta_\alpha(x,t) \overset{def}{=} \begin{cases} 1, & x_0 \le \underline{X}_\alpha(t) < x \\ 0, & \underline{X}_\alpha(t) < x_0 \quad \text{or} \quad \underline{X}_\alpha(t) \ge x \end{cases} \tag{3.6}$$

Let us emphasise that the instantaneous stream function is a *non-decreasing (in x), integer-valued stochastic process*. Assuming that the limits exists, the *concentration* $\kappa(x,t;n)$ of the traffic stream at x and instant t is defined by:

$$\kappa(x,t;n) \overset{def}{=} \lim_{\Delta x \to 0} \frac{1}{\Delta x} \Pr(\Psi(x+\Delta x,t) - \Psi(x,t) = n) \tag{3.7}$$

The value $\kappa(x,t;n)\Delta x$ (concentration multiplied by the interval length) equals the probability that an n-vehicle platoon is present on the infinitesimal interval $[x,x+\Delta x)$ at time instant t.

3.2 Velocity distributions and continuity relation

When we consider single vehicles, the assumption (cf. Leutzbach (1988)) of negligible probabilities that two (or more) vehicles pass cross-section x during an infinitesimal observation period $[t,t+dt)$, is justified. However, this assumption is *not* justified when describing traffic flow as a collection of zero-length n-vehicle platoons. Nevertheless, in this section we will show that the relation between flow-rate $m(x,t)$, density $r(x,t)$, and expected velocity $V(x,t)$ at location x and instant t also holds when we consider platoons rather than single vehicles:

$$m(x,t) = r(x,t)V(x,t) \tag{3.8}$$

3.2.1 Local and instantaneous velocity observations

Let us consider velocity observations at a specific time instant. These are called *instantaneous measurements* denoted with the subscript m. The underlying probability distribution function and probability density function for these instantaneous velocity measurements collected on lane j are denoted by $G_m(v) = G_m(v;x,t)$ and $g_m(v) = g_m(v;x,t)$ respectively. These probability distribution functions convey both the variations in the velocities in the population of drivers, as well as the within-driver variance in the velocities.

Measurements that are collected at a specific location are called *local measurements*, and denoted with the subscript l. The underlying probability distribution function and probability density function resulting for local observations collected on lane j are denoted by $G_l(v) = G_l(v;x,t)$ and $g_l(v) = g_l(v;x,t)$ respectively.

3.2.2 Empirical velocity distributions

Figure 3-2 shows the estimates of the velocity probability density functions of person-cars and trucks from measurements obtained at a two-lane motorway in the Netherlands (A9). The figure shows that the velocity distribution changes when the density increases. Also note that both the means and the variances of the distributions decrease with increasing density.

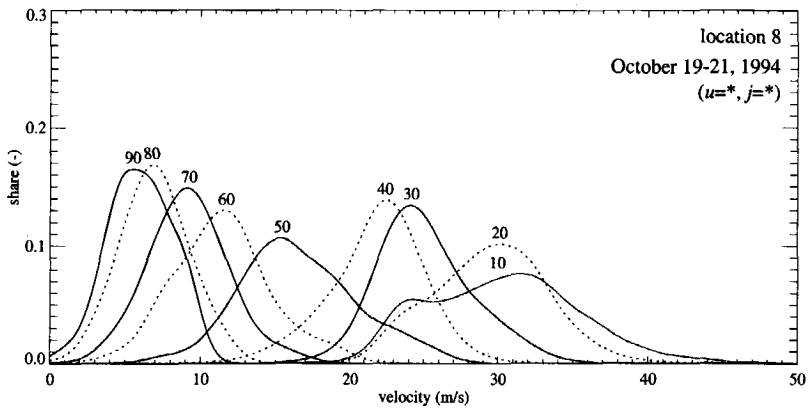

Figure 3-2: Velocity probability density function estimates for different average-lane densities (Kernel estimation technique). The numbers indicate class-mean densities (A9 two-lane motorway, 20th of October 1994, location 8).

3.2.3 Relation between concentration and intensity

The expression $\kappa(x,t;n)\mathrm{d}x$ by definition equals the probability that an n-vehicle platoon is present on the infinitesimal region $[x,x+\mathrm{d}x)$. By definition, the probability that an n-vehicle platoon located in $[x,x+\mathrm{d}x)$ is driving at a velocity in the infinitesimal interval $[v,v+\mathrm{d}v)$ equals $g_m(v)\mathrm{d}v$. In combining these results, the probability that at instant t, an n-vehicle platoon is present in $[x,x+\mathrm{d}x)$ having a velocity in $[v,v+\mathrm{d}v)$ equals:

$$\kappa(x,v,t;n)\mathrm{d}v\mathrm{d}x = \kappa(x,t;n)g_m(v)\mathrm{d}v\mathrm{d}x \tag{3.9}$$

Similarly, the probability that during the period $[t,t+\mathrm{d}t)$ an n-vehicle platoon passes the location point x having a velocity in $[v,v+\mathrm{d}v)$ equals:

$$\lambda(x,v,t;n)\mathrm{d}v\mathrm{d}t = \lambda(x,t;n)g_l(v)\mathrm{d}v\mathrm{d}t \tag{3.10}$$

A platoon driving with velocity v requires a period of $\mathrm{d}t = \mathrm{d}x/v$ to traverse $[x,x+\mathrm{d}x)$. As a consequence, the probability that during $[t,t+\mathrm{d}x/v)$ an n-vehicle platoon driving with velocity v passes the observation point x equals the probability that a n-vehicle platoon driving with velocity v is present in $[x,x+\mathrm{d}x)$ at instant t. In combining (3.9) and (3.10), we find:

$$v\kappa(x,t;n)g_m(v) = \lambda(x,t;n)g_l(v) \tag{3.11}$$

Integrating (3.11) with respect to the velocity v yields the fundamental equation:

$$\kappa(x,t;n)V(x,t;n) = \lambda(x,t;n) \tag{3.12}$$

where $V(x,t;n)$ denotes the *expected instantaneous velocity* of an n-vehicle platoon. Thus, the *intensity* $\lambda(x,t;n)$ equals the product of the concentration $\kappa(x,t;n)$ and the expected instantaneous velocity $V(x,t;n)$ of n-vehicle platoons.

3.2.4 *Density and flow-rate*

We define the *density* $r(x,t)$ on lane j by the *expected number of vehicles* present at an infinitesimal region $[x,x+dx)$ at instant t per unit roadway length, that is:

$$r(x,t) \overset{def}{=} \sum_{n=0}^{\infty} n \cdot \kappa(x,t;n) \tag{3.13}$$

while the *flow-rate* $m(x,t)$ is defined by the *expected number of vehicles* passing the observation location x during $[t,t+dt)$:

$$m(x,t) \overset{def}{=} \sum_{n=0}^{\infty} n \cdot \lambda(x,t;n) = \sum_{n=0}^{\infty} n \cdot \kappa(x,t;n) \cdot V(x,t;n) \tag{3.14}$$

The *expected instantaneous velocity* $V(x,t)$ equals:

$$V(x,t) = \sum n \cdot \kappa(x,t;n) \cdot V(x,t;n) / \sum n \cdot \kappa(x,t;n) = m(x,t) / r(x,t) \tag{3.15}$$

It appears that the fundamental equation also holds when considering n-vehicle platoons.

3.3 Desired velocity and other continuous attributes

In this section, we will show how the desired velocity of drivers can be accounted for in probabilistic terms, using the joint distribution function of the velocity and the desired velocity. We will also explain how other explanatory variables, such as the lateral discrete distribution of vehicles on the roadway, may be included in this approach.

3.3.1 *General continuous attributes*

Let us consider a vector $\underline{\mathbf{V}}^0 = (\underline{V}_1^0,\ldots,\underline{V}_n^0)$ of random variates reflecting the characteristics of the traffic at x at instant t. The associated joint probability *distribution* function and the joint probability *density* function of the vector of random variates $\underline{\mathbf{Y}} = (\underline{V},\underline{\mathbf{V}}^0)$ are respectively denoted by $G(v,\mathbf{v}^0;x,t)$ and $g(v,\mathbf{v}^0;x,t)$. Examples of random variates $\underline{V}_i^0$ are the desired velocity $\underline{V}^0$ and the acceleration time $\underline{\tau}$ of vehicles. Using this distribution function, we define the extended concentration $\kappa(x,v,\mathbf{v}^0,t;n)$ and the extended intensity $\lambda(x,v,\mathbf{v}^0,t;n)$ by:

$$\kappa(x,v,\mathbf{v}^0,t;n) \overset{def}{=} \kappa(x,t;n) g_m(v,\mathbf{v}^0;x,t) \tag{3.16}$$

and:

$$\lambda(x,v,\mathbf{v}^0,t;n) \overset{def}{=} \lambda(x,t;n) g_l(v,\mathbf{v}^0;x,t) \tag{3.17}$$

respectively, where the index m indicates instantaneous velocity observations, and the index l indicates the local velocity observations. Let us remark that $\kappa(x,v,\mathbf{v}^0,t;n)dxdvd\mathbf{v}^0$ equals the probability that an n-vehicle platoon is located on $[x,x+dx)$ at instant t, having a velocity in $[v,v+dv)$ and other flow properties ('continuous attributes') in $d\mathbf{v}^0$, for instance a desired velocity in $[v^0,v^0+dv^0)$. Expression $\lambda(x,v,\mathbf{v}^0,t;n)dtdvd\mathbf{v}^0$ equals the probability that an n-vehicle platoon passes the observation location x during the infinitesimal interval $[t,t+dt)$, having a velocity in $[v,v+dv)$ and continuous attributes in the region $d\mathbf{v}^0$.

3.3.2 Desired velocity

The *desired velocity* is a very important concept of the theory described in this thesis. It is defined by the *velocity* with which a *free-flowing* driver aims to traverse along the roadway.

Factors influencing the desired velocity

The desired velocity is determined by the velocity at which the driver wishes to travel on the one hand, and the constraints of his vehicle and the road on the other hand. The distribution of desired velocities in a traffic stream depends upon (Leutzbach (1988)):

- *Composition of the traffic stream* with respect to among other things user-classes, vehicle-types, and demographic characteristics.
- *External conditions*, such as ambient-, weather- and road-conditions.

Measurements of the desired velocity

Several methods have been developed for the determination of the desired velocities. In this respect, let us emphasise that in general only part of the drivers in a traffic stream will be able to drive at their desired velocity. The observed velocities of free-flowing vehicles are *not representative* of the mean desired velocity since the lower desired velocities are over-represented in the observations. This is caused by the fact that drivers with high desired velocities have a higher probability of being constrained in their speed choice by lower speed vehicles than drivers with lower desired speeds have.

Carlsson and Cedersund (1998) present a model for the determination of the desired velocity. They propose an additive model to describe the desired velocity as a function of the desired velocity under ideal conditions, and adjustment factors for respectively terrain type, lane width, distance to roadside obstacles (if less than 2 metres), cars with trailers, and width of the right hard shoulder. This model is calibrated using a simple regression analysis. In illustration, for motorway lanes (speed limit of 110*km/hr*), typical values for the *desired velocity under ideal conditions* are depicted in Table 3-1.

Table 3-1: Estimated mean desired velocities under ideal circumstances on the left-lane (L) and the right-lane (R) of a two-lane Swedish motorway for different speed limits (source: Carlsson and Cedersund (1998)).

speed-limit:	110*km/hr*		90*km/hr*		70*km/hr*	
Vehicle type:	L	R	L	R	L	R
person-car	116	105	106	94	85	76
non-articulate truck or bus	106	92	98	87	84	74
articulate truck	92	85	91.5	84.5	81	73

Branston (1979) presents a method to determine the desired velocity distribution based on an analytical model describing the distribution of the desired velocity for a road with negligible overtaking possibilities. Botma (1986) applied this method to a two-lane rural road in the Netherlands. He concludes that in this case, the desired velocity distribution changes during the day due to changing traffic composition (purpose of travel) and ambient conditions.

However, since overtaking possibilities cannot be neglected on a multilane motorway, this method is not applicable for our multilane case.

A simpler method to determine the desired velocities is to study the velocity distributions at very low traffic volumes. The Highway Capacity Manual (HCM,1994) suggests that these can adequately be observed for traffic volumes below 1400*veh/hr·lane*. In this respect note that the speed-limits differences* in the Netherlands cause *an increase* in the number of constrained vehicles at lower volumes. Nevertheless, we assume that the desired velocities can be observed when very dilute traffic is considered ($r < 4$*veh/km/lane*).

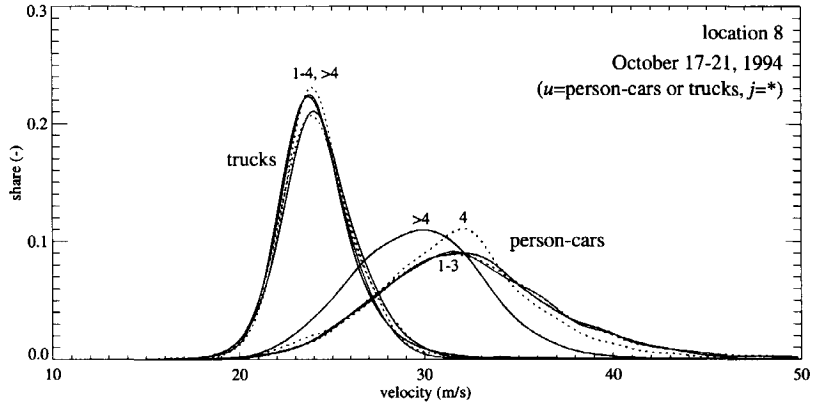

Figure 3-3: Velocity probability density functions for low *lane-average* densities (Kernel estimation technique). The densities indicate the class-mean density (A9 motorway data).

Figure 3-3 shows estimates for the velocity distribution at very low densities, determined from observations collected during the period 0:00AM – 6:00AM on two working weeks (Monday – Friday) in October 1994 at the A9 - 2×2 lane motorway in the Netherlands. The figure shows that the velocity distributions are nearly invariant for low densities. Note that assuming that these velocity distributions are representative for the desired velocity distribution implies that we extrapolate the desired velocity distribution measured during the evening or at night to other periods of the day, thereby neglecting the changes in the desired velocity distribution due to changes in the driver-population and ambient or weather-conditions.

Describing desired velocity

We will describe the distribution of the desired velocity by a random variate $\underline{V}^0$, conveying between drivers' variations in the desired velocity. In chapter 4 of this thesis we will show that only the platoon leader is able to accelerate towards his desired velocity; the followers accelerate together with the platoon leader towards the desired velocity of the latter vehicle, which will be referred to as the platoon's *acceleration velocity*. Clearly, the acceleration ve-

* Dutch legislation allows a maximum velocity of 120*km/hr* for person-cars, while the maximum velocity of trucks is 80*km/hr*.

locity only equals the desired velocity if all vehicles in the stream are free-flowing. Otherwise, the *acceleration velocity* changes when the fraction of constrained vehicle increases.

The desired velocity distribution is described in conjunction with the instantaneous velocity distribution. To this end, we consider the joint probability distribution function of the *instantaneous* $\underline{V}$ and the *desired velocity* $\underline{V}^0$ observed in the interval $[x,x+dx)$ at instant t, i.e. $\underline{\mathbf{Y}} = (\underline{V},\underline{V}^0)$. The joint distribution function of the velocity and the desired velocity plays an essential role in the sequel of this dissertation.

3.4 Phase-space traffic variables and conservative flow variables

Key to the derivation of the macroscopic multilane multiclass traffic flow model is the identification of the so-called *multilane multiclass Phase-Space Density* (MLMC-PSD). To introduce the concept, we consider in this section the Phase-Space Density (PSD) for a single user-class, without distinguishing roadway lanes or drivers' states. Later we will show the generalisation to all kinds of special classes.

In section 3.3.1 we have presented the notions of extended traffic concentration and traffic intensity by considering the distribution of among other things the velocity V and the desired velocity V^0 at location x at instant t. In this section, we will use this joint probability distribution function to define the so-called Phase-Space Density. Rather than considering general vectors $\underline{\mathbf{Y}}$ of stochastic variables $(\underline{V},\underline{V}_1^0,\underline{V}_2^0,\ldots,\underline{V}_n^0)$, we will only consider the joint probability of the velocity and the desired velocity, i.e. $\underline{\mathbf{Y}} = (\underline{V},\underline{V}^0)$. By doing so, we close the gap with other gas-kinetic flow modelling approaches (e.g. Paveri-Fontana (1975), Helbing (1996)) using the phase-space concept. Nevertheless, the topics discussed can be easily extended to general continuous attribute vectors $\underline{\mathbf{V}}^0$ (see section 3.3.1).

In macroscopic traffic flow description, the traffic flow variables are described as functions with two independent variables, namely location x and instant t. However, in the sequel of this chapter, we will introduce generalised flow variables that describe the dynamics of the flow in the *phase-space* Σ. That is, rather than only considering x and t, also velocity v and desired velocity v^0 are considered as *explanatory variables*. In the sequel we will refer to the space of all admissible values (x,v,v^0) as the *phase-space* Σ.

3.4.1 Phase-space density, reduced Phase-Space Density, and density

Let us consider $\underline{V}$ and $\underline{V}^0$ of vehicles at location x and instant t. Dropping the index m – indicating that we are considering the instantaneous velocity rather than local velocity observations – the Phase-Space Density ρ is then defined by:

$$\rho(x,v,v^0,t) \overset{def}{=} \sum_{n=0}^{\infty} n \cdot \kappa(x,v,v^0,t;n) = g(v,v^0 \mid x,t)\, r(x,t) \tag{3.18}$$

where $r(x,t)$ denotes the density at (x,t). Thus, $\rho(x,v,v^0,t)$ denotes the expected number of vehicles at (x,t) *per unit roadway length*, driving at velocity v while striving for desired velocity v^0. The Phase-Space Density has been introduced by Paveri-Fontana (1975) to derive gas-kinetic equations describing aggregate-lane aggregate-class flow operations (section 2.3.4).

From the Phase-Space Density the so-called *reduced Phase-Space Density* can be determined:

$$\tilde{\rho}(x,v,t) \overset{def}{=} \int \rho(x,v,v^0,t)\mathrm{d}v^0 \tag{3.19}$$

The reduced Phase-Space Density describes the expected number of vehicles at x and t per unit roadway length, currently driving with velocity v, irrespective of their desired velocity. Let us note that the density relates to the (reduced) Phase-Space Density according to:

$$r(x,t) = \iint \rho(x,v,v^0,t)\mathrm{d}v^0\mathrm{d}v = \int \tilde{\rho}(x,v,t)\mathrm{d}v \tag{3.20}$$

From relation (3.20) we observe that the Phase-Space Density can be considered as a *partial density*, in that it describes the contribution of the expected number of vehicles per unit roadway length driving with velocity v and having a desired velocity v^0 to the density r.

3.4.2 Phase-space momentum and phase-space energy

In analogy with the continuum theory of fluids and gasses, in the sequel, the so-called *conservative variables density*, *momentum*, and *energy* are introduced. These conservative variables play an essential role in the derivation of the presented multiclass flow theory. Similar to the density, we can also determine the traffic momentum and traffic energy from contributions of vehicles driving at a specific velocity. To this end, we define the *phase-space momentum* μ and the *phase-space energy* ε by the respective contributions to the total momentum and the total energy of vehicles driving at a distinct velocity v.

Momentum and phase-space momentum

Each particle in the stream has *momentum*, defined by the mass of the particle multiplied by its velocity. The *expected momentum* in a control volume equals the aggregate momentum of all particles in the volume divided by the volume. We define the momentum $M(x,v,t)$ of a vehicle driving with a velocity v at (x,t) by the 'mass' of the vehicle* – which equals one – multiplied by its velocity v:

$$M(x,v,t) \overset{def}{=} v \tag{3.21}$$

The momentum of a single vehicle leads to the *phase-space momentum* (PSM):

$$\mu(x,v,v^0,t) \overset{def}{=} v\rho(x,v,v^0,t) \tag{3.22}$$

and the reduced phase-space momentum:

$$\tilde{\mu}(x,v,t) \overset{def}{=} v\tilde{\rho}(x,v,t) = \int \mu(x,v,v^0,t)\mathrm{d}v^0 \tag{3.23}$$

* Note that the concept of vehicular mass used in this thesis has *no relation* with the physical mass of vehicles.

Energy and phase-space energy

In addition to *mass* and *momentum*, a particle in a stream also has *energy*. This *energy E* consists of three parts: *kinetic energy* E_{kin}, *internal energy* E_{int}, and *potential energy* E_{pot}. *Potential energy* is defined by the energy due to the location of particles (i.e. vehicles) in a 'force-field'. This type of energy is useless for one-dimensional vehicular flows, and is therefore neglected. Thus, *kinetic energy* E_{kin} and *internal energy* E_{int} form the total energy E of vehicles. The *kinetic energy* of a vehicle is defined by the energy contribution *of* the aggregate vehicular flow to which a vehicle belongs, i.e. the energy due to the expected velocity $V(x,t)$ of the vehicular flow at (x,t). The *internal energy* describes the additional energy due to the *deviation* $(v-V(x,t))$ from $V(x,t)$.

We will define the total energy $E = E(x,v,t)$ of a vehicle driving with velocity v according to the definition of the energy of a particle in a continuous medium. That is, the energy of a particle is the energy due to the particle's velocity and equals its mass times the square of its velocity divided by two. Setting the mass of a vehicle to 'one vehicle', the total energy of a single vehicle driving with velocity v at (x,t) equals:

$$E(x,v,t) \overset{def}{=} \tfrac{1}{2}v^2 \tag{3.24}$$

In accordance with the definition, E can be split-up into contributions E_{kin} and E_{int} (see Hirsch (1990a,b)). The *phase-space energy* (PSE) can then be defined in accordance with the definition of the PSD and the PSM, namely:

$$\varepsilon(x,v,v^0,t) \overset{def}{=} \tfrac{1}{2}v^2\rho(x,v,v^0,t) \tag{3.25}$$

while for the *reduced phase-space energy* we propose:

$$\tilde{\varepsilon}(x,v,t) \overset{def}{=} \tfrac{1}{2}v^2\tilde{\rho}(x,v,t) = \int \varepsilon(x,v,v^0,t)\mathrm{d}v^0 \tag{3.26}$$

3.5 Derivation of macroscopic variables

Let us recall that the aim of the thesis is to establish a traffic flow theory describing the dynamics of the macroscopic multilane multiclass traffic variables. Foundation of these equations will be the dynamics of the phase-space densities. Using these dynamics, equations describing the temporal changes in either the so-called conservative variables or the so-called primitive variables are established.

The *primitive variables* reflect *directly observable macroscopic quantities* of the traffic flow, such as the velocity and the velocity variance. Traditionally, these variables have been used to macroscopically describe traffic flow operations. The primitives have been interpreted from the viewpoint *of the individual driver* (e.g. Payne (1971), Kerner and Konhäuser (1995), Kerner *et al.* (1996), Lyrintzis *et al.* (1994), and Liu *et al.* (1998)) rather than from the viewpoint of the collective vehicular flow.

In contrast, the *conservative variables* reflect the state of the *collective heterogeneous flow*, such as traffic density, momentum and energy. Their name-giving reflects the conservative nature of the variables. That is, if only convective processes would be considered, traffic density, traffic momentum and traffic energy are *conserved* (i.e. 'storage = inflow – outflow').

Of course, processes such as acceleration, and deceleration due to interaction, cause this conservation of conservatives to be violated. Although the conservatives lack intuitive appeal from the viewpoint of a single driver, their use yields a number of advantages which become clear when deriving the macroscopic flow equations from the Phase-Space Density dynamics (sections 6.2, 6.3, and 6.4).

In this section we establish the macroscopic primitive traffic variables and conservative traffic variables from the Phase-Space Density, using the *mean-operator* $\langle\cdot\rangle$ and the *aggregation operator* $[\cdot]$ respectively (see Intermezzo I).

The mean operator $\langle\cdot\rangle$

In this thesis, the derivation of the *primitive* flow variables (density, velocity, velocity variance) from the phase-space densities is done using so-called *mean operators*. These mean operators provide the *expected* value of an arbitrary function $f(\mathbf{v},\mathbf{v}^0)$ of the velocity $\mathbf{v}\in I\!R^n$ (see section 3.2) and continuous attributes (e.g. desired velocity; see section 3.3) $\mathbf{v}^0\in I\!R^m$, given a joint probability density function $g(\mathbf{v},\mathbf{v}^0)$ of the velocity and the continuous attributes. The following expression defines the mean operator $\langle\cdot\rangle$ applied to the function f with respect to the probability density function g:

$$\left\langle f(\mathbf{v},\mathbf{v}^0)\right\rangle \stackrel{def}{=} \int\int f(\mathbf{w},\mathbf{w}^0)g(\mathbf{w},\mathbf{w}^0)\,\mathrm{d}\,\mathbf{w}^0\,\mathrm{d}\,\mathbf{w} \tag{i.1}$$

That is, since $g(\mathbf{w},\mathbf{w}^0)\mathrm{d}\mathbf{w}^0\mathrm{d}\mathbf{w}$ equals the probability that the velocity lies in the infinitesimal volume $\mathrm{d}\mathbf{w}$ while the continuous attributes are in the infinitesimal volume $\mathrm{d}\mathbf{w}^0$, the mean operator determines the *expected value* of the function f with respect to the velocity and continous attributes.

The aggregation operator $[\cdot]$

Alternatively, we will use *aggregation operators* to derive the *conservative* flow variables (density, momentum, energy) for the phase-space densities. These aggregation-operators provide the *expected total* value of contributions $f(\mathbf{v},\mathbf{v}^0)$ of vehicles driving with velocity $\mathbf{v}$, having continuous attributes $\mathbf{v}^0$. The following expression defines the aggregation operator $[\cdot]$ for general contributions f with respect to the phase-space density ρ:

$$[f(\mathbf{v},\mathbf{v}^0)] \stackrel{def}{=} \int\int f(\mathbf{w},\mathbf{w}^0)\rho(\mathbf{w},\mathbf{w}^0)\,\mathrm{d}\,\mathbf{w}^0\,\mathrm{d}\,\mathbf{w} \tag{i.2}$$

Note that the aggregation operator satisfies the following relation with the mean operator:

$$[f(\mathbf{v},\mathbf{v}^0)] = r\int\int f(\mathbf{w},\mathbf{w}^0)\frac{\rho(\mathbf{x},\mathbf{w},\mathbf{w}^0,t)}{r(\mathbf{x},t)}\,\mathrm{d}\,\mathbf{w}^0\,\mathrm{d}\,\mathbf{w} = r(\mathbf{x},t)\left\langle f(\mathbf{v},\mathbf{v}^0)\right\rangle \tag{i.3}$$

where $r(\mathbf{x},t)$ denotes the density at instant t and point $\mathbf{x}\in I\!R^n$.

Intermezzo I: Definition of mean operator and aggregation operator

3.5.1 *Determination of macroscopic primitive variables using mean operator*

The mean operator enables determination of various quantities reflecting specific characteristics of the joint probability density function $g(v,v^0)$. This can be done by choosing specific expressions for f. Let us now consider some of these specifications.

Identity relation. By choosing $f(v,v^0) = 1$, we can easily determine the identity relation:

$$\langle 1 \rangle \stackrel{def}{=} \int\int g(w,w^0)\mathrm{d}w^0\mathrm{d}w = 1 \tag{3.27}$$

Expected velocity. Let us consider the function $f(v,v^0) = v$. Then we can establish the following relation between the first order velocity moment $\langle v \rangle$ and the mean velocity V:

$$\langle v \rangle = \int\int wg(w,w^0)\mathrm{d}w^0\mathrm{d}w = V \quad \Leftrightarrow \quad V \stackrel{def}{=} \langle v \rangle \tag{3.28}$$

where we have dropped the dependence on (x,t) for notational convenience.

Expected velocity variance. Choosing $f(v,v^0) = v^2$, we can derive the relation between the second order velocity moment $\langle v^2 \rangle$ and the velocity variance Θ:

$$\langle v^2 \rangle = V^2 + \Theta \quad \Leftrightarrow \quad \Theta \stackrel{def}{=} \langle (v-V)^2 \rangle \tag{3.29}$$

Skewness of velocity distribution. Next, let us consider $f(v,v^0) = v^3$. Then, we can relate the third order velocity moment $\langle v^3 \rangle$ to the skewness Γ of the velocity distribution:

$$\langle v^3 \rangle = V^3 + 3V\Theta + \Gamma \quad \Leftrightarrow \quad \Gamma \stackrel{def}{=} \langle (v-V)^3 \rangle \tag{3.30}$$

Covariance between velocity and desired velocity. Choosing $f(v,v^0) = vv^0$ yields an expression for the covariance C between the velocity and the desired velocity:

$$\begin{gathered} \langle vv^0 \rangle = \int\int ww^0 g(w,w^0)\mathrm{d}w^0\mathrm{d}w = C + VV^0 \\ \Leftrightarrow \\ C \stackrel{def}{=} \langle vv^0 \rangle - VV^0 = \langle (v-V)(v^0-V^0) \rangle \end{gathered} \tag{3.31}$$

3.5.2 *Determination of macroscopic conservative variables using aggregation operator*

Similar to the approach used to determine primitive variables using the mean operator, we can determine the *conservative variables* using the *aggregation operator*.

Traffic density. In section 3.4.1 we have defined the *density* based on the PSD. Using the aggregation-operator, we can easily rewrite equation (3.20):

$$[1] = \int\int \rho(w,w^0)\mathrm{d}w^0\mathrm{d}w = r \tag{3.32}$$

Traffic momentum. Let us recall from section 3.4.2 that the momentum $M(x,v,t)$ of a vehicle driving with velocity v equals $M = v$. Then, similarly to the traffic density $r(x,t)$, we can determine the *traffic momentum* by aggregation of the partial momentum $\mu = v\rho$ using the aggregation operator $[\cdot]$:

$$m \overset{def}{=} [v] = \int\int w\rho(w, w^0)\mathrm{d}w^0\mathrm{d}w = r\langle v \rangle = rV \tag{3.33}$$

From (3.33) we see that traffic momentum m equals the *expected flow-rate* rV. Moreover, note that the traffic momentum can also be determined by aggregation of the reduced phase-space momentum $\tilde{\mu}$.

Traffic energy. In section 3.4.2 we have introduced the concept of the traffic energy $E(x,v,t)$ for vehicles driving with velocity v. By application of the aggregation operator $[\cdot]$ we can determine the total expected energy for the entire vehicular flow:

$$e \overset{def}{=} [E] = \tfrac{1}{2}\int\int w^2\rho(w, w^0)\mathrm{d}w^0\mathrm{d}w = \tfrac{1}{2}r\langle v^2 \rangle = \tfrac{1}{2}r(V^2 + \Theta) \tag{3.34}$$

If we again consider the distinction in contributions of the kinetic energy and the internal energy, we can respectively determine the expected kinetic and internal energy by:

$$e_{\text{kin}} = \tfrac{1}{2}rV^2 \quad \text{and} \quad e_{\text{int}} = \tfrac{1}{2}r\Theta = \tfrac{1}{2}P \tag{3.35}$$

where $P = r\Theta$ denotes the *traffic pressure*. Again, note that the traffic energy can also be determined by aggregation of the reduced phase-space energy $\tilde{\varepsilon}$.

Traffic enthalpy. The *flux of velocity variance* is defined by the third order velocity moment:

$$[v^3] = \int\int w^3\rho(w, w^0)\mathrm{d}w^0\mathrm{d}w = 2mH + J \tag{3.36}$$

where H denotes the stagnation of total traffic enthalpy, and J denotes the flux of velocity variance. The stagnation traffic enthalpy H is defined by:

$$H \overset{def}{=} e/r + \Theta = \tfrac{1}{2}V^2 + \tfrac{3}{2}\Theta \tag{3.37}$$

As will become clear in the remainder of this thesis, the stagnation traffic enthalpy H defines an expression for the convective flux. That is, it describes changes in the traffic energy caused by the inflow and outflow of vehicles.

Flux of velocity variance. The flux of velocity variance J is defined by:

$$J \overset{def}{=} r\Gamma = [(v - V)^3] \tag{3.38}$$

3.6 Generalisation of traffic flow variables

In this section we extend the approach presented in the previous sections to multiclass multilane traffic flow. To correctly model the differences between the lanes and the user-classes, several attributes delineating the differences in traffic flow behaviour of drivers and the resulting traffic flow conditions must be taken into account. In this dissertation, the following discrete attributes of vehicles are considered:

- *User-classes* $u \in \mathbf{U}$ (section 3.7.1).
- *Roadway lanes* $j \in \mathbf{J} = \{1,\ldots,M\}$ (section 3.7.2)
- *State-of-driving* $c \in \mathbf{C}$ (section 3.7.3)

The values of these attributes are both *non-overlapping* (*disjoint*) and *exhaustive*. That is, each vehicle in the stream belongs to *exactly one triple* $\mathbf{a} = (u,j,c)$ at the time.

An important issue discussed in the remainder of this chapter is that the distinction of drivers based on both discrete (e.g. user-types) and continuous (e.g. desired velocities) attributes results in the modification of the *vehicle-conservation* formalism. In other words, changes in the expected number of vehicles $\rho_{\mathbf{a}}(x,v,\mathbf{v}^0,t)dx$ in cell x^* characterised by the arbitrary discrete set $\mathbf{a}$ and the arbitrary continuous set $\mathbf{v}^0$ are *not only* governed by the balance between the inflow $\rho_{\mathbf{a}}(x,v,\mathbf{v}^0,t)vdt$ and outflow $\rho_{\mathbf{a}}(x+dx,v,\mathbf{v}^0,t)vdt$ during the interval dt (as would be the case for the traffic density $r(x,t)$). That is, the expected number of vehicles $\rho_{\mathbf{a}}(x,v,\mathbf{v}^0,t)dx$ in the roadway cell may change to transitions to other attribute sets $(\mathbf{a}',v',\mathbf{v}_0')$ as well.

Transitions between different attribute-values occur in an event-like manner. For instance, a driver suddenly becomes constrained when interacting with a slower vehicle. Based on the general notions introduced in section 3.1, we will introduce in the remainder the attribute-set specific local and instantaneous stream functions, intensity, and concentration respectively.

3.6.1 Generalised local and instantaneous stream functions

Let us now consider distinct discrete and continuous attributes in order to define the generalised local stream function and the generalised instantaneous stream function. To this end, we introduce vector $\mathbf{a}$ indicating drivers' discrete attribute-values (e.g. $\mathbf{a} = (u,j,c)$). Let $\mathbf{A}$ denote the set of all vectors $\mathbf{a}$ (e.g. $\mathbf{A} = \{\mathbf{U},\mathbf{J},\mathbf{C}\}$). The generalised local stream function $\Phi_{\mathbf{a}}(x,t)$ is defined by the number of vehicles sharing attribute-values $\mathbf{a}$, which pass x during interval $[t_0,t)$. Similarly, the instantaneous stream function $\Psi_{\mathbf{a}}(x,t)$ is defined by the number of vehicles of attribute-values $\mathbf{a}$ present in the region $[x_0,x)$ at instant t. Clearly, the following identities hold with respect to the aggregation of the respective discrete attributes:

$$\Phi(x,t) = \sum_{\mathbf{a}\in\mathbf{A}} \Phi_{\mathbf{a}}(x,t) \quad \text{and} \quad \Psi(x,t) = \sum_{\mathbf{a}\in\mathbf{A}} \Psi_{\mathbf{a}}(x,t) \tag{3.39}$$

3.6.2 Generalised intensity and concentration

If the limit exists, the *generalised* traffic intensity $\lambda_{\mathbf{a}}(x,t;n)$ is defined similar to eq. (3.4):

$$\lambda_{\mathbf{a}}(x,t;n) \overset{def}{=} \lim_{\Delta t\to 0} \Pr(\Phi_{\mathbf{a}}(x,t+\Delta t) - \Phi_{\mathbf{a}}(x,t) = n)/\Delta t \tag{3.40}$$

Considering the aggregation with respect to the attributes, we have the following identity:

$$\lambda(x,t;n) = \sum_{\mathbf{a}\in\mathbf{A}} \lambda_{\mathbf{a}}(x,t;n) \tag{3.41}$$

Similarly, assuming that the limit exists, we define the *generalised* concentration $\kappa_{\mathbf{a}}(x,t;n)$:

$$\kappa_{\mathbf{a}}(x,t;n) \overset{def}{=} \lim_{\Delta x\to 0} \Pr(\Psi_{\mathbf{a}}(x+\Delta x,t) - \Psi_{\mathbf{a}}(x,t) = n)/\Delta x \tag{3.42}$$

---

* Cell x is defined by the by the location interval $[x,x+\Delta x)$.

We can easily show that the fundamental equation (3.12) also holds for the generalised intensity and concentration:

$$\lambda_{\mathbf{a}}(x,t;n) = \kappa_{\mathbf{a}}(x,t;n)V_{\mathbf{a}}(x,t) \tag{3.43}$$

where $V_{\mathbf{a}}(x,t)$ denotes the *expected local velocity* of vehicles at (x,t) sharing attributes **a**. Using the generalised concentration and intensity, we can define the *generalised density* $r_{\mathbf{a}}$ and the *generalised momentum* $m_{\mathbf{a}}$:

$$r_{\mathbf{a}}(x,t) \overset{def}{=} \sum_{n=0}^{\infty} n \cdot \kappa_{\mathbf{a}}(x,t;n) \quad \text{and} \quad m_{\mathbf{a}}(x,t) \overset{def}{=} \sum_{n=0}^{\infty} n \cdot \lambda_{\mathbf{a}}(x,t;n) \tag{3.44}$$

3.6.3 Generalised velocity distributions and generalised PSD

Let us consider velocity $V_{\mathbf{a}}$ and desired velocity $V_{\mathbf{a}}^{0}$ at x at t of vehicles sharing attribute set **a**. The joint *probability* and *distribution* functions of the velocity and the desired velocity are denoted by $g_{\mathbf{a}}(v,v^0)$ and $G_{\mathbf{a}}(v,v^0)$ respectively. Then, the so-called generalised Phase-Space Density is defined by:

$$\rho_{\mathbf{a}}(x,v,v^0,t) \overset{def}{=} g_{\mathbf{a}}(v,v^0 \mid x,t) r_{\mathbf{a}}(x,t) \tag{3.45}$$

This generalised Phase-Space Density $\rho_{\mathbf{a}}$ denotes the expected number of vehicles per unit roadway length sharing attributes $\mathbf{a} \in \mathbf{A}$ present at x at t, while having velocity v and a desired velocity v^0. Although in this thesis we will only consider the velocity and the desired velocity, other explanatory variables can be easily introduced into the developed generalised framework (e.g. lateral position z on the roadway).

We can define the *reduced generalised PSD* similar to expression (3.19):

$$\tilde{\rho}_{\mathbf{a}}(x,v,t) \overset{def}{=} \int_{v^0} \rho_{\mathbf{a}}(x,v,v^0,t)\mathrm{d}v^0 \tag{3.46}$$

while the *generalised density* can be defined similar to relation (3.20):

$$r_{\mathbf{a}}(x,t) \overset{def}{=} \int_{v}\int_{v^0} \rho_{\mathbf{a}}(x,v,v^0,t)\mathrm{d}v^0\mathrm{d}v = \int_{v} \tilde{\rho}_{\mathbf{a}}(x,v,t)\mathrm{d}v \tag{3.47}$$

The *generalised phase-space momentum* and *generalised phase-space energy* can be defined for each attribute-set **a** in a similar manner.

3.6.4 Generalised mean operator and generalised aggregation operator

For each attribute-set **a**, we can define the *generalised mean-operator* indicated by subscript **a** in accordance to expression (i.1), given the velocity distribution function $g = g_{\mathbf{a}}$. The generalised mean $\langle\cdot\rangle_{\mathbf{a}}$ operator yields the generalised expected velocity $V_{\mathbf{a}}$, the variance $\Theta_{\mathbf{a}}$, the skewness $\Gamma_{\mathbf{a}}$, and the covariance $C_{\mathbf{a}}$ (equations (3.28), (3.29), (3.30), and (3.31) respectively).

We can also define the *generalised aggregation operator* $[\cdot]_{\mathbf{a}}$ with respect to the generalised Phase-Space Density $\rho_{\mathbf{a}}$ (expression (i.2)). By considering specific choices of f we can define the generalised momentum $m_{\mathbf{a}}$, energy $e_{\mathbf{a}}$, flux of velocity variance $J_{\mathbf{a}}$, and stagnation enthalpy $H_{\mathbf{a}}$ (equations (3.36), (3.38), (3.42), and (3.41) respectively).

3.6.5 *Multi-dimensional generalisation*

In addition to generalising the density concept with respect to the velocity v, general continuous attributes $\mathbf{v}^0$ and discrete attributes $\mathbf{a}$, the Phase-Space Density can also be generalised to describe the motion of traffic particles in two (or more dimensions). By doing so, the model can be adapted to describe the dynamics of alternative traffic systems, such as two-dimensional pedestrian traffic operations.

To this end, let us consider traffic particles moving in a n-dimensional subspace of $\mathbb{R}^n$. The location of these particles is denoted by the vector $\mathbf{x} = (x_1,\ldots,x_n)$, while their velocity is denoted by $\mathbf{v} = (v_1,\ldots,v_n)$. The *multi-dimensional generalised PSD* is denoted by $\rho_{\mathbf{a}}(\mathbf{x},\mathbf{v},\mathbf{v}^0,t)$, and describes the expected number of vehicles characterised by discrete attributes $\mathbf{a}$ per 'unit hypervolume', located at $\mathbf{x}$, that are moving at velocity $\mathbf{v}$, while being characterised by continuous attributes $\mathbf{v}^0$. For instance, for a two-dimensional traffic system (for instance, pedestrians moving in a railway station), the generalised PSD $\rho_{\mathbf{a}}(\mathbf{x},\mathbf{v},\mathbf{v}^0,t)$ denotes the expected number of traffic entities per unit area. Let us finally remark that by definition, the multi-dimensional generalised PSD equals:

$$\rho_{\mathbf{a}}(\mathbf{x},\mathbf{v},\mathbf{v}^0,t) \overset{def}{=} g_{\mathbf{a}}(\mathbf{v},\mathbf{v}^0 \mid x,t) r_{\mathbf{a}}(\mathbf{x},t) \tag{3.48}$$

where $g_{\mathbf{a}}(\mathbf{v},\mathbf{v}^0|\mathbf{x},t)$ denotes the probability density functions of the velocity-vector $\mathbf{v}$ and the continuous attributes $\mathbf{v}^0$ at $\mathbf{x}$ and instant t, and $r_{\mathbf{a}}(\mathbf{x},t)$ equals the generalised traffic density at $\mathbf{x}$ and instant t. In the remainder of this section we will concentrate on one-dimensional systems. However, the notions developed within this thesis can easily be generalised to describe the motion of traffic entities in two or higher dimensional spaces. For example, Hoogendoorn and Bovy (2000) describe the motion of pedestrians in $\mathbb{R}^2$ by considering the *Pedestrian Phase-Space Density* (P-PSD) $\rho(x_1,x_2,v_1,v_2,w,t)$.

3.7 Class, lane, and driver's state distinctions: empirical justification

In this section we will provide an overview of the flow-variables and the relevant attribute-sets. That is, we will exemplify the generalised traffic flow variables by considering the distinction of user-classes u, roadway lanes j, and drivers' states c. That is, the generalised PSD $\rho_{\mathbf{a}}$ is exemplified for $\mathbf{a} = (u,j,c)$, where $u \in \mathbf{U}$, $j \in \mathbf{J}$, and $c \in \mathbf{C}$, i.e. we will consider $\rho_{(u,j,c)}$.

3.7.1 *User-class distinction*

To accommodate the description of multiple user-class traffic flow, we consider the set $\mathbf{U}$ of user-classes u. This class-distinction in traffic flow is important because of the significant differences in vehicle performance and driving behaviour.

Motivation for user-class distinction

The distinction of user-classes is motivated by among other things:

1. Different control regimes may exist for different user-classes. Examples of such class-specific control options are pay-lanes, (dynamic) overtaking prohibition for trucks (see example section 10.7), class-dedicated lanes (HOV-lanes, truck-lanes, tidal flow-lanes). Class distinction is necessary to correctly describe resulting traffic operations.

2. Only if the model distinguishes different classes, control laws for the (automated) generation of class-specific dynamic control regimes can be determined.
3. We assume that by class-distinction, model potential for synthesis, analysis, and control of roadway traffic improves significantly. In other words, we have the strong belief that model performance improves by distinguishing user-classes and their distinct (driver-) characteristics.

Criteria for user-class distinction

User-classes can be categorised according the following criteria:

1. *Vehicle type characteristics.* Different types of vehicles may reveal differences in for instance size, maximum velocity, acceleration and deceleration capabilities, safe minimum distance to leading vehicle. Examples of vehicle-types are trucks, busses, person-cars, vans, and motorbikes.
2. *Driver characteristics.* Differences in driving characteristics reflect differences in among other things brisk and careful driving. That is, drivers maintaining different minimum distances with respect to the leading vehicle, different desired velocities, different anticipatory behaviour, different reaction times, etc. These differences may result from differences in experience, or familiarity with the route.
3. *Traveller-type characteristics.* User-classes can be identified by the purpose of travel, e.g. commuters, business-related, freight, recreational.
4. *Socio-economic characteristics.* Socio-economic differences are reflected by among other things value-of-time, and income. This categorisation enables differentiating between socially or economically important user-classes, such as police-cars, ambulances, and High Occupancy Vehicles (HOV's).
5. *Demographic characteristics.* Demographic differences are reflected by among other things age and sex.
6. *Level of route-information.* Some vehicles are equipped with on-board systems providing route information at various levels, while others have to rely on roadside information systems and driver's experience.
7. *Level of driver-support.* Automated systems are introduced, which provide various levels of support to the driving task. Lateral and longitudinal driving control systems can be distinguished.
8. *Driving direction.* E.g. contra-flow traffic.
9. *Travel destination.* The destination of a road-user on the motorway yields differences with respect to among other things lane-choice.

Let us emphasise that by admitting *negatively valued* velocities and desired velocities, a special user-class can be identified, namely traffic flowing into the *opposite direction.* That is, $\rho_{(u,j,c)}(x,v,v^0,t) > 0$ for some $v < 0$, and $v^0 < 0$. Identification of this user-class is of dominant importance when modelling traffic conditions on e.g. bi-directional two-lane roads, where overtaking using the left-lane containing the opposing traffic is allowed. Also, when model-

ling traffic operations of roadways where tidal flow is an available control option, the distinction of traffic flowing into the opposite direction is necessary.

Differences between user-classes from empirical studies

To illustrate some of the user-class characteristics, let us reconsider the velocity distributions given in Figure 3-2. The desired velocity probability density functions (i.e. the velocity probability distribution functions for small densities) have a *bimodal* character, which can be explained by studying the velocity distributions of person-cars and trucks separately.

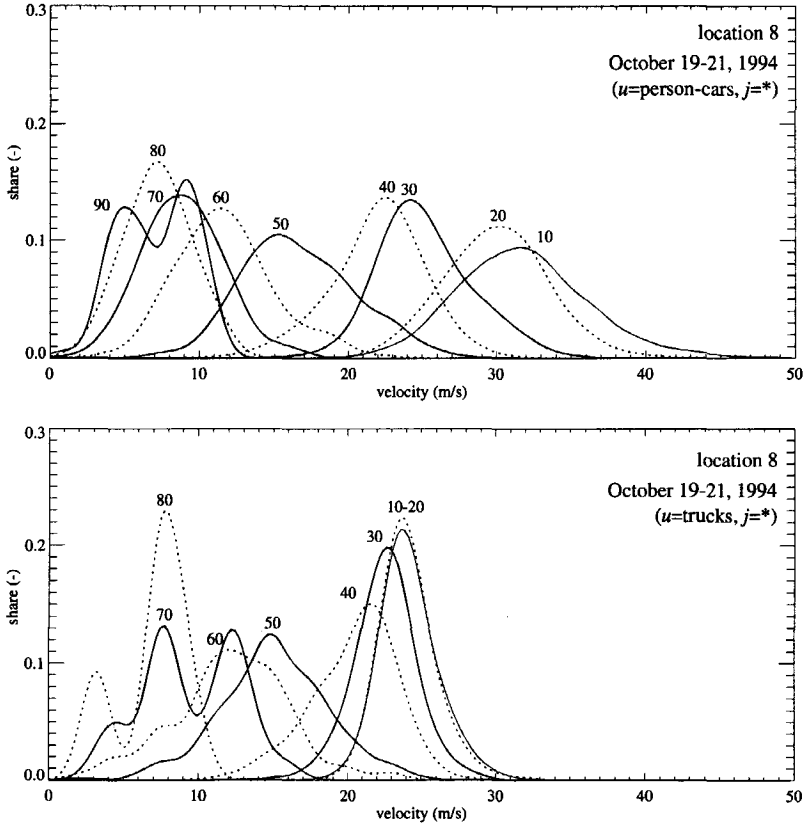

Figure 3-4: Two-lane velocity probability distribution functions by average-lane density for person-cars and trucks (kernel estimates).

Figure 3-4 shows the velocity probability density functions for person-cars and trucks at different density levels. The difference between the velocity distributions of person-cars and trucks is profound. That is, the mean velocity of person-cars is higher than the mean velocity of trucks. This holds equally for the velocity variance. Moreover, we can observe that the truck velocity remains the same within the range of density values from 0 to 30*veh/km*. Assuming that the desired velocity distribution can be derived by observing the velocity distri-

bution at very small density values reveals the differences between the user-classes with respect to the desired velocity.

Another example of a user-class specific parameter is the *minimum net time headway*. Figure 3-5 shows these minimum net time headways at high-densities, which reflect the differences between person-cars and trucks. Note that when the densities are high, most vehicles are platooning. When a driver is platooning, the net time headway equals the minimum safe time headway. Clearly, on average the trucks maintain a larger minimum net time headway than the person-cars (see also Dijker (1997a,b)). This is caused by the fact that truck-drivers consider the worse deceleration capabilities with respect to person-cars. In other words, when a person-car in front of the truck abruptly decelerates, the truck behind cannot decelerate to the same extent. Consequently, the truck will need more space to decelerate to the same velocity as the leading person-car. Similar results were found by Hoogendoorn and Bovy (1998e,f) and Hoogendoorn and Bovy (1999c) who studied the time headway distributions in mixed vehicle-type traffic on two-lane rural roads and two-lane motorways respectively.

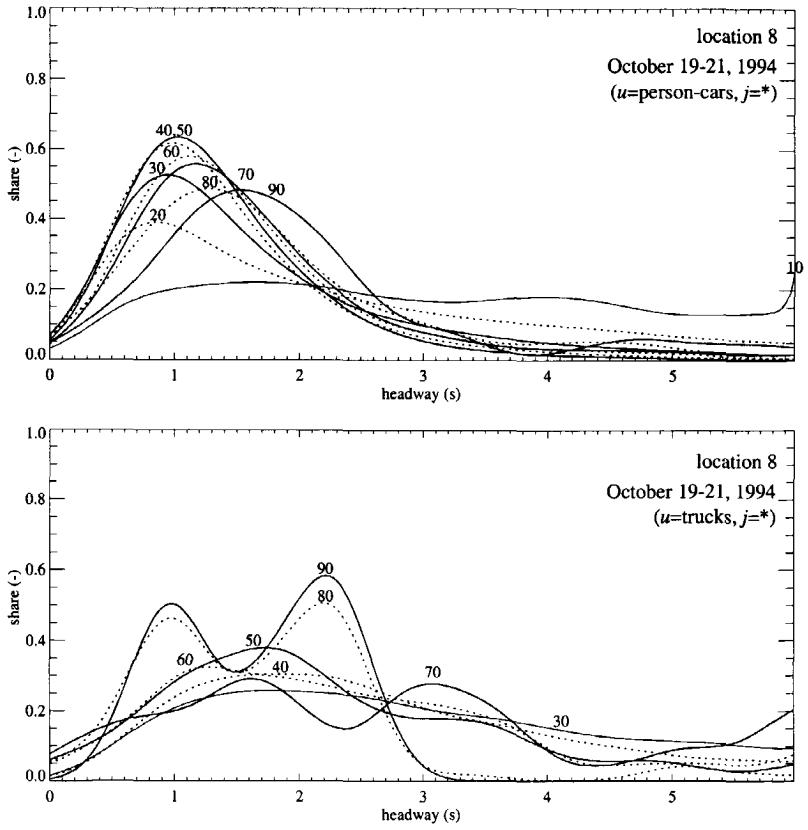

Figure 3-5: Distribution of the net time headway for different average-lane density values.

These examples show significant differences between user-classes. Therefore, distinguishing these classes is justified, and potentially improves model performance and consequent model application potential.

3.7.2 Lane distinction

In the previous section we have argued that the distinction of user-classes is beneficial, since these classes show very different behavioural characteristics of the driver-vehicle units. Let us now motivate the distinction of roadway lanes.

Motivation for lane distinction

The distinction of roadway lanes is motivated by a number of reasons:

1. Different control regimes exist for the different roadway lanes. Examples of such regimes are variable speed-limits (differences on lanes on the main carriage way and the on- and off-ramps, or in the case of diverging roads; see example section 10.7), dedicated lanes (HOV-lanes, truck-lanes, tidal flow-lanes). The distinction of lanes is necessary to model these differences.
2. Only if the model distinguishes these different lanes, control laws for the (automated) generation of lane-dedicated control regimes can be determined.
3. The merging, weaving and diverging possibilities are different for the different lanes of the roadway.
4. Due to traffic legislation ("drive on the right, overtake of the left", or high-speed lanes), the driver- and/or vehicle-composition is different on different roadway lanes.
5. We assume that by lane-distinction, the model potential for the synthesis, analysis, and control of roadway traffic improves significantly. In other words, we have the strong belief that the model performance improves by distinguishing roadway lanes.

Differences in flow operations on the roadway lanes

In addition to differences in desired velocities and minimum time net-headway, user-classes differ with respect to overtaking probabilities. Reasons for this are differences in lengths, velocities, and reaction times, and consequent gaps needed on the target-lane.

Additionally, vehicles with a lower desired velocity may be satisfied with the traffic conditions on the lane they are currently occupying, although they need to decelerate slightly, or are platooning. Differences in overtaking probabilities will be reflected by the distribution of vehicles across the lanes of the roadway. For instance, considering European legislation (drive-on-the-right, overtake-on-the-left) vehicles with poor overtaking capabilities seldom use the left roadway lane compared to vehicles with excellent overtaking performance. Thus, the distribution of vehicles over the roadway lanes will affect the average flow characteristics on the distinct roadway lanes. For instance, Figure 3-6 shows the aggregate-class velocity distributions on the left and the right lane of a 2×2 lane motorway. Note that these differences are less apparent if the density increases. Figures 3-7 and 3-8 show the velocity probability density functions for both person-cars and trucks on either of the two lanes of the A9 motor-

way. The figure clearly shows the combined differences between the classes and the motorway lanes.

Modelling roadway lanes

In order to accommodate lane-specific description of heterogeneous traffic, we dis-aggregate the PSD by distinguishing different motorway lanes. To this end, let the set $\mathbf{J} = \{1,\ldots,M\}$ denote the considered roadway lanes. Then, the mixed-state generalised PSD $\rho_{(u,j,*)}(x,v,v^0,t)$ – to which we will refer by the term mixed-state MLMC (i.e. *MultiLane MultiClass*) PSD – denotes the expected number of vehicles per unit road-length of user-class u at x on lane j at instant t which are currently driving at a velocity equal to v while aiming to traverse the road at a desired velocity equal to v^0, where $j = 1,\ldots,M$ and $u \in \mathbf{U}$. By definition, $j = 1$ denotes the rightmost lane while $j = M$ denotes the leftmost lane. We note that aggregation with respect to the roadway lanes yields total density for all lanes rather than average density per lane.

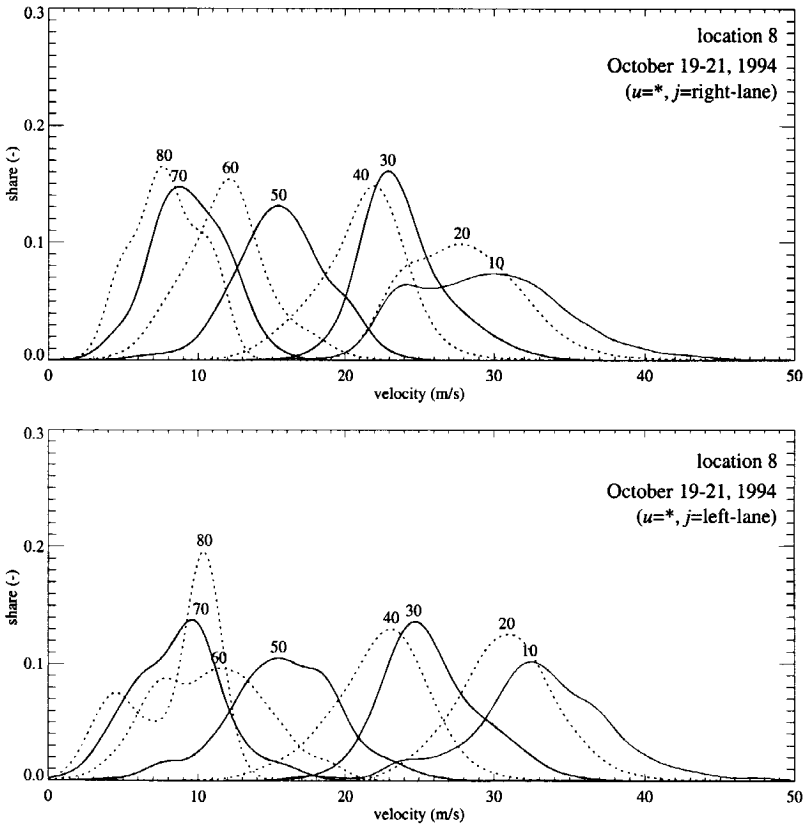

Figure 3-6: Aggregate-class velocity distributions by density on the left- and the right-lane of a two-lane motorway in the Netherlands (A9).

3.7.3 Distinction of drivers' states

Similar reasoning as for the lane and user-class distinction holds for the *state* of a driver – that is, whether he is constrained or free flowing – to a large extent determines the behavioural processes of the driver. That is, vehicle interaction, lane-changing behaviour, and acceleration behaviour are different for free-flowing and constrained drivers. For instance, whether or not a lane-change occurs and which lane is chosen is among other determined by the fact that a driver is either *constrained* or *unconstrained* (*free-flowing*): a driver impeded by the vehicle in front will not be able to accelerate towards his desired velocity. However, he may aim to change lanes to improve his driving conditions. Conversely, an unconstrained driver may not have any incentive to change to another lane. Instead, he aims to traverse the currently occupied lane at his desired speed and will therefore accelerate to do so.

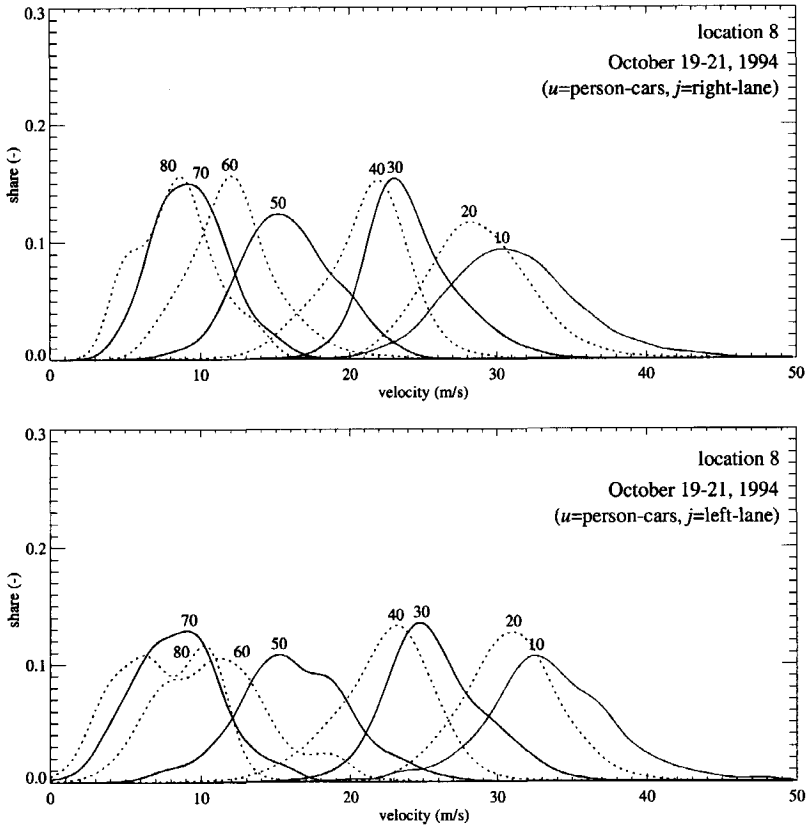

Figure 3-7: Person-car velocity distributions by density on the left- and the right-lane of a two-lane motorway in the Netherlands (A9).

Justification for bi-valued level of constrainedness

It is conceivable that the driver's *level of constrainedness c* varies between states 1 and 2. That is, a driver can be *partially constrained.* For instance, this partial constrainedness can describe a driver who is aware of vehicles in front, and anticipates on their behaviour, but is not a follower, in the sense that he maintains the same velocity at a specific distance. However, we will only consider two driver states, namely the extreme cases $c = 1,2$. On the one hand, this simplified classification is motivated by the fact that the distinction of free-flowing and platooning vehicles to improve traffic flow modelling has been successfully applied by a number of researchers.

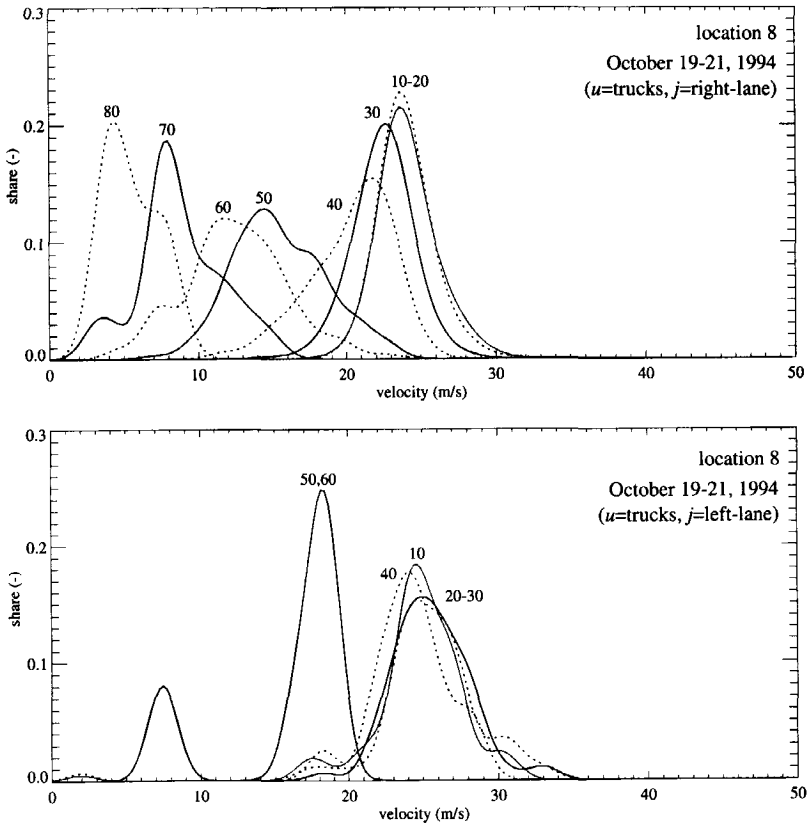

Figure 3-8: Truck velocity distributions by density on the left- and the right-lane of a two-lane motorway in the Netherlands (A9).

A good example is the *Generalised Queuing Model* (GQM) for headway distribution modelling (cf. Cowan (1975), Branston (1976), and Luttinen (1996)). In the GQM, headway observations are categorised as either *free-flowing* or *constrained.* Hoogendoorn and Botma (1997) developed a new estimation procedure to determine these distributions for free-flowing and constrained drivers from individual vehicle observations. Their approach has successfully been applied to two-lane rural roads in the Netherlands. Significant differences are found

between headways of free-flowing and platooning vehicles. Hoogendoorn and Bovy (1998e,f) established a *mixed vehicle-type* headway distribution model based on the GQM.

Modelling the driver's state

We will refer to any driver who has encountered a slower vehicle without being able to change to an adjacent lane as a *constrained* or a *platooning driver.* The inability to change to either of the adjacent lanes results in the formation of a *platoon.* An unconstrained vehicle leads the platoon. Additionally, the platoon consists of a nonnegative number of constrained vehicles, traversing along the roadway with the same velocity as their impeding predecessor. We assume that constrained drivers will try to relieve their constrained state – that is, *leave the platoon* – by changing to an adjacent lane, trying to travel at their desired speed.

Conversely, we will refer to any driver who is either not encountering any slow vehicle or is able to immediately overtake to an adjacent lane, without the need to decelerate as an *unconstrained, free,* or *platoon-leading* driver. We will assume that unconstrained drivers always aim to drive at their desired velocity, and will accelerate to do so. Moreover, unconstrained drivers may change lanes *spontaneously* to drive in the lane they prefer.

To correctly model these acceleration, interaction and lane-changing processes, we need to distinguish constrained and unconstrained drivers. Consequently, the set of drivers' states **C** consists of two elements, i.e. $\mathbf{C} = \{1,2\}$, where '1' indicates the free-flowing platoon leaders, and '2' indicates the constrained or platooning vehicles. Thus, the MLMC-PSD is disaggregated into $\rho_{(u,j,1)}(x,v,v^0,t)$ and $\rho_{(u,j,2)}(x,v,v^0,t)$, respectively denoting the contribution of unconstrained drivers and constrained drivers to the mixed-state MLMC-PSD.

In analogy to the mixed-state MLMC-PSD, we can again define the *reduced* MLMC-PSD, the conservative variables, and the primitive variables for free-flowing and constrained vehicles. The fraction of constrained vehicles in lane j of user-class u at (x,t) driving at velocity v while sustaining a desired velocity equal to v^0 is denoted by $\theta(x,v,v^0,t)$, which equals the *constrained* MLMC-PSD divided by the mixed-state MLMC-PSD:

$$\theta_{(u,j)}(x,v,v^0,t) \overset{def}{=} \rho_{(u,j,2)}(x,v,v^0,t) / \rho_{(u,j,*)}(x,v,v^0,t) \tag{3.49}$$

The fraction of constrained vehicles of user-class u in lane j driving at velocity v, irrespective of the desired velocity equals:

$$\tilde{\theta}_{(u,j)}(x,v,t) = \tilde{\rho}_{(u,j,2)}(x,v,t) / \tilde{\rho}_{(u,j,*)}(x,v,t) \tag{3.50}$$

3.8 Vector notation and attribute-aggregation*

In this section we present a new method of denoting the phase-space densities for all attributes **a** using a vector notation. This notation will enable compact notation, and simplifies the aggregation with respect to the attributes by reducing this aggregation to simple matrix multiplication. To this end, let us consider the *vector* $\vec{\rho}$ of $\rho_{\mathbf{a}}$ for all admissible attribute-sets

* This section discusses some technical details with respect to aggregation of the discrete attributes, and can be skipped by the first-time reader.

$\mathbf{a} \in \mathbf{A}$. Note that to clearly distinguish vectors from scalars, vectors of Greek-symbols vectors are indicated by an arrow '$\rightarrow$'.

$$\vec{\rho}(\mathbf{x}, \mathbf{v}, \mathbf{v}^0, t) \overset{def}{=} (\rho_{\mathbf{a}(1)} \quad \rho_{\mathbf{a}(2)} \quad \cdots \quad \rho_{\mathbf{a}(N)})^T \tag{3.51}$$

where $\mathbf{a}(i)$ is the i-th attribute-set and $N = |\mathbf{A}|$ denotes the cardinality of $\mathbf{A}$ (i.e. the number of *admissible attribute-sets* $\mathbf{a}$). Let $\mathbf{a} = (a_1,\ldots,a_D)$ denote the attribute-set consisting of values a_d indicating the a_d-th value of the discrete attribute d, where D is the *dimension* of the attribute-set $\mathbf{a}$. For example, when $\mathbf{A} = \{\mathbf{U},\mathbf{J},\mathbf{C}\}$, then the dimension D of $\mathbf{a}$ is 3, and $\mathbf{a} = (a_1,a_2,a_3) = (u,j,c)$. Moreover, for each attribute d, let n_d denote the number of admissible attribute-values. Clearly the cardinality of $\mathbf{A}$ is $N = \Pi_d n_d$. For instance, considering three classes, on a two-lane motorway, and two states ($n_1 = 3$, and $n_2 = n_3 = 2$) yields $N = 12$.

The mapping onto the vector $\vec{\rho}$ is defined by the index-function $I(\mathbf{a})$, relating the attribute-set $\mathbf{a}$ to the element-number in the vector $\vec{\rho}$:

$$I(\mathbf{a}) = I((a_1, a_2, \ldots, a_D)) = 1 + \sum_{d=1}^{D} \left((a_d - 1) \prod_{d'>d} n_{d'} \right) \tag{3.52}$$

In illustration, consider $\mathbf{a} = (u,j)$. Then, the vector $\vec{\rho}$ is defined by:

$$\vec{\rho}(x, v, v^0, t) \overset{def}{=} (\rho_{(1,1)} \quad \rho_{(1,2)} \quad \rho_{(2,1)} \quad \cdots \quad \rho_{(|\mathbf{U}|,2)})^T \tag{3.53}$$

where $n_1 = |\mathbf{U}|$ denotes the number of user-classes. We will see in the sequel of this thesis that the vector notation is very useful for the compact notation of the dynamic equations. Moreover, aggregation with respect to different attributes can be achieved by matrix manipulation.

3.8.1 Aggregation of attributes

In the sequel of this thesis, consistency of the derived MLMC traffic flow equations with other aggregate-lane and/or aggregate-class models is studied. To this end, the generalised (reduced) PSD, and derived conservative and primitive traffic variables are aggregated with respect to the relevant attributes. This can be achieved by simple matrix multiplication. In this respect, the following notational convention is chosen: when the respective generalised traffic flow variables are aggregated with respect to a specific attribute a_i of the attribute-set $\mathbf{a} = (a_1,\ldots,a_D)$, then the index is replaced by an asterix '*'.

Aggregation of the generalised PSD by matrix manipulation

The generalised PSD's are *additive*. That is, to aggregate with respect to a specific attribute, we can simply add the generalised PSD's associated with these attributes. For instance:

$$\rho_{(u,*,c)}(x, v, v^0, t) = \sum_{j \in \mathbf{J}} \rho_{(u,j,c)}(x, v, v^0, t) \tag{3.54}$$

equals the aggregate-lane generalised Phase-Space Density. The 'additivity' of the generalised PSD's is a result of the assumption that a vehicle can be described by an infinitesimal particle. Since these particles have no physical length, more than one particle can occupy a very small roadway cell dx. We can perform this aggregation by simple matrix manipulation. To this end, let $\mathbf{S}_d$ denote a $N \times N$ matrix that is defined by:

$$\mathbf{S}_d = \{s_{ij}\} \quad \text{where} \quad s_{ij} = \begin{cases} 1 & \exists a' \text{ such that } j = I((\ldots, a_{d-1}, a', a_{d+1}\ldots)) \\ 0 & \text{elsewhere} \end{cases} \tag{3.55}$$

In other words, for the i-th row of $\mathbf{S}_d$, the j-th column-element equals one if the column reflects the attribute-set for *specific* attributes values of $a_1,\ldots,a_{d-1},a_{d+1},\ldots,a_D$, independent of the value of the d-th attribute a_d. In defining the matrices $\mathbf{S}_d$, we can aggregate with respect to the d-th attribute in $\mathbf{a}$ by matrix multiplication. Let $\vec{\rho}^{\mathbf{d}}$ denote the vector of phase-space densities that are aggregated with respect to the attributes reflected by the vector $\mathbf{d}$, then:

$$\vec{\rho}^{\mathbf{d}} = \left(\prod_{d' \in \mathbf{d}} \mathbf{S}_{d'}\right) \cdot \vec{\rho} \tag{3.56}$$

Note that $\Pi_{d=1}^{D} \mathbf{S}_{d'}$ is a $N \times N$ matrix containing elements equal to one.

Example. Let us consider matrices $\mathbf{S}_d$ for $\mathbf{a} = (u,j)$, with $n_1 = n_2 = 2$, for $d = 1$ and $d = 2$ respectively. By definition, we have:

$$\mathbf{S}_1 = \begin{pmatrix} 1 & \cdot & 1 & \cdot \\ \cdot & 1 & \cdot & 1 \\ 1 & \cdot & 1 & \cdot \\ \cdot & 1 & \cdot & 1 \end{pmatrix} \quad \text{and} \quad \mathbf{S}_2 = \begin{pmatrix} 1 & 1 & \cdot & \cdot \\ 1 & 1 & \cdot & \cdot \\ \cdot & \cdot & 1 & 1 \\ \cdot & \cdot & 1 & 1 \end{pmatrix} \tag{3.57}$$

Suppose that we consider aggregation with respect to user-class ($d = 1$), e have:

$$\vec{\rho}^{1} = \mathbf{S}_1 \vec{\rho} = \begin{pmatrix} 1 & \cdot & 1 & \cdot \\ \cdot & 1 & \cdot & 1 \\ 1 & \cdot & 1 & \cdot \\ \cdot & 1 & \cdot & 1 \end{pmatrix} \cdot \begin{pmatrix} \rho_{(1,1)} \\ \rho_{(1,2)} \\ \rho_{(2,1)} \\ \rho_{(2,2)} \end{pmatrix} = \begin{pmatrix} \rho_{(1,1)} + \rho_{(2,1)} \\ \rho_{(1,2)} + \rho_{(2,2)} \\ \rho_{(1,1)} + \rho_{(2,1)} \\ \rho_{(1,2)} + \rho_{(2,2)} \end{pmatrix} = \begin{pmatrix} \rho_{(*,1)} \\ \rho_{(*,2)} \\ \rho_{(*,1)} \\ \rho_{(*,2)} \end{pmatrix} \tag{3.58}$$

□

For the reduced generalised PSD's, similar relations hold. For instance, if we consider the mixed-state generalised reduced PSD, we have:

$$\tilde{\vec{\rho}}^{\mathbf{d}} = \left(\prod_{d' \in \mathbf{d}} \mathbf{S}_{d'}\right) \cdot \tilde{\vec{\rho}} \tag{3.59}$$

In the sequel of this thesis, we frequently use the *diagonalisation operator* $\otimes$:

$$\mathbf{x}\otimes = \mathrm{diag}(x_1, x_2, \ldots, x_N) \tag{3.60}$$

Using this operator, we can determine the element-wise product of the vectors $\mathbf{x}$ and $\mathbf{y}$:

$$\mathbf{x} \otimes \mathbf{y} = \begin{pmatrix} x_1 & \cdot & \cdot \\ \cdot & \ddots & \cdot \\ \cdot & \cdot & x_N \end{pmatrix} \cdot \begin{pmatrix} y_1 \\ \vdots \\ y_N \end{pmatrix} = \begin{pmatrix} x_1 y_1 \\ \vdots \\ x_N y_N \end{pmatrix} \tag{3.61}$$

Aggregation of the conservative flow variables

In the previous section we have shown how the three conservative variables, that is generalised density r_a, generalised momentum m_a, and generalised traffic energy e_a can be determined by considering contributions of the generalised PSD ρ_a to these generalised macroscopic conservatives. By considering the definitions of these generalised conservative variables, additivity of the generalised PSD implies additivity of the generalised conservative variables. For instance, the aggregate-class traffic density is defined by:

$$r_{(*,j,c)}(x,t) = \sum_{u' \in \mathbf{U}} r_{(u',j,c)}(x,t) \tag{3.62}$$

Again, we can determine the attribute-aggregate conservatives by sequential multiplication by the matrices $\mathbf{S}_d$ with vectors of conservative variables.

The *additivity* of the conservatives is one of the advantages of using conservative variables rather than primitive variables. Let us finally remark that the generalised flux of velocity variance J_a and the generalised traffic pressure P_a are also additive variables.

Aggregation of the primitive flow variables

The primitive flow variables velocity and velocity variance are generally *not additive*: they need to be determined by using the relation with the conservative variables. For instance, aggregation (averaging) of the generalised velocity V_a is achieved using $V_a = m_a/r_a$. In illustration, the average-lane velocity equals (see equation (3.33)):

$$V_{(u,*,c)}(x,t) = \frac{m_{(u,*,c)}(x,t)}{r_{(u,*,c)}(x,t)} = \frac{\sum_{j \in \mathbf{J}} m_{(u,j,c)}(x,t)}{\sum_{j \in \mathbf{J}} r_{(u,j,c)}(x,t)} \tag{3.63}$$

For the velocity variance, the aggregation can be determined by considering relation (3.34). Similar expressions hold for aggregation of the stagnation enthalpy H_a, and the skewness of the velocity distribution Γ_a.

3.9 Summary

In this chapter, new theoretical notions have been introduced required for a multilane multiclass traffic flow theory to be developed in the sequel of this thesis. The main difference between traditional continuum traffic flow theory and the theory presented in this chapter is the description of flow using *platoons* rather than single vehicles. Moreover, the observed trajectories of vehicles in these platoons are assumed instances of random variates that describe the probability that a certain trajectory occurs.

Using the proposed theory, platoon-based flow variables were generalised to incorporate both continuous attributes, such as velocity and desired velocity, and discrete attributes, such as user-class, lane, and state of the driver, leading to the generalised Phase-Space Density $\rho_a(\mathbf{x},\mathbf{v},\mathbf{v}^0,t)$. A key variable in the sequel of the thesis is the so-called multiclass multilane (MLMC-) PSD $\rho_{(u,j,c)}(x,v,v^0,t)$. This mesoscopic flow variable describes the expected number of vehicles of class u and state c per unit roadway length, driving on lane j at velocity v, while having desired velocity v^0 at instant t.

The MLMC-PSD can be considered as a generalisation of the traditional density $r(x,t)$ in that the density is dis-aggregated into contributions of vehicles driving at distinct velocities v while striving for a specific desired velocity v^0 of class u on lane j in state c. Here state c indicates whether the vehicle is *free-flowing* ($c = 1$) or platooning ($c = 2$). For convenience of the reader, Table 3-2 summarises the concepts introduced in this chapter which will be used in model development in ensuing chapters.

In the remainder of this thesis we will establish dynamics of unconstrained, constrained, and mixed-state phase-space densities. These dynamics will be the foundation of the flow models describing dynamics of macroscopic *conservative* flow variables. In this chapter we have shown how these can be established from the generalised phase-space densities by application of the *aggregation operator*. This operator yields the density, the traffic momentum, the traffic energy, and the flux of velocity variance. Alternatively, the *mean operator* can be applied, yielding the *primitive variables* density, velocity, and velocity variance.

Table 3-2: Summary of MLMC traffic flow variables and aggregation operations for one-dimensional flows ($x \in \mathbb{R}$ and $v \in \mathbb{R}$), and single continuous attribute ($v^0 \in \mathbb{R}$)

Aggregation	phase-space $\sigma_{(u,j,c)}$ (1)	primitives $\vartheta_{(u,j,c)}$ (2)	conservatives $\xi_{(u,j,c)}$ (3)
		mean operator $\langle f \rangle_{(u,j,c)} = \iint f g_{(u,j,c)} \mathrm{d}w^0 \mathrm{d}w$	aggregation operator $[f]_{(u,j,c)} = \iint f \rho_{(u,j,c)} \mathrm{d}w^0 \mathrm{d}w$
state-specific MLMC	$\rho_{(u,j,c)}(x,v,v^0,t)$ (density)	$r_{(u,j,c)}(x,t)$ (density)	$r_{(u,j,c)}(x,t)$ (density)
	$\mu_{(u,j,c)}(x,v,v^0,t)$ (moment.)	$V_{(u,j,c)}(x,t)$ (velocity)	$m_{(u,j,c)}(x,t)$ (momentum)
	$\varepsilon_{(u,j,c)}(x,v,v^0,t)$ (energy)	$\Theta_{(u,j,c)}(x,t)$ (variance)	$e_{(u,j,c)}(x,t)$ (energy)
		$\Gamma_{(u,j,c)}(x,t)$ (skewness)	$J_{(u,j,c)}(x,t)$ (variance flux)
desired velocity	$\tilde{\sigma}_{(u,j,c)} = \int \sigma_{(u,j,c)}(x,v,w^0,t)\mathrm{d}w^0$ (reduced phase-space)	–	–
state aggregation	$\sigma_{(u,j,*)} = \sum_{c=\{1,2\}} \sigma_{(u,j,c)}$	$\vartheta_{(u,j,*)} = \frac{\sum_{c=\{1,2\}} r_{(u,j,c)} \vartheta_{(u,j,c)}}{\sum_{c=\{1,2\}} \vartheta_{(u,j,c)}}$	$\xi_{(u,j,*)} = \sum_{c=\{1,2\}} \xi_{(u,j,c)}$
class aggregation	$\sigma_{(*,j,c)} = \sum_{u \in \mathbb{U}} \sigma_{(u,j,c)}$	$\vartheta_{(*,j,c)} = \frac{\sum_{u \in \mathbb{U}} r_{(u,j,c)} \vartheta_{(u,j,c)}}{\sum_{u \in \mathbb{U}} r_{(u,j,c)}}$	$\xi_{(*,j,c)} = \sum_{u \in \mathbb{U}} \xi_{(u,j,c)}$
lane aggregation	$\sigma_{(u,*,c)} = \sum_{j=1}^{M} \sigma_{(u,j,c)}$	$\vartheta_{(u,*,c)} = \frac{\sum_{j=1}^{M} r_{(u,j,c)} \vartheta_{(u,j,c)}}{\sum_{j=1}^{M} r_{(u,j,c)}}$	$\xi_{(u,*,c)} = \sum_{j=1}^{M} \xi_{(u,j,c)}$

(1) Generic variables in the phase-space are indicated by the Greek symbol σ.
(2) Generic primitive variables are indicated by the Greek symbol ϑ.
(3) Generic conservative variables are indicated by the Greek symbol ξ.

4 GENERALISED GAS-KINETIC TRAFFIC FLOW EQUATIONS

Several very complex and interdependent processes influence the dynamic behaviour of vehicles in the multiclass traffic stream on multilane roadway facilities. For instance, platoon leaders accelerate towards their desired velocity, platooning vehicles accelerate towards the desired velocity of the platoon leader, vehicles interact yielding either a lane-change or deceleration, drivers change lanes to their preferred lane, or drivers adapt their desired velocity to prevailing road, weather or ambient conditions.

In this chapter, we will establish dynamic equations describing the evolution of traffic conditions for a multilane heterogeneous traffic stream. That is, we will describe and model processes, which yield changes in the generalised PSD, specifying the class-specific and lane-specific distribution of velocity and desired velocity, for both platoon leading vehicles, as well as platooning vehicles.

We show that these dynamics are governed by both *continuum* as well as *non-continuum* processes. In this context, *continuum processes* reflect *smooth changes* in the generalised PSD due to inflow and outflow of vehicles *in the phase-space* Σ. Examples of these continuum processes are longitudinal convection of vehicles and acceleration to the acceleration velocity. These continuum terms are similar irrespective of class, lane, and driving state. In opposition to continuum processes, *non-continuum processes* reflect *non-smooth* dynamic changes of the generalised PSD. These can either be *event-driven*, or *condition-driven*. Examples of event-driven processes are decelerations of vehicles due to interactions, and immediate lane-changing of faster vehicles. Examples of condition-driven processes are postponed lane-changing, and lane-changing to a preferred lane. Let us remark that both types of processes

are *state-specific*. Moreover, parameters characterising non-continuum processes depend on both user-class as well as roadway lane.

As a result of our deliberations, we present so-called *gas-kinetic equations* or *special continuity equations* describing the dynamics of the generalised PSD. Using expressions describing the continuum processes yields a formal expression for gas-kinetic equations for general traffic flows in the n-dimensional space, governed by convection, acceleration, adaptation of continuous attributes, event-driven non-continuum transitions, and condition-driven non-continuum transitions. These equations are consecutively specified for different user-classes, lanes, and driving-states (Figure 4-1).

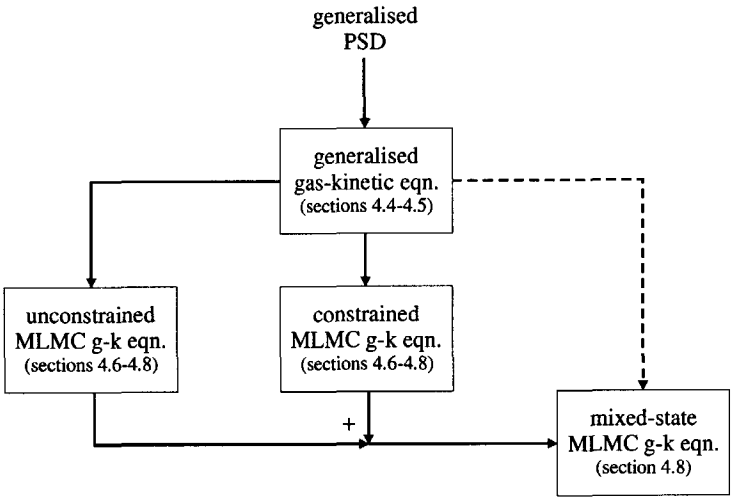

Figure 4-1: Overview of the gas-kinetic model derivation approach.

The (generic) gas-kinetic equations can be considered as a generalisation of the conservation equation (see section 2.4.1) that describes dynamic changes in traffic density due to the balance between vehicles flowing out of and into an infinitesimal roadway segment. Instead of only balancing inflow and outflow of vehicles, the generic gas-kinetic equations also reflect changes in the generalised PSD due to the aforementioned dynamic processes (e.g. lane-changing, deceleration caused by interactions with slower platoons, acceleration towards the drivers desired velocity, or the desired velocity of the platoon leader).

We propose an improved *collision equation* to describe the *expected number of interactions* per unit time. Let us recall that in the original gas-kinetic model (e.g. Prigogine and Herman (1971), Paveri-Fontana (1975), Helbing (1996)), the number of vehicular interactions per time unit is described by the *collision equation* which gives the expected number of interactions per unit time under the assumption of *vehicular chaos* (see section 2.3.3). The latter assumption implies that vehicles move independently of each other, thereby neglecting the correlation between for instance a platoon leader and the platooning vehicle following him. When traffic is dilute, the fraction of free-flowing vehicles is nearly one, and thus the vehicular chaos assumption is justified. However, when the density *increases*, the fraction of platooning vehicles *increases*. Since a platooning vehicle's position and velocity is predomi-

nantly determined by the position and the velocity of the platoon leader, the correlation between both the positions as well as the velocities of the vehicles in the flow increases, and cannot be neglected. Thus, we can conclude that the vehicular chaos assumption is flawed for non-dilute conditions. Moreover, in this chapter we will show that it leads to overestimation of the expected number of vehicle interactions per unit time.

Fortunately, the platoon-based traffic flow description presented in chapter 3 enables formulation of a correct collision equation, by assuming that *only* the *unconstrained platoon-leaders* (and thus the platoons) *move independently* of each other. However, this yields an unrealistically small number of vehicle interactions for dense traffic, which is easily remedied by considering the roadway-space use of vehicles, yielding an improved expression for the interaction rate. Finally, let us mention the result that by considering different user-classes having distinct velocity distributions, *asymmetric interaction* results. That is, fast classes experience relatively more interactions than the slow classes.

The chapter is outlined as follows. Section 4.1 discusses classification of dynamic processes into *lateral* and *longitudinal* processes. In section 4.2 we discuss these processes and their consequent dynamic effects on the MLMC-PSD from a qualitative perspective. Section 4.3 presents behavioural assumptions with respect to deceleration, acceleration, desired velocity adaptation, lane-changing, etc. In sections 4.4 and 4.5 we present generic gas-kinetic dynamic terms respectively describing continuum processes and non-continuum processes with respect to the generalised n-dimensional PSD introduced in the previous chapter. Sections 4.6 and 4.7 respectively specify *event-driven* non-continuum processes and *condition-driven* non-continuum processes for both unconstrained platoon leaders as well as constrained followers. Using these specifications, we derive separate gas-kinetic equations for both traffic states in section 4.8. In section 4.9 we discuss the relation between our MLMC gas-kinetic model and other models proposed in the literature. Finally, in section 4.10 we discuss the generalisability of the model equations to describe the motion of individual vehicles.

4.1 Classification of dynamic traffic processes

Key to the derivation approach is the proposed distinction of free-flowing and platooning traffic. Traffic behaviour, such as *acceleration*, *lane-changing*, and *deceleration* obviously differs for free-flowing and platooning drivers. In addition, the distinction is necessary to correctly describe *vehicular interaction* given the correlation between vehicles.

Traffic flow operations discussed in this thesis can be categorised by considering:

- *Continuum and non-continuum processes* (processes that either lead to continuous changes in the dependent variables or not). Non-continuum processes can be divided into *event-driven* and *condition-driven* non-continuum processes.
- *Convective and non-convective processes* (processes reflecting physical movement of vehicles or not).
- *Longitudinal* (car-following) and *lateral* (lane-changing) processes.

Cross-combining these criteria leads to a three-dimensional classification scheme. At this point, let us emphasise the difference between convective processes and continuum processes. *Continuum processes* reflect traffic 4processes yielding *smooth changes* in the depend-

ent variables. Examples of such processes are longitudinal convection of vehicles and (smooth) acceleration of vehicles. *Convective processes* reflect processes incorporating *physical transportation* of vehicles. Examples of such processes are longitudinal convection and lateral convection (lane-changing) of vehicles. Note that lateral processes are inherently convective.

4.1.1 Longitudinal processes

Longitudinal traffic flow processes describe *within-lane* (car-following) operations, such as acceleration, and deceleration. Table 4-1 presents an overview of these processes.

Table 4-1: Classification of longitudinal processes.

	continuum	**non-continuum processes**	
		event-driven	**condition-driven**
convective	longitudinal inflow and outflow of vehicles	N/A.	N/A.
non-convective	acceleration	deceleration after interaction with slower vehicle	N/A.

4.1.2 Lateral processes

Lateral traffic flow processes refer to vehicular exchange *between* lanes, on-ramps or off-ramps. Clearly, lateral processes are inherently convective, since they involve physical movement of vehicles from one lane to another. *Lane-changing* processes can be divided into two mutually exclusive lane-changing types, namely *discretionary* and *mandatory lane-changes* (see Ahmed *et al.* (1996)):

1. *Discretionary lane-change.* A discretionary lane-change occurs when a driver is not satisfied with the driving conditions on his current lane. Reasons for this dissatisfaction may be that the driver:
   - catches up with a slower platoon;
   - aims to escape from a platoon;
   - dislikes the high percentage of heavy vehicles on his current lane;
   - prefers using another lane, for instance, due to 'drive on the right – overtake on the left' traffic regulations.
2. *Mandatory lane-change.* A driver performs a mandatory lane-change if the currently used lane ceases to be an option. Causes for a mandatory lane-change may be:
   - traffic regulations (e.g. truck-, and HOV-lanes);
   - incidents and accidents blocking one or more roadway lanes;
   - reaching the end of a lane (e.g. at a lane drop or at the end of an on-ramp);
   - requirement to exit or change the current roadway using the off-ramp, or a fork.

With respect to *discretionary lane-changes*, we will categorise lane-changing manoeuvres into four *disjoint* and *exhaustive* lane-changing types (see Table 4-2). Since *mandatory lane-*

changes have a more insistent nature than *discretionary lane-changes*, the parameters describing the processes will be different. For instance, a driver will be more likely to accept a smaller – possibly unsafe – gap in the case of a mandatory lane-change than in case of a discretionary lane-change.

Table 4-2: Classification-scheme discretionary lane-changes.

	continuum	**non-continuum event-driven**	
		event-driven	**condition-driven**
convective	N/A.	*unconstrained*[*] and *constrained*[†] immediate lane-changes	*spontaneous*[‡] and *postponed*[§] lane-changes
non-convective	N/A.	N/A.	N/A.

4.2 Qualitative description of dynamic processes

We will provide a detailed account of longitudinal and lateral flow processes, and express their influence on the dynamics of the unconstrained and constrained MLMC-PSD. First, we will consider the different processes from a qualitative viewpoint.

4.2.1 Longitudinal processes influencing generalised PSD dynamics

Figure 4-2 shows the processes in cell x causing changes in the constrained or unconstrained MLMC-PSD due to inflow or outflow of vehicles, or changes within the cell.

Unconstrained traffic (white boxes)

Let us first consider the MLMC-PSD $\rho_{(u,j,1)}(x,v,v^0,t)$ reflecting platoon leaders in the flow.

Convection (1). In correspondence with the density $r(x,t)$ used in traditional traffic flow models $\rho_{(u,j,1)}$ changes due to free-flowing vehicles flowing from cell x–dx to cell x, or from cell x to cell x+dx.

However, in opposition to the density r, $\rho_{(u,j,1)}$ also changes due to other longitudinal processes, namely acceleration, deceleration, and relaxation:

Acceleration (2). Free-flowing vehicles of class u in cell x, driving at velocity v are *by definition* able to accelerate towards a higher velocity $w > v$ in order to achieve their desired ve-

[*] An *unconstrained immediate lane-change* occurs when a *free-flowing* vehicle *can immediately change* lanes when catching up with a slower platoon.

[†] A *constrained immediate lane-change* occurs when a *platooning* vehicle *can immediately change* lanes when interacting with a slower platoon. Note that a platooning vehicle interacts when *its platoon leader* interacts with a slower platoon.

[‡] A *spontaneous lane-change* is performed when a free-flowing vehicle changes lanes in order to drive on his preferred lane.

[§] When an interacting driver cannot change lanes, he will *join the platoon*. Assuming that the constrained state is an incentive for a driver to change lanes, a constrained driver performs a so-called *postponed lane-change* if the situation enables him to do so.

locity v^0. This causes a reduction in $\rho_{(u,j,1)}(x,v,v^0,t)$. However, unconstrained vehicles which were previously driving at a lower velocity $w < v$ may accelerate to a velocity v, which causes an *increase* in $\rho_{(u,j,1)}(x,v,v^0,t)$.

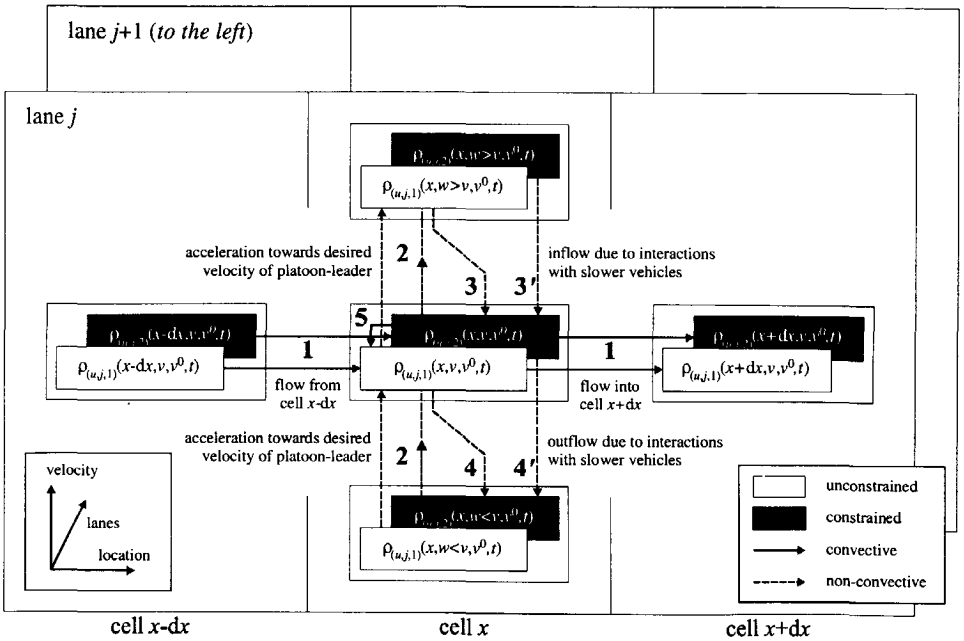

Figure 4-2: Longitudinal processes determining changes in state-specific MLMC-PSD on lane *j*.

Deceleration (4). Let us consider a free-flowing vehicle of class u on lane j driving at velocity v while having a desired velocity v^0. Let us assume that at (x,t) the faster vehicle catches up with a slower platoon with velocity $w < v$, but is unable to immediately change lanes. Then the free-flowing vehicle has to join the impeding platoon and to continue its trip with a lower velocity $w < v$. This deceleration causes an equally sized *decrease* and *increase* in $\rho_{(u,j,1)}(x,v,v^0,t)$ and $\rho_{(u,j,2)}(x,w,v^0,t)$, with $w < v$, respectively.

Relaxation of driver's state (5). If the leader of a platoon vanishes, for instance when changing lanes or accelerating, vehicles in the platoon may be relieved from their constrained state. This results in an *increase* in $\rho_{(u,j,1)}(x,v,v^0,t)$ at the expense of $\rho_{(u,j,2)}(x,v,v^0,t)$.

Constrained traffic (dark boxes)

Let us now consider the constrained vehicles reflected by $\rho_{(u,j,2)}(x,v,v^0,t)$.

Convection (1). Similar to free-flowing vehicles, the constrained MLMC-PSD $\rho_{(u,j,2)}(x,v,v^0,t)$ changes due to the balance of *inflow* of constrained vehicles from the upstream cell x–dx and *outflow* of constrained vehicles to the downstream cell x+dx.

Acceleration (2). Since movements of constrained vehicles are by definition *restricted* by other vehicles, we assume that they are unable to accelerate towards their *own* desired veloc-

ity. Rather, they accelerate to the desired velocity of the unconstrained vehicle leading their platoon, respecting the acceleration capabilities of the latter vehicle. The acceleration process yields an increase of $\rho_{(u,j,2)}(x,w,v^0,t)$ at the expense of $\rho_{(u,j,2)}(x,v,v^0,t)$ with $w > v$.

Deceleration (3+3'+4'). We have assumed that a platoon *has no physical length*, and that all constrained vehicles in the platoon drive *at the same velocity as the free-flowing platoon leader*. Thus, if the *platoon leader* interacts with a slower platoon, *all vehicles in the platoon* are affected in some way, yielding the incentive either to immediately change lanes or to decelerate to the velocity of the slower platoon. From this perspective, we define the concept of a *constrained interaction*.

When constrained vehicles driving at velocity v interact with slower platoons driving with velocity $w < v$, being *unable to immediately change lanes*, a decrease of $\rho_{(u,j,2)}(x,v,v^0,t)$, and an increase of $\rho_{(u,j,2)}(x,w,v^0,t)$, with $w < v$ results. However, $\rho_{(u,j,2)}(x,v,v^0,t)$ also *increases* due to deceleration: consider a vehicle in either driving state (i.e. $c = 1,2$) that was driving with velocity $w > v$ but needs to decelerate since it interacts with a slower platoon driving with velocity v, and is unable to immediately change lanes. This deceleration causes an increase in $\rho_{(u,j,2)}(x,v,v^0,t)$ at the expense of $\rho_{(u,j,c)}(x,w,v^0,t)$, for $c = 1,2$.

Relaxation of the driver's state (5). Finally, previously constrained vehicles able to relieve their constrained state due to changing traffic conditions may decrease $\rho_{(u,j,2)}(x,v,v^0,t)$.

4.2.2 Lateral processes influencing generalised PSD dynamics

Not all lane-change types are relevant for all drivers' states. Whether or not a lane-change type is relevant, depends on the state (i.e. free-flowing or platooning) of the vehicle. Table 4-3 depicts the different lane-changing types relevant for different drivers' states.

Table 4-3: Relevant lane-changing processes for free-flowing or platooning traffic. The numbers refer to the numbers indicated in Figure 4-3.

	free-flowing	*constrained*
unconstrained immediate lane-change	**(6)**	
constrained immediate lane-change		**(7)**
postponed lane-change		**(8)**
spontaneous lane-change	**(9)**	

Figure 4-3 shows these lane-changing processes for European traffic regulations given non-congested flow operations (driving on the right and lane-changing on the left). However, the developed model is *generic* with respect to lane-changing rules and legislation, so that other traffic regulations and the resulting lane-changing behaviours can be easily incorporated.

Unconstrained drivers (white boxes)

Unconstrained immediate lane-changing (6). We have already stated that if a *platoon leader* interacts, he either decelerates *or* – if possible – immediately changes to either of the adjacent lanes. In the latter case, we assume that the vehicle remains *unconstrained* and re-

tains its velocity. Let us remark that if we are considering European traffic regulations, the unconstrained immediate lane-changing always involves the left lane $j+1$, at least when traffic conditions are not congested. Clearly, unconstrained immediate lane-changes caused by interactions on lane j causes a reduction in $\rho_{(u,j,1)}(x,w,v^0,t)$. Alternatively, interactions causing immediate lane-changes to lane j cause an *increase* in the $\rho_{(u,j,1)}(x,w,v^0,t)$.

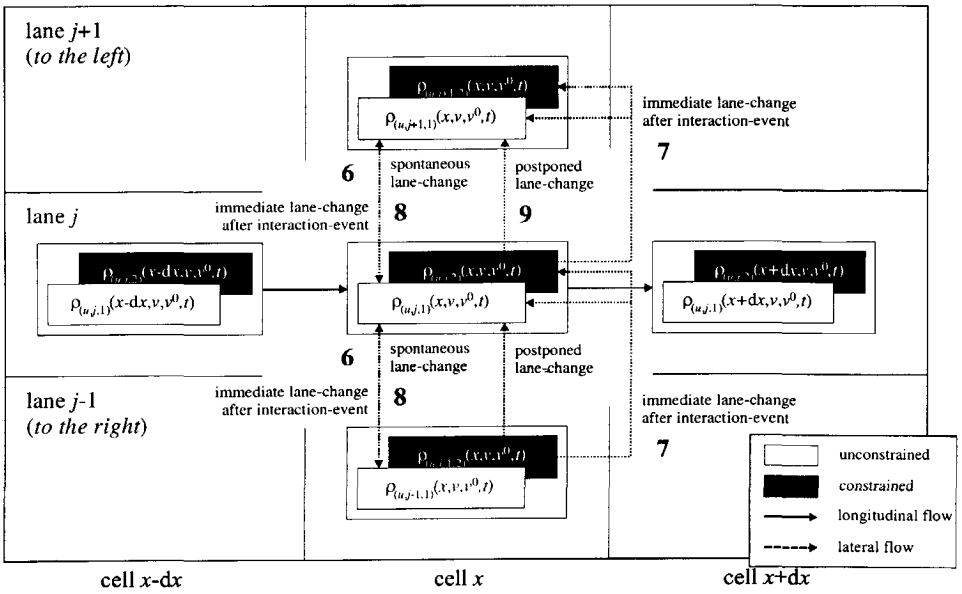

Figure 4-3: Lane-exchange processes on a roadway segment determining changes in the free-flowing or constrained MLMC-PSD on lane j (European traffic regulations).

Spontaneous lane-changing (9). Unconstrained vehicles currently driving on lane j may prefer an adjacent lane. As a consequence, they may change to either of these lanes $j\pm1$ if they are able to do so. This type of lane-changing is referred to as *spontaneous lane-change*. It causes a reduction in $\rho_{(u,j,1)}(x,v,v^0,t)$ on lane j. However, if unconstrained vehicles from either of the adjacent lanes prefer using lane j, spontaneously lane-changing vehicles cause an increase in $\rho_{(u,j',1)}(x,v,v^0,t)$. Note that in the case of European traffic regulations, vehicles are obliged to use the right-lane of the roadway. Consequently, reductions in $\rho_{(u,j,1)}(x,v,v^0,t)$ due to spontaneous lane-changes will mainly stem from lane-changes from the current lane j towards the right-lane $j-1$, whilst increases in $\rho_{(u,j,1)}(x,v,v^0,t)$ will mainly come from spontaneous lane-changing vehicles from the left-lane $j+1$.

Constrained drivers (dark boxes)

Constrained immediate lane-changing (7). When a platooning vehicle having velocity v interacts with a slower platoon at velocity w, the following options are possible:

- *The follower does not change lanes, irrespective of the actions of the leader.* In this case, the platooning vehicle must decelerate to w, yielding a flow from $\rho_{(u,j,2)}(x,v,v^0,t)$ to $\rho_{(u,j,2)}(x,w,v^0,t)$ (see section 4.2.1).

- *The leader and the follower immediately change to the same lane.* In this event, both the velocity and the state of the follower remain the same. This event yields a flux from $\rho_{(u,j,2)}(x,v,v^0,t)$ to $\rho_{(u,j',2)}(x,v,v^0,t)$ on the target-lane j'.
- *The follower immediately changes lanes, while the leader either does not change lanes or changes to another lane.* In this event, the velocity of the follower remains the same. However, we assume that the state of the driver is relieved. Thus, this event yields an increase of $\rho_{(u,j',1)}(x,v,v^0,t)$ on the target-lane j' at the expense of $\rho_{(u,j,2)}(x,v,v^0,t)$.

Postponed lane-changing (8). Alternatively, constrained vehicles may change to either of the adjacent lanes, thereby relieving their constrained state (at least temporarily). These lane-changes will be referred to as *postponed lane-changes*. Postponed lane-changing on the current lane j causes a reduction of $\rho_{(u,j,2)}(x,v,v^0,t)$ and an increase in $\rho_{(u,j',1)}(x,v,v^0,t)$ on either of the adjacent lanes j'.

Adaptation of desired velocity. Finally, let us remark that *adaptation of the desired velocity* can also cause changes in either the free-flowing or constrained MLMC-PSD. That is, due to changes in the desired velocity v^0, for instance caused by changing road, ambient or weather conditions, or by changing traffic regulations, the MLMC-PSD of vehicles striving for a velocity v^0 will change.

4.3 Behavioural assumptions

In the remainder of this chapter, equations describing the free-flowing, the constrained and the mixed-state MLMC-PSD are established. This is accomplished by careful consideration of the variety of convection, acceleration, and lane-changing processes discussed in the previous section. Before presenting these dynamic equations, let us summarise the behavioural assumptions made in this chapter.

However, let us first stress that a very important assumption underlying model development is that the notion that the *desired velocity* is a valid and traceable concept from the perspective of drivers. Moreover, we assume that it can be established empirically.

4.3.1 General model assumptions

The following summarises the general assumptions made in the model development:

1. *Infinitesimal vehicle and platoon length*[*]. During model derivation, we assume that vehicle lengths can be neglected. Also, we assume that a fast vehicle having interacted with a slower platoon, adopts the velocity of the slow vehicle and subsequently follows at zero distance. This implies that the formed platoon is a solid 'two-particle' block, which has no physical length.
2. *Independently moving platoons.* The dynamics of platoons are reflected by the platoon leader, which, by definition, moves freely in the vehicle stream. This justifies the

[*] In this stage of the model development, incorporation of these space requirements would unnecessarily complicate derivation of the model. Nevertheless, in the sequel of this chapter and chapter 6, vehicle spacing requirements are explicitly incorporated in the model dynamics.

assumption that movements of platoons that are led by this unconstrained leader are *uncorrelated.* In other words, the assumption of *vehicular chaos* holds for platoons.

3. *No user-class transitions.* Although the modelling approach allows transitions of drivers from one user-class to another, these are not specified in this dissertation research. For example, drivers unwilling to pay for using a lane at one time, are assumed not to switch to paying for the lane *during their trip.* Also, we assume that *individual* drivers do not change their desired velocity (or other continuous attributes) during their trip. However, the model does allow a shift of the *mean* desired velocity of an entire class.
4. *Acceleration of free-flowing vehicles.* Unconstrained vehicles driving at a velocity v lower than their desired velocity v^0 can and will always accelerate. An exponential relation considering a class dependent relaxation time τ_u is used to describe this acceleration process. We assume that this relaxation time is approximated adequately by a constant value τ_u^0.
5. *Acceleration of constrained vehicles.* Constrained vehicles are *unable* to accelerate towards their own desired velocity v_0. Instead, together with other vehicles in the platoon they accelerate towards the desired velocity of the unconstrained platoon-leading vehicle.
6. *Instantaneous deceleration.* Impeded free-flowing (or constrained) vehicles that are not able to immediately change lanes will become (or stay) constrained. Moreover, we assume that these vehicles will instantaneously adapt to the velocity of the impeding vehicle, while forming a vehicle platoon.

4.3.2 Behavioural assumptions with respect to lane-changing

The behavioural assumptions with respect to the various lateral processes are summarised by the following points:

General lane-changing assumptions

7. *Velocity unaffected by lane-changing.* We assume that lane-changing only indirectly affects the velocity of lane-changing vehicles. For instance, a previously constrained vehicle having performed a so-called postponed lane-changing manoeuvre will not arrive at the destination lane j' at a higher velocity. Instead, it relieves its constrained state, and subsequently accelerates towards its desired velocity v^0.
8. *Unaffected impeding vehicles (anisotropy assumption).* Neither a decelerating vehicle, nor a lane-changing vehicle influences the *impeding* platoon.

Immediate lane-changing assumptions

9. *Unconstrained immediate lane-changing state-transitions.* Some unconstrained vehicles impeded by slower platoons are able to perform *immediately lanes-changes.* After an immediate lane-change has occurred, the lane-changing vehicle *remains unconstrained* until it interacts with a slower platoon.

10. *Constrained immediate lane-changing state transitions.* Some of the constrained vehicles immediately change lanes when being impeded by a slower vehicle. A constrained immediate lane-change does *not necessarily* result in a state-transition. Whether or not a state-transition occurs depends on the actions of the other vehicles in the platoon. The constrained vehicle performing an immediate lane-change either stays *constrained* (e.g. when its leader chooses the same target-lane and is able to perform an immediate lane-change), or it becomes *unconstrained* (e.g. when its leader is unable to perform the immediate lane-change, or chooses a different target-lane). In either case, the velocity of the immediate lane-changing constrained vehicle is unaffected by the lane-change.

Spontaneous lane-changing

11. *Spontaneous lane-changing* to the preferred lane will only occur when the vehicle retains its unconstrained state. That is, we assume that unconstrained vehicles preferring to drive on either of the adjacent lanes will only perform an spontaneous lane-change manoeuvre if they will not be constrained on the destination lane, at least not directly upon arrival.

Postponed lane-changing

12. *Postponed lane-changing state-transitions.* The state of the driver provides a lane-changing incentive. That is, all constrained vehicles aim to change lanes to either of the adjacent lanes in order to improve their current condition. If a postponed lane-change has occurred, the driver will not immediately increase his velocity. A postponed immediate lane-change causes drivers to relieve their constrained state and become *unconstrained* on either of the adjacent lanes. After having changed states, they are able to accelerate towards their desired velocity until they again interact with a slower vehicle.

Target-lane choice behaviour

13. The probabilities that a vehicle changes lanes depend on the velocity of the vehicle, the user-class, the lane it is currently occupying, and its target lane. However, we assume that the lane-changing probabilities do *not* depend on the desired velocity of the lane-changing vehicles. Various factors influence the target-lane choice decision, and can be incorporated in the modelling approach. Nevertheless, *when explicitly specifying the model's lane-changing relations*, we will mainly consider traffic operations given European traffic regulations. Consequently we will assume that for a discretionary lane choice, the first choice option will always be the left roadway lane.

Gap acceptance behaviour

14. The probability that a gap on the chosen target lane is accepted depends on the joint probability distribution of *lead-gaps* and *lag-gaps* (see appendix C) on the target lane.
15. The *lag-gap* is sufficient if the gap between the vehicle that will follow the lane-changing vehicle *after the lane-change* suffices.

16. The *lead-gap* suffices if the required space in front of the lane-changing vehicle on the target-lane is smaller than the resulting space after the lane-change.

In the remainder of this chapter, we derive a gas-kinetic traffic flow model describing the dynamics of heterogeneous traffic flow on multilane roadways by adopting the assumptions presented in this section. Although these assumptions are cast from the viewpoint of the individual driver, they are employed to provide the probabilistic foundation of the mesoscopic model equations.

4.4 Continuum processes and gas-kinetic equations

The dynamics of the MLMC-PSD are governed by both *continuum* and *non-continuum* processes. In this section, we derive continuum terms specifying the influence of convection, acceleration, and adaptation of continuum attributes. In other words, we derive generalised gas-kinetic equations *without specifying the non-continuum processes*, and consequently describe the dynamics of the generalised PSD for n-dimensional flows for smoothly changing flows.

In chapter 3 we have stated that in order to realistically describe MLMC traffic flow operations using a gas-kinetic modelling approach, we need to distinguish classes u, roadway lanes j, and drivers' states c. However, derivation of the dynamics of the *generalised PSD* $\rho_a(x,v,v^0,t)$ is justified since the general form of the continuum terms is similar for free-flowing, constrained, and mixed-state traffic, and holds for each lane, and user-class (although the specific parameters will be different for each lane, class, and state).

4.4.1 Generalised dynamics following from continuum processes

Continuum terms reflect dynamic changes in the generalised PSD $\rho_a(\mathbf{x},\mathbf{v},\mathbf{v}^0,t)$ due to the *smooth inflow and outflow in the phase-space* $\Sigma = \mathbf{x} \times \mathbf{v} \times \mathbf{v}^0$, where $\mathbf{x},\mathbf{v} \in I\!R^n$ respectively are the (n-dimensional) location-vector and velocity-vector, and $\mathbf{v}^0 \in I\!R^m$ is the general continuous attribute vector. In this section, we present an expression equivalent to the conservation of vehicles equation for the generalised Phase-Space Density ρ_a. In appendix A we show that the following differential equation describes the dynamics of the generalised PSD ρ_a:

$$\partial_t \rho_a + \overbrace{\nabla_{\mathbf{x}} \cdot (\rho_a \dot{\mathbf{x}})}^{(I)} + \overbrace{\nabla_{\mathbf{v}} \cdot (\rho_a \dot{\mathbf{v}})}^{(II)} + \overbrace{\nabla_{\mathbf{v}^0} \cdot (\rho_a \dot{\mathbf{v}}^0)}^{(III)} = \overbrace{(\partial_t \rho_a)_{NC}}^{(IV)} \tag{4.1}$$

where the $\nabla_{\mathbf{x}}$-operator is defined by:

$$\nabla_{\mathbf{x}} \overset{def}{=} (\partial_{x_1} \quad \partial_{x_2} \quad \cdots \quad \partial_{x_n}) \tag{4.2}$$

and where $\nabla_{\mathbf{v}}$ and $\nabla_{\mathbf{v}^0}$ are defined similarly. We have used the notation $\dot{\mathbf{x}} = \mathrm{d}\mathbf{x}/\mathrm{d}t$ to indicate the total time derivative of $\mathbf{x}$; $\dot{\mathbf{v}}$ and $\dot{\mathbf{v}}^0$ denote the total time derivative of the velocity vector $\mathbf{v}$ and the continuous attributes $\mathbf{v}^0$ respectively. Finally, we have used the short-hand notation $\partial_t = \partial/\partial t$ to indicate the partial derivative with respect to t.

The generalised conservation equation (4.1) describes how the generalised PSD ρ_a *changes over time* by the balance of inflow and outflow of vehicles in the phase-space $\Sigma = \mathbf{x} \times \mathbf{v} \times \mathbf{v}^0$ (e.g. vehicles flowing into and out of cell x, vehicles smoothly accelerating) reflected by terms (I)-(III) of (4.1) on the one hand, and on the other hand, by non-smooth changes due to

non-continuum processes (vehicles decelerating after an interaction, lane-changing vehicles, etc.), reflected by term (IV) of (4.1). More specifically, the *continuum processes* (terms (I)-(III) of (4.1)) reflect the dynamic change, which are caused by convection (term (I)), smooth acceleration (term (II)), and adaptation of the continuous attributes (term (III)) respectively.

The 'source-like' term $(\partial_t \rho_{\mathbf{a}})_{NC}$ in the generalised continuity equation (4.1) (term (IV)) is equivalent to the non-continuum terms in the models of Paveri-Fontana (1975), and Helbing (1996). In the model specification presented in this thesis, it conveys both *longitudinal* and *lateral* traffic processes. E.g. the dynamics caused by lane-changing vehicles and vehicles interaction with other vehicles, without lane-changing opportunity. In section 4.5 we present a generalised description of these non-continuum processes. This description is based on the distinction between *event-driven* and *condition-driven* non-continuum processes. In sections 4.6 and 4.7 we specify these event-driven and condition-driven processes for unconstrained and platooning vehicles. However, first the terms $\dot{\mathbf{x}}$ and $\dot{\mathbf{v}}^0$ present in the generalised continuity equation (4.1) are specified. This is possible since the expressions specifying these terms are assumed to be independent of the attribute set **a**.

Let us now discuss the specification of the different terms reflecting the continuum processes in equation (4.1) both for generic n-dimensional flows as well as the one-dimensional case with $(\mathbf{x},\mathbf{v},\mathbf{v}^0,t) = (x,v,v^0,t)$.

Introducing velocity

By definition, the *total time derivative* $\dot{\mathbf{x}}$ in equation (4.1) equals the velocity $\mathbf{v}$ of the vehicles sharing attribute **a**, i.e.:

$$\dot{\mathbf{x}} = \mathbf{v} \tag{4.3}$$

Clearly, for the case $(\mathbf{x},\mathbf{v},\mathbf{v}^0,t) = (x,v,v^0,t)$, expression (4.3) remains unchanged.

Desired velocity adaptation

In general, the time-derivative $\dot{\mathbf{v}}^0$ reflects *smooth adaptation* of the continuous attributes $\mathbf{v}^0$. We will describe this process by the so-called *adaptation (vector-) function* $B_{\mathbf{a}}(\mathbf{x},\mathbf{v},\mathbf{v}^0,t)$, i.e.:

$$\dot{\mathbf{v}}^0 = B_{\mathbf{a}}(\mathbf{x}, \mathbf{v}, \mathbf{v}^0, t) \tag{4.4}$$

In this thesis we will mainly consider one-dimensional flows, where the only continuous attribute is desired velocity (i.e. $\mathbf{v}^0 = v^0$). For such traffic systems, let us consider the process of *adapting the desired-speed distribution* $P_0(v)$ to the *reasonable desired speed distribution* $Q_0(v)$. Helbing (1997a) proposes that the following relation adequately describes the contribution of this dynamic process with respect to dynamic changes in the PSD:

$$\dot{v}^0 = B_{\mathbf{a}}(x,v,v^0,t) = \tilde{\rho}(x,v,t)(Q_0(v;x,t) - P_0(v;x,t))/T_{adapt} \tag{4.5}$$

Assuming that the desired speed is adapted quickly to the reasonable desired speed (i.e. the adaptation time T_{adapt} is relatively small), the *adiabatic elimination* (see Helbing (1997a)*) justifies neglecting the adaptation process, i.e.:

$$Q_0(v;x,t) = P_0(v;x,t) \quad \Rightarrow \quad \dot{v}^0 = 0 \tag{4.6}$$

Assuming that the same holds for lane-specific multiclass traffic flow (i.e. $\mathbf{a} = (u,j,c)$), justifies omitting the dynamic effects of adaptation of the desired velocity distribution.

Acceleration to the desired velocity

In equation (4.1), the derivative $\dot{\mathbf{v}}$ reflects the *gradual acceleration behaviour* of traffic entities. In general terms, this acceleration behaviour is modelled by the *acceleration (vector-) function* $A_{\mathbf{a}}(\mathbf{x},\mathbf{v},\mathbf{v}^0,t)$:

$$\dot{\mathbf{v}} = A_{\mathbf{a}}(\mathbf{x},\mathbf{v},\mathbf{v}^0,t) \tag{4.7}$$

For the case $(\mathbf{x},\mathbf{v},\mathbf{v}^0,t) = (x,v,v^0,t)$, we assume that the acceleration characteristics vary between classes u, and between states c. This assumption is justified by observing the differences in acceleration performance between vehicle-types (e.g. person-cars, motorbikes, vans, and trucks). Moreover, the driver's state indicates whether a vehicle can accelerate to its own desired velocity, given its own acceleration capabilities, or if it is restricted by the acceleration characteristics of its platoon leader. Consequently, we will consider free-flowing vehicles ($c = 1$) and constrained vehicles ($c = 2$) of class u separately.

In either case, we derive *exponential expressions* for the acceleration function $A_{\mathbf{a}}$, which are of the following form:

$$\dot{v} = A_{\mathbf{a}}(x,v,v^0,t) = \frac{W_{\mathbf{a}}(v,v^0 \mid x,t) - v}{\tau_{\mathbf{a}}(v,v^0 \mid x,t)} \tag{4.8}$$

where $W_{\mathbf{a}}(v,v^0|x,t)$ denotes the *expected acceleration velocity* of vehicles characterised by attribute set $\mathbf{a}$, velocity v, and desired velocity v^0, and $\tau_{\mathbf{a}}(v,v^0|x,t)$ denotes the respective *acceleration time*.

Resulting gas-kinetic equations for one-dimensional flows

If we substitute relations (4.3), (4.4) and (4.7) into equation (4.1), we find the generalised gas-kinetic equations for n-dimensional flows:

$$\partial_t \rho_{\mathbf{a}} + \nabla_{\mathbf{x}} \cdot (\rho_{\mathbf{a}} \mathbf{v}) + \nabla_{\mathbf{v}} \cdot (\rho_{\mathbf{a}} A_{\mathbf{a}}(\mathbf{x},\mathbf{v},\mathbf{v}^0,t)) + \nabla_{\mathbf{v}^0} \cdot (\rho_{\mathbf{a}} B_{\mathbf{a}}(\mathbf{x},\mathbf{v},\mathbf{v}^0,t)) = (\partial_t \rho_{\mathbf{a}})_{NC} \tag{4.9}$$

Moreover, for one-dimensional systems with $\mathbf{v}^0 = v^0$, we find by substituting (4.3), (4.6), and (4.8) into equation (4.9), the so-called *generalised gas-kinetic equations* for one-dimensional traffic flow operations:

---

* The *adiabatic elimination* consists of assuming that the derivative of a variable with respect to time is approximately zero. Such an approximation is justified, when the considered variable quickly converges towards the 'equilibrium state', compared to the time scale of the process at hand. In this context, the variable $\tilde{\rho}(x,v,t)P_0(v;x,t)$ changes towards the equilibrium state $\tilde{\rho}(x,v,t)Q_0(v;x,t)$.

$$\partial_t \rho_{\mathbf{a}} + \partial_x (\rho_{\mathbf{a}} v) + \partial_v \left(\rho_{\mathbf{a}} \frac{W_{\mathbf{a}}(v, v^0 \mid x,t) - v}{\tau_{\mathbf{a}}(v, v^0 \mid x,t)} \right) = (\partial_t \rho_{\mathbf{a}})_{NC} \tag{4.10}$$

4.4.2 *Gas-kinetic dynamics for platoon-based multilane multiclass traffic flow*

Let us now consider the generalised gas-kinetic equations for one-dimensional traffic flows (equation (4.10)) for multiclass multilane traffic flow (i.e. $(\mathbf{x},\mathbf{v},\mathbf{v}^0) = (x,v,v^0)$ and $\mathbf{a} = (u,j,c)$).

Acceleration behaviour of free-flowing vehicles

We will assume that free-flowing drivers reflected by $\rho_{(u,j,1)}(x,v,v^0,t)$ accelerate towards their desired velocity v^0, given the acceleration capabilities of their vehicles. This is achieved in an *exponential fashion* while considering the user-class specific *relaxation time* τ_u. Let us remark that since unconstrained vehicles are by definition *not impeded* by any vehicle in front of them, they are *always able to accelerate towards their respective desired velocity* v^0. Consequently, we can propose the following simple expression describing the rate of adaptation towards the desired velocity:

$$W_{(u,j,1)}(v, v^0 \mid x,t) = v^0 \quad \rightarrow \quad \dot{v} = A_{(u,j,1)}(x,v,v^0,t) = \frac{v^0 - v}{\tau_u(v, v^0 \mid x,t)} \tag{4.11}$$

This expression is comparable to the relation proposed by Paveri-Fontana (1975). In the remainder of the thesis, we assume that $\tau_u(v,v^0|x,t)$ can be approximated by a constant τ_u^0, yielding an exponential acceleration law*. Substitution of expression (4.11) into equation (4.10) yields the gas-kinetic equations for unconstrained vehicles:

$$\partial_t \rho_{(u,j,1)} + v \partial_x \rho_{(u,j,1)} + \partial_v \left(\rho_{(u,j,1)} \frac{v^0 - v}{\tau_u^0} \right) = (\partial_t \rho_{(u,j,1)})_{NC} \tag{4.12}$$

Acceleration behaviour of platooning vehicles

To model the acceleration behaviour of vehicles that drive in platoons, two extreme cases are reported in the literature:

1. The modelling approach of Paveri-Fontana (1975) implies that also *platooning vehicles* accelerate towards their own desired velocity v^0, given their acceleration time τ_u^0. In generalising this assumption to the multiclass case, this yields the following expression for the acceleration function A for platooning vehicles ($c = 2$):

$$A_{(u,j,2)}(x,v,v^0,t) = \frac{W_{(u,j,2)}(v, v^0 \mid x,t) - v}{\tau_{(u,j,2)}(v, v^0 \mid x,t)} = \frac{v^0 - v}{\tau_u^0} \tag{4.13}$$

2. Helbing (1997a,b) assumes that platooning drivers are not able to accelerate at all. In other words, he assumes that the acceleration time $\tau_{(u,j,2)}(v,v^0|x,t) \rightarrow \infty$, implying that

* Other relaxation laws can be easily incorporated in the model. However, the assumption of an exponential relaxation seems to be in agreement with the real-life behaviour of drivers, since these in general gradually reduce their acceleration when approaching their desired velocity (cf. Helbing (1996,1997)).

platooning vehicles remain at the velocity of the *impeding vehicle* at the instant of interaction. Generalising this concept to the multiclass multilane case yields the following expression for the acceleration function A for platooning vehicles ($c = 2$):

$$A_{(u,j,2)}(x,v,v^0,t) = \frac{W_{(u,j,2)}(v,v^0 \mid x,t) - v}{\tau_{(u,j,2)}(v,v^0 \mid x,t)} = 0 \tag{4.14}$$

Neither of these extreme cases describes the acceleration behaviour of drivers realistically. It is likely that in real-life traffic flow operations, constrained vehicles accelerate together with their unconstrained platoon leaders, until the desired velocities of either the platoon leading vehicles or the following vehicles are reached. Note that the assumption that a constrained vehicle drives at a constant velocity, namely the velocity of the unconstrained slow vehicle at the instant of interaction, yields unrealistic results when the impeding vehicle is accelerating at the time the interaction occurs (see Figure 4-4). In this case, the interacting vehicle decelerates to the velocity of the impeding vehicle, and remains at its velocity until its constrained status is relieved. However, since the impeding vehicle is still accelerating, the latter vehicle drives away from the impeded vehicle.

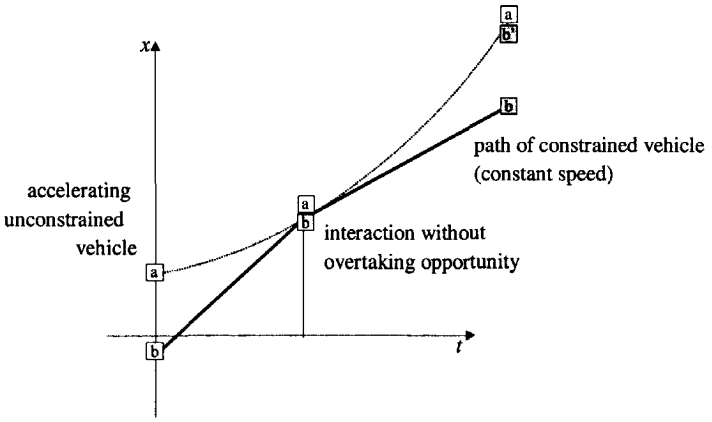

Figure 4-4: Interaction between accelerating unconstrained vehicles 'a' and 'b', given the assumption that the impeded vehicle is unable to accelerate. Vehicle 'b'' shows the position of the vehicle when it accelerates together with the impeding vehicle 'a'.

Summarising, we argue that platooning vehicles *can accelerate*, albeit not to their *own* desired velocity. Rather, they accelerate *simultaneously* (i.e. respecting the same acceleration time) to the *desired* velocities of their platoon leaders. To model this acceleration process, let us consider a platooning vehicle driving at location x and time t with velocity v having a desired velocity v^0. Let us consider the *expected desired velocity* $\tilde{V}^0_{(u,j,l)}(v \mid x,t)$ of *platoon leaders* of class u on lane j driving with velocity v. The probability density function of the desired velocity of this platoon leader equals:

$$\overline{g}_{(u,j,l)}(v^0 \mid x,v,t) = \rho_{(u,j,l)}(x,v,v^0,t) / \tilde{\rho}_{(u,j,l)}(x,v,t) \tag{4.15}$$

Thus, the expected desired velocity $\tilde{V}^0_{(u,j,1)}(v \mid x,t)$ equals*:

$$\tilde{V}^0_{(u,j,1)}(v \mid x,t) = \int v_0' \bar{g}_{(u,j,1)}(v_0' | x,v,t)\, \mathrm{d}\, v_0' \tag{4.16}$$

Let us now consider platooning vehicles $\rho_{(u,j,2)}(x,v,v^0,t)$. If we assume its platoon leader is of class u', then the expected acceleration velocity of the platoon leader and thus of the entire platoon equals $\tilde{V}^0_{(u',j,1)}(v \mid x,t)$, while the acceleration time of the platoon and the platoon equals $\tau_{u'}{}^0$. Thus, given that the platoon leader is of class u', the acceleration function becomes:

$$A_{(u,j,2)}(x,v,v_0,t \mid u') = (\tilde{V}^0_{(u',j,1)}(v \mid x,t) - v)/\tau^0_{u'} \tag{4.17}$$

Let us assume that platoon leaders are drawn randomly from the free-flowing vehicles with velocity v at (x,t). Let

$$\theta_{(u,j,1)}(x,v,t) = \tilde{\rho}_{(u,j,1)}(x,v,t)/\tilde{\rho}_{(*,j,1)}(x,v,t) \tag{4.18}$$

denote the probability that an unconstrained vehicles at (x,t) on lane j is of class u. Then, the acceleration function of constrained vehicles $\rho_{(u,j,2)}(x,v,v^0,t)$ equals:

$$A_{(u,j,2)}(x,v,v_0,t) = \sum_{u'} \theta_{(u',j,1)}(x,v,t) \cdot A_{(u,j,2)}(x,v,v_0,t \mid u') = \frac{W_{(u,j,2)}(v,v_0 \mid x,t) - v}{\tau_{(u,j,2)}(v,v_0 \mid x,t)} \tag{4.19}$$

where the *constrained acceleration time* $\tau_{(u,j,2)}(v,v_0|x,t)$ is defined according to:

$$\tilde{\rho}_{(*,j,1)}/\tau_{(u,j,2)}(v,v_0 \mid x,t) \overset{def}{=} \sum_{u'} (\tilde{\rho}_{(u',j,1)}/\tau^0_{u'}) \tag{4.20}$$

and the *constrained acceleration velocity* $W_{(u,j,2)}(v,v^0 \mid x,t)$ equals:

$$W_{(u,j,2)}(v,v_0 \mid x,t) = \frac{\sum_{u'} \tilde{\rho}_{(u',j,1)} \tilde{V}^0_{(u',j,1)}(v \mid x,t)/\tau^0_{u'}}{\sum_{u'} \tilde{\rho}_{(u',j,1)}/\tau^0_{u'}} \tag{4.21}$$

The assumption that platooning vehicles accelerate together with their platoon-leader towards the desired velocity of the latter, while respecting its acceleration time, yields the following *acceleration law* for constrained vehicles of user-class u:

$$\dot{v} = A_{(u,j,2)}(x,v,v^0,t) = \frac{W_{(u,j,2)}(v,v^0 \mid x,t) - v}{\tau_{(u,j,2)}(v,v^0 \mid x,t)} \tag{4.22}$$

By substituting expressions (4.6), and (4.22) into equation (4.1), we find the so-called *MLMC gas-kinetic equations for constrained vehicles:*

$$\partial_t \rho_{(u,j,2)} + v\partial_x \rho_{(u,j,2)} + \partial_v \rho_{(u,j,2)} \left(\frac{W_{(u,j,2)}(v,v^0 \mid x,t) - v}{\tau_{(u,j,2)}(v,v^0 \mid x,t)} \right) = (\partial_t \rho_{(u,j,2)})_{\mathcal{NC}} \tag{4.23}$$

---

* For notational convenience, the variable v^0 is on some occasions replaced by v_0.

Note that, in contrast to the original mesoscopic single user-class traffic flow models of Prigogine (1971) and macroscopic models discussed in chapter 2 (e.g. Lighthill and Whitham (1955), Payne (1971,1979), Papageorgiou (1989), Kerner *et al.* (1996)), the acceleration terms in (4.12) and (4.23) describes *individual relaxation* towards the (class-dependent) desired velocity of platoon leading vehicles, instead of *collective relaxation* towards a traffic composition dependent equilibrium velocity. This is a very important model feature: we argue that it is more realistic to assume that drivers aim to traverse the motorway at their desired velocity, while possibly being restricted due to interactions with slower vehicles, than to assume that drivers relax towards a velocity which they chose based on average traffic conditions.

4.4.3 Vector representation of generalised gas-kinetic equations

In section 3.6 we have defined the vector $\vec{\rho}(\mathbf{x}, \mathbf{v}, \mathbf{v}^0, t)$ with elements $\rho_{\mathbf{a}(i)}(x,v,v^0,t)$. Using this notation, the generalised gas-kinetic equation for generic one-dimensional traffic flows (4.10) can be recast in vector-notation, yielding:

$$\partial_t \vec{\rho} + v\partial_x \vec{\rho} + \partial_v \left(\vec{\rho} \otimes \frac{\mathbf{W}(v, v^0 \mid x,t) - v}{\vec{\tau}(v, v^0 \mid x,t)} \right) = (\partial_t \vec{\rho})_{NC} \tag{4.24}$$

where:

$$\vec{\tau} \overset{def}{=} (\tau_{(1,\ldots,1)} \quad \tau_{(1,\ldots,2)} \quad \cdots \quad \tau_{(n_1,\ldots n_D)}) \quad \text{and} \quad \mathbf{W} \overset{def}{=} (W_{(1,\ldots,1)} \quad W_{(1,\ldots,2)} \quad \cdots \quad W_{(n_1,\ldots n_D)}) \tag{4.25}$$

This vector formulation enables a compact representation of the gas-kinetic equations. Moreover, the aggregation of the equations with respect to user-classes, lanes, and states by using the aggregation matrices $\mathbf{S}_d$ (see section 3.8) is simplified significantly.

4.5 Generalised description of non-continuum traffic processes

The right-hand-side of the generic gas-kinetic equation (4.9) for n-dimensional flows reflects *non-continuum* processes that are by definition not caused by balancing smooth inflow and outflow of the differential hypervolume $\mathbf{S}$ in the phase-space $\Sigma = \mathbf{x} \times \mathbf{v} \times \mathbf{v}^0$. Non-continuum processes considered in this thesis are vehicles decelerating, immediate lane-changing, spontaneous lane-changing and postponed lane-changing, or state-relaxation, typically resulting in non-smooth changes of the generalised PSD $\rho_{\mathbf{a}}(\mathbf{x},\mathbf{v},\mathbf{v}^0,t)$. In the remainder of this chapter we will discuss these non-continuum processes. In this section we present generalised terms modelling dynamic influences of non-continuum processes, distinguishing between *event-driven* and *condition-driven* non-continuum processes, i.e.:

$$(\partial_t \rho_{\mathbf{a}}(\mathbf{x}, \mathbf{v}, \mathbf{v}^0, t))_{NC} = (\partial_t \rho_{\mathbf{a}}(\mathbf{x}, \mathbf{v}, \mathbf{v}^0, t))_{event} + (\partial_t \rho_{\mathbf{a}}(\mathbf{x}, \mathbf{v}, \mathbf{v}^0, t))_{condition} \tag{4.26}$$

4.5.1 Event-driven non-continuum processes

An event-driven non-continuum process is characterised by an event that yields a transition of the driver's discrete attributes $\mathbf{a} \rightarrow \mathbf{a}'$ (section 3.6) or non-smooth changes in the driver's velocity or continuous attributes $(\mathbf{v},\mathbf{v}^0) \rightarrow (\mathbf{v}',\mathbf{v}_0')$ (section 3.4). For instance, the state attribute c of a free-flowing driven catching up with a slower platoon (interaction event), while

being unable to immediately change lanes, changes from $c = 1$ to $c = 2$. The dynamic influences of these *events* are described using *event-rates*, defining the rate of occurrence of an event relevant for a specific class of vehicles. That is, if we consider vehicles characterised by discrete attributes **a**, velocity **v** and continuous attributes $\mathbf{v}^0$, the number of occurrences per unit time of a specific event α affecting a single vehicle is denoted by $\Pi_{\mathbf{a}}(\mathbf{x},\mathbf{v},\mathbf{v}^0,t;\alpha)$, where the set α uniquely characterises the event (e.g. $\alpha = (\mathbf{w},\mathbf{w}^0,\mathbf{b})$, where **w** denotes the velocity-vector, $\mathbf{w}^0$ denotes the continuous attributes, and **b** denotes the vector of discrete attributes of impeding vehicles). Since $\rho_{\mathbf{a}}(\mathbf{x},\mathbf{v},\mathbf{v}^0,t)$ denotes the expected number of vehicles sharing attributes **a**, **v** and $\mathbf{v}^0$, the *expected number of events* α per unit time equals:

$$\begin{aligned}\vec{\rho}(\mathbf{x},\mathbf{v},\mathbf{v}^0,t)\otimes\vec{\Pi}(\mathbf{x},\mathbf{v},\mathbf{v}^0,t;\alpha) &= \mathrm{diag}(\vec{\rho}(\mathbf{x},\mathbf{v},\mathbf{v}^0,t))\cdot\vec{\Pi}(\mathbf{x},\mathbf{v},\mathbf{v}^0,t;\alpha)\\ &= \{\rho_{\mathbf{a}(i)}(\mathbf{x},\mathbf{v},\mathbf{v}^0,t)\cdot\Pi_{\mathbf{a}(i)}(\mathbf{x},\mathbf{v},\mathbf{v}^0,t;\alpha)\}\end{aligned} \tag{4.27}$$

where $\mathbf{a}(i)$ denotes values **a** defined by index i, with $I(\mathbf{a}(i)) = i$ (section 3.8).

For each event-type α, $\pi_{\mathbf{a}}^{\mathbf{a}'}(\mathbf{v}',\mathbf{v}_0'|\mathbf{v},\mathbf{v}^0;\alpha)$ describes the probability that a vehicle involved in event α changes its velocity and discrete and continuous attributes from $(\mathbf{a},\mathbf{v},\mathbf{v}^0)$ to $(\mathbf{a}',\mathbf{v}',\mathbf{v}_0')$. The probability π describes a mixed conditional continuous/discrete random process. Using these probabilities, we can determine the so-called *event-driven transition matrix* $\mathbf{P}(\mathbf{v}',\mathbf{v}_0'|\mathbf{v},\mathbf{v}^0;\alpha) = \{p_{ij}(\mathbf{v}',\mathbf{v}_0'|\mathbf{v},\mathbf{v}^0;\alpha)\}$ for each event α, by considering the transition matrix **P** having the following elements:

$$\{p_{ij}(\mathbf{v}',\mathbf{v}_0' \mid \mathbf{v},\mathbf{v}^0;\alpha)\} \overset{def}{=} \pi_{\mathbf{a}(i)}^{\mathbf{a}(j)}(\mathbf{v}',\mathbf{v}_0' \mid \mathbf{v},\mathbf{v}^0;\alpha) \tag{4.28}$$

Let us consider the following matrix multiplication:

$$\begin{aligned}&\vec{\rho}(\mathbf{x},\mathbf{v},\mathbf{v}^0,t)\otimes\vec{\Pi}(\mathbf{x},\mathbf{v},\mathbf{v}^0,t;\alpha)\otimes\mathbf{P}(\mathbf{v}',\mathbf{v}_0' \mid \mathbf{v},\mathbf{v}^0;\alpha)\\ &\quad= \{\rho_{\mathbf{a}(i)}(\mathbf{x},\mathbf{v},\mathbf{v}^0,t)\otimes\Pi_{\mathbf{a}(i)}(\mathbf{x},\mathbf{v},\mathbf{v}^0,t;\alpha)\otimes\pi_{\mathbf{a}(i)}^{\mathbf{a}(j)}(\mathbf{v}',\mathbf{v}_0' \mid \mathbf{v},\mathbf{v}^0;\alpha)\}\end{aligned} \tag{4.29}$$

The elements of the resulting matrix reflect vehicles characterised by $(\mathbf{a}(i),\mathbf{v},\mathbf{v}^0)$ that switch to $(\mathbf{a}(j),\mathbf{v}',\mathbf{v}_0')$. Let us define the matrix-operator $\oplus$ that adds the matrix columns*:

$$\oplus\mathbf{A} \overset{def}{=} \mathbf{A}\cdot(1 \quad 1 \quad \cdots \quad 1)^T = (\Sigma_j a_{1,j} \quad \Sigma_j a_{2,j} \quad \cdots \quad \Sigma_j a_{N,j})^T \tag{4.30}$$

Using the operator $\oplus$ on the result (4.29) determines the total number of vehicles per unit time that switch from $\mathbf{a}(i)$ to any $\mathbf{a}(j)$ due to α by adding the *columns* of (4.29), yielding:

$$\begin{pmatrix} \Sigma_j(\pi_{\mathbf{a}(1)}^{\mathbf{a}(j)}(\mathbf{v}',\mathbf{v}_0' \mid \mathbf{v},\mathbf{v}^0;\alpha)\rho_{\mathbf{a}(1)}(\mathbf{x},\mathbf{v},\mathbf{v}^0,t)\Pi_{\mathbf{a}(1)}(\mathbf{x},\mathbf{v},\mathbf{v}^0,t;\alpha)) \\ \vdots \\ \Sigma_j(\pi_{\mathbf{a}(N)}^{\mathbf{a}(j)}(\mathbf{v}',\mathbf{v}_0' \mid \mathbf{v},\mathbf{v}^0;\alpha)\rho_{\mathbf{a}(N)}(\mathbf{x},\mathbf{v},\mathbf{v}^0,t)\Pi_{\mathbf{a}(N)}(\mathbf{x},\mathbf{v},\mathbf{v}^0,t;\alpha)) \end{pmatrix} \tag{4.31}$$

while the total number of vehicles per unit time that transfer *from any* $\mathbf{a}(j)$ *to* a *specific* $\mathbf{a}(i)$ by adding the *rows* of result (4.29) (or the *columns* of the transpose of (4.29)), that is:

* Note that the operator $\oplus$ is used in *prefix notation*, while the operator $\otimes$ is used in *suffix notation*.

$$\begin{pmatrix} \Sigma_j(\pi^{\mathbf{a}(1)}_{\mathbf{a}(j)}(\mathbf{v}',\mathbf{v}_0' \mid \mathbf{v},\mathbf{v}^0;\alpha)\rho_{\mathbf{a}(j)}(\mathbf{x},\mathbf{v},\mathbf{v}^0,t)\Pi_{\mathbf{a}(j)}(\mathbf{x},\mathbf{v},\mathbf{v}^0,t;\alpha)) \\ \vdots \\ \Sigma_j(\pi^{\mathbf{a}(N)}_{\mathbf{a}(j)}(\mathbf{v}',\mathbf{v}_0' \mid \mathbf{v},\mathbf{v}^0;\alpha)\rho_{\mathbf{a}(j)}(\mathbf{x},\mathbf{v},\mathbf{v}^0,t)\Pi_{\mathbf{a}(j)}(\mathbf{x},\mathbf{v},\mathbf{v}^0,t;\alpha)) \end{pmatrix} \tag{4.32}$$

The total expected number of vehicles of that switch *from* $(\mathbf{a},\mathbf{v},\mathbf{v}^0)$ due to the event α is determined by integrating (4.31) with respect $\mathbf{v}'$ and $\mathbf{v}_0'$. This yields the *decrease-rate* in the generalised PSD due to events causing a transition *from* $(\mathbf{a},\mathbf{v},\mathbf{v}^0)$:

$$(\partial_t\vec{\rho}(\mathbf{x},\mathbf{v},\mathbf{v}^0,t))^-_\alpha = \int \oplus(\vec{\rho}(\mathbf{x},\mathbf{v},\mathbf{v}^0,t) \otimes \vec{\Pi}(\mathbf{x},\mathbf{v},\mathbf{v}^0,t;\alpha) \otimes \mathbf{P}(\mathbf{v}',\mathbf{v}_0' \mid \mathbf{v},\mathbf{v}^0;\alpha))\,\mathrm{d}\,\mathbf{v}'\,\mathrm{d}\,\mathbf{v}_0' \tag{4.33}$$

Expression (4.33) shows how during an (infinitesimal) period $[t,t+\mathrm{d}t)$, the generalised PSD $\rho_{\mathbf{a}(i)}$ *reduces* by $\rho_{\mathbf{a}(i)}(\mathbf{x},\mathbf{v},\mathbf{v}^0,t)\Pi_{\mathbf{a}(i)}(\mathbf{x},\mathbf{v},\mathbf{v}^0,t;\alpha)\mathrm{d}t$ reflecting the number of vehicles during $[t,t+\mathrm{d}t)$ experiencing event α and changing states to $(\mathbf{a}(j),\mathbf{v}',\mathbf{v}_0')$. Clearly, aggregation with respect to all events α yields that the total decrease-rate in the generalised PSD equals*:

$$(\partial_t\vec{\rho}(\mathbf{x},\mathbf{v},\mathbf{v}^0,t))^-_{event} = \int (\partial_t\vec{\rho}(\mathbf{x},\mathbf{v},\mathbf{v}^0,t))^-_\alpha\,\mathrm{d}\,\alpha \tag{4.34}$$

The total expected number of vehicles that shift *to* $(\mathbf{a},\mathbf{v},\mathbf{v}^0)$ can be determined by integrating (4.32) with respect to $\mathbf{v}'$ and $\mathbf{v}_0'$, yielding the *increase-rate* in the generalised PSD due to events causing a transition *to* $(\mathbf{a},\mathbf{v},\mathbf{v}^0)$:

$$(\partial_t\vec{\rho}(\mathbf{x},\mathbf{v},\mathbf{v}^0,t))^+_\alpha = \int \oplus(\vec{\rho}(\mathbf{x},\mathbf{v}',\mathbf{v}_0',t) \otimes \vec{\Pi}(\mathbf{x},\mathbf{v}',\mathbf{v}_0',t;\alpha) \otimes \mathbf{P}(\mathbf{v},\mathbf{v}^0 \mid \mathbf{v}',\mathbf{v}_0';\alpha))^T\,\mathrm{d}\,\mathbf{v}'\,\mathrm{d}\,\mathbf{v}_0' \tag{4.35}$$

In other words, expression (4.35) shows the *increase* in the generalised PSD $\rho_{\mathbf{a}(i)}$ during the period $[t,t+\mathrm{d}t)$ due to vehicles $\rho_{\mathbf{a}(j)}(\mathbf{x},\mathbf{v}',\mathbf{v}_0',t)\Pi_{\mathbf{a}(j)}(\mathbf{x},\mathbf{v}',\mathbf{v}_0',t;\alpha)\mathrm{d}t$ with states $(\mathbf{a}(j),\mathbf{v}',\mathbf{v}_0')$ experiencing events α and consequently changing to $(\mathbf{a}(i),\mathbf{v},\mathbf{v}^0)$. Again, the increase in the generalised PSD due to any event α can be determined by aggregation with respect to the event α:

$$(\partial_t\vec{\rho}(\mathbf{x},\mathbf{v},\mathbf{v}^0,t))^+_{event} = \int (\partial_t\vec{\rho}(\mathbf{x},\mathbf{v},\mathbf{v}^0,t))^+_\alpha\,\mathrm{d}\,\alpha \tag{4.36}$$

The net-change in the generalised PSD due to events equals:

$$(\partial_t\vec{\rho}(\mathbf{x},\mathbf{v},\mathbf{v}^0,t))_{event} = (\partial_t\vec{\rho}(\mathbf{x},\mathbf{v},\mathbf{v}^0,t))^+_{event} - (\partial_t\vec{\rho}(\mathbf{x},\mathbf{v},\mathbf{v}^0,t))^-_{event} \tag{4.37}$$

4.5.2 Condition-driven non-continuum processes

A *condition-driven* non-continuum process β is characterised by vehicles relieving their state when the opportunity arises, rather than an *event-driven* process that yields a transition after an event has taken place. For instance, the state-attribute c and the lane-attribute j of a platooning vehicle on the right-lane $j = 1$ performing a postponed lane-change, change from $c = 2$ and $j = 1$ to $c = 1$ and $j = 2$. Instead of specifying *probabilities* that the vehicle's attributes change from $\mathbf{a}$, $\mathbf{v}$, and $\mathbf{v}^0$ to $\mathbf{a}'$, $\mathbf{v}'$ and $\mathbf{v}_0'$, we specify the *rates* at which transitions occur.

For each type of condition-driven process β, the rates ϕ are defined by the *expected number of state-transitions per vehicle per unit time* having attributes $\mathbf{a}$, $\mathbf{v}$ and $\mathbf{v}^0$, and are denoted by:

---

* Note the informal use of the intergral with respect to both the continuous attributes as well as the discrete attributes characterising events α. In the discrete case, integration in fact reflects *summation* with respect to the discrete attributes. This holds equally for conditions β.

$$\phi_{\mathbf{a}}^{\mathbf{a}'}(\mathbf{v}', \mathbf{v}_0' \mid \mathbf{v}, \mathbf{v}^0; \beta) \tag{4.38}$$

Using these rates, we can define the *condition-driven transition rates* $\mathbf{F} = \{f_{ij}\}$ by:

$$f_{ij}(\mathbf{v}', \mathbf{v}_0' \mid \mathbf{v}, \mathbf{v}^0; \beta) = \phi_{\mathbf{a}(i)}^{\mathbf{a}(j)}(\mathbf{v}', \mathbf{v}_0' \mid \mathbf{v}, \mathbf{v}^0; \beta) \tag{4.39}$$

The state-based non-continuum process β experienced by vehicles characterised by attributes $(\mathbf{v},\mathbf{v}^0;\mathbf{a})$ on the one hand yield a *decrease* of the generalised PSD's $\rho_{\mathbf{a}}(\mathbf{x},\mathbf{v},\mathbf{v}^0,t)$ due to vehicles changing their states *to* attributes $\mathbf{a}'$, $\mathbf{v}'$ and $\mathbf{v}_0'$, with a decrease-rate that equals:

$$(\partial_t \vec{\rho}(\mathbf{x}, \mathbf{v}, \mathbf{v}^0, t))_{\beta}^{-} = \int \oplus (\vec{\rho}(\mathbf{x}, \mathbf{v}, \mathbf{v}^0, t) \otimes \mathbf{F}(\mathbf{v}', \mathbf{v}_0' \mid \mathbf{v}, \mathbf{v}^0; \beta))\, \mathrm{d}\,\mathbf{v}'\, \mathrm{d}\,\mathbf{v}_0' \tag{4.40}$$

On the other hand, vehicles with attributes $(\mathbf{a}',\mathbf{v}_0')$ that shift to $(\mathbf{a},\mathbf{v}^0)$ cause an *increase* in the generalised PSD $\rho_{\mathbf{a}}(\mathbf{x},\mathbf{v},\mathbf{v}^0,t)$ with an increase-rate equal to:

$$(\partial_t \vec{\rho}(\mathbf{x}, \mathbf{v}, \mathbf{v}^0, t))_{\beta}^{+} = \int \oplus (\vec{\rho}(\mathbf{x}, \mathbf{v}', \mathbf{v}_0', t) \otimes \mathbf{F}(\mathbf{v}, \mathbf{w} \mid \mathbf{v}', \mathbf{v}_0'; \beta))^T\, \mathrm{d}\,\mathbf{v}'\, \mathrm{d}\,\mathbf{v}_0' \tag{4.41}$$

We can collect the contributions of the considered condition-driven processes β by integration with respect to β:

$$(\partial_t \vec{\rho}(\mathbf{x}, \mathbf{v}, \mathbf{v}^0, t))_{condition}^{-} = \int (\partial_t \vec{\rho}(\mathbf{x}, \mathbf{v}, \mathbf{v}^0, t))_{\beta}^{-} \mathrm{d}\beta \tag{4.42}$$

and:

$$(\partial_t \vec{\rho}(\mathbf{x}, \mathbf{v}, \mathbf{v}^0, t))_{condition}^{+} = \int (\partial_t \vec{\rho}(\mathbf{x}, \mathbf{v}, \mathbf{v}^0, t))_{\beta}^{+} \mathrm{d}\beta \tag{4.43}$$

The net-rate of change due to condition-driven non-continuum processes equals:

$$(\partial_t \vec{\rho}(\mathbf{x}, \mathbf{v}, \mathbf{v}^0, t))_{condition} = (\partial_t \vec{\rho}(\mathbf{x}, \mathbf{v}, \mathbf{v}^0, t))_{condition}^{+} - (\partial_t \vec{\rho}(\mathbf{x}, \mathbf{v}, \mathbf{v}^0, t))_{condition}^{-} \tag{4.44}$$

4.5.3 Generic gas-kinetic equations

Let us finally reconsider the gas-kinetic equations for the generalised PSD by collecting the continuum terms and the event-driven and condition-driven non-continuum terms. For the general, multi-dimensional PSD (i.e. flows of traffic entities in n-dimensions), we have:

$$\begin{aligned}
&\partial_t \vec{\rho} + \nabla_{\mathbf{x}} \cdot (\vec{\rho}\mathbf{v}) + \nabla_{\mathbf{v}} \cdot (\vec{\rho} \otimes \mathbf{A}(\mathbf{x}, \mathbf{v}, \mathbf{v}^0, t)) + \nabla_{\mathbf{v}^0} \cdot (\vec{\rho} \otimes \mathbf{B}(\mathbf{x}, \mathbf{v}, \mathbf{v}^0, t)) = \\
&\quad \int \oplus (\vec{\rho}(\mathbf{x}, \mathbf{v}', \mathbf{v}_0', t) \otimes \vec{\Pi}(\mathbf{x}, \mathbf{v}', \mathbf{v}_0', t; \alpha) \otimes \mathbf{P}(\mathbf{v}, \mathbf{w} \mid \mathbf{v}', \mathbf{v}_0'; \alpha))^T\, \mathrm{d}\,\mathbf{v}'\, \mathrm{d}\,\mathbf{v}_0'\, \mathrm{d}\,\alpha \\
&\quad - \int \oplus (\vec{\rho}(\mathbf{x}, \mathbf{v}, \mathbf{v}^0, t) \otimes \vec{\Pi}(\mathbf{x}, \mathbf{v}, \mathbf{v}^0, t; \alpha) \otimes \mathbf{P}(\mathbf{v}', \mathbf{v}_0' \mid \mathbf{v}, \mathbf{v}^0; \alpha))\, \mathrm{d}\,\mathbf{v}'\, \mathrm{d}\,\mathbf{v}_0'\, \mathrm{d}\,\alpha \\
&\quad + \int \oplus (\vec{\rho}(\mathbf{x}, \mathbf{v}', \mathbf{v}_0', t) \otimes \mathbf{F}(\mathbf{v}, \mathbf{v}^0 \mid \mathbf{v}', \mathbf{v}_0'; \beta))^T\, \mathrm{d}\,\mathbf{v}'\, \mathrm{d}\,\mathbf{v}_0'\, \mathrm{d}\beta \\
&\quad - \int \oplus (\vec{\rho}(\mathbf{x}, \mathbf{v}, \mathbf{v}^0, t) \otimes \mathbf{F}(\mathbf{v}', \mathbf{v}_0' \mid \mathbf{v}, \mathbf{v}^0; \beta))\, \mathrm{d}\,\mathbf{v}'\, \mathrm{d}\,\mathbf{v}_0' \mathrm{d}\beta
\end{aligned} \tag{4.45}$$

where $\mathbf{A}$ and $\mathbf{B}$ respectively denote the respective vectors of acceleration and adaptation functions for vehicles characterised by attribute-sets $\mathbf{a}(i)$.

For the specification of $\mathbf{x}$, $\mathbf{v}$, and $\mathbf{v}^0$ used in this thesis (i.e. $(\mathbf{x},\mathbf{v},\mathbf{v}^0,t) = (x,v,v^0,t)$), we have (in matrix-vector notation):

$$
\begin{aligned}
&\partial_t\vec{\rho} + v\partial_x\vec{\rho} + \partial_v\left(\vec{\rho}\otimes\frac{\mathbf{W}(v,v^0\mid x,t)-v}{\bar{\tau}(v,v^0\mid x,t)}\right) = \\
&\quad \int\oplus(\vec{\rho}(x,v',v_0',t)\otimes\vec{\Pi}(x,v',v_0',t;\alpha)\otimes\mathbf{P}(v,v^0\mid v',v_0';\alpha))^T\,\mathrm{d}v_0'\,\mathrm{d}v'\,\mathrm{d}\alpha \\
&\quad -\int\oplus(\vec{\rho}(x,v,v^0,t)\otimes\vec{\Pi}(x,v,v^0,t;\alpha)\otimes\mathbf{P}(v',v_0'\mid v,v^0;\alpha))\,\mathrm{d}v_0'\,\mathrm{d}v'\,\mathrm{d}\alpha \\
&\quad +\int\oplus(\vec{\rho}(x,v',v_0',t)\otimes\mathbf{F}(v,v^0\mid v',v_0';\beta))^T\,\mathrm{d}v_0'\,\mathrm{d}v'\,\mathrm{d}\beta \\
&\quad -\int\oplus(\vec{\rho}(x,v,v^0,t)\otimes\mathbf{F}(v',v_0'\mid v,v^0;\beta))\,\mathrm{d}v_0'\,\mathrm{d}v'\,\mathrm{d}\beta
\end{aligned}
\tag{4.46}
$$

Or, by expanding all matrix-vector terms, we find the equivalent system describing the dynamics of the MLMC-PSD $\rho_{\mathbf{a}}(x,v,v^0,t)$:

$$
\boxed{
\begin{aligned}
&\partial_t\rho_{\mathbf{a}} + \partial_x(\rho_{\mathbf{a}}v) + \partial_v\left(\rho_{\mathbf{a}}\frac{W_{\mathbf{a}}(v,v^0\mid x,t)-v}{\tau_{\mathbf{a}}(v,v^0\mid x,t)}\right) = \\
&\quad +\sum_{\mathbf{a}'}\int\rho_{\mathbf{a}'}(v',v_0')\Pi_{\mathbf{a}'}(v',v_0';\alpha)\pi^{\mathbf{a}}_{\mathbf{a}'}(v,v^0\mid v',v_0';\alpha))\,\mathrm{d}v_0'\,\mathrm{d}v'\,\mathrm{d}\alpha \\
&\quad -\sum_{\mathbf{a}'}\int\rho_{\mathbf{a}}(v,v^0)\Pi_{(u,j,c)}(v,v^0;\alpha)\pi^{\mathbf{a}'}_{\mathbf{a}}(v',v_0'\mid v,v^0;\alpha))\,\mathrm{d}v_0'\,\mathrm{d}v'\,\mathrm{d}\alpha \\
&\quad +\sum_{\mathbf{a}'}\int\rho_{\mathbf{a}'}(v',v_0')\phi^{\mathbf{a}}_{\mathbf{a}'}(v,v^0\mid v',v_0';\beta)\,\mathrm{d}\beta - \sum_{\mathbf{a}'}\int\rho_{\mathbf{a}}(v,v^0)\phi^{\mathbf{a}'}_{\mathbf{a}}(v',v_0'\mid v,v^0;\beta)\,\mathrm{d}\beta
\end{aligned}
}
\tag{4.47}
$$

Equation (4.46) (or (4.47)) shows the *generalised gas-kinetic equations*. It shows how the dynamic changes in the generalised PSD $\rho_{\mathbf{a}}(x,v,v^0,t)$ are governed by convection, acceleration, event-driven transitions, and condition-driven transitions. The right-hand side of (4.47) reflects these event-driven and condition-driven non-continuum changes. In the remainder of this chapter we specify these terms for $\mathbf{a} = (u,j,c)$, yielding the gas-kinetic dynamics of the free-flowing and the platooning MLMC-PSD $\rho_{(u,j,1)}$ and $\rho_{(u,j,2)}$ respectively. That is, by specifying expressions for the event-rates Π (section 4.6), the transition probabilities π (section 4.6), and the transition-rates ϕ (section 4.7), the dynamic equations for free-flowing and platooning vehicles of class u on lane j are established.

4.6 Specification of event-driven non-continuum processes

In this section, we will specify the *event-driven* non-continuum processes for the gas-kinetic MLMC traffic model presented in this thesis. We will only consider *interaction* events. First, we will discuss different interaction types for general flows in the n-dimensional space.

4.6.1 Interaction types for n-dimensional flows

Consider two vehicles a and b moving in $\mathbb{R}^n$, characterised by the triples (velocity, continuous attributes; discrete attributes), i.e. $(\mathbf{v},\mathbf{v}^0;\mathbf{a})$ and $(\mathbf{w},\mathbf{w}^0;\mathbf{b})$ respectively, with $\mathbf{v} \neq \mathbf{w}$. We define an *interaction* of a and b as the event that a and b are at the same location $\mathbf{x} \in \mathbb{R}^n$. *From the viewpoint of a*, three interaction types are distinguished:

1. *One-sided active interaction.* The conditions at the time the interaction occurs are such that vehicle *a* needs to take remedial actions in an attempt to avoid a collision, while *b* cannot influence the interaction outcome. That is, *a* is hindered by *b*, but *not* vice-versa. An example of a one-sided active interaction is vehicle *a* catching up with a slower vehicle *b*, assuming that the slow vehicle *b* is not influenced by the fast vehicle *a*. By the anisotropy assumption, *a* is called the active party and *b* is called the passive party of the interaction.
2. *One-sided passive-interaction.* In this case, vehicle *a* is *not* hindered by vehicle *b*, and consequently *a* cannot perform any remedial manoeuvres to prevent a collision. On the contrary, *b* is hindered by *a*. An example of a passive interaction is vehicle *a being caught up* by vehicle *b*, assuming that the slow vehicle *a* is not influenced by the fast vehicle *b*. In this case, *a* is the passive party, while *b* is the active party.
3. *Two-sided interaction.* In case of a two-sided interaction, both *a* as well as *b* are actively involved the interaction, i.e. both are likely to perform some remedial manoeuvre to avoid a collision. An example of a two-sided interaction is vehicle *a* and vehicle *b* meeting *head-on* (only in bi-directional flows, or two or higher dimensional flows (see Hoogendoorn and Bovy (2000)). For two-sided interactions, two active parties are identified.

4.6.2 *Interaction event for single dimensional flows*

In this thesis, we consider *uni-directional one-dimensional* flows. Based on the anisotropy assumption, the slow vehicle is not influenced by the interaction. Hence, only *one-sided interactions* (active and passive) are considered.

Thus for uni-directional one-dimensional flows, in terms of infinitesimal platoons moving in the phase-space Σ, an interaction event is equivalent to platoons *a* and platoons *b* being both present at (x,t) (see Figure 4-5). Unless stated otherwise, in this section we will use v, v' and w to describe the velocity of the impeded vehicle *before* the interaction, the velocity of the impeded vehicle *after* interacting and the velocity of the *impeding* vehicle respectively.

Interactions of platooning vehicles

We assume that vehicles having interacted with a slower platoon, while not having the opportunity nor the desire to change lanes, join the (*vertical*) *platoon* (Figure 4-6a). The velocity v' of the active party *after interaction* equals the velocity w of the platoon leader. Since we have assumed that vehicles have no physical length, and that the distance between interacting vehicles is zero, the formed platoon also has zero length*. When the active party is able to perform an immediate lane-change, the velocity v' of the active party *after* the interaction equals the velocity v of the active party *before* the interaction event (Figure 4-6b).

The concept of an interaction event experienced by a *platooning vehicle* seems to make no sense, since a constrained vehicle is by definition following and cannot directly interact with a slower platoon. However, since platooning vehicles follow their predecessor at zero dis-

* The *vertical platoon* assumption is remedied at a later stage in the model development (section 4.6.4 and section 6.8), by explicitly considering the finite space requirements of the vehicles.

tance, an interaction of the leader causes an interaction of the follower as well. In other words, if the leading vehicle interacts, it is either able to immediately change lanes *or* it needs to slow down. When the leader slows down, the follower needs to undertake remedial actions to prevent a collision. Then, the follower can either undertake a *constrained immediate lane-change* or *decelerate*. In the latter case, the follower decelerates to the velocity w of the passive party. When the leader is able to perform an unconstrained immediate lane-change, the infinitesimal length assumption yields that the following vehicle *immediately* interacts with the passive party. Again, the follower can undertake a constrained immediate lane-change, or it can reduce its velocity to the velocity of the passive party.

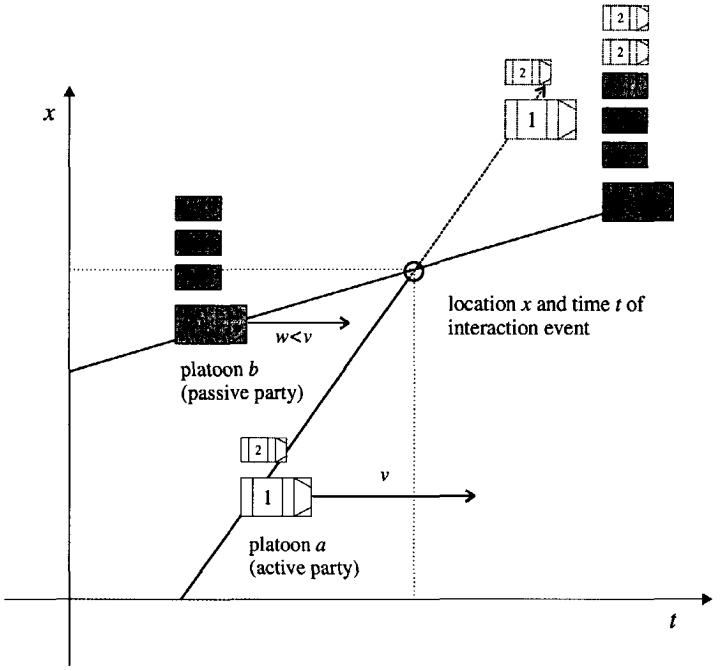

Figure 4-5: Schematics of an interaction event where a fast two-vehicle platoon *a* interacts with a slower four-vehicle platoon *b* (numbers indicate states of vehicles).

Concluding, given the vertical platoon assumption, the impeding vehicle yields the same effect for the constrained vehicle, irrespective of the action taken by the leader of this constrained vehicle. This shows that the concept of interaction makes sense for platooning vehicles as well.

Interaction-driven attribute-transitions

Let us consider interactions of vehicles of class u on lane j in state c driving with velocity v while having desired velocity v^0. We assume that these vehicles either change to the adjacent lanes *or* decelerate to avoid a collision. In either case, the interactions reduce $\rho_{(u,j,c)}(x,v,v^0,t)$.

However, interactions of vehicles of class u on lane j' in state c' driving with velocity v' having desired velocity v^0 may yield a transition to (u,j,c) and (v,v^0) causing $\rho_{(u,j,c)}(x,v,v^0,t)$ to *increase*. More specifically, in case of an immediate lane-change to an adjacent lane $j\pm1$, we have a transition $\rho_{(u,j\pm1,c)}(x,v,v^0,t) \rightarrow \rho_{(u,j,c)}(x,v,v^0,t)$, while a deceleration of a vehicle on lane j with state c yields the transition $\rho_{(u,j,c)}(x,w,v^0,t) \rightarrow \rho_{(u,j,2)}(x,v,v^0,t)$.

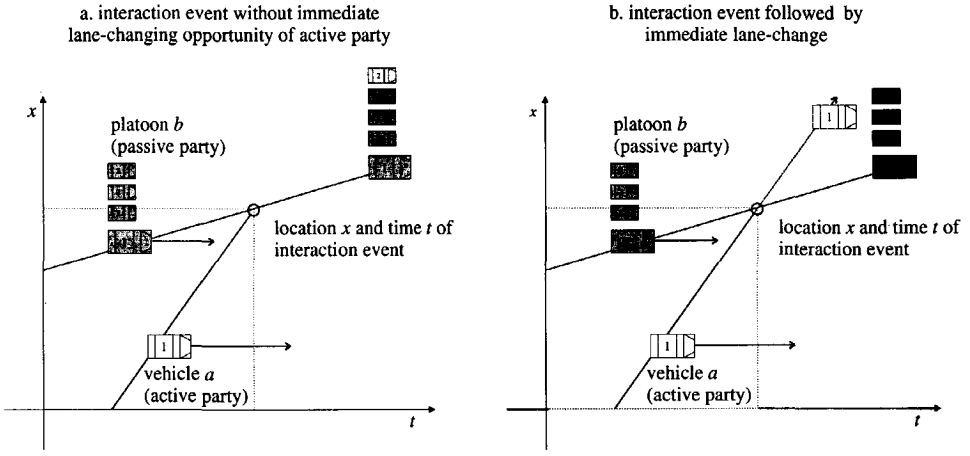

Figure 4-6: Interaction event without (*a*) and with (*b*) immediate lane-changing opportunity.

4.6.3 Interaction rates, deceleration and immediate lane-changing

In this thesis, we mainly consider the dynamics of one-dimensional traffic flows. However, the interaction event-rates $\Pi_a(\mathbf{x},\mathbf{v},\mathbf{v}^0,t;\alpha)$ are derived for the general n-dimensional case. To this end, let us consider *any* vehicle a which at instant t is located at $\mathbf{x}$ while moving with velocity $\mathbf{v}$. Let $\mathbf{w}$, $\mathbf{w}^0$ and $\mathbf{b}$ denote the velocity-vector, the vector of continuous attributes, and the vector of discrete attributes of *any* vehicle b that (possibly) interacts with a. We assume that the remedial actions of a (i.e. the transition probabilities) are *independent* on the continuous attributes $\mathbf{w}^0$ of b. This is justified by the fact that $\mathbf{w}^0$ (e.g. desired velocity) is generally unobservable by a. This implies that the remedial action of a after the interaction has occurred only depends on $\mathbf{w}$ and $\mathbf{b}$. Consequently, an interaction event can be specified by $\mathbf{w}$ and $\mathbf{b}$, an is in this case denoted by $\alpha = (\mathbf{w},\mathbf{b})$.

Specification of generic interaction-rates for n-dimensional flows

Let us define a parameterised curve $L = L(\mathbf{x},\mathbf{v},\mathbf{w},t|\Delta t)$ in the n-dimensional space by the curve where vehicles b that collide with a at some instant $s \in [t,t+\Delta t)$ are located at instant t. L is defined by (see Figure 4-7):

$$L \overset{def}{=} \{\mathbf{x}(s) \,|\, \mathbf{x}(s) = \mathbf{x} + (\mathbf{w} - \mathbf{v})\mathbf{s}, 0 \le s < \Delta t\} \tag{4.48}$$

In illustration, shows line L is case of a two-dimensional flow. In the figure, a traffic particle a is depicted with velocity $\mathbf{v}$ that is located at $\mathbf{x}$ at instant t. The expected number of interac-

tions that a experiences per unit time during period $[t,t+\Delta t)$ can be established by integrating along the line L:

$$\Pi_a(\mathbf{x},\mathbf{v},\mathbf{v}^0,t;\mathbf{w},\mathbf{b})\Delta t = \int_{L(\mathbf{x},\mathbf{v},\mathbf{w},t|\Delta t)} \tilde{\rho}_b(\mathbf{x}',\mathbf{w},t)\,\mathrm{d}\,\mathbf{x}' \tag{4.49}$$

By definition, we can rewrite the line-integral along the curve L as:

$$\int_{L(\mathbf{x},\mathbf{v},\mathbf{w},t|\Delta t)} \tilde{\rho}_b(\mathbf{x}',\mathbf{w},t)\,\mathrm{d}\,\mathbf{x}' = \int_t^{t+\Delta t} \tilde{\rho}_b(\mathbf{x}(s),\mathbf{w},s)\,|\,\dot{\mathbf{x}}(s)\,|\,\mathrm{d}\,s \tag{4.50}$$

with $\mathbf{x}(s) = \mathbf{x}+(\mathbf{w}-\mathbf{v})s$. Since $\dot{\mathbf{x}}(s) = \mathbf{w}-\mathbf{v}$ and when Δt is very small (i.e. $\Delta t \rightarrow \mathrm{d}t$) we have:

$$\Pi_a(\mathbf{x},\mathbf{v},\mathbf{v}^0,t;\mathbf{w},\mathbf{b}) = |\mathbf{w}-\mathbf{v}|\,\tilde{\rho}_b(\mathbf{x},\mathbf{w},t) \tag{4.51}$$

Eq. (4.51) depicts all interactions (active one-sided, passive one-sided, and two-sided). To determine the dynamic influence of interactions, correct specification of the transition probabilities is necessary.

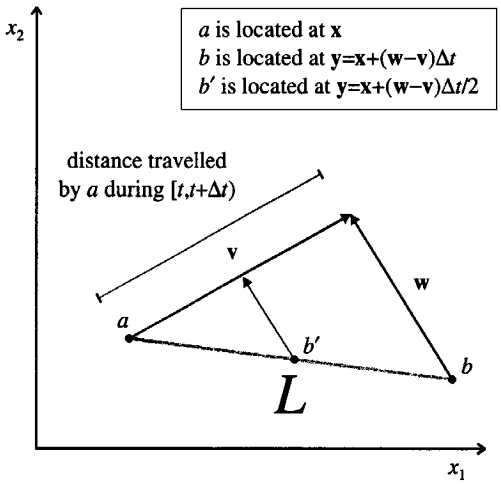

Figure 4-7: Example of line $L = L(\mathbf{x},\mathbf{v},\mathbf{w},t|\Delta t)$ in two dimensions, where traffic entities (e.g. b and b') having velocity w are located that interact (during interval $[t,t+\Delta t)$) with a that is located at x at instant t, while having velocity v.

Interaction rates for one-dimensional flows

For one-dimensional flows, eq. (4.51) becomes:

$$\Pi_a(x,v,v^0,t;w,\mathbf{b}) = |w-v|\,\tilde{\rho}_b(x,w,t) \tag{4.52}$$

This expression reflects *all interactions*, for instance, both interactions in which a is the *active party* ($v > w$) as well as the interactions in which a is the *passive party* ($v < w$). Moreover, also interactions which will not yield any counteractions of a are included (e.g. interactions with $\mathbf{b} = (u',j,2)$). To correctly describe the interaction process and the non-continuum

changes inferred by interaction-events, correct specification of the transition probabilities is of dominant importance. This is discussed in the following section.

Specification of the transition matrix

In this section, we discuss the transition rates reflecting transitions from $(\mathbf{a},v,v^0)$ to $(\mathbf{a}',v',v_0')$ with $\mathbf{a} = (u,j,c)$ due to interactions reflected by event $\alpha = (\mathbf{b},w)$. Table 4-4 summarises the possible transitions between these attributes, that is the non-zero elements of the matrix $\mathbf{P}(\mathbf{v}',\mathbf{w}'|\mathbf{v},\mathbf{w};\alpha)$. Note that transition probabilities for $\mathbf{b} = (s,j,2)$ are equal to zero. This implies that interactions with *constrained vehicles* ($c = 2$) will *not* result in a counteraction of a.

In other words, in opposition to the original model of Prigogine and Herman (1971), we only consider interactions with *platoon-leading vehicles* ($\mathbf{b} = (s,j,1)$), rather than with vehicles in both driving states 1 and 2. This is justified by the assumption that vehicles having interacted form a platoon of infinitesimal length. Since the expected number of platoons equals the expected number of platoon leaders, only the latter determines the interaction rate. Consequently, we can conclude that the *collision equation* of Prigogine and Herman (1971) (see also Paveri-Fontana (1975), Leutzbach (1988), Helbing (1996)) *overestimates* the number of interactions, caused by the fact that under the *vehicular chaos assumption*, it is unconvincingly assumed that the correlation between vehicles can be neglected. That is, when more vehicles in the flow are platooning, the vehicles' characteristics become more correlated.

Let us now briefly discuss the contents of Table 4-4. With respect to unconstrained vehicles, the table shows that for an unconstrained platoon leader, either of the following actions succeeds the interaction event:

1. *Deceleration.* The unconstrained vehicle is unable to overtake the impeding vehicle. We assume that the driver immediately decelerates to the velocity $w < v$ of the preceding vehicle, while becoming constrained: $\rho_{(u,j,1)}(x,v,v^0,t) \rightarrow \rho_{(u,j,2)}(x,w,v^0,t)$.
2. *Unconstrained immediate lane-changing.* The unconstrained vehicle is able to *immediately change lanes*, while staying unconstrained: $\rho_{(u,j,1)}(x,v,v^0,t) \rightarrow \rho_{(u,j\pm1,1)}(x,v,v^0,t)$.

For platooning vehicles, the following reactions are relevant after interacting:

1. *Deceleration.* In this case, the constrained vehicle decelerate instantaneously to the velocity w of the slow platoon: $\rho_{(u,j,2)}(x,v,v^0,t) \rightarrow \rho_{(u,j,2)}(x,w,v^0,t)$.
2. *Synchronous constrained immediate lane-change* (leader and follower immediately change to the same lane). Both the velocity and the state of the follower remain the same: $\rho_{(u,j,2)}(x,v,v^0,t) \rightarrow \rho_{(u,j\pm1,2)}(x,v,v^0,t)$.
3. *Asynchronous constrained immediate lane-change* (follower immediately changes lanes, while leader either does not change lanes or changes to another lane). The velocity of the constrained follower remains the same. However, we assume that the constrained state of the driver is relieved: $\rho_{(u,j,2)}(x,v,v^0,t) \rightarrow \rho_{(u,j\pm1,1)}(x,v,v^0,t)$.

Table 4-4: Non-zero probabilities reflecting all possible transitions from (a,v,v^0) to (a',v',v_0') after event $\alpha = (w;s,j,1)$ with $w < v$. For all other events α transition probabilities are zero.

TO: \ FROM:	unconstrained vehicles $\rho_{(u,j,1)}(x,v,v^0,t)$	constrained vehicles $\rho_{(u,j,2)}(x,v,v^0,t)$
constrained vehicles $\rho_{(u,j,2)}(x,w,v^0,t)$	deceleration + state transition $\pi^{(u,j,2)}_{(u,j,1)}(v',v_0' \mid v,v^0;\alpha)$	deceleration $\pi^{(u,j,2)}_{(u,j,2)}(v',v_0' \mid v,v^0;\alpha)$
unconstrained vehicles $\rho_{(u,j\pm1,1)}(x,v,v^0,t)$	unconstr. imm. lane-change $\pi^{(u,j\pm1,1)}_{(u,j,1)}(v',v_0' \mid v,v^0;\alpha)$	constr. imm. lane-change $\pi^{(u,j\pm1,1)}_{(u,j,2)}(v',v_0' \mid v,v^0;\alpha)$
constrained vehicles $\rho_{(u,j\pm1,2)}(x,v,v^0,t)$	N/A.	constr. imm. lane-change $\pi^{(u,j\pm1,2)}_{(u,j,2)}(v',v_0' \mid v,v^0;\alpha)$

Immediate lane-changing probability. The probability that after interaction α with a vehicle driving with velocity w, a vehicle is able to change lanes to either of the adjacent lanes, without needing to reduce its velocity v is described by the following specification of the transition probability for all events $\alpha = (w;\mathbf{b})$:

$$\pi^{(u,j',c')}_{(u,j,c)}(v',v_0' \mid v,v^0;w,\mathbf{b}) = \begin{cases} p^{(u,j',c')}_{(u,j,c)}(v,v^0 \mid x,t)\delta(v'-v)\delta(v_0'-v^0), & v > w, \mathbf{b} = (s,j,1) \\ 0, & \text{elsewhere} \end{cases} \quad (4.53)$$

where δ denotes the *delta-dirac* function, defined on any function $a(x)$ by the relation:

$$a(x) = \int a(y)\delta(y-x)\,\mathrm{d}\,y \quad (4.54)$$

Thus, the δ-dirac function in (4.53) delineates that an immediate lane-change does *not* affect the velocity v nor the desired velocity v^0 of the lane-changing vehicle. Note that the transition probability equals zero for all $v < w$ or $\mathbf{b} \neq (s,j,1)$ since these interactions do not require a remedial action of the interacting vehicle a, since a either interacts with a *faster vehicle* (passive interaction), or with a *constrained vehicle*.

Deceleration probability. The probability that a vehicle that interacts with a slower vehicle needs to decelerate, depends on the immediate lane-changing probability on the one hand, and the velocity w of the impeding platoon on the other hand. Let us define the probability that an immediate lane-change can occur irrespective of the destination lane j', by:

$$p^{*}_{(u,j,c)}(v,v_0 \mid x,t) = \sum_{c'=1,2} \sum_{j'=j\pm1} p^{(u,j',c')}_{(u,j,c)}(v,v_0 \mid x,t) \quad (4.55)$$

The magnitude of this probability depends on the probability that a driver wants to immediately change lanes when actively interacting with other vehicles. That is: does an immediate lane-change yield any benefits to the driver, and is the available gap on the target lane available and acceptable?

Let us now consider the event that a driver needs to reduce his velocity v to the velocity w of the impeding platoon. We find that the following specification of the transition probability models this instantaneous deceleration process for all events $\alpha = (w;\mathbf{b})$:

$$\pi^{(u,j,2)}_{(u,j,c)}(v',v'_0 \mid v,v^0;\alpha) = \begin{cases} (1-p^*_{(u,j,c)}(v,v^0 \mid x,t))\delta(w-v')\delta(v'_0-v^0), & v>w,\ \mathbf{b}=(s,j,1) \\ 0, & \text{elsewhere} \end{cases} \quad (4.56)$$

for $c = 1,2$, where we have assumed that the desired velocity v^0 of the impeded vehicle is unaffected by the interaction-event (as reflected by the second δ-dirac function). Again note that the transition probability equals zero for all $v < w$ or $\mathbf{b} \neq (s,j,1)$ since these interactions do not require a remedial action of the interacting vehicle a, since a either interacts with a *faster vehicle* (passive interaction), or with a *constrained vehicle*.

4.6.4 *Contribution to the MLMC gas-kinetic equations*

By considering all non-zero probabilities with respect to deceleration and immediate lane-changing (see Table 4-4), we can determine the resulting dynamics terms in the MLMC gas-kinetic equations (4.46). Let us first consider the result of interactions, followed by an instantaneous deceleration.

Deceleration

The *decrease-rate* due to vehicles with velocity v interacting with slower platoons with velocity w can be determined by substitution of (4.56) into expression (4.34), the *total decrease-rate due to vehicular interaction*:

$$(\partial_t \rho_{(u,j,c)})^-_{dec} = \int_{-\infty}^{v} \rho_{(u,j,c)}(x,v,v^0,t) \mid w-v \mid \tilde{\rho}_{(*,j,1)}(x,w,t)(1-p^*_{(u,j,c)}(v,v^0 \mid x,t))\,\mathrm{d}w \quad (4.57)$$

We often rewrite this expression by introducing the *event-type independent interaction-rate*:

$$\tilde{\Psi}_{(*,j)}(x,v,t) = \sum_{u'} \tilde{\Psi}_{(u',j)}(x,v,t) \text{ with } \tilde{\Psi}_{(u',j)}(x,v,t) \overset{def}{=} \int_{-\infty}^{v} \mid w-v \mid \tilde{\rho}_{(u',j,1)}(x,w,t)\,\mathrm{d}w \quad (4.58)$$

The event-type independent interaction rate describes the expected number of one-sided active interactions experienced by vehicles of $\mathbf{a} = (u,j,c)$ driving with velocity v with *slower vehicles* per vehicle per unit time, irrespective of the class and velocity of the *impeding vehicles*. Introducing this definition yields the following simplified expression for the decrease-rate due to deceleration:

$$(\partial_t \rho_{(u,j,c)})^-_{dec} = (1-p^*_{(u,j,c)}(v,v^0 \mid x,t))\rho_{(u,j,c)}(x,v,v_0,t)\tilde{\Psi}_{(*,j)}(x,v,t) \quad (4.59)$$

The *increase-rate* of $\rho_{(u,j,c)}$ due to deceleration is only relevant for constrained traffic, since for the transition probability to free-flowing traffic $p_{(u,j,c)}^{(u,j,1)} = 0$ holds (see Table 4-4). Substitution of expression (4.56) into (4.35) yields the increase-rate in $\rho_{(u,j,c)}(x,v,v_0,t)$ due to interactions of vehicles with velocity $w > v$, interacting with slower platoons driving with velocity $w = v$. Subsequent substitution into expression (4.36) yields the *total increase-rate due to vehicular interaction*:

$$(\partial_t \rho_{(u,j,c)})^+_{dec} = \sum_{c'=1,2} \int_{v}^{\infty} \rho_{(u,j,c')}(x,w,v^0,t) \mid w-v \mid \tilde{\rho}_{(*,j,1)}(x,v,t)(1-p^*_{(u,j,c')}(w,v_0 \mid x,t))\,\mathrm{d}w \quad (4.60)$$

Immediate lane-changing

With respect to immediate lane-changing, we find that $\rho_{(u,j,c)}$ *increases* due to vehicles changing lanes to either of the adjacent lanes $j\pm1$. The term reflecting the dynamic changes can be found by substituting the probability of an immediate lane-change $p_{(u,j,c)}^{(u,j',c')}$ into expression (4.33) yielding:

$$\begin{aligned}(\partial_t \rho_{(u,j,c)})^-_{ilc} &= \sum_{c'=1,2}\sum_{j'=j\pm1}\int_{-\infty}^{v}\rho_{(u,j,c)}(x,v,v_0,t)\,|\,w-v\,|\,\tilde{\rho}_{(*,j,1)}(x,w,t)(p_{(u,j,c)}^{(u,j',c')}(v,v_0\,|\,x,t))\,\mathrm{d}\,w \\ &= \sum_{c'=1,2}\sum_{j'=j\pm1}\rho_{(u,j,c)}(x,v,v_0,t)\,p_{(u,j,c)}^{(u,j',c')}(v,v_0\,|\,x,t)\tilde{\Psi}_{(*,j)}(x,v,t)\end{aligned} \tag{4.61}$$

By considering expression (4.35), we can determine the *increase* in the MLMC-PSD $\rho_{(u,j,c)}$ over time due to lane-changing:

$$\begin{aligned}(\partial_t \rho_{(u,j,c)})^+_{ilc} &= \sum_{c'=1,2}\sum_{j'=j\pm1}\int_{-\infty}^{v}\rho_{(u,j',c')}(x,v,v^0,t)\,|\,w-v\,|\,\tilde{\rho}_{(u,j',1)}(x,w,t)p_{(u,j',c')}^{(u,j,c)}(v,v_0\,|\,x,t))\,\mathrm{d}\,w \\ &= \sum_{c'=1,2}\sum_{j'=j\pm1}\rho_{(u,j',c')}(x,v,v^0,t)\,p_{(u,j',c')}^{(u,j,c)}(v,v_0\,|\,x,t)\,\tilde{\Psi}_{(*,j')}(x,v,t)\end{aligned} \tag{4.62}$$

4.6.5 Finite space requirements and modified interaction rate

In opposition to the relative size of particles in continuous media, the relative size of the *vehicular entities* is *not negligible*. The assumption that vehicles, and consequently vehicle platoons, have no physical length, leads to an *underestimation* of the number of interactions per unit time (see appendix B). To remedy this deficiency, appendix B shows how to incorporate the safe distance model described by Jepsen (1998), yielding the vehicle spacing correction factor $\delta_j(x,t) \geq 1$, which equals:

$$\delta_j(x,t) = (1-\textstyle\sum_{u'\in\mathbf{U}} r_{(u',j)}(d_{u'}^{min} + L_{u'} + V_{(u',j)}T_{u'} + (V_{(u',j)}^2 + \Theta_{(u',j)})F_{u'})^{-1} \tag{4.63}$$

In appendix B we also show that the *modified interaction rate*, describing the expected number of interactions $\alpha = (w,\mathbf{b})$ experienced by vehicles driving with velocity v on lane j with a slower platoons led by vehicles with discrete attributes $\mathbf{b} = (u'j,1)$ with velocity w equals:

$$\hat{\Pi}_{(u,j,c)}(x,v,v^0,t;w,\mathbf{b}) = \delta_j(x,t)\Pi_{(u,j,c)}(x,v,v^0,t;w,\mathbf{b}) \tag{4.64}$$

That is, the expected number of interactions events α is increased by the correction factor $\delta_j \geq 1$. The expected number of interactions events α per unit time and per unit unoccupied roadway space of vehicles of class u driving on lane j with velocity v, while having desired velocity v^0 and being of state c, equals:

$$\hat{\rho}_{(u,j,c)}(x,v,v^0,t)\hat{\Pi}_{(u,j,c)}(x,v,v^0,t;w,\mathbf{b}) = \delta_j^2(x,t)\rho_{(u,j,c)}(x,v,v^0,t)\Pi_{(u,j,c)}(x,v,v^0,t;w,\mathbf{b})^* \tag{4.65}$$

Note that when all space is used, we have $\delta_j \to \infty$. This case reflects traffic in which all vehicles are platooning. Let us consider a single vehicle that drives at a higher velocity than the

---

* In the remainder of this chapter, the hat is dropped for notational convenience. That is, unless explicitly stated the finite space requirements are incorporated in the model.

other vehicles. Since $\delta_j \to \infty$, the faster vehicle will instantaneously interact with slower vehicles, and will consequently need to adapt to the velocity of the slower vehicles.

4.7 Specification of condition-driven non-continuum processes

In addition to the event-driven immediate lane-changing process, also condition-driven processes are relevant in the description of MLMC traffic flow operations. In this respect, condition-driven processes are caused by the condition of a vehicle, reflected by the attributes $(\mathbf{a},\mathbf{v},\mathbf{v}^0)$. For example, the *condition* can either be the state of the vehicle, the lane it is occupying, or its longitudinal position (e.g. nearby an on-ramp).

In this section, we will specify the conditions causing changes in $\rho_{(u,j,c)}$. In this respect, we will distinguish between three types of transitions, namely *postponed lane-changes*, *spontaneous lane-changes*, and *relaxation of the constrained state*. The first is caused by drivers aiming to relieve their constrained state by lane-changing, while the second is caused by drivers' preferences for a particular lane. The latter type is a result of the disappearance of platoon leaders, for example due to lane-changing. Table 4-5 summarises the relevant non-zero transition-rates.

Table 4-5: Non-zero rates describing transitions from attributes a to attributes a'.

TO: \ FROM:	unconstrained vehicles $\rho_{(u,j,1)}(x,v,v^0,t)$	constrained vehicles $\rho_{(u,j,2)}(x,v,v^0,t)$
unconstrained vehicles $\rho_{(u,j\pm1,1)}(x,v,v^0,t)$	spontaneous lane-changing $\Delta^{(u,j\pm1,1)}_{(u,j,1)}(v;\beta)$	postponed lane-changing $\Delta^{(u,j\pm1,2)}_{(u,j,2)}(v;\beta)$
unconstrained vehicles $\rho_{(u,j,1)}(x,v,v^0,t)$	N/A.	relaxation $\Delta^{(u,j,1)}_{(u,j,2)}(v;\beta)$

4.7.1 Postponed lane-changing

We have described the process of vehicles being unable to perform an immediate lane-change after catching up with a slower platoon, instantaneously reduce their velocity and join the impeding platoon. Additionally, we assume that some of these platooning vehicles aim to change to either adjacent lane, as soon as the opportunity to improve their traffic conditions arises, by performing a so-called *postponed lane-change*. Figure 4-8 depicts a postponed lane-changing manoeuvre in the *xt*-plane. In this case, the postponed lane-change yields two transitions: first, the constrained vehicle changes to the adjacent lane j+1, while secondly, its constrained state is relieved. After the lane-change has occurred, the driver is able to accelerate towards his desired velocity, until he is impeded by another vehicle. We will model the postponed lane-changes using the *postponed lane-change rates*; $\Delta_{(u,j,2)}^{(u,j\pm1,1)}$ is the rate at which vehicles $\rho_{(u,j,2)}(x,v,v^0,t)$ can change lanes to either lane j–1 or lane j+1.

Principally, the constrained vehicle may join a faster platoon on the target-lane. However, since we do not allow discontinuous jumps in the velocity as a result of the lane-changing process, the vehicle performing a postponed lane-change is unable to instantaneously keep up with the faster platoon, and will consequently become unconstrained, almost immediately after the lane-change.

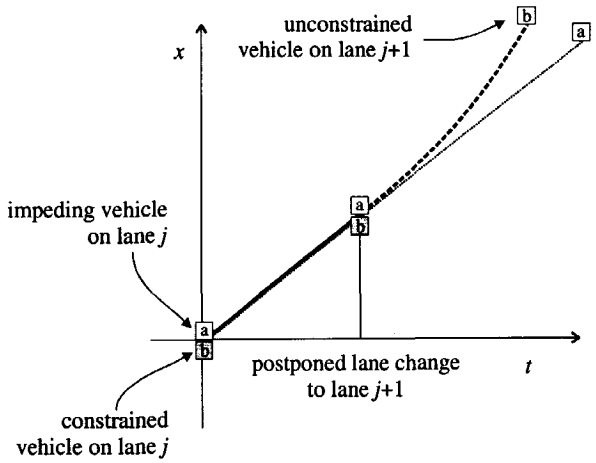

Figure 4-8: Postponed lane-change from lane *j* to lane *j*+1.

Again, we will determine the lane-changing rates by hypothesising that the constrained state of a driver yields the incentive for a lane-change. Thus, a constrained driver will only consider a postponed lane-change if the adjacent lanes are appropriate target lanes and if he can improve his driving conditions by performing a lane-change.

When either the left or the right lane is chosen, and if the gap on the target-lane is considered of adequate size, the driver performs a postponed lane-change. If he does not accept the gap on the destination lane, the driver will reconsider his primary target-lane choice and choose the secondary target-lane.

In opposition to the immediate lane-changing process, the postponed lane-change – and the spontaneous lane-change as well – has a *continuous* nature: the constrained driver will continuously check whether:

1. either of the adjacent lanes will improve his driving conditions, and
2. an acceptable gap is available.

Let us define the following events:

$A_{(u,j,2)}^{(u,j\pm1,1)}(v;\mathrm{d}t)$: a *platooning* vehicle of class u driving at velocity v *actually changes* from its current lane j to lane $j\pm1$ in an interval of (infinitesimal) length $\mathrm{d}t$;

$B_{(u,j,2)}^{(u,j\pm1,1)}(v;\mathrm{d}t)$: a *platooning* vehicle of class u driving at velocity v *can* change lanes from its current lane j to lane $j\pm1$ in an interval of (infinitesimal) length $\mathrm{d}t$, in the event that it is desired to do so.

The probability that a constrained vehicle on lane j can change to either of the adjacent lanes within an interval $\mathrm{d}t$ can be expressed in terms of the lane-changing intensities. That is:

$$\Pr(A_{(u,j,2)}^{(u,j\pm1,1)}(v;\mathrm{d}t)) \overset{def}{=} \Delta_{(u,j,2)}^{(u,j\pm1,1)}(v)\mathrm{d}t \tag{4.66}$$

Moreover, the probability that within an interval dt the opportunity arises for a vehicle on lane j to change to an adjacent lane equals:

$$\Pr(B^{(u,j\pm1,1)}_{(u,j,2)}(v;dt)) \overset{def}{=} \Lambda^{(u,j\pm1,1)}_{(u,j,2)}(v)dt \tag{4.67}$$

We can establish the following expression:

$$\Delta^{(u,j-1,1)}_{(u,j,2)}dt = \gamma_{(u,j)}\Lambda^{(u,j-1,1)}_{(u,j,2)}\Lambda^{(u,j+1,1)}_{(u,j,2)}dt^2 + \Lambda^{(u,j-1,1)}_{(u,j,2)}dt(1-\Lambda^{(u,j+1,1)}_{(u,j,2)}dt) \approx \Lambda^{(u,j-1,1)}_{(u,j,2)}dt \tag{4.68}$$

where $\gamma_{(u,j)} = \gamma_{(u,j)}(v)$ expresses the probability that the driver chooses lane j–1, while both lanes are available. From equation (4.68) we see that the probability that two lanes become available within the same infinitesimal period is negligible. Therefore, we also have:

$$\Delta^{(u,j+1,1)}_{(u,j,2)}(v)dt \approx \Lambda^{(u,j+1,1)}_{(u,j,2)}(v)dt \tag{4.69}$$

Note that since European traffic regulations only allow lane-changing on the left lane j+1, for dilute traffic we have:

$$\Delta^{(u,j-1,1)}_{(u,j,2)}(v) = \Lambda^{(u,j-1,1)}_{(u,j,2)}(v) = 0 \tag{4.70}$$

Of course, we also have:

$$\Delta^{(u,0,1)}_{(u,1,2)}(v) = \Lambda^{(u,0,1)}_{(u,1,2)}(v) = 0 \quad \text{and} \quad \Delta^{(u,M+1,1)}_{(u,M,2)}(v) = \Lambda^{(u,M+1,1)}_{(u,M,2)}(v) = 0 \tag{4.71}$$

Contributions to the MLMC gas-kinetic equations

To determine the contributions to the MLMC gas-kinetic equations, we must incorporate the assumption that a postponed lane-change does not result in a velocity change instantaneously. This is again modelled using the delta-dirac functions, yielding:

$$\phi^{(u',j',c')}_{(u,j,c)}(v', v_0' \mid v, v^0) = \Delta^{(u',j',c')}_{(u,j,c)}(v \mid x,t)\delta(v'-v)\delta(v_0'-v^0) \tag{4.72}$$

By substituting these expressions for the postponed lane-changing rate in equation (4.40), we find that the rate of change in $\rho_{(u,j,2)}(x,v,v_0,t)$ caused by postponed lane-changing is determined by the postponed lane-changing rate multiplied by $\rho_{(u,j,2)}(x,v,v_0,t)$:

$$(\partial_t\rho_{(u,j,2)})^-_{plc} = \sum_{j'=j-1,j+1}\Delta^{(u,j',1)}_{(u,j,2)}(v \mid x,t)\rho_{(u,j,2)}(x,v,v^0,t) \tag{4.73}$$

Previously constrained vehicles $\rho_{(u,j',2)}(x,v,v^0,t)$ able to execute a postponed lane-changing manoeuvre to j cause an increase in $\rho_{(u,j,1)}(x,v,v^0,t)$ (equation (4.41)):

$$(\partial_t\rho_{(u,j,2)})^+_{plc} = \sum_{j'=j-1,j+1}\Delta^{(u,j,1)}_{(u,j',2)}(v \mid x,t)\rho_{(u,j',2)}(x,v,v^0,t) \tag{4.74}$$

4.7.2 Spontaneous lane-changing

If an unconstrained driver prefers a specific lane, he may decide to perform a *spontaneous lane-change*. Since this process is similar to the postponed lane-changing process – although the reason for lane-changing is different – it yields comparable expressions.

For European traffic regulations, this 'spontaneous' lane-changing process to a large extent results from vehicles which have overtaken slower vehicles using the left lane returning to

their origin lane. In this case, no spontaneous lane-changes to the left lane occur. Thus, the *spontaneous lane-changing rates* $\Delta_{(u,j,1)}^{(u,j',1)}$ satisfy:

$$\Delta_{(u,j,1)}^{(u,j+1,1)}(v \mid x,t) = 0 \tag{4.75}$$

If we consider American traffic regulations, the spontaneous lane-changes result from drivers having a distinct preference for a specific lane. That is, a vehicle changes to the left lane if he prefers to be on any of lanes left of his current lane.

Contributions to the MLMC gas-kinetic equations

We have assumed that unconstrained drivers only change lanes if they remain unconstrained. Then spontaneous lane-changing yields the following contribution to the dynamics of the unconstrained MLMC-PSD (equation (4.40)):

$$(\partial_t \rho_{(u,j,1)})_{slc}^{-} = \Delta_{(u,j,1)}^{(u,j\pm1,1)}(v \mid x,t)\rho_{(u,j,1)}(x,v,v^0,t) \tag{4.76}$$

and thus (equation (4.41)):

$$\partial_t \rho_{(u,j,1)}{}_{slc}^{+} = \sum_{j'=j-1,j+1} \Delta_{(u,j',1)}^{(u,j,1)}(v \mid x,t)\rho_{(u,j',1)}(x,v,v^0,t) \tag{4.77}$$

4.7.3 Relaxation due to vanishing impeding vehicles

When an unconstrained platoon leader changes lanes to either adjacent lane, the constrained vehicle directly following the lane-changing vehicle is unconstrained. This can in itself yield a relaxation of other vehicles. Since this process is very complex, we will assume that the process can be modelled by taking:

$$\phi_{(u,j,2)}^{(u,j,1)}(v',v_0' \mid v,v_0) = \Xi(\Delta_{(u,j,1)}^{(u,*,1)}\rho_{(u,j,1)}(x,v,v_0,t))\delta(v'-v)\delta(v_0'-v_0) \tag{4.78}$$

yielding:

$$(\partial_t \rho_{(u,j,1)})_{rel}^{+} = \Xi(\Delta_{(u,j,1)}^{(u,j,1)}\rho_{(u,j,1)}(x,v,v_0,t))\rho_{(u,j,2)}(x,v,v_0,t) \tag{4.79}$$

and:

$$(\partial_t \rho_{(u,j,2)})_{rel}^{-} = \Xi(\Delta_{(u,j,1)}^{(u,*,1)}\rho_{(u,j,1)}(x,v,v_0,t))\rho_{(u,j,2)}(x,v,v_0,t) \tag{4.80}$$

where Ξ is a monotonically increasing function of the expected number of spontaneous lane-changes per unit time of unconstrained vehicles driving at a velocity equal to v.

4.8 MLMC gas-kinetic traffic flow equations

In this section we establish the gas-kinetic equations for unconstrained, constrained and mixed-state traffic, by combining the contributions of the continuum (section 4.4) and non-continuum processes (sections 4.6 and 4.7). In this way we establish three mesoscopic traffic flow models applicable to traffic in different states.

4.8.1 *Gas-kinetic equation for unconstrained traffic (c = 1)*

Let us first consider $\rho_{(u,j,1)}(x,v,v^0,t)$. Combining the special continuity equation (4.47) for unconstrained traffic with the specifications for the non-continuum processes derived in sections 4.6 and 4.7, yields the *special continuity equation for platoon-leaders* ($c = 1$)*:

$$\begin{aligned}
&\partial_t \rho_{(u,j,1)} + \underbrace{\partial_x(\rho_{(u,j,1)} v)}_{(1)} + \underbrace{\partial_v(\rho_{(u,j,1)}(v^0 - v)/\tau_u^0)}_{(2)} = \underbrace{-(1 - p^*_{(u,j,1)}(v))\,\tilde{\Psi}_{(*,j)}(v)\rho_{(u,j,1)}}_{(4)} \\
&\quad \underbrace{- \sum_{j'=j\pm1} (p^{(u,j',1)}_{(u,j,1)}(v)\tilde{\Psi}_{(*,j)}(v)\rho_{(u,j,1)} - p^{(u,j,1)}_{(u,j',1)}(v)\tilde{\Psi}_{(*,j')}(v)\rho_{(u,j',1)})}_{(6)} \\
&\quad + \underbrace{\sum_{j'=j\pm1} p^{(u,j,1)}_{(u,j',2)}(v)\tilde{\Psi}_{(*,j')}(v)\rho_{(u,j',2)}}_{(7)} + \underbrace{\sum_{j'=j\pm1} \Delta^{(u,j,1)}_{(u,j',2)}(v)\rho_{(u,j',2)}}_{(9)} \\
&\quad + \underbrace{\Xi(\Delta^{(u,*,1)}_{(u,j,1)}\rho_{(u,j,1)})\rho_{(u,j,2)}}_{(5)} - \underbrace{\sum_{j'=j\pm1} (\Delta^{(u,j',1)}_{(u,j,1)}(v)\rho_{(u,j,1)} - \Delta^{(u,j,1)}_{(u,j',1)}(v)\rho_{(u,j',1)})}_{(8)}
\end{aligned} \tag{4.81}$$

for all $u \in \mathbf{U}$ and $j = 1,\ldots,M$. The special continuity equations of $\rho_{(u,j,1)}(x,v,v^0,t)$ reflect the dynamics of processes causing dynamic changes. Let us briefly discuss these processes.

Longitudinal processes affecting the unconstrained MLMC-PSD are (see Figure 4-2):

1. *Convection.* Changes in the unconstrained MLMC-PSD due to the longitudinal inflow and outflow of unconstrained vehicles (equation (4.3)).
2. *Acceleration.* Changes caused by vehicles accelerating towards their desired velocity (equation (4.11)).
4. *Deceleration caused by interaction.* The unconstrained MLMC-PSD *decreases* due to actively interacting vehicles unable to immediately overtake the impeding vehicle or platoon (equation (4.60)).
5. *State transition.* The unconstrained MLMC-PSD *increases* due to state transitions from constrained traffic to unconstrained traffic (equation (4.79)).

Lateral processes governing the unconstrained MLMC-PSD dynamics are (Figure 4-3):

6. *Unconstrained immediate lane-changing.* Changes due to balancing the inflow and outflow of immediately lane-changing free-flowing vehicles to and from the adjacent lanes (expression (4.61) and (4.62)).
7. *Constrained immediate lane-changing.* Increases caused by the inflow of immediately lane-changing platooning vehicles from the adjacent lanes (expression (4.61) and (4.62)).

* The *numbering of terms* in this gas-kinetic equations is chosen such that the terms correspond to the terms depicted in Figure 4-2 and Figure 4-3; the *order of the terms* is the same as the order of the generalised gas-kinetic equation (4.46).

8. *Spontaneous lane-changing.* Changes due to balancing the inflow and outflow caused by spontaneously lane-changing vehicles to and from the adjacent lanes (equations (4.76) and (4.77)).
9. *Postponed lane-changing.* Increases due to postponed lane-changing vehicles from the adjacent lanes to the current lane (expression (4.74)).

4.8.2 *Gas-kinetic equation for constrained traffic (c = 2)*

Considering the special continuity equation (4.47) for $\rho_{(u,j,2)}(x,v,v^0,t)$ and the non-continuum processes influencing constrained traffic, the dynamics of $\rho_{(u,j,2)}(x,v,v^0,t)$ are:

$$\begin{aligned}\partial_t\rho_{(u,j,2)} &+ \underbrace{\partial_x(\rho_{(u,j,2)}v)}_{(1)} + \underbrace{\partial_v(\rho_{(u,j,2)}(W_{(u,j,2)}(v)-v)/\tau_{(u,j,2)})}_{(2)} = \underbrace{-(1-p^*_{(u,j,2)}(v))\rho_{(u,j,2)}\tilde{\Psi}_{(*,j)}(v)}_{(4)} \\ &+ \underbrace{\tilde{\rho}_{(*,j,1)}\sum_{c'=1,2}\int_v^\infty |w-v|(1-p^*_{(u,j,c')}(w))\rho_{(u,j,c')}(w,v^0)\,\mathrm{d}w}_{(3)} \\ &- \underbrace{\sum_{j'=j\pm1}(p^{(u,j',1)}_{(u,j,2)}\tilde{\Psi}_{(*,j)}(v)\rho_{(u,j,2)} - p^{(u,j,2)}_{(u,j',2)}\tilde{\Psi}_{(*,j')}(v)\rho_{(u,j',2)})}_{(7)} \\ &- \underbrace{\Xi(\Delta^{(u,*,1)}_{(u,j,1)}\rho_{(u,j,1)})\rho_{(u,j,2)}}_{(5)} - \underbrace{\sum_{j'=j\pm1}\Delta^{(u,j',1)}_{(u,j,2)}\rho_{(u,j,2)}}_{(8)}\end{aligned} \tag{4.82}$$

for all $u \in \mathbf{U}$ and $j = 1,\ldots,M$. From these special continuity equations we see that $\rho_{(u,j,2)}(x,v,v^0,t)$ changes, due to different processes. Let us briefly clarify these processes.

Longitudinal processes affecting the constrained MLMC-PSD are (Figure 4-2):

1. *Convection.* Changes due to the longitudinal inflow and outflow of constrained vehicles of user-class u on lane j (equation (4.3)).
2. *Platoon acceleration.* The constrained vehicles in the platoon are assumed to accelerate towards the expected desired velocity of platoon leaders (equation (4.22)).
3. *Deceleration of faster vehicles.* Increases due to interacting free-flowing and constrained vehicles decelerating *to* velocity v (equation (4.61)).
4. *Deceleration caused by slower vehicles.* Decreases caused by constrained vehicles decelerating to a lower velocity when interacting without being able to immediately change lanes (equation (4.61)).
5. *State transitions.* Decreases caused by previously constrained vehicles changing states (expression (4.80)).

Lateral processes governing the dynamics of $\rho_{(u,j,2)}(x,v,v^0,t)$ are (Figure 4-3):

7. *Constrained immediate lane-changing.* Changes due to the balance between immediately lane-changing constrained vehicles on lane j and lanes $j\pm1$ (equation (4.61) and (4.62)).

9. *Postponed lane-changing*. Decreases that are caused by postponed lane-changing vehicles (equation (4.74)).

*4.8.3 Special continuity equation for mixed-state traffic (c = *)*

The fraction of constrained vehicles is defined by:

$$\theta_{(u,j)}(x,v,v^0,t) \overset{def}{=} \rho_{(u,j,2)}(x,v,v^0,t)/\rho_{(u,j)}(x,v,v^0,t) \tag{4.83}$$

The gas-kinetic equation for *mixed-state traffic* can be determined easily from the matrix-vector expression (4.46) where the vector of event-rates $\vec{\Pi}$, and the matrices **P** and **F** are specified according to the relations discussed in this section, by right-multiplying with the aggregation-matrix $\mathbf{S}_3$ (see chapter 3). By doing so, we find the following equation for $\rho_{(u,j)}$:

$$\begin{aligned}
&\partial_t \rho_{(u,j)} + \underbrace{\partial_x(\rho_{(u,j)}v)}_{(1)} + \underbrace{\partial_v(\rho_{(u,j)}(W_{(u,j)}(v)-v)/\tau_{(u,j)})}_{(2)} = \underbrace{-(1-p^*_{(u,j)}(v,v^0))\tilde{\Psi}_{(*,j)}(v)\rho_{(u,j)}}_{(4)} \\
&\quad + \underbrace{(1-\theta_{(*,j)})\tilde{\rho}_{(*,j,1)}\int_v^\infty |w-v|(1-p^*_{(u,j)}(w,v^0))\rho_{(u,j)}(w,v^0)\,\mathrm{d}w}_{(3)} \\
&\quad - \underbrace{\sum_{j'=j\pm1}(p^{(u,j')}_{(u,j)}(v)\tilde{\Psi}_{(*,j)}(v)\rho_{(u,j)} - p^{(u,j)}_{(u,j')}(v)\tilde{\Psi}_{(*,j')}(v)\rho_{(u,j')})}_{(6+7)} \\
&\quad - \underbrace{\sum_{j'=j\pm1}(\Delta^{(u,j')}_{(u,j)}(v,v^0)\rho_{(u,j)} - \Delta^{(u,j)}_{(u,j')}(v,v^0)\rho_{(u,j')})}_{(8+9)}
\end{aligned} \tag{4.84}$$

for all $u \in \mathbf{U}$ and $j = 1,\ldots,M$, where we have used the following definition:

$$\Delta^{(u,j')}_{(u,j)}(v,v_0 \mid x,t) \overset{def}{=} \frac{1}{\rho_{(u,j)}(x,v,v_0,t)} \sum_{c'=1,2}(\Delta^{(u,j',1)}_{(u,j,c')}(v \mid x,t)\rho_{(u,j,c')}(x,v,v_0,t)) \tag{4.85}$$

describing the *state-independent lane-changing rates* of class u from lane j to lane, caused by both postponed lane-changing and spontaneous lane-changing. Moreover, we have defined the *state-independent* immediate lane-changing probability by:

$$p^{(u,j')}_{(u,j)}(v,v_0 \mid x,t) \overset{def}{=} \frac{1}{\rho_{(u,j)}(x,v,v_0,t)} \sum_{c'=1,2}(p^{(u,j',*)}_{(u,j,c')}(v \mid x,t)\rho_{(u,j,c')}(x,v,v_0,t)) \tag{4.86}$$

These reflect the unconditional probability that a vehicle is able to immediately change lanes after interacting with a slower platoon. Let us remark that $p_{(u,j)}{}^{(u,j')}$ equals the probability that a vehicle is either 1) free-flowing, and can perform an unconstrained immediate lane-change *or* 2) platooning, and can perform a constrained lane-change.

Let us again explain the different terms in the special continuity equation of the $\rho_{(u,j)}$. The *longitudinal processes* governing the dynamics of $\rho_{(u,j)}(x,v,v^0,t)$ are (Figure 4-2):

1. *Convection.* Changes caused by the inflow and outflow of state traffic.
2. *Acceleration.* Changes due to unconstrained vehicles, and the constrained vehicles following them, accelerating towards the desired velocity of the former vehicles.
3. *Deceleration of faster vehicles.* Decreases over time due to vehicles driving with velocity v slowing down to a lower velocity w.
4. *Deceleration caused by slower vehicles.* On the other hand, $\rho_{(u,j)}(x,v,v^0,t)$ *increases* over time by vehicles being slowed down to velocity v.

The *lateral processes* governing the dynamics of $\rho_{(u,j)}(x,v,v^0,t)$ are (Figure 4-3):

6^{+7}. *Immediate lane-changing.* Changes caused by the balancing the outflow to and the inflow from adjacent lanes, caused by actively interacting vehicles able to immediately overtake.

8^{+9}. *Postponed and spontaneous lane-changing.* Changes caused by balancing the outflow to and the inflow from adjacent lanes, caused by postponed lane-changing and spontaneous lane-changing.

4.9 Relation with aggregate-lane and aggregate user-class equations

In this section, we show that the multilane special continuity equations established in the previous sections are generalisations of earlier special continuity equations for both multiple user-class traffic flow and single user-class traffic flow. In this section, we will show that the aggregate-lane and single user-class conditions are special cases of the MLMC model presented in this thesis.

4.9.1 Aggregate-lane MLMC gas-kinetic equations

To show that the MLMC gas-dynamic model is a multilane multiclass generalisation of other gas-kinetic models presented in the literature, we *aggregate* (4.84) with respect to the lane, the user-class, or both.

Let us first consider the aggregation with respect to the roadway lanes. To this end, the gas-kinetic equations cast in vector-matrix notation (4.46) are left-multiplied with $\mathbf{S}_2\mathbf{S}_3$ (see section 3.8) yielding aggregation with respect to both the lanes and driver state. This yields the *multiclass gas-kinetic flow equations* for the $\rho_u(x,v,v^0,t)$:

$$\partial_t\rho_u + v\partial_x\rho_u + \partial_v(\rho_u(W_u(v)-v)/\tau_u) = \\ -(1-p_u^*)\sum_{u'\in U}\left(\rho_u(v,v^0)\int_{w<v}|w-v|\,\tilde{\rho}_{(u',*,1)}(w)\,\mathrm{d}w - \tilde{\rho}_{(u',*,1)}\int_{w>v}|w-v|\,\rho_u(w,v^0)\,\mathrm{d}w\right) \tag{4.87}$$

where the aggregate-lane mixed-state acceleration time τ_u and the aggregate-lane mixed-state acceleration velocity respectively satisfy:

$$\rho_u/\tau_u = \sum_j(\rho_{(u,j)}/\tau_{(u,j)}) \quad \text{and} \quad W_u(v) = \frac{\sum_j(\rho_{(u,j)}W_{(u,j)}(v)/\tau_{(u,j)})}{\sum_j(\rho_{(u,j)}/\tau_{(u,j)})} \tag{4.88}$$

for all $u \in \mathbf{U}$. Note that the terms describing the lane-changing processes cancel each other out. Consequently, the influence of lane-changing is only reflected by the interaction term, where p_u^* describes the probability that an immediate lane-change occurs.

The special continuity equations (4.87) are similar to the special continuity equations for heterogeneous traffic flow established by Hoogendoorn and Bovy (1998a,b). Nevertheless, they differ from the latter model in two respects. First, the term reflecting vehicular interactions is different. In the sequel we show that this holds equally for the traditional models of Prigogine and Herman (1971), Paveri-Fontana (1975), and Helbing (1996,1997). Secondly, the assumption that platooning vehicles accelerate towards the desired velocity of the platoon leader is included in the developed MLMC model (see also Hoogendoorn and Bovy (1999)).

4.9.2 Aggregate-lane aggregate-class special continuity equation

By left-multiplication of the gas-kinetic equations cast in vector-matrix notation (4.46) by the matrix $\mathbf{S}_1\mathbf{S}_2\mathbf{S}_3$, we find the gas-kinetic equations for the Phase-Space Density ρ:

$$\partial_t \rho + v\partial_x \rho + \partial_v(\rho(W(v)-v)/\tau) = \\ -(1-p^*)\left(\rho(v,v^0)\int_{w<v}|w-v|\tilde{\rho}_{(*,*,1)}(w)\mathrm{d}w - \tilde{\rho}_{(*,*,1)}(v)\int_{w>v}|w-v|\rho(w,v^0)\mathrm{d}w\right) \tag{4.89}$$

If we compare result (4.89) with the gas-kinetic equations of Paveri-Fontana (1975), and the aggregate lane single class of Helbing (1996,1997), we observe that the main difference are specification of the interaction term and the acceleration process. The latter difference is again caused by the assumption made by among others Paveri-Fontana (1975), and Helbing (1997a) that only constrained vehicles are able to accelerate.

We recall from chapter 2 that the interaction term in the Paveri-Fontana model equals:

$$(\partial_t \rho)_{int}^{active} = -(1-p^*)\left(\rho(v,v^0)\int_{w<v}|w-v|\tilde{\rho}(w)\mathrm{d}w - \tilde{\rho}(v)\int_{w>v}|w-v|\rho(w,v^0)\mathrm{d}w\right) \tag{4.90}$$

Paveri-Fontana assumes that vehicles have no physical length. Moreover, a vehicle located on x at instant t having interacted with a slower vehicle, immediately decelerates to the velocity of the impeding vehicle, thereby forming a two vehicle-platoon, which necessarily also has no physical length. From this viewpoint, the interaction term *must be a function of the number of platoons*, rather than the total number of vehicles. Rather, due to the infinitesimal vehicle length assumption, these platoons can be described by the free-flowing PSD. Consequently, we conclude that the Paveri-Fontana interaction paradigm yields *overestimation* of the number of interactions, especially when the fraction of constrained vehicles is high (e.g. during constrained traffic operations). This holds equally for the multiclass model of Hoogendoorn and Bovy (1998), and the multilane model of Helbing (1998).

4.10 Description of flow dynamics of individual vehicles

In the previous section, we have discussed the dynamics of aggregate-lane aggregate-class traffic flow. Let us now instead consider the reverse case. That is, we consider the mixed-state MLMC dynamics from the viewpoint of individual vehicles a, i.e. the case where each

vehicle represents a separate class. In the general case, the velocity and the desired velocity of vehicle a is represented by a distribution function $G_a(v,v^0;x,t)$. Let us assume that G_a is a continuous differentiable function of v and v^0. The Phase-Space Density $\rho_a(x,v,v^0,t)$ of an individual vehicle a is defined by this probability distribution function, i.e.:

$$\rho_a(x,v,v^0,t) = r_a(x,t)g_a(v,v^0;x,t) \tag{4.91}$$

where $r_a(x,t)$ is the density of vehicle a. The value $r_a(x,t)\mathrm{d}x$ can be interpreted as the probability that a is located at the interval $[x,x+\mathrm{d}x)$ at instant t. Clearly:

$$\lim_{x\to\infty} N_a(x,t) = 1, \quad \text{where} \quad N_a(x,t) \overset{def}{=} \int_{-\infty}^{x} r_a(x',t)\mathrm{d}x' \tag{4.92}$$

Thus, the Phase-Space Density of a can be considered as the joint probability density function of location x, velocity v and desired velocity v^0 at instant t. Moreover, by extending the Phase-Space Density by the lane index j, we can consider the probability density function of location x, velocity v, desired velocity v^0, and lane j at instant t. Let us remark that:

$$\rho_a(x,v,v^0,t) \overset{def}{=} \sum_{j'=1}^{M} \rho_{(a,j')}(x,v,v^0,t) \tag{4.93}$$

Let us now consider the special continuity equations for *mixed-state* traffic flow (4.83). For the sake of notational simplicity, let us assume that immediate lane-changing probabilities and lane-changing rates of vehicle a on lane j are independent on its velocity and desired velocity. Since the event-independent interaction rate equals:

$$\tilde{\Psi}_{(*,j)}(v) = \sum_b \int_{w<v} |w-v|(1-\tilde{\theta}_{(b,j)}(w))\tilde{\rho}_{(b,j)}(w)\,\mathrm{d}w \tag{4.94}$$

where $\tilde{\theta}_{(b,j)}(w)$ denotes the probability that vehicle b, driving with velocity w on lane j is platooning. Then, equation (4.95) describing dynamic changes in the ML-PSD of vehicle a can be established:

$$\begin{aligned}
&\partial_t \rho_{(a,j)} + \overbrace{\partial_x(v\rho_{(a,j)})}^{I} + \overbrace{\partial_v(\rho_{(a,j)}(W_{(a,j)}-v)/\tau_{(a,j)})}^{II} = \\
&\quad - \overbrace{(1-p^*_{(a,j)})\sum_b \rho_{(a,j)}(v,v^0)\int_{w<v}|w-v|(1-\tilde{\theta}_{(b,j)}(w))\tilde{\rho}_{(b,j)}(w)\,\mathrm{d}w}^{IVa} \\
&\quad + \overbrace{(1-p^*_{(a,j)})\sum_b (1-\tilde{\theta}_{(b,j)}(v)\tilde{\rho}_{(b,j,1)}(v)\int_{w>v}|w-v|\rho_{(a,j)}(w,v^0)\,\mathrm{d}w}^{IVa} \\
&\quad - \overbrace{\sum_{j'=j\pm1}(p^{(a,j')}_{(a,j)}\tilde{\Psi}_{(*,j)}(v)\rho_{(a,j)} - p^{(a,j)}_{(a,j')}\tilde{\Psi}_{(*,j')}(v)\rho_{(a,j')})}^{IVb} - \overbrace{\sum_{j'=j\pm1}(\Delta^{(a,j')}_{(a,j)}\rho_{(a,j)} - \Delta^{(a,j)}_{(a,j')}\rho_{(a,j')})}^{IVc}
\end{aligned} \tag{4.95}$$

Equation (4.95) shows how the ML-PSD $\rho_{(a,j)}(x,v,v^0,t)$ of vehicle a on lane j changes over time due to convection (I), acceleration (II), deceleration and immediate lane-changing after interaction with vehicles b (IVa and IVb), and postponed/spontaneous lane changing (IVc).

4.10.1 Reconsideration of interactions

When considering MLMC traffic flow, vehicles of class u may interact with both vehicles of class u as well as with vehicles of other classes s. However, considering the generalisation to single-vehicle classes, this is not longer the case. By definition, vehicle a can only interact with vehicles $b \neq a$ (i.e. other classes). However, both the deceleration term as well as the immediate lane-changing term (IVa and IVb of eq. (4.95)) show that also within vehicle interactions are considered ($b = a$). For the single-vehicle class case, this can be remedied by excluding class a from summation in term IVa of eq. (4.95) and in eq. (4.94).

This inconsistency is not an artefact of the transition to describing dynamics of individual vehicles. Principally, it is also present in the aggregate-vehicle model dynamics. That is, the number of interactions is modelled too high, due to fact that the model dynamics assume that vehicles also interact with themselves. To solve this incorrectness, within-vehicle interactions must be excluded. These modifications should lead to a (slightly) reduced influence of within class interaction. However, in this stage, no correct modification of the interaction process has been developed.

4.11 Use of generalised gas-kinetic equations

The potential applications of the MLMC gas-kinetic equations are various, and some of these applications are discussed in this section.

4.11.1 Mesoscopic simulation and particle discretisation

An interesting application is the use of the mesoscopic MLMC model for mesoscopic traffic flow simulation. To this end, the gas-kinetic equations need to be numerically approximated using dedicated solution approaches, for instance using a *finite volume approach* describing the dynamics of the average Phase-Space Density $\rho_{(u,j,c)}[i,n,m]$ in a discretisation volume defined in the phase-space (comparable to the finite volume approach applied to the macroscopic model equations presented in chapter 9).

Another option would be to apply a *particle discretisation method* to derive a numerical solution by *microscopic simulation* (cf. Hockney and Eastwood (1988)). Basically, the particle discretisation approach to gas-kinetic MLMC traffic flow equations is a mixed microscopic/mesoscopic approach. The time-space behaviour of each individual vehicle is distinguished and described separately. Based on the characteristics of these vehicles (e.g. position, velocity), the aggregate traffic situation on finite-size cells i defined by the region $[(i-1/2)\Delta x,(i+1/2)\Delta x)$ is approximated (e.g. traffic density, velocity distribution). Based on these aggregate traffic conditions, the stochastic behaviour of vehicles in the cell is established, based on for instance the probability that given prevailing cell conditions an interaction with another vehicle occurs. Hoogendoorn and Bovy (2000) have successfully applied a particle discretisation approach to gas-kinetic equations describing pedestrian flow.

4.11.2 Establishing equilibrium relations

Also, the generalised gas-kinetic model can be used to analyse the equilibrium joint probability distribution of the velocity and the desired velocity (compare Nelson (1995)) for the distinguished classes, lanes, and states. Moreover, establishing the moments of the velocity

distributions established relations between the moments (e.g. velocity, velocity variance) and the density. This is shown in section 6.4.5 of this thesis.

4.11.3 Foundation for macroscopic traffic flow models

In this thesis, the derived special continuity equations serve as the foundation for the macroscopic traffic flow model to be established in chapter 6. As an intermediate step, the special continuity equations are transformed into simplified equations in the following chapter. These *reduced special continuity equations* describe the dynamics of the reduced state-specific or mixed-state MLMC-PSD.

4.12 Summary

In this chapter we have established the so-called *special continuity equations* describing the dynamics of the unconstrained, constrained and mixed-state MLMC-PSD. We have shown that these equations can be considered to be generalisations of traditionally used continuity equations, describing the dynamics of the traffic density. The equations are 'special' since they do not only reflect changes caused by inflow and outflow of vehicles, but rather also reflect changes in the MLMC-PSD caused by acceleration to the class-dependent desired velocity, decelerations and immediate lane-changes caused by interactions between vehicles, postponed lane-changing and spontaneous lane-changing to the preferred lane.

To establish these gas-kinetic equations for MLMC traffic flow operations, generalised equations have been proposed describing the motion of traffic entities in an n-dimensional space. This is done by establishing dynamic equations for the *generalised Phase-Space Density* described in chapter 3. This generalised approach considers traffic entities characterised by an n-dimensional location-vector $\mathbf{x}$, velocity-vector $\mathbf{v}$, discrete attributes $\mathbf{a}$, and continuous attributes $\mathbf{v}^0$. We have shown how these dynamics are on the one hand governed by *continuum processes* (i.e. convection, acceleration, smooth adaptation of the continuous attributes), and on the other hand, are governed by *non-continuum processes* (i.e. event-driven and condition-driven processes). For each of these process-types, generic expressions are presented. The event-driven non-continuum processes are further specified in case of interaction events (i.e. traffic entities being on the same location at the same time). The generalised n-dimensional gas-kinetic equations are suited to describe various types of traffic systems (e.g. multiclass motorway traffic, pedestrian flows in a two-dimensional plane), depending on the specifications of the expressions describing continuum and non-continuum process.

In this chapter we have specified the generalised model to suit the *platoon-based* description of *multilane multiclass* traffic flow operations. Compared to other gas-kinetic traffic flow models presented in the literature, the established gas-kinetic model does not only constitute a MLMC generalisation: additionally, improved expressions applicable for aggregate-lane and/or aggregate-class gas-kinetic traffic flow models reflecting the interaction process yielding deceleration and lane-changes have been derived. Based on the assumption that constrained vehicles are able to accelerate towards the velocity of the unconstrained platoon leader, we also derived an improved relation to model the vehicle acceleration process.

5 REDUCED GENERALISED GAS-KINETIC TRAFFIC FLOW EQUATIONS

In this chapter we will derive the so-called *reduced generalised gas-kinetic equations* or *reduced generalised special continuity equations* These are subsequently specified further, describing the dynamics of the reduced MLMC-PSD for both platoon leaders and followers. The resulting equations present a MLMC generalisation of the aggregate user-class equations first proposed by Prigogine and Herman (1971). They form an intermediate step between the gas-kinetic equations described in chapter 4 and the macroscopic traffic flow equations established in chapter 6. These reduced generalised gas-kinetic equations model the dynamics of the reduced generalised PSD, defined by*:

$$\tilde{\rho}_a(\mathbf{x},\mathbf{v},t) = \int \rho_a(\mathbf{x},\mathbf{v},\mathbf{v}^0,t)\mathrm{d}\mathbf{v}^0 \tag{5.1}$$

Compared to the generalised PSD $\rho_a(\mathbf{x},\mathbf{v},\mathbf{v}^0,t)$, the term 'reduced' indicates independence of continuous attributes $\mathbf{v}^0$. The reduced gas-kinetic equations constitute a simplification of the gas-kinetic equations for generic n-dimensional flows established in chapter 4, because *expected* desired velocities are considered instead of desired velocity *distributions*.

In section 5.1 we establish the reduced generalised gas-kinetic equations for MLMC traffic flow. In sections 5.2 and 5.3 we specify these equations for unconstrained, constrained and mixed-state traffic respectively. In section 5.4 we show that the reduced model is a genuine generalisation of the reduced gas-kinetic model of Prigogine and Herman (1971).

* In a similar fashion, the reduced state-specific and mixed-state MLMC-PSD can be calculated by integrating the PSD's with respect to the desired velocity (see chapter 3).

5.1 Reduced generalised gas-kinetic equations

In this section, we will propose the *reduced generalised gas-kinetic equations* for the generic flow model describing the motion of traffic entities in the *n*-dimensional space, with general continuous attributes $\mathbf{v}^0$ (section 5.1.1). This result is then specified for one-dimensional flows and $\mathbf{v}^0 = v^0$ (section 5.1.2).

5.1.1 Generic n-dimensional flows

In this section, we will establish the reduced model describing the dynamics of the generalised reduced PSD defined by equation (5.1)*. In section 4.5.3, we have presented generic gas-kinetic equations describing the dynamics of the generalised PSD for *n*-dimensional flows governed by convection, acceleration, adaptation, event-driven non-continuum processes, and condition-driven non-continuum processes (equation (4.44)). In sections 4.6 and 4.7 we have assumed that the event-driven and condition-driven non-continuum processes do *not* change the continuous attributes $\mathbf{v}^0$ (i.e. the desired velocity v_0) of the drivers. Consequently, without loss of generality we can rewrite the transition probabilities π and transition-rates ϕ by introducing their reduced counterparts as:

$$\pi_a^{a'}(\mathbf{v}', \mathbf{v}_0' \mid \mathbf{v}, \mathbf{v}^0; \alpha) = \tilde{\pi}_a^{a'}(\mathbf{v}' \mid \mathbf{v}; \alpha)\, \delta(\mathbf{v}_0' - \mathbf{v}^0) \tag{5.2}$$

and:

$$\phi_a^{a'}(\mathbf{v}', \mathbf{v}_0' \mid \mathbf{v}, \mathbf{v}^0; \beta) = \tilde{\phi}_a^{a'}(\mathbf{v}' \mid \mathbf{v}; \beta)\, \delta(\mathbf{v}_0' - \mathbf{v}^0) \tag{5.3}$$

In recalling the definition of the δ-dirac function, eqn. (5.2) and (5.3) show that the continuous attributes $\mathbf{v}^0$ shift from $\mathbf{v}^0$ to $\mathbf{v}_0' = \mathbf{v}^0$ for both event-driven as well as condition-driven transitions. Substituting these relations into eq. (4.45), the generic dynamic equations for the generalised PSD $\rho_a(\mathbf{x},\mathbf{v},\mathbf{v}^0,t)$ for *n*-dimensional traffic flows become (scalar notation):

$$\begin{aligned}
&\overbrace{\partial_t \rho_a}^{(a)} + \overbrace{\nabla_x \cdot (\rho_a \mathbf{v})}^{(b)} + \overbrace{\nabla_v \cdot (\rho_a A_a)}^{(c)} + \overbrace{\nabla_{v^0} \cdot (\rho_a B_a)}^{(d)} = \\
&\overbrace{\sum_{a'} \int \rho_{a'}(\mathbf{v}', \mathbf{v}^0) \Pi_{a'}(\mathbf{v}', \mathbf{v}^0; \alpha) \tilde{\pi}_{a'}^{a}(\mathbf{v} \mid \mathbf{v}'; \alpha)\, d\mathbf{v}'\, d\alpha}^{(e)} + \overbrace{\sum_{a'} \int \rho_{a'}(\mathbf{v}', \mathbf{v}^0) \tilde{\phi}_{a'}^{a}(\mathbf{v} \mid \mathbf{v}'; \beta)\, d\mathbf{v}'\, d\beta}^{(g)} \\
&- \overbrace{\sum_{a'} \int \rho_a(\mathbf{v}, \mathbf{w}) \Pi_a(\mathbf{v}, \mathbf{v}^0; \alpha) \tilde{\pi}_a^{a'}(\mathbf{v}' \mid \mathbf{v}; \alpha)\, d\mathbf{v}'\, d\alpha}^{(f)} - \overbrace{\sum_{a'} \int \rho_a(\mathbf{v}, \mathbf{v}^0) \tilde{\phi}_a^{a'}(\mathbf{v}' \mid \mathbf{v}; \beta)\, d\mathbf{v}'\, d\beta}^{(h)}
\end{aligned} \tag{5.4}$$

The reduced model, describing the dynamics of the reduced PSD $\tilde{\rho}_a(\mathbf{x},\mathbf{v},t)$ can be derived easily from equation (5.4) by integration with respect to the respective elements in the continuous attribute-vector $\mathbf{v}^0$. For terms (*a*) and (*b*) we then find by changing the order of integration and differentiation:

(*a*): $$\int \partial_t \rho_a\, d\mathbf{v}^0 = \partial_t \int \rho_a\, d\mathbf{v}^0 = \partial_t \tilde{\rho}_a \tag{5.5}$$

* Rather than aggregation with respect to all continuous attributes in $\mathbf{v}^0$, similar results hold for generalisation with respect to a subset $\mathbf{v}_0^*$ of $\mathbf{v}^0$.

(*b*): $$\int \nabla_{\mathbf{x}} \cdot (\rho_a \mathbf{v})\, \mathrm{d}\,\mathbf{v}^0 = \nabla_{\mathbf{x}} \cdot \int (\rho_a \mathbf{v})\, \mathrm{d}\,\mathbf{v}^0 = \nabla_{\mathbf{x}} \cdot (\tilde{\rho}_a \mathbf{v}) \tag{5.6}$$

For term (*c*) we have:

(*c*): $$\int \nabla_{\mathbf{v}} \cdot (\rho_a A_a)\, \mathrm{d}\,\mathbf{v}^0 = \nabla_{\mathbf{v}} \cdot \int (\rho_a A_a)\, \mathrm{d}\,\mathbf{v}^0 = \nabla_{\mathbf{v}} \cdot (\tilde{\rho}_a \tilde{A}_a) \tag{5.7}$$

where the *reduced acceleration function* is defined by:

$$\tilde{A}_a(\mathbf{x},\mathbf{v},t) \overset{def}{=} \frac{1}{\tilde{\rho}_a(\mathbf{x},\mathbf{v},t)} \int \rho_a(\mathbf{x},\mathbf{v},\mathbf{v}^0,t) A_a(\mathbf{x},\mathbf{v},\mathbf{v}^0,t)\, \mathrm{d}\,\mathbf{v}^0 \tag{5.8}$$

With respect to term (*d*), let us first consider the case of an one-dimensional continuous attribute-vector $\mathbf{v}^0 = v^0$. Since $\rho_a(x,v,v^0,t) = 0$ at the boundaries V_{min} and V_{max} of admissible values v^0, the adaptation-term (*d*) yields:

$$\int_{v^0} \partial_{v^0} (\rho_a B_a)\, \mathrm{d}\, v^0 = \rho_a(x,v,v^0,t) B_a(x,v,v^0,t)\Big|_{v^0=V_{min}}^{V_{max}} = 0 \tag{5.9}$$

For a general *m*-dimensional continuous attribute-vector $\mathbf{v}^0$, this result holds equally:

(*d*): $$\int \nabla_{\mathbf{v}^0} \cdot (\rho_a B_a)\, \mathrm{d}\,\mathbf{v}^0 = 0 \tag{5.10}$$

For the remaining terms (*e*)-(*h*) we find:

(*e*): $$\begin{aligned} &\int \rho_{a'}(\mathbf{v}',\mathbf{v}^0) \Pi_{a'}(\mathbf{v}',\mathbf{v}^0) \tilde{\pi}_{a'}^{a}(\mathbf{v} \mid \mathbf{v}';\alpha)\, \mathrm{d}\,\mathbf{v}'\, \mathrm{d}\,\alpha\, \mathrm{d}\,\mathbf{v}^0 = \\ &\qquad \int \tilde{\rho}_{a'}(\mathbf{v}') \tilde{\Pi}_{a'}(\mathbf{v}') \tilde{\pi}_{a'}^{a}(\mathbf{v} \mid \mathbf{v}';\alpha)\, \mathrm{d}\,\mathbf{v}'\, \mathrm{d}\,\alpha \end{aligned} \tag{5.11}$$

where the *reduced interaction rate* for event α is defined by:

$$\tilde{\Pi}_a(\mathbf{x},\mathbf{v},t;\alpha) \overset{def}{=} \int \frac{\rho_a(\mathbf{x},\mathbf{v},\mathbf{v}^0,t)}{\tilde{\rho}_a(\mathbf{x},\mathbf{v},t)} \Pi_a(\mathbf{x},\mathbf{v},\mathbf{v}^0,t;\alpha)\, \mathrm{d}\,\mathbf{v}^0 \tag{5.12}$$

When only considering interaction events in the *n*-dimensional space, we have established eq. (4.51) for the event-rate of vehicle *a* (characterised by $(\mathbf{v},\mathbf{v}^0;\mathbf{a})$) interacting with vehicles characterised by $(\mathbf{w},\mathbf{w}^0;\mathbf{b})$. The reduced event-rate eq. (5.12) for event $\alpha = (\mathbf{w},\mathbf{b})$ becomes:

$$\tilde{\Pi}_a(\mathbf{x},\mathbf{v},t;\alpha) = \int \frac{\rho_a(\mathbf{x},\mathbf{v},\mathbf{v}^0,t)}{\tilde{\rho}_a(\mathbf{x},\mathbf{v},t)} |\mathbf{w}-\mathbf{v}|\, \tilde{\rho}_b(\mathbf{x},\mathbf{w},t)\, \mathrm{d}\,\mathbf{v}^0 = |\mathbf{w}-\mathbf{v}|\, \tilde{\rho}_b(\mathbf{x},\mathbf{w},t) \tag{5.13}$$

Moreover:

(*f*): $$\begin{aligned} &\int \rho_a(\mathbf{v},\mathbf{v}^0) \Pi_a(\mathbf{v},\mathbf{v}^0) \tilde{\pi}_a^{a'}(\mathbf{v}' \mid \mathbf{v};\alpha)\, \mathrm{d}\,\mathbf{v}'\, \mathrm{d}\,\alpha\, \mathrm{d}\,\mathbf{v}^0 = \\ &\qquad \int \tilde{\rho}_a(\mathbf{v}) \tilde{\Pi}_a(\mathbf{v}) \tilde{\pi}_a^{a'}(\mathbf{v}' \mid \mathbf{v};\alpha)\, \mathrm{d}\,\mathbf{v}'\, \mathrm{d}\,\alpha \end{aligned} \tag{5.14}$$

(*g*): $$\int \rho_{a'}(\mathbf{v}',\mathbf{v}^0) \tilde{\phi}_a^{a}(\mathbf{v} \mid \mathbf{v}';\beta)\, \mathrm{d}\,\mathbf{v}'\, \mathrm{d}\,\beta\, \mathrm{d}\,\mathbf{v}^0 = \int \tilde{\rho}_{a'}(\mathbf{v}') \tilde{\phi}_{a'}^{a}(\mathbf{v} \mid \mathbf{v}';\beta)\, \mathrm{d}\,\mathbf{v}'\, \mathrm{d}\,\beta \tag{5.15}$$

and finally:

(*h*): $$\int \rho_a(\mathbf{v},\mathbf{v}^0) \tilde{\phi}_a^{a'}(\mathbf{v}' \mid \mathbf{v};\beta)\, \mathrm{d}\,\mathbf{v}'\, \mathrm{d}\,\beta\, \mathrm{d}\,\mathbf{v}^0 = \int \tilde{\rho}_a(\mathbf{v}) \tilde{\phi}_a^{a'}(\mathbf{v}' \mid \mathbf{v};\beta)\, \mathrm{d}\,\mathbf{v}'\, \mathrm{d}\,\beta \tag{5.16}$$

In collecting the results, the following partial differential equation describe the dynamics of the reduced generalised PSD for generic n-dimensional traffic flows (in scalar-notation):

$$\begin{aligned}&\partial_t\tilde{\rho}_a+\nabla_x\cdot(\tilde{\rho}_a\mathbf{v})+\nabla_v\cdot(\tilde{\rho}_a\tilde{A}_a)=\\&\sum_{a'}\int\tilde{\rho}_{a'}(\mathbf{v}')\tilde{\Pi}_{a'}(\mathbf{v}';\alpha)\tilde{\pi}^a_{a'}(\mathbf{v}\,|\,\mathbf{v}';\alpha)\,d\mathbf{v}'d\alpha+\sum_{a'}\int\tilde{\rho}_{a'}(\mathbf{v}')\tilde{\phi}^a_{a'}(\mathbf{v}\,|\,\mathbf{v}';\beta)\,d\mathbf{v}'d\beta\\&-\sum_{a'}\int\tilde{\rho}_a(\mathbf{v})\tilde{\Pi}_a(\mathbf{v};\alpha)\tilde{\pi}^{a'}_a(\mathbf{v}'\,|\,\mathbf{v};\alpha)\,d\mathbf{v}'d\alpha-\sum_{a'}\int\tilde{\rho}_a(\mathbf{v})\tilde{\phi}^{a'}_a(\mathbf{v}'\,|\,\mathbf{v};\beta)\,d\mathbf{v}'d\beta\end{aligned}\tag{5.17}$$

Equation (5.17) shows how the reduced generalised PSD $\tilde{\rho}_a(\mathbf{x},\mathbf{v},t)$, changes due to convection, acceleration, event-driven and condition-driven continuum processes. Note that the influence of smooth adaptation of continuous attributes $\mathbf{v}^0$ has disappeared.

5.1.2 *Specification for one-dimensional traffic flows*

Let us now consider the reduced model equations (5.17) for one-dimensional flows (i.e. $\mathbf{x}=x$, and $\mathbf{v}=v$), with a scalar continuous attribute vector $\mathbf{v}^0=v^0$. In section 4.4.2 we have proposed the following expression describing the acceleration function $A_a(x,v,v^0,t)$:

$$A_a(x,v,v^0,t)=\frac{W_a(v,v^0\,|\,x,t)-v}{\tau(v,v^0\,|\,x,t)}\tag{5.18}$$

Using this exponential relation, the reduced acceleration function (5.8) becomes:

$$\tilde{A}_a(x,v,t)=\frac{\tilde{W}_a(v\,|\,x,t)-v}{\tilde{\tau}_a(v\,|\,x,t)}\tag{5.19}$$

In expression (5.19), the *reduced acceleration times* are defined by:

$$\tilde{\tau}_a^{-1}(v\,|\,x,t)\overset{def}{=}\int\tau_a^{-1}(v,v^0\,|\,x,t)\frac{\rho_a(x,v,v^0,t)}{\tilde{\rho}_a(x,v,t)}dv^0=\int\tau_a^{-1}(v,v^0\,|\,x,t)\bar{g}_a(v^0\,|\,v)\,dv^0\tag{5.20}$$

Note that the function $\bar{g}_a(v^0|v)=g_a(v,v^0)/\tilde{g}_a(v)$ is the *conditional probability density function* of the desired velocity $\underline{V}^0$ (cf. Grimmett and Stirzaker (1981)). Consequently, the inverse reduced acceleration time equals the conditional expected inverse acceleration time. In other words, the reduced acceleration time $\tilde{\tau}_a(v|x,t)$ is determined by the *harmonic expectation* of $\tau_a(v,\underline{V}^0|x,t)$. The *reduced acceleration velocity* is defined by:

$$\tilde{W}_a(v\,|\,x,t)\overset{def}{=}\int\frac{\tilde{\tau}_a(v\,|\,x,t)}{\tau_a(v,v_0\,|\,x,t)}W_a(v,v_0\,|\,x,t)\bar{g}_a(v_0\,|\,v)\,dv_0\tag{5.21}$$

Thus, for one-dimensional traffic flow, expression (5.19) becomes:

$$\begin{aligned}&\partial_t\tilde{\rho}_a+\partial_x(\tilde{\rho}_a v)+\partial_v\left(\tilde{\rho}_a\frac{\tilde{W}_a(v\,|\,x,t)-v}{\tilde{\tau}_a(v\,|\,x,t)}\right)=\\&+\sum_{a'}\int\tilde{\rho}_{a'}(v')\tilde{\Pi}_{a'}(v')\tilde{\pi}^a_{a'}(v\,|\,v';\alpha)\,dv'd\alpha+\sum_{a'}\int\tilde{\rho}_{a'}(v')\tilde{\phi}^a_{a'}(v\,|\,v';\beta)\,dv'd\beta\\&-\sum_{a'}\int\tilde{\rho}_a(v)\tilde{\Pi}_a(v)\tilde{\pi}^{a'}_a(v'\,|\,v;\alpha)\,dv'd\alpha-\sum_{a'}\int\tilde{\rho}_a(v)\tilde{\phi}^{a'}_a(v'\,|\,v;\beta)\,dv'd\beta\end{aligned}\tag{5.22}$$

Alternatively, the *reduced* generalised gas-kinetic equations can be cast in vector notation:

$$\begin{aligned}\partial_t\vec{\tilde{\rho}}+\partial_x(\vec{\tilde{\rho}}v)+\partial_v\left(\vec{\tilde{\rho}}\otimes\frac{\tilde{\mathbf{W}}(v\,|\,x,t)-v}{\vec{\tilde{\tau}}(v\,|\,x,t)}\right)=\\ +\int\oplus(\vec{\tilde{\rho}}(v')\otimes\vec{\tilde{\Pi}}(v')\otimes\tilde{\mathbf{P}}(v\,|\,v';\alpha))^T\,\mathrm{d}v'\,\mathrm{d}\alpha+\int\oplus(\vec{\tilde{\rho}}(v')\otimes\tilde{\mathbf{F}}(v\,|\,v';\beta))^T\,\mathrm{d}v'\,\mathrm{d}\beta\\ -\int\oplus(\vec{\tilde{\rho}}(v)\otimes\vec{\tilde{\Pi}}(v))\otimes\tilde{\mathbf{P}}(v'\,|\,v;\alpha)\,\mathrm{d}v'\,\mathrm{d}\alpha-\int\oplus(\vec{\tilde{\rho}}(v)\otimes\tilde{\mathbf{F}}(v'\,|\,v;\beta))\,\mathrm{d}v'\,\mathrm{d}\beta\end{aligned}\tag{5.23}$$

Using this expression, in section 5.2 we determine reduced gas-kinetic equations for both free-flowing and platooning drivers; section 5.3 considers mixed-state reduced dynamics.

5.2 Reduced equations for unconstrained and constrained vehicles

In this section, we will specify the generalised reduced model for one-dimensional traffic flows (expression (5.22)) for both platoon-leaders as well as platooning vehicles. In section 5.1, we have shown that in case of interaction events, the reduced event-rate of vehicles a characterised by $(\mathbf{v},\mathbf{v}^0;\mathbf{a})$ with vehicles b characterised by $(\mathbf{w},\mathbf{w}^0;\mathbf{b})$ equals eq. (5.13). Let us now specify the reduced transition probabilities and rates.

Reduced immediate lane-changing probability. If we combine eq. (4.53) and eq. (5.2), we conclude that the *reduced immediate lane-changing transition probability* equals:

$$\tilde{\pi}^{(u,j',c')}_{(u,j,c)}(v'\,|\,v;w,\mathbf{b})=\begin{cases}p^{(u,j',c')}_{(u,j,c)}(v\,|\,x,t)\delta(v'-v), & v>w,\mathbf{b}=(s,j,1)\\ 0, & \text{elsewhere}\end{cases}\tag{5.24}$$

Reduced deceleration probability. In combining eq. (4.56) and eq. (5.2), we find that the *reduced deceleration transition probability* (i.e. transition from (u,j,c) to (u,j',c') after interacting with a (slower) platoon with velocity w, and from v to v') equals:

$$\tilde{\pi}^{(u,j,2)}_{(u,j,c)}(v'\,|\,v;w,\mathbf{b})=\begin{cases}(1-p^{*}_{(u,j,c)}(v\,|\,x,t))\delta(v'-w), & v>w,\mathbf{b}=(s,j,1)\\ 0, & \text{elsewhere}\end{cases}\tag{5.25}$$

where $(1-p^{*}_{(u,j,c)}(v|x,t))$ denotes the probability that a vehicle driving with velocity v at (x,t) is unable to immediately changes to an adjacent lane after interacting with a slower vehicle.

Reduced lane-changing rates. The *reduced postponed and spontaneous lane-changing rates* are equal to (compare (4.72) and (5.14)):

$$\tilde{\phi}^{(u,j\pm1,1)}_{(u,j,c)}(v'\,|\,v)=\Delta^{(u,j\pm1,1)}_{(u,j,c)}(v\,|\,x,t)\delta(v'-v)\tag{5.26}$$

Reduced relaxation-rate. Finally, the *reduced relaxation rate* equals:

$$\tilde{\phi}^{(u,j,1)}_{(u,j,2)}(v'\,|\,v)=\tilde{\Xi}(\Delta^{(u,*,1)}_{(u,j,1)}\tilde{\rho}_{(u,j,1)}(x,v,v^0,t))\delta(v'-v)\tag{5.27}$$

where:

$$\tilde{\Xi}(\Delta^{(u,*,1)}_{(u,j,1)}\tilde{\rho}_{(u,j,1)}(x,v,t))=\int\Xi(\Delta^{(u,*,1)}_{(u,j,1)}\rho_{(u,j,1)}(x,v,v^0,t))g_{(u,j,1)}(v,v^0\,|\,x,t)\mathrm{d}v^0\tag{5.28}$$

We can now determine the reduced gas-kinetic equations for unconstrained ($c=1$) and constrained ($c=2$) vehicles by substituting expressions (5.24)-(5.28) into the generalised re-

duced gas-kinetic equations (5.22). We remark that these dynamic equations can also be established by direct integration of equation (4.81) and (4.82) with respect to v^0.

5.2.1 *Unconstrained vehicles (c = 1)*

Since (equation (5.20)):

$$\frac{1}{\tilde{\tau}_{(u,j,1)}(v \mid x,t)} \stackrel{def}{=} = \int \frac{1}{\tau_u^0} \bar{g}_{\mathbf{a}}(v^0 \mid v) \mathrm{d}v^0 = \frac{1}{\tau_u^0} \tag{5.29}$$

we have:

$$\tilde{W}_{(u,j,1)}(v \mid x,t) \stackrel{def}{=} \int v^0 \bar{g}_{\mathbf{a}}(v^0 \mid v)\, \mathrm{d}\, v^0 = \tilde{V}^0_{(u,j,1)}(v \mid x,t) \tag{5.30}$$

Note that is case of unconstrained vehicles, the reduced unconstrained acceleration velocity equals the expected desired velocity (section 4.4.2). Consequently, for the reduced MLMC-PSD of the unconstrained platoon leaders, we find:

$$\begin{aligned}
&\partial_t \tilde{\rho}_{(u,j,1)} + \underbrace{\partial_x(\tilde{\rho}_{(u,j,1)} v)}_{(1)} + \underbrace{\partial_v(\tilde{\rho}_{(u,j,1)}(\tilde{W}_{(u,j,1)}(v) - v)/\tau_u^0)}_{(2)} = \underbrace{-(1 - p^*_{(u,j,1)}(v))\tilde{\Psi}_{(*,j)}(v)\tilde{\rho}_{(u,j,1)}}_{(4)} \\
&\quad \underbrace{- \sum_{j'=j\pm1}(p^{(u,j',1)}_{(u,j,1)}(v)\tilde{\Psi}_{(*,j)}(v)\tilde{\rho}_{(u,j,1)} - p^{(u,j,1)}_{(u,j',1)}(v)\tilde{\Psi}_{(*,j')}(v)\tilde{\rho}_{(u,j',1)})}_{(6)} \\
&\quad + \underbrace{\sum_{j'=j\pm1} p^{(u,j,1)}_{(u,j',2)}(v)\tilde{\Psi}_{(*,j')}(v)\tilde{\rho}_{(u,j',2)}}_{(7)} + \underbrace{\sum_{j'=j\pm1}\tilde{\Delta}^{(u,j,1)}_{(u,j',2)}(v)\tilde{\rho}_{(u,k,2)}}_{(9)} \\
&\quad \underbrace{- \sum_{j'=j\pm1}(\Delta^{(u,j',1)}_{(u,j,1)}(v)\tilde{\rho}_{(u,j,1)} - \Delta^{(u,j,1}_{(u,j',1)}(v)\tilde{\rho}_{(u,j',1)})}_{(8)} + \underbrace{\tilde{\Xi}(\Delta^{(u,*,1)}_{(u,j,1)}\tilde{\rho}_{(u,j,1)})\tilde{\rho}_{(u,j,2)}}_{(5)}
\end{aligned} \tag{5.31}$$

for all $u \in \mathbf{U}$ and $j = 1,\ldots,M$. The respective terms (1)-(9) in this reduced equation stem from the same processes as the terms of the original equation (4.81). For a discussion of these terms, we refer to section 4.8.1.

5.2.2 *Constrained vehicles (c = 2)*

Let us now consider the generalised reduced gas-kinetic equations (5.22) for platooning vehicles of class u on lane j, i.e. $\mathbf{a} = (u,j,2)$. Using a similar approach applied to the unconstrained case, we find the following result.

$$\begin{aligned}
&\partial_t \tilde{\rho}_{(u,j,2)} + \underbrace{\partial_x(\tilde{\rho}_{(u,j,2)} v)}_{(1)} + \underbrace{\partial_v(\tilde{\rho}_{(u,j,2)}(\tilde{W}_{(u,j,2)}(v) - v)/\tilde{\tau}_{(u,j,2)}(v))}_{(2)} = \\
&\quad \underbrace{-(1 - p^*_{(u,j,2)}(v))\tilde{\rho}_{(u,j,2)}\tilde{\Psi}_{(*,j)}(v)}_{(4)} \underbrace{-\tilde{\Xi}(\Delta^{(u,*,1)}_{(u,j,1)}\tilde{\rho}_{(u,j,1)}(x,v,t))\tilde{\rho}_{(u,j,2)}}_{(5)} \\
&\quad \underbrace{+\tilde{\rho}_{(*,j,1)}\sum_{c=1,2}\int_{w>v}|w-v|((1-p^*_{(u,j,c)}(w))\tilde{\rho}_{(u,j,c)}(x,w,t)\,\mathrm{d}w}_{(3)} \\
&\quad \underbrace{-\sum_{j'=j\pm1}(p^{(u,j',2)}_{(u,j,2)}\tilde{\Psi}_{(*,j)}(v)\tilde{\rho}_{(u,j,2)} - p^{(u,j,2)}_{(u,j',2)}\tilde{\Psi}_{(*,k)}(v)\tilde{\rho}_{(u,j',2)})}_{(7)} \underbrace{-\sum_{j'=j\pm1}\Delta^{(u,j',1)}_{(u,j,2)}\tilde{\rho}_{(u,j,2)}}_{(8)}
\end{aligned} \tag{5.32}$$

for all $u \in \mathbf{U}$ and $j = 1,\ldots,M$. As with the reduced gas-kinetic equations for unconstrained traffic, the different terms of the reduced gas-kinetic equations for constrained traffic stem for equivalent processes as the terms in equation (4.82). For a discussion of these terms we refer to section 4.8.2.

5.3 Reduced gas-kinetic equations for mixed-state traffic (c = *)

The lane-specific reduced MLMC gas-kinetic equations can also be derived for mixed-state traffic, i.e. $\mathbf{a} = (u,j)$. To this end, we can either simply add equation (5.31) to (5.32), or we can specify the reduced expressions for the mixed-state transition rates. Either way, the reduced gas-kinetic equations for mixed-state traffic becomes:

$$\begin{aligned}
&\partial_t \tilde{\rho}_{(u,j)} + \underbrace{\partial_x(\tilde{\rho}_{(u,j)} v)}_{(1)} + \underbrace{\partial_v((\tilde{W}_{(u,j)}(v) - v)/\tau_{(u,j)}(v))}_{(2)} = \underbrace{-(1 - p^*_{(u,j)}(v))\tilde{\Psi}_{(*,j)}(v)\tilde{\rho}_{(u,j)}}_{(4)} \\
&\quad \underbrace{+(1-\tilde{\theta}_{(*,j)}(v))\tilde{\rho}_{(*,j)}(x,v,t)\int_{w>v}|w-v|(1-p^*_{(u,j)}(w))\tilde{\rho}_{(u,j)}(x,w,t))\,\mathrm{d}w}_{(3)} \\
&\quad \underbrace{-\sum_{j'=j\pm1}(p^{(u,j')}_{(u,j)}(v)\tilde{\Psi}_{(*,j)}(v)\tilde{\rho}_{(u,j)} - p^{(u,j)}_{(u,j')}(v)\tilde{\Psi}_{(*,j')}(v)\tilde{\rho}_{(u,j')})}_{(6+7)} \\
&\quad \underbrace{-\sum_{j'=j\pm1}(\Delta^{(u,j')}_{(u,j)}(v)\tilde{\rho}_{(u,j)} - \Delta^{(u,j)}_{(u,j')}(v)\tilde{\rho}_{(u,j')})}_{(8+9)}
\end{aligned} \tag{5.33}$$

In expression (5.33), we have used the following definitions:

$$p^{(u,j')}_{(u,j)}(v\,|\,x,t) \overset{def}{=} \frac{1}{\tilde{\rho}_{(u,j)}(x,v,t)}\sum_{c'=1,2} p^{(u,,j',1)}_{(u,j,c')}(v\,|\,x,t)\tilde{\rho}_{(u,j,c')}(x,v,t) \tag{5.34}$$

and:

$$\Delta^{(u,j')}_{(u,j)}(v \mid x,t) \overset{def}{=} \frac{1}{\tilde{\rho}_{(u,j)}(x,v,t)} \sum_{j'=1,2} \Delta^{(u,j',1)}_{(u,j,j')}(v \mid x,t)\tilde{\rho}_{(u,j,j')}(x,v,t) \tag{5.35}$$

The different terms present in this reduced equation stem from similar processes as the terms present in equation (4.84). For a discussion of the origin of these terms, see section 4.8.3.

5.4 Comparison with Prigogine-Herman model

Similar to the MLMC gas-kinetic equations, we can show that the reduced MUC model of Hoogendoorn (1997) and Hoogendoorn and Bovy (1998a,b) are special cases of the reduced MLMC gas-kinetic equations (5.33), by multiplication with the matrix $\mathbf{S}_2\mathbf{S}_3$ (see 3.8.1). Also, by multiplication of eq. (5.33) by the matrix $\mathbf{S}_1\mathbf{S}_2\mathbf{S}_3$, we can determine a reduced gas-kinetic model similar to the model of Prigogine and Herman (1971), yielding the following partial differential equations:

$$\begin{aligned} &\partial_t\tilde{\rho} + v\partial_x\tilde{\rho} + \partial_v(\tilde{\rho}(\tilde{W}(v) - v)/\tau(v)) = \\ &\qquad -\int_{w<v} |w-v|(1-p(v))\tilde{\rho}(v)(1-\tilde{\theta}(w))\tilde{\rho}(w)\,\mathrm{d}w \\ &\qquad +\int_{w>v} |w-v|(1-p(w))\tilde{\rho}(w)(1-\tilde{\theta}(v))\tilde{\rho}(v)\,\mathrm{d}w \end{aligned} \tag{5.36}$$

Comparing this result with the model of Prigogine and Herman, we conclude that the models differ in the handling of vehicle interaction. In the reduced model (5.36), interactions can only occur with platoon leaders representing the position and velocity of the platoon. In the model of Prigogine and Herman (1971), vehicles interact with all vehicles in the flow, thereby overestimating the expected number of interactions per unit time. This has been remedied by including suitable expressions for the reduced constrained vehicle fraction, and incorporating their space requirements (see section 4.6.5).

5.5 Use of reduced gas-kinetic equations

Aim of this study is to derive a traffic flow model enabling real-time simulation of multiple user-class traffic flow. To this end, the reduced gas-kinetic equations can be used directly by application of numerical solution approaches, similar to the gas-kinetic equations. Since our first attempts to numerically solve the (reduced) gas-kinetic equations are promising (e.g. Hoogendoorn and Bovy (2000)), it is envisaged that a suitable scheme for approximation solutions to these equations can be established (see section 4.11).

Nevertheless, keeping in mind the intended model applications, we are mainly interested in dynamic changes of collective (macroscopic) quantities, such as the traffic density $r_{(u,j)}(x,t)$. Consequently, the reduced gas-kinetic equations mainly serve as a foundation for the macroscopic MLMC traffic flow equations to be derived in the remainder of this dissertation.

5.6 Summary

In this chapter we have established the so-called *reduced gas-kinetic equations*, mesoscopically describing the dynamics of the reduced generalised PSD, which was subsequently specified for unconstrained, constrained and mixed-state traffic respectively. In the remainder

of this thesis, we will use these mesoscopic equations to derive the macroscopic traffic flow equations delineating the dynamics of the traffic density, momentum and energy of the classes on the respective lanes, for the different driver's states, by applying a derivation method similar to the method of moments.

Primitive moments of the velocity distribution

The *moments* of a joint probability distribution can be defined by application of the *generalised mean operator* (section 3.6.4) $\langle\cdot\rangle_a$. For traffic flows in the n-dimensional space, we define the $(\mathbf{k},\mathbf{l})$-*primitive moment* $M_a^{\mathbf{k},\mathbf{l}}(\mathbf{x},t)$ by:

$$M_a^{\mathbf{k},\mathbf{l}}(\mathbf{x},t) \overset{def}{=} \left\langle \prod_{j=1}^{m}\prod_{i=1}^{n}(v_i^{k_i}(v_j^0)^{l_j}) \right\rangle_a = \int\int \prod_{j=1}^{m}\prod_{i=1}^{n}(v_i^{k_i}(v_j^0)^{l_j}) g_a(\mathbf{v},\mathbf{v}^0 \mid \mathbf{x},t)\,\mathrm{d}\mathbf{v}\,\mathrm{d}\mathbf{v}^0 \qquad \text{(i.3)}$$

for vectors $\mathbf{k} \in \mathbb{N}^n$ and $\mathbf{l} \in \mathbb{N}^m$. The vector $\mathbf{M}^{\mathbf{k},\mathbf{l}}(\mathbf{x},t)$ indicates the vector of the $(\mathbf{k},\mathbf{l})$-primitive moments following from the vector $\tilde{\rho}(\mathbf{x},\mathbf{v},\mathbf{v}^0,t)$.

In section 3.5.2, we have shown how the primitive variables velocity V_a, velocity variance Θ_a, covariance between the velocity and the desired velocity C_a, and skewness of the velocity distribution Γ_a can be determined from the velocity distribution using the mean operator $\langle\cdot\rangle_a$ for $(\mathbf{x},\mathbf{v},\mathbf{v}^0,t) = (x,v,v^0,t)$,.

Conservative moments of the generalised PSD

Rather than using the joint velocity probability density function, the generalised PSD can be used directly to determine the *conservative moments*. To this end, section 3.6.5 introduced the *generalised aggregation operator* $[\cdot]_a$. Using this aggregation operator, the $(\mathbf{k},\mathbf{l})$-*conservative moment* $N^{\mathbf{k},\mathbf{l}}(\mathbf{x},t)$ is defined by:

$$N_a^{\mathbf{k},\mathbf{l}}(\mathbf{x},t) \overset{def}{=} \left[\prod_{j=1}^{m}\prod_{i=1}^{n}(v_i^{k_i}(v_j^0)^{l_j}) \right]_a = \int\int \prod_{j=1}^{m}\prod_{i=1}^{n}(v_i^{k_i}(v_j^0)^{l_j}) \rho_a(\mathbf{x},\mathbf{v},\mathbf{v}^0,t)\,\mathrm{d}\mathbf{v}\,\mathrm{d}\mathbf{v}^0 \qquad \text{(i.4)}$$

The vector $\mathbf{N}^{\mathbf{k},\mathbf{l}}(\mathbf{x},t)$ indicates the vector of the k^{th} primitive moments following from the vector $\tilde{\rho}(\mathbf{x},\mathbf{v},\mathbf{v}^0,t)$. In section 3.5.3, we have shown that the user-class specific density r_a, the momentum m_a and the energy e_a are determined by these conservation moments for $k = 0,1,$ and 2 and $l = 0$ respectively, using the aggregation operator $[\cdot]_a$ for $(\mathbf{x},\mathbf{v},\mathbf{v}^0,t) = (x,v,v^0,t)$.

Intermezzo II: Definition of primitive and conservative moments

6 MACROSCOPIC MLMC TRAFFIC FLOW MODEL

In this chapter, we will establish three new macroscopic multiclass multilane traffic flow models, namely for *unconstrained*, *constrained* and *mixed*-state traffic. In the derivation approach, the generalised gas-kinetic model presented in chapter 4 forms the basis for the derivation of the macroscopic equations – via the reduced model derived in chapter 5. That is:

$$\int\int \text{gas - kinetic model}\, d\,\mathbf{v}\, d\,\mathbf{v}^0 \quad \rightarrow \quad \text{macroscopic model}$$

The derivation of *macroscopic* traffic flow models from *gas-kinetic* traffic flow equations has been applied by a number of researchers (e.g. Herman *et al.* (1962), Prigogine and Herman (1971), Leutzbach (1990), Helbing (1996,1997a), Klar and Wegener (1998), Hoogendoorn (1997), and Hoogendoorn and Bovy (1998a,b,1999a)). Key to the derivation approach presented in these publications is the application of the *method of moments* to the gas-kinetic model equations. This method enables extracting specific moments from the probability density function of a distribution, such as the mean, the variance, and the skewness. In case of gas-kinetic models, application of the method of moments yields dynamic equations of the density, the expected velocity, the velocity variance, etc (the so-called *primitive moments*). However, this derivation approach is cumbersome.

In this chapter, we present an alternative derivation approach, which is shorter and less complicated. Key to the approach is the consideration of the *conservative moments* reflecting aggregate characteristics of the traffic flow rather than primitive moments reflecting mean characteristics. The derivation approach can be outlined as follows: first the dynamics of the *generalised conservative moments* are determined from the generic reduced gas-kinetic equations for n-dimensional traffic flows, derived in chapter 5. These generalised conservative moment

equations are specified for one-dimensional flows with $\mathbf{a} = (u,j,c)$, and $c = 1,2,*$ (i.e. free-flowing, constrained, and mixed-state). Subsequently, we consider the resulting multilane multiclass equations for the k-th conservative moment for $k = 0$, 1, and 2, respectively yielding the MLMC dynamics of density, momentum, and energy. Compared to the gas-kinetic flow equations, the resulting macroscopic flow model is a tractable flow model, which is more suitable for theoretical and numerical analysis of multilane heterogeneous traffic flow, as well as for real-time application in traffic estimation and control.

In addition to simplified model derivation, using conservatives rather than their primitive counterparts yields simplified model equations, enabling improved analytical and numerical analysis. The conservative MLMC-model derived in this chapter is recast in a *primitive model formulation* using density, velocity, and variance in chapter 7 of this thesis as well.

This chapter is organised as follows. Section 6.1 presents the dynamics of the generalised conservative moments. In sections 6.2–6.4 we present the dynamics of the macroscopic conservative variables for free-flowing, platooning, and mixed-state traffic respectively. The equilibrium relations that can be observed in these macroscopic equations are considered in section 6.5. In section 6.6 we introduce traffic viscosity, and present an expression for the flux of velocity variance. Finally, in section 6.7 we present the modifications in the model equations due to incorporation of vehicle spacing requirements.

6.1 Generalised conservative moments dynamics

In this section we present the dynamic equations describing temporal and spatial changes in the generalised conservative moments $N_{\mathbf{a}}^{\mathbf{k}} = N_{\mathbf{a}}^{\mathbf{k},0}$ for $\mathbf{k} \in \mathbb{N}^n$ (intermezzo II, page 124), for generic traffic flows in the n-dimensional space. This is achieved by multiplying the generic reduced flow equations by $\Pi_i v_i^{k_i}$ and integrating the result over v_i for $i = 1,\ldots,n$ respectively (section 6.1.1). This yields dynamic equations for the conservative moments $N_{\mathbf{a}}^{\mathbf{k}}(\mathbf{x},t)$. The resulting generic equations are then specified for generic flows in one-dimension (section 6.1.2), yielding the dynamic equations for conservative moments $N_{\mathbf{a}}^{k}(x,t)$ for $k = 0,1$ and 2. These moments respectively equal *generalised density* $r_{\mathbf{a}}$, *generalised momentum* $m_{\mathbf{a}}$, and *generalised energy* $e_{\mathbf{a}}$. In sections 6.2, 6.3, and 6.4, the generalised equations are specified for MLMC traffic flow for unconstrained, constrained, and mixed-state traffic respectively.

The proposed derivation approach differs from previous efforts to derive macroscopic flow equations from gas-kinetic traffic flow models: Prigogine and Herman (1971), Leutzbach (1989), Helbing (1996,1997a) applied the *mean operator* $\langle\cdot\rangle_{\mathbf{a}}$ to their gas-kinetic models. By doing so, dynamic equations for the mean and the variance (the so-called *primitive variables*) of the velocity distribution result. Instead, we determine aggregated conservative variables for the generalised Phase-Space Density, by considering *contributions* of vehicles driving at a specific velocity v to the respective conservative variables. Let us emphasise that, although both approaches are conceptually different, they are in fact equivalent, yielding partial differential equations that can be transformed into each other (see chapter 7).

6.1.1 Generalised moment equations for n-dimensional traffic flows

In section 5.1 we have derived reduced generalised gas-kinetic equations, describing the dynamics of the reduced generalised Phase-Space Density for n-dimensional traffic flows

(eqn. (5.17)). Appendix D shows how these reduced equations are used to derive partial differential equations describing the dynamics of the **k**-th generalised conservative moment:

$$N_{\mathbf{a}}^{\mathbf{k}}(\mathbf{x},t) \overset{def}{=} \int \mathbf{v}^{\mathbf{k}} \tilde{\rho}_{\mathbf{a}}(\mathbf{x},\mathbf{v},t)\,\mathrm{d}\,\mathbf{v} \quad \text{with} \quad \mathbf{v}^{\mathbf{k}} \overset{def}{=} (\Pi_i v_i^{k_i}) \tag{6.1}$$

where $\mathbf{k} = \{k_i\} \in \mathbb{N}^n$.

Let us define the **k**-th order (velocity-independent) acceleration time and acceleration velocity-vector by respectively:

$$\frac{1}{\mathrm{T}_{\mathbf{a}}^{\mathbf{k}}(\mathbf{x},t)} \overset{def}{=} \frac{1}{N_{\mathbf{a}}^{\mathbf{k}}(\mathbf{x},t)} \int \frac{\tilde{\rho}_{\mathbf{a}}(\mathbf{x},\mathbf{v},t)}{\tilde{\tau}_{\mathbf{a}}(\mathbf{x},\mathbf{v},t)} \mathbf{v}^{\mathbf{k}}\,\mathrm{d}\,\mathbf{v} \tag{6.2}$$

and the elements:

$$\{D_{\mathbf{a}}^{\mathbf{k}}(x,t)\}_j \overset{def}{=} \int \tilde{\rho}_{\mathbf{a}}(\mathbf{x},\mathbf{v},t)(\Pi_{i\neq j} v_i^{k_i}) v_j^{k_j-1} \{\tilde{W}_{\mathbf{a}}(\mathbf{x},\mathbf{v},t)\}_j \frac{\mathrm{T}_{\mathbf{a}}^{\mathbf{k}}(\mathbf{x},t)}{\tilde{\tau}_{\mathbf{a}}(\mathbf{x},\mathbf{v},t)} \mathrm{d}\,\mathbf{v} \tag{6.3}$$

In appendix D.1.2, the *expected event-aggregate probability* $p_{\mathbf{a}\to\mathbf{a}'}(\mathbf{x},t)$ and the ***k*-order moment-decreasing event-rate** $\mathcal{I}_{\mathbf{a}}^{\mathbf{k}}(\mathbf{x},t)$ are introduced: $p_{\mathbf{a}\to\mathbf{a}'}(\mathbf{x},t)$ denotes the average probability that any vehicle with attributes **a** changes its discrete attributes to **a**′; $\mathcal{I}_{\mathbf{a}}^{\mathbf{k}}(\mathbf{x},t)$ denotes change-rate in the **k**-order conservative moment $N_{\mathbf{a}}^{\mathbf{k}}(\mathbf{x},t)$ per vehicle of class **a**. Using these concepts, *decreases* of $N_{\mathbf{a}}^{\mathbf{k}}(\mathbf{x},t)$ due to events are factorised as follows:

$$p_{\mathbf{a}\to\mathbf{a}'}(\mathbf{x},t)\mathcal{I}_{\mathbf{a}}^{\mathbf{k}}(\mathbf{x},t) r_{\mathbf{a}}(\mathbf{x},t) = [\int\int \mathbf{v}^{\mathbf{k}} \cdot \tilde{\Pi}_{\mathbf{a}}(\mathbf{v};\alpha) \tilde{\pi}_{\mathbf{a}}^{\mathbf{a}'}(\mathbf{v}' \mid \mathbf{v};\alpha)\,\mathrm{d}\,\alpha\,\mathrm{d}\,\mathbf{v}']_{\mathbf{a}} \tag{6.4}$$

where we have used the following short-hand notation:

$$\mathbf{v}^{\mathbf{k}} = \prod_{i=1}^{n} v_i^{k_i} \tag{6.5}$$

In illustration, the **k**-order moment decreasing event-rate reflects decreases per vehicle per unit time due to events, provided that these events cause a shift from attribute-set **a**. For instance, the zero-order moment-decreasing event-rate $\mathcal{I}_{\mathbf{a}}^{\mathbf{0}}$ equals the expected number of vehicles with attributes **a** (reflected by $r_{\mathbf{a}}$) experiencing an interaction. When each of these vehicles would change their discrete attributes **a**, $r_{\mathbf{a}}\Pi_{\mathbf{a}}^{\mathbf{0}}$ expresses would the reduction in $r_{\mathbf{a}}$ per unit time caused by interaction.

In a similar fashion, *increases* of $N_{\mathbf{a}}^{\mathbf{k}}(\mathbf{x},t)$ due to events are factorised as follows:

$$r_{\mathbf{a}'}(\mathbf{x},t) p_{\mathbf{a}'\to\mathbf{a}}(\mathbf{x},t) \mathcal{X}_{\mathbf{a}'}^{\mathbf{k}}(\mathbf{x},t) = [\int\int (\mathbf{v}')^{\mathbf{k}} \tilde{\Pi}_{\mathbf{a}'}(\mathbf{v};\alpha) \tilde{\pi}_{\mathbf{a}'}^{\mathbf{a}}(\mathbf{v}' \mid \mathbf{v};\alpha)\,\mathrm{d}\,\mathbf{v}'\,\mathrm{d}\,\alpha]_{\mathbf{a}'} \tag{6.6}$$

where $\mathcal{X}_{\mathbf{a}}^{\mathbf{k}}(\mathbf{x},t)$ denotes the ***k*-order moment-increasing event-rate**.

Moreover, we have defined the **k**-order transition-rates by (appendix D.1.2):

$$f_{\mathbf{a}\to\mathbf{a}'}^{\mathbf{k}} = \frac{[\int \mathbf{v}^{\mathbf{k}} \cdot \tilde{\phi}_{\mathbf{a}}^{\mathbf{a}'}(\mathbf{v}' \mid \mathbf{v})\,\mathrm{d}\,\mathbf{v}']_{\mathbf{a}}}{N_{\mathbf{a}}^{\mathbf{k}}} \text{ and } g_{\mathbf{a}'\to\mathbf{a}}^{\mathbf{k}} = \frac{[\int (\mathbf{v}')^{\mathbf{k}} \tilde{\phi}_{\mathbf{a}'}^{\mathbf{a}}(\mathbf{v}' \mid \mathbf{v})\,\mathrm{d}\,\mathbf{v}']}{N_{\mathbf{a}'}^{\mathbf{k}}} \tag{6.7}$$

Moreover, let us assume that the *acceleration process* is described by an *exponential acceleration law*. Then, we can establish the following dynamic equation for traffic flows in n dimensions (appendix D.1.3):

$$\partial_t N_{\mathbf{a}}^{\mathbf{k}}(\mathbf{x},t) + \overbrace{\sum_j \partial_{x_j} N_{\mathbf{a}}^{\mathbf{k}+\mathbf{e}_j}(\mathbf{x},t)}^{(I)} - \overbrace{\sum_j k_j(\{D_{\mathbf{a}}^{\mathbf{k}}(\mathbf{x},t)\}_j - N_{\mathbf{a}}^{\mathbf{k}}(\mathbf{x},t))/T_{\mathbf{a}}^{\mathbf{k}}(\mathbf{x},t)}^{(II)} =$$
$$- \overbrace{\sum_{\mathbf{a}'} r_{\mathbf{a}}(\mathbf{x},t)\mathcal{I}_{\mathbf{a}}^{\mathbf{k}}(\mathbf{x},t)p_{\mathbf{a}\to\mathbf{a}'}(\mathbf{x},t)}^{(IVa)} + \overbrace{\sum_{\mathbf{a}'} r_{\mathbf{a}'}(\mathbf{x},t)\mathcal{X}_{\mathbf{a}'}^{\mathbf{k}}(\mathbf{x},t)p_{\mathbf{a}'\to\mathbf{a}}(\mathbf{x},t)}^{(IVb)} \tag{6.8}$$
$$- \overbrace{\sum_{\mathbf{a}'} N_{\mathbf{a}}^{\mathbf{k}}(\mathbf{x},t)f_{\mathbf{a}\to\mathbf{a}'}^{\mathbf{k}}(\mathbf{x},t)}^{(IVc)} + \overbrace{\sum_{\mathbf{a}'} N_{\mathbf{a}'}^{\mathbf{k}}(\mathbf{x},t)g_{\mathbf{a}'\to\mathbf{a}}^{\mathbf{k}}(\mathbf{x},t)}^{(IVd)}$$

where $\mathbf{e}_j$ is the j-th unit vector. Equation (6.8) reveals how the **k**-th conservative moment changes due to convection (II), acceleration (III), and event-driving (IV*a*,*b*) and condition-driven (IV*c*,*d*) non-continuum processes.

6.1.2 *Generalised moment equations for one-dimensional traffic flows*

Let us consider equation (6.8) describing the dynamics of the **k**-th order conservative moments, for one-dimensional traffic flow operations (see appendix D.1). In matrix-vector form, the dynamic equations for the conservative moments are given by:

$$\partial_t \mathbf{N}^k + \partial_x \mathbf{N}^{k+1} = k\frac{\mathbf{D}^k - \mathbf{N}^k}{\vec{\mathbf{T}}^k} - \oplus(\mathbf{r}\otimes\vec{\mathcal{I}}^k\otimes\mathbf{P}) - \oplus(\mathbf{N}^k\otimes\mathbf{F}^k)$$
$$+ \oplus(\mathbf{r}\otimes\vec{\mathcal{X}}^k\otimes\mathbf{P})^T + \oplus(\mathbf{N}^k\otimes\mathbf{G}^k)^T \tag{6.9}$$

where $\mathbf{N}^k = \{N_i^k\}$, $\vec{\mathbf{T}}^k = \{T_i^k\}$, $\mathbf{D}^k = \{D_i^k\}$, $\vec{\mathcal{I}}^k = \{\mathcal{I}_i^k\}$, $\vec{\mathcal{X}}^k = \{\mathcal{X}_i^k\}$, $\mathbf{P}^k = \{p_{ij}^k\}$, $\mathbf{Q}^k = \{q_{ij}^k\}$, $\mathbf{F}^k = \{f_{ij}^k\}$ and $\mathbf{G}^k = \{g_{ij}^k\}$ are defined by eqn. (6.1), (6.2), (6.3), (6.4), (6.6) and (6.7) respectively*. The generalised conservation of vehicle, momentum and energy equations can be determined easily from equation (6.9) by respectively considering $k = 0$, 1, and 2. In the remainder of this chapter, we will discuss specifying the conservative moment equation (6.9) for $\mathbf{a} = (u,j,c)$. More precisely, we specify dynamic equations for different states $c = 1,2,*$, i.e. for *unconstrained*, *platooning*, and *mixed-state* traffic of class u on lane j.

6.2 Macroscopic MLMC equations for free-flowing vehicles (c = 1)

In this section, we will specify the generalised conservative moment equation (6.9) for platoon-leading vehicles of class u on lane j, i.e. $\mathbf{a} = (u,j,1)$ (section 6.2.1). Using this equation, we can determine the generalised conservation-of-vehicle equation, momentum dynamics, and energy dynamics for free-flowing vehicles (sections 6.2.2-6.2.4).

* We have used the abbreviated notation $c_i = c_{\mathbf{a}(i)}$ and $c_{ij} = c_{\mathbf{a}(i)\to\mathbf{a}(j)}$.

6.2.1 *MLMC conservative moment dynamics for free-flowing traffic*

In appendix D.2 we specify the event-rates $\vec{\mathcal{I}}^k$ and $\vec{\mathcal{X}}^k$, the event-driven transition probabilities $\mathbf{P}$, and the condition-driven transition rates $\mathbf{F}^k$ and $\mathbf{G}^k$, using relations determined in chapters 4 and 5. Consequently, we show that by specification of these matrices, the generalised conservative moment equation (6.9) yields the following partial differential equation, describing the dynamics of unconstrained conservative moment:

$$\begin{aligned}\partial_t N^k_{(u,j,1)} + \underbrace{\partial_x N^{k+1}_{(u,j,1)}}_{(1)} &= \underbrace{k\frac{D^k_{(u,j,1)} - N^k_{(u,j,1)}}{\tau^0_u}}_{(2)} - \underbrace{(1-p^*_{(u,j1)})r_{(u,j,1)}\mathcal{I}^k_{(u,j,1)}}_{(3)} \\ &- \underbrace{\sum_{j'=j\pm1}(p^{(u,j',1)}_{(u,j,1)}r_{(u,j,1)}\mathcal{I}^k_{(u,j,1)} - p^{(u,j,1)}_{(u,j',1)}r_{(u,j',1)}\mathcal{I}^k_{(u,j',1)})}_{(6)} \\ &+ \underbrace{\sum_{j'=j\pm1}p^{(u,j,1)}_{(u,j',2)}r_{(u,j',2)}\mathcal{I}^k_{(u,j',2)}}_{(7)} - \underbrace{\sum_{j'=j\pm1}(\Delta^{(u,j',1)}_{(u,j,1)}N^k_{(u,j,1)} - \Delta^{(u,j,1)}_{(u,j',1)}N^k_{(u,j',1)})}_{(8)} \\ &+ \underbrace{[v^k\tilde{\Xi}(\Delta^{(u,*,1)}_{(u,j,1)}\tilde{\rho}_{(u,j,1)}(v))]_{(u,j,2)}}_{(5)} + \underbrace{\sum_{j'=j\pm1}\Delta^{(u,j,1)}_{(u,j',2)}N^k_{(u,j',1)}}_{(9)}\end{aligned} \tag{6.10}$$

The elements (1)–(9) correspond to the numbers in the Figures 4-2 and 4-3. Moreover, the k-th order *moment-decreasing interaction rate* is defined by:

$$\mathcal{I}^k_{(u,j,c)} \overset{def}{=} \left\langle \int_{w<v} v^k \,|\, w-v \,|\, \tilde{\rho}_{(*,j,1)}(w)\,\mathrm{d}\,w \right\rangle_{(u,j,c)} = \left\langle v^k \tilde{\Psi}_{(*,j)}(v) \right\rangle_{(u,j,c)} = \frac{[v^k\tilde{\Psi}_{(*,j)}(v)]_{(u,j,c)}}{r_{(u,j,c)}} \tag{6.11}$$

This interaction-moment describes the expected flux of the k-th moment from lane j per unit time per immediately overtaking vehicle.

6.2.2 *MLMC conservation of unconstrained vehicles equation ($k = 0$)*

Let us consider the dynamics of the traffic density reflecting the expected number of unconstrained vehicles of class u on lane j per unit road length. That is, let us consider equation (6.10) for $k = 0$*. We find:

* Alternatively, we can directly apply the method of conservative moments to the reduced gas-kinetic equations of free-flowing vehicles (5.23) to determine the conservative moment dynamics of $N^k_{(u,j,c)}$.

$$\begin{aligned}
&\partial_t r_{(u,j,1)} + \underbrace{\partial_x m_{(u,j,1)}}_{(1)} = \underbrace{-(1-p^*_{(u,j,1)}) r_{(u,j,1)} \mathcal{I}^0_{(u,j,1)}}_{(4)} + \underbrace{[\tilde{\Xi}(\Delta^{(u,*,1)}_{(u,j,1)} \tilde{\rho}_{(u,j,1)}(v))]_{(u,j,2)}}_{(5)} \\
&\underbrace{- \sum_{j'=j\pm1} (p^{(u,j',1)}_{(u,j,1)} r_{(u,j,1)} \mathcal{I}^0_{(u,j,1)} - p^{(u,j,1)}_{(u,j',1)} r_{(u,j',1)} \mathcal{I}^0_{(u,j',1)})}_{(6)} + \underbrace{\sum_{j'=j\pm1} p^{(u,j,1)}_{(u,j',2)} r_{(u,j',2)} \mathcal{I}^0_{(u,j',2)}}_{(7)} \\
&\underbrace{- \sum_{j'=j\pm1} (\Delta^{(u,j',1)}_{(u,j,1)} r_{(u,j,1)} - \Delta^{(u,j,1)}_{(u,j',1)} r_{(u,j',1)})}_{(8)} + \underbrace{\sum_{j'=j\pm1} \Delta^{(u,j,1)}_{(u,j',2)} r_{(u,j',2)}}_{(9)}
\end{aligned} \tag{6.12}$$

The elements (1)–(9) correspond to the numbers in the Figures 4-2 and 4-3. We can conclude that the expected number of vehicles of class u on lane j per unit roadway length changes over time due to convection (1) – balance of conservative momentum flux (flowrate) $m_{(u,j,1)}$ – deceleration (4), state-relaxation (5), and lane-changing (6)-(9). With respect to the latter lane-changing processes, the term (6) reflects the balance of unconstrained immediate lane-changing *to* and *from* the adjacent lanes $j\pm1$. The term (7) reflects the inflow of immediate constrained overtaking on the adjacent lanes. The terms (8) and (9) respectively depict the dynamics of the balance of spontaneously lane-changing vehicles *to* and *from* the adjacent lanes ($j\pm1$), and postponed lane-changing vehicles from the adjacent lanes ($j\pm1$).

6.2.3 *MLMC momentum dynamics for unconstrained vehicles (k = 1)*

If we aim to establish the momentum equations describing dynamics of expected momentum of unconstrained vehicles of class u on lane j per unit road length, we consider equation (6.10) for $k = 1$. We find:

$$\begin{aligned}
&\partial_t m_{(u,j,1)} + \underbrace{2\partial_x e_{(u,j,1)}}_{(1)} = \underbrace{(m^a_{(u,j,1)} - m_{(u,j,1)})/\tau^0_u}_{(2)} - \underbrace{(1-p^*_{(u,j,1)}) r_{(u,j,1)} \mathcal{I}^1_{(u,j,1)}}_{(4)} \\
&+ \underbrace{[v\tilde{\Xi}(\Delta^{(u,*,1)}_{(u,j,1)} \tilde{\rho}_{(u,j,1)}(v))]_{(u,j,2)}}_{(5)} - \underbrace{\sum_{j'=j\pm1} (p^{(u,j',1)}_{(u,j,1)} r_{(u,j,1)} \mathcal{I}^1_{(u,j,1)} - p^{(u,j,1)}_{(u,j',1)} r_{(u,j',1)} \mathcal{I}^1_{(u,j',1)})}_{(6)} \\
&+ \underbrace{\sum_{j'=j\pm1} p^{(u,j,1)}_{(u,j',2)} r_{(u,j',2)} \mathcal{I}^1_{(u,j',2)}}_{(7)} - \underbrace{\sum_{j'=j\pm1} (\Delta^{(u,j',1)}_{(u,j,1)} m_{(u,j,1)} - \Delta^{(u,j,1)}_{(u,j',1)} m_{(u,j',1)})}_{(8)} + \underbrace{\sum_{j'=j\pm1} \Delta^{(u,j,1)}_{(u,j',2)} m_{(u,j',2)}}_{(9)}
\end{aligned} \tag{6.13}$$

The dynamics equations describing the changes in the traffic momentum $m_{(u,j,c)}$ over time due to convection (1), acceleration (2), deceleration (4), state-relaxation (5), and immediate lane-changing, spontaneous lane-changing, and postponed lane-changing to and from the adjacent lanes (6)-(9). Apart from the acceleration term (2), these terms are similar to the terms present in the generalised conservation of unconstrained vehicles equation (6.12). With respect to the acceleration term (2), we observe that traffic momentum increases due to unconstrained vehicles accelerating towards their *acceleration velocity*. The expected acceleration velocity of unconstrained vehicles equals:

$$V^a_{(u,j,1)}(x,t) \overset{def}{=} \left\langle \tilde{W}_{(u,j,1)}(v \mid x,t) \right\rangle_{(u,j,1)} \tag{6.14}$$

where $\tilde{W}_{(u,j,1)}(v \mid x,t)$ is the reduced unconstrained acceleration velocity (eq. (5.21)). In case of unconstrained vehicles, the reduced unconstrained *acceleration* velocity equals the expected *desired* velocity $\tilde{V}^0_{(u,j,1)}(v \mid x,t)$. The so-called *acceleration momentum* is defined by:

$$m^a_{(u,j,1)}(x,t) \overset{def}{=} [\tilde{W}_{(u,j,1)}(v \mid x,t)]_{(u,j,1)} = r_{(u,j,1)}(x,t) V^a_{(u,j,1)}(x,t) \tag{6.15}$$

Unlike the results of Helbing (1996,1997a), the *expected acceleration velocity* is *not constant* but rather *depends on current traffic conditions*. That is, changes in traffic conditions changes the expected number of unconstrained vehicles driving with velocity v having desired velocity v^0. As a result, the conditional probability density function $\tilde{g}_{(u,j,1)}(v^0 \mid v)$ and consequently the expected acceleration velocity $\tilde{W}_{(u,j,1)}(v \mid x,t)$ change.

6.2.4 *MLMC energy dynamics for unconstrained vehicles (k = 2)*

If we consider the dynamics of the traffic energy reflecting the expected energy of unconstrained vehicles of class u on lane j per unit road length, we consider equation (6.10) for $k = 2$. We find:

$$\begin{aligned}
&\partial_t e_{(u,j,1)} + \underbrace{2\partial_x (m_{(u,j,1)} H_{(u,j,1)} + \tfrac{1}{2} J_{(u,j,1)})}_{(1)} = \underbrace{2(e^a_{(u,j,1)} - e_{(u,j,1)})/\tau^0_u}_{(2)} \\
&\underbrace{-\tfrac{1}{2}(1 - p^*_{(u,j,1)}) r_{(u,j,1)} \mathcal{I}^2_{(u,j,1)}}_{(4)} + \underbrace{\tfrac{1}{2}[v^2 \tilde{\Xi}(\Delta^{(u,*,1)}_{(u,j,1)} \tilde{\rho}_{(u,j,1)}(v))]_{(u,j,2)}}_{(5)} \\
&\underbrace{-\tfrac{1}{2} \sum_{j'=j\pm1} (p^{(u,j',1)}_{(u,j,1)} r_{(u,j,1)} \mathcal{I}^2_{(u,j,1)} - p^{(u,j,1)}_{(u,j',1)} r_{(u,j',1)} \mathcal{I}^2_{(u,j',1)})}_{(6)} + \underbrace{\tfrac{1}{2} \sum_{j'=j\pm1} p^{(u,j,1)}_{(u,j',2)} r_{(u,j',2)} \mathcal{I}^2_{(u,j',2)}}_{(7)} \\
&\underbrace{- \sum_{j'=j\pm1} (\Delta^{(u,j',1)}_{(u,j,1)} e_{(u,j,1)} - \Delta^{(u,j,1)}_{(u,j',1)} e_{(u,j',1)})}_{(8)} + \underbrace{\sum_{j'=j\pm1} \Delta^{(u,j,1)}_{(u,j',2)} e_{(u,j',2)}}_{(9)}
\end{aligned} \tag{6.16}$$

Processes similar to processes governing momentum dynamics govern the dynamics of the energy of unconstrained vehicles of class u on lane j. In the remainder of this thesis, we define *acceleration energy* as the sum of *covariance between velocity and acceleration velocity*:

$$C_{(u,j,1)}(x,t) \overset{def}{=} \left\langle v \cdot (\tilde{W}_{(u,j,1)}(v \mid x,t) - V^a_{(u,j,1)}(x,t)) \right\rangle_{(u,j,1)} \tag{6.17}$$

and the product of expected velocity and expected acceleration velocity, yielding:

$$e^a_{(u,j,1)} = \tfrac{1}{2} r_{(u,j,1)} (C_{(u,j,1)} + V_{(u,j,1)} V^a_{(u,j,1)}) \tag{6.18}$$

6.3 Macroscopic MLMC equations for constrained vehicles (c = 2)

Similar to dynamic equations of free-flowing vehicles, we can specify the generalised conservative moment equation (6.9) for platooning vehicles of class u on lane j (section 6.4.1). Using this equation, we can determine the generalised conservation of vehicles equation, momentum dynamics, and energy dynamics for free-flowing vehicles (sections 6.4.2-6.4.4).

6.3.1 MLMC conservative moment dynamics for constrained traffic

Similar to the case of free-flowing vehicles, in appendix D.2 we show how the conservative moment dynamics of platooning vehicles can be determined from equation (6.9), using the relations determined in chapters 4 and 5. It is shown that the following partial differential equation results for the conservative moments of constrained vehicles of class u on lane j:

$$\begin{aligned}\partial_t N^k_{(u,j,2)} + \underbrace{\partial_x N^{k+1}_{(u,j,2)}}_{(1)} &= \underbrace{k\frac{D^k_{(u,j,2)} - N^k_{(u,j,2)}}{\mathrm{T}^k_{(u,j,2)}}}_{(2)} + \underbrace{(1-p^*_{(u,j,1)})r_{(u,j,1)}\mathcal{X}^k_{(u,j,1)}}_{(3)} - \underbrace{\sum_{j'=j\pm1}\Delta^{(u,j',1)}_{(u,j,2)}N^k_{(u,j,2)}}_{(8)} \\ &\underbrace{-(1-p^*_{(u,j,2)})r_{(u,j,2)}\mathcal{R}^k_{(u,j,2)}}_{(3+4)} \underbrace{-\sum_{j'=j\pm1}p^{(u,j',1)}_{(u,j,2)}r_{(u,j,2)}\mathcal{I}^k_{(u,j,2)}}_{(7)} \\ &\underbrace{-\sum_{j'=j\pm1}(p^{(u,j',2)}_{(u,j,2)}r_{(u,j,2)}\mathcal{I}^k_{(u,j,2)} - p^{(u,j,2)}_{(u,j',2)}r_{(u,j',2)}\mathcal{I}^k_{(u,j',2)})}_{(7)} \underbrace{-[v^k\tilde{\Xi}(\Delta^{(u,*,1)}_{(u,j,1)}\tilde{\rho}_{(u,j,1)}(v))]_{(u,j,2)}}_{(5)}\end{aligned} \tag{6.19}$$

where the *k-th interaction rate* equals:

$$\mathcal{R}^k_{(u,j,c)} = \mathcal{I}^k_{(u,j,c)} - \mathcal{X}^k_{(u,j,c)} \tag{6.20}$$

and where the *k-th order moment-increasing interaction rate* is defined by:

$$\mathcal{X}^k_{(u,j,c)} \overset{def}{=} \left\langle \int_{w<v} w^k \,|\, w-v \,|\, \tilde{\rho}_{(*,j,1)}(w)\,\mathrm{d}\,w \right\rangle_{(u,j,c)} = \frac{[\int_{w<v} w^k \,|\, w-v \,|\, \tilde{\rho}_{(*,j,1)}(w)\,\mathrm{d}\,w]_{(u,j,c)}}{r_{(u,j,c)}} \tag{6.21}$$

Note that we can rewrite this expression by changing the order of integration:

$$r_{(u,j,c)}\mathcal{X}^k_{(u,j,c)} = \sum_{u'}\left[v^k \int_{w>v} |\, w-v \,|\, \tilde{\rho}_{(u,j,c)}(w)\,\mathrm{d}\,w \right]_{(u',j,c)} \tag{6.22}$$

6.3.2 MLMC conservation of constrained vehicles equation (k = 0)

Let us consider the dynamics of the traffic density reflecting the expected number of constrained vehicles of class u on lane j per unit road length. That is, let us consider equation (6.19) for $k = 0$. Since by definition we have:

$$\left[\int_{w<v} |\, w-v \,|\, \tilde{\rho}_{(*,j,1)}(w)\,\mathrm{d}\,w \right]_{(u,j,2)} = [\tilde{\Psi}_{(*,j)}(v)]_{(u,j,2)} \tag{6.23}$$

we have $\mathcal{I}^0_{(u,j,2)} = \mathcal{X}^0_{(u,j,2)}$, and thus equation (6.19) reduces to:

$$\partial_t r_{(u,j,2)} + \underbrace{\partial_x m_{(u,j,2)}}_{(1)} = \underbrace{(1-p^{*}_{(u,j,1)})r_{(u,j,1)}\mathcal{X}^{0}_{(u,j,1)}}_{(3)} - \underbrace{\sum_{j'=j\pm1} p^{(u,j',1)}_{(u,j,2)} r_{(u,j,2)}\mathcal{I}^{0}_{(u,j,2)}}_{(7)} - \underbrace{\sum_{j'=j\pm1}\Delta^{(u,j',1)}_{(u,j,2)} r_{(u,j,2)}}_{(9)}$$
$$- \underbrace{\sum_{j'=j\pm1}(p^{(u,j',2)}_{(u,j,2)} r_{(u,j,2)}\mathcal{I}^{0}_{(u,j,2)} - p^{(u,j,2)}_{(u,j',2)} r_{(u,j',2)}\mathcal{I}^{0}_{(u,j',2)})}_{(7')} - \underbrace{[\tilde{\Xi}(\Delta^{(u,*,1)}_{(u,j,1)}\tilde{\rho}_{(u,j,1)}(v))]_{(u,j,2)}}_{(5)} \tag{6.24}$$

for $k = 0$. From this result, we conclude that the density reflecting the expected number of constrained vehicles of class u on lane j, changes over time due to convection (1), unconstrained vehicles of class u on lane j decelerating after an interaction and joining the platoon (3), immediately overtaking constrained vehicles becoming unconstrained on the destination lane (7), balance between immediately overtaking vehicles staying constrained *to* and *from* the adjacent lanes (7), postponed lane-changing to the adjacent lanes (9), and finally state-relaxation (5).

6.3.3 *MLMC conservation of momentum for constrained vehicles equation (k = 1)*

In order to determine the momentum dynamics of platooning vehicles of class u on lane j, we consider equation (6.19) for $k = 1$. We find:

$$\partial_t m_{(u,j,2)} + \underbrace{2\partial_x e_{(u,j,2)}}_{(1)} = \underbrace{(m^{a}_{(u,j,2)} - m_{(u,j,2)})/\mathrm{T}^{1}_{(u,j,2)}}_{(2)} - \underbrace{(1-p^{*}_{(u,j,2)})r_{(u,j,2)}\mathcal{I}^{1}_{(u,j,2)}}_{(4)}$$
$$+ \underbrace{(1-p^{*}_{(u,j,1)})r_{(u,j,1)}\mathcal{X}^{1}_{(u,j,1)}}_{(3)} + \underbrace{(1-p^{*}_{(u,j,2)})r_{(u,j,2)}\mathcal{X}^{1}_{(u,j,2)}}_{(3')}$$
$$- \underbrace{\sum_{j'=j\pm1} p^{(u,j',1)}_{(u,j,2)} r_{(u,j,2)}\mathcal{I}^{1}_{(u,j,2)}}_{(7)} - \underbrace{\sum_{j'=j\pm1}(p^{(u,j',2)}_{(u,j,2)} r_{(u,j,2)}\mathcal{I}^{1}_{(u,j,2)} - p^{(u,j,2)}_{(u,j',2)} r_{(u,j',2)}\mathcal{I}^{1}_{(u,j',2)})}_{(7')} \tag{6.25}$$
$$- \underbrace{[v\tilde{\Xi}(\Delta^{(u,*,1)}_{(u,j,1)}\tilde{\rho}_{(u,j,1)}(v))]_{(u,j,2)}}_{(5)} - \underbrace{\sum_{j'=j\pm1}\Delta^{(u,j',1)}_{(u,j,2)} m_{(u,j,2)}}_{(9)}$$

Compared to the dynamics of the constrained density (6.24), the dynamics of the momentum of constrained vehicles are also affected by platooning vehicles that accelerate together with their platoon leader (term (2)), and decelerating constrained vehicles (terms (3′) and (4)).

The acceleration momentum $m^{a}_{(u,j,2)}$ is defined by the product of the density $r_{(u,j,2)}$ and the expected *acceleration velocity* $V^{a}_{(u,j,2)}$ of constrained vehicles. These are defined similar to the acceleration momentum $m^{a}_{(u,j,1)}$ and the expected acceleration velocity $V^{a}_{(u,j,1)}$ of platoon-leaders (eqn. (6.14) and (6.15)). However, in the constrained case, the reduced acceleration velocity $\tilde{W}_{(u,j,2)}(v|x,t)$ (eq. (5.21)) stems from the expected desired velocity $\tilde{V}^{0}_{(u,j,1)}(v|x,t)$ of platoon-leaders driving at velocity v (see section 4.4.2).

6.3.4 *MLMC conservation of energy for constrained vehicles equation (k = 2)*

In order to establish the expected energy dynamics of platooning vehicles of class u on lane j per unit road length, we consider eq. (6.19) for $k = 2$:

$$\begin{aligned}
&\partial_t e_{(u,j,2)} + \underbrace{\partial_x (m_{(u,j,2)} H_{(u,j,2)} + \tfrac{1}{2} J_{(u,j,2)})}_{(1)} = \underbrace{2(e^a_{(u,j,2)} - e_{(u,j,2)})/\mathrm{T}^2_{(u,j,2)}}_{(2)} \\
&+ \underbrace{\tfrac{1}{2}(1-p^*_{(u,j,1)}) r_{(u,j,1)} \mathcal{X}^2_{(u,j,1)}}_{(3)} + \underbrace{\tfrac{1}{2}(1-p^*_{(u,j,2)}) r_{(u,j,2)} \mathcal{X}^2_{(u,j,2)}}_{(3')} - \underbrace{\tfrac{1}{2}(1-p^*_{(u,j,2)}) r_{(u,j,2)} \mathcal{I}^2_{(u,j,2)}}_{(4)} \\
&- \underbrace{\tfrac{1}{2} \sum_{j'=j\pm1} p^{(u,j',1)}_{(u,j,2)} r_{(u,j,2)} \mathcal{I}^2_{(u,j,2)}}_{(7)} - \underbrace{\tfrac{1}{2} \sum_{j'=j\pm1} (p^{(u,j',2)}_{(u,j,2)} r_{(u,j,2)} \mathcal{I}^2_{(u,j,2)} - p^{(u,j,2)}_{(u,j',2)} r_{(u,j',2)} \mathcal{I}^2_{(u,j',2)})}_{(7')} \\
&- \underbrace{\tfrac{1}{2} [\nu^2 \tilde{\Xi}(\Delta^{(u,*,1)}_{(u,j,1)} \tilde{\rho}_{(u,j,1)}(v))]_{(u,j,2)}}_{(5)} - \underbrace{\sum_{j'=j\pm1} \Delta^{(u,j',1)}_{(u,j,2)} e_{(u,j,2)}}_{(9)}
\end{aligned} \tag{6.26}$$

The terms affecting the energy dynamics of constrained vehicles are comparable to terms of the momentum dynamics, and are consequently not discussed separately. The constrained acceleration energy $e^a_{(u,j,2)}$ is defined similar to eq. (6.18), by the sum of the covariance between velocity and acceleration velocity of platooning vehicles (see eq. (6.17)), and the product of expected velocity and expected acceleration velocity of constrained vehicles.

6.4 Macroscopic MLMC equations for mixed-state traffic (c = *)

In this section we will present the dynamics of the mixed-state density, momentum, and energy. These equations can be derived either by specifying the different terms in the generalised moments equations (6.9) for c = *. Alternatively, due to the *additivity* of the conservative flow variables, the dynamics equations for the unconstrained and constrained density, momentum, and energy can be totalled, adding up to the dynamic equations of the mixed-state density, momentum, and energy respectively. The latter approach is employed in this section. Moreover, the effects of *within-lane* processes (i.e. acceleration and deceleration) are combined into *equilibrium expressions* for the different conservative moments.

6.4.1 MLMC conservative moment equation for mixed-state traffic

By adding eqn. (6.10) and (6.19) we find the generalised conservative moment equations for mixed-state traffic:

$$\begin{aligned}
&\partial_t N^k_{(u,j)} + \partial_x N^{k+1}_{(u,j)} = k(N^{k,e}_{(u,j)} - N^k_{(u,j)})/\mathrm{T}^k_{(u,j)} \\
&\quad - \sum_{j'=j\pm1} (p^{(u,j')}_{(u,j,} r_{(u,j)} \mathcal{I}^k_{(u,j)} - p^{(u,j)}_{(u,j')} r_{(u,j')} \mathcal{I}^k_{(u,j')}) - \sum_{j'=j\pm1} (\Delta^{(u,j')}_{(u,j)} N^k_{(u,j)} - \Delta^{(u,j)}_{(u,j')} N^k_{(u,j')}))
\end{aligned} \tag{6.27}$$

where we have introduced the *k-th conservative equilibrium moment* $N^{k,e}_{(u,j)}$:

$$N^{k,e}_{(u,j)} \overset{def}{=} D^k_{(u,j)} - \frac{1}{k}(1-p^*_{(u,j)}) r_{(u,j)} \mathrm{T}^k_{(u,j)} \mathcal{R}^k_{(u,j)} \tag{6.28}$$

6.4.2 *MLMC conservation of vehicles for mixed-state traffic (k = 0)*

By adding the conservation equations for unconstrained traffic (6.12) and constrained traffic (6.24), the generalised conservation equation of vehicles for mixed-state traffic can be derived easily. We find the following, simple dynamic equation:

$$\partial_t r_{(u,j)} + \underbrace{\partial_x m_{(u,j)}}_{(1)} = \underbrace{-\sum_{j'=j\pm1}(p^{(u,j')}_{(u,j)} r_{(u,j)} \mathcal{I}^0_{(u,j)} - p^{(u,j)}_{(u,j')} r_{(u,j')} \mathcal{I}^0_{(u,j')})}_{(6+7)} \underbrace{-\sum_{j'=j\pm1}(\Delta^{(u,j')}_{(u,j)} r_{(u,j)} - \Delta^{(u,j)}_{(u,j')} r_{(u,j')})}_{(8+9)} \tag{6.29}$$

for all $u \in \mathbf{U}$, and $j \in \mathbf{J}$, where we have used that deceleration does not influence the traffic density $r_{(u,j)}$, i.e. $\mathcal{R}^0_{(u,j)} = \mathcal{I}^0_{(u,j)} - \mathcal{X}^0_{(u,j)} = 0$. Eq. (6.29) shows that the expected number of vehicles of class u on lane j changes due to the balance between inflow and outflow of vehicles in cell x (1), immediate lane-changing (6+7), and spontaneous and postponed lane-changing (8+9).

6.4.3 *MLMC conservation of momentum for mixed-state traffic (k = 1)*

Adding equations (6.13) and (6.25), yields the mixed-state momentum dynamics. By collecting the terms reflecting the traffic dynamics of vehicles accelerating towards the acceleration velocity on the one hand, and vehicles decelerating due to vehicle interactions on the other hand in a single *equilibrium momentum term*:

$$m^e_{(u,j)} \overset{def}{=} m^a_{(u,j)} - (1 - p^*_{(u,j)}) \mathrm{T}_{(u,j)} r_{(u,j)} \mathcal{R}^1_{(u,j)} \tag{6.30}$$

we find that the generalised conservation of momentum for mixed-state traffic equals:

$$\begin{aligned} \partial_t m_{(u,j)} + \underbrace{2\partial_x e_{(u,j)}}_{(1)} &= \underbrace{(m^e_{(u,j)} - m_{(u,j)})/\mathrm{T}_{(u,j)}}_{(2+3+4)} \\ &- \underbrace{\sum_{j'=j\pm1}(p^{(u,j')}_{(u,j)} r_{(u,j)} \mathcal{I}^1_{(u,j)} - p^{(u,j)}_{(u,j')} r_{(u,j')} \mathcal{I}^1_{(u,j')})}_{(6+7)} - \underbrace{\sum_{j'=j\pm1}(\Delta^{(u,j')}_{(u,j)} m_{(u,j)} - \Delta^{(u,j)}_{(u,j')} m_{(u,j')})}_{(8+9)} \end{aligned} \tag{6.31}$$

for all $u \in \mathbf{U}$, and $j \in \mathbf{J}$. Clearly, the traffic momentum of vehicles of class u on lane j changes over time due to the convection of traffic momentum (1), increase and loss of momentum due to accelerating and decelerating vehicles (2+3+4), immediately lane-changing vehicles (6+7), and spontaneous and postponed lane-changing (8+9).

Approximation of mixed-state acceleration time and acceleration velocity

In (6.31), the *mixed-state acceleration time* approximately equals:

$$1/\mathrm{T}_{(u,j)} \approx (1 - \theta_{(u,j)})/\tau^0_u + \theta_{(u,j)}/\mathrm{T}_{(u,j,2)} \tag{6.32}$$

where based on the assumption that platoon leaders are randomly from the population of unconstrained vehicles, the acceleration time of platooning vehicles approximately equals:

---

* We have implicitly assumed that $\mathrm{T}^k_{(u,j)} \approx \mathrm{T}_{(u,j)}$ for all k.

$$(1-\theta_{(*,j)})r_{(*,j)}/\mathrm{T}_{(u,j,2)} \approx \sum_{u'}(1-\theta_{(u',j)})r_{(u',j)}/\tau_{u'}^{0} \tag{6.33}$$

The *mixed-state acceleration momentum* equals:

$$m_{(u,j)}^{a} = r_{(u,j)}V_{(u,j)}^{a} \approx m_{(u,j,1)}^{a}(\mathrm{T}_{(u,j)}/\tau_{u}^{0}) + m_{(u,j,2)}^{a}(\mathrm{T}_{(u,j)}/\mathrm{T}_{(u,j,2)}) \tag{6.34}$$

enabling determination of the *mixed-state acceleration velocity* $V_{(u,j)}{}^{a}$. In section 8.4.7, we propose approximating the *fraction of constrained vehicles* $\theta_{(u,j)}$ by an explicit function of the total effective density.

6.4.4 *MLMC conservation of energy equation for mixed-state traffic (k = 2)*

Let us finally consider the energy dynamics by adding equations (6.16) and (6.26). We find:

$$\begin{aligned}\partial_t e_{(u,j)} + \underbrace{\partial_x(m_{(u,j)}H_{(u,j)} + \tfrac{1}{2}J_{(u,j)})}_{(1)} = \underbrace{2(e_{(u,j)}^{e} - e_{(u,j)})/\mathrm{T}_{(u,j)}}_{(2+3+4)} \\ \underbrace{-\tfrac{1}{2}\sum_{j'=j\pm1}(p_{(u,j)}^{(u,j')}r_{(u,j)}\mathcal{I}_{(u,j)}^{2} - p_{(u,j')}^{(u,j)}r_{(u,j')}\mathcal{I}_{(u,j')}^{2})}_{(6+7)} \underbrace{-\sum_{j'=j\pm1}(\Delta_{(u,j)}^{(u,j')}e_{(u,j)} - \Delta_{(u,j')}^{(u,j)}e_{(u,j')})}_{(8+9)}\end{aligned} \tag{6.35}$$

where the equilibrium traffic energy e^{e} is defined by:

$$e_{(u,j)}^{e} \overset{def}{=} e_{(u,j)}^{a} - \tfrac{1}{2}(1-p_{(u,j)}^{*})\mathrm{T}_{(u,j)}r_{(u,j)}\mathcal{R}_{(u,j)}^{2} \tag{6.36}$$

with:

$$e_{(u,j)}^{a} = \tfrac{1}{2}r_{(u,j)}(C_{(u,j)} + V_{(u,j)}V_{(u,j)}^{a}) \tag{6.37}$$

Concluding, the traffic momentum of vehicles of class u on lane j changes over time due to the convection of traffic momentum (1), increase and loss of momentum due to accelerating and decelerating vehicles (2+3+4), immediately lane-changing vehicles (6+7), and spontaneous and postponed lane-changing (8+9).

6.4.5 *Equilibrium relations*

The equilibrium momentum m^{e} and the equilibrium energy e^{e} can be considered as the multilane multiclass generalisation of the relations between speed and density (and in some cases speed variance and density), used in other traditional macroscopic traffic flow models (section 2.4). That is, the MLMC equilibrium traffic momentum m^{e} is comparable to the traditional relation between the traffic density r and the traffic flow (momentum) $m^{e} = rV^{e}$, where $V^{e} = V^{e}(r)$ is the equilibrium velocity-density relation (see section 2.4.2).

Let us emphasise that, rather than being *exogenous* to the model, the equilibrium momentum m^{e} is *endogenous*, in the sense that it results from the gas-kinetic derivation approach. This is an important result from the theoretical MLMC traffic flow analysis performed in the context of this study. In this section, we study the equilibrium momentum in more detail. To this end, let us first define the notion of *equilibrium conditions* for MLMC traffic flow operations.

Definition of equilibrium traffic operations

Let us define equilibrium conditions for multilane heterogeneous traffic by the case where:

1. The expected velocity $V_{(u,j)}$ and expected velocity variance $\Theta_{(u,j)}$ equal the equilibrium velocity $V^e_{(u,j)}$ and equilibrium velocity variance $\Theta^e_{(u,j)}$ for each u and j, and
2. The between-lane flows of the density, momentum, and energy due to lane-changing are balanced.

In other words, for any vector $\mathbf{r} = \{r_u\}$ of aggregate-lane densities for each class u, the velocities $V_{(u,j)}$ and the variances $\Theta_{(u,j)}$ satisfy:

$$V_{(u,j)} = V^e_{(u,j)}(\mathbf{r}, \mathbf{V}, \Theta) \qquad \Theta_{(u,j)} = \Theta^e_{(u,j)}(\mathbf{r}, \mathbf{V}, \Theta) \tag{6.38}$$

while for the lateral conservative-moment-flows, we have:

$$\sum_{j'=j\pm1}(p^{(u,j')}_{(u,j)} r_{(u,j)} \mathcal{I}^k_{(u,j)} - p^{(u,j)}_{(u,j')} r_{(u,j')} \mathcal{I}^k_{(u,j')}) + \sum_{j'=j\pm1}(\Delta^{(u,j')}_{(u,j)} N^k_{(u,j)} - \Delta^{(u,j)}_{(u,j')} N^k_{(u,j')}) = 0 \tag{6.39}$$

In illustration, let us consider expression (6.39) for $k = 0$ in case of a two-lane roadway. Then, dividing expression (6.39) by r_u, yields that the density fraction $\alpha_{(u,j)}$ on lane j satisfies:

$$\sum_{j'=j\pm1}(p^{(u,j')}_{(u,j)} \alpha_{(u,j)} \mathcal{I}^0_{(u,j)} - p^{(u,j)}_{(u,j')} \alpha_{(u,j')} \mathcal{I}^0_{(u,j')}) + \sum_{j'=j\pm1}(\Delta^{(u,j')}_{(u,j)} \alpha_{(u,j)} - \Delta^{(u,j')}_{(u,j)} \alpha_{(u,j')}) = 0 \tag{6.40}$$

Since $\alpha_{(u,2)} = 1 - \alpha_{(u,1)}$, we have:

$$\alpha_{(u,1)} = \frac{p^{(u,1)}_{(u,2)} \mathcal{I}^0_{(u,2)} + \Delta^{(u,1)}_{(u,2)}}{p^{(u,2)}_{(u,1)} \mathcal{I}^0_{(u,1)} + p^{(u,1)}_{(u,2)} \mathcal{I}^0_{(u,2)} + \Delta^{(u,2)}_{(u,1)} + \Delta^{(u,1)}_{(u,2)}} \tag{6.41}$$

That is, the fraction of vehicles of class u using the right lane $j = 1$ is determined by the ratio of the lane-changing rates from the left lane to the right lane, and the total number of lane-changing rates. That is, as the number of lane-changes per vehicle per unit time from lane 2 to lane 1 increases, the fraction of vehicles on lane 1 increases accordingly and vice versa. Note that similar expressions can be derived for motorways with more than two roadway lanes. Also, we can determine expressions for the lane-distribution of momentum and energy given equilibrium conditions. By doing so, in principle we are able to solve the spontaneous and postponed lane-changing rates Δ using the specification of the immediate lane-changing probabilities on the one hand, and the empirically established relations for the lane-distributions of density, momentum, and energy on the other hand.

Equilibrium traffic momentum and energy

The momentum of class u on lane j converges to the MLMC equilibrium traffic momentum $m^e_{(u,j)}$ with a rate equal to the acceleration time $T_{(u,j)}$. This equilibrium momentum is a result of two *competing processes*, namely 1) the *acceleration process* to the desired velocity of platoon-leading vehicles on the one hand, and 2) the *deceleration process* due to vehicular interaction. For both processes, the distinction of user-classes is important. For one, the acceleration velocity depends on the desired velocity of platoon leaders, which is biased towards the desired velocity of the slower vehicles in the traffic flow (generally, the trucks).

Secondly, the interaction process reveals both within and between user-class interactions. In illustration, let us consider the interaction term in the expression for the k-th conservative equilibrium moment (6.28). Considering the negative influence of the events, we have:

$$r_{(u,j)}\mathcal{I}^{k}_{(u,j)} = \sum_{u'\in U}\int_{v} v^{k}\tilde{\rho}_{(u,j)}(v)\int_{w<v}|w-v|\,\tilde{\rho}_{(u',j,1)}(w)\,\mathrm{d}w\,\mathrm{d}v \tag{6.42}$$

By changing the order of integration, we can show that the positive influence of events is:

$$r_{(u,j)}\mathcal{X}^{k}_{(u,j)} = \sum_{u'\in U}\int_{v} v^{k}\tilde{\rho}_{(u',j,1)}(v)\int_{w>v}|w-v|\,\tilde{\rho}_{(u,j)}(w)\,\mathrm{d}w\,\mathrm{d}v \tag{6.43}$$

Consequently, for the traffic momentum ($k = 1$), we find:

$$r_{(u,j)}\mathcal{R}^{k}_{(u,j)} = \sum_{u'\in U}\int_{v}\left(v\tilde{\rho}_{(u,j)}(v)\int_{w<v}|w-v|\,\tilde{\rho}_{(u',j,1)}(w)\mathrm{d}w + v\tilde{\rho}_{(u',j,1)}(v)\int_{w>v}|w-v|\,\tilde{\rho}_{(u,j)}(w)\mathrm{d}w\mathrm{d}v\right) \tag{6.44}$$

In illustration, Figure 6-1 shows the equilibrium traffic momentum ($k = 1$) of person-cars as a function of the (modified) density for various truck percentages on two lanes of a motorway*.

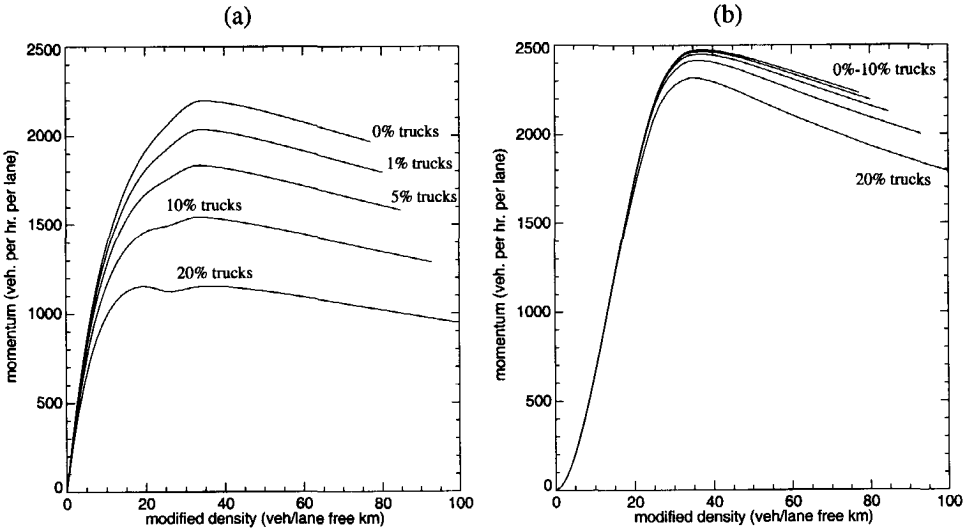

Figure 6-1: Equilibrium traffic momentum for person-cars on right-lane (a) and left-lane (b) of a two-lane roadway with various percentages of trucks.

6.4.6 Within and between user-class interactions

Expression (6.44) reveals how the velocity changes due to both *within* user-class interactions ($u' = u$), and *between* user-class interactions ($u' \neq u$).

Within user-class interactions

Since vehicles of the same user-class can drive at different velocities – reflected by the velocity variance $\Theta_{(u,j)}$ – fast vehicles from user-class u may interact with slow vehicles of user-

* The approach to determine the equilibrium conditions is presented in chapter 8.

class u. The influence of this within user-class interaction is present in both the MLMC traffic momentum dynamic equations and the MLMC traffic energy dynamic equations, as reflected by the equilibrium momentum and energy relations (6.30) and (6.36).

For the *traffic momentum*, we have, for $u' = u$ (equation (6.44)):

$$\begin{aligned}\int v\tilde{\rho}_{(u,j)}(v)\int_{w<v}|w-v|\,\tilde{\rho}_{(u,j,1)}(w)\,\mathrm{d}w\,\mathrm{d}v - \int v\tilde{\rho}_{(u,j,1)}(v)\int_{w>v}|w-v|\,\tilde{\rho}_{(u,j)}(w)\,\mathrm{d}w\,\mathrm{d}v \\ \approx (1-\theta_{(u,j)})\int v\tilde{\rho}_{(u,j)}(v)\int (w-v)\tilde{\rho}_{(u,j)}(w)\,\mathrm{d}w\,\mathrm{d}v \\ = (1-\theta_{(u,j)})r_{(u,j)}^2\Theta_{(u,j)}\end{aligned} \tag{6.45}$$

In other words, the influence of within class interactions on the equilibrium momentum is reflected by the expected rate at which fast vehicles in the class are impeded by slower vehicles of the same class. This *expected interaction rate* is expressed by the fraction of platoon-leading vehicles of class u on lane j, and the velocity variance of user-class u on lane j, which describes the within class velocity diffusion.

For the *energy*, a similar relation is found for $u' = u$. That is, we find that the *within user-class* influence on the magnitude of the equilibrium traffic energy is expressed by the term:

$$\begin{aligned}\int v^2\tilde{\rho}_{(u,j)}(v)\int_{w<v}|w-v|\,\tilde{\rho}_{(u,j,1)}(w)\,\mathrm{d}w\,\mathrm{d}v - \int v^2\tilde{\rho}_{(u,j,1)}(v)\int_{w>v}|w-v|\,\tilde{\rho}_{(u,j)}(w)\,\mathrm{d}w\,\mathrm{d}v \\ \approx (1-\theta_{(u,j)})r_{(u,j)}^2(\Gamma_{(u,j)}+2V_{(u,j)}\Theta_{(u,j)})\end{aligned} \tag{6.46}$$

where $\Gamma_{(u,j)} = J_{(u,j)}/r_{(u,j)}$ denotes the *skewness* of the velocities of class u on lane j.

The reader can easily verify that the influence of the within user-class interactions on the equilibrium traffic momentum and equilibrium traffic energy amounts to equivalent expressions derived by Helbing (1996,1997a) for his single-class flow model, although Helbing does not explicitly consider the correlation between platoon leaders and followers.

Between user-class interactions for disjoint velocity supports

To illustrate the influence of the between-class interactions, let us consider the equilibrium momentum for $u' \neq u$. The between-class interactions are reflected by the term:

$$\sum_{u'\neq u}\left(\int v\tilde{\rho}_{(u,j)}(v)\int_{w<v}|w-v|\,\tilde{\rho}_{(u',j,1)}(w)\,\mathrm{d}w\,\mathrm{d}v - \int v\tilde{\rho}_{(u',j,1)}(v)\int_{w>v}|w-v|\,\tilde{\rho}_{(u,j)}(w)\,\mathrm{d}w\,\mathrm{d}v\right) \tag{6.47}$$

In illustration, let us consider two classes (1 and 2) of slow and fast vehicles respectively. Moreover, let us assume that *all* vehicles of class 1 are slower than any vehicle of class 2. In this case, we can easily show that for class 1, the equilibrium momentum (and energy) are invariant with respect to the vehicles of class 2. This implies that the *supports*[*] of the velocity distribution functions of classes1 and 2 are disjoint. That is:

$$\int v\tilde{\rho}_{(1,j)}(v)\int_{w<v}(w-v)\tilde{\rho}_{(2,j,1)}(w)\,\mathrm{d}w\,\mathrm{d}v + \int v\tilde{\rho}_{(2,j,1)}(v)\int_{w>v}(w-v)\tilde{\rho}_{(1,j)}(w)\,\mathrm{d}w\,\mathrm{d}v = 0 \tag{6.48}$$

[*] The support of a probability density function $g(v)$ is defined by the set of all v such that $g(v) > 0$.

In this case, the expression for the equilibrium momentum m^e simplifies to:

$$m^e_{(1,j)} = m^a_{(1,j)} - (1 - p^*_{(1,j)})\mathrm{T}_{(1,j)}(1-\theta_{(1,j)})r^2_{(1,j)}\Theta_{(1,j)} \tag{6.49}$$

That is, the equilibrium momentum is determined by the *acceleration momentum* m^a, reduced by the influence of within user-class interactions of vehicles of class 1 on lane j.

Considering class 2, we can show that the between user-class interactions yield (see Hoogendoorn and Bovy (1998a)):

$$\begin{aligned}\int v\tilde{\rho}_{(2,j)}(v)\int_{w<v}|w-v|\,\tilde{\rho}_{(1,j,1)}(w)\,\mathrm{d}w\,\mathrm{d}v - \int v\tilde{\rho}_{(1,j,1)}(v)\int_{w>v}|w-v|\,\tilde{\rho}_{(2,j)}(w)\,\mathrm{d}w\,\mathrm{d}v \\ = (1-\theta_{(1,j)})r_{(1,j)}r_{(2,j)}(\Theta_{(1,j)}+\Theta_{(2,j)}+(V_{(2,j)}-V_{(1,j)})^2)\end{aligned} \tag{6.50}$$

Consequently, for class 2, the equilibrium momentum becomes:

$$\begin{aligned}m^e_{(2,j)} = m^a_{(2,j)} - (1-p^*_{(2,j)})\mathrm{T}_{(2,j)}r_{(2,j)} \\ \times((1-\theta_{(2,j)})r_{(2,j)}\Theta_{(2,j)} + (1-\theta_{(1,j)})r_{(1,j)}(\Theta_{(1,j)}+\Theta_{(2,j)}+(V_{(2,j)}-V_{(1,j)})^2))\end{aligned} \tag{6.51}$$

Clearly, for class 2 the acceleration momentum m^a is reduced by the within user-class interactions on the one hand, and the between user-class interactions on the other hand. The magnitude of the reduction due to the latter interaction depends on the velocity variance of either user-class, and the difference in the expected velocities of classes 1 and 2.

Between user-class interactions without disjoint velocity supports

Let us again consider the case where two classes are present. Let us assume that both classes have the same velocity variance. Figure 6-2 shows the magnitude of term (6.47) for different values of the expected velocity of class 1 and 2 respectively, given $\Theta = 10.0m^2/s^2$. From these figures we can observe that the velocity interaction moment of class 1 is *unaffected* by both one-sided active and passive interactions with vehicles of user-class 2, in the region characterised by $V_1 < V_2$. However, when the velocity of class 1 is larger than the velocity of class 2, both active and passive velocity interaction moments increase substantially. Note that lines with $V_1 - V_2 = c > 0$ yield different active and passive velocity interaction moments, while the total velocity interactions moments are constant for combinations with $V_1 - V_2 = c$.

6.5 Introducing traffic viscosity

In fluidic or gas-flows, *viscosity* expresses the influence of friction between the particles in the fluid or gas. The effect of the internal friction is expressed by a second order term with respect to the velocity present in the momentum dynamics. However, several authors (e.g. Helbing (1997a)) have argued that *traffic viscosity* cannot be plausibly interpreted from gas-kinetic theory, since due to the one-dimensionality of the traffic flow equations, the viscosity term cannot be shear viscosity (originating from friction between e.g. the boundaries of the flow-region). However, Helbing (1997a) argues that traffic viscosity may be interpreted from the viewpoint of transitions in the drivers' attitudes to prevailing traffic conditions. Hoogendoorn and Bovy (1998a) propose a similar relation for the multiclass case. This viscosity term can be considered to describe higher-order anticipation-behaviour of drivers. In other words,

it models that drivers travelling in a region of *spatially increasing velocities* will anticipate, and accelerate (Kerner *et al.* (1996)).

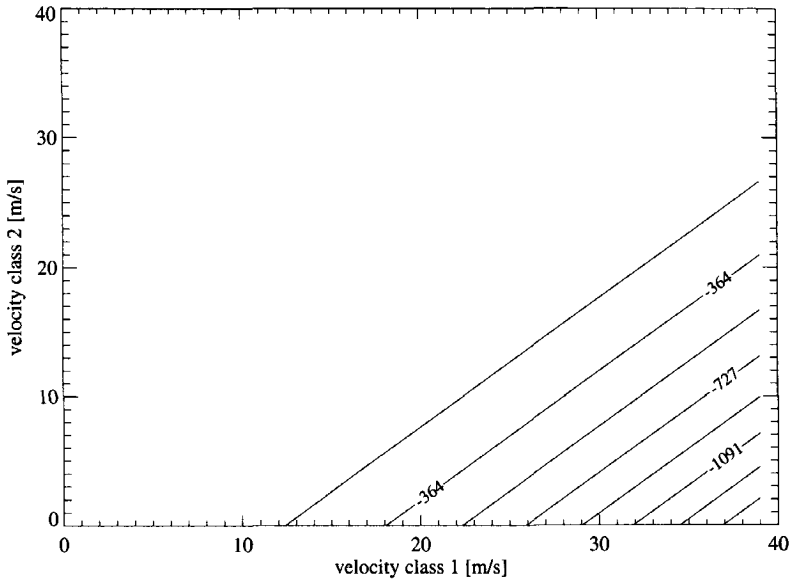

Figure 6-2: Total mean velocity interaction moment of user-class 1.

Let $\eta_{(u,j)}$ denote the so-called *bulk viscosity* for user-class u. Recall from section 3.5.2 that the energy $e_{(u,j)}$ can be expressed as follows:

$$e_{(u,j)} = \tfrac{1}{2}(r_{(u,j)}V^2_{(u,j)} + P_{(u,j)}) \tag{6.52}$$

where $P_{(u,j)} = r_{(u,j)}\Theta_{(u,j)}$ is the *traffic pressure*. This pressure reflects driver's anticipation-behaviour (see among others Kerner *et al.* (1996)). Assuming that traffic pressure $P_{(u,j)}$ is (among other things) a function of the transition rate X from *brisk* to *careful* driving, the additional pressure $\Delta P_{(u,j)}$ due to *changing driving states* yields (cf. Helbing (1996)):

$$\Delta P_{(u,j)} = -\eta_{(u,j)}\partial_x V_{(*,j)} \tag{6.53}$$

where the bulk viscosity equals:

$$\eta_{(u,j)} = r_{(u,j)}\nu_u = r_{(u,j)}\beta_{(u,j)}\partial_X \Delta P_{(u,j)}\big|_{X=0} \tag{6.54}$$

where $\beta_{(u,j)}$ denotes the fraction of brisk drivers.

By substitution of $e_{(u,j)}+\Delta P_{(u,j)}$ in both the traffic momentum equation (6.31) and the traffic energy equation (6.35), using (6.53) we find:

$$\partial_t m_{(u,j)} + \partial_x (2e_{(u,j)} - \eta_{(u,j)} \partial_x V_{(*,j)}) = (m^e_{(u,j)} - m_{(u,j)})/T_{(u,j)} - \sum_{j'=j\pm1} (p^{(u,j')}_{(u,j)} r_{(u,j)} \mathcal{I}^1_{(u,j)} - p^{(u,j)}_{(u,j')} r_{(u,j')} \mathcal{I}^1_{(u,j')}) - \sum_{j'=j\pm1} (\Delta^{(u,j')}_{(u,j)} m_{(u,j)} - \Delta^{(u,j)}_{(u,j')} m_{(u,j')}) \quad (6.55)$$

$$\partial_t e_{(u,j)} + \partial_x (m_{(u,j)} H_{(u,j)} + \tfrac{1}{2} J_{(u,j)} - \eta_{(u,j)} V_{(u,j)} \partial_x V_{(*,j)}) = 2(e^e_{(u,j)} - e_{(u,j)})/T_{(u,j,2)} - \tfrac{1}{2} \sum_{j'=j\pm1} (p^{(u,j')}_{(u,j)} r_{(u,j)} \mathcal{I}^2_{(u,j)} - p^{(u,j)}_{(u,j')} r_{(u,j')} \mathcal{I}^2_{(u,j')}) - \sum_{j'=j\pm1} (\Delta^{(u,j')}_{(u,j)} e_{(u,j)} - \Delta^{(u,j)}_{(u,j')} e_{(u,j')}) \quad (6.56)$$

The second order term introduces a *diffusion-effect*, causing damping of traffic momentum and traffic energy. This diffusion is similar to viscosity effects due to shear friction present in fluids and gasses. Then, ν_u denotes the *kinematic viscosity coefficient* of class u.

6.6 Flux of velocity variance

Additionally, a functional expression for the flux of velocity variance $J_{(u,j)} = r_{(u,j)}\Gamma_{(u,j)}$ is needed. Helbing (1996) proposes using the following relation for single user-class flow:

$$J = -\kappa \frac{\partial \Theta}{\partial x} \quad (6.57)$$

where $\kappa \geq 0$ denotes a *kinetic coefficient*, relating spatial changes in the velocity variance to the flux of velocity variance. In correspondence to this first-order approximation of Helbing (1996) for single class traffic, we propose the following relation for the MLMC case:

$$J_{(u,j)} = -\kappa_u \frac{\partial \Theta_{(u,j)}}{\partial x} \quad (6.58)$$

where $\kappa_u \geq 0$ denotes a user-class specific *kinetic coefficient*. The term stems from finite reaction and braking times of the vehicle-driver combinations, and results in a *spatial smoothing* of the velocity variance*.

6.7 Incorporating finite space requirements into macroscopic equations

We mentioned in section 4.6.4. that although vehicles moving in a traffic stream show some remarkable similarities between particles in a continuous medium, they cannot be considered as infinitesimal. Instead, the vehicles have a finite physical length restricting the total number of vehicles that can occupy a lane of the roadway. Moreover, to ensure safe and comfortable manoeuvring, the drivers take into account an *additional safety margin*, to which we will refer as the *minimal safe distance*. The sum of the vehicle length and the additional distance margin yields the total amount of roadway space occupied by the vehicle. Note that the distance gap of a *platooning vehicle* with respect to its leader equals the minimal safe distance.

In section 4.6 we stated that neglecting the finite space requirements would yield a severe underestimation of the expected number of vehicular interactions per unit time. To remedy this, we have proposed to describe traffic by consideration of the *modified MLMC-PSD*, de-

* Let us emphasise that when mathematically analysing the model equations (section 7.5), both the viscosity and the flux of velocity variance are neglected.

scribing the number of vehicles in the phase-space *per unused roadway space*, based on the safe-distance model of Jepsen (1998) (see section 2.2.1). The modified MLMC-PSD equals the regular MLMC-PSD multiplied by a factor $\delta_j \geq 1$ that is equal to the inverse of the unoccupied space on lane j per unit space on lane j.

6.7.1 Modified traffic flow variables

Similarly to the modified MLMC-PSD, we define the *modified* or *effective mixed-state conservative moments*:

$$\hat{N}^k_{(u,j)}(x,t) = \delta_j(x,t) N^k_{(u,j)}(x,t) \tag{6.59}$$

and the derived conservative variables. Appendix B discusses the effect of considering the finite space requirements on the expected number of vehicle interactions per unit time. We have shown that:

$$\hat{\tilde{\Psi}}_{(*,j)}(v) = \delta_j \tilde{\Psi}_{(*,j)}(v) \tag{6.60}$$

Consequently, we have:

$$\hat{\mathcal{I}}^k_{(u,j)} = \delta_j \mathcal{I}^k_{(u,j)}, \quad \hat{\mathcal{X}}^k_{(u,j)} = \delta_j \mathcal{X}^k_{(u,j)} \quad \text{and} \quad \hat{\mathcal{R}}^k_{(u,j)} = \delta_j \mathcal{R}^k_{(u,j)} \tag{6.61}$$

6.7.2 Finite space requirements in mixed-state flow model

Let us consider the influence of the finite space requirements on the dynamic equations of the MLMC conservative moments $N^k_{(u,j)}$. To this end, we first consider the MLMC dynamics of the mixed-state MLMC traffic density. In appendix B it is shown that given the premise of *adiabatic elimination*, incorporation of the finite space requirements yields the modified generalised *MLMC conservation-of-vehicle equation*:

$$\boxed{\partial_t \hat{r}_{(u,j)} + \partial_x \hat{m}_{(u,j)} = -\sum_{j'=j\pm1} (\hat{p}^{(u,j')}_{(u,j)} \hat{r}_{(u,j)} \hat{\mathcal{I}}^0_{(u,j)} - \hat{p}^{(u,j)}_{(u,j')} \hat{r}_{(u,j')} \hat{\mathcal{I}}^0_{(u,j')}) - \sum_{j'=j\pm1} (\hat{\Delta}^{(u,j')}_{(u,j)} \hat{r}_{(u,j)} - \hat{\Delta}^{(u,j)}_{(u,j')} \hat{r}_{(u,j')})} \tag{6.62}$$

where the *modified immediate lane-changing probability* and the *modified lane-changing rate* are defined by respectively:

$$\hat{p}^{(u,l)}_{(u,k)} \overset{def}{=} (\delta_j / \delta_k) \hat{p}^{(u,l)}_{(u,k)} \quad \text{and} \quad \hat{\Delta}^{(u,l)}_{(u,k)} \overset{def}{=} (\delta_j / \delta_k) \Delta^{(u,l)}_{(u,k)} \quad \text{for all } j,k,l \tag{6.63}$$

Equation (6.62) shows that the dynamics of the modified density of class u on lane j is governed by on the one hand the inflow and outflow of vehicles of class u on lane j in the consider roadway cell x (*convection*). On the other hand, immediate lane-changing, postponed lane-changing, and spontaneous lane-changing cause the modified density to change as well. In this respect, two important remarks must be made.

For one, the introduction of the finite space requirements yields an increase in the number of (active) interactions, causing an increased desire to change to either of the adjacent lanes. Secondly, since the multiplication factor δ_j is generally not equal for each lane j, the *decrease*

of the modified density on the vehicle-transmitting lane is not necessarily equal to the *increase* in the modified density on the vehicle-receiving lane.

Application of a similar method applied to the generalised MLMC conservation-of-vehicle equation, introduces the finite space requirements in the traffic momentum and traffic energy dynamics. To this end, we will show how traffic momentum, traffic energy, and flux-of-velocity variance are transformed into their modified counterparts:

$$m_{(u,j)} \to \hat{m}_{(u,j)}, \quad e_{(u,j)} \to \hat{e}_{(u,j)} \quad \text{and} \quad J_{(u,j)} \to \hat{J}_{(u,j)} \tag{6.64}$$

Clearly, the modified traffic momentum and the modified kinetic traffic energy equal:

$$\hat{m}_{(u,j)} = \hat{r}_{(u,j)} V_{(u,j)} \quad \text{and} \quad \hat{e}_{(u,j)} = \tfrac{1}{2}\hat{r}_{(u,j)}(V^2_{(u,j)} + \Theta_{(u,j)}) \tag{6.65}$$

The modified flux-of-velocity variance equals:

$$\hat{J}_{(u,j)} = \delta_j J_{(u,j)} = -\kappa_{(u,j)} \frac{\partial \Theta_{(u,j)}}{\partial x} \tag{6.66}$$

where the modified kinetic coefficient equals:

$$\hat{\kappa}_{(u,j)} = \delta_j \kappa_{(u,j)} \tag{6.67}$$

By defining the modified viscosity coefficient:

$$\hat{\eta}_{(u,j)} = \delta_j \eta_{(u,j)} \tag{6.68}$$

the second order viscosity term present in the momentum equations is replaced by:

$$\eta_u \frac{\partial^2 V_{(*,j)}}{\partial x^2} \to \hat{\eta}_{(u,j)} \frac{\partial^2 V_{(*,j)}}{\partial x^2} \tag{6.69}$$

Then, the presumption that the adiabatic elimination can be applied yields the following dynamics for the *modified MLMC traffic momentum*:

$$\begin{aligned} &\partial_t \hat{m}_{(u,j)} + \partial_x (2\hat{e}_{u,j} - \hat{\eta}_{(u,j)} \partial_x V_{(*,j)}) = (\hat{m}^e_{(u,j)} - \hat{m}_{(u,j)})/\mathrm{T}_{(u,j)} \\ &\quad - \sum_{j'=j\pm 1} (\hat{p}^{(u,j')}_{(u,j)} \hat{r}_{(u,j)} \hat{\mathcal{I}}^1_{(u,j)} - \hat{p}^{(u,j)}_{(u,j')} \hat{r}_{(u,j')} \hat{\mathcal{I}}^1_{(u,j')}) - \sum_{j'=j\pm 1} (\hat{\Delta}^{(u,j')}_{(u,j)} \hat{m}_{(u,j)} - \hat{\Delta}^{(u,j)}_{(u,j')} \hat{m}_{(u,j')}) \end{aligned} \tag{6.70}$$

where the *modified equilibrium momentum* is defined by:

$$\hat{m}^e_{(u,j)} \overset{def}{=} \hat{r}_{(u,j)} V^a_{(u,j)} - (1 - p^*_{(u,j)}) \mathrm{T}_{(u,j)} \hat{r}_{(u,j)} \hat{\mathcal{R}}^1_{(u,j)} \tag{6.71}$$

The dynamics of the *modified energy* are:

$$\begin{aligned} &\partial_t \hat{e}_{(u,j)} + \partial_x (\hat{m}_{(u,j)} H_{(u,j)} - \hat{\kappa}_{(u,j)} \partial_x \Theta_{(u,j)} - \hat{\eta}_{(u,j)} V_{(u,j)} \partial_x V_{(*,j)}) = 2(\hat{e}^e_{(u,j)} - \hat{e}_{(u,j)})/\mathrm{T}_{(u,j)} \\ &\quad - \tfrac{1}{2} \sum_{j'=j\pm 1} (\hat{p}^{(u,j')}_{(u,j)} \hat{r}_{(u,j)} \hat{\mathcal{I}}^2_{(u,j)} - \hat{p}^{(u,j)}_{(u,j')} \hat{r}_{(u,j')} \hat{\mathcal{I}}^2_{(u,j')}) - \sum_{j'=j\pm 1} (\hat{\Delta}^{(u,j')}_{(u,j)} \hat{e}_{(u,j)} - \hat{\Delta}^{(u,j)}_{(u,j')} \hat{e}_{(u,j')}) \end{aligned} \tag{6.72}$$

where:

$$\hat{e}^{e}_{(u,j)} \overset{def}{=} \hat{e}^{a}_{(u,j)} - \tfrac{1}{2}(1 - p^{*}_{(u,j)})\Gamma_{(u,j)}\hat{r}_{(u,j)}\hat{\mathcal{R}}^{2}_{(u,j)} \tag{6.73}$$

with:

$$\hat{e}^{a}_{(u,j)} = \tfrac{1}{2}\hat{r}_{(u,j)}(C_{(u,j)} + V_{(u,j)}V^{a}_{(u,j)}) \tag{6.74}$$

6.8 Summary

In this chapter, we have derived dynamic equations describing the dynamics of generalised conservative macroscopic traffic variables for generic n-dimensional traffic flows. Moreover, we have specified these relations for one-dimensional MLMC flows, yielding dynamic equations for traffic density, traffic momentum and traffic energy, for unconstrained, constrained traffic, and mixed-state traffic. In the sequel, we will focus on the dynamics of mixed-state traffic variables.

We have discussed within class interactions and the between class interactions reflected by the equilibrium relations for traffic momentum and traffic energy. We showed that within user-class interactions are reflected by the velocity variance. The between user-class interactions are a function of both the difference between mean velocities of the respective classes and accompanying velocity variances. From the expression describing the effect of class interaction in the equilibrium momentum and equilibrium energy, we concluded that slow vehicles remain virtually unaffected by faster vehicles.

The conservative formulation of the MLMC flow equations enables a clear interpretation of the traffic dynamics from the perspective of *collective* longitudinal and lateral vehicular flows of the respective classes on the different lanes. Additionally, the derivation of the model from the reduced gas-kinetic equations presented in chapter 5 is simple, and the dynamic equations are applicable to efficient numerical solution approaches (see chapter 9).

Nevertheless, since traditional macroscopic flow models are generally formulated using the primitive variables, describing the mean behaviour of the entities in the traffic flow, to improve the potential for cross-model comparison, in section 7.3 we will reformulate the model in its primitive form.

The mixed-state traffic dynamics are governed by a system of coupled partial differential equations. That is, the generalised conservation-of-vehicles equation depends on the momentum, the momentum dynamics depend on both the density and the energy, and the energy dynamics also depends on density, and momentum. This interdependence is complex and impairs mathematical analysis of the dynamical system. To this end, in section 7.4 we present a different model formulation in which the partial differential equations are *de-coupled*. The resulting characteristic equations describe the dynamics of the *characteristic variables*. Each equation describing the dynamics of the characteristic variable z_i is only (directly) dependent on that variable z_i. The de-coupling enables improved analysis of the model equations and reveals how disturbances are transported in the heterogeneous flow.

In chapter 8 we specify relations for the constrained vehicle fraction $\theta_{(u,j)}$ as a function of the density. In this chapter we also present specifications of immediate lane-changing probabilities, and postponed and spontaneous lane-changing rates. Also, we will establish relationships for the covariance between velocities and acceleration velocities.

7 PRIMITIVE AND CHARACTERISTIC FORMULATIONS OF MLMC MODEL

This chapter presents two alternative formulations of the developed macroscopic MLMC flow model presented in the previous chapter, which was cast using the so-called *conservative flow variables* ("*conservatives*") *density, momentum,* and *energy*. This conservative formulation enables a clear interpretation of the MLMC traffic dynamics from the viewpoint of the *collective* longitudinal and lateral flows of specific classes on different lanes. Moreover, the model derivation is significantly less cumbersome if using conservatives than when applying the traditional method of moments to derive the macroscopic model using *primitive traffic variables*. We will see in chapter 9 that the conservative model formulation is of dominant importance as well for the correct computation of numerical solutions to the MLMC model using flux-vector splitting schemes.

Nevertheless, the use of conservative flow variables is not widely accepted by the traffic engineering community. Rather, the macroscopic flow models that have been proposed during the long history of macroscopic modelling research have all been cast using the so-called *primitive traffic variables* ("*primitives*") *density, velocity,* and (sometimes) *velocity variance* (see section 2.4). In opposition to the conservatives that describe the aggregate characteristics of the flow, these primitives can be considered to describe the *mean behaviour* of the traffic flow. That is, primitives describe the *expected motion of the average driver*. It is widely accepted that the different terms present in the primitive formulation can be interpreted from the driver's viewpoint.

In order to establish the macroscopic MLMC model using primitives, we will first cast the model equations describing the dynamics of the conservatives in *quasi-linear* form using the

conservative flux Jacobian. This quasi-linear form is then recast into the primitive form. Compared to the conservative form, the primitive form cannot be used easily in numerical approximation approaches. Moreover, mathematical analysis of the form is more difficult (cf. Hoogendoorn and Bovy (1998d)). Nevertheless, the primitive form reveals the analogies with previous macroscopic traffic flow models. Moreover, in this chapter, the primitive MLMC model is considered from the driver's viewpoint. We conclude that behavioural interpretations presented by other authors, such as Payne (1979), Papageorgiou (1989), and Kerner *et al.* (1996), appear not applicable in the case of multiclass traffic flow.

For the purpose of mathematical analysis, neither the primitives nor the conservatives yield the most suitable model form. Therefore, a third type of variable is introduced, namely the so-called *Riemann* or *characteristic* variables. Contrary to the formulations using either primitives or conservatives, the characteristic model formulation is very well suited for both *mathematical* and *numerical analysis* of the continuum model. The Riemann variables cannot be interpreted easily. However, they provide excellent means for, among other things, shock wave analysis and gaining insight into the propagation of small disturbances in multilane heterogeneous flow that are characteristic for dominantly hyperbolic equations, such as the MLMC macroscopic model.

7.1 Conservative, primitive, and Riemann variables

In this section, we discuss the concepts and use of conservative, primitive, and Riemann variables from the viewpoint of model interpretation, comparison with alternative models, numerical solution techniques, and mathematical analysis.

7.1.1 Use of variable transformations

In this chapter we use variable transformations of the macroscopic mixed-state MLMC traffic flow model presented in chapter 6, which has been cast using the *conservative traffic flow variables* traffic density, traffic momentum, and traffic energy. These variables can be considered to describe the expected aggregate state of the vehicular flow in a small roadway segment. For instance, the density describes the expected number of vehicles, while the traffic momentum describes the aggregate momentum of all vehicles present.

The conservative formulation results from our modelling approach. The physical basis for the model is the conservation of density, momentum, and energy of each of the user-classes on the respective motorway lanes. We recall that the traffic density is conserved, that is, the number of vehicles of class u on a lane of a roadway segment changes due to the inflows from the upstream roadway segment and outflows to the downstream roadway segment on the one hand, and the balance of the inflow from and outflow to the adjacent roadway lanes on the other hand. We remark that momentum and energy are not conserved. They *do not* only change due to inflows and outflows from upstream and downstream roadway segments (*longitudinal convection*) and the adjacent lanes (*lateral convection*); non-conservative processes cause changes in traffic momentum and traffic energy as well. These non-conservative processes can be either *source-like* processes (acceleration and deceleration) or *diffusive processes* (viscosity and influence of finite reaction and braking time).

Apart from model derivation, the conservative formulation is also beneficial when establishing valid numerical solution approaches, such as the flux-vector splitting schemes (CIR, Van Leer, and Steger-Warming schemes; see Figure 7-1). These are discussed in section 9.2.

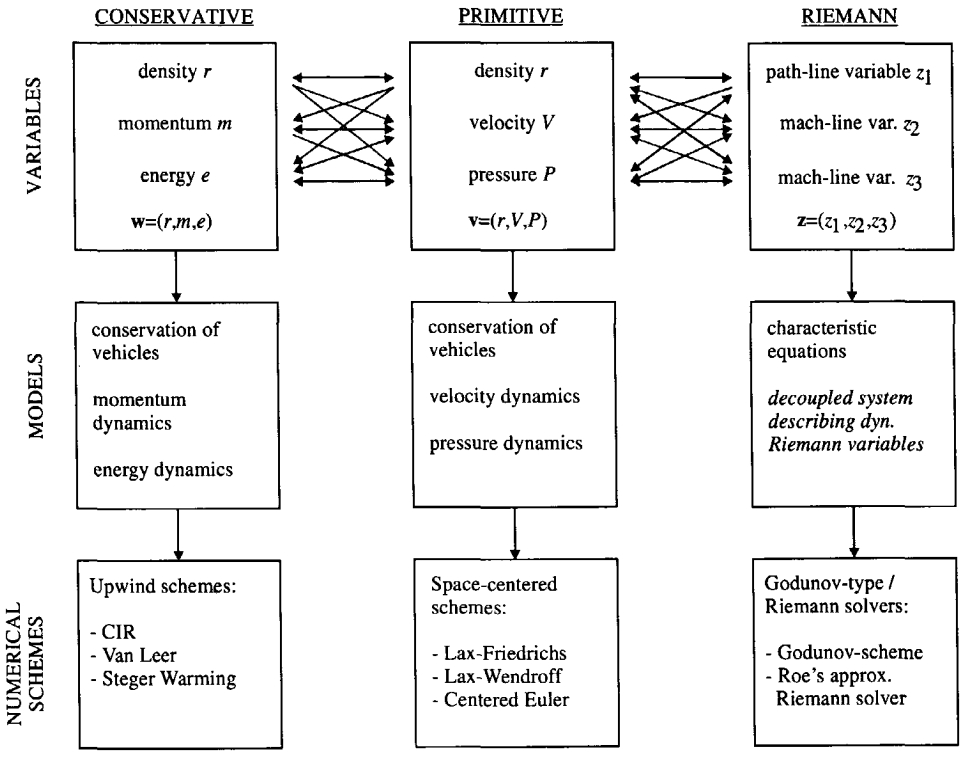

Figure 7-1: Different forms of the macroscopic MLMC-traffic flow model, their relevant variables, and the applicable numerical methods.

The *primitive variables* density, velocity and velocity variance are more 'direct' in the sense that they can be measured immediately from the traffic flow from individual observations. The primitive variables can be considered as describing the average behaviour of individual vehicles in the traffic stream. After recasting the model using primitives, we will analyse and interpret the different terms in the primitive formulation from the viewpoint of an average driver in the traffic stream. Also, since traditionally continuum models are formulated using primitive variables, the primitive formulation enables comparison of the developed model and other (aggregate-lane and aggregate-user-class) macroscopic traffic flow models. The use of the primitive model formulation for establishing valid numerical solution approaches however is limited (Figure 7-1).

In the closure of the previous chapter (section 6.8) we have mentioned that the established MLMC model is a system of coupled partial differential equations, where conservatives are the dependent variables. This coupling means that higher order conservative moments (such as m and e) appear as convective terms in the dynamic equations of lower order conservative

moments (r and m). The dynamic interdependence of conservatives implied by this coupling complicates mathematical analysis, since no clear insight into propagation of disturbances can be obtained. In this chapter, the model is therefore transformed using *Riemann* or *characteristic* variables as well. Key to the characteristic formulation is the *de-coupling* of the model equations, that is, in reformulating the MLMC traffic flow equations into equations describing the dynamics of the Riemann variables, which are independent of the *other* Riemann variables (at least with respect to the longitudinal convective terms). Although the Riemann variables lack a clear interpretation from a traffic engineering perspective, they do enable mathematical analysis (propagation of shock waves and discontinuities) of the heterogeneous traffic flow. Moreover, the characteristic formulation enables application of efficient Godunov-type numerical solution approaches (see Figure 7-1 and section 9.4).

7.2 Quasi-linear formulation of MLMC model

In this section we derive the so-called *quasi-linear* formulation of the MLMC traffic flow model cast using the conservative variables traffic density, momentum, and energy. As will be shown, this quasi-linear formulation will be the foundation of other model formulations. That is, this formulation enables simplified determination of the (pseudo-) primitive and characteristic model forms. Let us first recall the dynamics of mixed-state traffic of sections 6.7.2 and 6.7.3. For notational simplicity, we have dropped the '^' (indicating the *finite-space requirements form*) from notation.

Conservation of vehicles (equation (6.62)):

$$\partial_t r_{(u,j)} + \partial_x m_{(u,j)} = -\sum_{j'=j\pm1}(p^{(u,j')}_{(u,j)} r_{(u,j)} \mathcal{I}^0_{(u,j)} - p^{(u,j)}_{(u,j')} r_{(u,j')} \mathcal{I}^0_{(u,j')}) - \sum_{j'=j\pm1}(\Delta^{(u,j')}_{(u,j)} r_{(u,j)} - \Delta^{(u,j)}_{(u,j')} r_{(u,j')}) \tag{7.1}$$

Traffic momentum dynamics (equation (6.70)):

$$\begin{aligned}\partial_t m_{(u,j)} + \partial_x(2e_{(u,j)} - \eta_{(u,j)}\partial_x V_{(*,j)}) &= (m^e_{(u,j)} - m_{(u,j)})/\mathrm{T}_{(u,j)} \\ &- \sum_{j'=j\pm1}(p^{(u,j')}_{(u,j)} r_{(u,j)} \mathcal{I}^1_{(u,j)} - p^{(u,j)}_{(u,j')} r_{(u,j')} \mathcal{I}^1_{(u,j')}) - \sum_{j'=j\pm1}(\Delta^{(u,j')}_{(u,j)} m_{(u,j)} - \Delta^{(u,j)}_{(u,j')} m_{(u,j')})\end{aligned} \tag{7.2}$$

where the *equilibrium traffic momentum* m^e is defined by:

$$m^e_{(u,j)} \overset{def}{=} r_{(u,j)} V^a_{(u,j)} - (1 - p^*_{(u,j)})\mathrm{T}_{(u,j)} r_{(u,j)} \mathcal{R}^1_{(u,j)} \tag{7.3}$$

Energy dynamics (equation (6.72)):

$$\begin{aligned}\partial_t e_{(u,j)} + \partial_x(m_{(u,j)} H_{(u,j)} - \kappa_{(u,j)}\partial_x \Theta_{(u,j)} - \eta_{(u,j)} V_{(u,j)} \partial_x V_{(*,j)}) &= 2(e^e_{(u,j)} - e_{(u,j)})/\mathrm{T}_{(u,j)} \\ -\tfrac{1}{2}\sum_{j'=j\pm1}(p^{(u,j')}_{(u,j)} r_{(u,j)} \mathcal{I}^2_{(u,j)} - p^{(u,j)}_{(u,j')} r_{(u,j')} \mathcal{I}^2_{(u,j')}) - \sum_{j'=j\pm1}(\Delta^{(u,j')}_{(u,j)} e_{(u,j)} - \Delta^{(u,j)}_{(u,j')} e_{(u,j')})\end{aligned} \tag{7.4}$$

where the *equilibrium traffic energy* e^e is defined by:

$$e^e_{(u,j)} \overset{def}{=} e^a_{(u,j)} - \tfrac{1}{2}(1 - p^*_{(u,j)})\mathrm{T}_{(u,j)} r_{(u,j)} \mathcal{R}^2_{(u,j)} \tag{7.5}$$

In this section we will present the so-called *quasi-linear* formulation of these MLMC equations. This formulation is used to establish the set of MLMC equations cast in the primitive variables density, velocity and variance.

7.2.1 *Conservative-flux formulation*

Let us define the *vector of conservative variables* for traffic of user-class u on lane j:

$$\mathbf{w}_{(u,j)} \overset{def}{=} (w^{(1)}_{(u,j)} \quad w^{(2)}_{(u,j)} \quad w^{(3)}_{(u,j)})^T = (r_{(u,j)} \quad m_{(u,j)} \quad e_{(u,j)})^T \tag{7.6}$$

and let $\mathbf{W} = \{\mathbf{w}_{(u,j)}\}$ be the collection of conservative vectors $\mathbf{w}_{(u,j)}$ for all classes and all lanes. By introducing these vectors, we can recast our model equations (7.1)-(7.5) using the following simple vector-matrix formulation:

$$\partial_t \mathbf{w}_{(u,j)} + \partial_x(\mathbf{f}^C_{(u,j)}(\mathbf{w}_{(u,j)}) - \mathbf{f}^D_{(u,j)}(\mathbf{W})) = \mathbf{x}_{(u,j)}(\mathbf{W}) \tag{7.7}$$

where the *longitudinal convective-flux vector function* $\mathbf{f}^C$ is defined by:

$$\mathbf{f}^C_{(u,j)}(\mathbf{w}_{(u,j)}) \overset{def}{=} (m_{(u,j)} \quad 2e_{(u,j)} \quad m_{(u,j)}H_{(u,j)})^T \tag{7.8}$$

The *diffusive-flux vector function* $\mathbf{f}^D$ is defined by:

$$\mathbf{f}^D_{(u,j)}(\mathbf{W}) \overset{def}{=} (0 \quad \eta_{(u,j)}\partial_x V_{(*,j)} \quad \kappa_{(u,j)}\partial_x \Theta_{(u,j)} + \eta_{(u,j)}V_{(u,j)}\partial_x V_{(*,j)}) \tag{7.9}$$

Finally, the *innerforce*-term $\mathbf{x}_{(u,j)}$ (cf. Kerner *et al.* (1996)) summarises the right-hand-sides of eqn. (7.1) to (7.3), that is, effects of lateral convection, acceleration, and deceleration.

7.2.2 *Quasi-linear formulation*

Alternatively, we can reformulate model (7.7) in its *quasi-linear* form. That is, since:

$$\partial_x \mathbf{f}^C_{(u,j)} = \left(\frac{\partial \mathbf{f}^C_{(u,j)}}{\partial \mathbf{w}_{(u,j)}}\right) \cdot \partial_x \mathbf{w}_{(u,j)} = \mathbf{A}_{(u,j)}(\mathbf{w}_{(u,j)}) \cdot \partial_x \mathbf{w}_{(u,j)} \tag{7.10}$$

we can recast equation (7.7):

$$\boxed{\partial_t \mathbf{w}_{(u,j)} + \mathbf{A}_{(u,j)}(\mathbf{w}_{(u,j)})\partial_x \mathbf{w}_{(u,j)} = \mathbf{x}_{(u,j)}(\mathbf{W}) + \partial_x \mathbf{f}^D_{(u,j)}(\mathbf{W})} \tag{7.11}$$

where the so-called *conservative flux-Jacobian* $\mathbf{A}_{(u,j)}$ is defined by:

$$\mathbf{A}_{(u,j)} = \frac{\partial \mathbf{f}^C_{(u,j)}}{\partial \mathbf{w}_{(u,j)}} = \begin{pmatrix} \cdot & 1 & \cdot \\ \cdot & \cdot & 2 \\ V_{(u,j)}(V^2_{(u,j)} - H_{(u,j)}) & H_{(u,j)} - 2V^2_{(u,j)} & 3V_{(u,j)} \end{pmatrix} \tag{7.12}$$

The conservative flux-Jacobian $\mathbf{A}_{(u,j)}$ shows how small spatial changes in the conservative variables affect the model dynamics, assuming that the convective flux is dominant, i.e. the

diffusive processes are negligible. This implies that the influence of traffic viscosity and the finite reaction and braking times reflected respectively by η and κ is small.

As will be shown in the following section, the quasi-linear form is useful when recasting the model using different dependent traffic flow variables, such as the primitive variables density, velocity, and variance.

7.3 MLMC model in primitive variables

In this section we will show how we can transform the model in conservatives into a different model formulation, namely the MLMC model in *primitives* by using the quasi-linear model (7.11). By explicitly writing the conservative variables density, momentum, and energy as functions of the primitive variables density, velocity, and variance, a linearised relation between variations in the conservative vector $\mathbf{w}$ and variations in the primitive vector $\mathbf{v}$ can be determined. (i.e. $\delta\mathbf{v} = \mathbf{M}\delta\mathbf{w}$). In section 7.4, a similar relation is determined between the primitives and the characteristic variables. Figure 7-2 depicts an overview of the linearised relations between different variable-types.

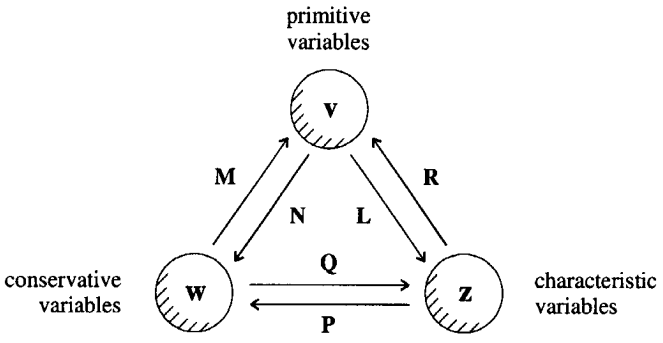

Figure 7-2: Linear transformation-relations among conservative, primitive, and characteristic variables (cf. Hirsch (1990b)).

7.3.1 Transformation of variables

Let us define the vector of *primitive variables* $\mathbf{v}_{(u,j)}$ by:

$$\mathbf{v}_{(u,j)} \overset{def}{=} (r_{(u,j)} \quad V_{(u,j)} \quad \Theta_{(u,j)})^T = (\nu^{(1)}_{(u,j)} \quad \nu^{(2)}_{(u,j)} \quad \nu^{(3)}_{(u,j)})^T \tag{7.13}$$

and let $\mathbf{V} = \{\mathbf{v}_{(u,j)}\}$ be the collection of primitive vectors $\mathbf{v}_{(u,j)}$ for all classes and all lanes. Our aim is to derive equations describing the dynamics of these primitive variables. To this end, we aim to derive these equations in the following quasi-linear form:

$$\partial_t \mathbf{v}_{(u,j)} + \mathbf{B}_{(u,j)}(\mathbf{v}_{(u,j)})\partial_x \mathbf{v}_{(u,j)} = \mathbf{y}_{(u,j)}(\mathbf{V}) + \partial_x \mathbf{g}^D_{(u,j)}(\mathbf{V}) \tag{7.14}$$

Let us reconsider the conservative variables $\mathbf{w}_{(u,j)}$. Note that the following relations between the primitive and the conservative variables can be established (section 3.5):

$$\begin{aligned} r_{(u,j)} = r_{(u,j)} \quad &\Leftrightarrow \quad w^{(1)}_{(u,j)} = v^{(1)}_{(u,j)} \\ m_{(u,j)} = r_{(u,j)} V_{(u,j)} \quad &\Leftrightarrow \quad w^{(2)}_{(u,j)} = v^{(1)}_{(u,j)} v^{(2)}_{(u,j)} \\ e^{j}_{u} = \tfrac{1}{2} r_{(u,j)} (V^2_{(u,j)} + \Theta_{(u,j)}) \quad &\Leftrightarrow \quad w^{(3)}_{(u,j)} = \tfrac{1}{2} v^{(1)}_{(u,j)} ((v^{(2)}_{(u,j)})^2 + v^{(3)}_{(u,j)}) \end{aligned} \tag{7.15}$$

Let us define the transformation matrix $\mathbf{M}_{(u,j)}$ by:

$$\mathbf{M}_{(u,j)} = \frac{\partial \mathbf{w}_{(u,j)}}{\partial \mathbf{v}_{(u,j)}} = \begin{pmatrix} 1 & \cdot & \cdot \\ V_{(u,j)} & r_{(u,j)} & \cdot \\ \tfrac{1}{2}(V^2_{(u,j)} + \Theta_{(u,j)}) & r_{(u,j)} V_{(u,j)} & \tfrac{1}{2} r_{(u,j)} \end{pmatrix} \tag{7.16}$$

Since:

$$\partial_t \mathbf{w}_{(u,j)} = \left(\frac{\partial \mathbf{w}_{(u,j)}}{\partial \mathbf{v}_{(u,j)}} \right) \cdot \partial_t \mathbf{v}_{(u,j)} = \mathbf{M}_{(u,j)} \partial_t \mathbf{v}_{(u,j)} \quad \text{and} \quad \partial_t \mathbf{w}_{(u,j)} = \mathbf{M}_{(u,j)} \partial_x \mathbf{v}_{(u,j)} \tag{7.17}$$

we can recast the quasi-linear form of the MLMC equations (7.11) as follows:

$$\begin{gathered} \mathbf{M}_{(u,j)} \partial_t \mathbf{v}_{(u,j)} + \mathbf{A}_{(u,j)} \mathbf{M}_{(u,j)} \partial_x \mathbf{v}_{(u,j)} = \mathbf{x}_{(u,j)}(\mathbf{W}) + \partial_x \mathbf{f}^D_{(u,j)}(\mathbf{W}) \\ \Leftrightarrow \\ \partial_t \mathbf{v}_{(u,j)} + \mathbf{B}_{(u,j)} \partial_x \mathbf{v}_{(u,j)} = \mathbf{y}_{(u,j)}(\mathbf{V}) + \partial_x \mathbf{g}^D_{(u,j)}(\mathbf{V}) \end{gathered} \tag{7.18}$$

where the *primitive flux-Jacobian* $\mathbf{B}_{(u,j)}$ and the *primitive source term* $\mathbf{y}_{(u,j)}$ satisfy:

$$\mathbf{B}_{(u,j)} = \mathbf{M}^{-1}_{(u,j)} \mathbf{A}_{(u,j)} \mathbf{M}_{(u,j)} \quad \text{and} \quad \mathbf{y}_{(u,j)}(\mathbf{V}) = \mathbf{M}^{-1}_{(u,j)} \mathbf{x}_{(u,j)}(\mathbf{W}) \tag{7.19}$$

respectively, and the *diffusive primitive flux* $\mathbf{g}^D$ equals:

$$\partial_x \mathbf{g}^D_{(u,j)}(\mathbf{V}) = \mathbf{M}^{-1}_{(u,j)} \partial_x \mathbf{f}^D_{(u,j)}(\mathbf{W}) \tag{7.20}$$

These can be determined by deriving the inverse matrix $\mathbf{N}_{(u,j)} = \mathbf{M}_{(u,j)}^{-1}$, which equals:

$$\mathbf{N}_{(u,j)} = \frac{\partial \mathbf{v}_{(u,j)}}{\partial \mathbf{w}_{(u,j)}} = \begin{pmatrix} 1 & \cdot & \cdot \\ -V_{(u,j)} / r_{(u,j)} & 1/r_{(u,j)} & \cdot \\ (V^2_{(u,j)} - \Theta_{(u,j)}) / r_{(u,j)} & -2V_{(u,j)} / r_{(u,j)} & 2/r_{(u,j)} \end{pmatrix} \tag{7.21}$$

Now, let us define the vector functions:

$$(\mathcal{F}^0_{(u,j,j')} \quad \mathcal{F}^1_{(u,j,j')} \quad \mathcal{F}^2_{(u,j,j')})^T \overset{def}{=} \mathbf{N}_{(u,j)} (\mathcal{I}^0_{(u,j')} \quad \mathcal{I}^1_{(u,j')} \quad \mathcal{I}^2_{(u,j')})^T \tag{7.22}$$

yielding:

$$\begin{aligned} \mathcal{F}^0_{(u,j,j')} &= \left\langle \tilde{\Psi}_{(*,j')}(v) \right\rangle_{(u,j')} \\ \mathcal{F}^1_{(u,j,j')} &= r^{-1}_{(u,j)} \left\langle (v - V_{(u,j)}) \tilde{\Psi}_{(*,j')}(v) \right\rangle_{(u,j')} \\ \mathcal{F}^2_{(u,j,j')} &= r^{-1}_{(u,j)} \left\langle (\Theta_{(u,j)} - (v - V_{(u,j)})^2) \tilde{\Psi}_{(*,j')}(v) \right\rangle_{(u,j')} \end{aligned} \tag{7.23}$$

For $k = 1$ and 2, the variables $\mathcal{F}^k$ describe the relative change in the k-th primitive variable for class u on lane j for each vehicle that immediately changes lanes to lane j' per unit time. Their primary use is to simplify the notation of the primitive model formulation.

7.3.2 *Macroscopic MLMC model in primitive traffic variables*

In this section we present the model cast using primitive variables. This is done by using the result (7.18) and substituting the definition (7.22). We can determine the following set of MLMC traffic flow equations:

Conservation of vehicles

The vehicle conservation equation remains the same (equation (7.1)).

Velocity dynamics:

$$\begin{aligned}\dot{V}_{(u,j)} &= \partial_t V_{(u,j)} + V_{(u,j)}\partial_x V_{(u,j)} \\ &= -r_{(u,j)}^{-1}\partial_x(r_{(u,j)}\Theta_{(u,j)}) + (V_{(u,j)}^e - V_{(u,j)})/\mathrm{T}_{(u,j)} \\ &\quad + r_{(u,j)}^{-1}\partial_x(\eta_{(u,j)}\partial_x V_{(*,j)}) - r_{(u,j)}^{-1}\sum_{j'=j\pm1}(p_{(u,j)}^{(u,j')} r_{(u,j)}\mathcal{F}_{(u,j,j)}^1 - p_{(u,j')}^{(u,j)} r_{(u,j')}\mathcal{F}_{(u,j,j')}^1) \\ &\quad + r_{(u,j)}^{-1}\sum_{j'=j\pm1}\Delta_{(u,j')}^{(u,j)} r_{(u,j')}(V_{(u,j')} - V_{(u,j)})\end{aligned} \tag{7.24}$$

where the equilibrium velocity of class u on lane j is defined by:

$$V_{(u,j)}^e \overset{def}{=} m_{(u,j)}^e / r_{(u,j)} = V_{(u,j)}^a - (1 - p_{(u,j)}^*)\mathrm{T}_{(u,j)}\mathcal{R}_{(u,j)}^1 \tag{7.25}$$

Velocity variance dynamics:

$$\begin{aligned}\dot{\Theta}_{(u,j)} &= \partial_t\Theta_{(u,j)} + V_{(u,j)}\partial_x\Theta_{(u,j)} \\ &= -2\Theta_{(u,j)}\partial_x V_{(u,j)} + 2(\Theta_{(u,j)}^e - \Theta_{(u,j)})/\mathrm{T}_{(u,j)} + 2\eta_{(u,j)} r_{(u,j)}^{-1}\partial_x V_{(u,j)}\partial_x V_{(*,j)} \\ &\quad + 2\partial_x(\kappa_{(u,j)} r_{(u,j)}^{-1}\partial_x\Theta_{(u,j)}) - r_{(u,j)}^{-1}\sum_{j'=j\pm1}(p_{(u,j)}^{(u,j')} r_{(u,j)}\mathcal{F}_{(u,j,j)}^2 - p_{(u,j')}^{(u,j)} r_{(u,j')}\mathcal{F}_{(u,j,j')}^2) \\ &\quad + r_{(u,j)}^{-1}\sum_{j'=j\pm1}\Delta_{(u,j')}^{(u,j)} r_{(u,j')}((V_{(u,j)} - V_{(u,j')})^2 - (\Theta_{(u,j)} - \Theta_{(u,j')}))\end{aligned} \tag{7.26}$$

where the equilibrium velocity variance is defined by:

$$\Theta_{(u,j)}^e \overset{def}{=} C_{(u,j)} + (1 - p_{(u,j)}^*)\mathrm{T}_{(u,j)}(\mathcal{F}_{(u,j)}^2 - 2V_{(u,j)}\mathcal{F}_{(u,j)}^1) \tag{7.27}$$

7.3.3 *Traffic pressure dynamics – pseudo-primitive form*

For mathematical analysis, a more suitable primitive form exists, namely using the traffic pressure P rather than the velocity variance Θ. To derive this model, let us denote the resulting vector of primitive variables by:

$$\tilde{\mathbf{v}}_{(u,j)} \overset{def}{=} (r_{(u,j)} \quad V_{(u,j)} \quad P_{(u,j)}) = (\tilde{v}_{(u,j)}^{(1)} \quad \tilde{v}_{(u,j)}^{(2)} \quad \tilde{v}_{(u,j)}^{(3)}) \tag{7.28}$$

where the traffic pressure equals $P_{(u,j)} = r_{(u,j)}\Theta_{(u,j)}$, then we can reformulate the adapted transformation matrices (7.16) and (7.21):

$$\tilde{\mathbf{M}}_{(u,j)} = \begin{pmatrix} 1 & \cdot & \cdot \\ V_{(u,j)} & r_{(u,j)} & \cdot \\ V_{(u,j)}^2/2 & r_{(u,j)}V_{(u,j)} & 1/2 \end{pmatrix} \text{ and } \tilde{\mathbf{N}}_{u,j} = \begin{pmatrix} 1 & \cdot & \cdot \\ -V_{(u,j)}/r_{(u,j)} & 1/r_{(u,j)} & \cdot \\ V_{(u,j)}^2 & -2V_{(u,j)} & 2 \end{pmatrix} \tag{7.29}$$

Using these transformation matrices, we can determine the adapted flux-Jacobian $\tilde{\mathbf{B}}$, the source vector $\tilde{\mathbf{y}}$, and the diffusive flux $\tilde{\mathbf{g}}^D$ similarly to the derivation approach of the primitive model formulation (section 7.3.1).

In casting the model in its pseudo-primitive form, the product $r\Theta$ in (7.24) is replaced by P. Otherwise, the generalised conservation equation (7.1) and the velocity dynamics (7.24) remain unchanged. The velocity variance dynamic equation (7.26) is replaced by the following partial differential equation describing the dynamics of the mixed-state traffic pressure $P_{(u,j)}$:

$$\begin{aligned} &\partial_t P_{(u,j)} + 3P_{(u,j)}\partial_x V_{(u,j)} + V_{(u,j)}\partial_x P_{(u,j)} = 2(P^e_{(u,j)} - P_{(u,j)})/\mathrm{T}_{(u,j)} + 2\eta_{(u,j)}\partial_x V_{(u,j)}\partial_x V_{(*,j)} \\ &\quad + 2\kappa_{(u,j)}\partial_x\Theta_{(u,j)} - \sum_{j'=j\pm1}(p^{(u,j')}_{(u,j)} r_{(u,j)}\mathcal{F}^2_{(u,j,j)} - p^{(u,j)}_{(u,j')} r_{(u,j')}\mathcal{F}^2_{(u,j,j')}) \\ &\quad - \sum_{j'=j\pm1}(\Delta^{(u,j')}_{(u,j)}P_{(u,j)} - \Delta^{(u,j)}_{(u,j')}P_{(u,j')}) + \sum_{j'=j\pm1}\Delta^{(u,j)}_{(u,j')} r_{(u,j')}(V_{(u,j)} - V_{(u,j')})^2 \end{aligned} \tag{7.30}$$

where the *equilibrium traffic pressure* equals:

$$P^e_{u,j} \overset{def}{=} r_{(u,j)}\Theta^e_{(u,j)} \tag{7.31}$$

The resulting system of partial differential equations is called the *pseudo-primitive form*. Its main use in this thesis is to simplify the derivation of the *characteristic form* (see section 7.4). It appears that using the pseudo-primitive rather than the conservative or the primitive form simplifies this derivation.

7.3.4 Comparison with aggregate-class aggregate-lane macroscopic models

The primitive model formulation enables comparison of the mixed-state model (equations (7.1), (7.24), and (7.26)) with other models. The *generalised conservation-of-vehicles* equation (7.1) is different from the conservation equation (2.24) in that it contains additional terms reflecting the between-lane density flows of vehicles of class u. Similarly, comparing the MLMC velocity dynamics (7.24) compared to the Payne/Helbing-type models (equation (2.33)) reveals a similar difference. This holds equally for the comparison of the MLMC velocity variance dynamic equation (7.26) and the variance equation (2.35).

7.3.5 Interpretation of MLMC equations in their primitive form

In this subsection we discuss the interpretation of the respective terms in the MLMC velocity equation (7.24). To this end, let us notice that $\partial_x P = r\partial_x\Theta + \Theta\partial_x r$ and consequently rewrite the right-hand-side of (7.24), thereby finding:

$$\dot{V}_{(u,j)} = \partial_t V_{(u,j)} + \overbrace{V_{(u,j)}\partial_x V_{(u,j)}}^{C} = \overbrace{-r_{(u,j)}^{-1}\partial_x(r_{(u,j)}\Theta_{(u,j)})}^{A_0} + \overbrace{(V_{(u,j)}^{e} - V_{(u,j)})/\mathrm{T}_{(u,j)}}^{R}$$
$$+ \overbrace{r_{(u,j)}^{-1}\partial_x(\eta_{(u,j)}\partial_x V_{(*,j)})}^{A_1} - \overbrace{r_{(u,j)}^{-1}\sum_{j'=j\pm1}(p_{(u,j)}^{(u,j')} r_{(u,j)}\mathcal{F}_{(u,j,j)}^{1} - p_{(u,j')}^{(u,j)} r_{(u,j')}\mathcal{F}_{(u,j,j')}^{1})}^{ILC} \qquad (7.32)$$
$$+ \overbrace{r_{(u,j)}^{-1}\sum_{j'=j\pm1}\Delta_{(u,j')}^{(u,j)} r_{(u,j')}(V_{(u,j')} - V_{(u,j)})}^{SLC+PLC}$$

From this equation we have concluded that the dynamic changes in the velocity experienced by an observer moving in the traffic flow along with the vehicles of class u on lane j are caused by *spatial changes* in the traffic pressure $P = r\Theta$ (term A_0). Several researchers have argued that the influences of these spatial changes on the dynamics of the velocity of the moving observer describes the *anticipatory behaviour* of drivers. We oppose to this interpretation: rather than describing driver's anticipation, the term A_0 is the result of a *convective process*, as can be seen from the original conservative model formulation.

Traffic pressure gradient and convection

To illustrate that the term A_0 stems from a convective process, let us consider the case of an increasing velocity variance $\partial_x\Theta_{(u,j)} > 0$, and a spatially constant traffic density $r_{(u,j)}$ and velocity $V_{(u,j)}$. As a result, we have $\partial_x P_{(u,j)} > 0$. If we consider cell x, the spatial increase in the velocity variance implies that at the upstream cell boundary, the variation in the velocity is less than at the downstream cell boundary, although the mean velocity is the same. For example, imagine that at the upstream cell boundary all vehicles have exactly the same velocity V, while at the downstream cell boundary, half of the vehicles has stopped, while the other half moves at $2V$. That is, while the expected velocity at the cell interfaces is equal, namely V, the variation increases spatially from 0 to V^2.

Clearly, at the upstream cell boundary, vehicles flow into cell x with a velocity V, while at the downstream cell interface, only vehicles having a velocity $2V$ flow out of the cell, while the motionless vehicles remain. Thus, at the upstream interface, the mean velocity remains *the same*, while at the downstream interface, the mean velocity *decreases*. As a consequence, the mean velocity in the whole cell x decreases as well.

Traffic relaxation processes, viscosity and lane-changing

The *relaxation term R* present in the velocity dynamics is a result of acceleration of unconstrained vehicles of class u on lane j towards their desired velocity, and acceleration of constrained vehicles to the desired velocity of the unconstrained platoon leader. In addition to the convective processes (terms C and A_0), and relaxation processes (term R), the *traffic viscosity* causes a 'dissipation flux' (term A_1), which results in a spatial smoothing of velocity.

Finally, the expected velocity of class u on lane j changes due to immediate lane-changing, postponed lane-changing, and spontaneous lane-changing. With respect to the latter two lane-changing types, the velocity of class u on lane j changes due to the inflow of vehicles from other lanes, which is reflected by the difference term $(V_{(u,j)}-V_{(u,j')})$ present in the velocity dynamics. Changes due to immediate lane-changing are of a comparable nature.

7.3.6 Validity of interpretation of pressure gradient from driver's anticipation viewpoint

We have already mentioned that it is generally believed (e.g. Payne (1971,1979), Smulders (1989), Kerner *et al.* (1996)) that the traffic pressure gradient (term A_0) in (7.32) can be correctly interpreted as describing drivers anticipation on downstream traffic conditions. Let us now motivate why this interpretation – which we have shown stems from *convection* of traffic with diverse velocities – from the viewpoint of anticipative behaviour is *incorrect* for (lane-specific) multiclass traffic flow. To this end, let us first recall the velocity dynamics of the single user-class, aggregate-lane traffic flow model of e.g. Kerner *et al.* (1996):

$$\partial_t V + V\partial_x V = \overbrace{-r^{-1}\partial_x(r\Theta_0)}^{A_0} + (V^e - V)/\mathrm{T} + r^{-1}\eta\partial_x^2 V \tag{7.33}$$

Kerner *et al.* (1996) argue that term A_0 of the right-hand-side of the velocity dynamics (7.33) describes changes in the mean velocity due to drivers *anticipating* on changing density conditions. That is, if the density r *increases* spatially ($\partial_x r > 0$), drivers *decelerate*, anticipating on the downstream traffic conditions. Alternatively, when the traffic density *decreases* spatially, drivers increase their velocity. Moreover, the second order viscosity term also describes drivers anticipatory behaviour ("*the higher order tendency of spatial traffic flow*"): when traffic is in a state of spatial acceleration ($\partial_x^2 V > 0$), drivers will "go along with the other drivers" and accelerate.

In the MLMC case (equation (7.32)), comparable 'anticipation' terms can be identified as in the single user-class aggregate-lane case (7.33). However, we can easily show that the interpretations of Kerner *et al.* (1996) are not justified, since in their model drivers of user-class u would only anticipate on changes in the density and velocity *of their own user-class u*. For instance, if the density of class u decreases spatially, drivers of class u will accelerate, *even if* the aggregate-class density $r_{(*,j)}$ does *not spatially decrease*. In illustration, consider a case where two user-classes are present: the first class consists of slow trucks and the second class consist of fast passenger-cars. Let us consider the case where the total traffic density is spatially homogenous, while the *traffic composition* changes with changing x. That is, we assume that the fraction of trucks increases with increasing x. Equation (7.32) shows that, since the passenger-car density decreases spatially, passenger-car drivers *anticipate* on the low passenger-car region and accelerate. However, in real-life traffic this is very unlikely to happen since the *total density* remains constant.

Concluding, in case of macroscopic multiclass (multilane) traffic flow, the interpretation of the term $\partial_x P$ from the perspective of drivers' anticipations is incorrect. Rather, the term stems from the convection of groups of vehicles with different variations in their velocities. However, if we extend this concept, the classical interpretation of the $\partial_x P$ is incorrect for *aggregate-class traffic* as well. That is, the term does not reflect driver's anticipative behaviour at all, conversely to what has been argued by among others Payne (1971,1979), Kerner *et al.* (1996), and Helbing (1996): describing the traffic process as a mixed stream of different user-classes rather than considering each class separately leads to the misinterpretation of the pressure term. In terms of gaining correct insights into the mechanisms of traffic flow operations, a multiclass distinction is hence invaluable.

7.4 MLMC model in Riemann variables

The convective character of the system of MLMC traffic flow equations is of dominant importance for the choice of correct numerical approximation schemes as well as for the mathematical formulation of the equations. That is, since the basic phenomena are of propagative or convective nature (i.e. properties of the traffic stream are transported due to convective processes), the *characteristics* of the system and their properties play an essential role in both the mathematical description and in many numerical discretisation schemes. For instance, the *characteristic* or *Riemann* form is important when applying so-called Godunov-type numerical approximation schemes. Moreover, the characteristic form is essential for mathematical analysis of among other things shock waves and discontinuities by showing how density, velocity and variance are transported in the vehicular flow.

In this section, we first introduce the concept of the characteristic variables. Secondly, we derive the characteristic MLMC model for the mixed-state MLMC traffic flow model. Using this formulation, and assuming that the diffusive processes (i.e. traffic viscosity and finite reaction times and braking times reflected by the flux-of-velocity variance) can be neglected, we show how disturbances propagate in the MLMC traffic flow. By doing so, we identify a new criterion to identify whether or not traffic flow operations are congested or not. Also, we discuss the formation of shock waves and contact discontinuities. Finally, we identify the correct number of boundary conditions needed to fully specify the MLMC traffic flow model.

7.4.1 Variable transformations and quasi-linear model formulation

In section 7.3 we have demonstrated how the conservative MLMC model can be recast using primitives. Before we discuss how the model can be recast using the characteristic variables, some additional remarks are made concerning the primitive variables.

Recall that the transformation matrix $\mathbf{M}$ is defined by (7.16). Let us assume that $\mathbf{w}$ (defined by (7.6)) is a solution of the conservative system (7.7), and let $\mathbf{v}$ be the corresponding solution using primitives. Let $\delta\mathbf{w}$ be an arbitrarily small variation of $\mathbf{w}$. Then, the corresponding variation $\delta\mathbf{v}$ of the solution $\mathbf{v}$ satisfies by definition:

$$\delta\mathbf{v}_{(u,j)} = \mathbf{M}^{-1}_{(u,j)}\delta\mathbf{w}_{(u,j)} \tag{7.34}$$

Moreover, since both the undisturbed solution $\mathbf{v}_{(u,j)}$ and the disturbed solution $\mathbf{v}_{(u,j)}+\delta\mathbf{v}_{(u,j)}$ satisfy (7.14), the disturbance $\delta\mathbf{v}_{(u,j)}$ also satisfies the quasi-linear equation (7.14).

Rather than using the *transformation matrix* $\mathbf{M}$ defined by (7.16), other matrices yielding different model formulations can be proposed. In the remainder of this chapter we discuss a specific *transformation matrix* $\mathbf{R}$, having the property that it *diagonalises* the flux Jacobian $\tilde{\mathbf{B}}$ of the *pseudo-primitive system*, that is (section 7.3.3):

$$\mathbf{R}^{-1}_{(u,j)}\tilde{\mathbf{B}}_{(u,j)}\mathbf{R}_{(u,j)} = \begin{pmatrix} \lambda^{(1)}_{(u,j)} & \cdot & \cdot \\ \cdot & \lambda^{(2)}_{(u,j)} & \cdot \\ \cdot & \cdot & \lambda^{(3)}_{(u,j)} \end{pmatrix} = \vec{\Lambda}_{(u,j)} \tag{7.35}$$

7.4.2 *Eigensystem of pseudo primitive model form*

Let us consider the pseudo-primitive form* of the MLMC traffic flow model:

$$\partial_t \tilde{\mathbf{v}}_{(u,j)} + \tilde{\mathbf{B}}_{(u,j)}(\tilde{\mathbf{v}}_{(u,j)})\partial_x \tilde{\mathbf{v}}_{(u,j)} = \tilde{\mathbf{y}}_{(u,j)}(\tilde{\mathbf{V}}) + \partial_x \tilde{\mathbf{g}}^D_{(u,j)} \tag{7.36}$$

where:

$$\tilde{\mathbf{v}}_{(u,j)} \overset{def}{=} (r_{(u,j)} \quad V_{(u,j)} \quad P_{(u,j)}) \tag{7.37}$$

and where $\tilde{\mathbf{V}} = \{\tilde{\mathbf{v}}_{(u,j)}\}$ is the vector of pseudo-primitive variables for all classes and lanes.

Let us consider the *eigenvalues* of the pseudo-primitive flux Jacobian, which is determined by substitution of (7.29) into (7.19) yielding:

$$\tilde{\mathbf{B}}_{(u,j)} = \begin{pmatrix} V_{(u,j)} & r_{(u,j)} & \cdot \\ \cdot & V_{(u,j)} & 1/r_{(u,j)} \\ \cdot & 3P_{(u,j)} & V_{(u,j)} \end{pmatrix} = \begin{pmatrix} V_{(u,j)} & r_{(u,j)} & \cdot \\ \cdot & V_{(u,j)} & 1/r_{(u,j)} \\ \cdot & r_{(u,j)}c^2_{(u,j)} & V_{(u,j)} \end{pmatrix} \tag{7.38}$$

where the *local sonic velocity* $c_{(u,j)} = (3\Theta_{(u,j)})^{1/2}$ is defined in analogy with flows in continuous media. In a fluid or a gas, the local sonic velocity describes the speed at which soundwaves (which are regions of changing pressure) propagate through the continuos medium. If we consider a moving particle in a continuous medium, specific properties of the particle are transported at the speed of sound (from the viewpoint of the moving entity). Interpretation of the local sonic velocity in traffic flow is similar: it depicts how specific properties of vehicles in the traffic stream are transported in the (MLMC) traffic stream. We will discuss this in more detail in section 7.5

The eigenvalues of the pseudo-primitive flux-Jacobian are the values λ satisfying:

$$\det(\tilde{\mathbf{B}}_{(u,j)} - \lambda\mathbf{I}) = (V_{(u,j)} - \lambda)((V_{(u,j)} - \lambda)^2 - c^2_{(u,j)}) = 0 \tag{7.39}$$

A direct calculation yields the eigenvalues:

$$\lambda^{(1)}_{(u,j)} = V_{(u,j)} \quad \lambda^{(2)}_{(u,j)} = V_{(u,j)} + c_{(u,j)} \quad \lambda^{(3)}_{(u,j)} = V_{(u,j)} - c_{(u,j)} \tag{7.40}$$

We will show in the sequel of this chapter, that the local sonic velocity $c_{(u,j)}$ yields a *congestion threshold value* that indicates when certain properties of the flow on a specific location and time instant are transported only downstream, or both downstream and upstream.

Let us now consider the *left row eigenvectors* $\mathbf{l}_{u,j}^{(i)}$ of the flux Jacobian $\tilde{\mathbf{B}}_{u,j}$ by:

$$\mathbf{l}^{(i)}_{(u,j)} \cdot (\tilde{\mathbf{B}}_{(u,j)} - \lambda^{(i)}_{(u,j)}\mathbf{I}) = \mathbf{0} \text{ such that } \mathbf{l}^{(i)}_{(u,j)} \neq \mathbf{0} \text{ for } i = 1,2,3 \tag{7.41}$$

Some straightforward computations yields these eigenvectors (arbitrarily normalised), which constitute the *left eigenvector matrix* $\mathbf{L}_{(u,j)}$:

---

* The *pseudo-primitive model form* (introduced in 7.3.3) is used rather than the *conservative* or the *primitive model forms*, since it yields simplified computations.

$$\mathbf{L}_{(u,j)} = \begin{pmatrix} \mathbf{l}^{(1)}_{(u,j)} \\ \mathbf{l}^{(2)}_{(u,j)} \\ \mathbf{l}^{(3)}_{(u,j)} \end{pmatrix} = \begin{pmatrix} 1 & \cdot & -1/c^2_{(u,j)} \\ \cdot & 1 & 1/r_{(u,j)}c_{(u,j)} \\ \cdot & 1 & -1/r_{(u,j)}c_{(u,j)} \end{pmatrix} \tag{7.42}$$

The *right eigenvectors* can be determined by inverting the left eigenvector matrix $\mathbf{L}_{(u,j)}$:

$$\mathbf{R}_{(u,j)} = \mathbf{L}^{-1}_{(u,j)} = \begin{pmatrix} 1 & r_{(u,j)}/2c_{(u,j)} & -r_{(u,j)}/2c_{(u,j)} \\ \cdot & 1/2 & 1/2 \\ \cdot & r_{(u,j)}c_{(u,j)}/2 & -r_{(u,j)}c_{(u,j)}/2 \end{pmatrix} \tag{7.43}$$

7.4.3 Definition of characteristic variables and characteristic equations

The eigenvector matrices are introduced to determine the characteristic form of the model. This is achieved by using the well known property (Strang (1980)) that **R** and **L** ((7.41) and (7.42) respectively) *diagonalise* the pseudo-primitive flux-Jacobian $\tilde{\mathbf{B}}$ (equation (7.38)):

$$\mathbf{L}_{(u,j)}\tilde{\mathbf{B}}_{(u,j)}\mathbf{R}_{(u,j)} = \begin{pmatrix} \lambda^{(1)}_{(u,j)} & \cdot & \cdot \\ \cdot & \lambda^{(2)}_{(u,j)} & \cdot \\ \cdot & \cdot & \lambda^{(3)}_{(u,j)} \end{pmatrix} = \vec{\Lambda}_{(u,j)} \tag{7.44}$$

Since $\mathbf{R}_{(u,j)}\mathbf{L}_{(u,j)} = \mathbf{I}$, left-multiplying (7.36) by $\mathbf{L}_{(u,j)}$, yields for the left-hand-side of (7.36):

$$\begin{aligned} \mathbf{L}_{(u,j)}\partial_t\tilde{\mathbf{v}}_{(u,j)} + \mathbf{L}_{(u,j)}\tilde{\mathbf{B}}_{(u,j)}\partial_x\tilde{\mathbf{v}}_{(u,j)} &= \mathbf{L}_{(u,j)}\partial_t\tilde{\mathbf{v}}_{(u,j)} + \mathbf{L}_{(u,j)}\tilde{\mathbf{B}}_{(u,j)}(\mathbf{R}_{(u,j)}\mathbf{L}_{(u,j)})\partial_x\tilde{\mathbf{v}}_{(u,j)} \\ &= (\mathbf{L}_{(u,j)}\partial_t + \vec{\Lambda}_{(u,j)}\mathbf{L}_{(u,j)}\partial_x)\tilde{\mathbf{v}}_{(u,j)} \end{aligned} \tag{7.45}$$

thus yielding:

$$(\mathbf{L}_{(u,j)}\partial_t + \vec{\Lambda}_{(u,j)}\mathbf{L}_{(u,j)}\partial_x)\tilde{\mathbf{v}}_{(u,j)} = \mathbf{L}_{(u,j)}(\tilde{\mathbf{y}}_{(u,j)} + \partial_x\tilde{\mathbf{g}}^D_{(u,j)}) \tag{7.46}$$

This vector equation (7.46) is a compact notation for the so-called *compatibility equations* for the eigenvalues $\lambda^{(k)}_{(u,j)}$. Note that this equation can also be expressed as functions of the conservatives $\mathbf{w}_{(u,j)}$ by replacing the left eigenvector matrix $\mathbf{L}_{(u,j)}$ by $\mathbf{L}_{(u,j)}\tilde{\mathbf{N}}_{(u,j)}$, yielding:

$$(\mathbf{L}_{(u,j)}\tilde{\mathbf{N}}_{(u,j)}\partial_t + \vec{\Lambda}_{(u,j)}\mathbf{L}_{(u,j)}\tilde{\mathbf{N}}_{(u,j)}\partial_x)\mathbf{w}_{(u,j)} = \mathbf{L}_{(u,j)}\tilde{\mathbf{N}}_{(u,j)}(\tilde{\mathbf{y}}_{(u,j)} + \partial_x\tilde{\mathbf{g}}^D_{(u,j)}) \tag{7.47}$$

The compatibility relations naturally lead to the introduction of the set of *characteristic variables*, which are defined by the relation valid for arbitrary variations in either the temporal direction (∂_t) or spatial direction (∂_x):

$$\delta\mathbf{z}_{(u,j)} = \mathbf{L}_{(u,j)}\delta\tilde{\mathbf{v}}_{(u,j)} \tag{7.48}$$

In other words, the k-th component of $\delta\mathbf{z}_{(u,j)}$ is obtained from a linear combination of the pseudo-primitive variables $\tilde{v}^{(i)}_{(u,j)}$ for $i = 1,2$ and 3, with coefficients that are equal to the components of the k-th left eigenvector. Then, let us formally define the *characteristic variable* $\mathbf{z}_{(u,j)}$ from these characteristic variations. For these characteristic variables we have:

$$\mathbf{L}_{(u,j)}\partial_t\tilde{\mathbf{v}}_{(u,j)} = \partial_t\mathbf{z}_{(u,j)} \quad \text{and} \quad \mathbf{L}_{(u,j)}\partial_x\tilde{\mathbf{v}}_{(u,j)} = \partial_x\mathbf{z}_{(u,j)} \tag{7.49}$$

Substituting relation (7.49) into the compatibility equations (7.46) yields that $\mathbf{z}_{(u,j)}$ is a solution of the following equation:

$$(\partial_t + \vec{\Lambda}_{(u,j)}\partial_x)\mathbf{z}_{(u,j)} = \mathbf{L}_{(u,j)}(\tilde{\mathbf{y}}_{(u,j)} + \partial_x \tilde{\mathbf{g}}^D_{(u,j)}) \tag{7.50}$$

7.4.4 Dynamic equations of characteristic variations

We can also explicitly determine the system of partial differential equations describing the dynamics of the characteristic variations. To this end, let us consider two solutions of the pseudo-primitive system (7.36) $\tilde{\mathbf{v}}_{(u,j)}$ and $\tilde{\mathbf{v}}_{(u,j)} + \delta\tilde{\mathbf{v}}_{(u,j)}$ respectively, with $\delta\tilde{\mathbf{v}}_{(u,j)}$ small.

Let us neglect diffusive processes. Then, by subtracting the respective equations (7.36) for these solutions from each other, it appears that the dynamics of the variation $\delta\tilde{\mathbf{v}}_{(u,j)}$ equals:

$$(\mathbf{L}_{(u,j)}\partial_t + \vec{\Lambda}_{(u,j)}\mathbf{L}_{(u,j)}\partial_x)\delta\tilde{\mathbf{v}}_{(u,j)} = \mathbf{L}_{(u,j)}\mathbf{C}_{(u,j)}\delta\tilde{\mathbf{v}}_{(u,j)} \tag{7.51}$$

with:

$$\mathbf{C}_{(u,j)} = \frac{\partial\tilde{\mathbf{y}}_{(u,j)}}{\partial\tilde{\mathbf{v}}_{(u,j)}} \tag{7.52}$$

where we have assumed that $\mathbf{L}_{(u,j)}$ is invariant to the first-order with respect to variations $\delta\tilde{\mathbf{v}}_{(u,j)}$ (which holds for all variations in $r_{(u,j)}$ and $V_{(u,j)}$).

Summarising the results from this section, characteristic variations $\delta\mathbf{z}_{(u,j)}$ are defined with respect to small variations on solutions of the macroscopic MLMC traffic flow model. In accordance to these equations, we can define the characteristic variables as those variables $\mathbf{z}_{(u,j)}$ that are a solution of the following equation (7.50). This equation is called the *characteristic equations* (*Riemann system equations*), and are well known in the analysis of the Euler-equations for inviscid flows in compressible fluids and gasses.

The characteristic variables lack intuitive appeal. Nevertheless, they are well suited for mathematical and numerical analysis of the higher-order traffic flow equations, due to the convective nature of the traffic flow equations. That is, the characteristics of the flow equations play an essential role in the mathematical description and numerical discretisation schemes. In this respect, section 7.5 shows how the propagation of disturbances in the traffic flow can be analysed using the characteristic formulation. In section 7.6 we show how the shock wave behaviour of the traffic stream follows from the characteristic formulation. In chapter 9 we show the importance of knowledge of this behaviour from the viewpoint of numerical solution techniques.

7.5 Analysis of inviscid flow equations using characteristic equations

This section discusses mathematical analysis of the higher-order traffic flow model. More precisely, we show how small perturbations in the multiclass traffic stream are transported in the flow. Since the process of disturbance propagation is of a convective nature – the higher order viscosity and flux-of-velocity variance term only cause a *smoothing* of these disturbances – to get a clear insight in the model behaviour we will consider the *inviscid flow equations*, i.e. $\tilde{\mathbf{g}}^D \equiv 0$. In other words, the traffic viscosity (section 6.5) and the finite reac-

tion and braking times (section 6.6) are neglected, implying that only the *convective* and *relaxation* processes are considered: we only consider acceleration towards the acceleration velocity, deceleration due to vehicles interacting, and changes in the traffic conditions in a cell due to the inflow and outflow of vehicles.

Having a clear understanding of these processes is of dominant importance, since they may cause shock waves in the traffic flow. It is well known (Payne (1971), Lyrintzis (1994)) that the *inviscid* (MLMC) flow equations always yield the occurrence of shocks in the flow, irrespective of the smoothness of the initial conditions. Introducing diffusion results in a spatial smoothing effect, potentially keeping shocks from appearing. Let us emphasise that neglecting diffusive processes introduces a drastic change in the *mathematical* formulation of the MLMC model, since the system of partial differential equations describing the inviscid MLMC traffic flow model reduces from second order to first order.

Neglecting higher-order terms yields the following system of equations (in conservatives):

$$
\begin{aligned}
&\partial_t r_{(u,j)} + \partial_x m_{(u,j)} = -\sum_{j'=j\pm1} (p^{(u,j')}_{(u,j)} r_{(u,j)} \mathcal{I}^0_{(u,j)} - p^{(u,j)}_{(u,j')} r_{(u,j')} \mathcal{I}^0_{(u,j')}) - \sum_{j'=j\pm1} (\Delta^{(u,j')}_{(u,j)} r_{(u,j)} - \Delta^{(u,j)}_{(u,j')} r_{(u,j')}) \\
&\partial_t m_{(u,j)} + 2\partial_x e_{(u,j)} = (m^e_{(u,j)} - m_{(u,j)})/\mathrm{T}_{(u,j)} \\
&\qquad - \sum_{j'=j\pm1} (p^{(u,j')}_{(u,j)} r_{(u,j)} \mathcal{I}^1_{(u,j)} - p^{(u,j)}_{(u,j')} r_{(u,j')} \mathcal{I}^1_{(u,j')}) - \sum_{j'=j\pm1} (\Delta^{(u,j')}_{(u,j)} m_{(u,j)} - \Delta^{(u,j)}_{(u,j')} m_{(u,j')}) \qquad (7.53) \\
&\partial_t e_{(u,j)} + \partial_x (m_{(u,j)} H_{(u,j)}) = 2(e^e_{(u,j)} - e_{(u,j)})/\mathrm{T}_{(u,j)} \\
&\qquad - \tfrac{1}{2} \sum_{j'=j\pm1} (p^{(u,j')}_{(u,j)} r_{(u,j)} \mathcal{I}^2_{(u,j)} - p^{(u,j)}_{(u,j')} r_{(u,j')} \mathcal{I}^2_{(u,j')}) - \sum_{j'=j\pm1} (\Delta^{(u,j')}_{(u,j)} e_{(u,j)} - \Delta^{(u,j)}_{(u,j')} e_{(u,j')})
\end{aligned}
$$

Another important issue is the correct formulation of the boundary conditions to operationalise the model. By studying the characteristic equations and the resulting information transportation mechanisms, we can determine how many boundary conditions need to be formulated at the entries and on-ramps on the one hand, and the exits and off-ramps of the roadway system at the other hand. This issue is discussed in section 7.7.

7.5.1 Propagation of disturbances and characteristic variables

Let us again consider a solution $(r_{(u,j)}, V_{(u,j)}, P_{(u,j)})$ of the pseudo-primitive system (7.36). Moreover, let us consider a small variation $(\delta r_{(u,j)}, \delta V_{(u,j)}, \delta P_{(u,j)})$ on this solution. Potential causes of such disturbances are abundant. For instance, they may result from the behaviour of a single driver in the stream (e.g. a driver who has been overtaken by another driver may decide to increase the gap with respect to his new leader, or a dawdling driver). Disturbances may also result from exogenous conditions (e.g. an incident in the opposite direction). Also, the results of traffic entering the roadway at an on-ramp results in perturbations in the density, velocity and pressure.

Characteristics in the LWR-model

Let us consider the characteristics of the LWR-model. To this end, we reformulate the LWR model (section 2.4.2) as follows:

$$\partial_t r + a(r)\partial_x r = 0 \quad \text{with} \quad a(r) = \mathrm{d}\, m^e(r)/\mathrm{d}\, r \tag{i.1}$$

with $m^e = rV^e$. Let us consider any point (x_0,t_0) in the (x,t)-plane. From this point, we define a parameterised curve $C = \{x(s),t(s)\}$ originating (by definition) from (x_0,t_0) for $s = 0$. Let us now define the curve C by the following set of differential equations defining the functions $x(s)$ and $t(s)$:

$$\mathrm{d}\, t/\mathrm{d}\, s = 1 \quad \text{and} \quad \mathrm{d}\, x/\mathrm{d}\, s = a(r(x(s),t(s))) \tag{i.2}$$

with $t(0) = t_0$ and $x(0) = x_0$. Then, for the *total derivative* with respect to s of the density at $r(x(s),t(s))$, we find, by using (i.2), that:

$$\mathrm{d}\, r/\mathrm{d}\, s = (\mathrm{d}\, t/\mathrm{d}\, s)\partial_t r + (\mathrm{d}\, x/\mathrm{d}\, s)\partial_x r = \partial_t r + a(r)\partial_x r \tag{i.3}$$

If we combine this result with the LWR-model (i.1), we find:

$$\mathrm{d}\, r/\mathrm{d}\, s = 0 \tag{i.4}$$

which implies that *along the curve* $C = \{x(s),t(s)\}$, the density $r(x(s),t(s))$ is *constant*. Since C originates from (x_0,t_0), the density along the curve equals $r(x_0,t_0)$. Due to the definition (i.3), the curve C is a straight line.

Congestion in the LWR model

It is well accepted that $M^e(r)$ has a *monotonically increasing arc* $(r < r_{crit})$ where $a(r) > 0$, and a *monotonically decreasing arc* $(r > r_{crit})$ where $a(r) < 0$ (see among others May (1990)). The decreasing branch reflects *congested traffic conditions*. That is, when $a(r) < 0$ traffic operations are congested. Thus, we can conclude that if traffic conditions are congested, that the characteristic curve C defined by (i.3) is directed *upstream*, while under free-flow conditions, C is directed *downstream*. In section 7.5.4 we show that a similar observation is valid for the MLMC model established in this thesis.

Intermezzo III: Characteristics of LWR model

By considering the characteristic system (7.50), we are able to analyse propagation of these small disturbances in the flow. To this end, we remark that the characteristic variation $\delta\mathbf{z}_{(u,j)}$ is defined by (combining (7.37) and (7.48)):

$$\delta\mathbf{z}_{(u,j)} = (\delta r_{(u,j)} - \delta P_{(u,j)}/c^2_{(u,j)} \quad \delta V_{(u,j)} + \delta P_{(u,j)}/r_{(u,j)}c_{(u,j)} \quad \delta V_{(u,j)} - \delta P_{(u,j)}/r_{(u,j)}c_{(u,j)}) \tag{7.54}$$

For inviscid MLMC flow equations, this characteristic equation (7.50) equals:

$$\partial_t \mathbf{z}_{(u,j)} + \tilde{\Lambda}_{(u,j)}\partial_x \mathbf{z}_{(u,j)} = \mathbf{L}_{(u,j)}\tilde{\mathbf{y}}_{(u,j)} \tag{7.55}$$

The characteristic equations are *de-coupled*. This means that *temporal variations* in $z_{(u,j)}^{(i)}$ depend only on *spatial variations* in $z_{(u,j)}^{(i)}$. They do *not* depend of spatial variations in $z_{(u,j)}^{(i')}$ for $i' \neq i$. This property enables simplified analysis of how disturbances propagate in MLMC traf-

fic flow. To show this, let us now consider the dynamics of characteristic variations $\delta z_{(u,j)}^{(i)}$ for $i = 1,2$ and 3 respectively.

7.5.2 *Path-lines in MLMC traffic flow (i = 1)*

Let us define the total time derivative $d_{(u,j)}/dt$ from the perspective of an observer moving along with the (average) vehicles of class u on lane j. Let $a(x,t)$ be any dependent variable. Then the following holds:

$$\frac{d_{(u,j)}\, a(x,t)}{dt} = \partial_t a(x,t) + \frac{d_{(u,j)}\, x}{dt}\partial_x a(x,t) = \partial_t a(x,t) + V_{(u,j)}(x,t)\partial_x a(x,t) \tag{7.56}$$

From the characteristic equation (7.55), we can observe how the quantities $z_{(u,j)}$ propagate in the (x,t)-plane:

$$\frac{d_{(u,j)}\, z_{(u,j)}^{(1)}}{dt} = \partial_t z_{(u,j)}^{(1)} + V_{(u,j)}\partial_x z_{(u,j)}^{(1)} = -c_{(u,j)}^{-2}\tilde{y}_{(u,j)}^{(3)} \tag{7.57}$$

That is, an observer who moves with the average vehicles of class u on lane j, only observes changes in the characteristic variable $\delta z_{(u,j)}^{(1)}$ described by the *right-hand-side source-term* of (7.57). The trajectory of this moving observer is defined by the so-called *characteristic curve* $C_{(u,j)}^{0} = \{x_{(u,j)}^{0}, t\}$, which is defined by:

$$C_{(u,j)}^{0} = \{x_{(u,j)}^{0}(t), t\} \quad \leftarrow \quad d\, x_{(u,j)}^{0}/dt = V_{(u,j)}(x_{(u,j)}^{0}(t), t) \tag{7.58}$$

Using this result, it appears that the first characteristic variation $\delta z_{(u,j)}^{(1)} = \delta r_{(u,j)} - c_{(u,j)}^{-2}\delta P_{(u,j)}$ propagates with velocity $V_{(u,j)}$ along the characteristic $C_{(u,j)}^{0}$. In fluid dynamics $C_{(u,j)}^{0}$ is called the *path-line* of the fluid. In MLMC traffic flow, this path-line represents the expected trajectory of vehicles of class u on lane j starting their trip at a location x_0 at the initial time t_0 on the path-line, defined by (see section 7.2):

$$x_{(u,j)}^{0}(t) = x_0(t) + \int_{t_0}^{t} V_{(u,j)}(x_{(u,j)}^{0}(s), s)\, ds \tag{7.59}$$

The path-line is always non-decreasing in the space-time plane (except when considering contra-flows). When the right-hand-side of (7.55) equals zero (i.e. when the MLMC traffic operations are in equilibrium), it appears that the variation $\delta z_{(u,j)}^{(1)}$ remains constant along this path-line. In this case, the characteristic variable (or Riemann variable) $z_{(u,j)}^{(1)}$ is referred to as the *Riemann invariant*.

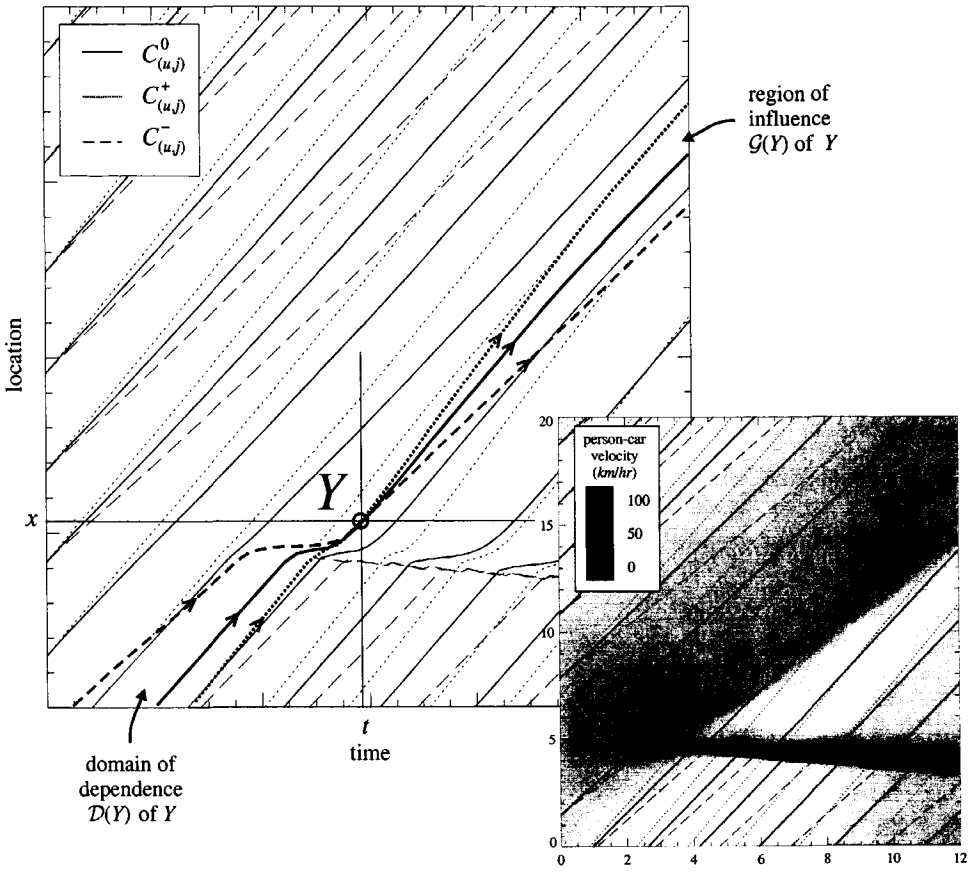

Figure 7-3: Characteristic curves (path-line and Mach-lines), region of influence, and the domain of dependence, in case of the occurrence of a jam (see section 10.2). The figure shows among other things the upstream propagating $C_{(u,j)}^-$ characteristics in the congested area.

7.5.3 Mach-lines in MLMC traffic flow (i = 2,3)

Let us now consider the second characteristic variable $z_{(u,j)}^{(2)}$. Using (7.55), the definition of both the eigenvalue (7.40) as well as the left-eigenvectors (7.42), we find that the dynamics of this variable are defined by the following partial differential equation:

$$\partial_t z_{(u,j)}^{(2)} + (V_{(u,j)} + c_{(u,j)})\partial_x z_{(u,j)}^{(2)} = \tilde{y}_{(u,j)}^{(2)} + \tilde{y}_{(u,j)}^{(3)} / r_{(u,j)} V_{(u,j)} \tag{7.60}$$

This corresponding variation $\delta z_{(u,j)}^{(2)} = \delta V_{(u,j)} + \delta P_{(u,j)} / (r_{(u,j)} c_{(u,j)})$ propagates along the characteristic curve $C_{(u,j)}^+ = \{x_{(u,j)}^+, t\}$, defined by (see Figure 7-3):

$$C_{(u,j)}^+ = \{x_{(u,j)}^+(t), t\} \quad \leftarrow \quad \mathrm{d}\, x_{(u,j)}^+ = (V_{(u,j)}(x_{(u,j)}^+(t), t) + c(x_{(u,j)}^+(t), t))dt \tag{7.61}$$

Finally, the dynamics of the third characteristic variable $z_{(u,j)}^{(3)}$ satisfy:

$$\partial_t z^{(3)}_{(u,j)} + (V_{(u,j)} - c_{(u,j)})\partial_x \delta z^{(3)}_{(u,j)} = \tilde{y}^{(2)}_{(u,j)} - \tilde{y}^{(3)}_{(u,j)} / r_{(u,j)} V_{(u,j)} \tag{7.62}$$

The characteristic variation $\delta z_{(u,j)}{}^{(3)} = \delta V_{(u,j)} - \delta P_{(u,j)}/(r_{(u,j)} c_{(u,j)})$ propagates along the characteristic curve $C_{(u,j)}{}^{-} = \{x_{(u,j)}{}^{-}, t\}$, which is defined by (see Figure 7-3):

$$C^{-}_{(u,j)} = \{x^{-}_{(u,j)}(t), t\} \quad \leftarrow \quad dx^{-}_{(u,j)} = (V_{(u,j)}(x^{-}_{(u,j)}(t), t) + c(x^{-}_{(u,j)}(t), t))dt \tag{7.63}$$

In fluid dynamics, the curves $C_{(u,j)}{}^{\pm}$ are referred to as the *Mach-lines* of the flow. The characteristic variations $\delta z_{(u,j)}{}^{(2)}$ and $\delta z_{(u,j)}{}^{(3)}$ propagate along these Mach-lines. When the right-hand-side of (7.55) is zero (i.e. when the MLMC traffic operations are in equilibrium), variations $\delta z_{(u,j)}{}^{(2)}$ and $\delta z_{(u,j)}{}^{(3)}$ are conserved along the Mach-lines of the MLMC traffic flow. In this case, the characteristic or Riemann variables are called characteristic or Riemann *invariants*.

From a traffic-engineering viewpoint, interpretation of the Mach-lines is not evident. We do know that the Mach-lines delimit the *domain of dependence* and the *region of influence* (see Figure 7-3) of the traffic flow properties in a point Y in the stream. For any point Y, the domain of dependence $\mathcal{D}(Y)$ is the collection of points Y' on which conditions in Y depend. In other words, the properties at any given point Y result from the quantities transported along the characteristics for points Y' in the domain of dependence. Each point Y is reached by one characteristic of each type. Therefore, flow operations at any location x at instant t only depend on the domain between Y^{+} and Y^{-}. (Figure 7-4). Alternatively, we can also define the *region of influence* $\mathcal{G}(Y)$ of Y, by considering the region included by characteristics emanating from Y. The region of influence delimits all possible points Y' which possible are influences by the traffic conditions in Y.

7.5.4 Identification of traffic congestion using the local sonic velocity

Let us consider an arbitrary point $Y = Y(x,t)$ in the (x,t) plane, for $t \geq t_0$ (see Figure 7-4). Traffic flow conditions in Y are determined by flow quantities (i.e. the *traffic entropy* $s_{(u,j)}$; see Hirsch (1990a,b)) transported along the path-line $C_{(u,j)}{}^{0}$ at velocity $V_{(u,j)}$. The velocity $V_{(u,j)}$ and the pressure $P_{(u,j)}$ or the density $r_{(u,j)}$ are determined from quantities $(V_{(u,j)} \pm c_{(u,j)})$ that are transported along the Mach-lines $C_{(u,j)}{}^{\pm}$ with velocities $(V_{(u,j)} \pm c_{(u,j)})$. If we neglect influences of source-terms (i.e. acceleration, deceleration, and lane-changing), we can show that entropy is conserved along the path-line of the flow (cf. Hirsch (1990b)). As a consequence, we have:

$$(V_{(u,j)} + c_{(u,j)})_Y = (V_{(u,j)} + c_{(u,j)})_{Y^{+}} \tag{7.64}$$

$$(V_{(u,j)} - c_{(u,j)})_Y = (V_{(u,j)} - c_{(u,j)})_{Y^{-}} \tag{7.65}$$

and for the entropy:

$$(s_{(u,j)})_Y = (s_{(u,j)})_{Y^0} \tag{7.66}$$

Figure 7-4 shows the domain of dependence for both *supersonic* and *subsonic* traffic flow operations. In this context, the term *supersonic* and *subsonic* are used in analogy with respectively supersonic and subsonic flows in continuous media. For these media, supersonic flow conditions occur when the velocity V of the particles is larger than the sound velocity c, while for subsonic conditions, the opposite holds. For the multiclass multilane traffic flow, we have adopted this definition. The states are defined by the slope of the $C_{(u,j)}{}^{-}$ characteris-

tics: if the $C_{(u,j)}^{-}$ characteristic has a negative slope, traffic flow is subsonic, while a positive slope indicates supersonic traffic flow conditions.

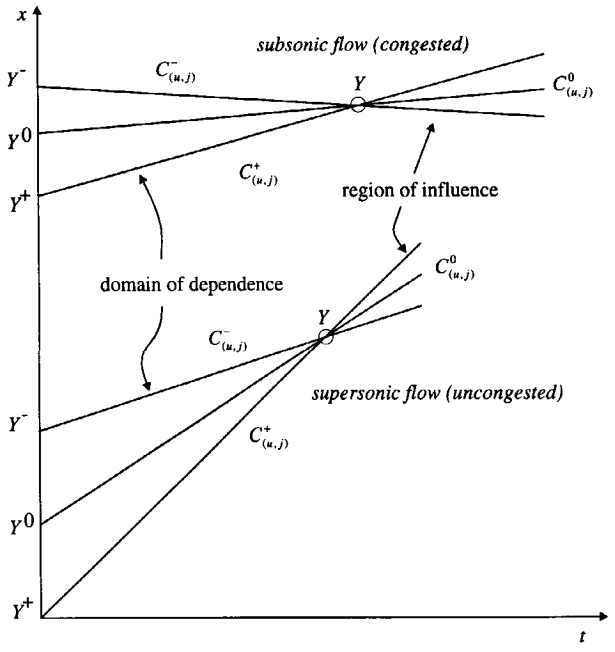

Figure 7-4: Propagation of flow quantities in inviscid MLMC traffic flow. The points Y^-, Y^+ and Y^0 indicate the origin of the respective unique characteristics C^-, C^+ and C^0 emanating from these points that reach the point Y. The combined effect of these characteristics determine the conditions in Y.

Intermezzo III recalls the definition of the (single) characteristic in the LWR-model. Moreover, Intermezzo III shows that the free-flow and the congested branch of the equilibrium flow relation $M^e(r)$ respectively yield downstream and upstream moving characteristics. In other words, when $r < r_{crit}$, the characteristic C has a positive slope $a(r) = \mathrm{d}M^e/\mathrm{d}r > 0$, while when $r > r_{crit}$, the characteristic C has a negative slope $a(r) < 0$. Extrapolating this observation to our more complex MLMC model, we conclude that *supersonic* traffic flow conditions are equivalent to *non-congested* traffic flow conditions, while *subsonic* traffic flow conditions are equivalent to *congested* traffic flow conditions.

In illustration, consider a situation where the expected velocity $V_{(u,j)}$ of class u on lane j is *smaller* than the local sonic speed $c_{(u,j)}$. In this case traffic operations are *subsonic*, since the slope of the characteristic $C_{(u,j)}^{-}$ is negative. As a result, characteristic moves *in the opposite direction of traffic*: density, velocity, and pressure are not only transported downstream – by the $C_{(u,j)}^{+}$ and $C_{(u,j)}^{0}$ characteristics – but also *upstream* along $C_{(u,j)}^{-}$. Drawing the analogy with the LWR-model, this situation reflects *congested* traffic conditions (Figure 7-4).

Thus, using the local sonic velocity, we have established a novel condition to classify the traffic state, based on the difference between the velocity of the traffic and the variance. That

is, whenever $V < c = (3\Theta)^{1/2}$, traffic conditions are congested, while if $V > c = (3\Theta)^{1/2}$ traffic is freely flowing.

7.5.5 Comparison with characteristics in the LWR-model and the Payne-models

Let us finally consider characteristics of the LWR-model and the Payne model. With respect to the LWR-model, we have observed (chapter 2.6.2 and Intermezzo III) that the kinematic model only has a single characteristic. To show the similarities and dissimilarities, let us consider the single user-class case of the MLMC model developed in this dissertation. In section 6.4.6 we have established the within-class interaction. Using the result presented there, we can determine the equilibrium momentum for the single user-class case:

$$M^e = rV^e = V^0 r - (1-p^*)(1-\theta)\tau\Theta r^2 \tag{7.67}$$

The single characteristic curve of the LWR-model is defined by $a(r) = \mathrm{d}M^e/\mathrm{d}r$, yielding:

$$\begin{aligned} a(r) &= \mathrm{d}_r M^e = V^0 - r^2\,\mathrm{d}_r((1-p^*)(1-\theta)\tau\Theta) - 2(1-p^*)(1-\theta)\tau\Theta r \\ &= V^e(r) - r((1-p^*)(1-\theta)\tau\Theta + \mathrm{d}_r((1-p^*)(1-\theta)\tau\Theta)) \\ &= V^e(r) - c_0(r) \end{aligned} \tag{7.68}$$

For the Payne-model, two characteristic curves can be identified, namely:

$$C^{\pm} = \{x^{\pm}(t), t\} \quad \leftarrow \quad \mathrm{d}_t x^{\pm} = V(x(t),t) \pm c_0 \tag{7.69}$$

where the anticipation term $c_0 > 0$ is assumed constant (see section 2.4.3). In case of the Payne-model, the anticipation constant is comparable to the standard deviation in the velocities, i.e. $c_0^2 = \Theta_0$. Considering this, the characteristics of the Payne model are enclosed by the characteristics of our model.

For both the LWR-model as well as Payne-type models, information is transported along these characteristic curves similar to the way in which information is transported in the MLMC flow model. However, the latter model has three characteristic curves, among which the path-line reflects trajectories of average vehicles (or a particular class u on lane j). Thus, our model-type appears to be the only model-type in which information is transported *physically with the average vehicles*. This reveals that including dynamics of the velocity variance (or equivalently, for traffic energy) yields a theoretically improved model form.

7.6 Shocks and contact discontinuities

It is a well know fact that the *Euler* equations, such as the inviscid MLMC-traffic flow model presented in this dissertation thesis, allow *discontinuous solutions* in certain cases. For the one-dimensional problem, these discontinuous solutions are the so-called contact discontinuities, and the *shock waves*. In this section, we discuss shock wave behaviour of the inviscid mixed-state MLMC-model. In appendix E we show that shock waves in traffic are formed by *intersecting C^- characteristics*. In this respect, traffic flow differs from the flow in a continuous media, where shocks are formed by intersection C^+ characteristics (Hirsch (1990b)).

Shocks in MLMC traffic flow

Shocks can be identified by a non-zero traffic flow through the discontinuity. As a consequence, the traffic pressure $P_{(u,j)}$ and the velocity $V_{(u,j)}$ undergo discontinuous variations. Appendix E shows how shocks can appear in the inviscid MLMC traffic flow. It is shown that the shocks appear due to intersecting $C_{(u,j)}^-$ characteristics if $\partial(V_{(u,j)}-c_{(u,j)})/\partial x < 0$. This can be seen by considering the fact that along each of the intersection characteristics different information $z_{(u,j)}^{(3)}$ is transported. Consequently, at the point of intersection an unphysical *multivalued* $z_{(u,j)}^{(3)}$ results, yielding the shock. In appendix E we show that the velocity $V_{(u,j)}^C$ of the shock is bounded by the velocities of the characteristic curves. Also let us remark that the shock formed by the intersecting $C_{(u,j)}^-$ characteristics can be either directed downstream, stationary, or directed upstream.

In appendix E we show that across the shock, the following condition holds for the discontinuous jumps in traffic density, traffic velocity, and traffic velocity variance:

$$[r_{(u,j)}] > 0 \;,\; [V_{(u,j)}] < 0 \;\text{ and }\; [\Theta_{(u,j)}] < 0 \tag{7.70}$$

That is, the jump in traffic density across the shock is *positive*, i.e. the traffic density increases spatially. Since the local sonic velocity decreases spatially, the velocity variance also decreases spatially. We can prove that the jump in the traffic pressure $P_{(u,j)}$ is also positive:

$$[P_{(u,j)}] > 0 \tag{7.71}$$

In addition to the shocks that might appear, *expansion fans* are observed in MLMC traffic flow. These expansion fans reflect regions where the variables change smoothly caused by vehicles accelerating towards different desired velocities. In opposition to shock waves, where C^- characteristics intersect at both sides of the shock wave, expansion waves are characterised by characteristics moving away from the discontinuity. Due to the origin of shocks and expansion waves in traffic flow, expansion waves *precede* shock waves. From a more elaborate discussion, we refer to Hirsch (1990b) and appendix E.

7.7 Physical boundary conditions

When we consider simulation of traffic flow operations using macroscopic models, we need to consider the initial conditions $\mathbf{w}_{(u,j)}(x,0)$ of the system at $t = 0$. However, if we consider a *non-closed system*, we also need to impose *boundary conditions* at the borders of the system. For instance, if we describe the MLMC flow operations at a motorway stretch with an on-ramp, the traffic demand at the entry of the stretch and at the on-ramps, as well as the velocity and the velocity variance of the inflow vehicles must be known. Moreover, at the exit of the stretch we need to know if vehicles can flow out of the stretch undisturbed, or that downstream traffic conditions influence the flow-conditions (e.g. under congested conditions). This section discusses the non-trivial problem of posing the correct boundary conditions on the modelled roadway stretch using the characteristics. The results explain the research-findings of among others Smulders (1989) who observed *undesirable model behaviour* when prescribing the boundary conditions at the exit incorrectly.

Let us consider a motorway section defined by the interval $[x_1,x_2]$ (Figure 7-5). Moreover, consider points R^0 and R^1 on respectively the entry and the exit of the motorway section at a

given instant t. The number of boundary conditions to be imposed will depend on the way the information is transported along the characteristics interacts with the boundaries.

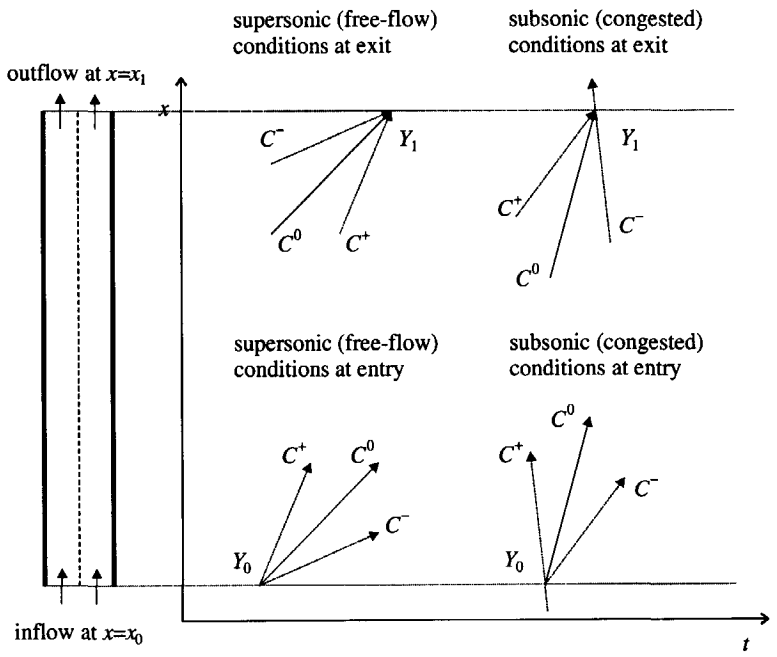

Figure 7-5: Boundary conditions for inviscid MLMC traffic flow equations

First consider the roadway entry. Here, the characteristics C^0 and C^+ always have positive slopes. Therefore, information is carried from the boundaries into the motorway, which requires specification of two boundary conditions on the motorway entry.

The slope of the C^- characteristic is dependent on the value of $V_{(u,j)}-c_{(u,j)}$ at the boundary. That is, if $V_{(u,j)}(x_0,t)-c_{(u,j)}(x_0,t) > 0$ (*supersonic* flow conditions at the boundary), the characteristic is directed from the boundary into the motorway. That is, information is carried from the boundary at x_0 into the motorway. This implies the specification of an appropriate boundary condition. However, if $V_{(u,j)}(x_0,t)-c_{(u,j)}(x_0,t) < 0$ (subsonic flow conditions at the boundary), the characteristic is directed in the opposite direction. Consequently, the characteristic carries information *from* the motorway *to* the boundary at the entry. In this case, no additional boundary condition needs to be specified. Similar considerations are valid for the motorway exit. Table 7-1 summarises the number of necessary boundary conditions at both the entry and the exit of a motorway. We have used the equivalence of subsonic and congested traffic operations on the one hand, and of supersonic and non-congested operations on the other hand.

From the analysis presented in this section, it is apparent why boundary conditions can impose problems for traffic flow analysis where different regimes at the boundaries can occur. Smulders (1989) presents simulation results with prescribing boundary conditions at the entry and the exit of the roadway. He states that prescribing the traffic conditions at the entrance

gives satisfactory results in general. However, prescribing the exit boundary conditions leads to "large fluctuations in the density in the last section, which then influences the whole freeway stretch". These phenomena can be explained by considering the direction of the characteristics of the underlying Riemann model formulation. Moreover, we can remedy such undesired phenomena by considering the correct number of boundary conditions at the entry and exit: two and one when the conditions at the entry respectively exit are congestion, and three and zero when the conditions at respectively the entry and the exit are free-flowing.

Table 7-1: Physical boundary conditions for inviscid MLMC equations

	Congested flow conditions	Non-congested flow conditions
motorway entry	*two conditions* $z_1(x_0,t)$ and $z_2(x_0,t)$ given	*three conditions* $z_1(x_0,t)$, $z_2(x_0,t)$ and $z_3(x_0,t)$ given
motorway exit	*one condition* $z_3(x_1,t)$ given	*no conditions*

7.8 Summary

In this chapter we have presented two different transformations of the mixed-state MLMC-model presented in chapter 6, namely in *primitive* or in *characteristic* variables. Primitives describe the dynamics of traffic flow using density, velocity and velocity variance (or traffic pressure). These can be considered as expressing the expected behaviour of individual drivers, that is the expected velocity and the mean deviation from the expected velocity. This formulation is valuable from an interpretation viewpoint and for model comparison purposes.

Also, we discussed the characteristic formulation of the flow model, using so-called characteristic variables. These variables enable de-coupling of the coupled system of multi-lane multiple user-class traffic flow equations. Although the Riemann variables lack intuitive appeal, the characteristic de-coupled form enables simplified mathematical analysis of the MLMC traffic flow equations. As a result, the way in which traffic density, velocity and pressure are transported in the traffic stream could be analysed. We revealed that *congested* and *free-flow* traffic operations are comparable to respectively *subsonic* and *supersonic* flow situations in fluidic or gas flows. Moreover, we showed that congested traffic conditions imply that density, velocity and pressure are transported both upstream and downstream. For non-congested traffic flow operations, density, velocity and velocity variance are only transported downstream. We showed that this among other things affects the appropriate number of boundary conditions to be used at the roadway exit and entry (section 7.7). Also, the formation of shocks has been described mathematically (section 7.6).

The main benefit of the Riemann formulation is the applicability of Godunov-type numerical schemes (see chapter 9). These are based on local exact solutions of the so-called Riemann problem. The latter is characterised by a single discontinuity in elsewhere constant traffic flow conditions. It can be shown that these discontinuous initial conditions result in a shock waves, a contact discontinuity and an expansion fan (see appendix D).

8 DATA ANALYSIS AND MODEL CALIBRATION

This chapter presents an empirical analysis of multiclass multilane traffic flow data. Its aim is threefold: to *gain insight into the real-life heterogeneous traffic behaviour* on the distinct motorway lanes, to *calibrate the model parameters*, such as desired velocities, average vehicle length for each user-class, and to *approximate functional equilibrium relations* between density on the one hand, and relevant dependent traffic flow variables.

In principle, gaining insight into both the dynamics of real-life MLMC traffic flow operations and the validity of the developed model requires dedicated data collection. That is, observations reflecting among other things velocities of vehicles, lane-changing behaviour and the fraction of constrained vehicles for each distinguished class are needed. Due to the complex nature of the phenomena of interest (e.g. class-specific lane-changing behaviour), data tailored for MLMC traffic data analysis was not available. Therefore, in this chapter we focus on other data-types and extract model parameters and functional relations from these data.

To this end, data of a two-lane motorway in the Netherlands is analysed. These data reveal the interdependencies of traffic flow variables, such as density, velocity, and velocity variance, on two lanes of the motorway for identified user-classes. To distinguish the dynamics of the expected flow variables from stochastic fluctuations, we propose a data *aggregation method* involving subsamples containing an equal number of observations, rather than covering periods of equal duration. Although this 'equal-sized samples' aggregation-method is superior to equal period length method, aggregation of measurements is observed to yield bias in some flow variables (e.g. velocity variance). To remedy this, we propose a new "discrete event" *filtering technique*, enabling determination of among other things velocity variance (see appendix G). We also propose an alternative method to correctly determine velocity

variances, based on differences in successive velocity observations. Both methods yield very similar results. By application of either method, it appears that the velocity variance is a monotonically decreasing function of the density. Moreover, it remains to be seen whether an observed increase in the variance be considered as predicting the on-set of congestion, as suggested by Kühne (1984a,b).

All relevant traffic flow parameters and relations are determined from available traffic data. That is, we have determined average vehicle lengths, reaction times, acceleration times, fractions of constrained vehicles, and velocity variances for each distinguished class and lane. Combining available free gaps and spaces needed by lane-changing vehicles establishes lane-changing probabilities and rates. Using these relations, an algorithm is developed that determines both the MLMC *equilibrium velocity* and the *lane-distribution* of vehicles given any configuration of aggregate-lane class-specific densities. We conclude that using the specifications based on real-life traffic observations, both the equilibrium velocities and lane-distribution are accurately reproduced.

8.1 Heterogeneous multilane traffic flow data requirements

Any traffic flow theory deemed suitable to realistically describe real-life phenomena in traffic flow must be compared with real-life observations. In this respect, numbers of data-types are available. In this section, we discuss some of them.

Ideally, the data consists of *vehicle trajectory observations* for the observed roadway stretch, for all vehicles in the stream of each class on each lane. Using these data, all relevant traffic flow variables (e.g. density, momentum) for each class can be established. Moreover, class-specific lane-changing behaviour (e.g. target-lane choice, gap-acceptance behaviour) can be studied, given conditions on the current lane and choice alternatives. However, trajectories of all vehicles in the stream are rarely available.

8.1.1 Infrastructure-based traffic detectors

The most common *infrastructure-based* traffic detectors collect *cross-section data*. Examples of these are pneumatic tube detectors, coaxial detectors, infrared detectors, radar detectors, ultrasonic detectors, and induction loop detectors. These detectors can usually determine passage time t_α, length l_α, and sometimes velocity v_α of the passing vehicle α. In some cases, the observations are lane-specific. Then, although several lane-specific variables can be derived (e.g. mean velocity per lane, distribution of classes with respect to the lanes), other lane-specific quantities *cannot be directly derived* from the observations (e.g. average number of immediate lane-changes per user-class).

Video camera detectors can be used as a substitution of the mentioned cross-section detectors. Conversely, it is also possible to register characteristics of a passing vehicle (e.g. vehicle-type, licence-plate, colour) enabling *Automated Vehicle Identification* (AVI). Using AVI we can observe that vehicle α passed an observation point on lane j_α at instant t_α with speed v_α. Then, when data from two subsequent measurement locations are available, (lower-bound) estimates of the number of lane-changes of each vehicle can be determined. This lower-bound is more likely to be an accurate estimate of the actual number of lane-changes, if the distance between the observation locations is adequately chosen. For instance, if vehicles are able to complete an *entire overtaking manoeuvre* (e.g. change to left-lane, overtake slower

vehicle, change back to right-lane) in the region between video detectors, it will pass the first detector on the same lane as the second detector. Since the time needed to complete an overtaking manoeuvre is in the order of $10s$, ideally the video detectors should be no more than $10s \times 30m/s = 300m$ apart.

Alternatively, using correctly positioned video cameras, the actual lateral movements of the vehicles can be observed. Then, it is possible to quantify the different lane-changing processes from one single detector. Drawbacks of this approach are the inaccuracy of the determined vehicle locations and speeds, and the relatively small observation region.

8.1.2 Non-infrastructure-based traffic detectors

To accurately monitor the multilane multiclass flow operations, information about both the *spatial* as well as *temporal fluctuations* are necessary to enable reconstruction of vehicle trajectories and observe class-specific lane-changing operations. However, infrastructure based detectors are designed to collect traffic data *at one specific and fixed location*. Let us now consider *non-infrastructure-based* traffic detectors.

Probe vehicles

In opposition to fixed detectors, vehicles can themselves be used for data collection purposes. Vehicles in the flow able to transmit information are referred to as *probes*. For heterogeneous multilane traffic flow analysis, these probes must at least be equipped with hardware that enables the determination of the *longitudinal* and the *lateral* position. Examples of such location determination techniques are *dead-reckoning*, *map-matching*, *proximity-beacon techniques*, *trilateration techniques*. Unless probes are also able to observe other vehicles in the flow (*moving observers*), other variables (e,g, flow-rate) must be established from other, for instance infrastructure based, detectors. In combining probe trajectories with fixed detector data, flow characteristics of non-equipped vehicles can be estimated (cf. Westerman (1995)).

Aerial photographs and video observations

Alternatively, aerial photographs or video observations can be collected. When these observations are available and sufficiently detailed, various MLMC flow variables, such as density, can be determined directly from the data. In the case of photographs, other quantities (e.g. space-mean-speeds, distance-headways) can be determined by comparing shots of consecutive time instants. For instance, the velocity of vehicles can be determined by comparing their longitudinal position, while an lower-bound approximation of the expected number of lane-changes can be determined by comparing lateral positions of vehicles. Similar to the AVI-observation technique, the time between two photographs should not be larger than the minimum time needed to perform a lane-change. Clearly, this does not apply to aerial video observations. Hence, detailed aerial video observations are suited for analysis of heterogeneous multilane traffic, since these data allow determination of flow variables and parameters.

However, for the research presented in this thesis, no such data was available. Rather, individual vehicle data from fixed detectors is combined with theoretical relations to determine the different parameters and quantities. These data and the approach used are presented in the ensuing of this chapter.

8.2 Individual vehicle measurements and derived quantities

In this section we discuss the direct individual vehicle observations used, and the individual quantities derived from these observations.

8.2.1 Description of the data

The data* that has been analysed was collected at the Dutch motorway A9, near the Dutch city of Badhoevedorp. The prevailing speed is $100km/hr$. The minimum width of the motorway lanes equals $3.5m$. The terrain is *level* to the extent, that the small grades do not influence traffic operations. Moreover, the curvature of the motorway does not influence traffic flow behaviour either.

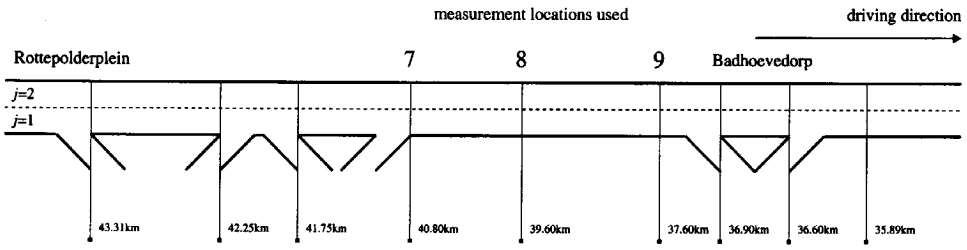

Figure 8-1: Measurement locations on the A9 motorway near the city of Badhoevedorp.

Individual vehicle data has been collected at a large number of observation points (see Figure 8-1). Also, in Figure 8-1 we have indicated the three measurement locations near the city of Badhoevedorp that have been used for MLMC data analysis and model calibration purposes. The datafile consist of arrival times, individual velocities and vehicle lengths. Using the vehicle length, an observation is classified as a person-car ($< 6m$) or a truck ($> 6m$). We will not distinguish articulated and non-articulated trucks, nor will we distinguish busses. These classes are gathered into the 'truck'-class.

In the remainder of this chapter, we will use measurement locations 7 ($x = 40.8km$), 8 ($x = 36.9km$) and 9 ($x = 37.6km$) for data analysis purposes. The location of measurement determines the range on the speed-density relation where measurements are found. For instance, it has been found that the number of observations of *synchronised* flow at location 7 (cf. Kerner and Rehborn (1996,1997a)) is very small. That is, the transition from free-flow to congested flow, and vice versa, occurs suddenly due to congestion-spillback caused by the downstream bottleneck at $x = 36.9km$. At location 8 longer lasting transition periods of synchronised operations and start-stop waves are observed. Therefore, this location is also used for data analysis. For a detailed discussion on the importance of the field location, we refer to May (1990; section 10.2.1).

Let us finally remark that we have found that traffic operations are prone to congestion during the morning peak-hour. Congestion almost never occurs during the evening peak-hour, or

* The data analysed in this thesis has been used at the courtesy of the Dutch Ministry of Transport, Public Works and Water management, Traffic Research Centre (AVV).

during other periods of the day. This congestion is formed by the major active bottleneck at the on-ramp near Badhoevedorp.

8.2.2 *Semi-direct measurements*

Semi-direct measurements are measurements that were available from the data-file. These data have been postprocessed from raw data containing instants when the front and the rear of the vehicles pass the first and second loop of the double-loop detectors*. Considering a vehicle α, following semi-direct measurements are available in the data:

1. Passing instant t_α.
2. Lane occupied j_α when passing the loop.
3. Velocity v_α at the passage moment.
4. Length L_α of the vehicle.

For a detailed description of the data and the way in which these are determined from the raw observations, we refer to Dijker *et al.* (1997).

Figure 8-2 depicts individual velocity measurements of person-cars and trucks on the two respective lanes of the roadway, collected during a typical morning peak period (6.00AM-11:00AM) on Thursday 20th of October 1994. The figure shows the relation between the filtered velocity† and the passage times. The velocity measurements have been filtered using the second order low-pass Butterworth filter (see appendix G) with cut-off frequency equal to $20\pi/N$, where N is the number of observations in the filtered sample. The figure clearly shows the dynamics of the expected velocity on the roadway lanes. On the left roadway lane, velocities are generally higher when traffic is freely flowing (I). When traffic conditions worsen, the velocity of the person-cars on the left-lane drops to the velocity of the person-cars on the right-lane (II). On the right-lane, a similar phenomenon is observed with respect to the person-car velocities on the one hand, and the truck velocities on the other hand (III). That is, when traffic becomes more congested, the expected velocity of the person-cars drops first to the velocity of the trucks, after which both drop at approximately the same rate.

Another interesting observation is made when considering velocity measurements during the congested period IV. During this period, velocities seem to cyclically increase and decrease, indicating stop-and-go traffic conditions. These so-called *stop-start waves* are characteristic for traffic flow where the density has surpassed a certain critical value. Other measurement data of these stop-start waves are reported by Leutzbach (1991), Verweij (1985), and Ferrari (1989). Each of these shows waves having a (more or less) regular shape and of reasonable long duration. In our case, the oscillation time is approximately $20min$, while the amplitude of the waves is in the order of $25km/hr$ (see also section 10.2). Note that in start-stop waves, truck velocities are lower than person-car velocities. Apparently, trucks are unable to in-

---

* Direct observations were not available.

† The filtering technique used in this thesis is a discrete-event filter, based on Butterworth-filtering in the frequency domain. The filter enables determining accurate estimates for time-varying traffic flow variables, such as expected velocity and velocity variance. With respect to the latter, the filter is especially valuable, as is discussed in the remainder of this chapter and appendix G.

crease their velocity during short 'go-waves' to the same extent as more agile person-cars, due to comparably poor acceleration and deceleration capabilities of trucks.

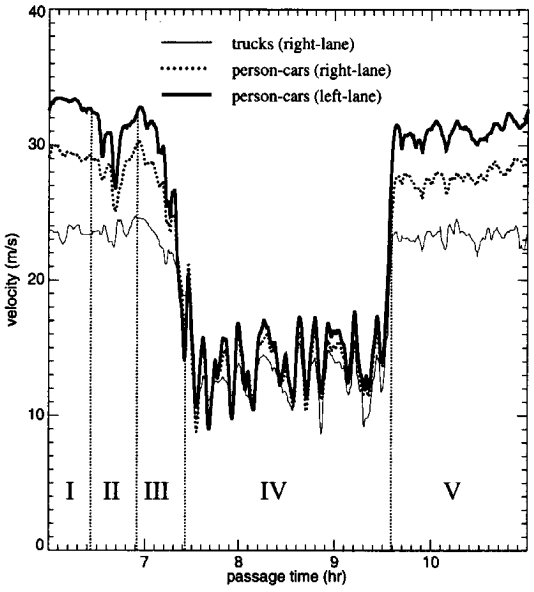

Figure 8-2: Filtered velocity measurements as a function of the passing times collected at the A9 motorway during the morning peak hour on Thursday, 20th of October, 1994. Truck velocity measurements on the left lane are discarded due to the little number of observations.

8.2.3 Indirect measurements

Indirect measurements represent individual quantities that can be determined from (semi-) direct measurements using simple computations. In other words, indirect observations can be established from direct observations using addition, subtraction, multiplication, and division, without needing to apply complex models, smoothing techniques, etc. that need fairly stringent behavioural assumptions. The determined indirect observations are (see Figure 8-3):

- Vehicle class u_α is determined from the length of the vehicle α.
- Gross time headway $H_\alpha = t_{\alpha'} - t_\alpha$ with respect to the preceding vehicle α'.
- Gross distance headway $D_\alpha = H_\alpha v_{\alpha'}$ with respect to the preceding vehicle α'.
- Distance *gap* $d_\alpha = D_\alpha - L_\alpha$ with respect to the preceding vehicle α'.
- Net time headway $h_\alpha = d_\alpha / v_{\alpha'}$ with respect to the preceding vehicle α'.

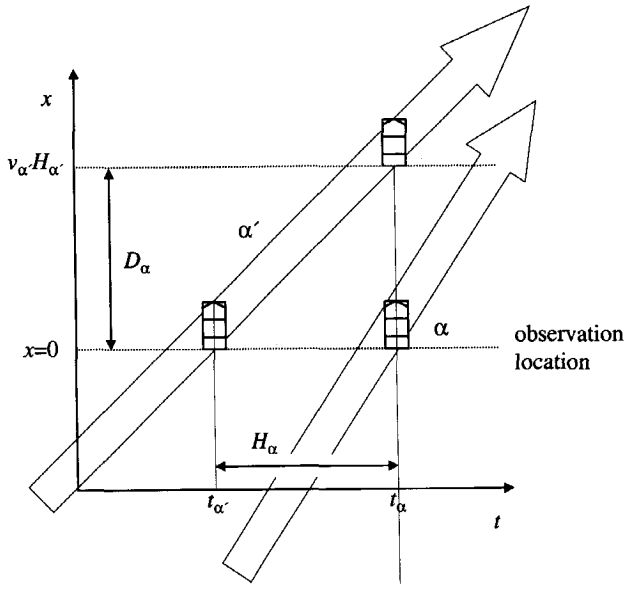

Figure 8-3: Definition of time and distance headways.

User-class specification

Due to the nature of the available data, only two user-classes can be distinguished, namely person-cars and trucks (including busses). This distinction is based on the differences in the length of the vehicles. We will use the following criteria (see Dijker *et al.* (1997)):

- Person-car: $0 \leq L_\alpha \leq 6m.$
- Truck: $L_\alpha \geq 6m.$

Other classes, such as motorbikes, are either to few to allow for a statistical significant analysis, or cannot be distinguished based on the available measurements (e.g. paying traffic, commutes, business-related traffic).

Distance headways and gaps

Figure 8-4 shows distance headways of person-cars and trucks on both lanes of the A9 motorway. Obviously, when traffic conditions become more congested (I–III), the distance headway decrease accordingly. The lowest values are attained during congestion (IV). The difference between the distance headways of person-cars and trucks is to a large extent dependent on differences in vehicle lengths of the two classes. Figure 8-5 shows gaps of both person-cars and trucks on two lanes. Differences in expected person-car gaps and expected truck gaps are clearly not as profound as when considering the distance headway. However, a significant difference remains (see Dijker *et al.* (1997)). Such differences may result from a large number of factors, such as better acceleration, deceleration, and lane-changing capabilities of person-cars, familiarity of drivers with the road, and so on.

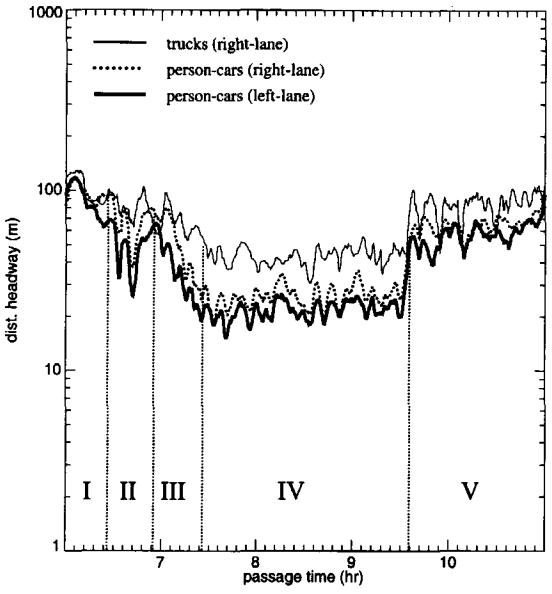

Figure 8-4: Filtered distance headway measurements.

8.2.4 Derived observations

Finally, *derived observations* are quantities derived from semi-direct and indirect observations using more complex algorithms. We can roughly distinguish variables that are – either directly or indirectly – determined using filtering techniques, or based on less obvious modelling or behavioural assumptions. Summarising, the derived observations are:

- The squared velocity deviation Θ_α.
- The level of constrainedness θ_α.

Filtered observations and the squared velocity deviation

The filtering approach is based on transforming a sequence of individual vehicle observations and enables estimating the expected velocity considering structural dynamic changes. The technique is based on transforming the *discrete-event signal*[*] $x[i]$, where i indicates the i-th vehicle, into the representation in the *frequency* or *Fourier* domain using the Fast Fourier Transform (FFT). Subsequently, *high-valued frequencies* – of which we presume that they reflect the high frequency noise present in the signal $x[i]$ – are filtered out, by application of either of the filters presented in appendix G (e.g. ideal low-pass filter, a linear low-pass filter, or a Butterworth filter). The resulting Fourier representation is transformed back into the discrete-event domain, yielding a smoothed signal $y[i]$ of $x[i]$.

[*] To avoid confusion, we stress that the term 'discrete-event signal' has no relation to the research field of 'discrete-event systems'.

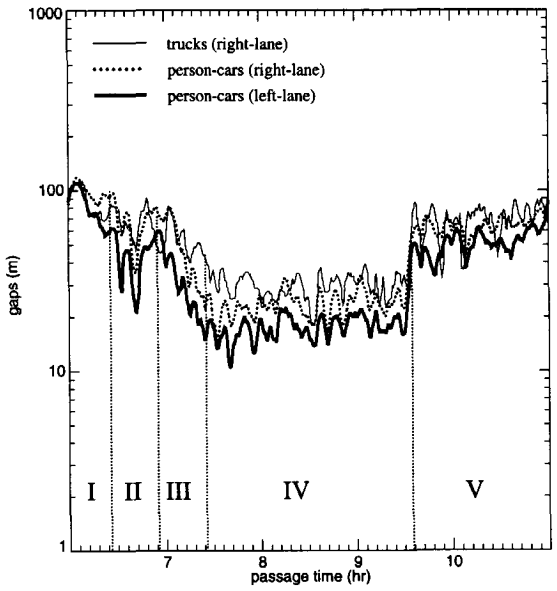

Figure 8-5: Smoothed gaps.

We assume that each velocity observation v_α of a vehicle of class u on lane j is a realisation of a random variate with expectation $V_{(u,j)}$. We apply the filter to estimate the expected velocity. Using the estimation of the expected velocity $V_{(u,j)}$ we can determine the *squared velocity deviation* by $\Theta_\alpha = (v_\alpha - V_\alpha)^2$ for each vehicle that has passed the observation point. Clearly, the *cut-off value* ω_C and the order n_{BC} of the Butterworth filter applied to the velocity measurements influence the magnitude of Θ_α.

In illustration, Figure 8-6 depicts the histogram plots of the standard velocity deviation determined by application of the Butterworth filter for various parameter values (ω,n_{BC}). In other words, the figure shows how frequently a specific standard deviation occurs. From the results depicted in this picture, we conclude that an increase in the cut-off frequency (less smoothing of the velocity) yields both a lower velocity deviation average and less spread of the velocity deviations. This is most profound when stop-and-go traffic conditions can be identified (period IV). In this case, the low-valued cut-off frequency causes the approximation of the expected velocity to react to slowly to changing traffic conditions. In other words, the filter is unable to delineate dynamic changes in the expected velocity $V_{(u,j)}$ from the high-frequency noise. Choosing a higher cut-off frequency remedies this problem. Similar remarks can be made with respect to the order n_{BC} of the Butterworth filter.

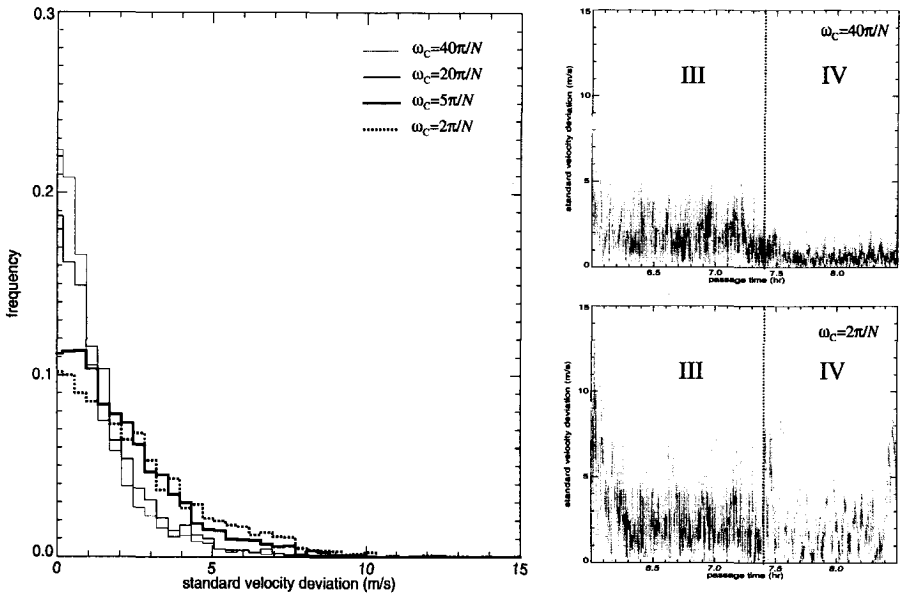

Figure 8-6: Frequency plots of the standard velocity deviations $\sigma_\alpha = \Theta_\alpha^{1/2}$ of person-cars on the right-lane of the A9 motorway (left figures) determined using various levels of smoothing using 4th order Butterworth filter. Clearly, the relative number of high-standard deviation observations *increases* when the cut-off frequency of the filter *decreases* (more smoothing of average velocity).

Vehicle's state

We also need to determine the state of the vehicle. Several criteria that allow determination of the vehicle's state have been proposed in the literature, varying from very simple to very complex methods. Dijker *et al.* (1997) defined a constrained vehicle according to their *net time headway* t_α, which should be less than $5s$. Additionally, when the velocity is less than $20km/hr$, a vehicle is unconditionally constrained. Wiersma *et al.* (1996) use both a speed-difference criterion (velocity difference with the preceding vehicle is smaller than $1m/s$) and a time headway (should be smaller than $5s$).

More elaborate methods are possible as well. For instance, Hoogendoorn *et al.* (1997) present a method to estimate the Generalised Queuing Model (CGM; cf. Cowan (1975) and Branston (1976)) to individual vehicle data. By doing so, the constrained vehicle fraction, which is a parameter of the CGM, is estimated as well. Moreover, Hoogendoorn and Bovy (1998,1999c) have also applied their approach on vehicle-type specific data and lane-specific data. They concluded among other things that the fraction of constrained trucks was lower than the fraction of constrained person-cars.

Fuzzy-set approach to determine the level of constrainedness

The approach used in this dissertation is a fuzzy two-criteria technique. In this respect, the term *fuzzy* indicates that a driver does not have to be either constrained or unconstrained. Rather, the driver's state can also be *partially constrained.* This is reflected by the *level of constrainedness* θ_α of vehicle α. By using a fuzzy approach rather than an approach with crisp thresholds, constrainedness levels can be determined from the data. In other words, the fraction of constrained vehicles can be approximated by the *average level of constrainedness.* We argue that to describe the level of constrainedness, the fuzzy-set paradigm is useful, due to its ability to describe inherently vague traffic variables (see Hoogendoorn *et al.* (1997))

This vagueness is a result of the vague observations and perceptions of drivers (see among others Rekersbrink (1995)). To determine the level of constrainedness, we have used two criteria:

1. The *gap* is approximately equal to the distance needed for safe driving.
2. The *speed difference* with respect to the leading vehicle is near zero.

For both criteria we determine the extent to which these criteria are met. For criterion 1 this is performed by determining the distance gap. If this gap lies within certain fuzzy bounds (Figure 8-7), criterion (1) holds to a certain degree. Similarly, we determine the degree to which criterion (2) holds by considering the velocity difference with respect to the leading vehicle. The overall level is determined by taking the minimum, indicating the AND operation in fuzzy-set terms (see Zadeh (1965)).

In illustration, Figures 8-8 and 8-9 show estimates of both the gap probability density function, as well as the probability density function of the velocity-difference of the leading and the following vehicle. Also, Figures 8-8 and 8-9 depict the fuzzy bounds (indicated by the partially constrained regions) for both criteria.

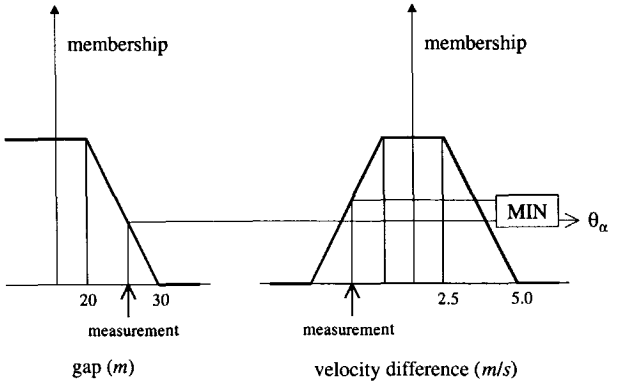

Figure 8-7: Determination of constrainedness-level θ_α using fuzzy sets.

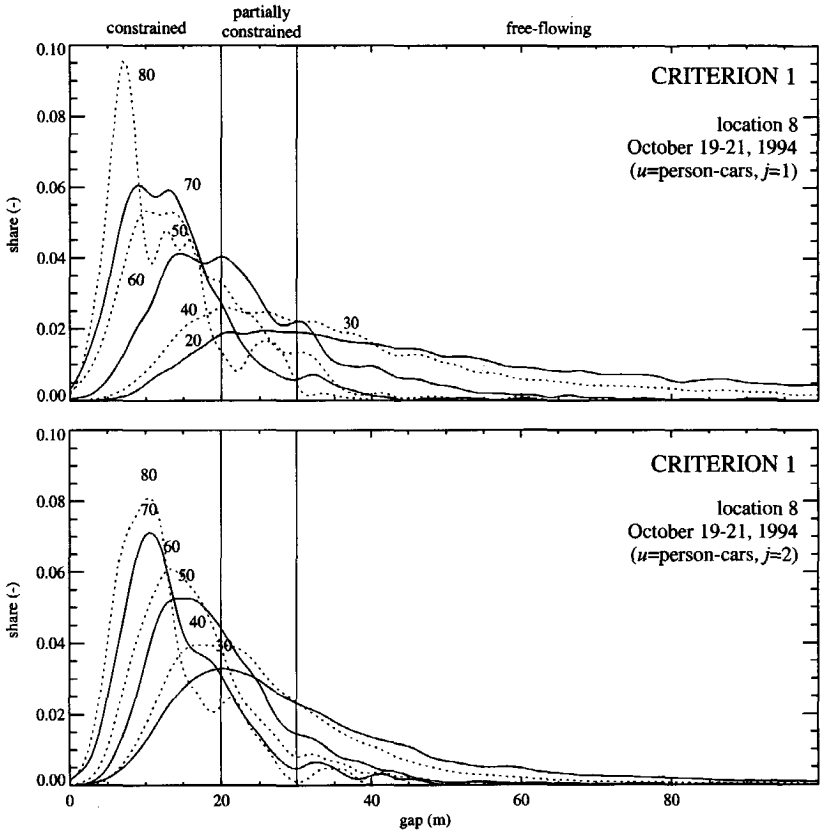

Figure 8-8: Distribution of person-car gaps for different values of total density per lane, for the right-lane and the left-lane (kernel estimates).

8.3 Data aggregation approach

Aggregation of individual vehicle observations is necessary for multilane heterogeneous traffic flow analysis. By doing so, we can approximate various MLMC flow variables such as density, velocity, momentum, and pressure.

8.3.1 Approach to data-aggregation

However, we have observed that the traditional approach of aggregating data collected during equal-length periods is unsuitable for MLMC traffic for two reasons. First, since the number of observations is different from one period to another, the statistical accuracy with which flow variables are estimated cannot be determined a priori*. Secondly, since some vehicle counts of some classes are less in number than others, a minimal number of observations of a

* This holds equally for non-MLMC traffic flow analysis.

specific class *cannot be guaranteed.* In other words, periods occur where observations for a specific class are absent.

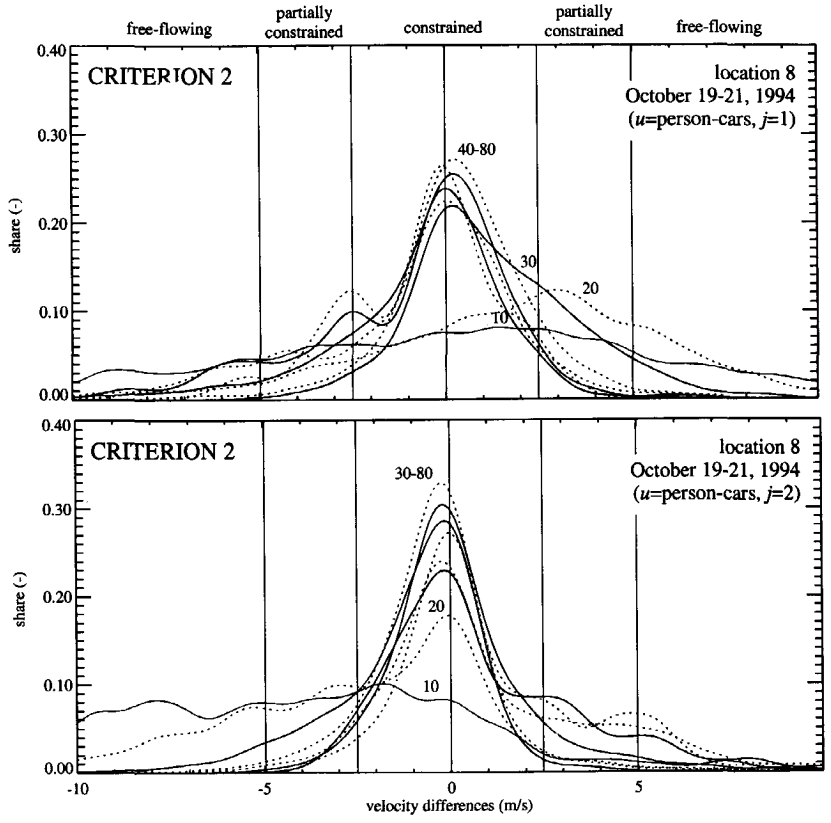

Figure 8-9: Distribution of person-car velocity differences for different total density values, for right-lane and left-lane (kernel estimates).

To remedy these problems, we propose to classify the observations into equally-sized subsamples. This assures non-zero samples sizes on the one hand, while on the other hand the statistical accuracy of the derived estimates can be estimated a priori. With respect to the approximation of the expected velocity for person-cars and trucks, we have observed that the *Coefficient of Variation* (CV) of person-car velocities is approximately *two times higher* than the CV of truck velocities. As a consequence, the number of person-cars observations per subsample must be *four* times higher for person-cars than for trucks, to attain the same level of confidence for the estimates. For details, see appendix F.

8.3.2 Determination of local and instantaneous averages

Whilst some variables are typically *local* (e.g. time headways, time-mean-speeds), other variables are *instantaneous* (distance headways, space-mean-speeds). In appendix F we show that *local variables* can be approximated by the *arithmetic mean* of the observations:

$$y_{\mathbf{a}}[k] = \mathrm{avg}_{\mathrm{A}}(y_{\mathbf{a}}; k, M_{\mathbf{a}}) \overset{def}{=} \frac{1}{M_{\mathbf{a}}} \sum_{i=0}^{M_{\mathbf{a}}-1} y_{\mathbf{a}}(i + kM_{\mathbf{a}}) \tag{8.1}$$

where $y_{\mathbf{a}}(i)$, $M_{\mathbf{a}}$, and $y_{\mathbf{a}}[k]$ respectively denote the observation of 'y' of the i-th passing vehicle, the number of observations per subsample, and the average of $y_{\mathbf{a}}(i)$ for the k-th subsample, with respect to discrete attribute-set **a**.

It is well known that for *instantaneous variables* the arithmetic mean overestimates contributions of vehicles with higher velocities (cf. Leutzbach (1988)). To remedy this, the *harmonic average* can be used, written as a *weighted sum* of individual velocity measurements:

$$z_{\mathbf{a}}[k] = \mathrm{avg}_{\mathrm{H}}(z_{\mathbf{a}}; k, M_{\mathbf{a}}) \overset{def}{=} \frac{1}{M_{\mathbf{a}}} \sum_{i=0}^{M_{\mathbf{a}}-1} \beta_{\mathbf{a}}(i;k) z_{\mathbf{a}}(i + kM_{\mathbf{a}}) \tag{8.2}$$

where the weighting parameters $\beta_{\mathbf{a}}(i;k)$ are determined using the velocity measurements:

$$\beta_{\mathbf{a}}(i;k) = \left(\frac{1}{M_{\mathbf{a}}} \sum_{j=0}^{M_{\mathbf{a}}-1} \frac{v_{\mathbf{a}}(i + kM_{\mathbf{a}})}{v_{\mathbf{a}}(j + kM_{\mathbf{a}})} \right)^{-1} \tag{8.3}$$

and $v_{\mathbf{a}}(i)$ is the observed velocity of the i-th vehicle with the attribute-set **a** that has passed the observation cross-section.

8.3.3 Determination of the velocity variance

The velocity variance Θ can be either determined by averaging 'individual variances' determined by the differences with the filtered velocity (section 8.2.4) or using a standard technique to determine the sample deviation of measured velocities. However, the latter approach does not yield the correct results. This is caused by sudden transition of traffic operations from free-flow to synchronised flow, stop-and-go flow, or congested flow (i.e. upstream propagating shock waves) and the occurrence of start-stop waves (e.g. Figure 8-2). If such a sudden transition occurs during sample period k, deviations of individual velocity measurements with respect to the period-average velocity are large due to the change in the real expected velocity. In other words, velocity observations obtained during the period can not be considered instances of the same distribution, yielding unrealistically high velocity variances. To remedy this, the number of vehicles in a sample can be reduced, thereby resulting in a shorter sample period and consequent lower probability that sudden transitions will affect the determined velocity variance. However, to cancel out the biasedness in estimated variances altogether, the number of observations in the sample needs to be reduced to the extent that no statistically reliably estimates can be inferred from the sample.

In illustration, Figure 8-10 shows the velocity variance-estimates for person-cars on the right roadway lane established using the 'traditional approach' for $N = 40$ and $N = 80$. Clearly, at moderate total *effective* or *modified density* values, the velocity variance increases. Figure 8-10 also shows estimates for the variance determined using by averaging the individual deviations of the average velocity (section 8.2.4). Using the filter-approach reveals that velocity variance is a *monotonically decreasing function* of total effective density.

Velocity variance estimation using the method of successive velocity measurements

To validate the results of the filtering method, we have developed a third method to establish estimates for the velocity variance. This method is based on the assuming that the observed velocities are instances of a Gaussian-distributed random variate, that is:

$$\underline{V}_n \sim \mathcal{N}(V_{(u,j)}, \Theta_{(u,j)}) \tag{8.4}$$

If we assume that two successive velocities v_n and v_{n+1} are observations that are both instances of two $\mathcal{N}(V_{(u,j)},\Theta_{(u,j)})$-distributed random variates $\underline{V}_n$ and $\underline{V}_{n+1}$, then the difference $(v_{n+1}-v_n)$ is also Gaussian distributed:

$$\underline{V}_{n+1} - \underline{V}_n \sim \mathcal{N}(0, 2\Theta_{(u,j)}) \tag{8.5}$$

By determining the difference between two successive observations we are able to determine an approximation of the variance $\Theta_{(u,j)}$ by determining the harmonic mean of the squared difference of successive velocities:

$$\hat{\Theta}_{(u,j)}[k] = \frac{1}{2M_{(u,j)}} \sum_{i=0}^{M_a-1} \beta_{(u,j)}(i;k)\left(v_{(u,j)}(i+1+kM_{(u,j)}) - v_{(u,j)}(i+kM_{(u,j)})\right)^2 \tag{8.6}$$

In illustration, Figure 8-10 finally shows the results using the estimator (8.6).

8.4 Empirical multiclass multilane relations

Traditional traffic flow data analysis has mainly concentrated on determination and analysis of relations between density r on the one hand, and dependent traffic flow variables (e.g. the velocity V or the momentum m) on the other hand. That is, data analysis aims to empirically determine relations for equilibrium velocity $V^e(r)$ and equilibrium momentum $m^e(r) = rV^e(r)$. In contrast, we aim to establish relations between densities $r_\mathbf{a}$ for specific choice of $\mathbf{a} = (u,j,c)$ on the one hand, and dependent traffic flow variables describing traffic conditions for vehicles having attribute set $\mathbf{a}$ on the other hand (sections 3.6 and 3.9). For instance, we establish relations between aggregate-lane person-car density r_1 and aggregate-lane truck density r_2, and average-lane equilibrium velocity $V_1^e(r_1,r_2)$ of person-cars.

In doing so, we have observed that the independent variables describing the MLMC empirical relations can be reasonably approximated by a single explanatory variable, namely *the effective* or *modified density*. As was shown in section 6.7, the latter variable is a function of the densities and velocities of the distinguished user-classes, and describes the *average number of vehicles per unoccupied unit roadway length.*

8.4.1 Theoretical considerations

In this section, we will determine an empirical relationship between average velocities of both person-cars and trucks on the one hand, and the person-car and truck densities on the other hand. By doing so, we aim to *approximate* the equilibrium velocity $V^e_{(u,j)} = V^e_{(u,j)}(\mathbf{r}_j,\mathbf{V}_j,\Theta_j)$, derived in chapter 7, by a function of the densities $r_{(1,j)}$ and $r_{(2,j)}$ only. This is justified by assuming for any density configuration $\mathbf{r}$ – indicating the densities of the different user-classes on the different lanes – which the dependent variables satisfy:

$$(V^e_{(u,j)}, \Theta^e_{(u,j)}) = (V^e_{(u,j)}(\mathbf{r}, \mathbf{V}^e, \Theta^e), \Theta^e_{(u,j)}(\mathbf{r}, \mathbf{V}^e, \Theta^e)) \tag{8.7}$$

when traffic operates under equilibrium conditions. This yields a fixed point problem that, given it has a unique solution, can be determined for any **r**. Moreover, assuming that for a specific density configuration, the distribution of vehicles of a specific user-class also evolves to an equilibrium value, enables us to cast the equilibrium velocity and velocity variance as a function of the lane-aggregate traffic densities of the respective user-classes only.

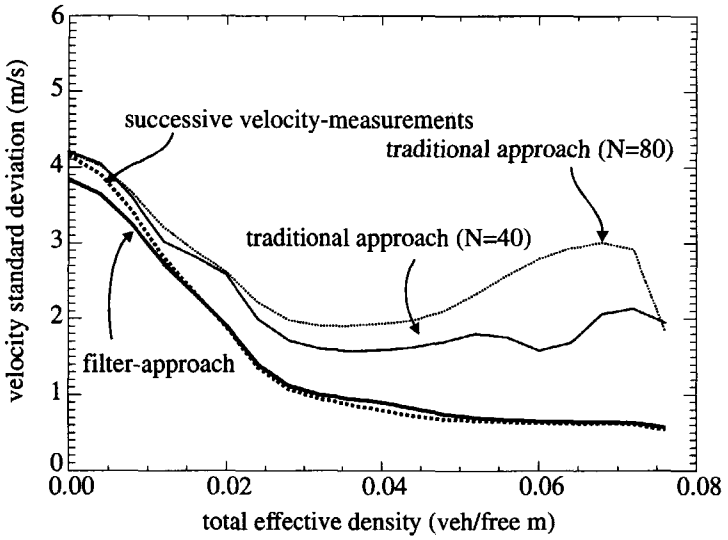

Figure 8-10: Velocity variance estimates using different approaches as a function of the total effective density per lane. The figure clearly reveals the deficiency of the traditional method to accurately determine the variance, especially for moderate to high densities. The estimates obtained by both the filter-approach as well as the successive velocity-measurement approach are almost identical.

Multiclass equilibrium velocity

Let us first consider the equilibrium velocity for the aggregate-lane case in further detail. When densities are very low, we assume that the average velocity for either user-class is approximately equal to the average desired velocity, that is $V_{(u,j)}{}^e(\mathbf{0}) = V_{(u,j)}{}^0$. When either density increases, the increase in the number of vehicle interactions, and thereby the resulting number of vehicles decelerating, increases. As a result, the expected velocity decreases. Thus, the equilibrium velocity is a monotonically decreasing function of the densities:

$$\partial V^e_u / \partial r_{u'} \leq 0 \quad \text{for all } u \in \mathbf{U} \text{ and } u' \in \mathbf{U} \tag{8.8}$$

When densities increase to the extent that almost no vehicle is able to move around anymore, the velocity is zero. Motionless vehicles occupy $L_u + d_u^{min}$ space on the roadway lane, where L_u denotes the length of the vehicle, and d_u^{min} denotes the margin describing the distance between vehicles standing still (see section 2.2.2). Then, if we consider the total amount of available roadway space, this space is entirely occupied if:

$$\mathbf{r}^T\mathbf{L} = \sum_{u' \in U} r_{u'}(L_{u'} + d_{u'}^{\min}) = 1 \tag{8.9}$$

This relation specifies the *jam-density space* $\mathbf{R}_{jam}$, defining the *space of vectors* $\mathbf{r}$ where no roadway space is left unoccupied, and all vehicles have stopped. For each $\mathbf{r} \in \mathbf{R}_{jam}$, the equilibrium velocity variance equals zero:

$$V_u^e(\mathbf{r}) = 0 \quad \text{for all} \quad \mathbf{r} \in \mathbf{R}_{jam} \quad \text{where} \quad \mathbf{R}_{jam} = \{\mathbf{r} \mid \mathbf{r}^T(\mathbf{L} + \mathbf{d}^{min}) = 1\} \tag{8.10}$$

In other words, rather than prescribing a scalar-valued jam-density, we specify an entire plane of density configurations $\mathbf{R}_{jam}$. Kühne (1991) reports aggregate-class jam-densities that are in the range between 160*veh/km* and 180*veh/km*. Similar observations can be made with respect to the equilibrium velocity variance as for the equilibrium velocity variance.

8.4.2 *Aggregate-lane average velocity*

Let us now consider the case of two user-classes, namely person-cars and trucks. Let us first consider the average-lane equilibrium velocity for both classes as a function of the average-lane densities (that is, the average number of vehicles per unit roadway length per lane, average across the roadway lanes). Figure 8-11 shows the relation between the densities and the velocities of these user-classes, determined from data collected during the period 17-21 October 1994, and 24-28 October 1994. In the figure *iso-density lines* are indicated so that the possible asymmetric velocity reduction can be clearly observed. These lines reflect these combinations of person-car densities and truck densities that amount to the same total (average-lane) density per lane.

To derive the relations, data is processed as follows. First, the sample is categorised into small equally sized subsamples k. These subsamples contain both person-cars and trucks. For each k velocities $v_{(u,*)}[k]$ and densities $r_{(u,*)}[k]$ are determined for $u = 1,2$. The pair $(r_{(1,*)},r_{(2,*)})$ is a point in a two-dimensional plane for which values $v_{(u,*)}$ are known. Since data is sparse in the two-dimensional class-density plane, we assume that velocity observations known in point $(r_{(1,*)},r_{(2,*)})$ contain information in a small neighbourhood of the point $(r_{(1,*)},r_{(2,*)})$. This *information diffusion* is modelled by introducing *weighting functions* $\omega(r_1,r_2;k)$ that are defined for each pair $(r_{(1,*)}[k],r_{(2,*)}[k])$ by the following two-dimensional function:

$$\omega(r_1, r_2; k) = \max\{0, \exp(-(r_1 - r_{(1,*)}[k])^2 / \sigma_1^2 - (r_2 - r_{(2,*)}[k])^2 / \sigma_2^2) - c\} \tag{8.11}$$

where σ_1, σ_2, and c are parameters determining the information diffusion. The approximation of the equilibrium velocity can be determined by the following equation:

$$\hat{V}_{(u,*)}^e(r_1, r_2) = \frac{\sum_{k=0}^{N-1} \omega(r_1, r_2; k) \cdot v_{(u,*)}[k]}{\sum_{k=0}^{N-1} \omega(r_1, r_2; k)} \tag{8.12}$$

A similar approach is used to establish relations between the velocity, variance, constrained vehicle fraction, etc. on the one hand, and the effective density per lane on the other hand.

Figure 8-11a clearly shows that the dependency of person-car velocity on the person-car densities and the truck densities is *asymmetrical*: the iso-velocity curves decline non-proportionally with respect to the straight iso-density curves, especially in the low density ($r < 10$*veh/km*) regions and the high-density regions ($r > 30$*km/hr*). That is, the decrease in

the person-car equilibrium velocity due to an additional person-car per unit roadway length is smaller than the decrease caused by an additional truck per unit roadway length. This can be explained by the following observations:

- An additional truck will occupy more space than an additional person-car, since trucks are on average longer than person-cars. Moreover, the minimal safe distance of a truck is likely to be larger due to the impaired deceleration capabilities of trucks compared to those of person-cars.
- An additional truck impedes more vehicles than an additional *faster* person-car. If we assume that the overtaking probability of the impeded vehicle does not depend on the velocity of the vehicle that is caught up, more vehicles will need to decelerate. Moreover, once in a while a truck will change to the left-lane, thereby having an even more profound effect on the average velocity of the person-cars.

However, in reality the process of person-cars interacting with other person-cars is more subtle than the arguments above. For example, a person-car interacting with another, slightly slower, person-car may find the velocity drop too insignificant to undertake a lane-change. Interacting with a much slower truck however may provide the incentive to change lanes (the so-called *heavy vehicle factor* (see Ahmed *et. al* (1996)). In the first case, the average velocity would drop, while in the second case, it would not. Moreover, it can be argued that drivers do not like following a truck, for instance due to reduced sight. Consequently, the vehicle following the truck is more likely to change lanes than a vehicle following a person-car. These effects may reduce the asymmetry in the relation between the equilibrium velocity and the density-pair.

Figure 8-11b shows how the truck velocity relates to the person-car densities and the truck densities. We can observe that for a very large region, the truck velocities are nearly constant. That is, neither an increase in the number of person-cars, nor an increase in the number of trucks affects the average truck velocity. On the one hand, this can be explained by the fact that nearly all person-cars are faster than trucks. Consequently, the number of interaction events of trucks with person-cars is low. On the other hand, since we can observe that the velocity variance of trucks is very low, i.e. all trucks drive at nearly the same velocity, it follows that the number of interactions among trucks is also very small (see the expression for the equilibrium velocity). This explains why the average truck velocity does not decrease with increasing truck density.

When we consider density-pairs in this *unaffected truck-velocity* region, we find that truck velocities decrease *in approximately the same extent* as person-car velocities of the same density-pair. Moreover, average velocities of person-cars and trucks are approximately equal in this *region of synchronised flow*. Independently of the research reported in this thesis, Helbing and Huberman (1998a,b) observed a similar phenomenon. Both by simulation and analysis of motorway traffic data they observed a transition into a highly coherent state while the average-lane density increases. This state is characterised by *all* vehicles having an approximately equal velocity. Moreover, they observed that the number of lane-changes is minimal in this traffic state. The authors qualify this state as the motion of a solid block.

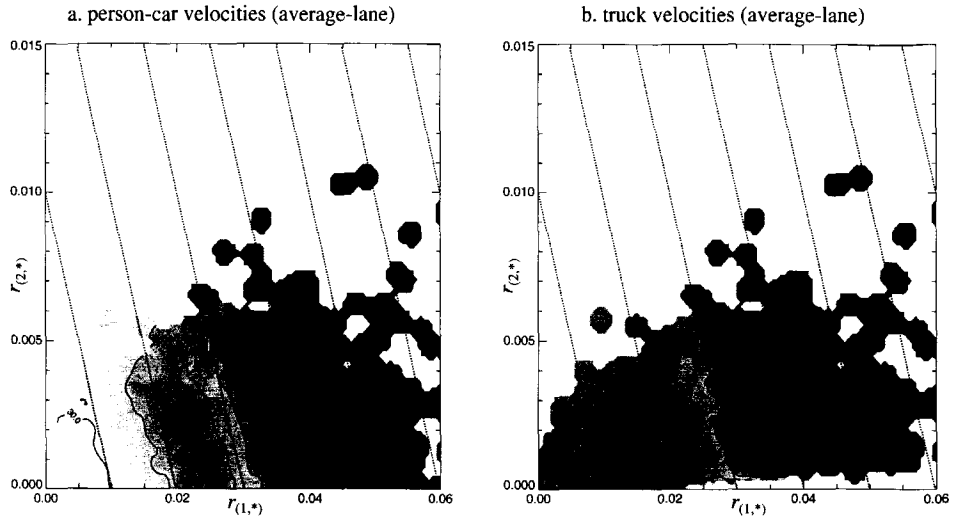

Figure 8-11: Relation between lane-aggregate velocity measurements of person-cars ($u = 1$;a) and trucks ($u = 2$;b), and their respective densities $r_{(1,*)}$ and $r_{(2,*)}$.The velocity-difference between two iso-velocity curves is 2.5*m/s*.

8.4.3 Lane-specific empirical equilibrium velocity relation

Figure 8-12a-d shows the relations between the average velocities of person-cars and trucks, and the person-car and truck densities on the right and the left-lane of the A9 motorway. Clearly, when considering the lanes separately, the asymmetric effect is more profound.

Figure 8-12a shows that the reduction in the average person-car velocity due to an additional truck is more profound. The reason for this is two-fold: first, increased truck numbers increase the interaction frequency and the subsequent number of person-cars needing to reduce velocity. Secondly, in the population of person-cars that *are able* to change lanes, faster vehicles are over-represented. In other words, since a fast person-car is more likely to interact with a slower truck, the number of fast person-cars that perform an immediate lane-change is larger than the number of slow person-cars. Since the number of fast person-cars on the right-lane decreases, the arithmetic mean velocity also decreases.

8.4.4 Average velocity

Let us first consider the average velocities for each of the subsamples. Figure 8-16 (page 204) shows the relation between the average velocity and the total effective density on each lane of the A9 motorways, for person-cars and trucks respectively, collected at locations 7, 8 and 9 during the morning period. Recall that the *total effective density* or *total modified density* is defined by the expected number of vehicles on all lanes per unit non-used roadway space, divided by the number of lanes.

Figure 8-16 shows that the average velocity of person-cars and trucks show some important differences, especially in the low-density region. Here, the average velocity of trucks is nearly unaffected by a small increase in the number of vehicles per unit unoccupied roadway

length, whereas the person-car velocity drops approximately linearly with an increasing number of vehicles. When a certain critical density is reached person-car velocities and truck velocities decrease together at an equal rate, albeit truck velocities are slightly lower.

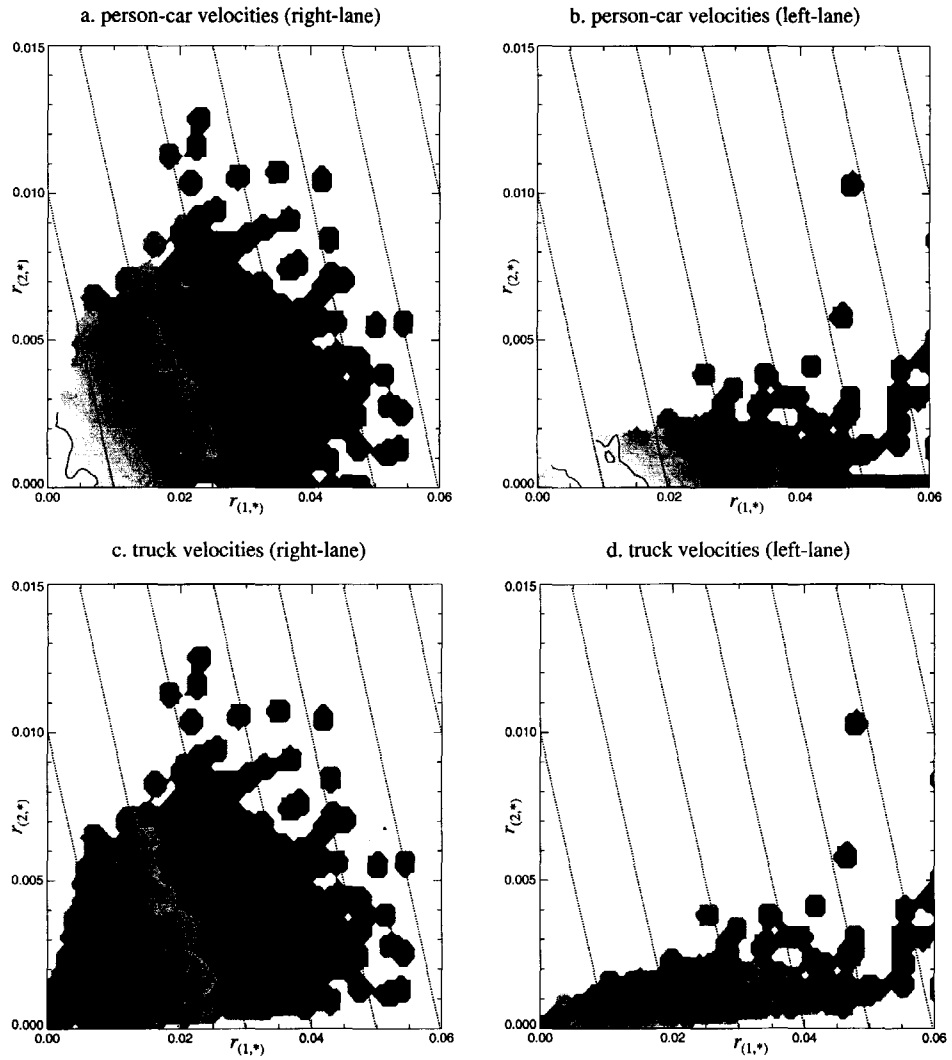

Figure 8-12: Average truck velocities on the right- and the left-lane of the A9 motorway as a function of the person-car densities and truck densities on the left lane. The dotted lines are the iso-total density lines.

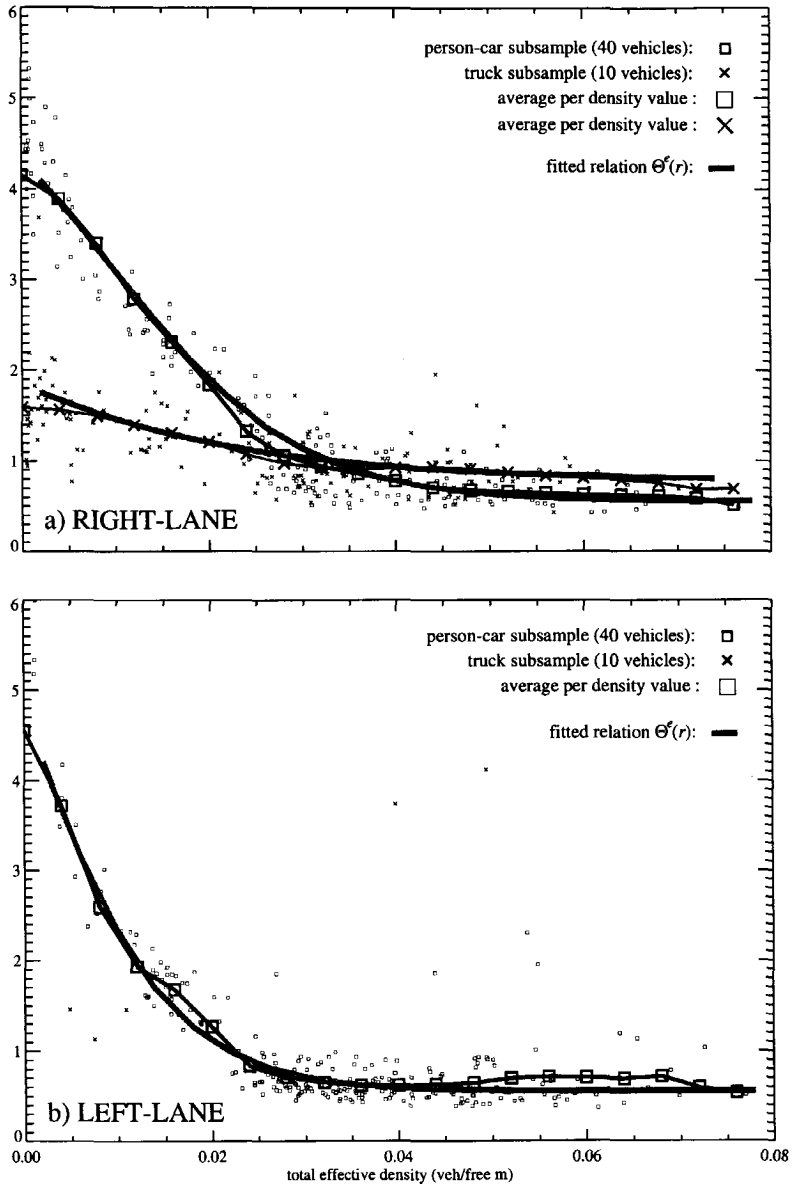

Figure 8-13: Empirical relation between the velocity standard deviation and the total effective density (locations 7-9).

8.4.5 Average velocity variance and velocity standard deviation

Let us now consider the empirical relation between the standard velocity deviation on the one hand, and the total effective density on the other hand. In addition to the aggregated observations, we have fitted the following relation (see Kerner *et al.* (1996)):

$$\Theta^{e}_{(u,j)}(\hat{r}) = \frac{\Theta^{0}_{(u,j)}}{1+\exp((\hat{r}-a_{(u,j)})/b_{(u,j)})} - c_{(u,j)} \tag{8.13}$$

where a, b, and c are parameters to be estimated. Figure 8-13 shows the relation between the total effective density and the velocity standard deviation at collected at locations 7-9, and the fitted relation (8.13).

8.4.6 Lane-distribution of vehicles

Let us now consider the class-specific distribution of vehicles across the lanes as a function of total effective density (see Figure 8-17, page 205). As can be expected when the total density is low, only a small fraction of person-cars use the left roadway lane. When the total effective density increases, the fraction of person-cars using the left lane increases. It appears that the fraction of trucks using the left lane remains approximately the same.

We have shown in chapter 6 that under equilibrium conditions, the distribution of vehicles of a user-class across the lanes of the motorway can be determined from the lane-changing probabilities and rates. Consequently, we can check whether the model is able to realistically describe the lane-changing processes by comparing the *theoretical* and the *empirically established* vehicle distributions.

8.4.7 Fraction of constrained vehicles

Figure 8-14 depicts the constrained vehicle fraction on the two lanes of the A9 motorway for both person-cars and trucks.

8.4.8 Free gap

Let us now reconsider the available space left on the lane. To this end, let us consider the *free gap*. This gap is defined by the gross gap minus the space effectively used by the vehicle.

The latter space equals the vehicle length and an additional safety margin. In chapter 6 we have discussed several models (e.g. Jepsen (1998), Leutzbach (1988), Forbes (1958)) that prescribe this safety margin. In this chapter, we will use the model of Jepsen (1998) and assume that the additional safe distance equals the sum of a *fixed constant value* d_u^{min}, a *linear term* depending on the velocity v and the reaction time T_u of the driver, and finally *a second order term* $v^2 S_u$ modelling the way in which a driver takes into account the severity of a collision. Motivated by the small value of the second order term $v^2 S_u$ ($\approx 0.022v^2$) the latter term is neglected in the ensuing. The reaction time T_u can be determined from data by considering the *net time headway* of vehicles of class u at very low velocity values. By doing so, we have observed that $T_{car} \approx 1.6s$ and $T_{truck} = 2.8s$ (see Figure 8-15).

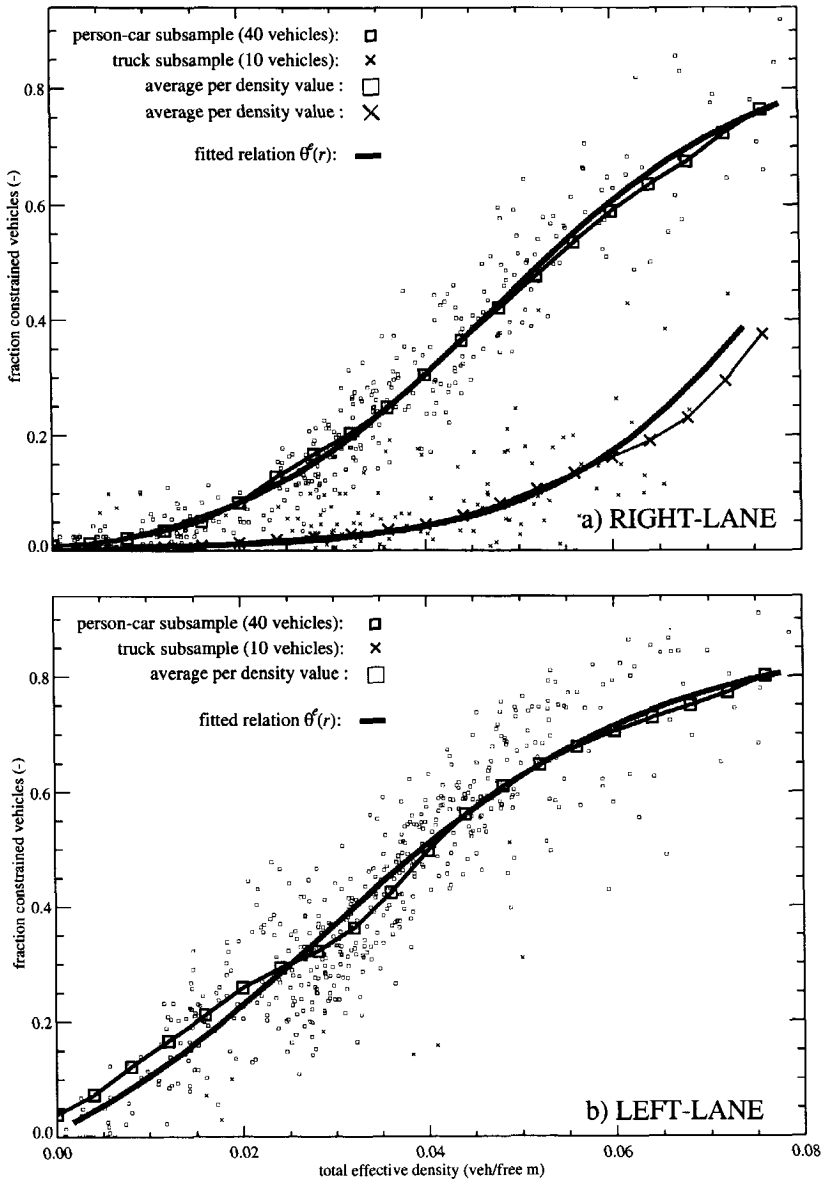

Figure 8-14: Fractions of constrained person-cars and trucks as a function of the effective density on both lanes of A9 motorway (locations 7-9, morning period).

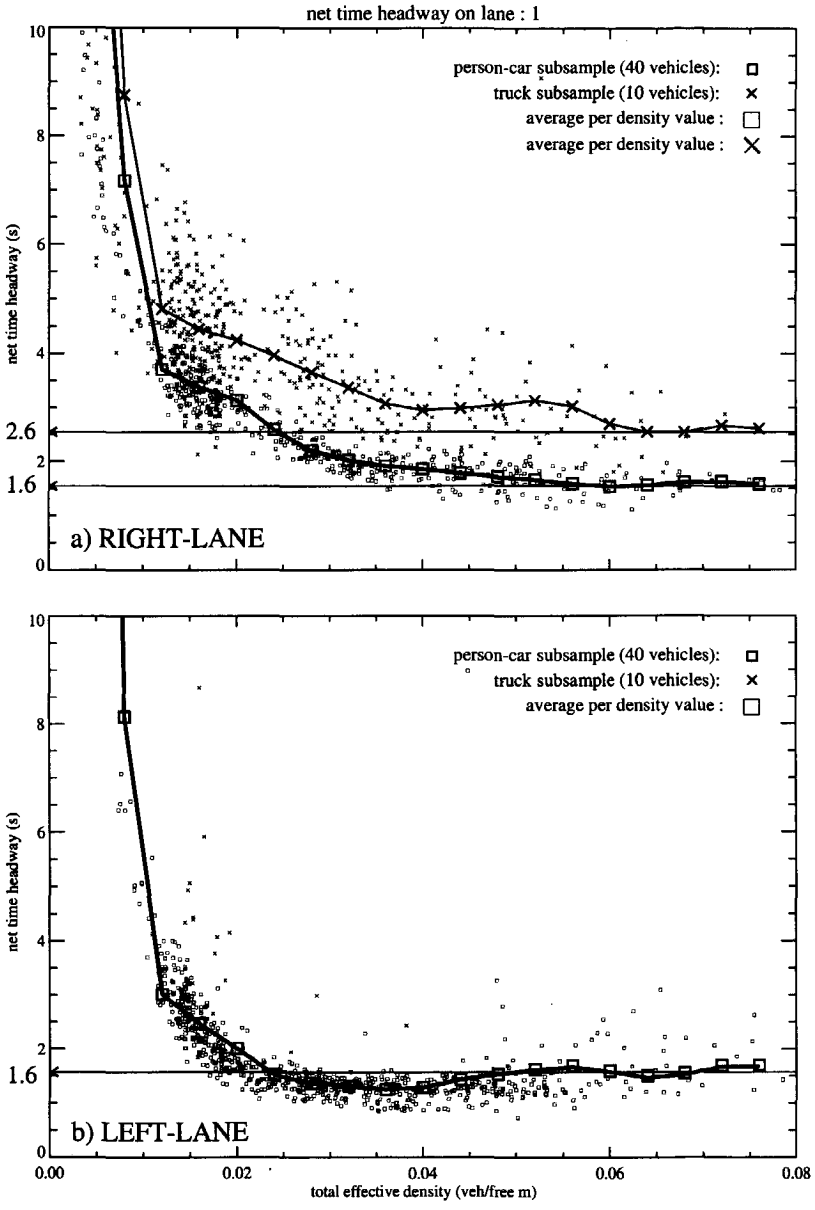

Figure 8-15: Net time headway (gross time headway minus time-headway requirements) of person-cars and trucks on both lanes of the A9 motorway (locations 7-9).

According to the *Generalised Queuing Model* (GQM) for *time-headway* distributions (cf. Cowan (1975), Branston (1976), Luttinen (1997), Hoogendoorn and Bovy (1997,1998)*), the total *time-headway* $\underline{H}$ is the sum of the *empty zone* $\underline{X}$ and the *free headway* $\underline{Q}$. The latter headway, reflecting the 'available time' on the destination lane, is described by an exponential distribution function characterised by the arrival frequency λ of free-flowing vehicles.

By using the effective gap $\underline{S}$ (m) rather than the free time headway $\underline{Q}$ (s) we can determine the probability density function of the space not used by unconstrained vehicles on lane j. This is achieved by considering the distribution functions of the free headway $\underline{Q}$ and the velocity of unconstrained vehicles:

$$\begin{aligned} \Pr(s \le \underline{S}_{(*,j)} < s + \mathrm{d}\, s) &= \Pr(s \le \underline{Q}_{(*,j,1)} \underline{V}_{(*,j,1)} < s + \mathrm{d}\, s) \\ &= \int_v \lambda \exp(-\lambda(s/v)) g_{(*,j,1)}(v)\, \mathrm{d}\, v \end{aligned} \tag{8.14}$$

If we neglect the velocity variance of unconstrained vehicles, i.e. $g_{(*,j,1)}(v) = \delta(v - V_{(*,j)})$ distribution, the unused roadway space of unconstrained vehicles on lane j is approximately exponentially distributed with parameter $\kappa = \lambda / V_{(*,j)}$. The parameter $1/\kappa$ equals the expected space that is not used by an unconstrained vehicle, i.e. $s_{(*,j)}$.

8.5 Distribution of velocities and desired velocities

In this section we will establish approximations for the class- and lane-specific distributions of the velocity and the desired velocity. To this end, we propose that both distributions for a user-class are Gaussian, which can consequently be described by its mean and its variance. Moreover, we will derive the desired velocity distribution for the individual roadway lanes by considering the gas-kinetic equations of the mixed-state traffic.

8.5.1 Aggregate-lane velocity distributions for low density values

Let us discuss some properties of the multidimensional equilibrium velocity $V_u^e(r_1, r_2)$. When traffic is dilute, that is, when drivers can move freely, the equilibrium velocity approximately equals the average desired velocity of the vehicles of the user-class. In other words, velocity observations for $r_1 \approx 0$, and $r_2 \approx 0$ constitute the desired velocity, and the spread in the desired velocity. In illustration, Figure 3-4 (page 62) shows the velocity probability density functions for person-cars and trucks for different values of the total density. From the figure we observe that the aggregate-lane velocity distribution for person-cars and trucks differs significantly. The average velocity of person-cars is much higher than the average velocity of trucks. Moreover, the velocity variance is much higher. Figure 3-6 (page 65) shows the velocity distributions of person-cars for different values of the total density. Clearly, the desired velocity distributions (r small) differ for the different lanes of the A9 motorway. This difference is caused by the fact that at low-density values, only the fastest person-cars – having a

* Branston (1976) assumes that the movement of traffic passing an observation point can be compared to the output of a M/G/1 *queuing system* having random input. The *server* produces empty zones $\underline{X}$ (the *server-time*) as long as the server is busy (i.e. there is a queue). The probabilities that the server is either busy or idle respectively equal θ and $(1-\theta)$. Then, the length of an interdeparture time equals the sum of the server time X and the interarrival time $\underline{Q}$. Assuming that the interarrival time is exponentially distributed results in the GQM.

relatively high desired velocity – interact with slower person-cars and trucks. Thus, the slow person-cars occupy the right lane of the motorway, while the fast person-cars use the left-lane of the motorway.

8.5.2 Aggregate-lane and lane-specific desired velocity distributions

In the previous section we proposed that the aggregate-lane desired velocity distribution can be approximated by observing the velocity distribution at very low values of the density. On the one hand, this is justified by the invariability of the velocity distribution with respect to different small densities (see Figure 3-3, page 51). On the other hand, small densities usually occur only during off-peak hours (e.g. at night). The population of drivers using at these off-peak periods is generally *not representative* for other periods. For instance, traffic composition with respect to purpose of travel will change during the day. Nevertheless, we will use the velocity distributions at low densities to approximate the desired velocity distribution. Note that we are mainly interested in desired velocities of unconstrained vehicles, since we have assumed that these determine acceleration processes in the traffic flow.

Based on the shape of this distribution, we have assumed that aggregate-lane desired velocity distribution is Gaussian. Since we have assumed that drivers do not adapt their desired velocity during their trip, the aggregate-lane desired velocity distribution is invariant. However, this does not hold for lane-specific desired velocity distributions. Considering European traffic legislation, when density – and thus the number of interactions – increases, more vehicles use the left roadway lane. Since fast vehicles (with a high desired velocity) are more likely to interact at low-density values, the left roadway lane will contain a larger number of vehicles with a high desired velocity than the right roadway lane. As a result, the expected desired velocity on the left lane will be considerably higher than on the right lane, at low densities. As density increases, the number of relatively slower vehicle interaction increases equally. As a result, the expected desired velocity on the left lane *decreases*. The expected desired velocity on the right lane will first decrease (more fast vehicle will change lanes), while at a certain density value it will increase again, due to slow vehicle changes lanes. Concluding, in opposition to the aggregate-lane desired velocity distribution, the lane-specific desired velocity distribution are not invariant, but changes with increasing density.

If $g^0_{(u,j,1)}(v^0 \mid x,t)$ denotes the desired velocity probability density function of free-flowing vehicles at (x,t) then the following holds:

$$r_{(u,*,1)}(x,t)\,g^0_{(u,*,1)}(v^0 \mid x,t) = \sum_{j'} r_{(u,j',1)}(x,t)\,g^0_{(u,j',1)}(v^0 \mid x,t) \tag{8.15}$$

If we consider a two-lane roadway, the aggregate-lane desired velocity distribution is the weighted mean of the lane-specific desired velocity distributions, i.e.:

$$r_{(u,*,1)}(x,t)\,g^0_{(u,*,1)}(v^0 \mid x,t) = r_{(u,1,1)}(x,t)\,g^0_{(u,1,1)}(v^0 \mid x,t) + r_{(u,2,1)}(x,t)\,g^0_{(u,2,1)}(v^0 \mid x,t) \tag{8.16}$$

yielding:

$$r_{(u,*,1)}V^0_{(u,*,1)} = r_{(u,1,1)}V^0_{(u,1,1)} + r_{(u,2,1)}V^0_{(u,2,1)} \tag{8.17}$$

and:

$$r_{(u,*,)}((V^0_{(u,*,1)})^2 + \Theta^0_{(u,*,1)}) = r_{(u,1,1)}((V^0_{(u,1,1)})^2 + \Theta^0_{(u,1,1)}) + r_{(u,2,1)}((V^0_{(u,2,1)})^2 + \Theta^0_{(u,2,1)}) \tag{8.18}$$

When the density is approximately zero, let us assume that the expected desired velocity of the lanes equals:

$$V^0_{(u,1,1)} = V^0_{(u,*,1)} \quad \text{and} \quad V^0_{(u,2,1)} = V^0_{\max} \tag{8.19}$$

where $V^0_{\max}$ is the maximum possible velocity. In other words, when the total density is approximately zero, only the fastest vehicles will use the left motorway lane. Moreover:

$$\Theta^0_{(u,1,)} = \Theta^0_{(u,*,1)} \quad \text{and} \quad \Theta^0_{(u,2,1)} = 0 \tag{8.20}$$

If the density increases, then the expected velocity on the left lane will decrease. This decrease is modelled using the function $b(r_1,r_2)$ of person-car density r_1 and truck density r_2:

$$V^0_{(u,2,1)}(r_1,r_2) = V^0_{\max} - b(r_1,r_2) \quad \text{with} \quad b(\mathbf{0}) = 0 \quad \text{with} \quad b(\mathbf{r}_{jam}) \le V^0_{\max} - V^0_{(u,*,1)} \tag{8.21}$$

Consequently using (8.17) we have:

$$V^0_{(u,1,1)} = r_{(u,*,1)} V^0_{(u,*,1)} / r_{(u,1,1)} - r_{(u,2,1)}(V^0_{\max} - b(r_1,r_2)) / r_{(u,1,1)} \tag{8.22}$$

In absence of any empirical results, we will assume that b can be approximated by a function of the total effective density, namely:

$$b(r_1,r_2) = b(\hat{r}) = (V^0_{\max} - V^0_{(u,*,1)})(1 - \exp(-\alpha\hat{r})) \tag{8.23}$$

where α is an unknown parameter.

8.6 Specification of model parameters and relations

This section discusses the specification of the model parameters. That is, we will specify the different model parameters and relations using simplified expressions. The average vehicle length for each user-class are easily derived from the available traffic data. By relating them to the density, constrained vehicle fractions, and so on, we approximate the desired velocity, the acceleration time, and the equilibrium velocity variance. The immediate lane-changing probabilities are determined by considering the expected number of vehicles that, while having interacted on their lane j, accept the gap on lane j', given that the *free-gaps* on the target lane j' are exponentially distributed. Similarly, we specify the lane-changing rates.

8.6.1 Acceleration velocity

The acceleration velocity $V^a_{(u,j)}(x,t)$ describes the *expected velocity* to which state-aggregate vehicles of class u on lane j accelerate. In section 6.4.3 we presented an approximation of both the acceleration time $T_{(u,j)}$ of mixed-state traffic as well as the acceleration velocity $V^a_{(u,j)}$ (via the acceleration momentum), based on the acceleration times and expected desired velocities of unconstrained vehicles. The lane-specific class-specific expected desired velocity of unconstrained vehicles changes when density increases, due to two reasons.

At first mainly fast vehicles – with a high desired velocity – will use the left motorway lane. If the density increases then so does the number of slower vehicles using the left lane. As a consequence, the expected desired velocity on the right lane increases, at the expense of the desired velocity on the left-lane. This was modelled in the previous section by introducing the function b (see eq. (8.21))

Moreover, when the number of constrained vehicles increases, the expected desired velocity of the unconstrained vehicles also decreases, since the number of unconstrained faster vehicles will in general decrease *faster* than the number of slow unconstrained vehicles. Eventually, when nearly all vehicles but the slowest are constrained, the desired velocity of the unconstrained vehicles will equal the minimum desired velocity of the vehicles in the class. This can be adequately modelled by describing the desired velocity as a monotonically decreasing function of the fraction of constrained vehicles, i.e.:

$$V^0_{(u,*,1)} = V^0_{(u,*,1)}(\theta_{(u,*)}(x,t)) \tag{8.24}$$

8.6.2 *Acceleration time*

When traffic is dilute, i.e. when neither of the vehicles is constrained, the acceleration times τ_u reflect the acceleration capabilities of the vehicles. The acceleration law for unconstrained traffic is (see section 4.4.2):

$$\dot{v} = (v^0 - v)/\tau^0_u \tag{8.25}$$

When a stopped vehicle accelerates, its acceleration equals $a_u = v^0/\tau_u{}^0$. May (1990) reports accelerations from standstill of respectively person-cars and trucks that are equal to $3.5m/s^2$ and $0.9m/s^2$, yielding:

$$\begin{aligned} a_{car} &\approx 3.5m/s^2 \quad \rightarrow \quad \tau^0_u \approx 33.3/3.5 = 9.5s \\ a_{truck} &\approx 0.9m/s^2 \quad \rightarrow \quad \tau^0_u \approx 22.2/0.9 = 24.7s \end{aligned} \tag{8.26}$$

We assume that the acceleration time is the same for all vehicles within a certain class. Thus, the distribution of vehicles over the roadway lanes does not influence the acceleration time, in opposition to the desired velocity of vehicles. Moreover, we have determined that only free-flowing *platoon leaders* can accelerate to their respective desired velocity considering the acceleration time $\tau_u{}^0$. Platooning vehicles accelerate along with the platoon leader, while considering the acceleration time of the latter. In section 6.4.3 we presented an approximation of acceleration times $T_{(u,j,2)}$ and $T_{(u,j)}$ of constrained and mixed-state traffic respectively.

8.6.3 *Immediate overtaking probabilities*

Let us assume that fast vehicles that interact on the right lane of the two-lane motorway always aim to change to the left motorway lane. Whether an immediate lane-change actually occurs depends on the available gap distribution on the left motorway lane.

Let us consider the safe distance model of Jepsen (1998). Neglecting the influence of the speed-risk factor, the space $l_u(v)$ needed on the target-lane by a vehicle of class u driving with velocity v equals:

$$l_u(v) = d_u^{min} + L_u + vT_u \tag{8.27}$$

The parameter $d_u{}^{min}$ reflects the minimum spacing between vehicles in a jam (approximately $1m$; Jepsen (1998)). The parameter T_u describes the additional speed-dependent safety margin that a driver needs to accept the gap on the target lane; L_u are the class-dependent vehicle lengths. From the collected data we have established that average vehicle lengths of person-cars and trucks are respectively equal to $3.7m$, and $11.2m$. The reaction time can be estab-

lished by considering the net-time headway for high densities. It was found that reaction times of trucks drivers are considerably higher than reaction times of person-cars drivers. Reasonable values of these reaction times for person-cars and trucks appeared to be 1.6*s* and 2.8*s* respectively (see Figure 8-15, page 196).

Let $\underline{S}_{(*,j')}$ denote a random variate delineating the available *free gap* of a unconstrained vehicle on the target-lane j'. Then, if we assume that this free-gap is exponentially distributed, we can determine that the probability that a vehicle driving with velocity v accepts an available gap on lane j' equals:

$$(1-\theta_{(*,j')})\Pr(\underline{S}_{(*,j')} > L_u + vT_u) = (1-\theta_{(*,j')})\exp(-(L_u + vT_u)/s_{(*,j')}) \tag{8.28}$$

where $s_{(*,j')}$ is the expected available gap of unconstrained vehicles on lane j'.

We have shown that the expected number of vehicles of class u driving with velocity v on lane j that interact with slower vehicles per unit time equals $\rho_{(u,j)}(x,v,t)\Psi_{(*,j)}(x,v,t)$ (section 4.6). Thus, the expected number of vehicles on the *right-lane* ($j = 1$) per unit time that immediately changes lanes to the left-lane equals:

$$\begin{aligned}(1-\theta_{(*,j')})r_{(u,j)}&\left\langle \exp(-(L_u + vT_u)/s_{(*,j')})\tilde{\Psi}_{(*,j)}(v)\right\rangle_{(u,j)} \\ &= (1-\theta_{(*,j')})r_{(u,j)}\left(\exp(-L_u/s_{(*,j')})\left\langle \exp(-vT_u/s_{(*,j')})\tilde{\Psi}_{(*,j)}(v)\right\rangle_{(u,j)}\right)\end{aligned} \tag{8.29}$$

Since the arrival intensity $\lambda = V\kappa$ of unconstrained vehicles on lane j' is in general smaller than the capacity of lane j', usually we have:

$$\lambda_{j'}T_u = V_{(*,j')}T_u/s_{(*,j')} < 1 \tag{8.30}$$

Therefore, using only the zeroth and first Taylor term yields a reasonable approximation:

$$\left\langle \exp(-vT_u/s_{(*,j')})\tilde{\Psi}_{(*,j)}(v)\right\rangle_{(u,j)} \approx \left\langle \tilde{\Psi}_{(*,j)}(v)\right\rangle_{(u,j)} - T_u/s_{(*,j')}\left\langle v\tilde{\Psi}_{(*,j)}(v)\right\rangle_{(u,j)} \tag{8.31}$$

Finally, we have observed that $1/s_{(*,j)} = \zeta_j/d_{(*,j)} \approx 1.2r_{(*,j)}$.

The immediate overtaking probability can be determined by considering the expected number of vehicles changing to the left lane (8.29), divided by the expected number of interacting vehicles, i.e.:

$$\pi_{(u,1)} \approx (1-\theta_{(*,2)})\exp(-L_u\zeta_2 r_2)\left(1 - T_u\zeta_2 r_2\left\langle v\tilde{\Psi}_{(*,1)}(v)\right\rangle_{(u,1)}/\left\langle \tilde{\Psi}_{(*,1)}(v)\right\rangle_{(u,1)}\right) \tag{8.32}$$

Note that $\langle v\Psi_{(*,1)}\rangle_{(u,1)}/\langle\Psi_{(*,1)}\rangle_{(u,1)}$ equals the expected velocity of the interacting vehicles of class u on lane 1. With respect to immediate overtaking to the right-roadway lane, similar relations hold. However, since we are considering European legislation, overtaking using the right roadway lane is prohibited when traffic is not congested. Thus, we assume that $\pi_{(u,j)} = 0$, for $V > 80km/hr$.

8.6.4 Equilibrium velocity variance

In the remainder of this thesis, we assume that a suitable explicit relation can approximate the MLMC equilibrium velocity variance. To this end, we employ equation (8.13).

8.6.5 *Lane-changing rates*

Let us finally specify the lane-changing rates. Basically, this is done using a similar approach as applied to specify the immediate lane-changing probabilities. That is, we assume that for a vehicle of class u driving with velocity v, the probability that the gap on the target-lane suffices equals (8.28). The number of vehicles attempting a spontaneous or postponed lane-change is described by the *expected number of unconstrained and constrained vehicles*, and the *average decision time* for a spontaneous or postponed lane-change, respectively denoted by T_u^{spon} and T_u^{post}. Then, the number of vehicles able to perform a spontaneous or postponed lane-change equal respectively:

$$(1-\theta_{(*,j')})\exp(-L_u / s_{(*,j')})(1-\theta_{(u,j)})r_{(u,j)}(1-V_{(u,j)}T_u / s_{(*,j')})/T_u^{spon} \tag{8.33}$$

and:

$$(1-\theta_{(*,j')})\exp(-L_u / s_{(*,j')})\theta_{(u,j)}r_{(u,j)}(1-V_{(u,j)}T_u / s_{(*,j')})/T_u^{post} \tag{8.34}$$

8.7 Model validation using equilibrium equations

In this section we will show how the equilibrium traffic conditions can be determined using a simple iterative procedure. In doing so, we can compare the equilibrium conditions to empirical estimates of the equilibrium conditions. More precisely, using the model relations specified in the preceding sections, the equilibrium velocity and the density distributions are compared to the empirical relations established from the A9 traffic data. Although the parameters are not optimised to fit the data, we can conclude that the equilibrium relations fit the observations well.

8.7.1 *Equilibrium conditions*

In section 6.4.5 we have shown that a two-lane motorway operating under equilibrium conditions satisfies:

$$V_{(u,j)} = V^e_{(u,j)}(\mathbf{r},\mathbf{V},\Theta) \qquad \Theta_{(u,j)} = \Theta^e_{(u,j)}(\mathbf{r},\mathbf{V},\Theta) \tag{8.35}$$

while the fraction of vehicles on the right-lane $j = 1$ equals:

$$\alpha_{(u,1)} = \frac{p^{(u,1)}_{(u,2)}\mathcal{I}^0_{(u,2)} + \Delta^{(u,1)}_{(u,2)}}{p^{(u,2)}_{(u,1)}\mathcal{I}^0_{(u,1)} + p^{(u,1)}_{(u,2)}\mathcal{I}^0_{(u,2)} + \Delta^{(u,2)}_{(u,1)} + \Delta^{(u,1)}_{(u,2)}} \tag{8.36}$$

That is, the fraction of vehicles of class u using the right lane $j = 1$ is determined by the ratio between the lane-changing rates from the left lane to the right lane, and the total number of lane-changing rates. That is, as the number of lane-changes per vehicle per unit time from lane 2 to lane 1 increases, the fraction of vehicles on lane 1 increases accordingly and vice versa. Note that similar expressions can be derived for motorways with more than two roadway lanes. Also, we can determine expressions for the lane-distribution of momentum and energy given equilibrium conditions (see section 6.4.5).

8.7.2 *Approach to determine equilibrium conditions*

In this section, the approach used to determine the equilibrium velocity and the equilibrium traffic density distribution for any configuration $\mathbf{r} = \{r_u\}$ is presented. The procedure consists of the following steps:

1. Let l indicate the l-th iteration step.
2. For any vector $\mathbf{r} = \{r_u\}$ choose an initial estimate for the lane-distribution of vehicles for each class u, yielding $\mathbf{r}^{(l)} = \{r^{(l)}_{(u,j)}\}$. This is performed by applying an empirical relation between the total density and the fraction of vehicles of class u using lane j (section 8.4.3). Using this initial estimate, the effective densities are determined for each lane j. An initial estimate $V_{(u,j)}^{(0)}$ for the *equilibrium velocity* is determined by using an empirically established relation between the effective density per lane, and the equilibrium velocity (see section 8.4.1).
3. Using the effective density, the velocity variance is determined by using relation (22). This yields the estimate $\Theta_{(u,j)}^{(l)}$ for each class u on lane j. Another empirical relation is used to determine the fraction of constrained vehicles $\theta_{(u,j)}^{(l)}$ for each class u and lane j (see section 8.4.5).
4. Using these estimates $\{\mathbf{r}^{(l)}, \mathbf{V}^{(l)}, \Theta^{(l)}, \theta^{(l)}\}$, we can determine the acceleration velocity $V_{(u,j)}^{a,(l)}$ and acceleration time $\mathrm{T}_{(u,j)}^{(l)}$, using expressions (6.34) and (6.32) respectively.
5. Subsequently, $\mathcal{I}_{(u,j)}^{0}$, $\mathcal{I}_{(u,j)}^{1}$, and $\mathcal{X}_{(u,j)}^{1}$ can be determined for step l, by assuming that the velocities are Gaussian distributed random variates.
6. The probabilities that an immediate lane-change, a spontaneous lane-change, or a postponed lane-change is performed is determined by using the approximate expressions (8.32), (8.33), and (8.34) respectively.
7. Using these approximations, we can determine the equilibrium velocity using:

$$V^{e}_{(u,j)} = V^{a,(l)}_{(u,j)} - (1 - p^{(l)}_{(u,j)}) r^{(l)}_{(u,j)} \mathrm{T}^{(l)}_{(u,j)} \mathcal{R}^{1}_{(u,j)}(\mathbf{r}^{(l)}, \mathbf{V}^{(l)}, \Theta^{(l)}) \tag{8.37}$$

8. We also determine the balance of the number of vehicles of class u changing from lane j to j' and vice-versa yielding:

$$\delta r^{(l)}_{(u,j)} = r^{(l)}_{(u,j)} (p^{(l)}_{(u,j)} \mathcal{I}^{1}_{(u,j)}(\mathbf{r}^{(l)}, \mathbf{V}^{(l)}, \Theta^{(l)}) + \Delta^{(l)}_{(u,j)}) \tag{8.38}$$

9. Next, we update both the estimate of the equilibrium velocity and the number of vehicles per lane by using the weighing parameters a and b:

$$V^{(l+1)}_{(u,j)} = aV^{(l)}_{(u,j)} + (1-a)V^{e}_{(u,j)} \quad \text{and} \quad r^{(l+1)}_{(u,j)} = br^{(l)}_{(u,j)} + (1-b)\delta r^{(l)}_{(u,j)} \tag{8.39}$$

10. Set $l = l+1$ and proceed to step 2 until the error is sufficiently small*.

Choosing appropriate values for the parameters a and b poses a trade-off between convergence-speed of the algorithm (larger values) and the convergence (smaller values). We have found that choosing $a = 0.1$ and $b = 0.05$ yield good results.

* Comparing the differences of the successive iterations approximates the error.

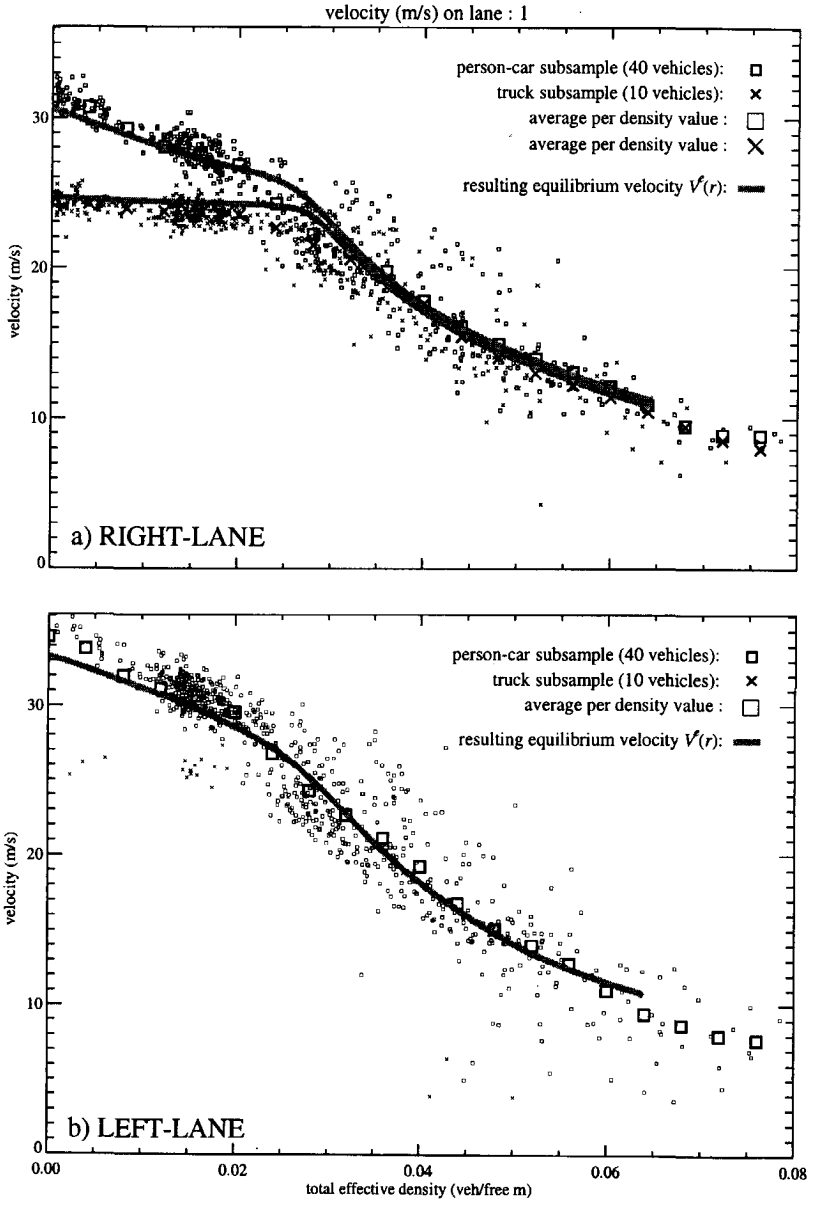

Figure 8-16: Estimated equilibrium velocity relations for person-cars and trucks for a two-lane motorway and data collected on the (A9 – loc. 7-9).

8.7.3 Equilibrium velocity

Note that the equilibrium velocity is not a function of the spontaneous and postponed lane-changing rates. As a consequence, we can see if the choice of the model relations and pa-

rameters yields good results independently of the relations for the spontaneous and postponed lane-changing rates. The algorithm presented in the previous section was applied to determine the equilibrium velocity for the two-lane A9 motorway. Figure 8-16 shows the results of applications of the algorithm with 20% trucks, using the parameters and relations presented in the preceding sections of this chapter, compared to the person-car and truck velocity observations collected at the A9 test-site. Clearly, the comparison reveals the adequacy of the chosen model relations to describe the equilibrium velocities.

8.7.4 Distribution of vehicles

Application of the algorithm also gives the distribution of person-cars and trucks across the lanes of the motorway. Figure 8-17 shows the results of this exercise compared to the observations collected on the A9 motorway. We conclude that the estimated distribution of vehicles is sufficiently accurate.

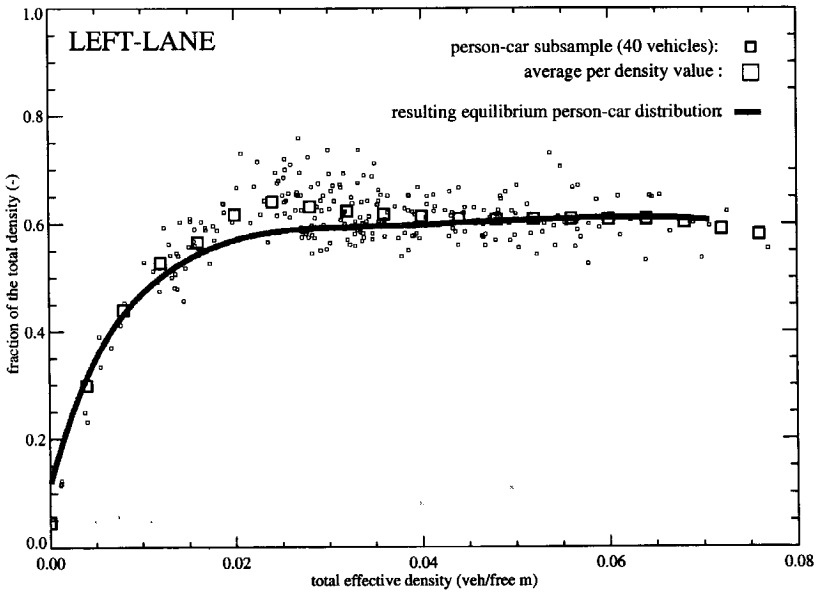

Figure 8-17: Estimated distribution of person-cars and trucks due to immediate, spontaneous and postponed lane-changing, compared to collected data (A9 – loc. 8).

We have observed that the number of trucks using the left lane is too high. Closer examination of the lateral truck flows reveals that this is caused by trucks able to perform an immediate lane-change after having interacted with a slower vehicle. Since we have assumed that *each vehicle* that experiences an interaction attempts to change lanes, irrespective whether its situation improves, attempts to change to either adjacent motorway lane. However, it is likely that, although the interaction will reduce the truck velocity slightly, the truck's situation on the target lane will not improve significantly. In real-life, trucks will then probably accept a certain deceleration, before attempting an immediate lane-change, explaining differences between the model's equilibrium distribution and real-life measurements.

8.8 Summary and conclusions

In this chapter we have discussed the empirical analysis of multilane heterogeneous traffic data. To this end, different MLMC traffic flow variables derived from measurements on the two-lane A9 motorway in the Netherlands have been considered, such as the class- and lane-specific density, velocity, and velocity variance. To enable the correct approximation of the velocity variance a new filtering technique has been developed. The latter technique eliminates the effects of the length of the sample interval on the magnitude of the velocity variance. As a consequence, it is found that the empirically determined velocity variance is a monotonically decreasing function of person-car and truck densities.

Rather than aggregating observations collected during fixed time intervals, we have determined the aggregate flow variables *for fixed sample sizes* for both person-cars and trucks on the respective motorway lanes. By doing so, statistical accuracy can be attained for the determined estimates. Moreover, the approach ensures that reasonably sized samples are also collected for classes and lanes with only a small traffic demand.

Relationships between the effective density and the dependent traffic flow variables velocity variance $\Theta_{(u,j)}$ and constrained vehicle fraction $\theta_{(u,j)}$ were obtained from the data. Also approximations for the average vehicle length L_u per class, and the reaction time T_u were obtained. Using these traffic parameters and relations, the acceleration time $T_{(u,j)}$ and the acceleration velocity $W_{(u,j)}$ were determined. The immediate lane-changing probabilities $p_{(u,j)}$ and the combined spontaneous and postponed lane-changing rates $\Delta_{(u,j)}$ were specified by consideration of the probability that a free-gap on the target-lane is accepted.

Using these specifications, a dedicated algorithm was applied to determine both the MLMC equilibrium velocity and lane-distribution of the vehicles. Although we have not optimised the parameters and relationships, it was concluded that the resulting relations fitted the A9 observations sufficiently well.

Since the equilibrium velocity and the distribution of the vehicles across the roadway lanes is determined by the interdependency of several processes, such as acceleration, interaction, immediate lane-changing, postponed and spontaneous lane-changing, they are dependent on the traffic legislation (e.g. driving on the left – overtaking on the right, speed-limits, truck overtaking prohibition, etc.). In other words, it is foreseen that the model needs to be recalibrated for different traffic rules. We envisage that the number of lanes and the location will play a significant role as well. However, the relationships presented in this sections are to a large extent independent of the number of lanes and the locations. Hence, we believe that the estimated parameters and relations can be generalised to describe multilane facilities at a high accuracy level. Nevertheless, this hypothesis needs to be validated using data.

In the ensuing of this thesis, the flow variables and relations determined in this chapter are used for model simulations for two-lane motorways. Moreover, since the relations employed are not a result from optimally fitting the relations to the available two-lane motorway data, but rather the result of theoretical analysis of the heterogeneous multilane flow processes, it is envisaged that the estimated model parameters can be readily applied to simulate more general multilane motorway facilities.

9 NUMERICAL SOLUTION APPROACHES

Several numerical approximation schemes have been developed in the past proposed to determine solutions to a variety of macroscopic models (see Lyrintzis *et al.* (1994), Lui *et al.* (1998), Lebaque (1996), Kerner *et al.* (1996), Papageorgiou (1989), Helbing (1996), Daganzo (1994)). Table 9-1 shows relationships between numerical schemes and model types. Because the recently developed higher-order traffic flow model of Helbing (1996,1997a), as well as the multiclass multilane generalisation discussed in this dissertation have significantly increased the complexity of the macroscopic flow models, there is a need for more efficient numerical approaches to approximate solutions.

The numerical treatment of the hyperbolic (dominantly convective) multidimensional and highly non-linear traffic flow model presented in this thesis is quite cumbersome, which requires dedicated techniques incorporating the physical properties of the underlying traffic flow process. In this chapter we present two types of approaches to numerically solve the higher-order flow models. The first type is based on the MLMC flow model cast using the *conservative variables* (chapter 6), while the second type is based on the *Riemann* or *characteristic* formulation of the MLMC flow equations (chapter 7).

The physical basis for the *inviscid* MLMC flow equations is the expression for conservation laws for density, momentum and energy. Hirsch (1990a) showed that this conservation form is essential to correctly compute the propagation speed and intensity of discontinuities or shocks that can occur in inviscid flows. Consequently, we will mainly focus on so-called *upwind schemes*, since these consider the physical propagation of perturbations along the characteristics, which are typical for dominantly hyperbolic equations, such as the MLMC flow model presented in this thesis. In this respect, we emphasise that so-called central difference schemes frequently used for discretisation of traffic flow equations (cf. Payne (1971,1979), Kerner *et. al.* (1995,1996)) *are not suitable* because they yield results that do not satisfy the physical properties of underlying traffic flow processes on the one hand, and potentially

cause stability-problems on the other hand. Rather, upwind schemes (cf. Daganzo (1994), Lyrintzis *et al.* (1994)) and Godunov-type schemes (cf. Lebaque (1996)) are more suitable. However, these schemes have only been applied to the LWR-model and the (primitive) viscous Payne-type models (see Table 9-1). The schemes presented in this chapter present a theoretically founded generic approach to correctly discretise higher-order flow equations.

Table 9-1: Numerical solution approaches applied in macroscopic traffic flow modelling.

MODEL-TYPE	NUMERICAL SCHEME	APPLICATIONS
LWR-model	upwind methods	Leo and Pretty (1992)
[vehicle]	space-centred schemes	
	implicit Euler	Chronopoulos *et al.* (1992)
	Godunov-scheme (Hirsch (1990b))	Lebaque (1996), Daganzo (1994)*, Leo and Pretty (1992)
Payne-type model	space-centred schemes	
[vehicle, speed]	explicit Euler (Hirsch (1990b))	Payne (1971,1979), Lyrintzis *et al.* (1994)
	Lax-scheme (1954)	Lyrintzis *et al.* (1994)
	implicit Euler (Hirsch (1990b))	Kerner *et al.*(1995,1996)
	upwind schemes	
	flux-vector splitting	Leo and Pretty (1992), Lyrintzis *et al.* (1994), Liu *et al* (1998)
	ad-hoc discretisation	Papageorgiou *et al* (1989,1991), Van Maarseveen (1982), Smulders (1989) (*semi-discrete*)
Helbing-type model	space-centred schemes	
[vehicle, speed,	Lax-Friedrichs scheme	Hoogendoorn and Bovy (1998c)
variance]	MacCormack (1972,1975) predictor/ corrector scheme	Helbing (1997a)
	upwind schemes	
	flux-vector splitting	Hoogendoorn and Bovy (1998d)
	Godunov-scheme (Hirsch (1990b)	Hoogendoorn and Bovy (1998c)

The choice of the numerical solution approach is essential to correctly compute solutions to the macroscopic traffic flow equations (see Lebaque and Lesort (1999)). In this context we should remark that although it is well understood that a finite-difference method can affect the computational accuracy of the macroscopic flow model, the importance of the proper choice of finite-difference methods has not been properly addressed in the past. Consequently, some improper finite difference methods have been applied. For example, Lyrintzis *et al.* (1994) argue that, although the Payne-model is superior to the simple kinematic model, Payne (1979) fails to show that this is due to the poor choice of numerical solution approach, namely, explicit Euler-like space-centred finite differen Lyrintzis *et al.* (1994) propose some corrective finite difference schemes for inviscid and viscous Payne-type models. Let us finally remark that a different class of numerical solution approaches is the so-called particle discretisation approach. This simulation-based approach has been discussed in sections 2.2.5 and 2.6. We refer to Van Aerde (1984) and Hoogendoorn and Bovy (2000) for details.

* Lebaque (1996) shows that the Cell-Transmission model of Daganzo (1994a,b) is a special case of the general Godunov-scheme applied to the LWR-model.

9.1 Governing equations

Starting point of our discussion are the MLMC-equations describing the dynamics of the *conservative variables* $\mathbf{w}_{(u,j)} = (r_{(u,j)}, m_{(u,j)}, e_{(u,j)})$ (see section 6.7)). Using the conservative vector notation presented in section 7.2.1, we have summarised the system of partial differential equations by the following equation:

$$\partial_t \mathbf{w}_{(u,j)} + \partial_x (\mathbf{f}^C_{(u,j)}(\mathbf{w}_{(u,j)}) - \mathbf{f}^D_{(u,j)}(\mathbf{W})) = \mathbf{x}_{(u,j)}(\mathbf{W}) \tag{9.1}$$

This formulation is called the *conservative form*, where $\mathbf{f}^C$ denotes the *conservative flux-vector*. We have also shown that we can recast this equation into the so-called *quasi-linear form* (section 7.2.2):

$$\partial_t \mathbf{w}_{(u,j)} + \mathbf{A}_{(u,j)}(\mathbf{w}_{(u,j)}) \partial_x \mathbf{w}_{(u,j)} = \mathbf{x}_{(u,j)}(\mathbf{W}) + \partial_x \mathbf{f}^D_{(u,j)}(\mathbf{W}) \tag{9.2}$$

In the remainder of this chapter, we emphasise the discretisation of the inviscid flux. That is, we will assume that $\partial_x \mathbf{f}^D \approx \mathbf{0}$.

9.2 Finite volume formulation

In order to numerically approximate solutions for the MLMC traffic flow model, we will divide *each lane j* of the modelled motorway into *finite cells i*. For each of these cells, the *total* density, momentum and energy is approximated for each class *u*. Note that this *finite volume approach* is different from *finite difference approaches* in that we approximate the *total* conservative variables in the cell, rather than the values of conservatives at specific points.

Cell *i* is defined by the location interval $[x_{i-1/2}, x_{i+1/2}]$. We will assume that the mesh is *equidistant*, with cell length Δx and $x_i = i\Delta x$. Moreover, we let t_k denote the time instant $k\Delta t$.

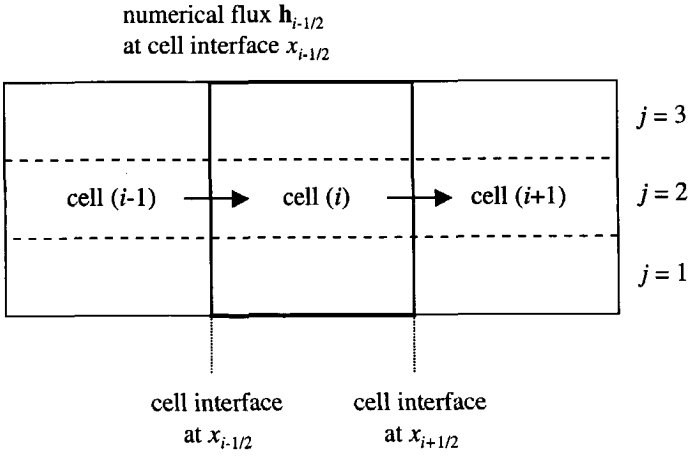

Figure 9-1: Definition of cells and cell-interfaces.

Let us define the *space-averaged* conservative vector over cell *i* at time instant t_k by:

$$\tilde{\mathbf{w}}_{(u,j)}^{i,k} \overset{def}{=} \frac{1}{\Delta x}\int_{x_{i-1/2}}^{x_{i+1/2}} \mathbf{w}_{(u,j)}(x',t_k)\mathrm{d}x' \tag{9.3}$$

These values represent the mean conservative variables density, momentum, and energy per unit roadway length for class u on lane j. The *time-averaged* conservative flux over the k-th time interval $[t_k,t_{k+1})$ at location x_i is defined by:

$$\bar{\mathbf{f}}_{(u,j)}^{i,k} \overset{def}{=} \frac{1}{\Delta t}\int_{t_k}^{t_{k+1}} \mathbf{f}_{(u,j)}^{C}(x_i,t')\mathrm{d}t' \tag{9.4}$$

Finally, the *time-space-averaged* source-term over the i-th location interval and the k-th time interval is defined by:

$$\hat{\mathbf{x}}_{(u,j)}^{i,k} \overset{def}{=} \frac{1}{\Delta x\Delta t}\int_{x_{i-1/2}}^{x_{i+1/2}}\int_{t_k}^{t_{k+1}} \mathbf{x}_{(u,j)}(x',t')\mathrm{d}t'\mathrm{d}x' \tag{9.5}$$

Using these definitions, the following set of equations is an *exact* discrete formulation of the conservative MLMC equations:

$$\boxed{(\tilde{\mathbf{w}}_{(u,j)}^{i,k+1} - \tilde{\mathbf{w}}_{(u,j)}^{i,k})\Delta x = (\bar{\mathbf{f}}_{(u,j)}^{i+1/2,k} - \bar{\mathbf{f}}_{(u,j)}^{i-1/2,k})\Delta t + \hat{\mathbf{x}}_{(u,j)}^{i,k}\Delta x\Delta t} \tag{9.6}$$

The remaining problem is to find appropriate expressions for both the time-averaged flux and time-space averaged source-term such that the space-averaged conservative variables can be determined using (9.6). This requires two types of approximation, that is approximation associated with *space averaging* and with *time evolution*. Since the spatial approximation was found to be the most challenging, the main part of this chapter will concern determining approximations $\mathbf{h}_{(u,j)}{}^{i}(t)$ for the time-averaged conservative flux vector, based on the available average conservative variables of each cell. That is, by describing the conservative flux at $x_{i+1/2}$ by a suitable function $\mathbf{h}_{(u,j)}$ of the average conservative variables for the distinguished cells, we aim to approximate $\bar{\mathbf{f}}_{(u,j)}^{i+1/2}(t)$. By doing so, a semi-discretised system results.

9.3 Flux-splitting schemes using conservative variables

By using the physical properties of the MLMC traffic flow, appropriate numerical schemes can be developed. In this section we discuss the so-called *flux-vector splitting schemes* (see Figure 7-1). These schemes are determined by considering the direction in which information is transported in the heterogeneous traffic flow.

For numerical analysis of flows in continuous media, a large number of schemes exists (see Hirsch (1999a,b)). We have found that *Steger-Warming splitting*, *Van Leer splitting*, and *Roe's Approximate Rieman solver* are very suitable schemes for numerically solving the conservative MLMC equations in traffic flow modelling. Before we present these schemes, we will briefly discuss the *Lax-Friedrichs* scheme, which is used for the purpose of comparison.

9.3.1 Lax-Friedrichs scheme

Lax-Friedrichs schemes (see Hirsch (1990b)) are generally not applied anymore, due to their poor first order accuracy. They do, however, form a good base for comparisons with other schemes. Basically, the Lax-Friedrichs scheme is defined by the numerical flux definition:

$$\mathbf{h}_{(u,j)}^{i+1/2} = (\mathbf{f}_{(u,j)}^{C}(\mathbf{w}_{(u,j)}^{i}) + \mathbf{f}_{(u,j)}^{C}(\mathbf{w}_{(u,j)}^{i+1}))/2 - (\mathbf{w}_{(u,j)}^{i+1} - \mathbf{w}_{(u,j)}^{i})/(2\Delta t/\Delta x) \tag{9.7}$$

where we have omitted the dependence on t. The scheme is based on *central space discretisation*. As with all central space discretisation schemes, it does not take the differences between upstream and downstream influences into account. As a consequence, the physical propagation of perturbations along the characteristics, which is typical of the hyperbolic traffic flow equations, are not considered by this numerical approximation scheme.

Higher-order central difference schemes such as the *Lax-Wendroff* scheme, are able to approximate solutions of the traffic flow equations very accurately in the smooth regions of the flow. However, near discontinuities, higher-order schemes generate oscillations. These non-physical fluctuations occur whenever the effect of the continuum processes of a convective nature outweighs the dissipation effects caused by drivers' higher-order anticipatory behaviour (viscosity) and finite reaction and braking times. As a consequence, the higher-order terms present in the flow equations are necessary when using these higher-order central space discretisation schemes.

9.3.2 Conservative flux splitting

In opposition to the central space discretisation schemes, the *upwind-type schemes* presented in this section are directed towards introducing physical properties of traffic flow, discussed in chapter 7, into the discretised formulation. In our case, only the signs of eigenvalues of the flux-Jacobian $\mathbf{A}_{(u,j)}$ (see equation (7.12)) are used. These indicate directions along which the traffic density, momentum and energy are transported.

Flux splitting schemes are based on decomposition of the flux vector $\mathbf{f}_{(u,j)}$. Basically, two types of flux vector splitting approaches are known: conservative and non-conservative splitting. *Conservative splitting* is based on decomposition of the conservative flux $\mathbf{f}$ into flux-contributions $\mathbf{f}^+$ and $\mathbf{f}^-$, such that we have $\mathbf{f} = \mathbf{f}^+ + \mathbf{f}^-$. *Non-conservative splitting* amounts to splitting the Jacobian $\mathbf{A}$ into two contributions, $\mathbf{A}^+$ and $\mathbf{A}^-$.

Let us now discuss how to exploit the flux splitting in a finite volume approach. To this end, the numerical flux function associated with a flux vector splitting is expressed as:

$$\mathbf{h}_{(u,j)}^{i+1/2} = \mathbf{h}_{(u,j)}^{i+1/2}(\mathbf{w}_{(u,j)}^{i}, \mathbf{w}_{(u,j)}^{i+1}) \overset{def}{=} \mathbf{f}^{+}(\mathbf{w}_{(u,j)}^{i}) + \mathbf{f}^{-}(\mathbf{w}_{(u,j)}^{i+1}) \tag{9.8}$$

Clearly, 'blind splitting' ($\mathbf{f}^{\pm} = \mathbf{f}/2$) would inaccurately estimate the time integral of the flux through the finite volume boundary points. Conversely, constructing a splitting where $\mathbf{f}^+$ and $\mathbf{f}^-$ *coincide* with contributions that depend, respectively, upon $\mathbf{w}_{(u,j)}^{i}$ and $\mathbf{w}_{(u,j)}^{i+1}$ in an *adaptive* way yields a better evaluation of the time integral of the flux. This would require that the eigenvalues of the Jacobians of the split-fluxes $\mathbf{f}^+$ (respectively $\mathbf{f}^-$) are real and positive (respectively negative). However, determination of a flux splitting that automatically fulfils the above requirement is not trivial.

9.3.3 General adaptive flux splitting

Let us consider a class of flux decomposition schemes, which are obtained by defining the numerical flux:

$$\mathbf{f}^{\pm}(\mathbf{w}) = \mathbf{A}^{\pm}\mathbf{w} \tag{9.9}$$

where:

$$\mathbf{A}^{\pm} = (\mathbf{A} \pm g(\mathbf{A}))/2 \tag{9.10}$$

where g(**A**) is any matrix having right eigenvectors $\mathbf{R}_A$ and left eigenvectors $\mathbf{L}_A$ coinciding with those of **A**. That is:

$$g(\mathbf{A}) = \mathbf{L}_A \Lambda_g \mathbf{R}_A \tag{9.11}$$

where $\Lambda_g = \text{diag}(g_1,g_2,g_3)$. Then, the eigenvalues of $\mathbf{A}^{\pm}$ are equal to $\lambda_i^{\pm} = (\lambda_i \pm g_i)/2$, that is:

$$\lambda_1^{\pm} = (V \pm g_1)/2 \qquad \lambda_{21}^{\pm} = ((V+c) \pm g_1)/2 \qquad \lambda_3^{\pm} = ((V-c) \pm g_1)/2 \tag{9.12}$$

To ensure the correct adaptive behaviour, that is $\lambda_i^{+} \geq 0$ and $\lambda_i^{-} \geq 0$, the following condition must be satisfied:

$$g_1 \geq |V| \qquad g_2 \geq |V+c| \qquad g_3 \geq |V-c| \tag{9.13}$$

9.3.4 Steger-Warming splitting

Let us first consider the approximation scheme that was first applied by Steger and Warming (1981) to numerically approximate solutions of the so-called Euler equations (see Hirsch (1990b)). Applying the scheme to the inviscid MLMC flow equations yields choosing:

$$g_1 = |V_{(u,j)}| \qquad g_2 = |V_{(u,j)} + c_{(u,j)}| \qquad g_3 = |V_{(u,j)} - c_{(u,j)}| \tag{9.14}$$

This choice amounts to the following specification of the conservative flux contributions:

$$\mathbf{f}^{+} = \frac{r_{(u,j)}}{6}\begin{pmatrix} 4V_{(u,j)} + (V_{(u,j)} + c_{(u,j)}) \\ 4V_{(u,j)}^2 + (V_{(u,j)} + c_{(u,j)})^2 \\ \frac{1}{2}\left(4V_{(u,j)}^3 + (V_{(u,j)} + c_{(u,j)})^3\right) \end{pmatrix} \quad \text{and} \quad \mathbf{f}^{-} = \frac{r_{(u,j)}}{6}\begin{pmatrix} V_{(u,j)} - c_{(u,j)} \\ (V_{(u,j)} - c_{(u,j)})^2 \\ \frac{1}{2}(V_{(u,j)} - c_{(u,j)})^3 \end{pmatrix} \tag{9.15}$$

for $V_{(u,j)} < c_{(u,j)}$, while otherwise:

$$\mathbf{f}^{+} = \mathbf{f}_{(u,j)}^{C} \quad \text{and} \quad \mathbf{f}^{-} = \mathbf{0} \tag{9.16}$$

In section 7.5.4 we have shown that if the traffic operations are not congested ($V_{(u,j)} > c_{(u,j)}$), all *characteristics* traverse in the same direction as the traffic stream. That is, no momentum or energy is transported upstream. In this case, the Steger-Warming splitting scheme yields the following specification of the numerical flux at the cell interface $x_{i+1/2}$:

$$\mathbf{h}_{(u,j)}^{i+1/2} = \mathbf{f}_{(u,j)}^{C}(\mathbf{w}_i) \tag{9.17}$$

Thus, the numerical flux at the cell interface is only dependent of traffic conditions in the transmitting cell *i*. However, if traffic operations are congested $V_{(u,j)} < c_{(u,j)}$, the Mach-line $C_{(u,j)}^{-}$ traverses the opposite direction of the traffic stream: momentum or energy are also transported *upstream*. In this case, the numerical flux at the cell interface due to the transmitting cell is corrected according to the traffic conditions in the receiving cell.

9.3.5 *Van Leer splitting*

The Steger-Warming scheme yields discontinuous behaviour of the split-fluxes at $V_{(u,j)} = c_{(u,j)}$. These discontinuities may yield a discontinuity in the *slope* in the transition region from non-congested to congested traffic operations. To resolve these discontinuities, Van Leer (1982) proposed changing these split fluxes to modify their functional dependence on $V_{(u,j)}/c_{(u,j)}$. The splitting proposed by Van Leer is then the following:

$$\mathbf{f}^{+} = \frac{r_{(u,j)}}{4c_{(u,j)}}(V_{(u,j)} + c_{(u,j)})^2 \begin{pmatrix} 1 \\ \frac{2}{3}(V_{(u,j)} + c_{(u,j)}) \\ \frac{1}{4}(V_{(u,j)} + c_{(u,j)})^2 \end{pmatrix} \tag{9.18}$$

and:

$$\mathbf{f}^{-} = -\frac{r_{(u,j)}}{4c_{(u,j)}}(V_{(u,j)} - c_{(u,j)})^2 \begin{pmatrix} 1 \\ \frac{2}{3}(V_{(u,j)} - c_{(u,j)}) \\ \frac{1}{4}(V_{(u,j)} - c_{(u,j)})^2 \end{pmatrix} \tag{9.19}$$

for $V_{(u,j)} < c_{(u,j)}$, while otherwise:

$$\mathbf{f}^{+} = \mathbf{f}^{C}_{(u,j)} \quad \text{and} \quad \mathbf{f}^{-} = \mathbf{0} \tag{9.20}$$

Hänel modifies the Van Leer splitting function by requiring that the split-mass and energy flux components are scaled by the total enthalpy mH, thereby satisfying the constant enthalpy constraint (see Hänel *et al.* (1987)).

9.4 Godunov-type schemes for traffic flow equations

This section discusses the Godunov-type schemes to numerically solve systems of traffic flow equations. Lebaque (1996) was the first to apply a Godunov scheme to traffic flow equations, by numerically approximating solutions to the LWR-model using Godunov's original scheme. In this section, we generalise this approach to suit traffic flow models that consist of dynamic equations for density, velocity, and velocity variance (or density, momentum, and energy). Moreover, the approach adapted to suit numerical approximation of our multilane multiclass traffic flow model. To this end, we present the so-called *approximate Riemann solver* for the macroscopic MLMC traffic flow model developed in this thesis.

Before establishing Godunov-type schemes for traffic flow equations, we refer to appendix E that discusses the so-called *Riemann problem* for traffic flow. This *Riemann* problem is characterised by a discontinuity in the initial conditions that are constant elsewhere. Using the characteristic formulation, we can analytically solve the Riemann problem for the inviscid equilibrium traffic flow. We show that the discontinuity yields a *shock wave*, a *contact discontinuity*, and an *expansion fan*.

Godunov-type schemes introduce information from the local exact solutions of the inviscid flow equations, yielding a high interaction level with the physical properties of the flow equations. The solution at time t_k is approximated by a *piecewise constant* function for each cell i. Each cell interface separates two homogeneous regions (see Figure 9-2). For each cell pair $(i,i+1)$ a Riemann problem is present. The solution at t_{k+1} is determined by analytically

solving this Riemann problem at each cell interface and subsequently approximating the new state at t_{k+1} by a piecewise constant function. This requires solving a complex non-linear equation at each cell interface, which can be quite time consuming. However, since the Godunov scheme is only first order accurate, Roe (1981) was able to establish an approximate solution to the Riemann problems at the cell interfaces without decreasing the accuracy. His approach is based on the characteristic decomposition of the conservative flux while ensuring the conservation properties of the scheme.

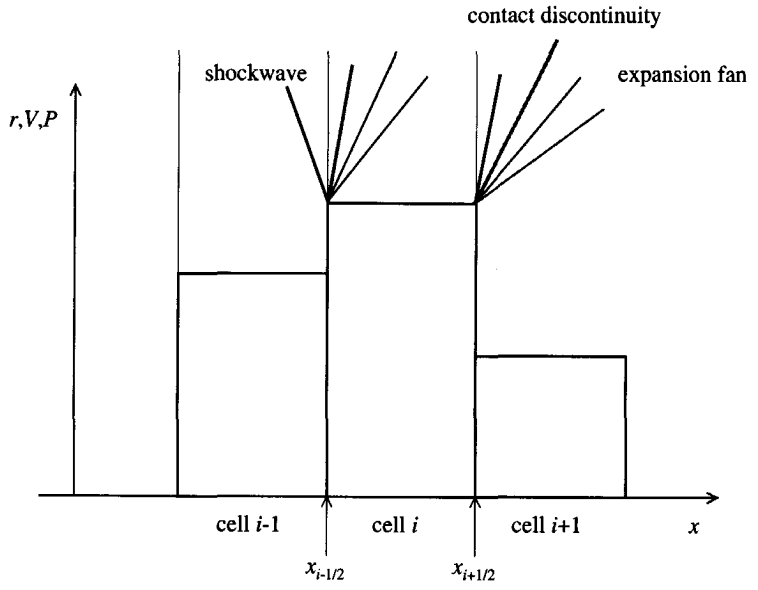

Figure 9-2: Determining the solution of the Riemann problem at the cell interfaces

9.4.1 Description of Godunov original scheme

Godunov-type schemes introduce information from the local exact solutions to the inviscid flow equations yielding a high level of interaction of the discretisation method and the physical properties Godunov-type schemes present.

The solution at time $t_k = k\Delta t$ is approximated by a function which is *piecewise constant* for each cell. The flow dynamics originate from the wave interactions at the cell interfaces. At these interfaces, two flow states are present. The resulting problem is the Riemann problem, which can be solved analytically (see appendix E). The original Godunov method is based on this exact solution. However, approximate solutions can be applied as an alternative.

Let $\mathbf{v}^{(R)}(x/t,\mathbf{v}_L,\mathbf{v}_R)$ denote the exact solution of the Riemann problem with initial conditions:

$$\tilde{\mathbf{v}}(x,0) = \tilde{\mathbf{v}}_L \quad \text{for} \quad x<0 \quad \text{and} \quad \tilde{\mathbf{v}}(x,0) = \tilde{\mathbf{v}}_R \quad \text{for} \quad x>0 \tag{9.21}$$

which can be determined using the procedure discussed in section E.2. The solution of the Riemann problem at the cell interface between cell i and cell i+1 becomes:

$$\tilde{\mathbf{v}}(x,t) = \tilde{\mathbf{v}}^{(R)}((x-(i+1/2)\Delta x)/(t-k\Delta t), \tilde{\mathbf{v}}_i^k, \tilde{\mathbf{v}}_{i+1}^k) \tag{9.22}$$

Finally, the obtained state variables are averaged over each cell i, yielding the piecewise approximation at k+1:

$$\tilde{\mathbf{v}}^{i,k+1} = \frac{1}{\Delta x}\int_{x_{i-1/2}}^{x_{i+1/2}} \tilde{\mathbf{v}}(x,(k+1)\Delta t)\mathrm{d}x \tag{9.23}$$

We mentioned that application of the Godunov scheme necessitates solving the Riemann problem following the procedure outlined in appendix E. This requires solving non-linear equations at each of the cell interfaces, which can be quite time consuming. However, since we average the exact solution of each cell, approximating it by a constant function, the Godunov scheme is only first order accurate. Consequently, we might consider approximate solutions to the Riemann problems at the cell interfaces without decreasing the accuracy of the scheme but requiring much less computational work. To this end, the following section discusses Roe's approximate Riemann solver.

9.4.2 *Roe's Approximate Riemann Solver for Traffic Flow models*

Roe's approach is based on the characteristic decomposition of the flux differences while ensuring the conservation properties of the scheme. Basically, the method determines approximations of the solution of the Riemann problem at the cell interfaces.

Roe's approximate Riemann solver (cf. Roe (1981)) is directly applicable to discretise the *convective flux* of the mixed-state MLMC flow model. However, the respective terms in the source, reflecting the influence of acceleration, deceleration and overtaking, need to be considered sequentially (see section 9.8). In this section, we will only present the equations delineating Roe's approximate solver.

9.4.3 *Summary of Roe's approximate Riemann solver*

Roe's scheme is now completely determined. We can summarise it as follows:

1. At each cell interface i+1/2 determine

$$\hat{r}_{i+1/2} = \sqrt{r_{i+1}r_i} = R_{i+1/2}r_i \qquad \hat{V}_{i+1/21} = \frac{R_{i+1/2}V_{i+1} + V_i}{R_{i+1/2}+1}$$
$$\hat{H}_{i+1/21} = \frac{R_{i+1/2}H_{i+1} + H_i}{R_{i+1/2}+1} \tag{9.24}$$

   where $R_{i+1/2} = (r_{i+1}/r_i)^{1/2}$, and the associated average local sonic speed:

$$\hat{c}^2 = 2(\hat{H} - \hat{V}^2/2)^* \tag{9.25}$$

2. Compute the eigenvalues and eigenvectors of the linearised matrix $\hat{\mathbf{A}}(\mathbf{w}_i, \mathbf{w}_{i+1})$ by respectively determining:

---

* The hat '^' indicates the so-called Roe-averages (average weighted by the square root of the densities; cf. Roe (1981)).

$$\hat{\lambda}_{(1)} = \hat{V} \quad \hat{\lambda}_{(2)} = \hat{V} + \hat{c} \quad \hat{\lambda}_{(3)} = \hat{V} - \hat{c} \tag{9.26}$$

$$\hat{s}^{(1)} = \begin{pmatrix} 1 \\ \hat{V} \\ \hat{V}^2/2 \end{pmatrix} \quad \hat{s}^{(2)} = \frac{\hat{r}}{2\hat{c}} \begin{pmatrix} 1 \\ \hat{V} + \hat{c} \\ \hat{H} + \hat{c}\hat{V} \end{pmatrix} \quad \hat{s}^{(3)} = \frac{\hat{r}}{2\hat{c}} \begin{pmatrix} 1 \\ \hat{V} - \hat{c} \\ \hat{H} - \hat{c}\hat{V} \end{pmatrix} \tag{9.27}$$

3. Determine the wave amplitudes ∂z_j:

$$\partial z_1 = \delta r - \delta P / \hat{c}^2 \quad \partial z_2 = \delta V + \delta P / \hat{r}\hat{c} \quad \partial z_3 = \delta V - \delta P / \hat{r}\hat{c} \tag{9.28}$$

$$\delta r_{i+1/2} = r_{i+1} - r_i \quad \delta V_{i+1/2} = V_{i+1} - V_i \quad \delta P_{i+1/2} = P_{i+1} - P_i \tag{9.29}$$

4. Evaluate the numerical flux of Roe's scheme:

$$\mathbf{h}_{i+1/2} = \mathbf{f}(\mathbf{w}_i) + \sum_j \lambda^-_{(j)} \partial z_j s^{(j)} = \mathbf{f}(\mathbf{w}_{i+1}) - \sum_j \lambda^+_{(j)} \partial z_j s^{(j)} \tag{9.30}$$

We remark that the numerical flux at the cell interface depends on the magnitude of $\hat{V} - \hat{c}$, which is evaluated using Roe's average. This average depends on both the traffic conditions of the transmitting cell *i and* the receiving cell *i*+1.

9.5 Temporal discretisation

In the previous sections we have discussed several approaches to determine approximations for the conservative flux **f**. The resulting system is a so-called *lumped system* of ordinary non-linear differential equations. That is:

$$\frac{\partial \mathbf{w}}{\partial t} + \frac{\partial \mathbf{f}}{\partial x} = \mathbf{y} \quad \rightarrow \quad \frac{\mathrm{d}}{\mathrm{d}t} \mathbf{w}_i(t) = (\mathbf{h}_{i+1/2}(t) - \mathbf{h}_{i-1/2}(t)) / \Delta x + \mathbf{y}_i(t) \tag{9.31}$$

Here, $\mathbf{w}_i$ is the vector consisting of approximations of the space-averaged conservative variables density, momentum, and energy in cell *i*. The next step is the time integration of the resulting lumped system. Since the speed of computation is of dominant importance in traffic flow simulations, we have only considered *explicit methods* (Hirsch (1990b)).

The most straightforward explicit approach is to approximate to a first order accurate forward difference to approximate the derivative $\partial \mathbf{w}/\partial t$. By application of *Von Neumann's stability analysis*, we can show that both the Steger-Warming scheme as well as the Van Leer scheme applied to the inviscid flow equations are *conditionally stable*. That is, the schemes are stable when Δt satisfies:

$$\Delta t \leq \Delta x / (V + c)_{\max} \tag{9.32}$$

9.6 Choice of numerical approximation approach

In this section we will illustrate the numerical schemes presented in the previous sections by two test-case scenarios, namely the removal of a blockade and the occurrence of an incident. Although in these cases we numerically approximate solutions of the aggregate-lane aggregate-class flow model, the results can be generalised to the multilane heterogeneous case. In order to compare different numerical solution approaches, we have implemented the schemes

of Lax-Friedrichs, Steger-Warming, Van Leer, and Roe (see sections 9.3 and 9.4) in the Interactive Data Language (IDL version 5.2 (Win32 x86). © Research Systems, Inc.).

The scenarios that are chosen reflect typical traffic flow conditions where occurrences of *non-smooth* solutions of the flow model equations are likely. Since these non-smooth solutions are inevitable for *inviscid* traffic flow equations, the numerical approximation scheme must be able to adequately reproduce these discontinuities. Let us note that for the viscous models these discontinuous solutions will also occur if the influence of the dissipative flux is too small compared to the conservative flux.

For both scenarios, results of the numerical solution approaches are compared by on the one hand considering mathematical properties of the exact solutions, and on the other hand a reference solution. These reference solutions have been obtained by comparing numerical solutions following from the different implemented schemes for a very fine mesh. It appeared that solutions of the different schemes converged to the same solution in the limiting case. We have made the (arbitrary) decision to use the approximate Riemann solver to determine the reference solution using a very fine mesh. Based on comparison between the reference solution, and the mathematically derived properties of the solution, we aim to determine which numerical scheme yields the best approximation and is hence most suitable.

We apply the approximation approaches discussed in previous sections to aggregate-lane aggregate-class flow ($u = j = *$). We will test different numerical approaches using two test-case scenarios, namely:

1. Removal of a blockade (section 9.6.1).
2. Occurrence of an incident (section 9.6.2).

The scenarios concern the traffic conditions on a ringroad of $20km$ having two lanes and three lanes for case 1 and case 2 respectively. By considering a ringroad, the (non-trivial) problem of determining appropriate boundary conditions is avoided (see section 7.7). The following parameter values have been chosen for the single class:

$$\begin{aligned} V^0 &= 30m/s \qquad \tau = 8s \qquad r_{jam} = 200veh/km/lane \\ &\eta = 15m/s \qquad \kappa = 15m/s \end{aligned} \tag{9.33}$$

Both the equilibrium velocity variance and the immediate overtaking probability are assumed to be functions of the density r, i.e. $\Theta^e = \Theta^e(r) = 20+40\cdot(1-5r)^{3/2}$ and $\pi = \pi(r) = \exp(-(40r)^2)$. The equilibrium velocity is a function of both the density r, the current immediate overtaking probability π and the velocity variance Θ. Nevertheless, we approximate the equilibrium velocity by substituting $\Theta^e(r)$ and $\pi(r)$ into $V^e(r)$, i.e. $V^e(r) = V^0-\tau(1-\pi(r))r\Theta^e(r)$. By doing so, the critical density r_{crit} indicating the threshold between non-congested and congested traffic operations (i.e. $V(r_{crit}) = c(r_{crit})$) is also approximated. Consequently, also the equilibrium flow-rate m^e can be approximated.

9.6.1 Removal of a blockade

We consider the situation where at $t < 0$ a queue is present in the region $x = [2.5km, 7.5km]$ (see Figure 9-3). The velocity in the queue is approximately zero. This queue can be formed due to the closure of a bridge or the occurrence of a serious incident. At $t = 0$, the blockade at $x = 7.5km$ is removed and vehicles in the queue flow into the empty roadway.

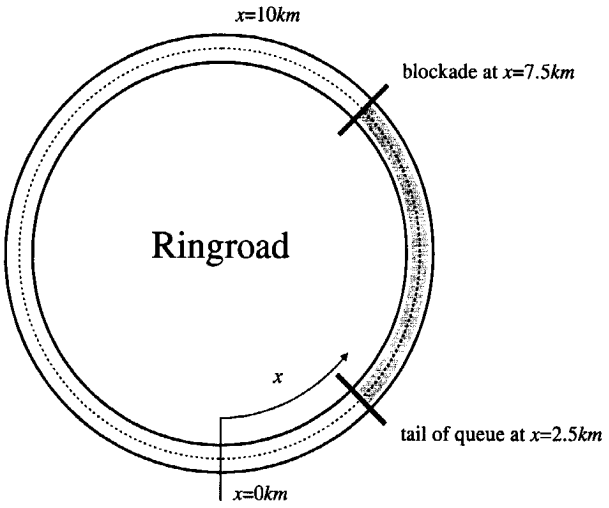

Figure 9-3: Initial conditions for 'removal of blockade' scenario. The head of the queue is located at x = 7.5, while the tail of the queue is located at x = 2.5km.

Before we discuss the results of the numerical schemes, let us first consider the expected traffic operations by considering the characteristics. We refer to chapter 7 for explanations of the theory. To this end, we consider the discontinuity in the density at the *tail of the queue* ($x = 2.5km$). Here, the velocity V equals the desired velocity V^0, while the variance Θ equals the free-flow variance (which equals $\Theta^e(0)$) which equals the variance in the desired velocities of the drivers. Since $r = 0 < r_{crit}$, we have $V \pm c > 0$. That is, all characteristics emanating from (x,t_0) for $0 \leq x < 2.5$ propagate downstream. In the region upstream of the queue tail, the velocity is approximately zero. Since the velocity variance is small, albeit positive, the C^- characteristic move *upstream*. The C^0 characteristic, defined by $x = x_0$, and the C^+ characteristics move *downstream*. The C^- characteristics upstream and downstream of the queue tail intersect, leading to the formation of a shock wave (sections 7.5 and 7.6).

The velocity of the shock depends on the upstream and downstream traffic conditions. To determine the shock velocity, the *Rankine-Hugoniot* conditions (see appendix E) can be applied. These state that the jump $[r]$ across the shock, multiplied by the shock velocity V_C equals the jump $[m]$ in the traffic momentum. Since the latter equals zero, we have $V_C = 0$. That is, the shock at the queue tail is stationary.

Next, let us consider the traffic conditions at the *head of the queue* ($x = 7.5km$). In front of the queue head, the characteristic C^- moves *upstream*, the C^0 characteristic is a vertical line, and the C^+ characteristic moves *downstream*. Downstream of the head of the queue, all characteristics move in the same direction as the traffic. If we assume that the C^+ characteristic emanating from the queue has a slope $V+c$ smaller than the slope of the C^- characteristic emanating from the region downstream of the queue, i.e. $2(3\Theta_{jam})^{1/2} < V^0$, none of the characteristics will intersect. As a result, an expansion fan results characterised by continuous changes in the traffic variables. Note that in this particular case, the C^+ characteristics emanating from the downstream region of the queue head separates the downstream empty region

and the upstream region where vehicles are present. As a consequence, we can interpret this characteristic as the path of the fastest vehicles discharging from the queue.

Numerical approximation results

Figure 9-4 depicts the results of numerical approximation using the various proposed techniques. Among other things, the figure shows that applying Lax-Friedrichs' scheme (with $\Delta x = 100m$) results in vehicles at the tail of the queue flowing into the empty road upstream. That is, they flow backwards, *violating the anisotropy condition.* Moreover, vehicles driving into the empty road downstream of the head of the queue have already arrived at the end of the road after three minutes. Note that some vehicles move along the C^+ characteristics emanating upstream of the queue head. Since the slope of this characteristic equals $V^0+(3\Theta^0)^{1/2} \approx 43.8 m/s$, after three minutes these vehicles arrive at $x = 15.4km$. That is, vehicles are propagating too fast in the Lax-Friedrichs scheme.

These effects are caused by the presence of *artificial dissipation* effects in the Lax-Friedrichs scheme. That is, an artificial second order term is introduced in the flow equations, which effect is of order Δx^2. Figure 9-4 shows clearly that with decreasing magnitude of Δx, the effect of numerical dissipation is reduced.

Concluding, on the one hand, the Lax-Friedrichs scheme is stable due to this dissipation effect. That is, problems caused at for instance discontinuities by intersecting characteristics are remedied. On the other hand, the smoothing in the results is unrealistic, since apparently some vehicles *drive backwards* into the empty region. That is, although the continuous model satisfies the anisotropy conditions, the use of Lax-Friedrichs scheme results in a numerical scheme violating this anisotropy.

In opposition to the Lax-Friedrichs scheme, the Steger-Warming splitting scheme, the Van Leer splitting scheme, and the approximate Riemann solver appear to yield no numerical dissipation. In other words, after 'releasing' the vehicles, drivers at the head of the queue drive away at a realistic velocity, while vehicles at the queue tail remain at their location. The velocity at which the fastest vehicles at the queue head drive into the empty region is in accordance with the slope of the C^+ characteristics along which these vehicles move. However, the Steger-Warming scheme yields some artefacts at the queue tail. Some vehicles are able to drive into the jammed region. This unrealistic effect is caused by the discontinuity in the numerical flux function. The Van Leer flux splitting approach, and the approximate Riemann solver yield most plausible results.

Finally, we remark that the conservative splitting schemes produce a very high valued velocity variance at the queue tail (not shown). This high variance indicates the sharp transition between traffic states, i.e. from non-congested to congested traffic; it 'spatially' predicts the occurrence of congestion. The Lax-Friedrichs scheme is not able to produce this high-valued velocity variance accurate enough.

9.6.2 *Occurrence of an incident*

As a second scenario, let us consider an incident at $x = 10km$ where for 5 minutes one lane of a three-lane roadway is blocked in a region of $250m$. When the incident occurs at $t = 1min$, the density on the blocked roadway stretch increases instantaneously from $20veh/km$ to $30veh/km$ per lane. Vehicles upstream of the incident, having a higher velocity, will flow into

the incident region. Since they do not adapt their velocity instantaneously, the interaction rate that is expressed by the traffic pressure $P = r\Theta$ increases. The increase in the velocity variance causes a reduction in the equilibrium velocity, and consequently a decrease in the velocity. Due to the decreased velocity, the interaction between inflowing fast vehicles will become even more significant. This avalanche-like process yields a region of high densities upstream of the incident. In this region, the velocity will be low, while the velocity variance will be considerable. Moreover, provided the reduction in velocity is large enough, the traffic conditions upstream of the incident may become congested. As a consequence, characteristics emanating from the congested region propagate upstream, possibly causing a backward-propagating shock wave.

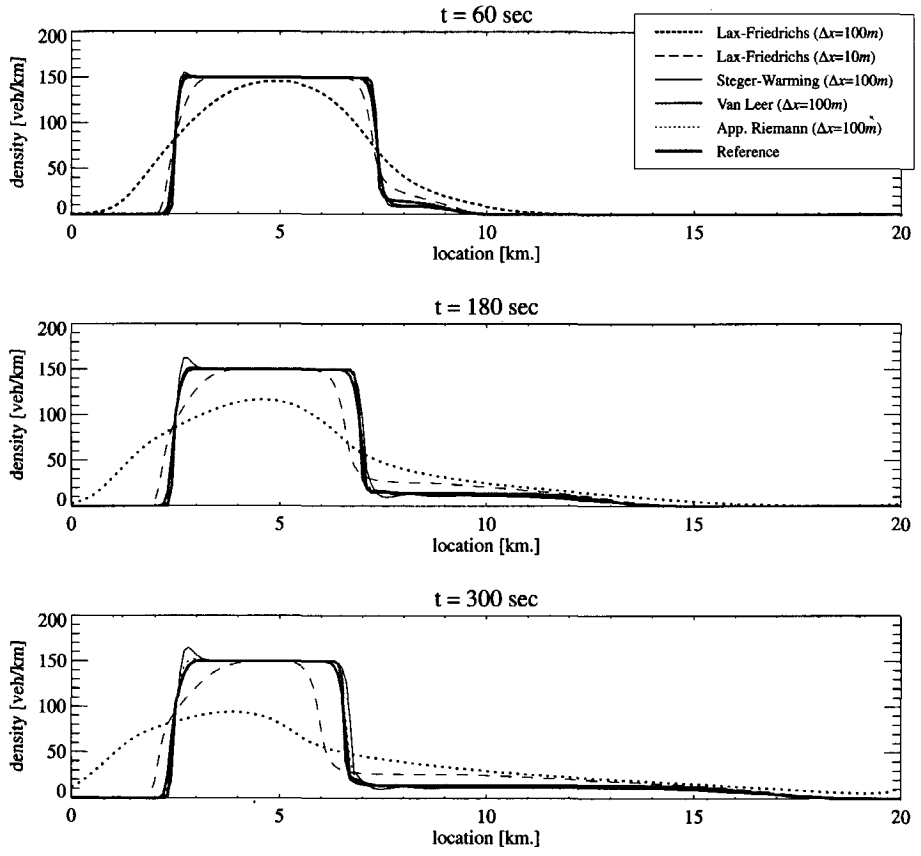

Figure 9-4: Removal of blockade approximation of density at different time instants, using different discretisation schemes.

Numerical approximation results

Figure 9-5 shows the results from application of the different schemes to the incident scenario. Again, numerical dissipation causes the Lax-Friedrichs scheme to provide unrealistically smooth results. The effect of the incident is very moderate. Also, when the incident is removed (at $t = 6min$), the effect soon vanishes. Neither a shock wave is formed, nor does congestion occur.

Application of the proposed conservative numerical approaches yields completely different results compared to the Lax-Friedrichs scheme. The Steger-Warming scheme, the Van Leer scheme, and the approximate Riemann solver all result in congesting occurring upstream of the incident. Initially, the Steger-Warming scheme shows two upstream moving shock waves, emerging from the high-density incident region at $t = 2.7min$ and $t = 5.0min$ respectively. These merge into one single shock wave at approximately $t = 7.2min$. The shock wave has a velocity of approximately $5.8m/s$. In addition, the Van Leer scheme shows two shock waves originating from the incident region. However, the second shock wave is somewhat slower than the first shock wave. Consequently, rather than merging into a single shock wave, they diverge. The first shock wave has a velocity of approximately $4.4m/s$, while the second shock has a velocity of approximately $4.2m/s$. The Riemann scheme shows similar results.

Compared to the reference solution, the shocks move upstream too fast. The reference solution shows two shock waves, one of which dissolves, moving with an approximate velocity of $2.9m/s$. Nevertheless, the schemes reproduce the shock waves to a certain extent. Compared to the reference solution, the Van Leer scheme seems to be the best approximation.

The seemingly large differences between the results of the different schemes can be explained by considering the *chaotic-like* behaviour of traffic flow. Among others, Kerner *et al.* (1996) and Bovy and Hoogendoorn (1998) have stressed that the traffic flow process is highly non-linear in nature. That is, provided that traffic operates under 'metastable conditions', small variations at some time instant tend to grow exponentially, possibly resulting in a so-called phantom-jam. Since the different schemes yield different, albeit comparable results, the small differences in the approximations of the traffic conditions at a certain instant, potentially yield very large differences at a later instant in time. This explains the seemingly large differences in the results for the incident scenario.

9.7 Multistep determination of innerforces

The so-called *innerforce*-vector $\mathbf{x}_{(u,j)}$ in (9.2) describes the influence of acceleration, deceleration due to interaction, immediate, postponed and spontaneous lane-changing. With respect to the different lane-changing types, in chapter 4 we have argued that these processes are *mutually exclusive*. This is true when considering periods Δt of infinitesimal duration. However, when we consider a finite size period length Δt, this is not generally true.

Preliminary numerical simulations using the MLMC traffic flow model developed in chapter 6 of this thesis revealed that by *simultaneously* determining effects of *immediate lane-changes*, *postponed* lane-changing and *spontaneous lane-changes* during period $[t,t+\Delta t)$ based on the situation at t, may result in more vehicles flowing out of the lane segment than currently occupy the lane segment.

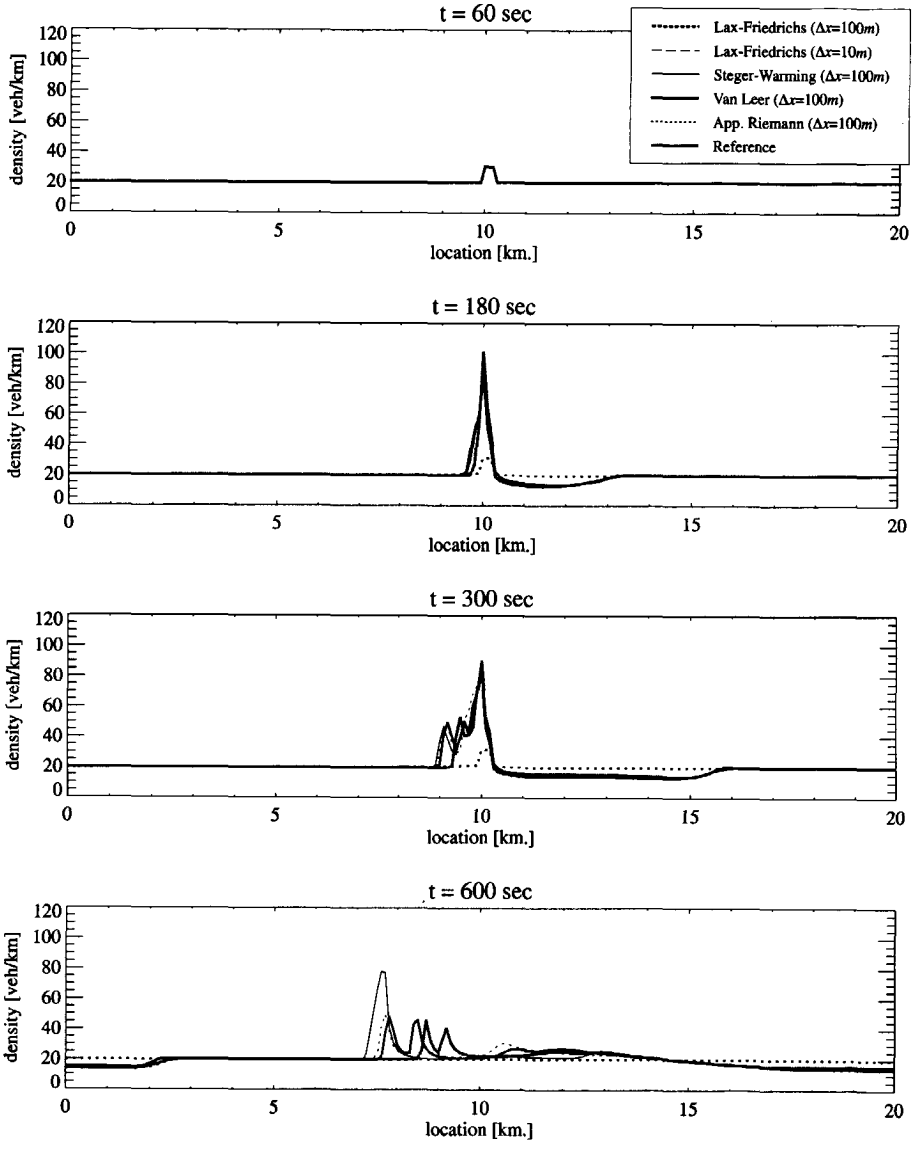

Figure 9-5: The effect of an incident blocking one lane of a three-lane freeway using different numerical schemes.

To remedy this side effect, a multistep approach to determine the number of lane-changes is proposed: rather than simultaneously considering the various non-continuum processes in MLMC traffic flow, we consider them *consecutively*. That is, we first determine the effects of acceleration, deceleration due to interaction, and immediate overtaking $\Delta \mathbf{w}^*[i,k]$ to determine the number of vehicles, their momentum, and their energy per class, left after these processes would have taken place. Based on this intermediate result $\mathbf{w}^*[i,k] = \mathbf{w}[i,k]+\Delta \mathbf{w}^*[i,k]$, we de-

termine the between-lane flux $\Delta \mathbf{w}^{**}[i,k]$ due to postponed and spontaneous lane-changing. Then total between-lane flux due to the non-continuum processes equals $\Delta \mathbf{w}^{*}[i,k]+\Delta \mathbf{w}^{**}[i,k]$. For a more detailed discussion, we refer to appendix H.

9.8 Resulting numerical solution approach

Before presenting the conclusions of this chapter, let us summarise the resulting numerical solution approach used to determine the results presented in the following chapter. The numerical approximation scheme can be roughly divided into the following five steps:

- Determination of the cell width Δx and the time-step Δt;
- Determination of the initial conditions ($k = 0$);
- Discretised approximation of the source-term:
  - effect of diffusion*, acceleration and deceleration;
  - effect of immediate lane-changing;
  - effect of postponed and spontaneous lane-changing;
- Discretised approximation of the *convective flux* $\mathbf{f}^{C}$ using Van Leer's flux vector splitting scheme;
- Updating the approximation for the new time step (k: = k+1) and continue (step 2).

For a detailed discussion, we refer to appendix H.

9.9 Conclusions

In this chapter we have discussed theoretically and compared experimentally a number of numerical approximation schemes. From the viewpoint of numerical analysis of the flow equations, we have observed that the conservative form is essential to correctly compute the propagation velocity and the intensity of discontinuities such as shock waves that are characteristic in traffic flow. The finite volume representation enables direct discretisation of the exact integral equations, thereby ensuring that traffic density, momentum, and energy are also conserved at the discretised level, at least with respect to the convective processes in traffic flow.

We have shown that by applying *flux vector splitting schemes* the physical properties of the traffic flow equations were introduced in the numerical approximation schemes, resulting in an improved solution compared to the usually applied basic central difference scheme. By applying different numerical approximation schemes to different test-case scenarios, some of the advantages of the proposed schemes were revealed.

For instance, by considering traffic conditions after the removal of a blockade, it was observed that since central discretisation approaches do not take the direction in which traffic variables 'move' into account, they violate the *anisotropy condition* of traffic flow, even

* The term *diffusion* indicates the higher-order processes in the MLMC flow-model.

when the model *does* yield anisotropy. Moreover, we observed that vehicles tend to flow too fast in low-density regions. Instead, application of the flux splitting schemes does result in satisfying this fundamental condition, while vehicles do not flow too fast into the low-density region. In this case, *anisotropy* is not a model characteristic, but rather a characteristic of the numerical approximation approach. From the 'removal of a blockade' scenario, it was concluded that the Van Leer splitting scheme and the approximate Riemann solver yielded the best results.

Considering the results from an incident scenario, the splitting schemes correctly reproduce the occurrence of congestion due to the incident. However, the chaotic-like behaviour of the traffic system results in significant differences in the results of the different schemes. That is, since small variations tend to 'blow up' under specific circumstances, and consequently yield very dissimilar results, the discretisation approach used affects the exact location and duration of formed shock waves and traffic jams.

In the remainder of this thesis, the Van Leer splitting scheme is employed for macroscopic multiclass multilane traffic flow simulation, since it is concluded that this method yields accurate and reliable results – even in non-smooth traffic conditions – on the one hand, and is computationally very efficient.

10 MULTICLASS MACROSCOPIC SIMULATION OF MULTILANE TRAFFIC

In this chapter we present macroscopic simulation results of MLMC traffic flow. The aim of this chapter is two-fold: on the one hand, we show that the model meets the fundamental modelling-issues presented in section 2.8 of this thesis, and is able to realistically describe multiclass traffic flow operations on multilane roadways. That is, we show that the developed model remedies the flaws of other higher-order macroscopic flow models with respect to the *anisotropic* behaviour of drivers and *slow vehicles* that should be *virtually unaffected* by faster vehicles (section 10.1). The *invariant personality critique*, i.e. drivers have personalities which are unaffected by prevailing traffic conditions, is remedied *to a certain extent.* At the same time, we will show that the model can describe *hysteresis phenomena* and the occurrence of phantom-jams in the multiclass traffic flow (section 10.2).

On the other hand, we will show typical practically relevant problems in traffic engineering that advantageously can be handled and solved with the MLMC model developed in this thesis. The outcomes of these cases will show the functioning and plausibility of the model. Moreover, we show the increased application area of macroscopic modelling following from the multilane multiclass generalisation. That is, we discuss the ability of the model to macroscopically describe specific situations that are characterised by class or lane-specific behaviour and conditions. For instance, we present how jams can result seemingly spontaneously from mixing slow and fast traffic streams (section 10.3); we will consider the effects of a lane-drop (section 10.4) and incidents that block a lane of the motorway for a specific time duration (section 10.5). Finally, other practical cases show the model's applicability to assess

lane and class-specific (dynamic) traffic management measures, and the consequent lane and class-specific impacts. To this end, we will also show the effect of overtaking prohibition of trucks (section 10.6), and lane-specific speed-limits (section 10.7).

10.1 Fundamental modelling issues; preliminary model validation

In section, 2.8 we have discussed some issues of interest in the ongoing debate between the LWR-modelling stream and the Payne-type modelling stream. In this discussion, we have presented some points of criticism of each of the streams. In this first section, we will discuss the relevant issues for section 2.8 for the viewpoint of the discrete MLMC flow model. That is, we show that the *discrete* MLMC flow model (= continuum MLMC traffic flow model + Van Leer splitting approach) presented in this thesis meets the fundamental issues. Three of these issues, i.e. the finite-space requirements, incorporation of velocity variance, finite reaction and braking times (section 2.8.3), have been *explicitly considered* in the model development phase, and these need not to be discussed in this section. Rather, in this section we show that our model remedies the fundamental flaws of higher-order macroscopic traffic flow models identified by Daganzo (section 2.8.2), i.e. we demonstrate the anisotropic nature of drivers, unaffected slow drivers, and (to a certain extent) drivers' invariant personalities. We apply the numerical approximation scheme proposed in section 9.8 (based on the Van Leer) to show that the discrete model satisfies the anisotropy requirements. Moreover, we show that in principle the model also supports the unchanged personality of drivers. The same holds for the unaffected slow vehicles. Some macroscopic simulation results with respect to hysteresis and the occurrence of phantom-jams are presented in section 10.2.

The cases considered describe the MLMC traffic flow operations on a twenty-kilometre two-lane motorway ringroad without on- and off-ramps. This ringroad is divided into 200 equally sized cells i of length $\Delta x = 100m$. The time-step equals $\Delta t = 0.1s$. Moreover, we only consider two classes, namely person-cars and trucks. The class-specific parameters and relationships for each of these classes have been discussed in section 8.6, and are applied in this chapter. By considering a ringroad, the non-trivial problem of providing boundary conditions at the entry and the exit section (section 7.6.3) is omitted. To assure that vehicles cannot drive around the ringroad during the simulation period, the ratio between the length of the ringroad and the duration of the simulation is restricted by the maximal velocity.

Let us note that the model applications presented in this section intent to show the validity of the discrete MLMC model. We therefore emphasise that these cases are not intended to be of major practical relevance.

10.1.1 Drivers' anisotropy

To study the drivers' anisotropic behaviour (among other things implying that drives will not show negative speeds in any situation), let us consider a MLMC-version of the case similar to the removal of a blockade example presented in section 9.7. That is, we assume that at $t < 0$ a queue of *virtually motionless*[*] vehicles is present in the region $[2km,6km)$. At $t = 0$, the blockade at the queue head is removed and vehicles flow into the empty roadway lanes.

[*] The vehicles in the queue have a *very* low velocity (approximate $0.5km/hr$).

Similar to the aggregate-lane aggregate-class case, we expect that the discontinuity at the tail of the queue ($x = 2km$) remains nearly stationary due to the low in-queue velocities. At the head at $x = 6km$, vehicles accelerate and drive away from the queue. The number of person-cars and trucks in the queues on the roadway lanes will reduce according to the *queue-discharge flows*. In opposition to the aggregate-lane aggregate-class case (cf. Hall *et al.* (1992)), the queue-discharge flow is both lane-specific and traffic-composition dependent. The fastest vehicles of the class will head the discharging vehicles. These move into the empty region along the $C^{+}_{(u,j)}$ characteristic. Consequently, a region of high velocities will be present. These velocities are even higher than the average desired speeds of the respective classes. The latter is caused by the assumption that the desired velocity is a random variate with a specific mean and variance (section 3.3.2). Hence, some vehicles have an above-average desired velocity. These vehicles will have the highest velocity and will head the vehicles discharging from the queue.

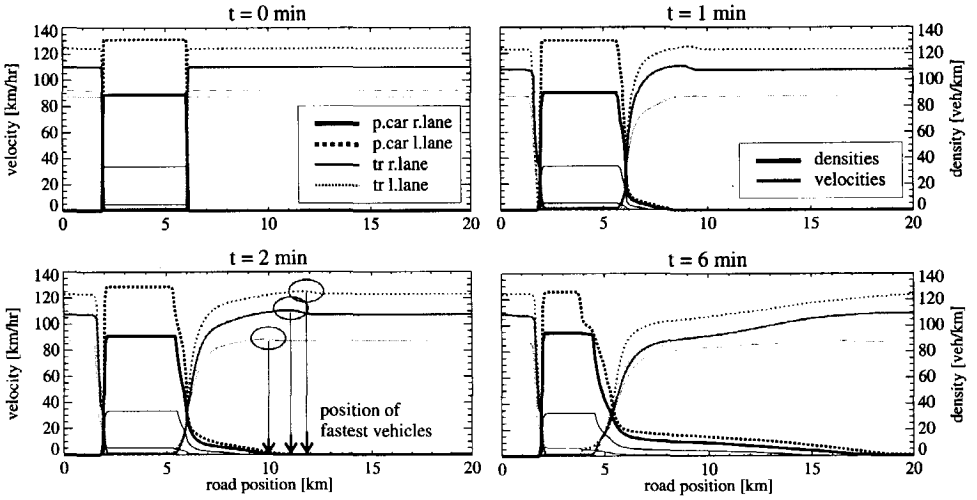

Figure 10-1: Density and velocity dynamics by lane for person-cars and trucks for the "removal of blockade" scenario. Note that in the regions where initially no vehicles are present ($X = [0km,2km] \cup [6km,20km]$), the velocity is assumed to be equal to mean desired velocity.

Figure 10-1 shows the dynamics of the class- and lane-specific densities, which reveal clearly that the vehicles at the tail of the queue ($x = 2km$) remain motionless at their location, while the vehicles at the head of the queue ($x = 6km$) flow into the empty roadway. Since at the queue-tail, no vehicle flows into the upstream empty roadway, the higher-order effects described by Daganzo (1995) do not occur. This can also be observed by studying Figure 10-2, which shows among other things the *characteristic curves* (path-lines $C^{0}_{(u,j)}$ and Mach-lines $C^{\pm}_{(u,j)}$) for person-cars that emanate from the high-density region on the right lane of the roadway. The figure reveals clearly that driver's anisotropy is met by the continuum macroscopic MLMC model. Clearly, since our numerical solution approach respects the physical properties of the equations, the discrete model also respects the anisotropy condition.

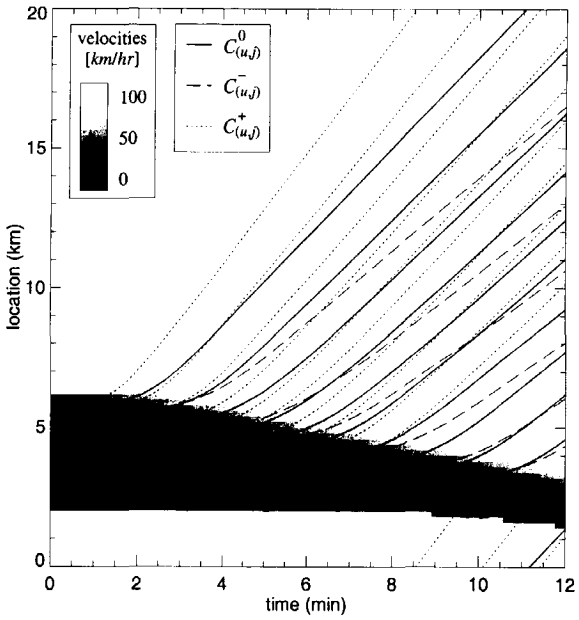

Figure 10-2: *Characteristics* and *iso-velocity contour-plot* of person-cars on right lane for "removal of blockade" scenario.

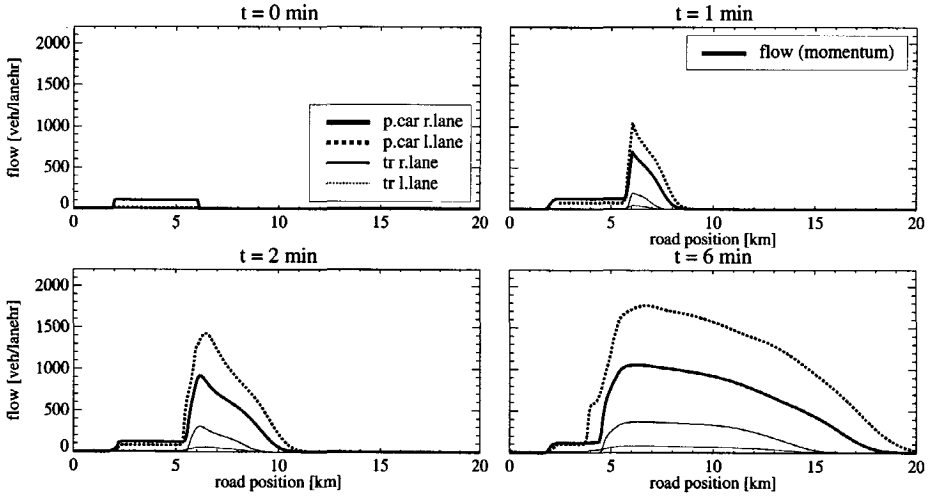

Figure 10-3: Traffic momentum dynamics by lane for person-cars and trucks for the "removal of blockade" scenario. Note that since the vehicles in the queue have a positive, albeit very low velocity, within-queue momentum is not equal to zero.

Notice that from the characteristics we can observe that vehicles do not instantaneously accelerate, but rather accelerate towards the desired velocity in a gradual way. Finally, let us observe that Figure 10-2 also shows how the fast vehicles in the stream traverse along the

$C^{+}_{(u,j)}$ characteristics. Figure 10-3 shows class-specific and lane-specific momentum dynamics. The figure shows the queue-dissipation behaviour at the queue-head ($x = 6km$). Notice that the momentum is a continuous function of x. In other words, the flow-rate is not discontinuous at the head of the queue where vehicles flow out of the queue respecting the queue discharge rate. This is caused by non-instantaneous acceleration behaviour of vehicles. That is, vehicles *gradually* accelerate from standstill to the acceleration velocity (Figure 10-2).

10.1.2 Unaffected slow vehicles

Daganzo's second criticism is the observed influence of the faster vehicles in the flow on the slower ones. In chapter 6 we have proved that the MLMC model developed in this thesis has the property that the slower vehicles (i.e. trucks) are not affected by the faster vehicles in the stream. Although we will not explicitly devote a simulation experiment to show the invariance of slower vehicles (cf. Hoogendoorn and Bovy (1998d)), the cases presented in sections 10.2-10.7 clearly reveal this model property.

10.1.3 Unchanged driver's personality

Daganzo also noted that drivers, unlike particles in a fluid or a gas, have *personalities* that remain virtually unchanged by the prevailing traffic conditions. He argues that macroscopic flow models do not satisfy this particularity of vehicular traffic. Let us briefly discuss the extent to which this condition is met by our model.

To this end, consider (comparable to the situation discussed above) a region (region I) of non-zero traffic densities of different user-classes. Moreover, let us assume that downstream of this region, a zero-density region is present (region II). We have observed that the fastest vehicles of region I flow into region II along Mach-line $C^{+}_{(u,j)}$. If we then assume that at some time t_1, these vehicles have reached location x_1, then we would expect that while the velocity is considerably higher than the expected desired velocity (see Figure 10-1), the *velocity variance* would be quite small, since vehicles that have arrived first approximately have the same velocity. That, slow vehicles – which combined with the presence of faster vehicles cause a relatively high velocity variance – have not yet arrived at x_1. However, the velocity variance in x_1 is approximately the covariance between the velocity and the desired velocity. This high variance in vehicular speeds indicates that of the fast vehicles having arrived at x_1, at least some *suddenly aim to drive at a lower velocity*. Consequently, the *personality* of drivers appears to have changed.

However, distinguishing user-classes does remedy this to a certain extent, since by class-distinction the velocity diffusion is reduced. Consequently, the velocity variance at x_1 *is considerably lower* in the multiclass case than in the aggregate-class case. Moreover, we can disaggregate the classes even further, for instance by considering the slow and fast drivers in a class, or even a more refined classification. In this limiting case, the velocity variance converges to a small value, reflecting the variability of the speeds of individual drivers. Concluding, in principle the model satisfies the 'unchanged driver personality', provided that an adequate number of user-classes are distinguished.

From another viewpoint, the developed model does convey user-class personalities, by explicitly considering several *class-specific parameters* such as desired speeds, acceleration times, vehicle lengths, and within-class velocity variances. Since these characteristics are *in-*

variant to prevailing traffic conditions, in this context, the MLMC model established in this thesis does reflect constant personalities of drivers.

10.2 Traffic hysteresis and phantom-jams

In section 2.7.1 we have discussed the disability of LWR-type models to describe some phenomena observed in real-life traffic flow (e.g. hysteresis and phantom-jams. In addition, we have recalled that Payne-type and Helbing-type models *are* able to describe these phenomena. For instance, the latter models allow fluctuations around the equilibrium state, smooth shocks, traffic hysteresis, and the occurrence of localised structures and phantom-jams. In this section, we show that the discrete MLMC flow model is able to reproduce these (we will only discuss the non-trivial traffic hysteresis and phantom-jams).

10.2.1 Concepts of traffic hysteresis, localised structure, and phantom-jam

We have discussed how the dynamics of traffic flow result in the so-called hysteresis phenomenon. This phenomenon is characterised by drivers showing different behaviour when emerging *from a disturbance* compared to the behaviour of the same drivers approaching the disturbance (e.g. increasing headways). In other words, traffic flow and density are different after emerging from a kinematic disturbance compared with the platoon approaching the disturbance (Treiterer and Myers (1974)). Verweij (1989), Ferrari (1989), and Leutzbach (1991) have experimentally observed transients and the formation of start-stop waves.

These critical phenomena and phase-transitions that are the fundamental properties of a huge number of physical systems, may also occur in traffic flow when the vehicular density exceeds some critical value. Kerner and Rehborn (1997) show *the non-linear theory of a traffic cluster* effect in traffic flow, i.e. the effect of the appearance of a region of high densities and low velocities in initially homogeneous traffic flow. Kerner *et al.* (1996) use a macroscopic flow model to describe the occurrence of phantom-jams in the flow. These seemingly spontaneously occurring jams are the result of an *avalanche-like* process in traffic flow. In other words, their theory describes how a small perturbation in the traffic stream grows and yields the formation of a *localised structure*, eventually resulting in traffic breakdown.

10.2.2 Hysteresis and phantom-jams in MLMC traffic flow model

Figure 10-4 shows the formation of a phantom-jam described by the discrete MLMC model. The figure depicts the average-lane momentum (i.e. flow) in the multiclass stream, where the dark regions indicate a low momentum, while the light areas indicate high momentum areas. Figure 10-4 also shows the trajectories of person-cars and trucks respectively.

For one, Figure 10-4 shows how the flow upstream is higher than downstream of the congestion, while the velocity of the vehicles is approximately equal. This implies that drivers maintain a *larger time headway* when emerging *from* a disturbance than when approaching one. In other words, we can conclude that the discrete MLMC traffic flow model plausibly reproduces traffic hysteresis.

Secondly, the Figure 10-4 shows the spontaneous formation of congestion due to a small but critical perturbation (cf. Kerner and Konhäuser (1995)), in initial truck densities. The formed *nearly stationary* moving cluster has some characteristic features. At first, the amplitude of

the critical perturbation increases *very slowly* in time. However, the shape of this perturbation is gradually deformed. At some instant t near the maximum of $r(x,t)$, a local perturbation of density and average velocity is self-formed. This results from the increased number of interactions in the higher-density region, yielding a lower mean velocity. If the finite reaction and braking times of the drivers, having a *smoothing effect*, are dominant, then the localised disturbances will disappear. If not, the localised structure will continue to grow, eventually leading to traffic breakdown. The resulting local vehicle cluster is thus self-formed, and is surrounded by only slightly perturbed homogeneous traffic flow conditions.

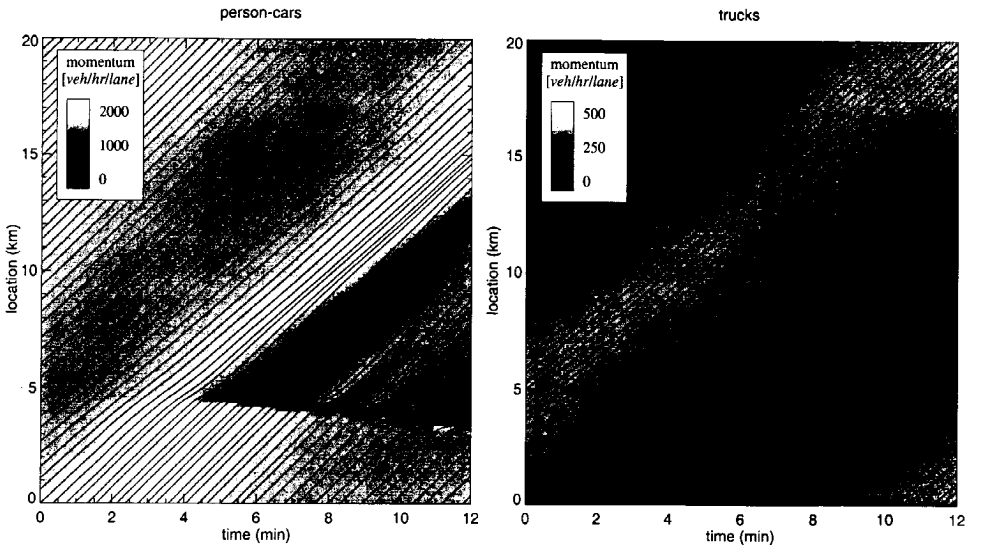

Figure 10-4: Iso-momentum contour-plot and average-lane trajectories of person-cars and trucks in case of the occurrence of a localised structure.

When this traffic breakdown has occurred, the vehicles that arrive in the high-density region are *held back* due to the low in-region velocities. This results in the formation of a low-density region *downstream* of the phantom jam. Further downstream, a *transition layer* is formed between this low-density region and the region of slightly disturbed homogeneous flow (Figure 10-5). In this transition layer, other localised structures can form, which eventually may lead to the formation of other phantom-jams. Kerner and Konhäuser (1996) show the kinetics of the cluster formation in the (r,m)-phase plane. They show that in this phase-space, the localised structure has roughly the shape of a triangle.

In the scenarios that are described in the remainder of this chapter, the formation of localised clusters and the resulting phantom-jams will arise in a number of different occasions. Since the model describes *multilane multiclass traffic flow*, reasons and the effects of cluster formation that can not be described by the aggregate-lane aggregate-class models of Kerner and Konhäuser (1995) and Kerner *et al.* (1996) can be studied. For instance, we will show that the *mixture of homogeneous regions of different traffic types* will cause the on-set of congestion. Moreover, we will also show the effect of traffic regulations (overtaking prohibition for trucks) and traffic management (variable speed limits) on the formation of localised struc-

tures in the flow. An interesting result is the increased traffic system's sensitivity for phantom-jam formation due to truck overtaking prohibition strategies.

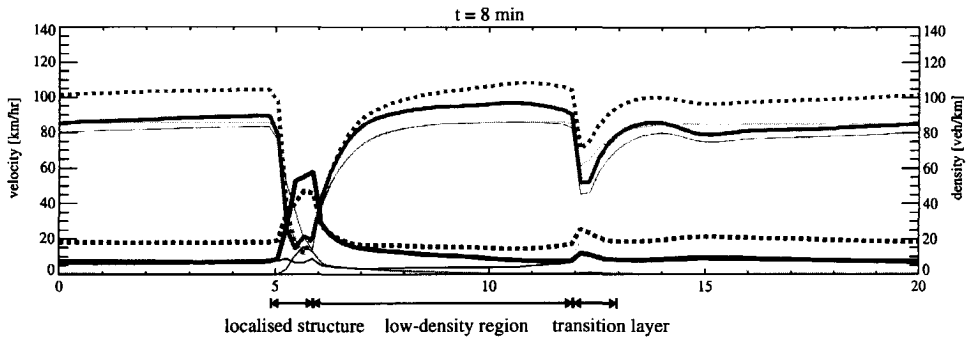

Figure 10-5: Localised structures in multiclass multilane traffic flow.

10.3 Mixing of vehicle classes

In this section, we will illustrate some of the multiclass mechanisms by a test-case in which we study the effects on the flow operations due to mixing vehicle classes. To this end, let us reconsider the twenty kilometre two-lane ringroad, and *three* homogeneous regions present at $t = 0$ (see Figure 10-6).

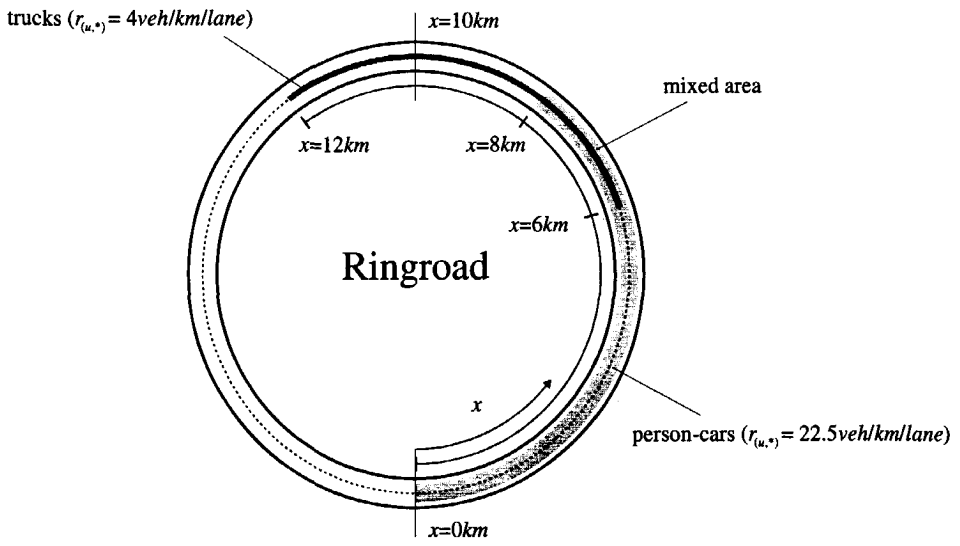

Figure 10-6: Schematics of the two-lane ringroad and the initial distribution of person-cars and densities.

The first region I = [0*km*,6*km*) consists of person-cars only. The second region II = [6*km*,8*km*) consists of both person-cars and trucks, while the third region III = [8*km*,12*km*) consists of trucks only. We assume that initially, traffic is in equilibrium. We will now study the traffic operations resulting from the model for $t > 0$. Let us emphasise that this scenario cannot be described by traditional aggregate-class flow models.

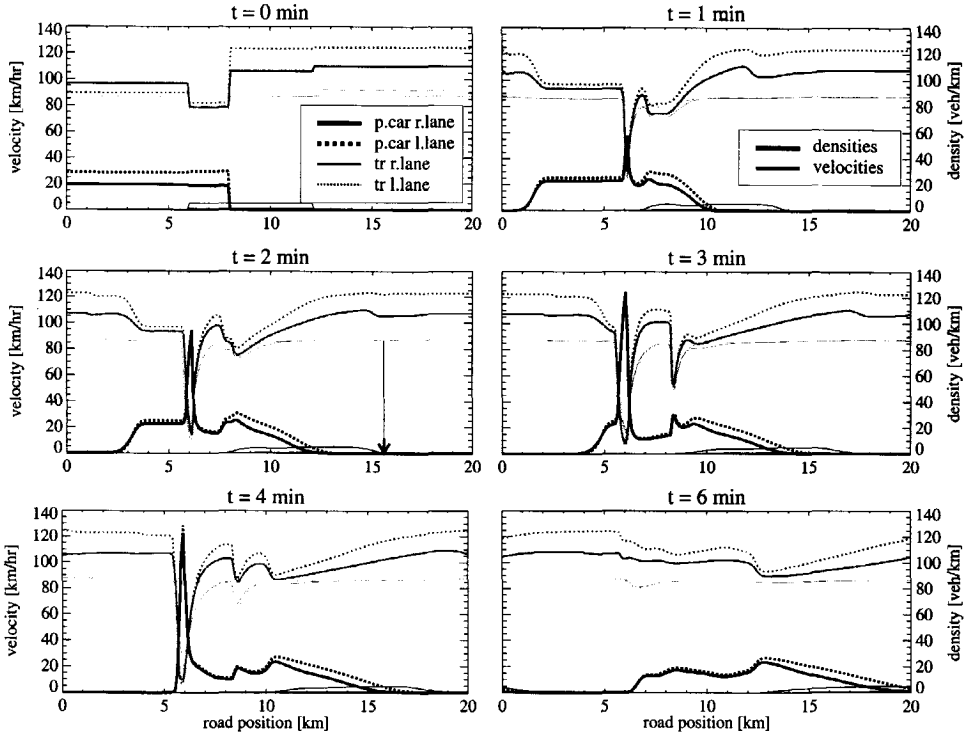

Figure 10-7: The occurrence of congestion due to merging traffic flows.

Figure 10-7 shows the results of macroscopic simulation for the mixing traffic scenario. Let us discuss some of the resulting phenomena. First, we observe that the trucks at $x = 12km$ flow into the empty roadway section, headed by the fastest trucks within the truck-class. In illustration, considering instant $t = 2min$, the trucks are located at approximately $x = 15km$. These vehicles have travelled at a velocity of approximately $90km/hr$, which is considerably higher than the average desired speed of trucks. They have travelled along the Mach-line $C^{+}_{(u,j)}$ of the flow, defined by $dx/dt = (V_{(u,j)}+(3\Theta_{(u,j)})^{1/2})$ (see section 7.5 and Figure 10-8).

Secondly, note that the fast person-cars flowing from the mixed traffic region II into the truck only region III *do not affect the velocities of the slower trucks*[*]. Clearly, the opposite is not true: the velocities of the person-cars flowing from the person-car only region I into the mixed region II are reduced due to the interaction with slower trucks and person-cars. Due to

[*] This model behaviour shows that the MLMC model meets the *unaffected slow-vehicles requirements*.

fast person-cars flowing from the upstream region I into the lower velocity mixed region I, a jam forms between I and II. That is, fast person-cars from region I interact with trucks and slow person-cars, resulting both in a decreased velocity and an increased density. The extent of this decrease and this increase in respectively the velocity and the density is such that more interactions with slower vehicles result, yielding an avalanche-like process that causes the formation of a traffic jam in the transitional area between the two regions. The mechanisms behind the seemingly spontaneously occurrence of congestion are similar to the mechanisms described by Kerner *et al.* (1996) with respect to aggregate-lane aggregate-class traffic flow.

Figure 10-8 shows the trajectories of trucks and the characteristics of person-cars on the left-lane for the "mixing of vehicle classes" scenario. The figure shows among other things how the fast person-cars flow into the truck-only region (thick-lined trajectories). Moreover, we observe that the congestion is formed downstream of the trucks region, and that the latter are consequently unaffected by the jam.

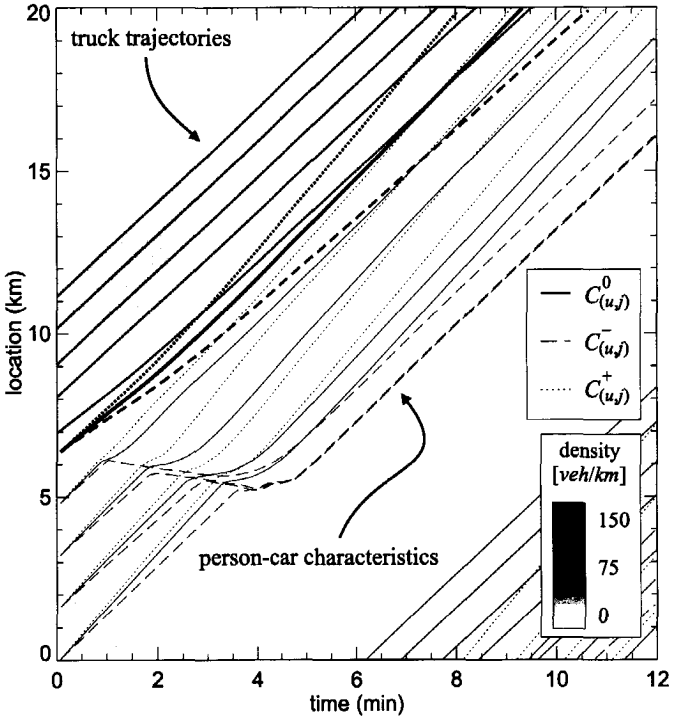

Figure 10-8: Truck density contour plot, truck trajectories, and person-car densities on the right-lane for "mixing of classes" scenario.

10.4 Two lane drop scenarios

The second test case describes the traffic conditions on the $20km$ two-lane ringroad at lane drops. The lane drop area is located at $X = [10km, 13km]$ (see Figure 10-9). We will consider

both a right-lane and a left-lane drop. In either case, upstream of the lane drop, both person-cars and trucks are present. We assume that at $t = 0$, traffic conditions are in equilibrium. The lane-drop is modelled by placing *motionless phantom-cars* (see appendix I) on the right and left-lane respectively. The merging area $X_1 = [10km, 10.5km]$ contains an increasing number of phantom vehicles, while the region $X_3 = [12.5km, 13km]$ contains a decreasing number of phantom vehicles on the right and left lane respectively. The presence of these phantom-vehicles causes an increased interaction-rate, yielding on the one hand an increase in the number of lane-changes to the left lane, and on the other hand, a decrease in the expected velocity on the right-lane. The actual lane-drop is located in the region $X_2 = [10.5km, 12.5km]$. In this area, no vehicles may be present.

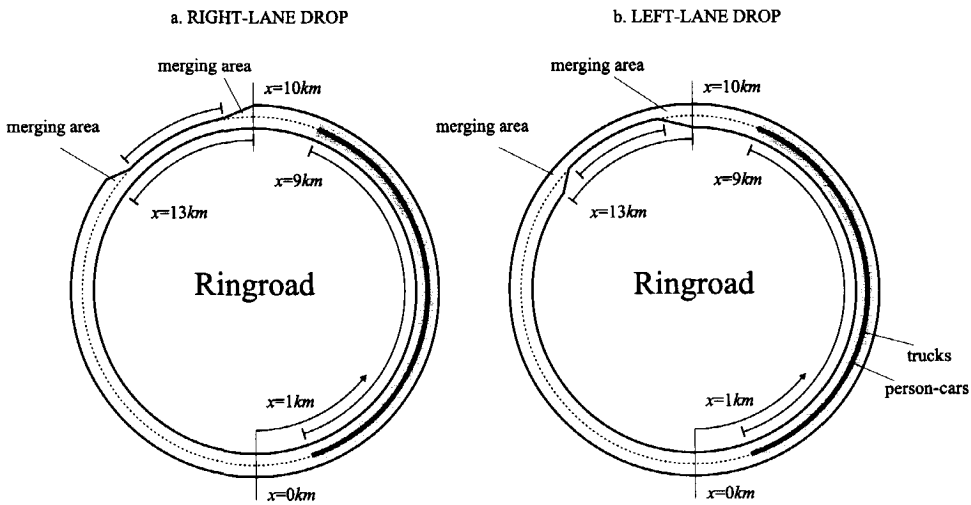

Figure 10-9: Schematics of the right-lane drop (a), the left-lane drop (b), and the initial distribution of person-cars and trucks on two-lane ringroad.

10.4.1 Right-lane drop

Figure 10-10 shows macroscopic simulation results for the right-lane drop. The figure indicates both densities, path-lines C^0 and Mach-lines $C^{\pm}$ of person-cars and trucks. As was shown in section 7.5, the characteristics show how disturbances are transported in the MLMC stream. The path-lines are the trajectories of the average vehicles of the class. The Mach-lines C^+ reflect the influence of the fastest vehicles of the class on the downstream traffic conditions. Finally, the C^- characteristic reflect the way in which information is transported.

Figure 10-11 shows density surface plots for the same case. Let us briefly elaborate upon these results. The figure shows that when person-cars arrive at the lane-drop ($t \approx 1min$), vehicles manage to manoeuvre themselves onto the left-lane, causing the (person-car) density on this lane to increase, while emptying the right-lane. Trucks arrive at the lane-drop at a later instant. Initially, these are also able to change to the left-lane. From the trajectories of these vehicles, we can conclude that these vehicles are able to pass the lane-drop nearly unaffected.

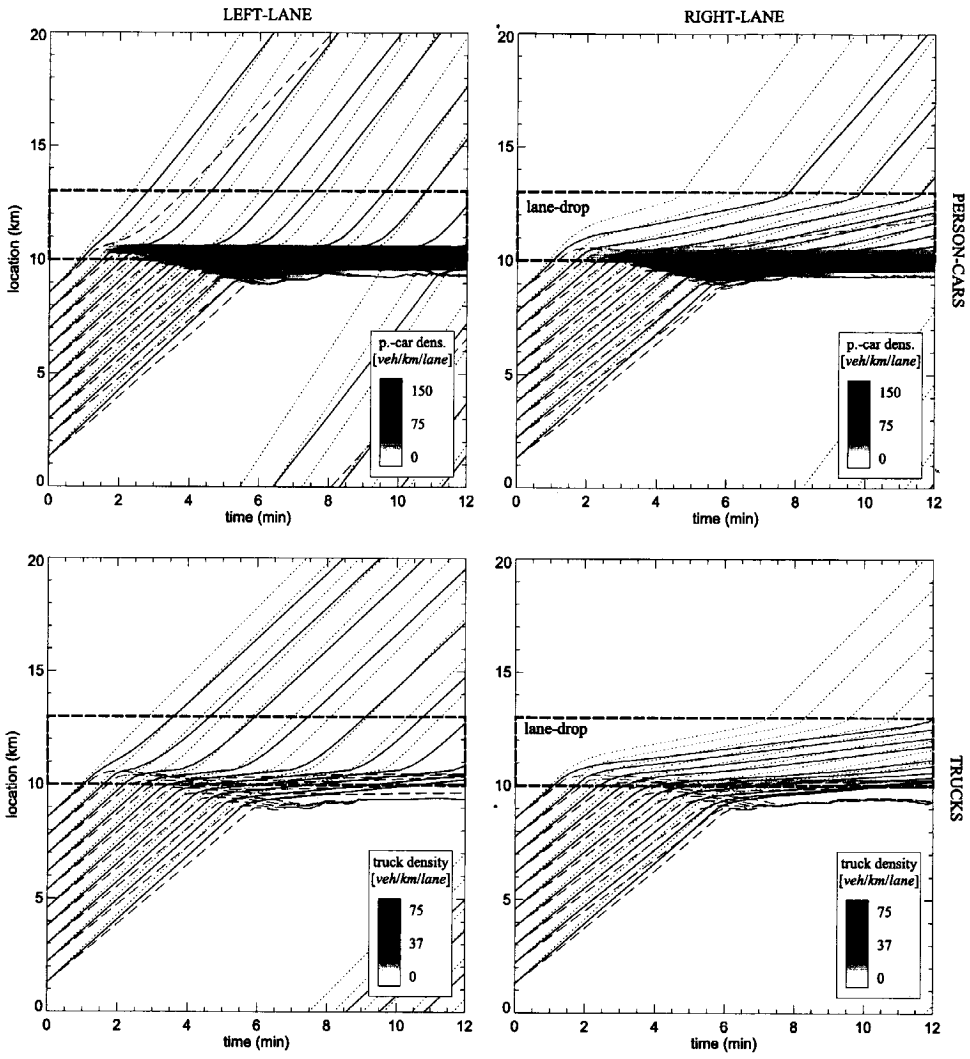

Figure 10-10: Density contour plots and characteristic curves for right-lane drop scenario. Although no vehicles occupy the right-lane in the lane-drop area, both values of the velocity and the variance have been determined, resulting in the characteristic curves in the lane-drop region. Note that in the congested region, the intersection C^- characteristics move upstream.

However, after some time ($t > 2min$) the density on the *left-lane* increases to such an extent, that not all vehicles are able to immediately change lanes and flow into the bottleneck-area. Moreover, since the density on the left-lane increases, the resulting increase in the number of vehicular interactions causes the left-lane velocity to decrease as well. Note that the region of high left-lane densities is located *in the bottleneck* (at $x \approx 10.7km$) rather than upstream of it (see Figure 10-10). Since the vehicular spacing on the left-lane decreases, so will the probability that a driver on the right-lane can immediately change lanes to the left. Consequently,

the density and the velocity on the *right-lane increases* respectively *decreases* as well, resulting in congested traffic conditions on the right-lane. Note that this queue is located *upstream of the bottleneck* ($t = 4min$). As time goes by, the queue on the respective lanes increases (until $t \approx 6min$; see Figure 10-10). When all vehicles present have joined the queue, the queue will slowly dissipate.

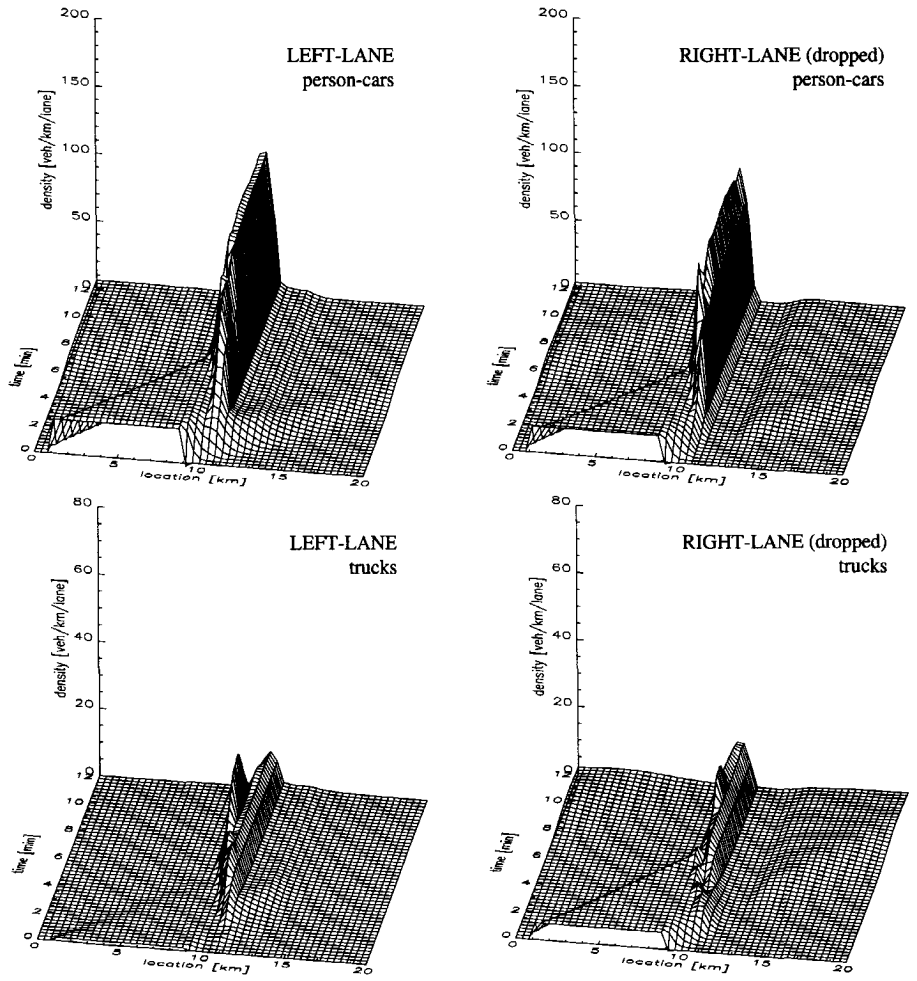

Figure 10-11: Density surface plots for person-cars and trucks on two-lane ringroad in case of a right-lane drop.

Finally, note that some of the person-cars that arrive at the end of the lane-drop ($x = 13km$) change back to the right roadway lane. The same holds for the trucks (after some time *nearly all* vehicles of the truck-class change back to the right-lane).

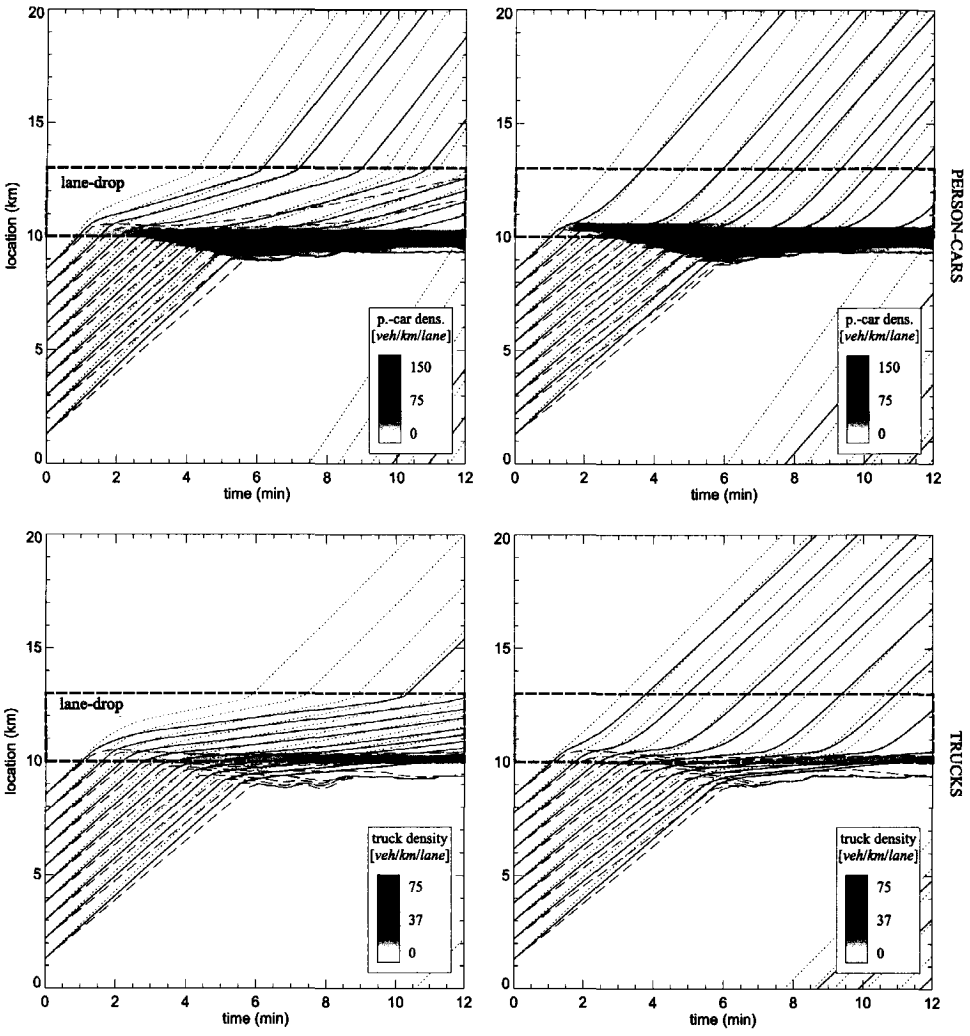

Figure 10-12: Density contour plots and characteristic curves for left-lane drop scenario. Although no vehicles occupy the left-lane in the lane-drop area, both values of the velocity and the variance have been determined, resulting in the characteristic curves in the lane-drop region. Note that in the congested region, the intersection C^- characteristics move upstream.

10.4.2 Left-lane drop

Similarly, we have considered the resulting traffic operations in case of a left-lane drop. We predict that the left-lane drop will yield improved truck operations, since the impaired lane-changing performance of the trucks will not be of much influence. Figure 10-12 shows the densities and the characteristics of the respective classes in case of a left-lane drop. From this figure, similar conclusions can be drawn as in the right-lane drop scenario.

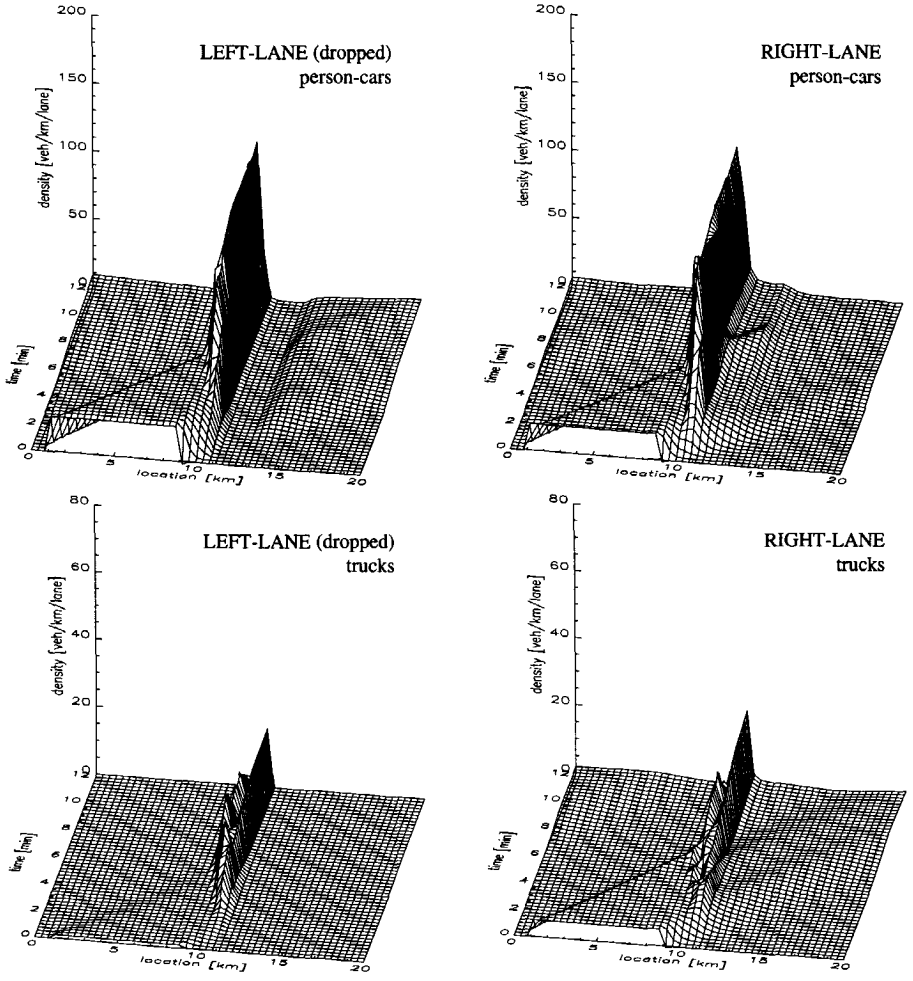

Figure 10-13: Density surface plots for person-cars and trucks on two-lane ringroad in case of a left-lane drop.

Figure 10-13 shows densities of person-cars and trucks on the respective ringroad lanes. The figure clearly shows how the left-lane is cleared of person-cars upstream of the lane-drop at $x = 10.5km$. In addition, the figure shows that some person-cars change back onto the left-lane after having passed the bottleneck at $x = 13km$.

One remarkable observation is the increased truck density on the left motorway lane. The reason for this is twofold: on the one hand, the small numbers of trucks that are present on the left-lane drive into an low-velocity area upstream of the lane-drop. The poor overtaking performance of the trucks, and the need to slow-down yields the formation of a high-density truck region. On the other hand, trucks on the right-lane that flow into the congested area starting at the beginning of the bottleneck extending its tail in the upstream direction. The

trucks take remedial actions, resulting in some trucks changing to the left-lane *right in front of the bottleneck*. That is, since vehicles are modelled as unconscious particles that do not anticipate on future events, the truck drivers have no incentive to keep their lane right in front of the bottleneck. This problem can however be easily remedied by assuming that vehicles at a certain upstream distance of the bottleneck do not change lanes.

Table 10-1: Average velocities [*km/hr*] and velocity standard deviations [*km/hr*] of person-cars and trucks on the lanes of the ringroad in the right-lane drop and left-lane drop scenarios.

	user-class:	*person-cars*			*trucks*			*overall*		
scenario	lane:	1	2	*	1	2	*	1	2	*
right-lane drop	V	56.9	68.8	62.3	61.6	22.2	52.1	57.6	65.7	61.1
	$\Theta^{1/2}$	40.3	45.3	43.1	31.12	27.4	34.7	39.0	45.9	42.3
left-lane drop	V	56.3	63.9	61.0	62.5	36.9	52.9	57.4	61.9	60.2
	$\Theta^{1/2}$	41.8	45.4	44.2	30.6	33.2	34.0	40.1	45.2	43.2

Table 10-1 shows the average simulation period results for both scenarios. This table shows that the mean velocity of all vehicles is slightly decreased in case of a left-lane drop instead of a right-lane drop. However, if we consider class-specific results, we see that the right-lane situation is only better for the person-cars (having adequate overtaking capabilities). The trucks' velocities are slightly higher in the left-lane drop case*.

10.5 Effects of an incident

In this section, we macroscopically simulate the effects on an incident. To this end, let us again consider the ringroad. In this case, we assume initially homogeneous traffic conditions, with lane-average densities $r_{person\text{-}car}(x,0) = 15 veh/km/lane$ and $r_{truck}(x,0) = 2 veh/truck/lane$ for $0 \le x \le L$. Let us assume that the incident occurring at $t = 1 min$ blocks the right-lane of the two-lane motorway during a two minute period $T = [60s, 180s)$. Figure 10-14 shows the resulting MLMC traffic dynamics for this incident scenario.

Only a few sections after the occurrence of the incident, all vehicles have changed lanes to the left roadway lane. The mechanisms that cause this have been described in section 10.4 describing the traffic conditions in case of a lane-drop. However, in opposition to the lane-drop scenario, the incident is cleared at $t = 3min$.

Nevertheless, the increase in the density and the resulting decrease in the velocity upstream of the incident ($x = 9km$) cause a traffic jam to occur. This jam persists during the entire simulation period. Similarly to the results reported by Kerner and Rehborn (1997), the MLMC model identifies the jam as an intrinsic traffic state. Note that the jam moves upstream at a low velocity (at approximately $7.5 km/hr$).

As with the other scenarios, the formation of the traffic jam is dependent on the region in which the system operates at the time a disturbance occurs: if the system operates in the *sta-*

* Differences are only moderate due to the immediate lane change activities of trucks upstream of the bottleneck.

ble region, a small disturbance will not result in a persisting traffic jam. However, if the traffic system is operating in *metastable region*, the jam resulting from the disturbance will persist during a considerable time.

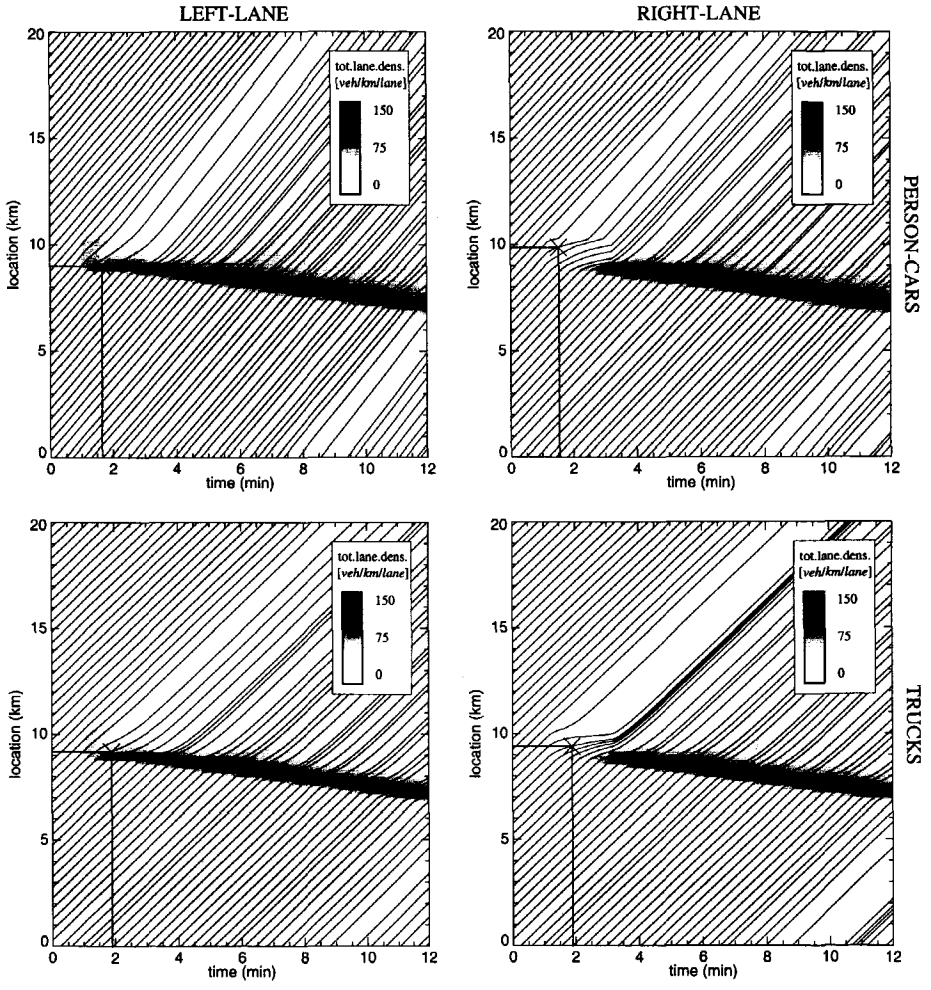

Figure 10-14: Trajectories of person-cars and trucks on the left-lane and the right-lane of the two-lane ringroad, and the aggregate-class lane-specific densities for the incident-scenario. The figure indicates the moment and location at which congested conditions occur, based on the criterion proposed in section 7.5.

In illustration, the predicted effects of the incident have been determined for different initial conditions, leading to very dissimilar results. Considering the MLMC traffic conditions at very low initial densities (Figure 10-15; $r_{person\text{-}car} = 8 veh/km/lane$ and $r_{trucks} = 1 veh/km/lane$), the effects of the incident rapidly dissolve. However, when the initial densities are higher

(Figure 10-16; $r_{person\text{-}car} = 30veh/km/lane$ and $r_{trucks} = 2veh/km/lane$), the incident leads to the occurrence of several localised traffic clusters.

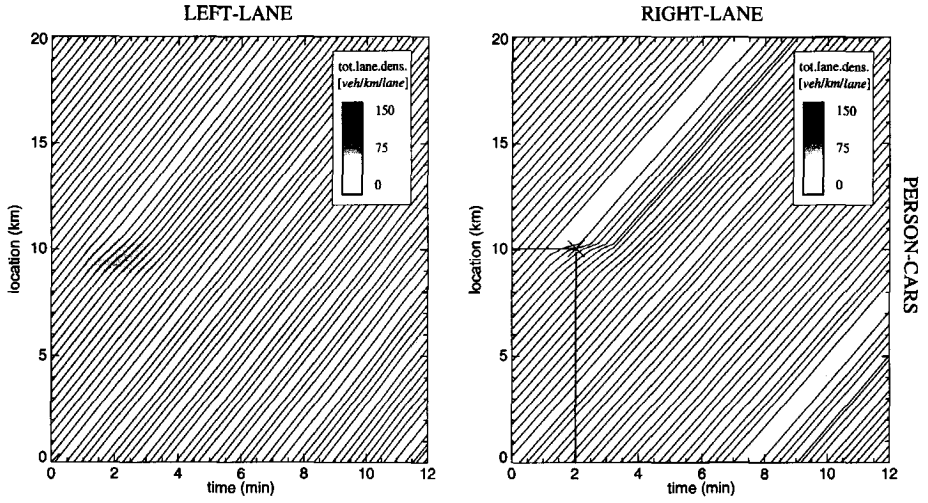

Figure 10-15: Trajectories of person-cars for incident scenario with low-density initial conditions. Clearly, the effects of the incident dissipate rapidly.

Finally, we have also considered results of a longer-lasting incident (5 minutes instead of 2 minutes). As is shown in Figure 10-17, the width of the formed congestion is larger compared to the two-minute incident scenario (compare Figure 10-14).

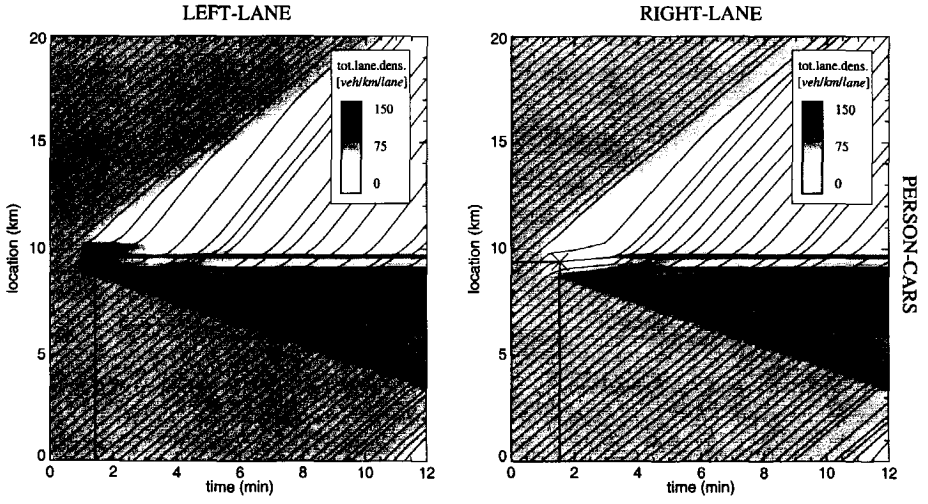

Figure 10-16: Trajectories of person-cars for incident scenario with higher-density initial conditions. The figure shows clusters moving upstream from the incident region.

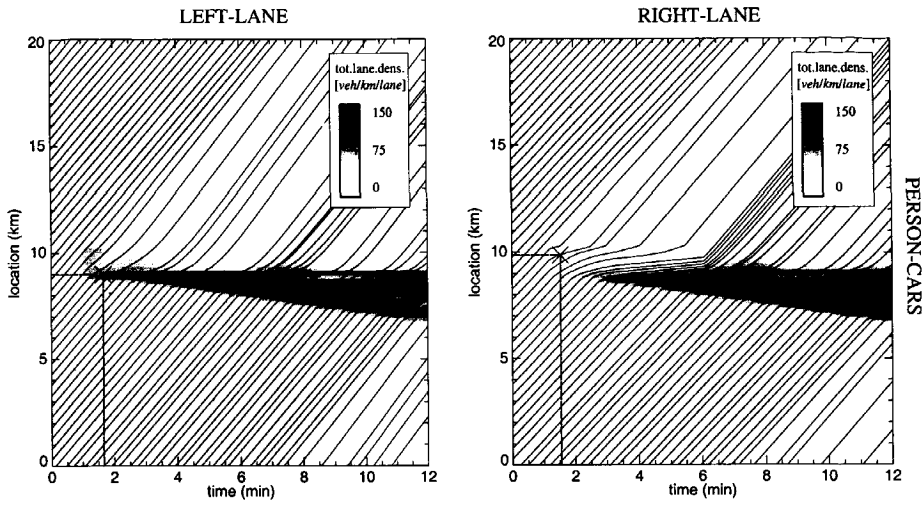

Figure 10-17: Person-car trajectories in case of a five-minute incident blocking the right lane of the ringroad.

10.6 Overtaking prohibition for trucks

In the remainder of this chapter, we will consider some practical applications of the MLMC model from an *impact assessment perspective*. For instance, in this section we will study the effects of a truck overtaking prohibition on a two-lane motorway. This is done by comparing traffic operations for two different situations (trucks either being allowed to use the left 'overtaking-lane' or not). The truck overtaking prohibition is incorporated in the model by setting the truck overtaking probabilities from the right lane to the left lane equal to zero.

In studying effects of truck overtaking prohibitions by macroscopic simulation, several cases have been considered. In this section, we discuss the most interesting findings.

10.6.1 Real-life studies and empirical findings

The objective of this traffic management measure is two-fold:

1. Improve traffic flow operations (increase traffic flow and capacity).
2. Increase traffic safety.

The overtaking prohibition can be operationalised in a number of ways. In the Netherlands, the most common option is to employ a static sign indicating the prohibition, in some cases completed with an additional sign indicating the period when the prohibition is active.

It is generally believed that a truck overtaking-prohibition yields a positive effect on traffic flow operations, based on the notion that an overtaking truck may cause the appearance of a shock wave. However, in practice, overtaking prohibitions for trucks have resulted in mixed

outcomes. Table 10-2 summarises evaluation results with respect to truck overtaking prohibition on Dutch motorways. The differences in findings are remarkable.

Table 10-2: Overview of empirical truck overtaking prohibition evaluation studies in the Netherlands.

case*	ref.	time†	quantitative effects	qualitative effects	add. remarks
t A2 Limburg	Goudappel Coffeng (1996a)	a	• total flow slightly increased • slight increase velocity person-cars at expense of trucks • changes in capacity unknown	• homogeneous flow operations • less disturbances	no periods with congestion during pilot
s A2 Limburg	Goudappel Coffeng (1996b)	a	• no effect on flow • changes in capacity unknown	• homogeneous flow operations • less disturbances	no periods with congestion during pilot
s A50 Arnhem	Heidemij (1996)	a	• slight increase in capacity • moderate decrease of velocity	• decreasing number overtakings on right • formation of truck-platoons	
s A50 Arnhem	Goudappel Coffeng (1998)	e	• slight improvement flow conditions (increased velocity 7-9%)‡ • moderate decrease of velocity	• very poor acceptance	other factors present during pilot study
s A9 Badhoevedorp	Goudappel Coffeng (1998)	n	• worsening traffic conditions (decreases velocity 16-18%) • decrease capacity (4%)	• no apparent differences	accelerated onset congestion
d A16	AGV (1999)	e + m	• increase capacity (3.6%) • velocity small volumes / high volumes (-1% / +2%)	• positive effect flow operations and safety • generally good acceptance	

Similar studies have been performed in Germany. By considering a pilot study in Nordhein-Westfalen, Lühder (1990) shows empirically that for traffic volumes below 1500*veh/lane/hr*, overtaking prohibitions are not useful. The author recommends installing overtaking prohibitions only when volumes are higher than 1500*veh/lane/hr*, and only when the fraction of trucks is below 6%. Another pilot study in Germany (*Baden-Württemberg*) reveals a moderately positive effect with respect to both the velocity and the traffic volumes, while other studies show negative effects, such as the formation of truck-platoons (*Hessen*). For an overview of these German studies, we refer to Drews (1996).

* Static, time-of-day dependent, or dynamic truck overtaking prohibitions.

† Restricted to morning period, evening period, or all day.

‡ Due to the presence of other factors, this increase can only be partially attributed to the overtaking prohibition.

Initial conditions

The initial conditions are determined by assuming that the aggregate-lane person-car density $r_{(1,*)}(x,0)$ for cells i at time $k = 0$ equals $24veh/km$. Initially, the trucks are confined to the right roadway lane. The spatial density distribution of trucks is given by the conditions $r_{(2,1)}(x,0) = r+\delta r\cdot(1+\sin(2\pi x/L))$ and $r_{(2,2)}(x,0) = 0$, where r and δr are constants determining the truck density. Using the calibration approach presented in chapter 8, we can determine the lane-specific density, momentum, and energy for both the trucks and the person-cars. These serve as initial conditions $\mathbf{r}(x,0)$ for $0 \le x \le L$ for our simulation experiments.

10.6.2 Case 1: effects of truck overtaking prohibition for non-congested operations

In the first case, the values $(r,\delta r) = (3,0.25)$ have been used. In this case, neither for the regular scenario, nor for the truck overtaking prohibition scenario, congestion occurs. For both strategies the density $r_{(u,j)}[i,k]$, the momentum $m_{(u,j)}[i,k]$, and the energy $e_{(u,j)}[i,k]$ are recorded for each cell i and period k. By addition of these conservatives with respect to location i and period k, the total density, momentum, and energy $r_{(u,j)}$, $m_{(u,j)}$ and $e_{(u,j)}$ can be determined, which can consequently be used to determine the average velocities and velocity variances of the respective classes during the simulation period. Using this approach, the macroscopic simulation outcomes shown in Table 10-3 have been determined during a twelve-minute simulation period.

Table 10-3: Mean velocities [*km/hr*] and velocity standard deviations [*km/hr*] with and without overtaking prohibition for trucks for non-congested situation.

	user-class:	*person-cars*			*trucks*			*overall*		
scenario	lane:	1	2	*	1	2	*	1	2	*
no prohibition	V	89.0	101.5	97.3	82.5	85.7	82.5	86.5	101.4	94.8
	$\Theta^{1/2}$	8.8	7.0	9.6	4.5	3.7	4.5	8.1	7.1	10.6
prohibition	V	88.8	101.5	97.4	82.3	-	82.3	86.4	101.5	94.8
	$\Theta^{1/2}$	9.0	7.1	9.8	4.8	-	4.8	8.3	7.1	10.7

Results shown in Table 10-3 reflect *very moderate* effects of the truck overtaking prohibition. As is foreseen, the average velocity of person-cars on the left motorway lane increases slightly at the expense of a slight decrease in average speeds of person-cars and trucks on the right motorway lane. Overall, there is a very small increase in velocities of person-cars at the expense of a small decrease in truck speeds, primarily occurring on the left roadway lane. The velocity on the right lane decreases slightly. The main reason for these *modest* changes is that given near free-flow traffic conditions, the number of lane-changing trucks is very small. In other words, the number of interactions of faster trucks and slower ones are very few due to the small velocity variance of the trucks. Thus, the average number of trucks on the left roadway lane is very small, even if no overtaking prohibition is active.

Let us also notice that the overtaking prohibition has a *negative effect* on the velocity variances. This small increase in the velocity variance can be explained by noticing that due to the overtaking prohibition, the smoothing effect which the trucks have on the between lane velocity difference disappears: although the number of fast trucks is very small (due to the low value of the velocity variance), the (slightly) faster trucks are not allowed to use the fast-

lane, yielding the following consequences. This increases the number of interacting trucks that need to decelerate, which then yields a decrease in the average velocity of trucks. That is, a truck 'bunching' effect appears. Due to this bunching effect, the number of interactions of fast person-cars with the slower trucks increases, resulting in an increased number of immediate lane-changes to the left motorway lane on the one hand, and on the other hand an increased number of person-cars unable to immediately change lanes, thereby increasing the velocity differences between the left-lane and the right-lane. Due to these larger differences in lane-speeds, lane-changing manoeuvres *increase the velocity variance*, since vehicles will not be able to immediately adapt their velocity after a lane-change*. Finally, the increased velocity variances will again result in more interactions between vehicles.

Concluding, for the non-congested regime, the overtaking prohibition causes only a slight increase in average person-car velocities at the expense of average truck velocities. At the same time, velocity variances increase, resulting in a chain of processes that yield an increase in the velocity variance of respective classes, and an increased between-lane velocity difference. In the following section, we will show that under critical conditions (i.e. density exceeds some critical value), the avalanche-like process causing aforementioned effects may result in more elaborate differences between the non-prohibition and prohibition strategies.

10.6.3 Case 2: accelerated occurrence of localised congestion

Let us now consider the case that the truck density is increased to the extent that the increased number of interactions of person-cars with these slower trucks yield the on-set of a jam. To this end, the truck constants $(r,\delta r)$ were set at (4,0.5), and the initial conditions were determined. For both the 'non-prohibition' as well as 'prohibition' scenario, these initial conditions cause spontaneous formation of a phantom-jam.

Table 10-4: Mean velocities [*km/hr*] and velocity standard deviations [*km/hr*] with and without overtaking prohibition for trucks for phantom-jam situation (large perturbation).

	user-class:	*person-cars*			*trucks*			*overall*		
scenario	lane:	1	2	*	1	2	*	1	2	*
no prohibition	V	83.4	94.9	90.5	80.3	61.0	79.4	82.7	94.5	89.1
	$\Theta^{1/2}$	19.3	17.6	19.1	8.6	29.6	11.5	17.3	18.1	18.7
prohibition	V	82.7	94.9	90.3	78.5	-	78.5	81.6	94.9	88.9
	$\Theta^{1/2}$	20.7	18.3	20.1	12.7	-	12.7	19.0	18.3	19.8

Figure 10-18 shows iso-velocity curves for person-car and truck velocities when trucks are allowed to use the left roadway lane. In the figure time and location of the on-set of congestion computed using the proposed congestion indicator (section 7.5.4) are indicated by a cross. Figure 10-19 shows the same curves when trucks are *not* allowed to use the left roadway lane. Clearly, congestion occurs approximately two minutes earlier (and approximately 500*m* upstream) in case of the overtaking prohibition. We also remark that in these cases, congestion occurs first on the right-lane. Table 10-4 shows results with respect to average

* This effect can be quantified by considering the dynamic equation for the velocity variance presented in section 7.2 of this thesis.

velocities and velocity variances of person-cars and trucks on the respective roadway lanes during the simulation period.

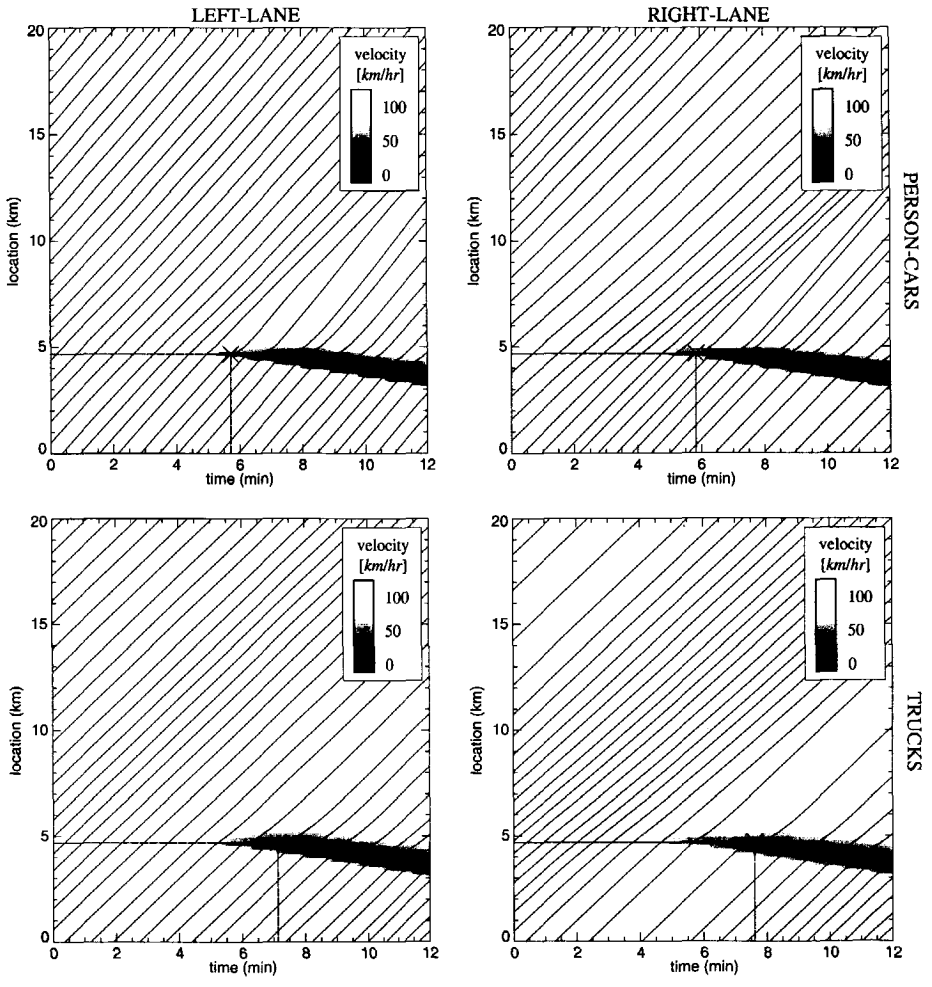

Figure 10-18: Velocity contour plot for person-cars and trucks when trucks are allowed to overtake slower vehicles using the left roadway lane. The cross indicates the location and time of the on-set of congestion.

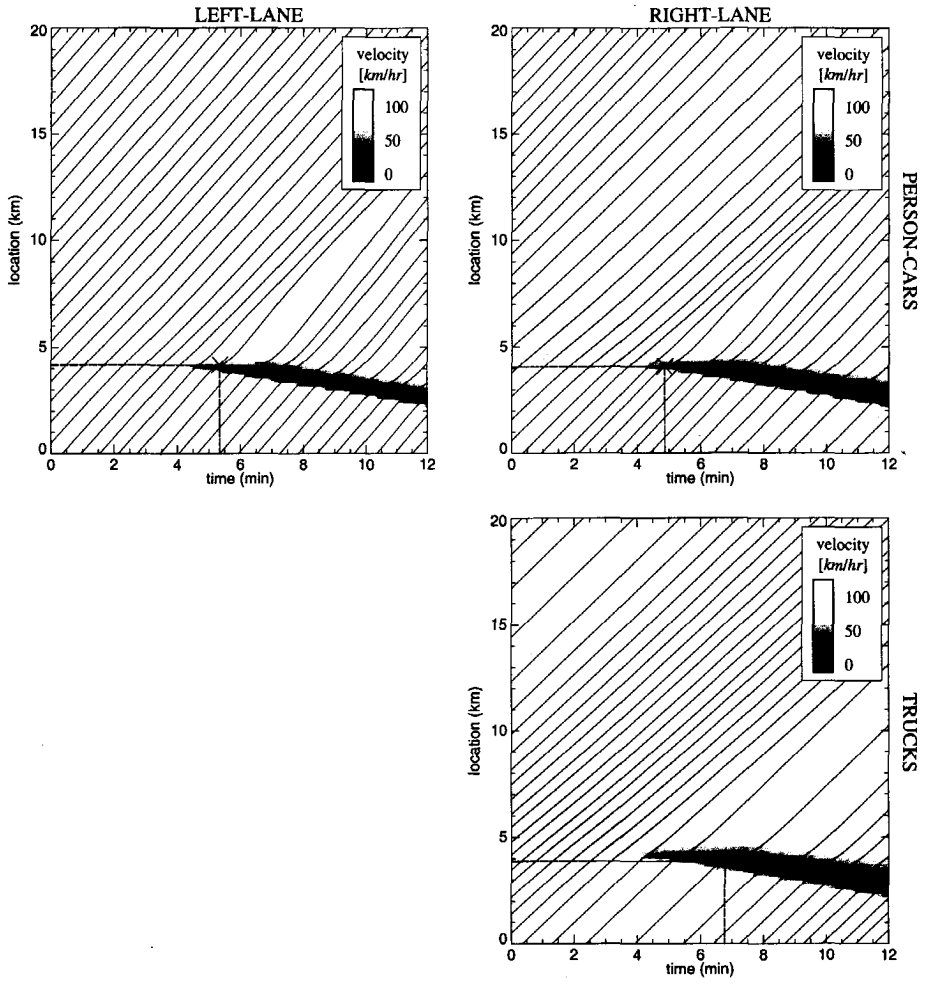

Figure 10-19: Iso-velocity curves for person-cars and trucks when the trucks-overtaking prohibition strategy is active. The cross indicates the location and time of the on-set of congestion.

We have also considered similar, but slightly less perturbed initial conditions. In this case, in the non-prohibition case, the disturbance dissolves after some time (Figure 10-20). However, for the overtaking prohibition scenario, the small disturbance in the truck density grows into a localised traffic jam (Figure 10-21). Table 10-5 depicts the results for both cases. Note that the negative impacts of the truck overtaking prohibition are even more clear in this case.

Table 10-5: Mean velocities [*km/hr*] and velocity standard deviations [*km/hr*] with and without overtaking prohibition for trucks for phantom-jam situation (small perturbation).

	user-class:	*person-cars*			*trucks*			*overall*		
scenario	lane:	1	2	*	1	2	*	1	2	*
no prohibition	V	88.8	101.4	97.2	82.3	85.7	82.3	86.3	101.3	94.7
	$\Theta^{1/2}$	8.9	7.1	9.7	4.7	3.7	4.7	8.2	7.1	10.7
prohibition	V	84.8	99.2	94.4	80.4	-	80.4	83.1	99.1	92.0
	$\Theta^{1/2}$	19.1	16.0	18.4	10.9	-	10.9	16.6	16.0	18.1

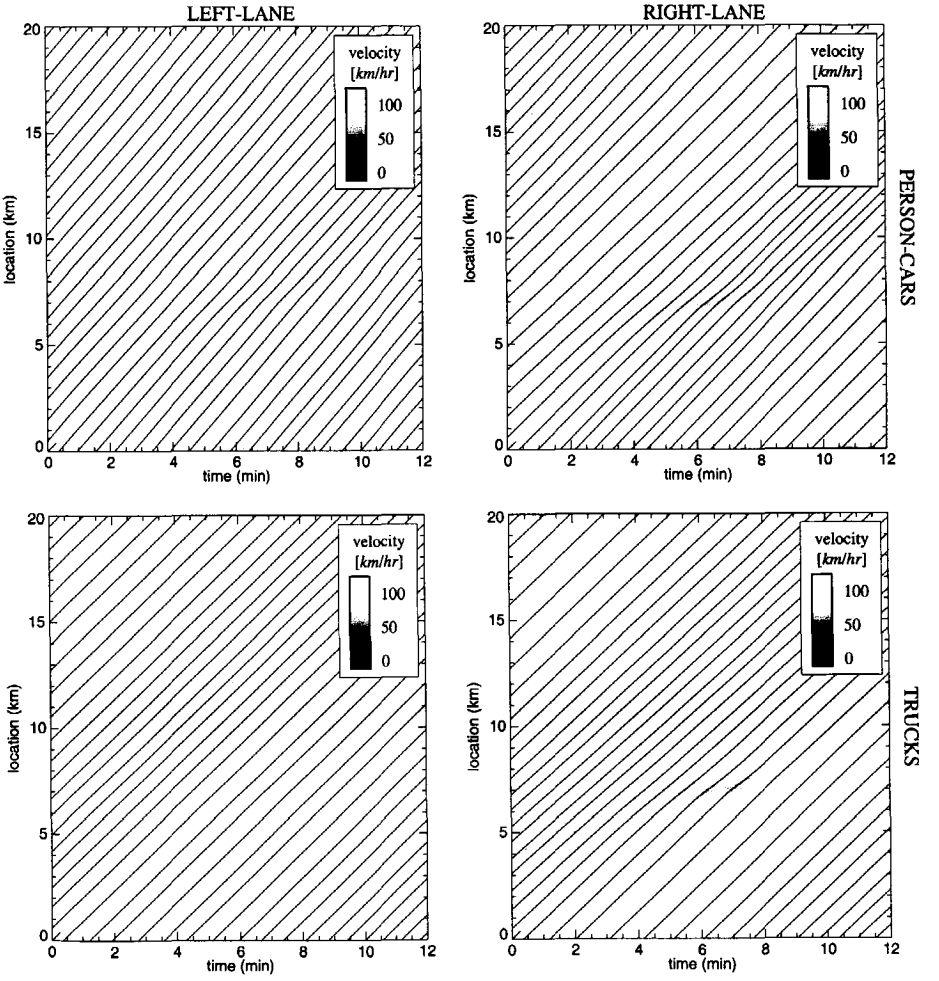

Figure 10-20: Velocity contour plot and trajectories for person-cars and trucks in case of slightly disturbed non-critical traffic conditions.

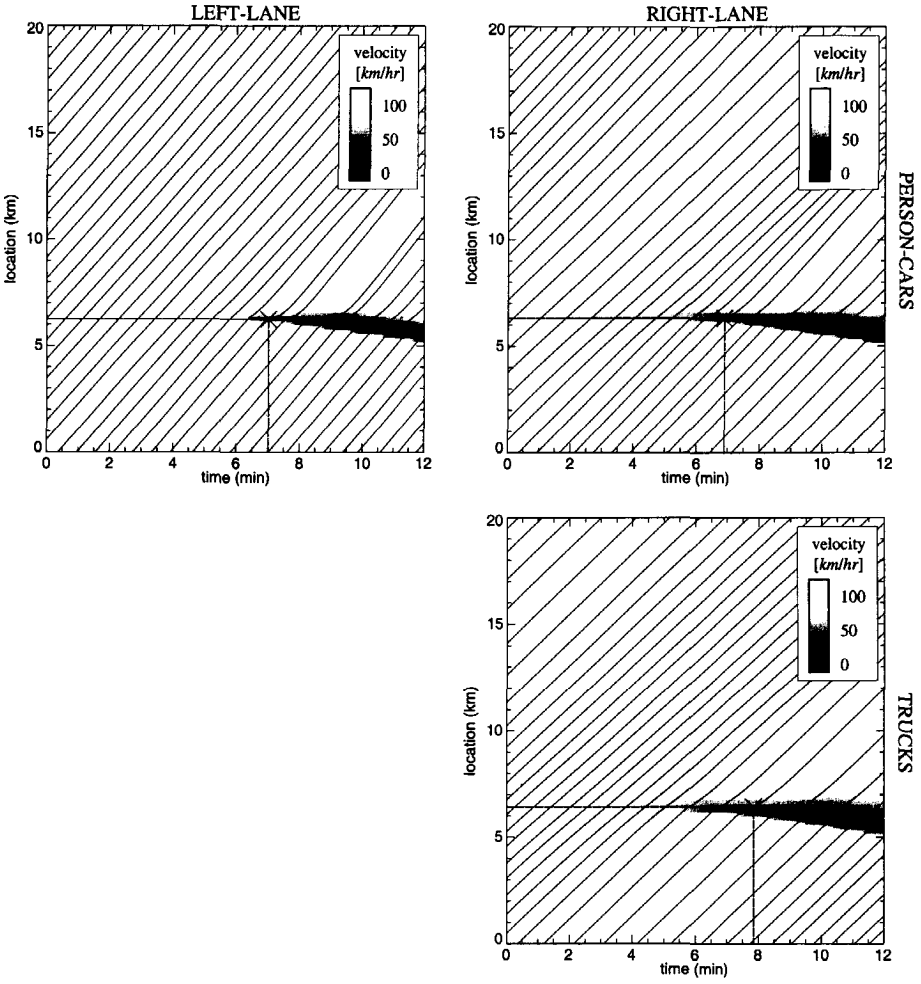

Figure 10-21: Velocity contour plot and trajectories for person-cars and trucks in case of slightly disturbed non-critical traffic conditions, when truck-overtaking prohibition is active.

Concluding, in this section we have considered the effects of a truck overtaking prohibition by macroscopic simulation. The MLMC model developed in this thesis predicts that such a prohibition is unfavourable, due to the increased observed velocity variances, and the increase in the between-lane velocity differentials. We have shown that these increased variances accelerate the on-set of congestion due to the increase in the number of interactions. Moreover, the macroscopic model predicts increases in the velocity variances and the increased differences in mean lane-speeds, which are undesirable from a safety perspective. However, the impacts are very moderate and may critically depend on the chosen model parameters (viscosity and kinematic coefficient, reaction time, etc.).

These results are not in accordance to the general belief that an overtaking prohibition for trucks will improve traffic operations and safety. We note that this belief is founded on the idea that under capacity-conditions, an overtaking truck may cause a shock wave thereby having a negative impact on traffic operations. However, when the traffic system is operating at its capacity, velocities of person-cars and trucks are (nearly) identical (see Helbing and Huberman (1998a)). In this case, an overtaking truck will not yield a shock wave.

However, we do stress that some of the aspects that may either be beneficial for the traffic system or not, have not been considered. For instance, we have implicitly assumed that minimal following distances of person-cars (or trucks) are independent of the followed vehicle. In real-life flow operations, person-cars (or trucks) following person-cars may very maintain different distance headways that person-cars (or trucks) following trucks. Clearly, this will have an effect on the capacity that is not considered by the model.

10.7 Variable speed control

A popular option in dynamic traffic management is *variable speed control* using Variable Message Signs. These VMS's display either a *speed limit* or a *speed advice*. The objectives of the system are among other things the detection of incidents, improved utilisation of the existing capacity, achieving greater safety, and enabling road repair works. In this respect, Van Toorenburg (1983) studied the effect of *homogenisation* (advisory speeds), aiming to achieve a traffic stream that is homogeneous with respect to velocity, distribution over lanes, etc. The following impacts were reported:

- The instability of traffic flow, measured by the number of serious speed drops, significantly decreases during homogenising control (about 50%).
- During control the capacity of the roadway increased slightly (about 1-2%).
- No significant effect was measured in other traffic characteristics (mean speed, speed differences, distribution over lanes, etc.).

In other words, the control has a double effect. Firstly, there is an (apparently fairly slight) effect on the average speed of the stream since the velocity of the (fastest) vehicles is affected. Secondly, there is a psychological response reflected by the increased driver's awareness, resulting in smoother linking-up when the queue tail comes into view (cf. Van Toorenburg and Van Der Linden (1996)). Therefore, variable speed control decreases both the spatial velocity derivative $\partial V/\partial x$ (smoothing the traffic by providing information on the conditions downstream) as well as the variance (slowing-down of the fastest vehicles in the stream). Consequently, homogenising may prevent the on-set of spontaneously appearing traffic jams. If so, the impacts of homogenising are likely to be very significant.

The benefits of variables speed control when congestion has already set-in is less clear, since the queue-dissipation rate at the head of the queue cannot be positively influenced by providing speed information. Rather, care should be taken *not to decrease* the dissipation rate by providing speed-limits at the queue-head that are below the critical velocity at capacity. Nevertheless, we will also consider the effect of homogenising at capacity situations.

10.7.1 Real-life studies and empirical findings

Variable speed control has been applied on several locations on Dutch motorways. Table 10-6 shows some results of field studies where VMS's have been used for variable speed control. Generally, it was found that speed homogenising control is not effective near bottlenecks. On the contrary, it is effective for busy, unsafe motorway sections (e.g. directly downstream of a bottleneck) (cf. Smulders and Van Den Hoogen (1994)).

Table 10-6: Variable speed limit control findings in the Netherlands.

case	ref.	quantitative results	qualitative results	add. remarks
A2	HEIDEMIJ (1993), GRONTMIJ (1999)	• decrease in velocity variance • no effects on capacity, or start-stop waves • small reduction in the frequency and severity of shockwaves	• traffic calmer • high user-acceptance • small shifts in traffic using the right roadway lane	
A20	De Kroes *et al.* (1983)	small reduction in average velocity.	-	speed-limits non-mandatory
A12	Kuipers *et al.* (1983)	capacity nearly unchanged	• increased stability of traffic	speed-limits non-mandatory

In the remainder of this section, we will study the effect of dynamic speed limit control using the developed MLMC traffic flow model. In doing so, several aspects of speed limit control will be studied. For instance, we will consider effects of among other things location of detectors with respect to the gantries, and driver's response to displayed speed limits.

10.7.2 Control strategy

Let us first discuss the control strategy employed. In this respect, let us assume that inductive loop detectors at distinct locations equip the considered two-lane motorway. These loops 'measure' the lane-specific velocity at the respective cross-sections. This is approximated by determining density and momentum of the lanes j of cells i where detectors are located. These lane-specific measurement are aggregated into average-lane observations (lane-specific speed limit control is discussed in section 10.8). The default distance between two consecutive loops is $500m$. Based on the measurements, each VMS displays a variable speed limit. The strategy implemented in this test-case example is similar to the strategy used on motorways in the Netherlands. The VMS displays a speed limit that is identical for all lanes. These speed limits are based on measurements from the downstream detector. That is, the displayed speed limit equals $50km/hr$, $70km/hr$, or $90km/hr$, if the measured velocity downstream is below $50km/hr$, $70km/hr$, or $90km/hr$ respectively. In addition, if the downstream sign displays a velocity of $50km/hr$, or $70km/hr$, then the upstream detector displays a speed limit of $70km/hr$, or $90km/hr$ respectively, provided measurements at the current detector do not indicate otherwise*.

* A more refined speed-control strategy is developed and analysed by Smulders (1989), and Mason and Woods (1998).

10.7.3 Driver's response to speed limits

The messages on the VMS's will have two consequences. Firstly, the mean velocity of the drivers decreases. Secondly, the velocity variance decreases. With respect to the changes in the velocity, we will assume that speed limit affects the desired velocity of the platoon-leaders. That is, we assume that this desired velocity is changed according to the following mechanism:

$$\overline{V}^0_{(u,j)}(x,t) = \min(V^0_{(u,j)}(x,t), V_{SL}(x,t) + \Delta V) \tag{10.1}$$

where $V_{SL}(x,t)$ is the speed limit indicated by the VMS. Since assessment studies of variable speed limits show drivers' ill-responsiveness (Van Toorenburg and Van Der Linden (1996)), the constant $\Delta V > 0$ is incorporated.

Due to the absence of adequate models describing the reduction in the velocity variance due to speed-homogenisation, we assume that the variance reduces to the same extent as the velocity. In other words, we assume that the *Coefficient of Variation* (CV) remains constant (see appendix F; figure F-1). Consequently, the controlled velocity variance becomes:

$$\overline{\Theta}^e_{(u,j)} = \Theta^e_{(u,j)} \sqrt{\overline{V}^0_{(u,j)} / V^0_{(u,j)}} \tag{10.2}$$

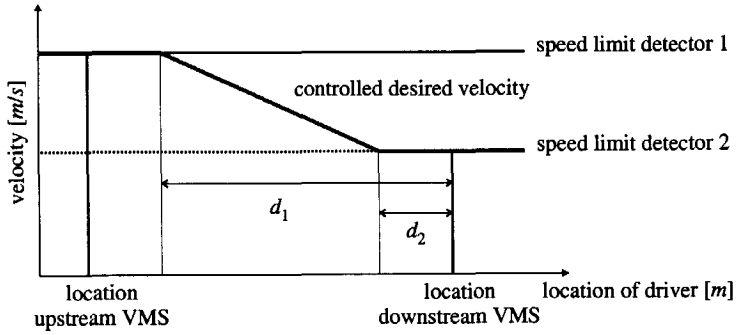

Figure 10-22: Driver's reaction to downstream VMS messages. A driver will consider the speed limit on the upstream VMS. When drivers approach the downstream VMS, they gradually adapt their desired velocity to the speed limit on the downstream sign.

Let us consider the *anticipation behaviour* of the drivers, reflecting the fact that drivers will look ahead to the downstream VMS and anticipate on the messages displayed on that sign. Let the constants d_1 and d_2, with $d_1 > d_2$ denote the *anticipation boundaries*. Let x_{DS} denote the location of the *downstream* VMS sign. Then, the following equation describes the effective speed limit that is considered by the drivers:

$$V_{SL}(x,t) = \begin{cases} V_{US} & x \le x_{DS} - d_1 \\ \alpha(x)V_{US} + (1-\alpha(x))V_{DS} & \text{elsewhere, where } \alpha(x) = (x - d_2)/(d_1 - d_2) \\ V_{DS} & x > x_{DS} - d_2 \end{cases} \tag{10.3}$$

where V_{US} and V_{DS} respectively denote the speed limits on the upstream and the downstream VMS signs. In other words, at $x = x_{DS}-d_1$ the influence of speeds displayed by the down-

stream VMS is zero, while on $x = x_{DS}-d_2$, the desired velocity of the drivers is completely determined by the message on the downstream VMS (see Figure 10-22).

In the remainder of this section, we will consider two scenarios. Firstly, we will reconsider the occurrence of phantom-jams resulting from small perturbations in the homogenous flow. Secondly, we will study the effects of speed-homogenising control in the case of incidents. Unless explicitly stated otherwise, we will use $\Delta V = 10km/hr$, $d_1 = 500m$ and $d_2 = 0m$ (default situation).

10.7.4 Phantom-jam prevention

Let us reconsider the scenario described in section 10.6 for the non-prohibition case. We have observed that due to perturbation in the truck densities a phantom jam emerged. The process of jam-formation due to localised structures has been explained in section 10.1. Figure 10-23 shows the results of a small perturbation in truck-densities on velocities of person-cars on the left roadway lane. The figure clearly indicates how the traffic jam persists during the entire simulation period.

However, when dynamic speed limit control is implemented, the phantom jam does not appear, since drivers are warned about downstream traffic conditions and are able to anticipate. In other words, the drivers do not drive into the high-density region as vigorously, where they would cause an increase in the traffic density and a decrease in the velocity. Rather, they slow down at the upstream location. Consequently, the phantom jam that would otherwise have occurred is not formed when dynamic speed limits are operational (Figure 10-23).

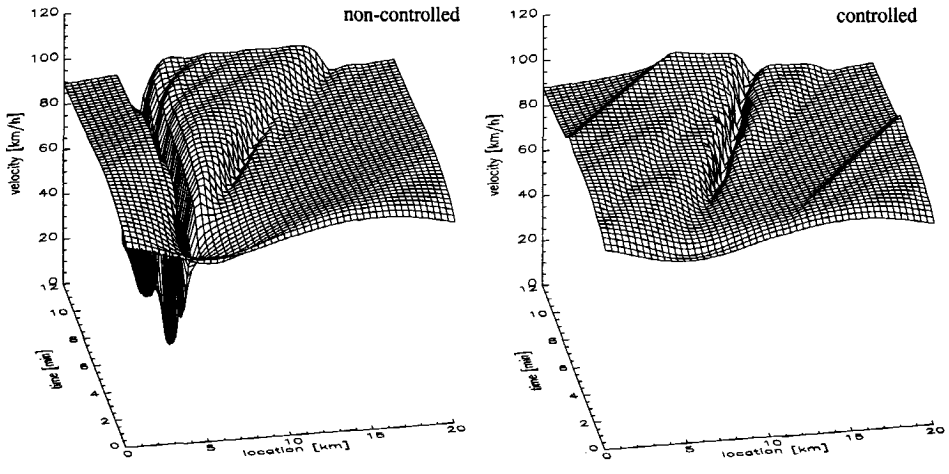

Figure 10-23: Velocity surface plot of person-cars on the right motorway lane for non-controlled traffic flow operations (left) and VMS-controlled flow operations (right).

If we compare the resulting performance of the system with and without variable speed limits, we can observe that the ability to withhold the on-set of congestion results in a very significant improvement of the system. From Table 10-7 we can observe that both average velocities of person-cars and trucks are increased significantly (from 94.7*km/hr* to 97.9*km/hr*,

and from 78.3*km/hr* to 83.5*km/hr*). Note that the increase is most noticeable on the *right roadway lane* (which is the lane where congestion occurs first; see section 10.6.3). Therefore, the between-lane velocity differentials are decreased, causing the variance to decrease further since the velocity of vehicles changing lanes is not that different from the velocities of the vehicles on the lane. The variance also decreases due to the variable speed limit itself. Both the decrease in the variances and the decrease in the between-lane speed differential are beneficial from a safety perspective.

Table 10-7: Mean velocities [*km/hr*] and velocity standard deviations [*km/hr*] with and without variable-speed limit control.

	user-class:	*person-cars*			*trucks*			*overall*		
scenario	lane:	1	2	*	1	2	*	1	2	*
no control	V	82.8	101.5	95.7	81.1	61.1*	80.0	82.0	100.5	92.2
	$\Theta^{1/2}$	25.2	19.7	23.2	8.8	29.9	12.1	19.3	21.0	22.2
control	V	90.7	100.2	97.3	83.4	85.2	83.4	87.1	100.1	94.4
	$\Theta^{1/2}$	8.9	8.0	9.3	4.4	3.9	4.4	7.9	8.1	10.3

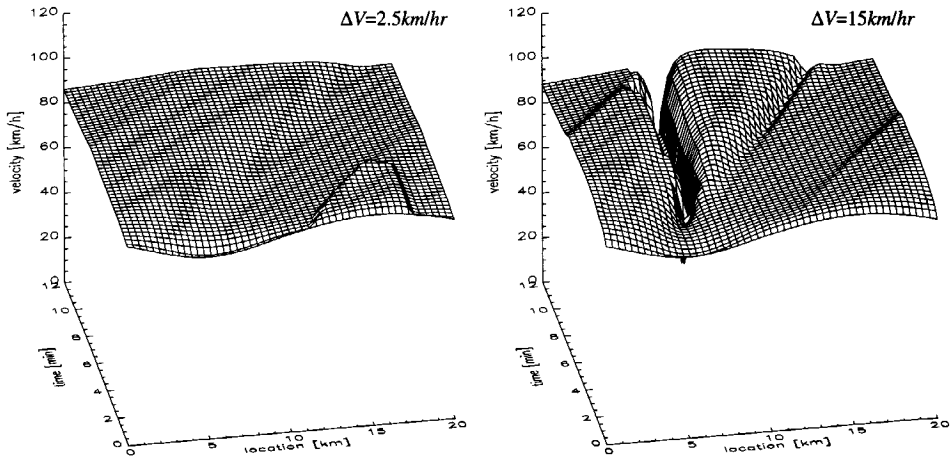

Figure 10-24: Effect of response-shift ΔV on the effectiveness of the speed-homogenising control.

Influence of driver's response

We have studied the effect of both the response-shift ΔV and the anticipation distances d_1 and d_2. With respect to the former, we have observed that high-valued ΔV has a negative impact on controller effectiveness. That is, while choosing ΔV small yields improved traffic condi-

* The average velocity is determined by considering average velocities during the simulation period, weighted by the number of vehicles having these velocities. Since trucks only use the left lane when traffic conditions have worsened to the extent that the number of truck interactions become significant, those trucks using the left lane on average have a relatively low velocity. This explains the low average truck velocity on the left-lane.

tions, a larger ΔV will disable the controller to suspend the congestion (although traffic conditions are improved compared to the no-control case). Considering the influence of anticipation distances d_1 and d_2, it is concluded that the influence of d_1 and d_2 are very moderate.

The fact is that the response-shift is of dominant importance for the effectiveness of speed-homogenising control. This provides useful insights into the way to improve the control measure, namely by somehow changing the relation between the measured velocities and the displayed speed limits.

Influence of detector location

The described case showed the effect of speed-homogenising control when the VMS's provides speed-information collected at *downstream* inductive loops. However, the relative location of the detectors with respect to the VMS plays an essential role. To show this, let us first consider the case where the VMS provides information on the velocities collected from the inductive loops below (distance $d = 0m$ downstream of the VMS) the VMS. Figure 10-25 depicts results of this strategy on person-car velocity of on the right-lane. We conclude that, although the on-set of congestion is *postponed* for some time, the controller is unable to avoid the formation of a jam. Secondly, let us assume that the detectors are located at a distance $d = 200m$ downstream of the VMS's. In this case, no congestion occurs (see Figure 10-25). With $d = 100m$, the phantom-jam *did* occur.

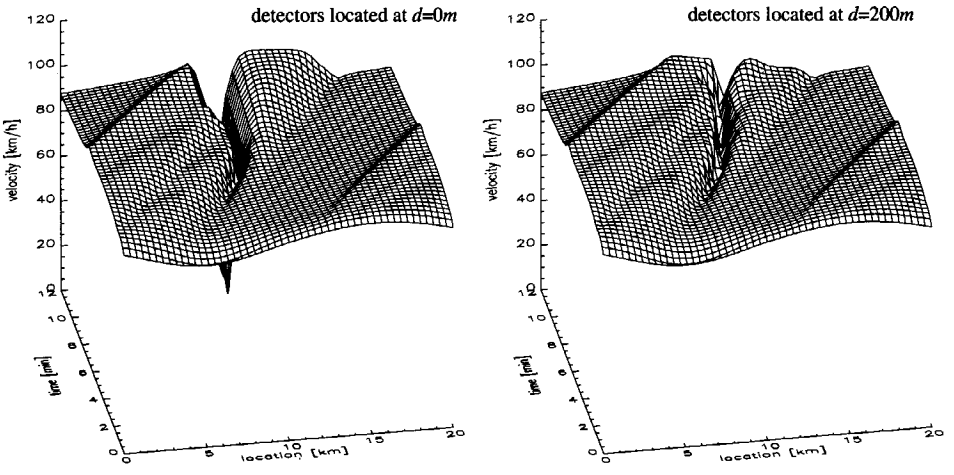

Figure 10-25: Influence of relative location of speed detector with respect to VMS sign upon congestion.

Concluding, the relative location of the detector with respect to the VMS influences the effectiveness of the control measure. That is, if the VMS's provide information that is based on data from a detector that is too near the VMS, the effectiveness of the strategy will be limited.

10.7.5 Results of a small incident

Let us now consider the effects of homogenising in case of a very small incident. To this end, let us consider homogeneous traffic conditions with $r_{(1,*)}(x,0) = 30veh/km$ and $r_{(2,*)} = 3veh/km$. During the very short period $T = [1min, 1.5min)$, an incident blocks the left-lane of the two-lane roadway. Let us assume that the incident blocks the region $X = [9.25, 9.75km)$. The incident is modelled using phantom-cars (appendix I). Rather than considering a ringroad, we have considered a roadway stretch with constant inflow at the entry of the roadway, while vehicles are able to exit the roadway undisturbed.

Table 10-8: Mean velocities [*km/hr*] and velocity standard deviations [*km/hr*] with and without variable-speed limit control (30-second incidents).

	user-class:	*person-cars*			*trucks*			*overall*		
scenario	lane:	1	2	*	1	2	*	1	2	*
no control	V	87.7	99.5	94.7	83.7	63.5	82.0	87.0	99.0	93.6
	$\Theta^{1/2}$	24.8	23.2	24.6	9.8	28.0	13.7	22.9	23.6	24.1
speed-control	V	95.1	104.6	100.9	85.4	84.9	85.4	93.2	104.5	99.5
	$\Theta^{1/2}$	7.7	7.1	8.7	4.6	6.5	4.7	8.1	7.2	9.5
lane-specific	V	95.2	104.9	101.1	85.4	85.4	85.4	93.2	104.8	99.7
speed-control*	$\Theta^{1/2}$	7.7	6.6	8.5	4.7	5.3	4.7	8.2	6.7	9.4

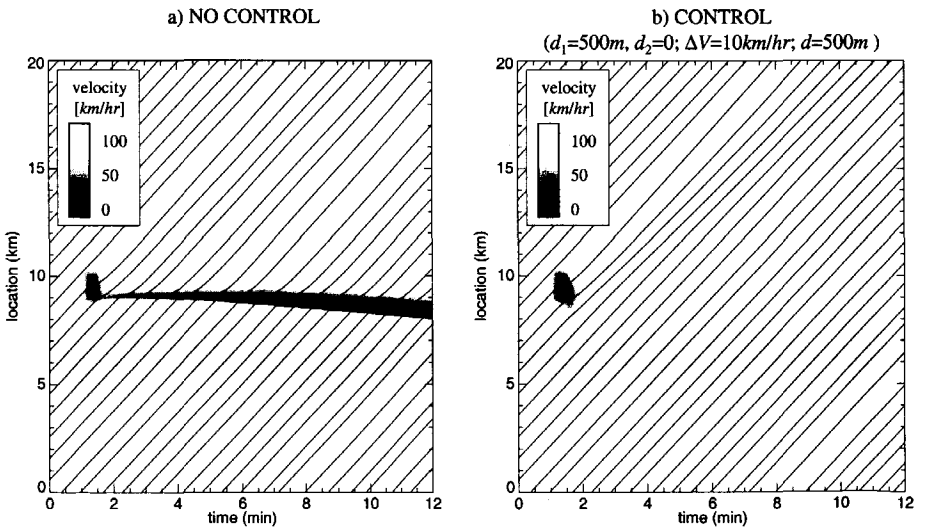

Figure 10-26: Velocity contour plot and trajectories of person-cars on the right-lane in case of a very short incident (30*sec*) for non-controlled scenario (a) and VMS-controlled scenario (b).

* The results on lane-specific speed-limits are discussed in section 10.8.

Considering non-controlled traffic operations, the incident causes a disturbance in the traffic flow that actuates a jam, which persists during the entire simulation period. Figure 10-26 shows the self-organised growth of the traffic jam. Note that the head of the queue is nearly stationary, while the tail of the queue grows. Table 10-8 shows the mean velocities and velocity variances for each (class/lane) pair during the simulation period $T = [0min, 12min)$.

Table 10-9: Mean velocities [*km/hr*] and velocity standard deviations [*km/hr*] with and without variable-speed limit control (1-minute incident).

	user-class:	*person-cars*			*trucks*			*overall*		
scenario	lane:	1	2	*	1	2	*	1	2	*
no control	V	86.3	98.4	93.4	83.3	62.0	81.1	85.7	97.7	92.3
	$\Theta^{1/2}$	26.6	25.0	26.3	11.2	28.7	15.4	24.6	25.5	25.8
speed-control	V	94.1	103.5	99.8	84.9	82.7	84.8	92.3	103.4	98.4
	$\Theta^{1/2}$	9.2	8.9	10.1	6.0	10.7	6.2	9.4	9.1	10.7
lane-specific	V	87.3	98.3	93.9	81.4	69.7	80.6	86.2	98.0	92.7
speed-control*	$\Theta^{1/2}$	22.5	21.6	22.6	13.5	22.0	14.5	21.3	21.8	22.3

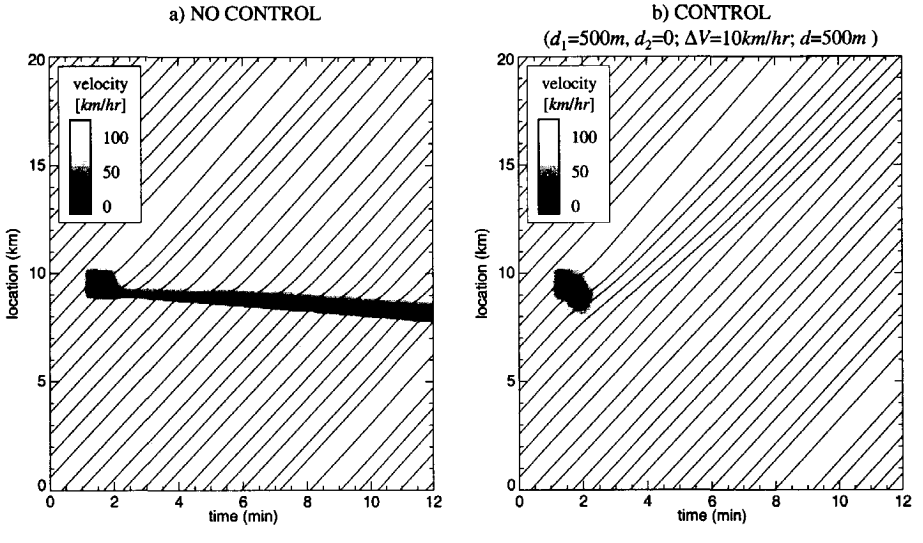

Figure 10-27: Velocity contour plot and trajectories of person-cars on the right-lane in case of a short incident (1*min*) for non-controlled scenario (a) and VMS-controlled scenario (b).

Variable speed limit control also has a positive impact in case of an incident, as indicated by the values of the average velocities and velocity variances in Table 10-8. These large differ-

* The results on lane-specific speed-limits are discussed in section 10.8.

ences are caused by the fact that the ability of the controller to dissolve the congestion, which would otherwise have persisted (Figure 10-26).

We have also considered the effects of a slightly longer incident of 1*min* (Table 10-9 and Figure 10-27). Again, using variable-speed limit control the otherwise persisting congestion dissolves quickly.

10.7.6 Impact of a VMS in case of a larger incident

Let us now consider an incident of longer duration, namely two minutes. This case is interesting since under variable speed-limit control the effects of the incident do not dissolve. Figure 10-28 shows how the structure of the jam changes: its length *increases*, while its amplitude *decreases*. Moreover, the high-density area formed upstream of the incident location due to VMS-control is irregular. That is, within this high-density region, regions can be identified with even higher densities. In these regions, the mean velocities are significantly lower than in other parts of the formed high-density region.

Table 10-10: Mean velocities [*km/hr*] and velocity standard deviations [*km/hr*] with and without variable-speed limit control (2-minute incident).

	user-class:	*person-cars*			*trucks*			*overall*		
scenario	lane:	1	2	*	1	2	*	1	2	*
no control	V	85.1	97.2	92.2	82.8	60.3	80.1	84.7	96.5	91.1
	$\Theta^{1/2}$	27.9	26.5	27.7	12.6	29.7	17.3	25.9	27.0	27.2
speed-control	V	86.0	96.2	92.1	80.0	68.0	79.2	84.9	95.9	90.9
	$\Theta^{1/2}$	22.7	22.5	23.1	15.1	22.3	16.0	21.6	22.7	22.9
lane-specific	V	87.1	98.2	93.7	81.7	68.9	80.8	86.1	97.9	92.6
speed-control*	$\Theta^{1/2}$	22.0	20.1	21.6	11.8	24.1	13.4	20.6	20.4	21.3

Table 10-10 shows the impact of the variable speed control on average velocities and velocity-variances during the 12-minute simulation period. While the traffic conditions on lane 1 (right lane) improve slightly, the conditions on lane 2 worsen. Overall, variable speed limit control is unfavourable from the perspective of the traveller optimising his velocity. On the other hand, the velocity variance is decreased significantly, yielding an *improvement* from the perspective of traffic safety. However, with respect to this safety, we remark that the high-density region formed by the control-law reflects regions of spatial deceleration and acceleration, while in case of the non-controlled scenario, only a single high-density region exists. Since these high-density regions imply the necessity of a driver to decelerate very quickly, the presence of more of these regions is unfavourable from a safety perspective.

We have also considered changing the response shift ΔV, and the distance d between the gantry and the detector. With respect to the former, we have observed that different response-shifts do not relieve the congestion, even when $\Delta V = 0$. In addition, the downstream distance d of the detector with respect to the gantry could not be chosen such that the congestion resulting from the incident dissolved.

* The results on lane-specific speed-limits are discussed in section 10.8.

If we consider Figure 10-28b, we observe that the high-density regions are located at approximately equal distances, namely 500*m*. This leads us to believe that these local high-density regions are formed since their on-set is not noticed by the detectors (which are located at 500*m*). To illustrate this belief, we have considered placing using more detectors. In this case, the speed-limit on the VMS is based on the minimum velocity measured at the distinct detectors. When one detector was located on each cell *i* (i.e. inter-detector distance of 100*m*), the congestion resulting from the two-minute incident did dissolve (Figure 10-29).

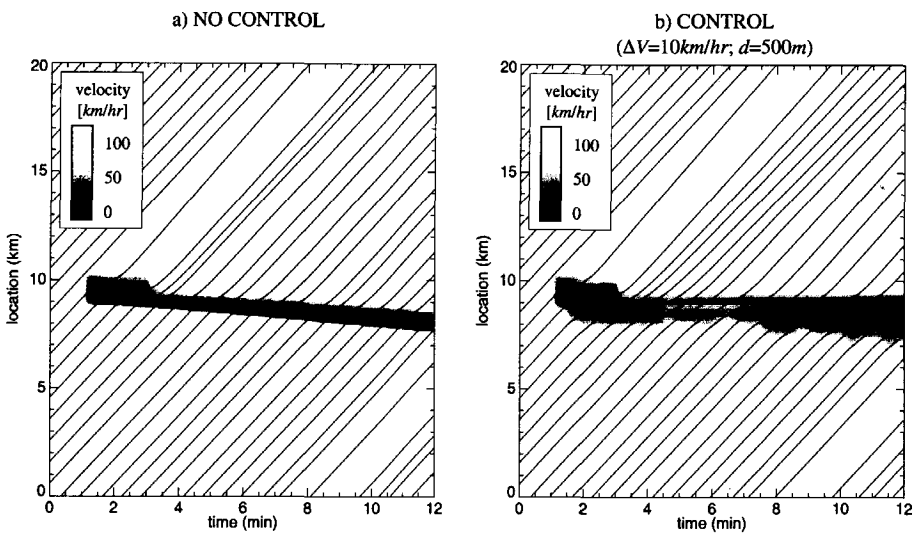

Figure 10-28: Velocity contour plot and trajectories of person-cars on the right-lane in case of an incident (2*min*) for non-controlled scenario (a) and VMS-controlled scenario (b).

In conclusion, we have seen that dynamic speed limits are useful in preventing the on-set of phantom-jams due to their longitudinal homogenising effect (section 10.7.4). We have also seen that under specific conditions, this control can also diminish the effects of a small incident (section 10.7.5). When the incident is more severe (section 10.7.6), beneficial effects of dynamic speed limits is less obvious. That is, neither the congestion is resolved, nor are the conditions smoother than without speed control.

10.8 Lane-specific variable speed control

As an alternative to applying equal dynamic speed limits for all lanes of the roadway, we can consider *lane-specific speed homogenising control*. In this case, lane-specific data collected at measurement locations downstream of the gantries are employed to provide lane-specific variable speed limits. The lane-specific speed limits are coupled in that we assume that the speed-difference between adjacent lanes is not larger than 20*km/hr*.

Lane-specific variable speed limit control approach may improve the efficiency of the control, since the velocity control is only applied to the lane where the disturbances or localised

congestion occurs. That is, the undisturbed lane is not affected by the variable speed limits (at least not in the same extent as aggregate-lane speed control).

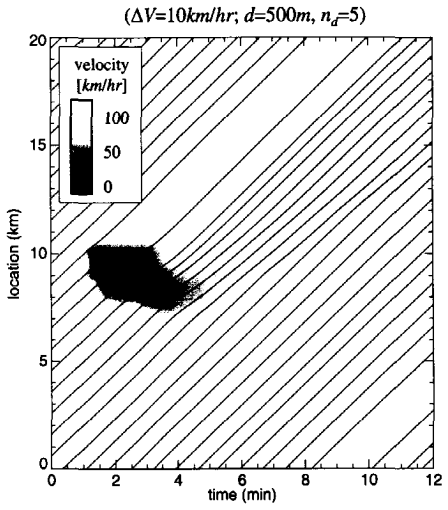

Figure 10-29: Velocity contour plot and trajectories of person-cars on the right-lane for VMS-controlled 2-minute incident scenario, with detector spacing of 100*m*.

10.8.1 Lane-specific speed-control and incidents

Table 10-8 (page 257) shows the results of lane-specific speed control on the traffic conditions in case of a thirty-second incident. From the results, we can see that the lane-specific variable speed limit slightly improves the aggregate-lane approach. However, this improvement is only very moderate.

However, if we consider an incident that is slightly longer (i.e. one minute), we find that for the default lane-specific VMS strategy the congestion resolving effect of the VMS control is precluded, in opposition to the aggregate-lane dynamic speed-limit control (see Table 10-9). Rather, the localised jam resulting in the uncontrolled scenario also persists in the lane-specific speed-limit case.

We have observed that choosing a different value for the measurement location relative to the VMS ($d = 1000m$), using more detectors to determine speed limits on the gantries, or modifying the driver's response shift ΔV are all adequate to realise congestion dissolving by lane-specific speed limits (see Table 10-11). Compared to the results depicted in Table 10-9, the results of lane-specific control (Table 10-11) improve traffic operations very modestly. Best results are obtained by changing the location of measurement for $500m$ to $1000m$ downstream of the gantries.

Finally, we have considered the 'large'-incident scenario (Table 10-11). Similar to the aggregate-lane case, the congestion resulting from the incident was only cleared when the number of detectors per gantry n_d was increased significantly.

Table 10-11: Mean velocities [*km/hr*] and velocity standard deviations [*km/hr*] using *lane-specific* variable speed control (1-minute incident) for different control variable sets (default: $d = 500m$, $n_d = 1$, and $\Delta V = 10m/s$).

	user-class:	*person-cars*			*trucks*			*overall*		
scenario	lane:	1	2	*	1	2	*	1	2	*
lane-specific	V	94.5	104.3	100.4	85.0	84.3	85.0	92.6	104.2	99.0
contr. ($d = 1000$)	$\Theta^{1/2}$	8.9	7.5	9.4	6.1	7.6	6.1	9.2	7.6	10.1
lane-specific	V	94.3	104.0	100.2	84.9	83.7	84.9	92.4	103.9	98.8
contr. ($n_d = 5$)	$\Theta^{1/2}$	9.2	7.9	9.7	6.2	8.8	6.3	9.5	8.1	10.4
lane-specific	V	94.0	103.9	100.0	84.8	83.5	84.8	92.2	103.8	98.6
contr. ($\Delta V = 5$)	$\Theta^{1/2}$	9.5	8.2	10.0	6.3	9.3	6.4	9.7	8.4	10.6

Table 10-12: Mean velocities [*km/hr*] and velocity standard deviations [*km/hr*] using *lane-specific* variable speed control (2-minute incident) for different control variable sets (default: $d = 500m$, $n_d = 1$, and $\Delta V = 10m/s$).

	user-class:	*person-cars*			*trucks*			*overall*		
scenario	lane:	1	2	*	1	2	*	1	2	*
lane-specific	V	87.1	98.2	93.7	81.7	68.9	80.8	86.1	97.9	92.6
contr. ($d = 1000$)	$\Theta^{1/2}$	22.0	20.1	21.6	11.8	24.1	13.4	20.6	20.4	21.3
lane-specific	V	86.9	97.3	93.1	79.7	73.9	79.4	85.5	97.1	91.9
contr. ($n_d = 5$)	$\Theta^{1/2}$	20.2	19.4	20.4	14.4	17.1	14.7	19.5	19.6	20.3
lane-specific	V	81.0	93.6	88.4	79.0	57.4	77.0	80.7	93.1	87.4
contr. ($\Delta V = 5$)	$\Theta^{1/2}$	29.5	28.2	29.4	17.0	27.5	19.3	27.7	28.5	28.8

10.9 Summary and conclusions

In this chapter, we have presented several applications of the MLMC traffic flow model established in this thesis. In the first part of the chapter, we have discussed the extent to which the MLMC model remedies the fundamental criticisms cast by among other Daganzo (1995) on higher order macroscopic model by means of numerical analysis. We have concluded that the model satisfies both the anisotropy condition and the unaffected slow vehicles condition. The invariant personality critique is relieved to a certain extent. Additionally, we have discussed the model's ability to describe formation of localised structures in multilane multiclass traffic flow.

Judging from the results presented in the sections 10.1–10.4, it appears that the developed MLMC model is able to describe observed phenomena on motorways adequately. Moreover, in opposition to other macroscopic models that also have this ability (e.g. the models of Payne (1971), Kerner *et al.* (1996), Helbing (1996,1997a), etc.), our model is able to describe these phenomena for each distinguished user-class and each lane *specifically*. Consequently, the model yields improved insights into causes and mechanisms underlying these phenomena (interaction between the user-classes, dependencies between the lanes).

The second part of the chapter discussed some practically relevant application of the model. Among other things, we have shown the effects of mixture of different vehicle-types, the traffic operations near a lane-drop, and the effects of an incident. In each of these examples, the occurrence of congestion played an essential role. Similar to the aggregate-class aggregate-lane traffic theory of Kerner and Konhäuser, perturbations in the heterogeneous traffic flow may cause the on-set of congestion consisting of nearly stationary moving jams that can persist for a very long duration, and are an intrinsic characteristic of traffic flow. However, due to the multiclass multilane nature of the model, the disturbances causing these jams can be of a different nature (mixing of traffic, presence of slower trucks). Moreover, the impacts can be assessed for the individual classes and lanes separately.

In the final part of this chapter, we have used the MLMC model to assess the impacts of three traffic management measures, namely (1) overtaking prohibition for trucks (2) aggregate-lane variable speed limits and (3) lane-specific variable speed limits. With respect to the first, we conclude, based on model-predictions, that an overtaking prohibition for trucks is not beneficial, not from a safety perspective (increased velocity variances and between-lane velocity differentials) nor from an efficiency perspective (accelerated occurrence of traffic jams).

The impact of both aggregate-lane as well as lane-specific dynamic speed limits provided by Variable Message Signs shows the ability of this measure to postpone the occurrence of congestion during metastable traffic operations. That is, the model predicts that informing the drivers that the velocity downstream is lower enables drivers to anticipate and reduce their velocity in time. Consequently, fast vehicles will not drive into the high-density region with very high speeds, preventing localised disturbances to grow to traffic jams.

11 CONCLUSIONS AND RECOMMENDATIONS

In this closing chapter, we present the main conclusions of the work presented in this thesis, categorised into conclusions with respect to traffic flow theory, continuum modelling, numerical schemes, estimation techniques, and finally results of applications of the developed MLMC model. In section 11.2 we show some promising practical short-term model applications. In section 11.3 we propose some scientifically challenging future research directions for the long-term.

11.1 Conclusions

The work presented in this dissertation has evolved into a broad scope. We have established a new traffic flow theory, developed several models on various levels of aggregation, described suitable numerical approximation schemes, analysed MLMC traffic flow data, and presented some interesting macroscopic simulation results. Therefore, the conclusions presented in this section are categorised into five groups, namely theory development, gas-kinetic and macroscopic flow modelling, numerical approximation schemes, data analysis and estimation techniques, and model applications.

Overall, in opposition to current aggregate-class aggregate-lane macroscopic models, the multiclass multilane generalisation presented in this thesis enables macroscopic model application to problems where class and lane distinction is necessary. For instance, the model is able to predict the effect of a truck overtaking prohibition (which is a lane- and class-specific traffic management measure). In addition, both aggregate-lane variable speed control as well as lane-specific variable speed control have been assessed using the multilane macroscopic model. Neither of these measures could have been assessed using traditional aggregate-lane

and aggregate-class macroscopic flow models. Moreover, model-based applications of class and/or lane-specific control measures can also be embarked upon using the newly developed MLMC traffic flow model. This can be achieved by employing it as a traffic operation prediction module in model-based MLMC traffic control (e.g. dynamic lane allocation). Additionally, the model provides insight into the response behaviour of MLMC traffic flow operations, thereby bringing MLMC traffic flow theory to a higher level of descriptive detail.

In this section, we provide a systematic summary of the main conclusions drawn for the work done within the scope of this dissertation.

11.1.1 Theory development

The main result of the thesis research is the development of a realistic and tractable traffic flow model, accurately describing the multiclass traffic flow operations on multilane roadways, given the complexity of the asymmetric interactions between the classes and the lanes. This model provides insight into both the interactions between the distinct user-classes and the interaction between the lanes of the motorway thereby yielding a better understanding of the response of heterogeneous traffic flows to multiple control measures.

During the model development, we concluded that in order to be able to realistically describe the various processes (such as acceleration of platooning vehicles, and interaction of fast with slower vehicles) between the vehicles, on top of the user-class and lane-distinction, a *third* classification is essential, namely the distinction between *platoon-leaders* and *followers*. This distinction has led to the development a new *probabilistic platoon-based continuum* traffic flow theory describing the multiclass traffic flow operations on multilane roadways. The theory captures the correlation between the vehicular particles which is essential to correctly describe the interaction process between vehicles on the one hand, and the acceleration of platoons given the desired velocity and the acceleration capabilities of the platoon leader.

The new theory has been shown to be very general, even in the sense that it can deal with flows in opposite directions or in two or higher dimensional systems (e.g. pedestrian flows). Additionally, characteristics other than desired velocity, class, lane, and state can be incorporate as well (e.g. acceleration time, destination of pedestrians).

11.1.2 Gas-kinetic equations for generic traffic systems in n-dimensions

In this thesis, we have established generic gas-kinetic equations describing the motion of general traffic entities (e.g. vehicles, cyclist, and pedestrians) in n-dimensional space. It appeared that the dynamics of n-dimensional traffic flows are governed by *continuum* and *non-continuum* processes. Continuum processes reflect effects of convection, acceleration, and smooth adaptation of continuous attributes (e.g. desired velocity, acceleration time). Non-continuum processes, yielding non-smooth changes in velocities or continuous attributes, are divided into *event-driven* and *condition-driven* processes. Event-driven processes are *stimulus-response*-like processes, where changes in velocities or continuous attributes are caused by an event, usually an interaction between traffic entities. Condition-driven processes reflect non-smooth changes due to the conditions in which traffic entities are (e.g. platooning conditions for vehicles on the motorway).

11.1.3 Multiclass gas-kinetic modelling of multilane traffic flow

The developed theory and generic gas-kinetic model enables establishing gas-kinetic equations that describe the multilane dynamics of multiclass mesoscopic quantities in traffic flow by considering convection, acceleration, deceleration, and various types of lane-changing processes for platoon-leaders and followers separately. In opposition to traditional flow models, these equations clearly reflect the asymmetric interaction between vehicles from different driving-states on the one hand, and different user-classes on the other hand. Comparing the derived interaction term (the so-called *collision equation*) with the interaction terms used in traditional gas-kinetic models (e.g. Prigogine and Herman (1971), Paveri-Fontana (1975)) reveals that the latter models *do not correctly describe the interaction processes*. This results from the so-called *vehicular chaos assumption* that implies that the correlation between the vehicles (i.e. the free-flowing platoon leaders and the constrained followers) can be neglected. To prevent underestimation of the number of vehicular interactions, it appeared that the roadway-space requirements of vehicles had to be explicitly considered.

Moreover, since these models assume that either *all* vehicles are able to accelerate towards their desired velocity, or assume that only the unconstrained vehicles are able to accelerate towards their desired velocity, we have concluded and remedied the implication that these models do no correctly incorporate the acceleration processes of the *platooning* vehicles.

Concluding, based on a platoon-based probabilistic representation of multilane multiclass traffic flow, we have established a multiclass gas-kinetic flow model for both free-flowing, constrained, and mixed-state traffic flow on multilane roadway facilities. We have shown that these models can be considered as true generalisations of the original efforts of Prigogine and Herman (1971) and Paveri-Fontana (1975). The model is directly applicable to (stochastic) simulation of multilane flow operations of heterogeneous traffic by application of suitable numerical solution approaches, for instance by particle discretisation approaches (Hoogendoorn and Bovy (2000)).

11.1.4 Multiclass macroscopic modelling of multilane traffic flow

The number of unknown model parameters in the mesoscopic generalised gas-kinetic equations is too high to enable effortless and tractable model-application. Therefore, to establish at a tractable macroscopic model, a method similar to the method of moments has been developed and applied. Application of the method has resulted in lane-specific dynamic equations for the conservative multiclass traffic flow variables density, momentum and energy. This conservative model-form constitutes a new type of macroscopic traffic flow model that is excellently suited for efficient numerical solution approaches.

In addition, the resulting macroscopic model has been transformed into two other model formulations, namely the traditional primitive formulation using density, velocity and velocity variance, and the characteristic formulation, using the characteristic or *Riemann* variables. The model formulations are equivalent. Nevertheless, each has its own merits and drawbacks.

Although its use in mathematical and numerical model analysis is limited, the *primitive formulation* is very well suited for comparison with currently available macroscopic models. By doing so, we observe that the main differences between the developed model and the traditional macroscopic models are:

1. Expression for equilibrium velocity and variance (which are *endogenous* rather than *exogenous* and depend on the interaction and immediate lane-changing processes).
2. Model terms reflecting lane-changing processes.

Moreover, by comparing the specifications of these models and the MLMC model developed in this thesis, the multiclass formulation reveals that the *behavioural interpretation* of the *pressure term* in traditional macroscopic models in terms of driver's anticipation-behaviour is flawed. That is, the *traffic pressure gradient* $\partial P/\partial x$ (with $P = r\Theta$) does *not reflect the anticipation behaviour of drivers*. Rather, it is a result of differences in velocity distributions of groups of vehicles flowing in to, respectively out of an infinitesimal roadway section.

From the system of dynamic equations we have derived equilibrium relations describing the equilibrium momentum and energy (conservative formulation), as well as the equilibrium velocity and velocity variance (primitive formulation). These reflect the influences of two *competitive* processes, namely *acceleration to the desired velocity* on the one hand, and *deceleration due to vehicular interactions*. The latter process reflects the *asymmetric interaction* between the slow and fast user-classes.

Considering equilibrium traffic flow operations, we show that the class-dependent lane-distribution of density, momentum, and energy can be expressed by on the one hand a function of the expected number of immediate lane-changing vehicles, and on the other hand the expected number of postponed lane-changing, and spontaneous lane-changing vehicles.

Finally, using the *characteristic formulation*, the way in which perturbations propagate in the multiclass flow has been analysed. We show that these (small) disturbances traverse along the *characteristic curves*. For each class and lane, *three* characteristic curves have been established, namely the trajectory of the average vehicles (the so-called *path-line*), and two so-called *Mach-lines*. In comparison, the LWR-model and the Payne-type models only have one and two characteristics respectively. Neither of the latter models describes how disturbances are transported along the trajectories of the vehicles.

Similar to the behaviour of fluids and gasses, expansion fan, shock waves and contact discontinuities are identified. The *expansion fan* reflects the vehicular diffusion due the vehicles accelerating towards different acceleration velocities (due to differences in desired velocities of platoon-leading vehicles). The *shock wave* describes sharp transitions in the (worsening) traffic conditions. We have shown that in opposition to fluidic flows, the expansion fan *precedes* the shock wave.

Finally, we have observed that when traffic is operating under congested conditions, perturbations are transported in both the downstream and the upstream direction, while in free-flow conditions, the effects of a perturbation are transported downstream only. These congested traffic conditions are equivalent to subsonic flows in fluids or gasses, while free-flow traffic conditions are equivalent to supersonic flow conditions.

11.1.5 Numerical solution techniques

We have shown that insights into the way disturbances move in the flow is of dominant importance to correctly compute numerical solutions of the system of partial differential equations describing the MLMC traffic operations. Therefore, by using these insights, improved numerical solution approaches were developed. These solution approaches are based on re-

spectively *flux-vector splitting schemes* and the *approximate Riemann solver* used to solve systems of hyperbolic equations (the so-called Euler-equations), describing the dynamics of inviscid fluids. In this thesis we have developed and applied an adapted scheme to suit multilane traffic flow simulation.

To evaluate different numerical solution approaches, we have compared the central difference Lax-Friedrichs scheme with several other schemes. It appeared that, although the Lax-Friedrichs scheme is able to accurately compute solutions in smooth regions of the flow, it fails to do so near sharp transitions from one state of traffic to another. Among other things this results in vehicles propagating backwards into the flow, violating the anisotropy condition. We argued that this is true for general *central-difference* approximation schemes. Hence, these are *not suited* to numerically determine solutions of *dominantly convective* traffic flow equations.

By considering the accuracy of solutions and the computational efficiency, we recommend to use the Van Leer flux-splitting scheme to serve as foundation of the numerical solution approach for the MLMC traffic flow equations. The developed solution approach consists of an adapted Van Leer scheme, characterised by a sequential consideration of the acceleration, immediate lane-changing, spontaneous lane-changing, and postponed lane-changing.

11.1.6 Multiclass data analysis and estimation

We argue that for accurate determination of the model parameters and relations, video observations combined with automated vehicle identification are well suited and cost-effective. However, since no video observations were available at the time, individual cross-section vehicle observations from a two-lane motorway in the Netherlands have been analysed.

We have observed that to correctly identify the structural changes in the mean traffic flow variables (e.g. velocity), traditional averaging approaches of the observation are unsuitable. To remedy this, an event-driven low-pass filter has been proposed to distinguish the structural changes in the variables from the noise. The signal $u[k]$ consists of observations (e.g. velocities) of the k-th vehicle passing the observation point. This 'signal' is represented in the Fourier domain, after which the high-frequency noise is filtered out. Subsequently, the resulting Fourier representation is transformed back into the discrete domain, yielding a smoothed signal $u^*[k]$ (e.g. smoothed velocity observation of the k-th vehicle). It has been observed that the separation of structural changes and the noise is of dominant importance to obtain realistic estimates for the velocity variance.

To ensure comparable statistical significance, observations were classified into equal-sized subsamples of vehicles of class u on lane j instead of equal-period samples. For these subsamples we have determined relevant flow variables and relationships (e.g. equilibrium velocity variance, fraction of platooning vehicles, acceleration times and acceleration velocities, reaction times, overtaking probabilities, and vehicle lengths), and used these observations to estimate the relevant parameters and relationships in the developed flow model. The data analysis clearly showed the relevance of distinguishing classes and lanes in the modelling approach. Plausible parameter values resulted for distinct classes and processes.

11.1.7 Results from model application

In chapter 10 of this dissertation we have presented results of model application to a number of test-cases, which on the one hand were intended to show the validity of the model in remedying the criticisms on higher-order flow models, while on the other hand aimed at showing the plausibility of the new model by calculating outcomes of practical interest.

The discrete macroscopic MLMC model remedies both the anisotropy as well as the unaffected slow vehicle criticism. We have shown that the extent to which the invariant personality condition is resolved depends on the level of class-aggregation. Moreover, the model captures the observed differences between user-classes and lanes plausibly (although more elaborate model calibration and validation is required). We have shown that by macroscopic simulation a number of interesting phenomena observed in real-life traffic flow, such as hysteresis and phantom jams, are captured convincingly.

It was also shown that traffic management measures have an impact on the occurrence of these phenomena. For example, the model predicts that speed-homogenising control postpones the occurrence of congested flow caused by hysteresis-effects. In opposition, we have also demonstrated the unexpected outcome that an overtaking prohibition for trucks *accelerates* the occurrence of congestion.

11.2 Model application perspectives

Let us propose some fruitful application areas of the newly developed macroscopic model. In this respect, the proposals are restricted to applications of the model *as is*. That is, apart from additional model calibration and validation (e.g. for a multiple-lane case), the model can be readily applied with only moderate development effort. The application areas are among other things:

1. Dynamic multiclass travel time estimation.
2. Model based predictive control of corridors (e.g. speed homogenisation, on-ramp control, and dynamic lane allocation control).
3. Automated incident and congestion detection.
4. Multiclass multilane data checking and completion.
5. Travel time functions for multiclass dynamic assignment.

This list is not exhaustive but rather provides some directions in which model applications can be sought. In the ensuing, we discuss the application proposals in more detail.

11.2.1 Dynamic multiclass travel time estimation

Provision of travel time information on freeway-sections is currently implemented in various situations. Estimates of *instantaneous* travel times are frequently based on *unreliable* estimates of numbers of vehicles occupying considered sections. Consequently, reliable methods to estimate these numbers and consequent instantaneous or experienced travel times are needed to provide accurate and reliable information to road-users.

We envisage that by applying Kalman-like filtering techniques to combine real-life measurements and results from *macroscopic simulation* using the developed model, improved ac-

curacy of travel-time estimates can be achieved. Moreover, these estimates are class-specific, and will therefore convey significant differences in experienced travel times of the different classes the observed in real-life traffic flow.

Implicitly, application of dynamic models describing traffic operations on the section introduces correlation in both the time and space dimensions. In other words, measurement of the upstream, current and downstream detectors are correctly combined in estimating the conditions at the current detector location. This results in *extrapolation* of measurements in the time domain, and in either interpolation or extrapolation of measurements in the space domain, depending on the location of data collection. In addition to providing more reliable and accurate estimates, a by-product resulting from application of the Kalman-algorithm is a *performance indicator* reflecting the accuracy of estimation-results. Moreover, the extent of correlation in the time- and space-domain can be assessed directly.

11.2.2 Model-based optimal control of corridors

From a traffic control perspective, contemporary policies pursue a more efficient use of available infrastructure. The mixed user-class multilane traffic control problem is characterised by multiple objectives (efficiency, safety, etc.), multiple target-groups, and a high complexity. This complexity is caused by interaction between the user-classes and interplay of the available control instruments (e.g. co-ordinated ramp-metering and speed-homogenising control). We argue that to handle this complexity, a model-based approach is required. In this respect, application of the MLMC model developed in this thesis is beneficial.

The model can be applied either by the operator to predict the impacts of a specific control strategy (*Decision Support Systems*), or in a model-based controller at various levels of automation. In the latter case, the controller determines a control strategy describing the settings over time of the different control actuators present at the corridor that optimise the impacts predicted by the model. In this respect, traffic demand predictions at the boundaries of the controlled corridor are required to forecast the MLMC traffic conditions.

11.2.3 Automated incident detection

By comparing real-time traffic data with the discrete MLMC model outcomes, deviations from the expected traffic conditions described by the model can be identified. If these deviations are large, it is likely that the real-life situation is different from the situation predicted by the model. For example, the number of available lanes is smaller due to an incident. Thus, these large deviations may indicate the occurrence of an incident blocking one or more lanes of the roadway. Even if no lanes are blocked, but the incident causes changes in the traffic operations (e.g. due to 'rubber-necking'), the resulting capacity drop and the consequent deviations may yield the detection of the incident.

The MLMC flow model developed in this dissertation is very well suited for application in automated incident detection algorithms. This is motivated by the accuracy with which the model describes heterogeneous traffic operations on multilane roadways. Additionally, not only can we detect exceptional deviations with respect to the flow, also unexpected changes in the traffic composition caused by an incident can be identified.

11.2.4 Multiclass checking and completion of multilane data

Traffic detectors are never faultless. When for some reason, traffic data at a specific location is not available, the functioning of traffic monitoring and traffic control systems may decline. Providing accurate estimates for these missing data may be of dominant importance.

By on-line estimation of the traffic conditions on the roadway using the available data, estimates of the traffic conditions (in terms of density, velocity, and variance per class per lane) are available for each cell i of the roadway. This provides useful information at the non-observed locations.

By comparing detector data and model results, and identifying large deviations between them, the correctness of the data and the consequent functioning of the detector can be checked. When a detector fails, the missing data can be completed with model results.

11.2.5 Travel time functions in multiclass dynamic assignment

Bliemer (1998) establishes the generalisation of the traditional car-based or PCE (person-car equivalents) based *speed-density* relation to multiple user-classes in order to establish travel time functions for the multiclass dynamic traffic assignment problem (MUC-DTA). Bliemer shows the improvements following from a MUC-DTA approach in realistically assigning multiclass traffic to a road network, as well as the implications when assessing the impacts in case of multiclass dynamic traffic management measures. Bliemer discusses the applicability of the multiclass travel time functions following from the equilibrium velocity relations of the aggregate-lane model developed in this thesis. Although he uses downgraded equilibrium model relations, he concludes that currently the multiclass speed-density relations of the MLMC-model is the only multiclass speed-density relations that satisfies the theoretical conditions the author imposes on the multiclass speed-density relations.

11.3 Future research directions

In this final section we contemplate upon the future research directions that naturally follow from the research described in this thesis. First, we will consider several model improvements which are expected to improve either the accuracy or application potential of the model. Secondly, we briefly consider application of the modelling approach to alternative traffic systems. Finally, we will consider a *network generalisation* of the macroscopic MLMC model at hand, and the consequent development of a *suitable control theory for network-wide control of heterogeneous multilane traffic flow* operations.

11.3.1 Macroscopic modelling of alternative traffic systems

The generic model developed in this thesis has been applied to describe heterogeneous traffic on multilane motorways. This MLMC model can be easily adapted such that it suits other areas of application as well, for instance two-lane bi-directional roadways, and mixed (bi-directional) pedestrian and bicycle streams.

With respect to the former, traffic in opposite directions, we have briefly noted in the thesis that the model can incorporate traffic with negative velocities $v < 0$, i.e. traffic in *the opposite direction*. Let us consider two classes reflecting vehicles driving in different directions. Each

class primarily uses the right, respectively the left lane. If a vehicle interacts with a vehicle of the same class, it will attempt an immediate lane-change. If the gap on the target-lane is of sufficient size, the impeded vehicle will change to the left roadway lane.

When the vehicle is on the left lane it will either spontaneously move back to the right-lane if the opportunity to do so arises, or it will experience an interaction with a vehicle on the left-lane *that is driving in the opposite direction*. Note that since the vehicular spacing requirements are incorporated in the model, an active interaction does not (necessarily) imply a collision. Similar to the uni-directional case, this interaction is followed either by an immediate lane-change or by a deceleration. In the latter case, the vehicle decelerates to the velocity of the oncoming vehicles (while the oncoming vehicles will do the same). Clearly in the case of oncoming traffic, the urge to undertake an immediate lane-change will be considerable. Note that by allowing an immediate overtaking probability that is not equal to one, the vehicles that have changed to the left lane yield *a reduction in the equilibrium velocity* of vehicles driving in the opposite direction. That is, in the presence of an opposing lane, the average velocity on the right-lane will be decreased, similar to observed traffic operations on bi-directional two-lane roads.

With respect to mixed pedestrian and bicycle flows, we assume that movements of pedestrians and bicycles are confined to a finite number of imaginary lanes*. The classes reflect the different types of pedestrians (for instance fast and slow pedestrians, elderly, and people with luggage), and/or bicycles (e.g. regular bicycles, riskjas, etc.). For these classes, different parameters must be estimated (e.g. desired velocities, overtaking probabilities). Note that the manoeuvrability of pedestrians and bicycles is much better than the manoeuvrability of vehicles. The ability to model traffic in different directions is clearly very important in this case.

11.3.2 Pedestrian flows in two dimensions

In this dissertation we have proposed gas-kinetic equations, describing the dynamics of the generalised Phase-Space Density $\rho_a(\mathbf{x},\mathbf{v},\mathbf{v}^0,t)$, where $\mathbf{x}$ and $\mathbf{v}$ respectively denote the n-dimensional location and velocity vector, and $\mathbf{v}^0$ denotes the m-dimensional vector of continuous attributes. The gas-kinetic equations have been specified for one-dimensional vehicular flows ($\mathbf{x} = x$ and $\mathbf{v} = v$) with $\mathbf{a} = (u,j,c)$ and $\mathbf{v}^0 = v^0$. However, other model specifications are conceivable as well.

The generic model has been specified to capture the movements of pedestrians in two dimensions by Hoogendoorn and Bovy (2000). They derive pedestrian gas-kinetic equations by specifying both the acceleration function, as well as the transition probabilities describing the response of pedestrians to different interaction types. The *acceleration function* reflects the combined result of pedestrians smoothly accelerating towards their desired velocity on the one hand, while on the other hand it reflect pedestrians smoothly changing their angle of movement in order to reach their destination. *Transition probabilities* reflect pedestrians' remedial manoeuvres after an interaction. These are specified such that the *interaction type* is realistically considered. For instance, pedestrians meeting other pedestrians 'head-on' react differently from fast pedestrians catching up with slow pedestrians.

---

* This is also assumed when modelling pedestrian flows by *Cellular Automata models* (Blue and Adler (1998)).

Hoogendoorn and Bovy (2000) have carefully considered possible response actions of pedestrians, thereby determining plausible transition probabilities. It appeared the pedestrian model based on the generic gas-kinetic equations reproduce empirical speed-density relations established for pedestrian data analysis accurately.

11.3.3 Semi-microscopic simulation of MLMC traffic

In this thesis, solutions of the (macroscopic) MLMC model were numerically approximated using finite volume approaches. This yields approximations of the expected number of vehicles, the expected velocity, etc., of the respective user-classes on different roadway lanes.

However, a different approach would be to use the *macroscopic* MLMC flow equations as foundation for a (stochastic) microscopic simulation model. In this case, the dynamics of the individual traffic entities are governed by the macroscopic flow equations (see Hockney and Eastwood (1988), Van Aerde (1984)). Alternatively, instead of the macroscopic equations, the gas-kinetic equations can be used straightaway in the particle approach.

The approach is not restricted to describe vehicular flow. For instance, Hoogendoorn and Bovy (2000) have shown that application of particle discretisation methods to numerically approximate solutions of a gas-kinetic pedestrian flow model yields a stochastic microscopic pedestrian flow model able to describe pedestrian flows in large infrastructural facilities.

11.3.4 Network extension of macroscopic MLMC model

Current network-traffic flow theory is deficient in the sense that it does not deal adequately with heterogeneously composed traffic on multilane motorways networks. In order to cope with the complex traffic control task, a suitable traffic control theory is required that can deal with the multiplicity of control objectives and target groups, while for its application a much more elaborate theory of traffic flow operations on motorway networks is necessary.

To advance the work presented in this thesis, we propose adhering to the following steps:

1. *Furthering of a generic traffic flow theory* for the synthesis and analysis of *multiclass multilane* traffic flow. In particular, the lane choice and the lane-changing behaviour of drivers for each of the distinct classes need to be underpinned empirically.
2. *Furthering of a control theory for co-ordinated heterogeneous traffic flow control on motorway networks* considering the multitude of control instruments and options, while establishing a quantitative modelling approach for the optimisation problem.
3. *Establishing* a theory-based operational traffic flow model for the analysis of multilane heterogeneous flow operations in multiclass traffic networks.

The developed theory must provide a genuine extension and generalisation of traditional macroscopic traffic flow theory in multiclass networks. We envisage that the model provides insight into both the interactions between the distinct user-classes and the nature of the control problem at hand, given complex traffic network configurations and traffic control instruments, yielding a better understanding of the response of heterogeneous traffic flows to multiple control measures.

The aim of the proposed research can roughly be divided into three objectives:

1. The analysis of the problem of optimising *co-ordinated traffic control on motorway networks*, considering the multitude of interacting control instruments and options, while establishing a quantitative model for the optimisation problem.
2. An operational traffic flow network model suitable for estimating behavioural parameters as well as for unconditional and control-dependent flow predictions.
3. Empirical underpinning of the developed theory and models aimed at application in real-life situations on motorway networks. This should deliver the building blocks for the operational model for respectively off-line and real-time traffic control.

We envisage that the proposed research will yield improved models for operational traffic control. Moreover, the distinction between lanes and user-classes will enable new and superior control strategies. This potentially yields a more efficient utilisation of both the scarcely available infrastructure and the available traffic control instruments.

REFERENCES

AGV (1993), *Empirical Research of Truck Overtaking Prohibition A28* (in Dutch). Report. Dutch Ministry of Transport, Public Works and Water Management, Regional Directorate Utrecht.

AGV (1999), *Evaluation Truck Overtaking Prohibition A16* (in Dutch). Evaluation Report. Dutch Ministry of Transport, Public Works and Water Management, Regional Directorate Utrecht and Traffic Research Centre (AVV).

Ahmed, K.I., M.E. Ben-Akiva, H.N. Koutsopoulos, and R.G. Mishalani (1996). Models of Freeway Lane-changing and Gap-Acceptance Behaviour. *Proceedings of the 13th International Symposium of Transportation and Traffic Theory*, INRETS, Lyon, 1996, 501-515.

Anderson, R.L., R. Herman, and I. Prigogine (1962). On the Statistical Distribution Function Theory of Traffic Flow. *Operations Research* **10**, 180-196.

Babcock, P.S. (1982). *Freeway Simulation and Control.* University of California at Berkely, Institute of Transportation Studies.

Barceló J., J. Casas, J.L. Ferrer, and D. García (1998). Modelling Advanced Transport Telematic Applications with Microscopic Simulators: The Case with AIMSUN2. *Proceedings of the workshop Verkehr und Mobilität, Forschungsverbund Verkehrssimulation und Umweltswirkungen*, 137-143.

Ben-Akiva, M., and S. Lerman (1995), *Discrete Choice Analysis.* MIT Press, Cambridge, MA.

Bliemer, M.C.J., (1998). Multi-User Class Speed-Density Functions for Macroscopic Dynamic Traffic Assignment Models. *Proceedings of the 4th TRAIL Annual Congres.*

Botma, H. (1978), *State-of-the-Art report "Traffic Flow Models"* (in Dutch). Research Report R-78-40, SWOV.

Botma, H. (1985), *Evaluation Method of Branston for Desired Velocity Estimation* (in Dutch). Research Report, Delft University of Technology.

Bovy, P.H.L., and S.P. Hoogendoorn. (1998), The Ill-Predictability of the Occurrence of Road-Traffic Congestion.. In: *Limits To Predictability In Traffic And Transport*, J. van Geenhuizen (ed.), Delft University of Technology, Delft.

Branston, D. (1976). Models of Single Lane Time Headway Distributions. *Transportation Science* **10**, 125-148.

Branston, D. (1979). A Method for Estimating the Free Speed Distribution for a Road. *Transportation Science* **13**(2), 130-145.

Brilon, W., and N. Wu (1998). Evolution of Cellular Automata for Traffic Flow Simulation on Freeways and Urban Streets. *Proceedings of the workshop Verkehr und Mobilität, Forschungsverbund Verkehrssimulation und Umweltwirkungen*, 111-117.

Buckley, D.J. (1968). A Semi-Poisson Model of Traffic Flow. *Transporation Science* **2**(2), 107-132

Bui, D.D, P. Nelson, A. Sopasakis (1996) The Generalised Bimodal Stream Model and Two-Regime Flow Theory. *Proceedings of the 13th ISTTT*, 680-695.

Carlsson, A., and Cedersund, H.-A. (1998). A Macro Speed-Flow Model for Multi-lane Roads. *Proceedings of the Third International Symposium on Highway Capacity*, 297-319, Copenhagen, Denmark.

Chandler, R.E., R. Herman, and E.W. Montroll, *Traffic Dynamics: Studies in car following.* Operations Research 6, pp. 165-184, 1958.

Chronopoulos, A., A.S. Lyrintzis, P.G. Michalopoulos, C. Rhee, and P. Yi (1993). Traffic Flow Simulation through High-Order Traffic Modelling. *Mathematical Computation and Modelling* **17**(8), 11-22.

Chronopoulos, A., P.G. Michalopoulos, and Donohoe (1992). Efficient Traffic Flow Simulation Computations. *Mathematical Computation and Modelling* **16**(5), 107-120.

Cowan, R.J. (1975). Useful Headway Models. *Transportation Research* **9**, 371-375.

Daganzo, C.F. (1994a). The Cell Transmission Model: A Dynamic Representation of Highway Traffic Consistent with Hydrodynamic Theory. *Transportation Research B* **28**(4), 269-287.

Daganzo, C.F. (1994b). The Cell Transmission Model, Part II: Network Traffic. *Transportation Research B* **28**(2), 279-93.

Daganzo, C.F. (1995). Requiem for Second-Order Fluid Approximations of Traffic Flow. *Transportation Research B* **29**(4), 277-286.

Daganzo, C.F. (1997a). A Continuum Theory of Traffic Dynamics for Freeways with Special Lanes. *Transportation Research B* **31**(2), 83-102.

Daganzo, C.F. (1997b), *Fundamentals of Transportation and Traffic Operations*, Pergamon-Elsevier, Oxford, U.K.

Daganzo, C.F. (1999). The Lagged Cell-Transmission Model. *Proceedings of the 14th Internation Symposium on Transportation and Traffic Theory*, 81-104.

De Kroes, Donk and De Klein (1983). *Evaluation of the External Effects of Speed Homogenising Control for Highways* (in Dutch). Dutch Ministry of Transport, Public Works and Water Management, Traffic Research Centre (AVV).

Dijker, T., P.H.L. Bovy, and R.G.M.M. Vermijs (1997a). *Car-following under non-congested and congested conditions.* Research Report VK2206.301, Delft University of Technolgy.

Dijker, T., P.H.L. Bovy, R.G.M.M. Vermijs (1997b), Car-following under congested Conditions: empirical Findings. *Transportation Research Record* 1644, 20-28.

Drews, O. (1996). *Verkehrliche Auswirkung der Anordnung vor Ueberholverboten fuer LKW auf Autobahnen.* Schriftenreihe Lehrstuhl fuer Verkehrswesen, Ruhr-Universitaet Bochum.

Edie, L.C. and R.S. Foote (1958). Traffic Flow in Tunnels. *Proceedings of the Highway Research Board* **37**, 334-344.

Edie, L.C. and R.S. Foote (1960). Effect of Shock Waves on Tunnel Traffic Flow. *Proceedings of the Highway Research Board* **39**, 492-505.

Esser, J., L. Neubert, J. Wahle, and M. Schreckenberg (1999). Microscopic online Simulations of Urban Traffic. *Proceedings of the 14th International Symposium of Transportation and Traffic Theory*, 517-534.

Ferrari, P. (1989). The Effect of Driver Behaviour on Motorway Reliability. *Transportation Research B* **23**, 139-150.

Forbes, T.W., H.J. Zagorski, E.L. Holshouser, and W.A. Deterline (1958), *Measurement of Driver Reactions to Tunnel Conditions.* Highway Research Board, Proceedings 37, 345-357.

Gazis, D.C., R, Herman, and R.W. Rothery (1961). Nonlinear Follow the Leader Models of Traffic Flow. *Operations Research* **9**, 545-567.

GOUDAPPEL COFFENG (1996a). *Evaluation of Dynamic Overtaking Prohibition for Trucks A2 Roosteren-Born* (in Dutch). Evaluation report. Dutch Ministry of Transport, Public Works and Water Management, Traffic Research Centre (AVV)

GOUDAPPEL COFFENG (1996b). *Evaluation of Overtaking Prohibition for Trucks A2 Roosteren-Born* (in Dutch). Evaluation report. Dutch Ministry of Transport, Public Works and Water Management, Regional Directorate Zuid-Holland.

GOUDAPPEL COFFENG (1998). *Monitoring Truck Overtaking Prohibition* (in Dutch). Evaluation report. Dutch Ministry of Transport, Public Works and Water Management, Traffic Research Centre (AVV).

GRONTMIJ (1999). *Evaluation Dynamic Speed Adaptation / Trajectory Control* (in Dutch). Ministry of Transport, Public Works and Water Management, Traffic Research Centre (AVV).

Haken, H. (1983). *Advanced Synergetics*. Springer, Berling.

Hall, F.L., V.F. Hurdle, and J.H. Banks (1992). Synthesis of Recent Work on the Nature of Speed-Flow and Flow-Occupancy (or Density) Relationships on Freeways. *Transportation Research Record* 1365, 12-18.

Hänel, D., R. Schwane, and G. Seider (1987). On the Accuracy of Upwind Schemes for the Solution of the Navier-Stokes Equations. *AIAA paper* **87**-1105, 42-46

HEIDEMIJ (1993), *Evaluation of Pilot Speed Homogenising Control A2* (in Dutch). Evaluation Report.

HEIDEMIJ (1996). *Overtaking Prohibition for Trucks A50: Final Report* (in Dutch). Evaluation report. Dutch Ministry of Transport, Public Works and Water Management, Directorate Oost-Nederland.

Helbing, D. (1997a). *Verkehrsdynamik – Neue Physikalische Modellieringskonzepte*. Springer-Verlag.

Helbing, D. (1997b). Modeling Multi-lane Traffic Flow with Queuing Effects. *Physica A* **242**, 175-194.

Helbing, D. (1996). Gas-kinetic derivation of Navier-Stokes-like traffic equations. *Physical Review* E **53**(3), 2266-2381.

Helbing, D., and B.A. Huberman. (1998a). Moving like a solid Block. *Nature*.

Helbing, D., and B.A. Huberman (1998b), Coherent Moving States in Highway Traffic. **396**, 738-740.

Helbing, D. A. Hennecke, V. Shvetsov, and M. Treiber (1999). MASTER: Macroscopic traffic simulation based on a gas-kinetic, non-local traffic model. *Transportation Research B*, in print.

Herman, R., E.W. Montroll, R. Potts, and R.W. Rothery. (1959). Traffic Dynamics: Analysis of Stability in Car-Following. *Operations Research* **1**(7), 86-106, 1959.

Herman, R., T. Lam, and I. Prigogine (1972). Kinetic Theory of Vehicular Traffic: Comparison with Data. *Transportation Science* **6**, 440-452.

Hirsch, C. (1990a). *Numerical Computation of Internal and External Flow. Volume 1: Fundamentals of Numerical Discretisation*. John Wiley and Sons.

Hirsch, C. (1990b). *Numerical Computation of Internal and External Flow. Volume 2: Computational Methods for Inviscid and Viscous Flows*. John Wiley and Sons.

Hockney, R.W., and J.W. Eastwood (1988). *Computer Simulations using Particles*. Adam Higler, Bristol, New York.

Hoogendoorn, S.P., and H. Botma (1997). Modeling and estimation of headway distributions. *Transportation Research Record* 1591. 14-22.

Hoogendoorn, S.P. (1997). A Macroscopic Model for Multiple User-Class Traffic Flow. *Proceedings of the 3rd TRAIL PhD. Congress*, TRAIL Research School, part I.

Hoogendoorn, S.P., and P.H.L. Bovy (1998a). *Multiple User-Class Traffic Flow Modelling – Derivation, Analysis and Numerical Results.* Research Report VK2205.328, Delft University of Technology.

Hoogendoorn, S.P., and P.H.L. Bovy (1998b). *Continuum Modelling of multi-lane Heterogeneous Traffic Flow Operations.* Research Report VK2205.330, Delft University of Technology.

Hoogendoorn, S.P., and P.H.L. Bovy (1998c), Modeling Multiple User-Class Traffic. *Transportation Research Record* 1644, 57-69.

Hoogendoorn, S.P., and P.H.L. Bovy (1998d). Macroscopic Modelling of Multiple User-Class Traffic Flow using Conservative Variables. *Proceedings of the 6th Meeting of the EURO Working group*, Gothenburg.

Hoogendoorn, S.P., and P.H.L. Bovy (1998e). Mixed Traffic Headway Distributions. *Motorway Traffic Flow Analysis – New Methodologies and Recent Empirical Findings* (ed. P.H.L. Bovy), Delft University Press, 71-96.

Hoogendoorn, S.P. and P.H.L. Bovy (1998f). A New Estimation Technique For Vehicle-Type Specific Headway Distributions. *Transportation Research Record* 1646, 18-28.

Hoogendoorn, S.P., and P.H.L. Bovy (1999a). Multiclass Macroscopic Traffic Flow Modelling: A Multilane Generalisation Using Gas-Kinetic Theory. *Proceedings of the 14th International Symposium of Transportation and Traffic Theory,* 27-50.

Hoogendoorn, S.P., and P.H.L. Bovy (1999b). Continuum Modeling of Multiclass Traffic Flow. To appear in *Transportation Research B.*

Hoogendoorn, S.P., and P.H.L. Bovy (1999c). Estimation and Analysis of Multilane Multiclass Headway Distribution. *Proceedings of the 27th European Transport Forum Annual Meeting.*

Hoogendoorn, S.P. and P.H.L. Bovy (2000). Gas-Kinetic Modeling and Simulation of Pedestrian Flows. Submitted to *Transportation Research Board* 2000.

Hoogendoorn, S.P., G. Copinga, and U. Kaymak (1998). *Perspectives of Fuzzy Logic in Traffic Engineering.* Research Report Dutch Ministry of Transport, Public Works and Water Management, Rotterdam, The Netherlands.

Jepsen, M. (1998), On the Speed-Flow Relationships in Road Traffic: A Model of Driver Behaviour. *Proceedings of the Third International Symposium on Highway Capacity*, 297-319, Copenhagen, Denmark.

Kerner, B.S. (1999). Theory of Congested Traffic Flow: Self-Organization without Bottlenecks. *Proceedings of the 14th International Symposium of Transportation and Traffic Theory*, 147-172.

Kerner, B.S., and H. Rehborn (1996), Experimental Features and Characteristics of Traffic Jams. *Physical Reviews* E **53**(2), 1297-1300.

Kerner, B.S., and H. Rehborn (1997), Experimental Properties of Phase-Transitions in Traffic Flow. *Physical Review Letters* **79**(20), 4030-4033.

Kerner, B.S., and Konhäuser, P. (1995), Cluster effect in initially homogenous traffic flow, *Physical Review* E, vol. 48(4).

Kerner, B.S., Konhäuser, P., and Schilke, M. (1996), A new approach to problems of traffic flow theory, *Proceedings of the 13th International Symposium of Transportation and Traffic Theory,* INRETS, Lyon, 119-145.

Klar, A., and Wegener (1998), *A Hierarchy of Models for Multilane Vehicular Traffic I & II: Modelling*. SIAM Journal of Applied Mathematics.

Kotsialos, A., C. Diakaki, Y. Pavlis, M. Papageorgiou, G. Vardaka, (1998). Short-term Traffic Forecasting using the Macroscopic Simulation Tool METANET. *Proceedings of the DACCORD Short-term Forecasting Workshop*, 13-29.

Kotsialos, A., M. Papageorgiou, and A. Messmer, (1999). Optimal Co-ordinated and Integrated Motorway Network Traffic Control. *Proceedings of the 14th International Symposium of Transportation and Traffic Theory*, 621-644.

Kühne, R.D. (1984a), Freeway speed distribution and acceleration noise - calculations from a stochastic continuum theory and comparison with measurements, *Proceedings of the 10th International Symposium on Transportation and Traffic Theory*, Gartner & Wilson (ed.), Elsevier, New-York.

Kühne, R.D. (1984b), Fernstraßenverkehrbeeinflussuing und Physik der Phasenübergängen. *Physik in unsere Zeit* **15**(3), 84-93.

Kühne, R.D. (1991). Traffic Patterns in unstable Traffic Flow on Freeways. *Highway Capacity and Level of Service*. Brannolte (ed.), Rotterdam.

Kuipers, Bos, Broekhuizen, Van Donkelaar, Grilk, and Jenezon (1985), *Evaluation Traffic Signalling systems A13, A2 and A12* (in Dutch). Dutch Ministry of Transport, Public Works and Water Management, Traffic Research Centre (AVV).

Lax, P.D. (1954). Weak Solutions of Nonlinear Hyperbolic Equations and their Numerical Computations. *Communications on pure applied Mathematics* **7**, 159-173.

Lebaque, J.P. (1993). Les Modèles Macroscopiques de Trafic. *Annales des Ponts* **67**, 28-45.

Lebaque, J.P.(1996). The Godunov scheme and what it means for first order traffic flow models. *Proceedings of the 13th International Symposium of Transportation and Traffic Theory*, INRETS, Lyon, 647-677.

Lebaque, J.P., and J.B. Lesort (1999). Macroscopic Traffic Flow Models: a Question of Order. *Proceedings of the 14th International Symposium of Transportation and Traffic Theory*, 3-26.

Leo, C.J., and R.L. Pretty (1992). Numerical Simulation of Macroscopic Continuum Traffic Flow Models. *Transportation Research B* **26**(3), 207-220.

Leutzbach, W. (1988), *An introduction to the theory of traffic flow*, Springer-Verlag, Berlin.

Leutzbach, W. (1991). *Measurements of Means Speed Time Series Autobahn A5 near Karlsruhe, Germany.* Institute of Transport Studies, University of Karlsruhe, Germany.

Lighthill, M.H., and G.B. Whitham (1955). On kinematic waves II: a theory of traffic flow on long, crowded roads. *Proceedings of the Royal Society of London series A*, **229**, 317-345.

Liu, G., A.S. Lyrintzis, , P. G. Michalopoulos (1998), Improved High-Order Model for Freeway Traffic Flow. *Transportation Research Record* 1644, 37-46.

Ludmann, J. (1998), *Beeinflussung des Verkehrsablaufs auf Straßen – Analyse mit dem fahrzeugorientierten Verkehrssimulationsprogramm PELOPS*. Schriftenreihe Automobiltechnik, Institut für Kraftfahrwesen, Aachen.

Lühder, M.R. (1990). *Truck Overtaking Prohibition on German Motorways* (in German). Straßenverkehrstechnik **2**.

Luttinen, R.T. (1996), *Statistical Analysis of Vehicle Time Headways*, PhD. thesis, Teknillinen korkeakoulu, Liikennetekniika, Julkaisu 87, Gummerus Printing, Saarijärvi.

Lyrintzis, A.D., G. Liu, P.G. Michalopoulos. (1994). Development and comparative evaluation of high-order traffic flow models, *Transportation Research Record* **1547**, 174-183.

Lyrintzis, A.S., P.G. Michalpoulos, A. Chronopoulos, P. Yi, G. Liu, and C. Rhee, (1992). *Development of Advanced Traffic Flow Models and Implementation in Parallel Processing (phase 1)*. Final report. Centre of Transportation Studies, University of Minnesota.

MacCormack, R.W., and A.J. Paullay (1972). Computational Efficiency achieved by Time-Splitting of Finite-Difference Operators. *AIAA paper* 72-154.

MacCormack, R.W., and B.S. Baldwin (1975). A Numerical Method for Solving the Navier-Stokes Equations with Application to Shock-Boundary Layer Interaction. *AIAA paper* 75-81.

Mason, A.D., A.W. Woods (1998). The Effect of Speed Controls on Traffic. *Mathematics in Transport Planning and Control* (ed. J.D. Griffiths), 351-360.

May, A.D. (1990). *Traffic Flow Fundamentals*. Prentice Hall, Englewood Cliffs, NJ.

Minderhoud, M.M. (1999). *Supported Driving: Impacts on Motorway Traffic Flow*. Dissertation Thesis, Delft University of Technology. Delft University Press.

Montrol, E.W. (1961). Acceleration Noise and Clustering Tendency of Vehicular Traffic. *Theory of Traffic Flow* (ed. R. Herman), 147-157.

Munjal, P., and J. Pahl (1969). An Analysis of the Boltzmann-type Statistical Models for Multi-Lane Traffic Flow. *Transportation Research* **3**, 151-163.

Nagel, K. (1996). Particle Hopping Models and Traffic Flow Theory. *Physical Review E* **53**, 4655-4672.

Nagel, K., P. Simon, M. Rickert, and J. Esser, (1998). Iterated Transportation Simulation for Dallas and Portland. *Proceedings of the workshop Verkehr und Mobilität, Forschungsverbund Verkehrssimulation und Umweltswirkungen*, 95-99

Nagel, K. (1998). From Particle Hopping Models to Traffic Flow Theory. *Transportation Research Record 1644*, 1-9.

Nelson, P. (1995). A Kinetic Theory of Vehicular Traffic and its Associated Bimodal Equilibrium Solutions. *Transport Theory and Statistical Physics* **24**(1-3), 383-409.

Nelson, P., D.D. Bui. and A. Sopasakis (1997). A Novel Traffic Stream Model deriving from a Bimodal Kinetic Equilibrium. *Proceedsing of the IFAC conference*, 799-804.

Newell, C.F. (1993). A Simplified Theory of Kinematic Waves (I: general theory; II: queuing at freeway bottlenecks; III: multi-destination flows). *Transportation Research* B **27**, 281-314.

Newell, G.F. (1961). A Theory of Traffic Flow in Tunnels. *Theory of Traffic Flow* (ed. R. Herman), 193-206.

Papageorgiou, M. (1989), Dynamic modelling, assignment, and route guidance in traffic networks. *Transportation Research B* **23**, 29-48.

Papageorgiou, M., M.J. Blosseville, H. Hadj-Salem (1989). Macroscopic Modelling of Traffic Flow on the Boulevard Peripherique in Paris. *Transportation Research B* **23**, 29-47

Papageorgiou, M. (1998). Some Remarks on Macroscopic Traffic Flow Modelling. *Transportation Research A* **32**(5), 323-329.

Paveri-Fontana, S.L. (1975). On Boltzmann-Like treatments for traffic flow: a critical review of the basic model and an alternative proposal for dilute traffic analysis. *Transportation Research B* **9**, 225-235.

Payne, H.J. (1971). Models for Freeway Traffic and Control. *Mathematical Models of Public Systems* (ed. G.A. Bekey) **1**, 51-61.

Payne, H.J. (1979). FREFLO: A Macroscopic Simulation Model of Freeway Traffic. *Transportation Research Record* **722**, 68-77.

Philips, W.F. (1979), Kinetic Model for Traffic Flow with Continuum Implications. *Transportation Research Planning and Technology* 5, 131-138.

Pignataro, L.J. (1973), *Traffic Engineering – Theory and Practice.* Prentice-Hall Inc., Englewood Cliffs.

Pipes, L.A. (1953), An Operational Analysis of Traffic Dynamics. *Journal of Applied Physics*, vol. 24, no.1, 274-287.

Prigogine, I., and R. Herman (1971). Kinetic Theory of Vehicular Traffic. *American Elsevier* New-York.

Prigogine, I.. (1961). A Boltzmann-like Approach to the Statistical Theory of Traffic Flow. *Theory of Traffic Flow* (ed. R. Herman).

Rekersbrink, A (1995). Mikroskopische Verkehrssimulation mit Hilfe der Fuzzy Logik *Straßenverkehrstechnik* **2**.

Richards, P.I (1956), Shock waves on the highway, *Operations Research 4*, 42-51.

Roe (1981). The use of the Riemann problem in finite difference schemes. *Lecture notes in physics* **141**, Springer-Verlag, 354-359,

Shapiro, A.H. (1953). *The Dynamics and Thermodynamics of Compressible Fluid Flow.* New York, Ronald Press.

Smulders, S. (1989). *Control of Freeway Traffic Flow.* Ph.D. Thesis, University of Twente.

Smulders, S. and E. Van Den Hoogen (1994). Control by Variable Speed Signs – Results of the Dutch Experiment. *Proceedings of the 7th Conference on Road Traffic Monitoring and Control.* London, 145-149.

Smulders, S. (1996). *Control of Freeway Traffic Flow*. CWI Trans 80, Centre for Mathematics and Informatics (CWI), Amsterdam.

Steger, J.L. and R.F. Warming (1981). Flux vector splitting of the inviscid gas-dynamic equations with applications to finite difference methods. *Journal of Computational Physics* **40**, 263-293.

Strang, G. (1980), *Linear algebra and its applications*. New York : Academic Press.

Todosiev, E.P., and L.C. Barbosa (1964) A Proposed Model for the Driver-Vehicle System. *Traffic Engineering* **34**, 17-20.

Treiterer, J. and J.A. Myers (1974), The Hysteresis Phenomena in Traffic Flow. *Proceedings of the 6th International Symposium on Transportation and Traffic Flow Theory*, 13-38.

Van Aerde, M. (1994). *INTEGRATION: A Model for Simulating Integrated Traffic Networks*. Transportation System Research Group.

Van Arem, B., J.H. Hogema (1995). *The Microscopic Simulation Model MIXIC 1.2*. TNO-INRO report 1995-17b, Delft.

Van Leer (1982). Flux vector splitting for the Euler equations. *Proceedings 8th International Conference in Numerical Methods in Fluid Dynamics*, Berlin, Springer-Verlag, 1982.

Van Maarseveen, M.F.A.M. (1982). *The Theory of Martingales in Stochastic Systems Theory – Surveillance and Control of Freeway Traffic Flow. PhD Thesis*, University of Twente, Enschede.

Van Toorenburg, J.A.C. (1986). *Homogenising. Effect of adapted recommeded Speeds on Traffic Flow Operations* (in Dutch). Report, Traffic Engineering Division, Dutch Ministry of Transport.

Van Toorenburg, J.A.C., and R.J.P van der Linden (1996), *Predictive Control in Traffic Management*, Research Report, TRANSPUTE, Gouda.

Vermijs, R.G.M.M., Papendrecht, H.J., Lutje Spelberg, R.F., and Toetenel, W.J. (1995). Short term forecasting of the level of service on a motorway network, by using a microscopic simulation model. *Proceedings of the 2nd Erasmus-Network conference on transportation and traffic engineering*, Kerkrade.

Verweij, H.D. (1985). *Congestion Warning and Traffic Flow Operations* (in Dutch). Dutch Ministry of Traffic and Transportation, Delft, The Netherlands.

Westerman, M. (1995). *Real-time Traffic Data Collection for Transportation Telematics*. PhD. thesis, Delft University of Technology.

Whitham, G.B. (1974). *Linear and Nonlinear Waves*. Wiley, New York, 1974.

Wu, N., and W. Brilon (1999). Cellular Automata for Highway Traffic Flow Simulation. *Proceedings 14th International Symposium on Transportation and Traffic Theory (Abbreviated presentations)*, 1-18.

Wiedemann, R. (1974). *Simulation des Straßenverkehrsflußes*. Technical Report, Institute for Traffic Engineering, Univisity of Karlsrühe.

Wiersma, J.M.F., T. Heijer. (1996). Safety Criteria for Motorway Traffic Control. *Studies of the Second TRAIL Annual Congress*.

Yserentant, H. (1997). A New Class of Particle Methods. *Numerical Mathematics* **76**, 87-109.

Zadeh, L.A. (1965). Fuzzy Sets. *Information and Control* **89**, 3238-3532.

Zhang, H.M. (1999). A Mathematical Theory of Traffic Hysteresis. *Transportation Research B* **33**, 1-23.

A MATHEMATICAL DERIVATION OF THE GAS-KINETIC EQUATIONS

In this appendix, we present some theoretical results regarding the derivation of the MLMC gas-kinetic equations. More precisely, we show how the *generalised special continuity equations* can be determined using a probabilistic approach. In addition, we specify an expression for the *MLMC collision equations*.

We will first present the conservation equations in two dimensions x and t. Then, we consider the continuity equation in the four-dimensional phase-space of vectors (x,v,v^0,t). Finally, we will show the generic continuity equations for vectors $(\mathbf{x},\mathbf{v},\mathbf{v}^0,t)$ for generic flows in the n-dimensional space $I\!R^n$.

A.1 Probabilistic derivation of the conservation equations

Let us first recall the regular *conservation* of vehicle equation. To this end, let us consider a differential plane $d\mathbf{S}$ that is defined by all pairs (x,t) in the region defined by the Cartesian product $[x,x+dx)\times[t,t+dt)$. The boundaries of this region are denoted by $d\Omega$, which is the union of lines $d\Omega_1(x)$, $d\Omega_1(x+dx)$, $d\Omega_2(t)$, and $d\Omega_2(t+dt)$, defined by:

$$d\Omega_i(z) \overset{def}{=} \{(\omega_1,\omega_2) \,|\, \omega_i = z, s_j \le \omega_j < s_j + ds_j \text{ for all } j \neq i\} \tag{A.1}$$

for $i = 1,2$ (see Figure A-1). If we consider the trajectory of an n-vehicle platoon, then we can define the following events:

A. *Entry events.* The platoon is located on the boundary line $d\Omega_1(x)$ (event A_1), that is, the vehicle enters the region at x during the interval $[t,t+dt)$, *or* the vehicle is located

on the boundary line $d\Omega_2(t)$ (event A_2). The latter event is equivalent to the event that the vehicle is located on the infinitesimal region $[x,x+dx)$ at instant t.

B. *Exit events.* The platoon is either located on the boundary line $d\Omega_1(x+dx)$ (event B_1), i.e. the vehicle is present at location $x+dx$ in the interval $[t,t+dt)$, *or* the vehicle is on the boundary line $d\Omega_2(t+dt)$ (event B_2), that is, the vehicle is located in the region $[x,x+dx)$ at instant $t+dt$.

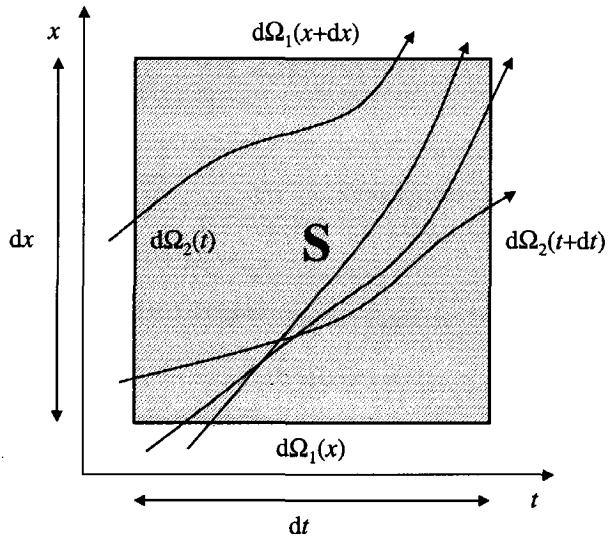

Figure A-1: Trajectories in the small region S in the *xt*-space.

The entry events A_1 and A_2 are *mutually exclusive*, yielding:

$$\Pr(A_1 \cup A_2) = \Pr(A_1) + \Pr(A_2) \tag{A.2}$$

This holds equally for the events B_1 and B_2. Moreover, the events A and B are *equivalent*. That is, if a platoon is either present in the region $[x,x+dx)$ at instant t, or it enters the region at x during the period $[t,t+dt)$, then it must either still be present at the instant $t+dt$, or it has left the region at $x+dx$ during the period $[t,t+dt)$. Thus, using relation (A.2), the condition $\Pr(A_1 \cup A_2) = \Pr(B_1 \cup B_2)$ yields the following expression:

$$\Pr(A_1) + \Pr(A_2) = \Pr(B_1) + \Pr(B_2) \tag{A.3}$$

Let us recall that the probability that an n-vehicle platoon is present in the region $[x,x+dx)$ at instant t is defined by the concentration, and equals $\kappa(x,t;n)dx$. Moreover, the probability that an n-vehicle platoon enters the region at x during $[t,t+dt)$ is reflected by the intensity, and equals $\lambda(x,t;n)dt$. Thus, we find:

$$\Pr(A_1) = \lambda(x,t;n)dt, \quad \Pr(A_2) = \kappa(x,t;n)dx,$$
$$\Pr(B_2) = \lambda(x+dx,t;n)dt, \quad \text{and} \quad \Pr(B_2) = \kappa(x,t+dt;n)dx \tag{A.4}$$

Substituting eqn. (A.4) into eq. (A.3) yields the *continuity equation* for n-vehicle platoons:

$$\lambda(x,t;n)dt + \kappa(x,t;n)dx = \lambda(x+dx,t;n)dt + \kappa(x,t+dt;n)dx$$
$$\Leftrightarrow \tag{A.5}$$
$$\partial_t \kappa(x,t;n) + \partial_x \lambda(x,t;n) = 0$$

A.1.1 Probabilistic derivation of conservation equations in the phase-space

To derive the continuum terms in the gas-kinetic equations of the generalised PSD, let us consider a differential (hyper-) volume d**S** in the phase-space that is defined by the Cartesian product $[x,x+dx)\times[v,v+dv)\times[v^0,v^0+dv^0)\times[t,t+dt)$. At this point, let us emphasise that the results of this section hold equally when other continuous attributes are present in the generalised PSD, such as the lateral position z.

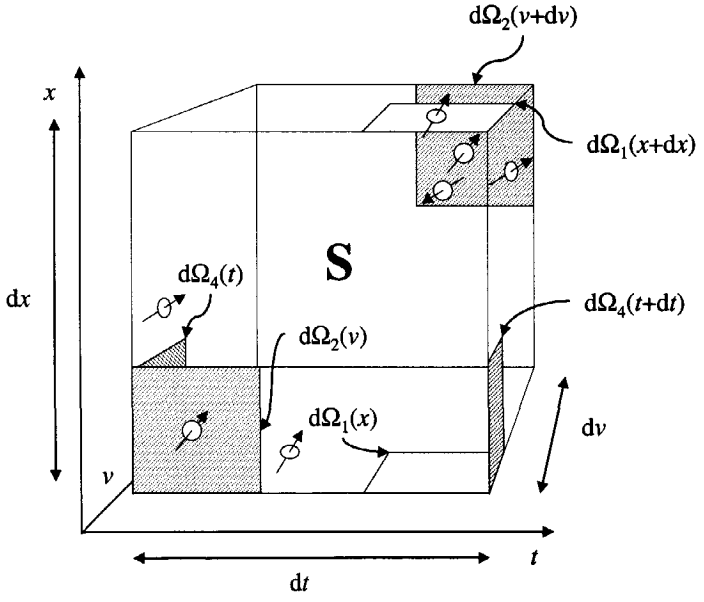

Figure A-2: Volume S in the reduced phase-space (x,v,t) with possible entry- and exit-events.

The *infinitesimal hypervolume* **S** is bounded by the infinitesimal hyperplanes denoted by $d\Omega_i(z)$. These hyperplanes are defined by:

$$d\Omega_i(z) = \{(\omega_1,\omega_2,\omega_3,\omega_4) \,|\, \omega_i = z, s_j \le \omega_j < s_j + ds_j \text{ for all } j \ne i\} \tag{A.6}$$

Let us now reconsider the equivalent events presented in the previous subsection. To this end, let us consider the path defined by $(x(t),v(t),v^0(t),t)$ of a platoon in the phase-space. In oppo-

sition to location $x(t)$ and time t, velocity $v(t)$ and desired velocity $v^0(t)$ of the vehicles in a platoon *may be* decreasing functions over time[1]. However, let us first consider the case where both the v and v^0 are monotonically non-decreasing functions of time, i.e. $dv/dt \geq 0$, and $dv^0/dt \geq 0$. The results presented in the sequel hold equally for $dv/dt < 0$, and/or $dv^0/dt < 0$. If we consider the differential volume **S**, we can again define equivalent entry and exit events, which can be split up respectively in *mutually exclusive* subevents (see Figure A-2):

A. *Entry events*. Either of the following events convey the entry of the n-vehicle platoon into the differential volume:

- *The platoon is located on the boundary hyperplane $d\Omega_1(x)$.* That it, the platoon driving with a velocity in the region $[v,v+dv)$, while having a desired velocity in the region $[v^0,v^0+dv^0)$ enters the region at x during interval $[t,t+dt)$ (event A_1).
- *The platoon is located on the boundary hyperplane $d\Omega_4(t)$.* I.e., the platoon driving with a velocity in the interval $[v,v+dv)$ while having a desired velocity in the interval $[v^0,v^0+dv^0)$, is present on the interval $[x,x+dx)$ at instant t (event A_4).
- *The platoon is located on the boundary hyperplane $d\Omega_2(v)$.* This implies that a platoon located in the region $[x,x+dx)$, during the interval $[t,t+dt)$, while maintaining a desired velocity in the interval $[v^0,v^0+dv^0)$, accelerates to a velocity v (event A_2).
- *The platoon is located on the boundary hyperplane $d\Omega_3(v^0)$.* That is, a platoon located in the region $[x,x+dx)$, during the interval $[t,t+dt)$, with a velocity in the interval $[v,v+dv)$, collectively increases its desired velocity to v^0 (event A_3).

B. *Exit events*. With respect to exit event, equivalent subevents can be determined as for the entry events. Summarising, we have the following mutually exclusive events:

- *The platoon is located on the boundary hyperplane $d\Omega_1(x+dx)$.* That it, the platoon driving with a velocity in the region $[v,v+dv)$, while having a desired velocity in the region $[v^0,v^0+dv^0)$ leaves the region **S** at $x+dx$ during interval $[t,t+dt)$ (event B_1).
- *The platoon is located on the boundary hyperplane $d\Omega_4(t+dt)$.* That is, the platoon driving with a velocity in the interval $[v,v+dv)$ while having a desired velocity in the interval $[v^0,v^0+dv^0)$, is present on the interval $[x,x+dx)$ at instant $t+dt$ (event B_4).
- *The platoon is located on the boundary hyperplane $d\Omega_2(v+dv)$.* This implies that a platoon located in the region $[x,x+dx)$, during the interval $[t,t+dt)$, while maintaining a desired velocity in the interval $[v^0,v^0+dv^0)$, accelerates to a velocity $v+dv$ (event B_2).
- *The platoon is located on the boundary hypeplane $d\Omega_3(v^0+dv^0)$.* That is, a platoon located in the region $[x,x+dx)$, during the interval $[t,t+dt)$, with a velocity in the interval $[v,v+dv)$, collectively increases its desired velocity to v^0+dv^0 (event B_3).

Since the events A_i and B_i ($i = 1,\ldots,4$) are mutually exclusive, we find:

---

[1] Although in this thesis we assume that the desired velocity of a vehicle is *invariant* over time, the modelling approach allows driver's adaptation of the desired velocity.

$$\Pr(\bigcup_{i=1}^{4} A_i) = \sum_{i=1}^{4} \Pr(A_i) \quad \text{and} \quad \Pr(\bigcup_{i=1}^{4} B_i) = \sum_{i=1}^{4} \Pr(B_i) \tag{A.7}$$

yielding:

$$\sum_{i=1}^{4} \Pr(A_i) = \sum_{i=1}^{4} \Pr(B_i) \tag{A.8}$$

Let us recall from chapter 3 that the *generalised intensity* $\lambda_{\mathbf{a}}$ expresses the probability that a platoon of vehicles sharing properties **a**, while having a velocity in the region $[v,v+dv)$ and a desired velocity $[v^0,v^0+dv^0)$, enters the region $[x,x+dx)$ at x during the period $[t,t+dt)$. That is:

$$\Pr(A_1) = \lambda_{\mathbf{a}}(x,v,v^0,t;n)dtdvdv^0 \quad \text{and} \quad \Pr(B_1) = \lambda_{\mathbf{a}}(x+dx,v,v^0,t;n)dtdvdv^0 \tag{A.9}$$

Moreover, the probability that an n-vehicle platoon sharing the properties **a** is present in the region $[x,x+dx)$ having a velocity in the region $[v,v+dv)$ and a desired velocity $[v^0,v^0+dv^0)$ at instant t is defined by the *generalised concentration* $\kappa_{\mathbf{a}}$, i.e.:

$$\Pr(A_4) = \kappa_{\mathbf{a}}(x,v,v^0,t;n)dxdvdv^0 \quad \text{and} \quad \Pr(B_4) = \kappa_{\mathbf{a}}(x,v,v^0,t+dt;n)dxdvdv^0 \tag{A.10}$$

Similarly, we can define the probabilities of the events A_2, A_3, B_2, and B_3, by defining *generalised acceleration intensity* $\lambda_{\mathbf{a}}^{v}$ and *generalised intensity of changes in desired velocity* $\lambda_{\mathbf{a}}^{v0}$:

$$\Pr(A_2) = \lambda_{\mathbf{a}}^{v}(x,v,v^0,t;n)dxdtdv^0 \quad \text{and} \quad \Pr(B_2) = \lambda_{\mathbf{a}}^{v}(x,v+dv,v^0,t;n)dxdtdv^0 \tag{A.11}$$

and:

$$\Pr(A_3) = \lambda_{\mathbf{a}}^{v^0}(x,v,v^0,t;n)dxdtdv \quad \text{and} \quad \Pr(B_3) = \lambda_{\mathbf{a}}^{v^0}(x,v,v^0+dv^0,t;n)dxdtdv \tag{A.12}$$

By substituting the expressions (A.9)-(A.12) into equation (A.8), we find:

$$\partial_t \kappa_{\mathbf{a}} + \partial_x \lambda_{\mathbf{a}} + \partial_v \lambda_{\mathbf{a}}^{v} + \partial_{v^0} \lambda_{\mathbf{a}}^{v^0} = 0 \tag{A.13}$$

Equation (A.13) is the generalised continuity equation for n-vehicle platoons. It shows how the generalised concentration $\kappa_{\mathbf{a}}$ changes over time due to the balance between the intensities at cell boundaries of a small cell **S** in the phase-space.

A.1.2 Relating concentration κ to intensities λ

In this subsection, we will present expressions describing the relation between the generalised concentration and the generalised intensities. To this end, let us consider the platoons sharing the properties reflected by the attribute-set **a** that are driving at velocity v while having a desired velocity v^0, that are located on the interval $[x-\Delta x,x)$ at instant t. Let the length Δx of this region satisfy $\Delta x = v\Delta t$. For this particular choice of Δx, we observe the following.

Platoons having velocity v, which are in the interval $[x-\Delta x,x)$ at time instant t all pass the cross-section x during the interval $[t,t+\Delta t)$. Thus, we have:

$$\int_{x-\Delta x}^{x} \kappa_{\mathbf{a}}(y,v,v^0,t;n)dy = \int_{t}^{t+\Delta t} \lambda_{\mathbf{a}}(x,v,v^0,s;n)ds \tag{A.14}$$

Replacing Δt with an infinitesimal value dt, and the region length Δx by the infinitesimal value dx, (A.14) yields:

$$\frac{\partial \lambda_a}{\partial \kappa_a} = \dot{x} \tag{A.15}$$

Analogously we find:

$$\frac{\partial \lambda_a^v}{\partial \kappa_a} = \dot{v} \quad \text{and} \quad \frac{\partial \lambda_a^{v^0}}{\partial \kappa_a} = \dot{v}^0 \tag{A.16}$$

and thus:

$$\partial_x \lambda_a = \partial_x \kappa_a \dot{x} \qquad \partial_v \lambda_a^v = \partial_v \kappa_a \dot{v} \qquad \partial_{v^0} \lambda_a^{v^0} = \partial_{v^0} \kappa_a \dot{v}^0 \tag{A.17}$$

Then, (A.13) yields:

$$\partial_t \kappa_a + \partial_x (\kappa_a \dot{x}) + \partial_v (\kappa_a \dot{v}) + \partial_{v^0} (\kappa_a \dot{v}^0) = 0 \tag{A.18}$$

Recall from chapter 3 that the generalised PSD ρ_a satisfies:

$$\rho_a(x, v, v^0, t) = \sum_{n=1}^{\infty} n \cdot \kappa_a(x, v, v^0, t; n) \tag{A.19}$$

yielding the generalised conservation equation for the generalised PSD:

$$\partial_t \rho_a + \partial_x (\rho_a \dot{x}) + \partial_v (\rho_a \dot{v}) + \partial_{v^0} (\rho_a \dot{v}^0) = 0 \tag{A.20}$$

A.1.3 Generalised continuity equations

Let us consider the motion of traffic particles in the *n*-dimensional subspace of $I\!R^n$. The location of these particles is denoted by the vector $\mathbf{x}$, while their velocity is denoted by $\mathbf{v}$, with $\mathbf{x}, \mathbf{v} \in I\!R^n$. Moreover, let $\mathbf{v}^0 \in I\!R^m$ denote the vector of general continuous attributes of the considered traffic particles. The *multi-dimensional generalised PSD* is denoted by $\rho_a(\mathbf{x}, \mathbf{v}, \mathbf{v}^0, t)$, and describes the expected number of vehicles characterised by the discrete attributes $\mathbf{a}$ per 'unit hypervolume' at $\mathbf{x}$, moving at velocity $\mathbf{v}$, being characterised by continuous attributes $\mathbf{v}^0$.

Let the $\nabla_{\mathbf{x}}$-operator be defined by:

$$\nabla_{\mathbf{x}} \overset{def}{=} (\partial_{x_1} \quad \partial_{x_2} \quad \cdots \quad \partial_{x_n}) \tag{A.21}$$

Similarly, we define the operators $\nabla_{\mathbf{v}}$ and $\nabla_{\mathbf{v}0}$. Using these operators, we can generalise the result presented in the previous section A.1.2 (equation (A.20)), yielding:

$$\partial_t \rho_a + \nabla_{\mathbf{x}} \cdot (\rho_a \dot{\mathbf{x}}) + \nabla_{\mathbf{v}} \cdot (\rho_a \dot{\mathbf{v}}) + \nabla_{\mathbf{v}^0} \cdot (\rho_a \dot{\mathbf{v}}^0) = 0 \tag{A.22}$$

Here '$\cdot$' defines the *inner product* or *dot product*, defined by $\mathbf{x} \cdot \mathbf{y} = \Sigma_i x_i y_i$.

Non-continuum processes reflecting non-smooth changes in the velocity $\mathbf{v}$ or the continuous attributes $\mathbf{v}^0$, can be modelling by adding a source-like term to the right-hand-side of (A.22), yielding the generic gas-kinetic equations for *n*-dimensional traffic flows:

$$\partial_t \rho_a + \nabla_{\mathbf{x}} \cdot (\rho_a \dot{\mathbf{x}}) + \nabla_{\mathbf{v}} \cdot (\rho_a \dot{\mathbf{v}}) + \nabla_{\mathbf{v}^0} \cdot (\rho_a \dot{\mathbf{v}}^0) = (\partial_t \rho_a)_{NC} \tag{A.23}$$

B EFFECTS OF VEHICULAR SPACE REQUIREMENTS

In this appendix, we will determine the correction factor describing the necessary modification of the interaction rates in order to incorporate finite space requirements of vehicles. Moreover, we will show how the dynamic model equations determined in chapter 6 change by considering drivers' space requirements. That is, assuming that we may apply adiabatic approximation to the model equations, we propose dynamic equations for *modified* or effective density, momentum, and energy.

B.1 Expected amount of occupied space

If we assume that vehicle lengths and reaction times are equal for all vehicles of a class, then we can show that the *modified* or *effective* MLMC-PSD, reflecting the expected number of vehicles *per unit non-occupied roadway space* rather than the expected number of vehicles per unit gross roadway space, equals:

$$\hat{\rho}_{(u,j,1)}(x,v,v^0,t) \stackrel{def}{=} \delta_j(x,t)\rho_{(u,j,1)}(x,v,v^0,t) \tag{B.1}$$

where the *space-requirement correction factor* $\delta_j(x,t)$ equals:

$$\delta_j(x,t) = (1 - \sum_{u' \in \mathbf{U}} r_{(u',j)}((L_{u'} + d_{u'}^{min}) + V_{(u',j)}T_{u'} + (V_{(u',j)}^2 + \Theta_{(u',j)})F_{u'})^{-1} \tag{B.2}$$

with $\delta_j \geq 1$, where L_u is the length of the vehicle, T_u is the *reaction time* T_u of a driver of class u, F_u is the so-called *speed-risk factor*, and d_u^{min} is the *minimal distance headway*.

In the remainder of this section, we will consider the derivation of this correction factor δ_j. To this end, let us consider the required amount of roadway space of a vehicle of class u driving at a velocity v. In addition, let us assume that the total amount of roadway space occupied by a vehicle of class u driving with velocity v is given by (Leutzbach (1988) and Jepsen (1998); see section 2.2.1):

$$l_u(v) = (L_u + d_u^{min}) + v(T_u + vF_u) \tag{B.3}$$

For the sake of simplicity, we will assume that all vehicles of user-class u have equal lengths L_u, reaction times T_u, and speed-risk factors F_u. If we consider cell x of length dx, then the *expected amount of space used by vehicles of class u* driving at velocity v on lane j equals:

$$\tilde{\rho}_{(u,j)}(x,v,t)l_u(v)\mathrm{d}x \tag{B.4}$$

The total amount of space ds of cell x of lane j used by all vehicles (irrespective of their velocity v and the user-class u) equals:

$$\mathrm{d}\,s = \sum_{u'\in\mathbf{U}}\int \tilde{\rho}_{(u',j)}(x,v',t)l_{u'}(v')\mathrm{d}v' = \mathrm{d}\,x\sum_{u'\in\mathbf{U}}(r_{(u',j)}(L_{u'} + d_{u'}^{min}) + m_{(u',j)}T_{u'} + 2e_{(u',j)}F_{u'}) \tag{B.5}$$

If we consider the amount of *non-occupied roadway space dy = dx–ds of cell x*, we find:

$$\mathrm{d}\,y = \mathrm{d}\,x(1 - \textstyle\sum_{u'\in\mathbf{U}}(r_{(u',j)}(L_{u'} + d_{u'}^{min}) + m_{(u',j)}T_{u'} + 2e_{(u',j)}F_{u'})) \tag{B.6}$$

Then, we can define the so-called *vehicle-spacing requirement factor* $\delta_j(x,t)$ by:

$$\delta_j(x,t) \overset{def}{=} \mathrm{d}\,x/\mathrm{d}\,y = (1 - \textstyle\sum_{u'\in\mathbf{U}} r_{(u',j)}(L_{u'} + d_{u'}^{min}) + m_{(u',j)}T_{u'} + 2e_{(u',j)}F_{u'})^{-1} \tag{B.7}$$

Then, clearly $\mathrm{d}x/\mathrm{d}y = \delta_j(x,t)$. In other words, the correction factor equals the *inverse of the expected unused space* on the lane per unit lane space. Consequently $\delta_j(x,t) \geq 1$.

B.2 Modified MLMC-PSD

Using this expression, we can compute the *modified MLMC-PSD* (indicated by the *hat* '^'), determined by the *expected number of vehicles per unit non-occupied roadway space dy*. That is, the expected number of vehicles of class u driving on lane j with velocity v, while having desired velocity v^0 *per unit unoccupied roadway space dy* is equal to:

$$\hat{\rho}_{(u,j,c)}(x,v,v^0,t) \overset{def}{=} (\mathrm{d}\,x/\mathrm{d}\,y)\rho_{(u,j,c)}(x,v,v^0,t) = \delta_j(x,t)\rho_{(u,j,c)}(x,v,v^0,t) \tag{B.8}$$

Similarly, we define the modified reduced phase-space density by $\hat{\tilde{\rho}}_{(u,j,c)} = \delta_j\tilde{\rho}_{(u,j,c)}$.

B.3 Modified interaction rates

The assumption that vehicles, and consequently vehicle platoons, have no physical length, leads to an *underestimation* of the number of interactions per unit time. Let us clarify this by an example.

Figure B-1 shows two cases. Case I deals with traffic operations for very dilute traffic: all vehicles are freely flowing. Clearly, from the amount of space that is (physically) left on the roadway, a fast vehicle entering the roadway stretch will be able to traverse a certain distance without interacting with any of the slower vehicles. In case II the same vehicles are leaders of platoons exhibiting more congested traffic conditions. In this case, little roadway-space is left for manoeuvring. Therefore, a faster vehicle on the roadway will not be able to traverse a very long distance, without interacting with a slower vehicle. Clearly, the real-life interaction-rate in case I should be considerably lower than in case II. However, since we only consider unconstrained platoon-leaders, the interaction rate $\Pi_{(u,j,c)}(x,v,v^0,t;w,\mathbf{b})$ (equation (4.52), section 4.6.3) yields the same value of both cases I and II, caused by the fact that on the one hand, we only consider the free-flowing platoon-leaders, while on the other hand, spacing-requirements of the vehicles are not considered.

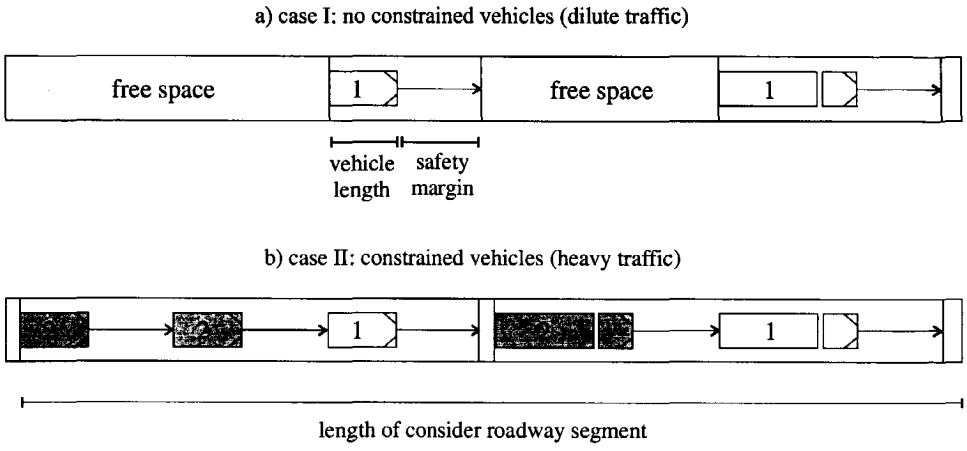

Figure B-1: Different traffic conditions for which the interaction-rates Π are equal, due to an equal number of free-flowing vehicles. Case I shows the *interaction-free* (*unused*) roadway space when traffic conditions are free-flow. Case II shows this roadway space for congested traffic conditions.

By introducing finite space requirements of vehicles, the expected number of interactions increases. That is, the expected number of interactions with vehicles with discrete attributes $\mathbf{b} = (s,j,1)$ having velocity w experienced by a vehicle with discrete attributes $\mathbf{a} = (u,j,c)$ driving with velocity v on lane j equals:

$$\begin{aligned}\hat{\Pi}_{\mathbf{a}}(x,v,v^0,t;w,\mathbf{b}) &= |w-v|\hat{\tilde{\rho}}_{\mathbf{b}}(x,w,t) \\ &= \delta_j(x,t)\,|w-v|\tilde{\rho}_{\mathbf{b}}(x,w,t) \\ &= \delta_j(x,t)\Pi_{\mathbf{a}}(x,v,v^0,t;w,\mathbf{b})\end{aligned} \tag{B.9}$$

The modified event-independent interaction rate, describing the expected number of slower platoons caught up by a vehicle driving with velocity v when incorporating the finite-space requirements of the vehicles is defined by (see equation (4.58)):

$$\hat{\tilde{\Psi}}_{(u',j)}(x,v,t) \overset{def}{=} \int_{-\infty}^{v} \delta_j(x,t)\,|\,w-v\,|\,\hat{\tilde{\rho}}_{(u',j,1)}(x,w,t)\,\mathrm{d}\,w = \delta_j(x,t)\tilde{\Psi}_{(u',j)}(x,v,t) \tag{B.10}$$

and:

$$\hat{\tilde{\Psi}}_{(*,j)}(x,v,t) = \sum_{u'\in U} \hat{\tilde{\Psi}}_{(u',j)}(x,v,t) \tag{B.11}$$

Consequently, the expected number of interactions experienced by vehicles of class u on lane j driving at velocity v, while having a desired velocity equal to v^0 and state c, equals:

$$\hat{\rho}_{(u,j,c)}(x,v,v^0,t)\hat{\tilde{\Psi}}_{(*,j)}(x,v,t) = \delta_j^2(x,t)\rho_{(u,j,c)}(x,v,v^0,t)\tilde{\Psi}_{(*,j)}(x,v,t) \tag{B.12}$$

In other words, the number of interactions increases by the square of δ_j, reflecting the mapping from gross roadway space to unoccupied roadway space. In other words, incorporation of the finite space requirements of the vehicles on the roadway drastically increases the expected number of interactions.

B.4 Introducing finite-space requirements in macroscopic equations

In section B.2, we have introduced the *modified MLMC-PSD*. We have seen that consideration of the expected number of vehicles per unit unused roadway length amounts to multiplying the regular MLMC-PSD by a correction factor δ_j which equals the inverse of the expected unused space on the lane per unit lane space. We can also consider the modified aggregate-state conservative moments, defined by:

$$\hat{N}^k_{(u,j)}(x,t) \overset{def}{=} \delta_j(x,t)N^k_{(u,j)}(x,t) \tag{B.13}$$

Section B.3 discusses the effect of considering the finite space requirements on the expected number of vehicle interactions per unit time. Since expression (B.9) holds, we also have (compare equation (6.12)):

$$\hat{\mathcal{I}}^k_{(u,j)}(x,t) \overset{def}{=} \left\langle \int_{w<v} v^k\,|\,w-v\,|\,\hat{\tilde{\rho}}_{(*,j,1)}(x,v,t)\,\mathrm{d}\,w \right\rangle_{(u,j)} = \delta_j(x,t)\mathcal{I}^k_{(u,j)}(x,t) \tag{B.14}$$

and (compare equation (6.22)):

$$\mathcal{X}^k_{(u,j)}(x,t) \overset{def}{=} \left\langle \int_{w<v} w^k\,|\,w-v\,|\,\hat{\tilde{\rho}}_{(*,j,1)}(x,w,t)\,\mathrm{d}\,w \right\rangle_{(u,j)} = \delta_j(x,t)\mathcal{X}^k_{(u,j)}(x,t) \tag{B.15}$$

B.4.1 Finite space requirements for aggregate-lane aggregate-class density dynamics

Let us now consider the influence of the finite space requirements on the dynamic equations of the MLMC conservative moments $N^k_{(u,j)}$. To this end, consider the MLMC dynamics of the aggregate-state MLMC traffic density (see section 6.4.2):

$$\begin{aligned}\frac{\partial r_{(u,j)}}{\partial t} + \frac{\partial m_{(u,j)}}{\partial x} = &-\sum_{j'=j\pm1}\left(p^{(u,j')}_{(u,j,}r_{(u,j)}\mathcal{I}^0_{(u,j)} - p^{(u,j)}_{(u,j')}r_{(u,j')}\mathcal{I}^0_{(u,j')}\right)\\ &-\sum_{j'=j\pm1}\left(\Delta^{(u,j')}_{(u,j)}r_{(u,j)} - \Delta^{(u,j)}_{(u,j')}r_{(u,j')}\right)\end{aligned} \tag{B.16}$$

Note that:

$$\frac{\partial \hat{r}_{(u,j)}}{\partial t} = \delta_j \frac{\partial r_{(u,j)}}{\partial t} + r_{(u,j)} \frac{\partial \delta_j}{\partial t} \quad \text{and} \quad \frac{\partial \hat{m}_{(u,j)}}{\partial x} = \delta_j \frac{\partial m_{(u,j)}}{\partial x} + m_{(u,j)} \frac{\partial \delta_j}{\partial x} \tag{B.17}$$

We also have:

$$\begin{aligned} \frac{\partial \delta_j}{\partial t} &= \sum_{u'} \left(\frac{\partial \delta_j}{\partial r_{(u',j)}} \frac{\partial r_{(u',j)}}{\partial t} + \frac{\partial \delta_j}{\partial m_{(u',j)}} \frac{\partial m_{(u',j)}}{\partial t} + \frac{\partial \delta_j}{\partial e_{(u',j)}} \frac{\partial e_{(u',j)}}{\partial t} \right) \\ &= -\delta_j^2 \sum_{u' \in U} \left(L_{u'} r_{(u',j)} \frac{\partial r_{(u',j)}}{\partial t} + T_{u'} m_{(u',j)} \frac{\partial m_{(u',j)}}{\partial t} + 2F_{u'} e_{(u',j)} \frac{\partial e_{(u',j)}}{\partial t} \right) \end{aligned} \tag{B.18}$$

and:

$$\frac{\partial \delta_j}{\partial x} = -\delta_j^2 \sum_{u' \in U} \left(L_{u'} r_{(u',j)} \frac{\partial r_{(u',j)}}{\partial x} + T_{u'} m_{(u',j)} \frac{\partial m_{(u',j)}}{\partial x} + 2F_{u'} e_{(u',j)} \frac{\partial e_{(u',j)}}{\partial x} \right) \tag{B.19}$$

Then, we can find the following result:

$$\begin{aligned} r_{(u,j)} \frac{\partial \delta_j}{\partial t} + m_{(u,j)} \frac{\partial \delta_j}{\partial x} &= -\delta_j^2 r_{(u,j)} \sum_{u' \in U} \left(L_{u'} r_{(u',j)} \left(\frac{\partial r_{(u',j)}}{\partial t} + V_{(u,j)} \frac{\partial r_{(u',j)}}{\partial x} \right) + \right. \\ &\left. + T_{u'} m_{(u',j)} \left(\frac{\partial m_{(u',j)}}{\partial t} + V_{(u,j)} \frac{\partial m_{(u',j)}}{\partial x} \right) + 2F_{u'} e_{(u',j)} \left(\frac{\partial e_{(u',j)}}{\partial t} + V_{(u,j)} \frac{\partial e_{(u',j)}}{\partial x} \right) \right) \\ &= -\delta_j^2 r_{(u,j)} \sum_{u' \in U} \left(L_{u'} r_{(u',j)} \left(\frac{\mathrm{d}_{(u,j)} r_{(u',j)}}{\mathrm{d}t} \right) + T_{u'} m_{(u',j)} \left(\frac{\mathrm{d}_{(u,j)} m_{(u',j)}}{\mathrm{d}t} \right) + 2F_{u'} e_{(u',j)} \left(\frac{\mathrm{d}_{(u,j)} e_{(u',j)}}{\mathrm{d}t} \right) \right) \end{aligned} \tag{B.20}$$

where $\mathrm{d}_{(u,j)}/\mathrm{d}t$ indicates the total time derivative of an observer moving along with vehicles of class u on lane j. Assuming that the *adiabatic elimination* (cf. Haken (1983)) can be applied for the observer moving along with the vehicle of class u on lane j, yields:

$$\frac{\mathrm{d}_{(u,j)} r_{(u',j)}}{\mathrm{d}t} \approx 0, \quad \frac{\mathrm{d}_{(u,j)} m_{(u',j)}}{\mathrm{d}t} \approx 0 \quad \text{and} \quad \frac{\mathrm{d}_{(u,j)} e_{(u',j)}}{\mathrm{d}t} \approx 0 \tag{B.21}$$

As a consequence,

$$\begin{aligned} \frac{\partial \hat{r}_{(u,j)}}{\partial t} + \frac{\partial \hat{m}_{(u,j)}}{\partial x} &= \delta_j \left(\frac{\partial r_{(u,j)}}{\partial t} + \frac{\partial m_{(u,j)}}{\partial x} \right) + r_{(u,j)} \frac{\partial \delta_j}{\partial t} + m_{(u,j)} \frac{\partial \delta_j}{\partial x} \\ &\approx \delta_j \left(\frac{\partial r_{(u,j)}}{\partial t} + \frac{\partial m_{(u,j)}}{\partial x} \right) \end{aligned} \tag{B.22}$$

Substitution of the conservation of vehicle equation (B.14), yields the following dynamic equation for the modified MLMC density:

$$\frac{\partial r_{(u,j)}}{\partial t}+\frac{\partial m_{(u,j)}}{\partial x}=-\sum_{j'=j\pm1}\left(p_{(u,j)}^{(u,j')}\frac{\delta_j}{\delta_j}r_{(u,j)}\mathcal{I}_{(u,j)}^{0}-p_{(u,j')}^{(u,j)}\frac{\delta_j}{\delta_{j'}}r_{(u,j')}\mathcal{I}_{(u,j')}^{0}\right)$$
$$-\sum_{j'=j\pm1}\left(\Delta_{(u,j)}^{(u,j')}\frac{\delta_j}{\delta_j}r_{(u,j)}-\Delta_{(u,j')}^{(u,j)}\frac{\delta_j}{\delta_{j'}}r_{(u,j')}\right)) \tag{B.23}$$

By defining the modified immediate lane-changing probability and the modified lane-changing rate respectively by:

$$\hat{p}_{(u,k)}^{(u,l)}\overset{def}{=}\delta_j/\delta_k\hat{p}_{(u,k)}^{(u,l)}\quad\text{and}\quad\hat{\Delta}_{(u,k)}^{(u,l)}\overset{def}{=}\delta_j/\delta_k\Delta_{(u,k)}^{(u,l)}\quad\text{for all } j,k,l \tag{B.24}$$

we can rewrite:

$$\frac{\partial \hat{r}_{(u,j)}}{\partial t}+\frac{\partial \hat{m}_{(u,j)}}{\partial x}=-\sum_{j'=j\pm1}(\hat{p}_{(u,j)}^{(u,j')}\hat{r}_{(u,j)}\hat{\mathcal{I}}_{(u,j)}^{0}-\hat{p}_{(u,j')}^{(u,j)}\hat{r}_{(u,j')}\hat{\mathcal{I}}_{(u,j')}^{0})$$
$$-\sum_{j'=j\pm1}(\hat{\Delta}_{(u,j)}^{(u,j')}\hat{r}_{(u,j)}-\hat{\Delta}_{(u,j')}^{(u,j)}\hat{r}_{(u,j')}) \tag{B.25}$$

Equation (B.25) shows that the dynamics of the modified density of class u on lane j is governed by on the one hand the inflow and outflow of vehicles of class u on lane j in cell x (*convection*). On the other hand, immediate lane changing, postponed lane changing, and spontaneous lane changing cause the modified density to change as well. In this respect, two important remarks must be made.

For one, the introduction of the finite space requirements yields an increase in the number of interactions, causing an increased desire to immediately change to either of the adjacent lanes. Secondly, since the multiplication factor δ_j is generally not equal for each lane j, the *decrease* of the modified density on the vehicle-transmitting lane is not necessarily equal to the *increase* in the modified density on the vehicle-receiving lane.

Application of a similar method applied to the generalised MLMC conservation of vehicle equation discussed in this appendix yields the introduction of finite space requirements in the MLMC traffic momentum and energy dynamics.

C SPECIFICATION OF LANE CHANGING PROBABILITIES

In this appendix, the lane-changing model is described in detail. This model yields the lane changing probabilities for both the unconstrained platoon leaders on the one hand, and the constrained followers on the other hand. This is done by assuming that drivers aim to maximise the utility of their trip, and may consequently attempt to change to another lane to improve their experienced traffic conditions. However, when the gap on the selected target lane does not suffice and is not accepted, the driver may reconsider his target-lane choice and attempt again. In the analysis, we distinguish discretionary and mandatory lane-changes. Before we will propose the description of these processes, we will first consider the structure of the lane changing process in some detail.

C.1 Discretionary lane changing process

Discretionary lane changes occur when a driver is not satisfied with the driving conditions on the currently used lane. With respect to the discretionary lane-changes, we identify four lane-changing types, namely:

1. An *unconstrained immediate lane-change* occurs when a free-flowing vehicle can immediately change to the adjacent lane when actively interacting with a slower vehicle. Thus, we will assume that each interaction will yield the desire to perform an immediate lane-change.
2. A *constrained immediate lane-change* is defined from the perspective of a constrained driver travelling in a platoon of which the platoon leader interacts with a slower platoon. If the platooning vehicle is able to immediately change lanes, thereby

preventing deceleration to an even lower velocity, a constrained immediate lane-change occurs. Again, we assume that an interaction of the platoon leader is an incentive for a constrained vehicle to change to an adjacent lane, since otherwise the interaction results in a speed reduction.

3. When an impeded driver cannot change to either of the adjacent lanes, he will become constrained. We assume that the constrained state is an incentive for a driver to change lanes. When a constrained driver is able to change lanes, a *postponed lane-change* occurs. We will assume that when a postponed lane change has occurred, that the driver – at least temporarily – assumes the free-flowing state, and can thus accelerate to a higher velocity.
4. Finally, a *spontaneous lane-change* occurs when an unconstrained vehicle changes lanes in order to drive on his preferred lane.

C.1.1 Hypothesised model hierarchy

Figure C-1 depicts an overview of the hypothesised model hierarchy for the discretionary lane changing process.

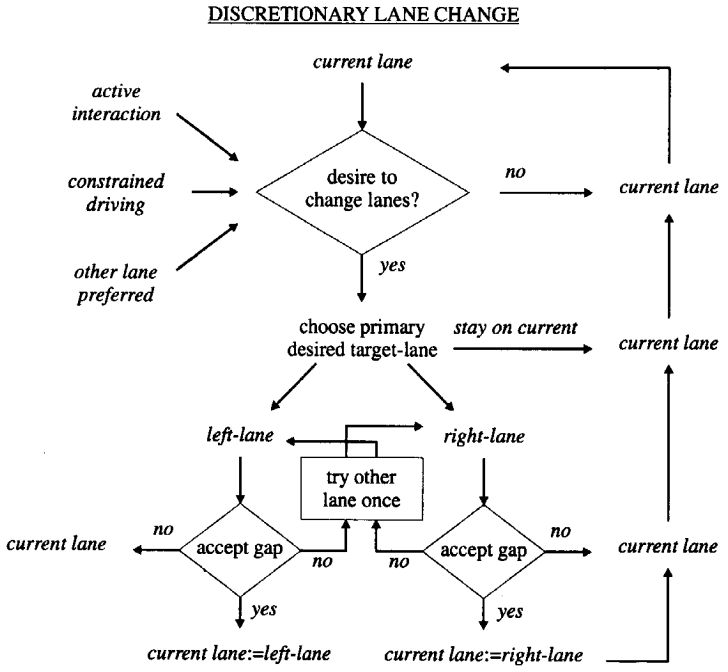

Figure C-1: The discretionary lane-changing decision-model structure.

We have assumed that the probabilities that a vehicle changes lanes depend on the vehicle's velocity vehicle, the driver's desired velocity, the user-class, the lane, and the target lane.

C.1.2 Target-lane choice behaviour

When the incentive for a lane-change is present, the driver first chooses a target-lane. This choice is based on a number of factors, such as the fraction of heavy vehicles, the velocity-differentials between the target-lane and the current lane, and an adjacent ramp indicator (disutility of a lane when adjacent to an on-ramp). When the traffic conditions of the driver do not improve, the driver may also decide to stay on the currently used lane.

Various factors influence the target-lane choice decision, and can be incorporated in the modelling approach. Nevertheless, *when explicitly specifying the model's lane-changing relations*, we will mainly consider traffic operations given European traffic regulations. Consequently, we will assume that for a discretionary lane choice, the first choice option will always be the left roadway lane.

C.1.3 Gap-acceptance behaviour

When the target-lane is selected, the driver looks into the rear-view mirror and decides whether the available gap on the lane is acceptable. In reality, this decision is based on the distance to the vehicle which will be in front on the lane-changing vehicle (the *lead-gap*), and the distance to the vehicle which will be behind the lane-changing vehicle (the *lag-gap*). When both gaps suffice, the lane change will be performed (see Figure C-1). That is, the probability that a gap on the chosen target lane is accepted depends on the joint probability distribution of *lead-gaps* and *lag-gaps* on the target lane (see Figure C-3).

We assume that the lag-gap suffices if the space required by the vehicle on the target-lane, which is behind the lane-changing vehicle, is smaller than the resulting space after the lane-change. The lead-gap suffices if the *required* or minimal space *in front* of the lane-changing vehicle on the target-lane is smaller than the resulting space after the lane-change.

C.2 Mandatory lane-changing process

The focus in this dissertation thesis is on uninterrupted motorway stretches. Nevertheless, we will briefly discuss the *mandatory lane-changing process*. In this respect, the reasons to perform a mandatory lane-change may be among others a lane-drop or closure, merging at a motorway entry or exit, a weaving section, or (class-specific traffic) lane-specific control measures. In these cases, the target-lane will be fixed. However, in case of an incident that blocks a lane, the driver will need to choose a target-lane.

Figure C-2 depicts an overview of the structure of the mandatory lane changing process. The mandatory lane-changing process is considered as a sequence of driver-decisions, potentially leading to a lane change. First, in the rare occasion that the driver's target-lane choice set contains more than one target-lane, the driver chooses the desired lane. In opposition to the discretionary lane-change, the driver considering the mandatory lane change is inclined to accept relatively bad traffic conditions on the target lane. As a consequence, the probability that the driver decides to stay on the current lane will be very small.

When the target-lane is determined, the driver considers if the available gap on the target-lane is acceptable. Compared to the discretionary lane change, the driver might be satisfied with a smaller gap, thereby disturbing the traffic on the target lane considerably.

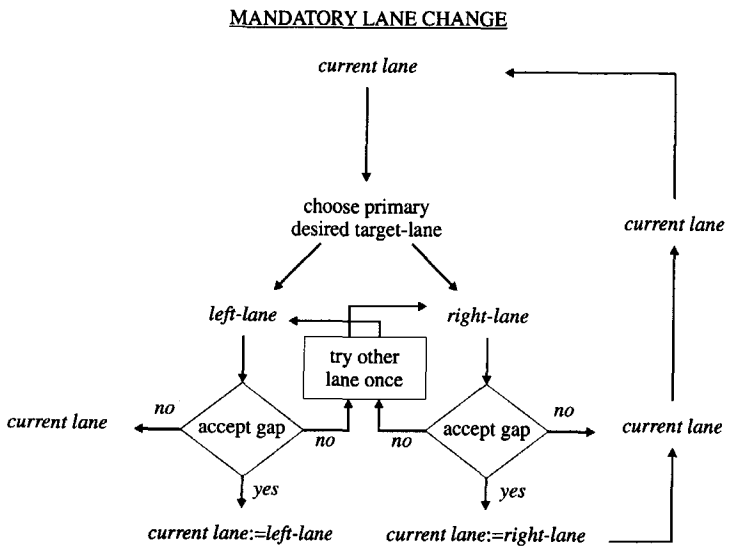

Figure C-2: The mandatory lane-changing decision-model structure.

C.3 Specification of lane-change probabilities

Let us now consider the immediate lane change probability for vehicles of class u driving with velocity v on lane j, which are in state c.

Attribute transitions due to lane-changing

When a lane change occurs, we assume that vehicles undergo an attribute change. That is, the discrete attribute set $\mathbf{a} = (u,j,c)$ changes to $\mathbf{a}' = (u',j',c')$, with $j' \neq j$. The probability of this lane change is denoted by:

$$p_{\mathbf{a}}^{\mathbf{a}'}(v \mid x,t) = p_{(u,j,c)}^{(u',j',c')}(v \mid x,t) \tag{C.1}$$

For instance, if we take the lane-changing process of unconstrained vehicles ($c = 1$) of class u on lane j, then the probability that these vehicles change to the right lane j–1 while staying unconstrained is denoted by $p_{(u,j,1)}^{(u,j-1,1)}(v)$.

Also user-class changes are conceivable. That is, when a constrained vehicle of class $u = \{non\text{-}paying\}$ changes to lane j–1 to make use of the neighbouring pay-lane, while becoming unconstrained, this probability is denoted by $p_{(non-paying,j,2)}^{(paying,j-1,1)}(v)$.

The notational convention that the asterix '*' denotes aggregation with respect to the relevant discrete attribute holds equally for the lane-change probabilities. Moreover, when the notation is unambiguous, the asterix is dropped from notation. In addition, although class transitions can be described using the proposed modelling approach, we will assume that a lane change does not affect the class of a vehicle in this phase of the research.

Target lane choice behaviour

We stated that an *interaction* yields an incentive for a driver to change lanes. That is, when a driver catches up with a slower vehicle, he will consider changing lanes to improve his driving conditions. To this end, he will first choose a *target lane*. This target lane can be the left, right, or even the current lane. In the latter case, a driver decides that he cannot improve his traffic conditions by changing to either of the adjacent lanes. Reasons for this are for instance a high percentage of heavy vehicles, the fact that an on-ramp or off-ramp is nearby, and the likelihood that the driver will catch up with an (even) slower vehicle on the target lane.

The choice for a target-lane is modelled by a discrete choice model (Ben-Akiva (1985)). If we assume that the target-lane choice process can be adequately described by a logit-type model (cf. Ahmed *et al.* (1996)), the probability that target lane j is chosen equals:

$$\Pr(A^{(*,j',*)}_{(u,j,c)}(x,v,v^0,t)) = \frac{\exp(\mathbf{w}^T \mathbf{y}_{(u,j,c)})}{\sum_{k=j-1,j,j+1} \exp(\mathbf{w}^T \mathbf{y}_{(u,k,c)})} \tag{C.2}$$

where $\mathbf{y}_{(u,j,k)} = \mathbf{y}_{(u,j,k)}(x,v,v^0,t)$ denotes the set of lane-change explanatory variables, such as gap to the leader, desired velocity, speed differential between the lanes, the heavy vehicle indicator, the ramp-indicator, and $\mathbf{w}$ denotes a weighing factor, and $A^{(*,j',*)}_{(u,j,c)}(x,v,v^0,t)$ denotes the event that a vehicle characterised by attributes $\mathbf{a} = (u,j,c)$ and (v,v^0) at location x at instant t chooses target-lane j'.

Gap-acceptance behaviour

When a driver chooses either of the adjacent lanes, he will look for a gap on the target lane. We will assume that this gap is composed of two parts, namely the *lead-gap* and the *lag-gap* (see Ahmed *et al.* (1996)). Figure C-3 depicts the definition of the different gaps.

For a *discretionary lane change*, we assume that a vehicle will only change to the target-lane, if both the lag-gap and the lead-gap are large enough, and the gap to the leader is small enough. If we consider a *mandatory lane change*, the accepted lag-gaps and lead-gaps will be considerably smaller.

Let $B^{(*,j',*)}_{(u,j,c)}(x,v,v^0,t)$ denote the probability that a vehicle at x driving at velocity v with desired velocity v^0 at instant t, of class u on lane j with state c accepts the gap on the target-lane j'. Let $\underline{H}$ denote the random variate indicating the *gross total gap*, which is defined by the sum of the *total gap* and *the length of the following vehicle*, on the target lane. In illustration, Figure 8.8 (section 8.2.4) depicts the gross total gap distributions on respectively the left-lane and the right-lane of a two-lane motorway in the Netherlands, for various total density values.

The lead-gap and the lag-gap can be determined from the total gap and the length of the vehicle, if the position x of the vehicle at the time the decision to change to the target-lane is made, is known. However, the MLMC-PSD does not provide information on the exact location of the lane-changing vehicle.

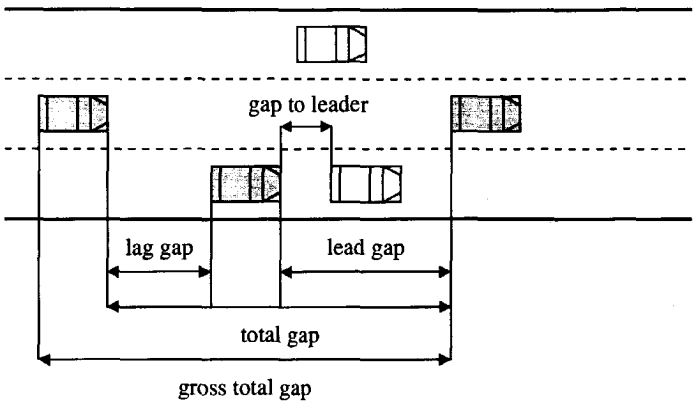

Figure C-3: Definition of gross total gap, total gap, lead gap, and lag gap for a vehicle with target lane = left-lane.

As a consequence, we assume that total target-lane gap is accepted if:

1. The *gross total gap* $\underline{H}^{j'}$ available on the target-lane j' is larger than the total space needed by the lane-changing vehicle (including safety distance).
2. The space that is needed for safe driving by the vehicle on the target that will follow the lane-changing vehicle once the lane-change is completed.

These spaces equal the sum of the length of the vehicles and a velocity-dependent safety margin, for both the vehicle attempting a lane-change as well as the following vehicle. The safety margin equals the velocity of the respective vehicles, multiplied by the user-class specific reaction time of the drivers. Consequently, the probability that the gross-gap on the target-lane suffices equals:

$$
\begin{aligned}
\Pr(B_{(u,j,c)}^{(*,j',*)}) &= \sum_{u'} \Pr(B_{j'} \mid X_{u'}) \times \Pr(X_{u'}) \\
&= \sum_{u'} \Pr(L_u + T_u v + L_{u'} + T_{u'} \underline{V}_{u'}^{j'} \le \underline{H}^{j'}) \times \frac{r_{u'}^{j'}}{r^{j'}} \\
&= \sum_{u'} \frac{r_{u'}^{j'}}{r^{j'}} \int_{h=0}^{\infty} \Pr(L_u + T_u v + L_{u'} + T_{u'} \underline{V}_{u'}^{j'} \le \underline{H}^{j'} \mid \underline{H}^{j'} = h) f_{H^{j'}}(h) \mathrm{d}h \\
&= \sum_{u'} \frac{r_{u'}^{j'}}{r^{j'}} \int_{h=0}^{\infty} \Pr(L_u + T_u v + L_{u'} + T_{u'} \underline{V}_{u'}^{j'} \le h) f_{H^{j'}}(h) \mathrm{d}h \\
&= \sum_{u'} \frac{r_{u'}^{j'}}{r^{j'}} \int_{h=0}^{\infty} \Pr(\underline{V}_{u'}^{j'} \le (h - L_u - T_u v - L_{u'})/T_{u'}) f_{H^{j'}}(h) \mathrm{d}h \\
&= \sum_{u'} \frac{r_{u'}^{j'}}{r^{j'}} \int_{h=0}^{\infty} G_{u'}^{j'}((h - L_u - T_u v - L_{u'})/T_{u'}) f_{H^{j'}}(h) \mathrm{d}h
\end{aligned}
\tag{C.3}
$$

where $f_H(h)$ denotes the gross-gap density function, $G_{u'}^{j'}(v)$ the velocity distribution function of vehicles of class u' on lane j', and $X_u = X_u(x,t)$ is the probability that a vehicle is of class u. Note that when the reaction times T_u are negligible, then Pr(B) equals:

$$\Pr(B_{j'})) = \sum_{u'}(1 - F_{H^{j'}}(L_u + L_{u'}))(r_{u'}^{j'} / r^{j'}) \tag{C.4}$$

Combining primary target-lane choice and gap-acceptance probabilities

By combining the probabilities that a driver chooses a particular target lane j', and the event that a driver accepts the gap on the target-lane, we can determine an immediate overtaking probability. To this end, let us reconsider the probability that lane j' is chosen by the driver. This probability equals the sum of the probability that lane j' is the *primary target lane* of the driver, and the probability that lane j' is the secondary lane choice, while lane $k \neq j'$ is the primary target lane of which the available gap was rejected.

The probability that a driver of class u driving on lane j at a velocity v chooses lane j' and subsequently accepts the gap on this target-lane j' equals:

$$p_{(u,j,c)}^{(*,j',*)}(x, v, v^0, t) = \Pr(A_{(u,j,c)}^{(*,j',*)}) \times \Pr(B_{(u,j,c)}^{(*,j',*)}) \tag{C.5}$$

Note that when the target-lane equals the current lane, that $\Pr(B) = 1$.

Secondary lane choice

If the primary target-lane is either the left lane $j' = j+1$, or the right-lane $j' = j-1$, then with a certain probability, the gap on the primary destination lane is not accepted. When this event occurs, we assume that the driver reconsiders his target lane choice, and chooses a secondary target lane j''. The probability that lane j'' is chosen is denoted by $\Pr(A_{(u,j,c)}^{(*,j''|j',*)})$.

Let us now specify the probability for the event that the left lane $j+1$ is the secondary lane choice, which is accepted for the lane-change manoeuvre. The probability that a driver chooses the left-lane, but cannot accept the gap on this lane, equals:

$$\Pr(A_{(u,j,c)}^{(*,j+1,*)}) \times (1 - \Pr(B_{(u,j,c)}^{(*,j+1,*)})) \tag{C.6}$$

Consequently, the probability that the left lane is the secondary target-lane choice, and is accepted for the lane-change equals:

$$\Pr(A_{(u,j,c)}^{(*,j+1,*)}) \times (1 - \Pr(B_{(u,j,c)}^{(*,j+1,*)})) \times \Pr(A_{(u,j,c)}^{(*,j-1|j+1,*)}) \times \Pr(A_{(u,j,c)}^{(*,j-1,*)}) \tag{C.7}$$

Consequently, the probability that the right lane is chosen and accepted for the lane-changing manoeuvre (either as primary or secondary target lane) by a driver of class u driving on lane j with velocity v equals:

$$p_{(u,j,c)}^{(*,j-1,*)}(v) = \{\Pr(A_{(u,j,c)}^{(*,j-1,*)}) + \Pr(A_{(u,j,c)}^{(*,j+1,*)})(1 - \Pr(B_{(u,j,c)}^{(*,j+1,*)}))\Pr(A_{(u,j,c)}^{(*,j-1|j+1,*)})\}\Pr(B_{(u,j,c)}^{(*,j-1,*)}) \tag{C.8}$$

The probability that the left lane is chosen and accepted for the lane-change equals:

$$p_{(u,j,c)}^{(*,j+1,*)}(v) = \{\Pr(A_{(u,j,c)}^{(*,j+1,*)}) + \Pr(A_{(u,j,c)}^{(*,j-1,*)})(1 - \Pr(B_{(u,j,c)}^{(*,j-1,*)}))\Pr(A_{(u,j,c)}^{(*,j+1|j-1,*)})\}\Pr(B_{(u,j,c)}^{(*,j+1,*)}) \tag{C.9}$$

Note that, for the leftmost lane $j = 1$:

$$p_{(u,1,c)}^{(*,0,*)}(v) = 0 \quad \text{and} \quad p_{(u,1,c)}^{(*,2,*)}(v) = \Pr(A_{(u,1,c)}^{(*,2,*)}) \times \Pr(B_{(u,1,c)}^{(*,2,*)}) \tag{C.10}$$

and the rightmost lane $j = M$, we have:

$$p^{(*,M+1,*)}_{(u,M,c)}(v) = 0 \quad \text{and} \quad p^{(*,M-1,*)}_{(u,M,c)}(v) = \Pr(A^{(*,M-1,*)}_{(u,M,c)}) \times \Pr(B^{(*,M-1,*)}_{(u,M,c)}) \tag{C.11}$$

Moreover, when we consider European traffic regulations, overtaking on the left is prohibited when traffic is not congested. That is, as long as $v>80km/hr$, then:

$$p^{(*,j-1,*)}_{(u,j,c)}(v) = 0 \quad \text{and} \quad p^{(*,j+1,*)}_{(u,j,c)}(v) = \Pr(A^{(*,j+1,*)}_{(u,j,c)}) \times \Pr(B^{(*,j+1,*)}_{(u,j,c)}) \tag{C.12}$$

Finally, the probability that the driver remains on his current lane equals:

$$\begin{aligned} p^{(*,j,*)}_{(u,j,c)}(v) &= \Pr(A^{j}) + (1-\Pr(B^{j-1}))\Pr(A_j^{-j-1}) + (1-\Pr(B^{j+1}))\Pr(A_j^{-j+1}) \\ &= 1 - p^{*}_{(u,j,c)}(v) \end{aligned} \tag{C.13}$$

where:

$$p^{*}_{(u,j,c)}(v) \stackrel{def}{=} p^{(*,j-1,*)}_{(u,j,c)}(v) + p^{(*,j+1,*)}_{(u,j,c)}(v) \tag{C.14}$$

Let us remark that this equals the probability that a driver does not perform an immediate lane change.

D SPECIFICATION OF GENERALISED CONSERVATIVE MOMENT EQUATIONS

In this appendix, we derive the generalised conservative moment equations. Moreover, we specify these terms to describe one-dimensional flow dynamics for free-flowing, platooning, and mixed-state traffic.

D.1 Derivation of the generalised moment equations

In section 5.1, we have established the *reduced generalised gas-kinetic equations* (5.17), describing the dynamics of traffic flows in n-dimensions. Our objective is to use these dynamic equations to derive partial differential equations describing the dynamics of the $\mathbf{k}$-th conservative moments, defined by (see intermezzo II):

$$\begin{aligned} N_a^{\mathbf{k}}(\mathbf{x},t) &\overset{def}{=} N_a^{\mathbf{k},0}(\mathbf{x},t) = [\mathbf{v}^{\mathbf{k}}]_a \\ &= \int\int \mathbf{v}^{\mathbf{k}} \rho_a(\mathbf{x},\mathbf{v},\mathbf{v}^0,t)\,\mathrm{d}\,\mathbf{v}\,\mathrm{d}\,\mathbf{v}^0 = \int \mathbf{v}^{\mathbf{k}} \tilde{\rho}_a(\mathbf{x},\mathbf{v},t)\,\mathrm{d}\,\mathbf{v} \end{aligned} \tag{D.1}$$

where $\mathbf{k} \in I\!N^n$, and where we have used the shorthand notation:

$$\mathbf{v}^{\mathbf{k}} = \prod_{i=1}^{n} v_i^{k_i} \tag{D.2}$$

In multiplying equation (5.17) with $\mathbf{v}^{\mathbf{k}}$ we find:

$$\underbrace{\mathbf{v}^{\mathbf{k}}\partial_t\tilde{\rho}_{\mathfrak{a}}}_{(a)}+\underbrace{\mathbf{v}^{\mathbf{k}}\nabla_{\mathbf{x}}\cdot(\tilde{\rho}_{\mathfrak{a}}\mathbf{v})}_{(b)}+\underbrace{\mathbf{v}^{\mathbf{k}}\nabla_{\mathbf{v}}\cdot(\tilde{\rho}_{\mathfrak{a}}\tilde{A}_{\mathfrak{a}})}_{(c)}=$$
$$\underbrace{-\mathbf{v}^{\mathbf{k}}\sum_{\mathfrak{a}'}\int\int\tilde{\rho}_{\mathfrak{a}}(\mathbf{v})\tilde{\Pi}_{\mathfrak{a}}(\mathbf{v};\alpha)\tilde{\pi}_{\mathfrak{a}}^{\mathfrak{a}'}(\mathbf{v}'\mid\mathbf{v};\alpha)\,\mathrm{d}\,\mathbf{v}'\mathrm{d}\,\alpha}_{(d)}$$
$$\underbrace{+\mathbf{v}^{\mathbf{k}}\sum_{\mathfrak{a}'}\int\int\tilde{\rho}_{\mathfrak{a}'}(\mathbf{v}')\tilde{\Pi}_{\mathfrak{a}'}(\mathbf{v}';\alpha)\tilde{\pi}_{\mathfrak{a}'}^{\mathfrak{a}}(\mathbf{v}\mid\mathbf{v}';\alpha)\,\mathrm{d}\,\mathbf{v}'\mathrm{d}\,\alpha}_{(e)} \tag{D.3}$$
$$\underbrace{-\mathbf{v}^{\mathbf{k}}\sum_{\mathfrak{a}'}\int\int\tilde{\rho}_{\mathfrak{a}}(\mathbf{v})\tilde{\phi}_{\mathfrak{a}}^{\mathfrak{a}'}(\mathbf{v}'\mid\mathbf{v};\beta)\,\mathrm{d}\,\mathbf{v}'\mathrm{d}\,\beta}_{(f)}+\underbrace{\mathbf{v}^{\mathbf{k}}\sum_{\mathfrak{a}'}\int\int\tilde{\rho}_{\mathfrak{a}'}(\mathbf{v}')\tilde{\phi}_{\mathfrak{a}'}^{\mathfrak{a}}(\mathbf{v}\mid\mathbf{v}';\beta)\,\mathrm{d}\,\mathbf{v}'\mathrm{d}\,\beta}_{(g)}$$

To determine the conservative moment equations, we will integrate (D.3) with respect to $\mathbf{v}$. Let us consider terms (a)-(g) consecutively.

D.1.1 Continuum processes

For term (a) we find[2]:

$$\int\mathbf{v}^{\mathbf{k}}\partial_t\tilde{\rho}_{\mathfrak{a}}\,\mathrm{d}\,\mathbf{v}=\partial_t\int\mathbf{v}^{\mathbf{k}}\tilde{\rho}_{\mathfrak{a}}\,\mathrm{d}\,\mathbf{v}=\partial_t N_{\mathfrak{a}}^{\mathbf{k}}(\mathbf{x},t) \tag{D.4}$$

For term (b) we have:

$$\begin{aligned}\int\mathbf{v}^{\mathbf{k}}\nabla_{\mathbf{x}}\cdot(\tilde{\rho}_{\mathfrak{a}}\mathbf{v})\,\mathrm{d}\,\mathbf{v}&=\int\mathbf{v}^{\mathbf{k}}\textstyle\sum_j(\partial_{x_j}(\tilde{\rho}_{\mathfrak{a}}v_j))\,\mathrm{d}\,\mathbf{v}\\&=\int\textstyle\sum_j(\partial_{x_j}\mathbf{v}^{\mathbf{k}}(\tilde{\rho}_{\mathfrak{a}}v_j))\,\mathrm{d}\,\mathbf{v}=\textstyle\sum_j\partial_{x_j}N_{\mathfrak{a}}^{\mathbf{k}+\mathbf{e}_j}(\mathbf{x},t)\end{aligned} \tag{D.5}$$

where $\mathbf{e}_j$ is the j-th unit vector, with $j=1,\ldots,n$.

Let us now consider term (c). We have:

$$\begin{aligned}\int\mathbf{v}^{\mathbf{k}}\nabla_{\mathbf{v}}\cdot(\tilde{\rho}_{\mathfrak{a}}\tilde{A}_{\mathfrak{a}})\,\mathrm{d}\,\mathbf{v}&=\int\mathbf{v}^{\mathbf{k}}\textstyle\sum_j(\partial_{v_j}(\tilde{\rho}_{\mathfrak{a}}\{\tilde{A}_{\mathfrak{a}}\}_j))\,\mathrm{d}\,\mathbf{v}\\&=\textstyle\sum_j\int\mathbf{v}^{\mathbf{k}}(\partial_{v_j}(\tilde{\rho}_{\mathfrak{a}}\{\tilde{A}_{\mathfrak{a}}\}_j))\,\mathrm{d}\,\mathbf{v}\end{aligned} \tag{D.6}$$

where $\{A_{\mathfrak{a}}\}_j$ denotes the j-th element of $A_{\mathfrak{a}}$. We rewrite $\Pi_i v_i^{k_i}=v_j^{k_j}\Pi_{i\neq j}v_i^{k_i}$. Consider the integration-range $[a,b]$ of v_j. Then, for any j, we have for $k_j=0$:

$$\begin{aligned}\int(v_j^{k_j}\Pi_{i\neq j}v_i^{k_i})(\partial_{v_j}(\tilde{\rho}_{\mathfrak{a}}\{\tilde{A}_{\mathfrak{a}}\}_j))\,\mathrm{d}\,\mathbf{v}&=\int(\Pi_{i\neq j}v_i^{k_i})(\partial_{v_j}(\tilde{\rho}_{\mathfrak{a}}\{\tilde{A}_{\mathfrak{a}}\}_j))\,\mathrm{d}\,\mathbf{v}\\&=\int_{v_i\neq v_j}(\Pi_{i\neq j}v_i^{k_i})\left(\int_{v_j}(\partial_{v_j}(\tilde{\rho}_{\mathfrak{a}}\{\tilde{A}_{\mathfrak{a}}\}_j))\,\mathrm{d}\,v_j\right)\mathrm{d}\,v_i\\&=\int_{v_i\neq v_j}(\Pi_{i\neq j}v_i^{k_i})\left(\tilde{\rho}_{\mathfrak{a}}\{\tilde{A}_{\mathfrak{a}}\}_j\Big|_{v_j=a}^{b}\right)\mathrm{d}\,v_i\end{aligned} \tag{D.7}$$

while for $k_j\geq 1$, we have by partial integration:

---

[2] If the dependence on $(\mathbf{x},t)$ is unambiguous, in some cases $\mathbf{x}$ and t are dropped from notation.

$$\begin{aligned}\int (v_j^{k_j}\Pi_{i\neq j}v_i^{k_i})(\partial_{v_j}(\tilde{\rho}_a\{\tilde{A}_a\}_j))\mathrm{d}\,\mathbf{v} &= \int (\Pi_{i\neq j}v_i^{k_i})v_j^{k_j}(\partial_{v_j}(\tilde{\rho}_a\{\tilde{A}_a\}_j))\mathrm{d}\,\mathbf{v}\\ &= \int_{v_i\neq v_j}(\Pi_{i\neq j}v_i^{k_i})\left(\int_{v_j} v_j^{k_j}(\partial_{v_j}(\tilde{\rho}_a\{\tilde{A}_a\}_j))\mathrm{d}\,v_j\right)\mathrm{d}\,v_i\\ &= \int_{v_i\neq v_j}(\Pi_{i\neq j}v_i^{k_i})\left(v_j^{k_j}\tilde{\rho}_a\{\tilde{A}_a\}_j\Big|_{v_j=a}^{b} - k_j\int_{v_j=a}^{b} v_j^{k_j-1}(\tilde{\rho}_a\{\tilde{A}_a\}_j)\mathrm{d}\,v_j\right)\mathrm{d}\,v_i\end{aligned} \tag{D.8}$$

By letting $a \to -\infty$ and $b \to \infty$, we find for all k_j:

$$v_j^{k_j}\tilde{\rho}_a\{\tilde{A}_a\}_j\Big|_{v_j=a}^{b} = 0 \tag{D.9}$$

Consequently, for $k_j \geq 1$, we have:

$$\int (v_j^{k_j}\Pi_{i\neq j}v_i^{k_i})(\partial_{v_j}(\tilde{\rho}_a\{\tilde{A}_a\}_j))\mathrm{d}\,\mathbf{v} = -\int (\Pi_{i\neq j}v_i^{k_i})v_j^{k_j-1}(\tilde{\rho}_a\{\tilde{A}_a\}_j)\mathrm{d}\,\mathbf{v} \tag{D.10}$$

For exponential acceleration functions of the form:

$$\{\tilde{A}_a\}_j = \frac{\{\tilde{W}_a(\mathbf{v}\,|\,\mathbf{x},t)\}_j - v_j}{\tilde{\tau}_a(\mathbf{v}\,|\,\mathbf{x},t)} \tag{D.11}$$

expression (D.10) becomes:

$$\begin{aligned}\int (\Pi_i v_i^{k_i})\left(\partial_{v_j}\left(\tilde{\rho}_a\frac{\{\tilde{W}_a(\mathbf{v})\}_j - v_j}{\tilde{\tau}_a(\mathbf{v})}\right)\right)\mathrm{d}\,\mathbf{v} &= -\int (\Pi_{i\neq j}v_i^{k_i})v_j^{k_j-1}\left(\tilde{\rho}_a\frac{\{\tilde{W}_a(\mathbf{v})\}_j - v_j}{\tilde{\tau}_a(\mathbf{v})}\right)\mathrm{d}\,\mathbf{v}\\ &= -\int (\Pi_{i\neq j}v_i^{k_i})v_j^{k_j-1}\left(\frac{\tilde{\rho}_a(\mathbf{x},\mathbf{v},t)\{\tilde{W}_a(\mathbf{v})\}_j}{\tilde{\tau}_a(\mathbf{v})}\right)\mathrm{d}\,\mathbf{v} + \int\frac{\tilde{\rho}_a(\mathbf{x},\mathbf{v},t)}{\tilde{\tau}_a(\mathbf{v})}(\Pi_i v_i^{k_i})\,\mathrm{d}\,\mathbf{v}\end{aligned} \tag{D.12}$$

Let us define the *velocity-independent acceleration time* of vehicles with attribute-set **a** by:

$$\frac{1}{\mathrm{T}_a^{\mathbf{k}}(\mathbf{x},t)} \overset{def}{=} \frac{1}{N_a^{\mathbf{k}}(\mathbf{x},t)}\int\frac{\tilde{\rho}_a(\mathbf{x},\mathbf{v},t)}{\tilde{\tau}_a(\mathbf{x},\mathbf{v},t)}\mathbf{v}^{\mathbf{k}}\,\mathrm{d}\,\mathbf{v} \tag{D.13}$$

which is the *harmonic expected value* of the reduced generalised acceleration time $\tilde{\tau}_a(\mathbf{v}) = \tilde{\tau}_a(\mathbf{x},\mathbf{v},t)$, weighted with the contributions of powers of the velocity given the velocity distribution. Moreover, let us define the *expected acceleration convervative moment-vector* $D_a^{\mathbf{k}}$ with elements:

$$\{D_a^{\mathbf{k}}(x,t)\}_j \overset{def}{=} \int\tilde{\rho}_a(\mathbf{x},\mathbf{v},t)(\Pi_{i\neq j}v_i^{k_i})v_j^{k_j-1}\{\tilde{W}_a(\mathbf{x},\mathbf{v},t)\}_j\frac{\mathrm{T}_a^{\mathbf{k}}(\mathbf{x},t)}{\tilde{\tau}_a(\mathbf{x},\mathbf{v},t)}\mathrm{d}\,\mathbf{v} \tag{D.14}$$

Then, we can recast the result (D.12) as follows: for $k_j = 0$:

$$\int\mathbf{v}^{\mathbf{k}}\left(\partial_{v_j}\left(\tilde{\rho}_a\frac{\{V_a^0(\mathbf{v})\}_j - v_j}{\tilde{\tau}_a(\mathbf{v})}\right)\right)\mathrm{d}\,\mathbf{v} = 0 \tag{D.15}$$

while for $k \geq 1$, we have:

$$\int \mathbf{v}^{\mathbf{k}} \left(\partial_{v_j} \left(\tilde{\rho}_{\mathbf{a}} \frac{\{\tilde{W}_{\mathbf{a}}(\mathbf{v})\}_j - v_j}{\tilde{\tau}_{\mathbf{a}}(\mathbf{v})} \right) \right) \mathrm{d}\mathbf{v} = -k_j \frac{\{D_{\mathbf{a}}^{\mathbf{k}}(\mathbf{x},t)\}_j - N_{\mathbf{a}}^{\mathbf{k}}(\mathbf{x},t)}{T_{\mathbf{a}}^{\mathbf{k}}(\mathbf{x},t)} \tag{D.16}$$

D.1.2 Non-continuum processes

Let us consider contributions of transitions caused by events. If we integrate term (*d*) of eq. (D.3) with respect to the elements of **v**, we have:

$$\int \mathbf{v}^{\mathbf{k}} \int\int \tilde{\rho}_{\mathbf{a}}(\mathbf{v}) \tilde{\Pi}_{\mathbf{a}}(\mathbf{v};\alpha) \tilde{\pi}_{\mathbf{a}}^{\mathbf{a}'}(\mathbf{v}' \mid \mathbf{v};\alpha) \mathrm{d}\mathbf{v}' \mathrm{d}\alpha = [\mathbf{v}^{\mathbf{k}} \int\int \tilde{\Pi}_{\mathbf{a}}(\mathbf{v};\alpha) \tilde{\pi}_{\mathbf{a}}^{\mathbf{a}'}(\mathbf{v}' \mid \mathbf{v};\alpha) \mathrm{d}\mathbf{v}' \mathrm{d}\alpha]_{\mathbf{a}} \tag{D.17}$$

We will assume that this term can be factorised as follows:

$$[\mathbf{v}^{\mathbf{k}} \int\int \tilde{\Pi}_{\mathbf{a}}(\mathbf{v};\alpha) \tilde{\pi}_{\mathbf{a}}^{\mathbf{a}'}(\mathbf{v}' \mid \mathbf{v};\alpha) \mathrm{d}\mathbf{v}' \mathrm{d}\alpha]_{\mathbf{a}} = r_{\mathbf{a}}(\mathbf{x},t) p_{\mathbf{a}\to\mathbf{a}'}(\mathbf{x},t) \mathcal{I}_{\mathbf{a}}^{\mathbf{k}}(\mathbf{x},t) \tag{D.18}$$

where $r_{\mathbf{a}}(\mathbf{x},t)$ denotes the traffic density, $p_{\mathbf{a}\to\mathbf{a}'}(\mathbf{x},t)$ denotes the *expected event-aggregate probability* that, i.e. the probability that a vehicle **a** experiencing an event changes its attributes to **a**′. The *k-order moment-decreasing event rate* $\mathcal{I}_{\mathbf{a}}^{\mathbf{k}}(\mathbf{x},t)$ denotes resulting changes in the **k**-order conservative moment $N_{\mathbf{a}}^{\mathbf{k}}(\mathbf{x},t)$ per vehicle of class **a**. We will explain this factorisation in more detail in the ensuing of this appendix. Let us note that the expected probabilities $p_{\mathbf{a}(i)\to\mathbf{a}(j)}$ constitute a transition matrix transition matrix $\mathbf{P}(\mathbf{x},t) = \{p_{ij}(\mathbf{x},t)\}$.

For term (*e*) of (D.3), we can establish similar relations. By interchanging **v** and **v**′, we find:

$$\int \mathbf{v}^{\mathbf{k}} \int\int \tilde{\rho}_{\mathbf{a}'}(\mathbf{v}') \tilde{\Pi}_{\mathbf{a}'}(\mathbf{v}';\alpha) \tilde{\pi}_{\mathbf{a}'}^{\mathbf{a}}(\mathbf{v} \mid \mathbf{v}';\alpha) \mathrm{d}\mathbf{v}' \mathrm{d}\alpha \mathrm{d}\mathbf{v} = [\int\int (\mathbf{v}')^{\mathbf{k}} \tilde{\Pi}_{\mathbf{a}'}(\mathbf{v};\alpha) \tilde{\pi}_{\mathbf{a}'}^{\mathbf{a}}(\mathbf{v}' \mid \mathbf{v};\alpha) \mathrm{d}\mathbf{v}' \mathrm{d}\alpha]_{\mathbf{a}'} \tag{D.19}$$

In this case, we assume that this result can be factorised as follows:

$$[\int\int (\mathbf{v}')^{\mathbf{k}} \tilde{\Pi}_{\mathbf{a}'}(\mathbf{v};\alpha) \tilde{\pi}_{\mathbf{a}'}^{\mathbf{a}}(\mathbf{v}' \mid \mathbf{v};\alpha) \mathrm{d}\mathbf{v}' \mathrm{d}\alpha]_{\mathbf{a}'} = r_{\mathbf{a}'}(\mathbf{x},t) p_{\mathbf{a}'\to\mathbf{a}}(\mathbf{x},t) \mathcal{X}_{\mathbf{a}'}^{\mathbf{k}}(\mathbf{x},t) \tag{D.20}$$

With respect to the dynamic influences on the *k*-th conservative moment due to condition-driven transitions (terms (*f*) and (*g*)), let us define the velocity-independent *k*-th order average condition-driven transition-rate from attribute-set **a**(*i*) to **a**(*j*) by:

$$f_{\mathbf{a}\to\mathbf{a}'}^{\mathbf{k}} = \frac{[\int\int \mathbf{v}^{\mathbf{k}} \tilde{\phi}_{\mathbf{a}}^{\mathbf{a}'}(\mathbf{v}' \mid \mathbf{v};\beta) \mathrm{d}\mathbf{v}' \mathrm{d}\beta]}{N_{\mathbf{a}}^{\mathbf{k}}} \quad \text{and} \quad g_{\mathbf{a}'\to\mathbf{a}}^{\mathbf{k}} = \frac{[\int\int (\mathbf{v}')^{\mathbf{k}} \tilde{\phi}_{\mathbf{a}'}^{\mathbf{a}}(\mathbf{v} \mid \mathbf{v}') \mathrm{d}\mathbf{v}' \mathrm{d}\beta]}{N_{\mathbf{a}'}^{\mathbf{k}}} \tag{D.21}$$

Using the definitions of the condition driven transition coefficients for the *k*-th conservative moment enables recasting terms (*f*) and (*g*) as follows:

$$\int (\Pi_i v_i^{k_i}) \sum_{\mathbf{a}'} \int \tilde{\rho}_{\mathbf{a}}(\mathbf{v}) \tilde{\phi}_{\mathbf{a}}^{\mathbf{a}'}(\mathbf{v}' \mid \mathbf{v}) \mathrm{d}\mathbf{v}' \mathrm{d}\mathbf{v} = \sum_{\mathbf{a}'} f_{\mathbf{a}\to\mathbf{a}'}^{\mathbf{k}} N_{\mathbf{a}}^{\mathbf{k}} \tag{D.22}$$

$$\int (\Pi_i v_i^{k_i}) \sum_{\mathbf{a}'} \int \tilde{\rho}_{\mathbf{a}'}(\mathbf{v}') \tilde{\phi}_{\mathbf{a}'}^{\mathbf{a}}(\mathbf{v} \mid \mathbf{v}') \mathrm{d}\mathbf{v}' \mathrm{d}\mathbf{v} = \sum_{\mathbf{a}'} g_{\mathbf{a}'\to\mathbf{a}}^{\mathbf{k}} N_{\mathbf{a}'}^{\mathbf{k}} \tag{D.23}$$

D.1.3 Dynamic equations for n-dimensional traffic flows

In combining these results for terms (*a*)-(*g*), we find the following macroscopic dynamic equations for the **k**-th order conservative moment:

$$\underbrace{\partial_t N_{\mathbf{a}}^{\mathbf{k}}(\mathbf{x},t)}_{(a)} + \underbrace{\sum_j \partial_{x_j} N_{\mathbf{a}}^{\mathbf{k}+\mathbf{e}_j}(\mathbf{x},t)}_{(b)} - \underbrace{\sum_{j=1}^{n} k_j \frac{\{D_{\mathbf{a}}^{\mathbf{k}}(\mathbf{x},t)\}_j - N_{\mathbf{a}}^{\mathbf{k}}(\mathbf{x},t)}{T_{\mathbf{a}}^{\mathbf{k}}(\mathbf{x},t)}}_{(c)} =$$
$$- \underbrace{\sum_{\mathbf{a}'} r_{\mathbf{a}}(\mathbf{x},t)\mathcal{I}_{\mathbf{a}}^{\mathbf{k}}(\mathbf{x},t)p_{\mathbf{a}\to\mathbf{a}'}(\mathbf{x},t)}_{(d)} + \underbrace{\sum_{\mathbf{a}'} r_{\mathbf{a}'}(\mathbf{x},t)\mathcal{X}_{\mathbf{a}'}^{\mathbf{k}}(\mathbf{x},t)p_{\mathbf{a}'\to\mathbf{a}}(\mathbf{x},t)}_{(e)} \qquad \text{(D.24)}$$
$$- \underbrace{\sum_{\mathbf{a}'} N_{\mathbf{a}}^{\mathbf{k}}(\mathbf{x},t)f_{\mathbf{a}\to\mathbf{a}'}^{\mathbf{k}}(\mathbf{x},t)}_{(f)} + \underbrace{\sum_{\mathbf{a}'} N_{\mathbf{a}'}^{\mathbf{k}}(\mathbf{x},t)g_{\mathbf{a}'\to\mathbf{a}}^{\mathbf{k}}(\mathbf{x},t)}_{(g)}$$

D.1.4 Dynamic equations for one-dimensional traffic flows

For one-dimensional traffic flows, the dynamic equations of the k-th order conservative moment $N_{\mathbf{a}}{}^{k}(x,t)$ can be cast in matrix-vector notation, by defining the vectors $\mathbf{N}^k$ of conservative moments $N_{\mathbf{a}}{}^{k}$:

$$\underbrace{\partial_t \mathbf{N}^k}_{(a)} + \underbrace{\partial_x \mathbf{N}^{k+1}}_{(b)} = \underbrace{k\frac{\mathbf{D}^k - \mathbf{N}^k}{\bar{T}^k}}_{(c)} - \underbrace{\oplus(\mathbf{r}\otimes\bar{\mathcal{I}}^k\otimes\mathbf{P})}_{(d)} - \underbrace{\oplus(\mathbf{N}^k\otimes\mathbf{F}^k)}_{(f)}$$
$$+ \underbrace{\oplus(\mathbf{r}\otimes\bar{\mathcal{X}}^k\otimes\mathbf{P})^T}_{(e)} + \underbrace{\oplus(\mathbf{N}^k\otimes\mathbf{G}^k)^T}_{(g)} \qquad \text{(D.25)}$$

D.2 Conservative moments equation for free-flowing vehicles (c = 1)

Let us first consider the case $\mathbf{a} = (u,j,c)$ for $c = 1$ (*unconstrained vehicles*). Let us specify the terms of the conservative moment equation (D.25) for *platoon leaders* ($\mathbf{a} = (u,j,1)$).

D.2.1 Continuum processes

The terms (a) and (b) in equation (D.25) remain unchanged. With respect to term (c), let us recall that the acceleration time τ_u^0 of free-flowing vehicles is constant. Consequently, the acceleration time $T^k_{(u,j,1)}$ equals:

$$T^k_{(u,j,1)} = \tau_u^0 \quad \text{for all } k \qquad \text{(D.26)}$$

Then, the expected acceleration moment simplifies to:

$$D^k_{(u,j,1)} \overset{def}{=} \int \tilde{\rho}_{(u,j,1)} v^{k-1} \tilde{W}_{(u,j,1)}(v)\,\mathrm{d}\,v \qquad \text{(D.27)}$$

D.2.2 Non-continuum processes

Next, let us consider term (d), depicting the dynamics caused by event-driven transitions. We only consider interaction events. An interaction-event with a slow vehicle either yields a deceleration, or an immediate lane-change of the fast vehicle. Let us respectively discuss both processes.

Deceleration. Let us consider an unconstrained vehicle driving with velocity v interacting with another unconstrained vehicle of class s on lane j that is driving with velocity w (referred to as event $\alpha = (w,(s,j,1))$). In section 5.2 we have shown that the reduced deceleration probability equals:

$$\tilde{\pi}^{(u,j,2)}_{(u,j,1)}(v' \mid v;w,(s,j,1)) = \begin{cases} (1-p^{*}_{(u,j,1)}(v \mid x,t))\delta(v'-w), & v > w \\ 0, & \text{elsewhere} \end{cases} \tag{D.28}$$

We have also determined the *event-rate* for events $\alpha = (w,(s,j,1))$:

$$\tilde{\Pi}_{(u,j,c)}(v;w,(s,j,1)) = \mid w-v \mid \tilde{\rho}_{(s,j,1)}(x,w,t) \tag{D.29}$$

Using (D.28) (D.29), we can determine:

$$\begin{aligned} &\int\int \tilde{\Pi}_{(u,j,1)}(v;w,(*,j,1))\tilde{\pi}^{(u,j,2)}_{(u,j,1)}(v' \mid v;w,(*,j,1))\,\mathrm{d}\,\mathbf{v}'\,\mathrm{d}\,w \\ &= (1-p^{*}_{(u,j,1)}(v))\int_{v'<v} \mid v'-v \mid \rho_{(*,j,1)}(x,v',t)\,\mathrm{d}\,v' = (1-p^{*}_{(u,j,1)}(v))\tilde{\Psi}_{(*,j)}(x,v,t) \end{aligned} \tag{D.30}$$

For deceleration, let us define the **k**-order aggregate-event rate by:

$$\mathcal{I}^{k}_{(u,j,1)}(x,t) = \frac{[v^{k}(1-p^{*}_{(u,j,1)}(v))\tilde{\Psi}_{(*,j)}(x,v,t)]_{(u,j,1)}}{r_{(u,j,1)}(x,t)\cdot p_{(u,j,c\to 2)}(x,t)} \tag{D.31}$$

where we have defined the expected aggregate-event probability by:

$$p_{(u,j,c\to 2)}(x,t) = \left\langle (1-p^{*}_{(u,j,1)}(v)) \right\rangle_{(u,j,1)} \tag{D.32}$$

Note that if the immediate lane-changing probabilities are independent of the velocity v, then:

$$\mathcal{I}^{k}_{(u,j,1)}(x,t) = \frac{1}{r_{(u,j,1)}(x,t)}[v^{k}\tilde{\Psi}_{(*,j)}(x,v,t)]_{(u,j,1)} \tag{D.33}$$

The contribution of the *deceleration process* thus becomes:

$$r_{(u,j,1)}\mathcal{I}^{k}_{(u,j,1)}p_{(u,j,1\to 2)} = [(1-p^{*}_{(u,j,1)}(v))v^{k}\tilde{\Psi}_{(*,j)}(v)]_{(u,j,1)} \tag{D.34}$$

Immediate lane-changing. In section 5.2, we have determined the reduced immediate lane-changing transition probability:

$$\tilde{\pi}^{(u,j',c')}_{(u,j,c)}(v' \mid v;w,(s,j,1)) = \begin{cases} p^{(u,j',c')}_{(u,j,c)}(v \mid x,t)\delta(v'-v), & v > w, \mathbf{b} = (s,j,1) \\ 0, & \text{elsewhere} \end{cases} \tag{D.35}$$

yielding:

$$\int\int \tilde{\Pi}_{(u,j,1)}(v;w,(*,j,1))\tilde{\pi}^{(u,j',1)}_{(u,j,1)}(v' \mid v;w,(*,j,1))\,\mathrm{d}\,\mathbf{v}'\,\mathrm{d}\,w = p^{(u,j',1)}_{(u,j,1)}(v)\tilde{\Psi}_{(*,j)}(x,v,t) \tag{D.36}$$

For immediate lane-changing, we define the **k**-order aggregate-event rate by:

$$\mathcal{I}^{k}_{(u,j,1)}(x,t) = \frac{[v^{k}p^{(u,j',1)}_{(u,j,1)}(v)\tilde{\Psi}_{(*,j)}(x,v,t)]_{(u,j,1)}}{r_{(u,j,1)}(x,t)\cdot p_{(u,j\to j',1)}(x,t)} \tag{D.37}$$

where we have defined the expected aggregate-event probability by:

$$p_{(u,j\to j',1)}(x,t) = \left\langle p^{(u,j',1)}_{(u,j,1)}(v) \right\rangle_{(u,j,1)} \tag{D.38}$$

The contribution of the *deceleration process* thus becomes:

$$\sum_{j'=j\pm1} r_{(u,j,1)} \mathcal{I}^k_{(u,j,1)} p_{(u,j\to j',1)} = \sum_{j'=j\pm1} [p^{(u,j',1)}_{(u,j,1)}(v) v^k \tilde{\Psi}_{(*,j)}(v)]_{(u,j,1)} \tag{D.39}$$

Thus, considering of these active event-driven transitions, we can specify term (*d*) of the dynamic equation (D.25) as follows:

$$\begin{aligned} &\sum_{\mathbf{a}'} r_{\mathbf{a}}(x,t) \mathcal{I}^k_{\mathbf{a}}(x,t) p_{\mathbf{a}\to\mathbf{a}'}(x,t) \quad \Rightarrow \\ &\qquad [(1 - p^{*}_{(u,j,1)}(v)) v^k \tilde{\Psi}_{(*,j)}(v)]_{(u,j,1)} + \sum_{j'=j\pm1} [p^{(u,j',1)}_{(u,j,1)}(v) v^k \tilde{\Psi}_{(*,j)}(v)]_{(u,j,1)} \end{aligned} \tag{D.40}$$

Let us now consider term (*e*) of (D.25). Since faster vehicles decelerating to a lower velocity v also undergo a state-change (c:1→2), the positive influence of deceleration caused by interactions is non-existent for unconstrained vehicles. However, immediate lane-changing vehicles on adjacent lanes $j\pm1$ *do* cause the conservative moments to increase. We find for (*e*):

$$\begin{aligned} &\sum_{\mathbf{a}'} r_{\mathbf{a}'}(x,t) \mathcal{X}^k_{\mathbf{a}'}(x,t) p_{\mathbf{a}'\to\mathbf{a}}(x,t) \quad \Rightarrow \\ &\qquad \sum_{j'=j\pm1} [p^{(u,j,1)}_{(u,j',1)}(v) v^k \tilde{\Psi}_{(*,j')}(v)]_{(u,j',1)} + \sum_{j'=j\pm1} [p^{(u,j,1)}_{(u,j',2)}(v) v^k \tilde{\Psi}_{(*,j')}(v)]_{(u,j',2)} \end{aligned} \tag{D.41}$$

Spontaneous and postponed lane-changing. With respect to term (*f*) of expression (D.25), let us consider the reduction in the conservative moments due to spontaneous lane changing. For the elements of $\mathbf{F}^k$ we find:

$$f^k_{(u,j\to j\pm1,1)} = [v^k \Delta^{(u,j\pm1,1)}_{(u,j,1)}(v)]_{(u,j,1)} / N^k_{(u,j,1)} \tag{D.42}$$

which yields:

$$\sum_{\mathbf{a}'} N^k_{\mathbf{a}}(x,t) f^k_{\mathbf{a}\to\mathbf{a}'}(x,t) \quad \Rightarrow \quad \sum_{j'=j\pm1} [v^k \Delta^{(u,j',1)}_{(u,j,1)}(v)]_{(u,j,1)} \tag{D.43}$$

Finally, with respect to term (*g*) of expression (D.25), we note that the unconstrained conservative moments increase due to vehicles of class u on the adjacent lanes $j\pm1$ able to change to lane j, due to either postponed or spontaneous lane changing. Moreover, constrained vehicles 'unconstraining' also cause an increase over time. For the spontaneous and postponed dynamics, we find for the elements of $\mathbf{G}^k$:

$$g^k_{(u,j\pm1\to j,c')} = [v^k \Delta^{(u,j,1)}_{(u,j\pm1,c')}(v)]_{(u,j\pm1,c')} / N^k_{(u,j\pm1,c')} \tag{D.44}$$

while for the relaxation process we have:

$$g^k_{(u,j,2\to1)} = [v^k \tilde{\Xi}(\Delta^{(u,*,1)}_{(u,j,1)} \tilde{\rho}_{(u,j,1)}(v))]_{(u,j,2)} / N^k_{(u,j,2)} \tag{D.45}$$

Consequently, we find:

$$\sum_{\mathbf{a}'} N^k_{\mathbf{a}'}(x,t) g^k_{\mathbf{a}'\to\mathbf{a}}(x,t) \Rightarrow$$
$$\sum_{j'=j\pm1} [v^k \Delta^{(u,j,1)}_{(u,j',1)}(v)]_{(u,j',1)} + \sum_{j'=j\pm1} [v^k \Delta^{(u,j,1)}_{(u,j',2)}(v)]_{(u,j',2)} + [v^k \tilde{\Xi}(\Delta^{(u,*,1)}_{(u,j,1)} \tilde{\rho}_{(u,j,1)}(x,v,t))]_{(u,j,2)} \quad \text{(D.46)}$$

D.2.3 Resulting conservative moment dynamics for free-flowing traffic

In collecting terms (*a*)-(*g*), we can specify the conservative moments dynamics for unconstrained vehicles of class u on lane j. Assuming that event-driven transition probabilities and condition-driven transition-rates can be adequately approximated by quantities that are independent of velocity v, we find the following simplified expression for the dynamics of the conservative moments of unconstrained vehicles of class u on lane j:

$$\begin{aligned}
&\partial_t N^k_{(u,j,1)} + \underbrace{\partial_x N^{k+1}_{(u,j,1)}}_{(1)} = \underbrace{k \frac{D^k_{(u,j,1)} - N^k_{(u,j,1)}}{\tau^0_u}}_{(2)} - \underbrace{(1 - p^*_{(u,j1)}) r_{(u,j,1)} \mathcal{I}^k_{(u,j,1)}}_{(3)} \\
&\quad - \underbrace{\sum_{j'=j\pm1} (p^{(u,j',1)}_{(u,j,1)} r_{(u,j,1)} \mathcal{I}^k_{(u,j,1)} - p^{(u,j,1)}_{(u,j',1)} r_{(u,j',1)} \mathcal{I}^k_{(u,j',1)})}_{(6)} \\
&\quad + \underbrace{\sum_{j'=j\pm1} p^{(u,j,1)}_{(u,j',2)} r_{(u,j',2)} \mathcal{I}^k_{(u,j',2)}}_{(7)} - \underbrace{\sum_{j'=j\pm1} (\Delta^{(u,j',1)}_{(u,j,1)} N^k_{(u,j,1)} - \Delta^{(u,j,1)}_{(u,j',1)} N^k_{(u,j',1)})}_{(8)} \\
&\quad + \underbrace{[v^k \tilde{\Xi}(\Delta^{(u,*,1)}_{(u,j,1)} \tilde{\rho}_{(u,j,1)}(v))]_{(u,j,2)}}_{(5)} + \underbrace{\sum_{j'=j\pm1} \Delta^{(u,j,1)}_{(u,j',2)} N^k_{(u,j',1)}}_{(9)}
\end{aligned} \quad \text{(D.47)}$$

for all $u \in \mathbf{U}$ and $j = 1,\ldots,M$, where the k-th order interaction moment is defined by:

$$\mathcal{I}^k_{(u,j,c)} \overset{def}{=} \left\langle v^k \tilde{\Psi}_{(*,j)}(v) \right\rangle_{(u,j,c)} = [v^k \tilde{\Psi}_{(*,j)}(v)]_{(u,j,c)} / r_{(u,j,c)} \quad \text{(D.48)}$$

This moment describes the expected flux of the k-th moment from lane j per unit time per immediately overtaking vehicle.

D.3 Conservative moments equation for platooning vehicles (c = 2)

Let us now consider the specification of the conservative moment dynamic equations (D.25) for the constrained platooning vehicles $\mathbf{a} = (u,j,2)$.

D.3.1 Continuum processes

The terms (*a*) and (*b*) of equation (D.25) remain unchanged. Let us now consider the acceleration process of the platooning vehicles (term (*c*)). In chapter 4 we have proposed expressions describing the dynamics of platooning vehicles able to accelerate with the platoon leader to the desired velocity of the latter. Using these specifications, we can determine the velocity-independent acceleration time $T^k_{(u,j,2)}$ using equation (6.10). Moreover, we determine the k-th expected desired moment for platooning vehicles using equation (6.11).

D.3.2 Non-continuum processes

Let us consider term (*d*) of equation (D.25). This term depicts the dynamics caused by event-driven transitions.

Deceleration. The dynamic changes caused by platooning vehicles decelerating is equivalent to the effect of deceleration on free-flowing vehicles (equation (D.34)). That is, the contribution of the deceleration processes with respect to the conservative moment equations for platooning vehicles equals (equation (D.25) for $\mathbf{a} = (u,j,2)$):

$$r_{(u,j,2)}\mathcal{I}^k_{(u,j,2)}p_{(u,j,2\to 2)} = [(1-p^*_{(u,j,2)}(v))v^k\tilde{\Psi}_{(*,j)}(v)]_{(u,j,1)} \tag{D.49}$$

where $p^k_{(u,j,2\to 2)}$ is 'velocity independent' probability that a platooning vehicles is unable to immediately change lanes after interacting with a slower platoon. Similarly, the contribution of platooning vehicles immediately changing to an adjacent lane j' equals:

$$\sum_{j'=j\pm 1} r_{(u,j,2)}\mathcal{I}^k_{(u,j,2)}(k)p_{(u,j\to j',2)} = \sum_{c'=1,2}\sum_{j'=j\pm 1}[p^{(u,j',c')}_{(u,j,2)}(v)v^k\tilde{\Psi}_{(*,j)}(v)]_{(u,j,2)} \tag{D.50}$$

Thus, term (*d*) of equation (D.25) yields:

$$\begin{aligned}&\sum_{\mathbf{a}'} r_{\mathbf{a}}(x,t)\mathcal{I}^k_{\mathbf{a}}(x,t)p_{\mathbf{a}\to\mathbf{a}'}(x,t) \quad \Rightarrow \\ &\quad [(1-p^*_{(u,j,2)}(v))v^k\tilde{\Psi}_{(*,j)}(v)]_{(u,j,2)} + \sum_{c'=1,2}\sum_{j'=j\pm 1}[p^{(u,j',c')}_{(u,j,2)}(v)v^k\tilde{\Psi}_{(*,j)}(v)]_{(u,j,2)}\end{aligned} \tag{D.51}$$

Deceleration and immediate-lane changing. Term (*e*) of equation (D.25) reflects the *increase* in the unconstrained conservative moments due to *events*. For platooning vehicles, these may either be caused by:

1. Vehicles that decelerate to velocity v.
2. Constrained vehicles of class u on the adjacent lanes j' performing an immediate lane change to lane j.

For events $\alpha = (w,(*,j,1))$ (i.e. interactions with unconstrained vehicles on lane j that are driving with velocity w), we find for $c' = 1,2$:

$$r_{(u,j,c')}\mathcal{X}^k_{(u,j,c')}p_{(u,j,c'\to 2)} = (1-p^*_{(u,j,c')}(v\,|\,x,t)[w^k\textstyle\int_{v>w}|\,w-v\,|\,\tilde{\rho}_{(*,j,1)}(w)\,\mathrm{d}\,w]_{(u,j,c')} \tag{D.52}$$

where we have used:

$$\tilde{\pi}^{(u,j,2)}_{(u,j,c')}(v'\,|\,v;w,(*,j,1)) = (1-p^*_{(u,j,c')}(v\,|\,x,t))\delta(v'-w) \tag{D.53}$$

Considering the constrained vehicles on the adjacent lanes that are able to change to lane j, but remain constrained, we find an expression equivalent to (D.39). In combining these results, we find that for term (*e*) of equation (D.25):

$$\begin{aligned}&\sum_{\mathbf{a}'} r_{\mathbf{a}'}(x,t)\mathcal{X}^k_{\mathbf{a}'}(x,t)p_{\mathbf{a}'\to\mathbf{a}}(x,t) \quad \Rightarrow \\ &\qquad \sum_{c'=1,2}[(1-p^*_{(u,j,c')}(v)\textstyle\int_{w<v}w^k\,|\,w-v\,|\,\tilde{\rho}_{(*,j,1)}(w)\,\mathrm{d}\,w]_{(u,j,c')} \\ &\qquad + \sum_{j'=j\pm 1}[p^{(u,j,2)}_{(u,j',2)}(v)v^k\tilde{\Psi}_{(*,j')}(v)]_{(u,j',2)}\end{aligned} \tag{D.54}$$

Spontaneous and postponed lane-changing. With respect to the condition-driven transition rates for constrained vehicles (terms (*f*) and (*g*) of equation (D.25)), similar remarks can be made as for unconstrained vehicles. Similarly, we find:

$$\sum_{\mathbf{a}'} N^k_{\mathbf{a}'}(x,t) g^k_{\mathbf{a}'\to\mathbf{a}}(x,t) = \sum_{j'=j\pm 1} [v^k \Delta^{(u,j',1)}_{(u,j,2)}(v)]_{(u,j,2)} + [v^k \tilde{\Xi}(\Delta^{(u,*,1)}_{(u,j,1)} \tilde{\rho}_{(u,j,1)}(v))]_{(u,j,2)} \tag{D.55}$$

Since none of the condition-driven processes cause an increase in the conservative moments of the platooning vehicles, we have:

$$\sum_{\mathbf{a}'} N^k_{\mathbf{a}}(x,t) f^k_{\mathbf{a}\to\mathbf{a}'}(x,t) = 0 \tag{D.56}$$

D.3.3 Resulting conservative moment dynamics for free-flowing traffic

In collecting terms (*a*)-(*g*), we find the equation describing the *k*-th conservative moments dynamics for the constrained vehicles of class *u* on lane *j*. By assuming that the event-driven transition probabilities and the condition-driven can be adequately approximated by quantities that are independent on the velocity *v*, we find the following simplified expression for the dynamics of the conservative moments of constrained vehicles of class *u* on lane *j*:

$$\begin{aligned}
&\partial_t N^k_{(u,j,2)} + \underbrace{\partial_x N^{k+1}_{(u,j,2)}}_{(1)} = \underbrace{k \frac{D^k_{(u,j,2)} - N^k_{(u,j,2)}}{T^k_{(u,j,2)}}}_{(2)} + \underbrace{(1-p^*_{(u,j,1)}) r_{(u,j,1)} \mathcal{X}^k_{(u,j,1)}}_{(3)} - \underbrace{\sum_{j'=j\pm 1} \Delta^{(u,j',1)}_{(u,j,2)} N^k_{(u,j,2)}}_{(8)} \\
&\quad \underbrace{-(1-p^*_{(u,j,2)}) r_{(u,j,2)} \mathcal{R}^k_{(u,j,2)}}_{(3+4)} - \underbrace{\sum_{j'=j\pm 1} p^{(u,j',1)}_{(u,j,2)} r_{(u,j,2)} \mathcal{I}^k_{(u,j,2)}}_{(7)} \\
&\quad \underbrace{- \sum_{j'=j\pm 1} (p^{(u,j',2)}_{(u,j,2)} r_{(u,j,2)} \mathcal{I}^k_{(u,j,2)} - p^{(u,j,2)}_{(u,j',2)} r_{(u,j',2)} \mathcal{I}^k_{(u,j',2)})}_{(7)} - \underbrace{[v^k \tilde{\Xi}(\Delta^{(u,*,1)}_{(u,j,1)} \tilde{\rho}_{(u,j,1)}(v))]_{(u,j,2)}}_{(5)}
\end{aligned} \tag{D.57}$$

where the *k-th order balanced interaction moment* equals:

$$\mathcal{R}^k_{(u,j,c)} = \mathcal{I}^k_{(u,j,c)} - \mathcal{X}^k_{(u,j,c)} \tag{D.58}$$

and where the *k-th order increasing interaction moment* is defined by::

$$\mathcal{X}^k_{(u,j,c)} \overset{def}{=} \left\langle \int_{w<v} w^k \,|\, w-v \,|\, \tilde{\rho}_{(*,j,1)}(w) \mathrm{d}\, w \right\rangle_{(u,j,c)} = \frac{[\int_{w<v} w^k \,|\, w-v \,|\, \tilde{\rho}_{(*,j,1)}(w) \mathrm{d}\, w]_{(u,j,c)}}{r_{(u,j,c)}} \tag{D.59}$$

Note that we can rewrite this expression by changing the order of integration:

$$r_{(u,j,c)} \mathcal{X}^k_{(u,j,c)} = \sum_{u'} \left[v^k \int_{w>v} |w-v| \tilde{\rho}_{(u,j,c)}(w) \mathrm{d}\, w \right]_{(u',j,c)} \tag{D.60}$$

E SHOCK-WAVES, EXPANSION-FANS AND THE RIEMANN PROBLEM

In this appendix we discuss the formation of shocks and expansion fans in MLMC traffic flow operations in more detail. Also, we discuss the so-called *Riemann problem* for the inviscid macroscopic mixed-state flow equations. This problem is defined by a single discontinuity in elsewhere homogeneous and equilibrium traffic flow conditions. The results presented in this appendix are similar but not equal to the results from analysing the Riemann problem in a continuous medium. That is, the formation of shocks in traffic flow is different from similar processes in continuum media.

E.1 Shocks and contact discontinuities

In this appendix, we first discuss the formation of contact discontinuities and shocks in the MLMC traffic flow. That is, we will discuss the well know fact that inviscid Navier-Stokes-like or *Euler* equations, such as the MLMC-traffic flow model presented in this dissertation thesis, allow *discontinuous solutions* is certain cases. For the one-dimensional problem, these discontinuous solutions are the *contact discontinuities* and the *shock waves*.

We show that shock-waves in traffic are formed by *intersecting C^- characteristics*. In this respect, traffic flow differs from the flow in continuous media, where shocks are formed by intersecting C^+ characteristics (Hirsch (1990b)): in opposition to flows in fluids or gases, a *decrease* in the density is (in equilibrium circumstances) accompanied by an *increase* in the velocity and velocity variance. The extent to which these increases/decreases relate depends on the traffic regime (free-flow, congested).

E.1.1 The Rankine-Hugoniot relations

Let $\Sigma_{(u,j)}(x,t) = 0$ define a discontinuity (a sudden jump in the traffic density, velocity, and/or pressure) moving with velocity $V_{(u,j)}{}^{C}$. Moreover, let '$[a]$' indicate the *jump* in the quantity a across the discontinuity. Then, the *Rankine-Hugoniot relations* can be used to determine the magnitude in the jump of the traffic flow variables, given the velocity $V_{(u,j)}{}^{C}$ of the discontinuity (cf. Hirsch (1990a)):

$$[m_{(u,j)}] = [r_{(u,j)} V_{(u,j)}] = V^{C}_{(u,j)} [r_{(u,j)}] \tag{E.1}$$

$$[2e_{(u,j)}] = [r_{(u,j)} V^{2}_{(u,j)} + P_{(u,j)}] = V^{C}_{(u,j)} [m_{(u,j)}] \tag{E.2}$$

and

$$[m_{(u,j)} H_{(u,j)}] = V^{C}_{(u,j)} [e_{(u,j)}] \tag{E.3}$$

E.1.2 Shocks

The most important type of discontinuity is probably the shock. Shocks can be identified by a non-zero traffic flow through the discontinuity. As a consequence, the traffic pressure $P_{(u,j)}$ and the velocity $V_{(u,j)}$ undergo discontinuous variations:

$$[r_{(u,j)}] \neq 0 \qquad [V_{(u,j)}] \neq 0 \qquad [P_{(u,j)}] \neq 0 \tag{E.4}$$

Let us now explain how shocks can appear in MLMC traffic flow. To this end, let us assume that we can neglect the source terms in the inviscid MLMC traffic flow equations. This is justified when the MLMC traffic flow operations are in equilibrium.

Intersection of the $C_{(u,j)}{}^{+}$ characteristics

Let us consider the case where the slopes of the characteristic curves decrease with increasing x. In particular, let us consider $\nabla(V_{(u,j)}+c_{(u,j)})<0$. In this case, the situation illustrated in Figure E-1 occurs. Here, the $C_{(u,j)}{}^{+}$ characteristic emanating from Y^{+} intersects the $C_{(u,j)}{}^{+}$ characteristic issuing from $Y_1{}^{+}$. Since the variations on the quantity $V_{(u,j)}+c_{(u,j)}$ are transported along the $C_{(u,j)}{}^{+}$ characteristics, a multi-valued quantity would occur in Y_1.

If we neglect the source terms in the flow, the Riemann variables are conserved along the characteristics. In this case, we have:

$$(V_{(u,j)} + c_{(u,j)})_{Y_1} = (V_{(u,j)} + c_{(u,j)})_{Y^{+}} \text{ and } (V_{(u,j)} + c_{(u,j)})_{Y_1} = (V_{(u,j)} + c_{(u,j)})_{Y_1^{+}} \tag{E.5}$$

where:

$$(V_{(u,j)} + c_{(u,j)})_{Y^{+}} \neq (V_{(u,j)} + c_{(u,j)})_{Y_1^{+}} \tag{E.6}$$

This impossible situation leads to discontinuous flow called a *shock wave*. Shapiro (1953) shows that the shock velocity $V_{(u,j)}{}^{C}$ satisfies:

$$(V_{(u,j)} + c_{(u,j)})_{Y_1^{+}} < V^{C}_{(u,j)} < (V_{(u,j)} + c_{(u,j)})_{Y^{+}} \tag{E.7}$$

That is, the velocity of the shock wave lies between the slopes of the $C_{(u,j)}{}^{+}$ characteristics. Let us consider the case where:

$$(V_{(u,j)})_{Y_1^+} < (V_{(u,j)})_{Y^+} \tag{E.8}$$

That is, the expected velocity of class *u* on lane *j decreases* spatially. We will now show that, unlike the shock wave behaviour in inviscid fluids, it is unlikely that the intersection C_{uj}^+ characteristics yield a discontinuity in the traffic flow, given equilibrium traffic conditions.

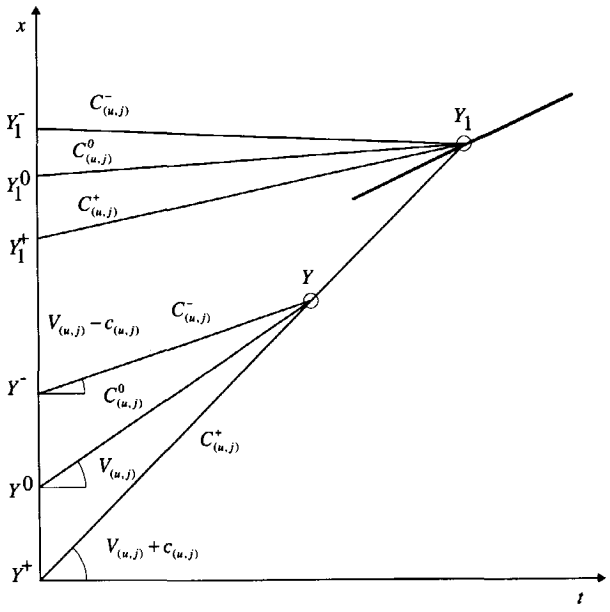

Figure E-1: Intersecting characteristics of class u on lane j for $\nabla(V_{(uj)}+c_{(uj)})<0$.

To this end, let us reconsider the first Rankine-Hugoniot condition:

$$[r_{(u,j)}V_{(u,j)}] = V^C_{(u,j)}[r_{(u,j)}] \tag{E.9}$$

Since the Riemann variables are conserved along the C_{uj}^+ characteristics, we can rewrite:

$$[r_{(u,j)}V_{(u,j)}] = (r_{(u,j)}V_{(u,j)})_{Y_1^+} - (r_{(u,j)}V_{(u,j)})_{Y^+} = (V_{(u,j)})_{Y_1^+}[r_{(u,j)}] + (r_{(u,j)})_{Y^+}[V_{(u,j)}] \tag{E.10}$$

Using this result, for the shock-velocity $V_{(uj)}{}^C$, we have the following relation:

$$\begin{aligned} &V^C_{(u,j)} > (V_{(u,j)} + c_{(u,j)})_{Y_1^+} \quad \Rightarrow \\ &V^C_{(u,j)} - (V_{(u,j)})_{Y_1^+} > (V_{(u,j)} + c_{(u,j)})_{Y_1^+} - (V_{(u,j)})_{Y_1^+} = (c_{(u,j)})_{Y_1^+} > 0 \end{aligned} \tag{E.11}$$

The Rankine-Hugoniot relations yields:

$$[r_{(u,j)}V_{(u,j)}] = V^C_{(u,j)}[r_{(u,j)}] \quad \Rightarrow \quad (r_{(u,j)})_{Y^+}[V_{(u,j)}] = (V^C_{(u,j)} - (V_{(u,j)})_{Y_1^+})[r_u^j] \tag{E.12}$$

Since $[V_{(uj)}]<0$, and $r_{(uj)}>0$, we find the necessary condition:

$$[r_{(u,j)}] > 0 \tag{E.13}$$

That is, in order for the shock caused by intersecting $C_{(u,j)}^{+}$ characteristics, both the velocity *and* the density should decrease spatially. In equilibrium MLMC traffic flow, this can only occur if the traffic composition changes spatially. Specifically, when the traffic densities of the other classes spatially increases to the extent that the equilibrium velocity of class u decreases while the traffic density of class u decreases. However, when the traffic composition remains (approximately) constant, this *cannot occur*. That is, the condition $[r_{(u,j)}]$ necessary for a discontinuity in the solution of the MLMC inviscid flow equations is not satisfied.

Intersection of the $C_{(u,j)}^{-}$ characteristics

The other delimiting case is the case of intersection $C_{(u,j)}^{-}$ characteristics. Similar to the occurrence of the compression shock discussed in the previous section, we assume that the slopes of the $C_{(u,j)}^{-}$ characteristics decrease with increasing x, that is, we assume that $\partial(V_{(u,j)} - c_{(u,j)}) < 0$. As a consequence, the $C_{(u,j)}^{-}$ characteristics will intersect. The Riemann variables are conserved along the characteristics. In this case, we have:

$$(V_{(u,j)} - c_{(u,j)})_{Y_1} = (V_{(u,j)} - c_{(u,j)})_{Y^-} \text{ and } (V_{(u,j)} - c_{(u,j)})_{Y_1} = (V_{(u,j)} - c_{(u,j)})_{Y_1^-} \tag{E.14}$$

where:

$$(V_{(u,j)} - c_{(u,j)})_{Y^-} \neq (V_{(u,j)} - c_{(u,j)})_{Y_1^-} \tag{E.15}$$

We can again show that, if a shock is formed by these intersecting characteristics, the velocity of the shock $V_{(u,j)}^{C}$ would be between the velocities of the characteristic curves, that is:

$$(V_{(u,j)} - c_{(u,j)})_{Y_1^-} < V_{(u,j)}^{C} < (V_{(u,j)} - c_{(u,j)})_{Y^-} \tag{E.16}$$

Let us remark that, in opposition to the shock formed by intersection $C_{(u,j)}^{+}$ characteristics, the shock formed by the intersecting $C_{(u,j)}^{-}$ characteristics can not only be directed downstream, but can also be stationary, or directed in the upstream direction.

Let us assume that the expected velocity $V_{(u,j)}$ decreases spatially. Generally, in equilibrium traffic flow, the local sonic velocity decreases as well. The assumption that the slopes of the characteristics intersect puts restraints on the magnitude of the spatial decreases in the local sonic velocity. Thus, across the shock we have:

$$[V_{(u,j)}] < 0 \quad \text{and} \quad [c_{(u,j)}] < 0 \tag{E.17}$$

Since we neglect the source terms in the flow, the Riemann variables are conserved along these characteristics. In this case, we have:

$$(V_{(u,j)} - c_{(u,j)})_{Y_1} = (V_{(u,j)} - c_{(u,j)})_{Y^-} \text{ and } (V_{(u,j)} - c_{(u,j)})_{Y_1} = (V_{(u,j)} - c_{(u,j)})_{Y_1^-} \tag{E.18}$$

where:

$$(V_{(u,j)} - c_{(u,j)})_{Y^-} \neq (V_{(u,j)} - c_{(u,j)})_{Y_1^-} \tag{E.19}$$

Thus, if the $C_{(u,j)}^{-}$ characteristics intersect, a shock occurs at the point of intersection. In this case, the velocity of the shock lies somewhere between the velocities of the characteristics (cf. Shapiro (1953)), i.e. the velocity $V_{(u,j)}^{C}$ satisfies :

$$(V_{(u,j)} - c_{(u,j)})_{Y_1^-} < V_{(u,j)}^C < (V_{(u,j)} - c_{(u,j)})_{Y^-} \tag{E.20}$$

We can rewrite the first Rankine-Hugoniot condition to obtain:

$$\begin{aligned} [r_{(u,j)}V_{(u,j)}] &= (r_{(u,j)})_{Y_1^-}[V_{(u,j)}] + (V_{(u,j)})_{Y^-}[r_{(u,j)}] = V_{(u,j)}^C[r_{(u,j)}] \\ &\Leftrightarrow \\ (r_{(u,j)})_{Y_1^-}[V_{(u,j)}] &= (V_{(u,j)}^C - (V_{(u,j)})_{Y^-})[r_{(u,j)}] \end{aligned} \tag{E.21}$$

In combining this result with:

$$\begin{aligned} &V_{(u,j)}^C < (V_{(u,j)} - c_{(u,j)})_{Y^-} \quad \Rightarrow \\ &V_{(u,j)}^C - (V_{(u,j)})_{Y^-} < (V_{(u,j)} - c_{(u,j)})_{Y^-} - (V_{(u,j)})_{Y^-} = -(c_{(u,j)})_{Y^-} \end{aligned} \tag{E.22}$$

and since, $r_{(u,j)}>0$, and $[V_{(u,j)}]<0$, we have the following necessary condition for a discontinuity across the shock:

$$[r_{(u,j)}] > 0 \tag{E.23}$$

That is, the traffic density jump across the shock wave $\Sigma_{(u,j)}$ is *positive*, i.e. the traffic density increases spatially. Since the local sonic velocity decreases spatially, the velocity variance also decreases spatially.

The jump in the traffic pressure is dependent on the direction of the shock wave. The direction of the shock wave depends on the flowrates at either side of the discontinuity. That is:

$$[r_{(u,j)}V_{(u,j)}] = V_{(u,j)}^C[r_{(u,j)}] \quad \text{with} \quad [r_{(u,j)}] > 0 \quad \Rightarrow \quad \text{sign}(V_{(u,j)}^C) = \text{sign}([r_{(u,j)}V_{(u,j)}]) \tag{E.24}$$

We can prove that the jump in the traffic pressure $P_{(u,j)}$ is also positive:

$$[P_{(u,j)}] > 0 \tag{E.25}$$

Contact discontinuities

Another discontinuity that potentially arises is the *contact discontinuity*. A contact discontinuity is characterised by the conditions that no vehicles flow through the discontinuity $\Sigma_{(u,j)}$. This implies that the velocity $V_{(u,j)}$ is equal on both sides of the discontinuity. Also, the velocity of the contact discontinuity equals the velocity of the expected velocity of the vehicles of class u on lane j. Using the Rankine-Hugoniot condition (E.2), we can conclude that since $V_{(u,j)}{}^C = V_{(u,j)}$, that:

$$\begin{aligned} [r_{(u,j)}V_{(u,j)}^2 + P_{(u,j)}] &= [r_{(u,j)}V_{(u,j)}^2] + [P_{(u,j)}] \\ &= V_{(u,j)}^C[m_{(u,j)}] = V_{(u,j)}[r_{(u,j)}V_{(u,j)}] = V_{(u,j)}^2[r_{(u,j)}] \end{aligned} \tag{E.26}$$

yielding:

$$[P_{(u,j)}] = 0 \tag{E.27}$$

That is, the traffic pressure $P_{(u,j)}$ is continuous on the discontinuity. This implies that there is a jump in the density $r_{(u,j)}$ across the discontinuity $\Sigma_{(u,j)}$:

$$[r_{(u,j)}] \neq 0 \tag{E.28}$$

Concluding, a contact discontinuity represents an interface between two fluid regions of different densities but equal pressure. However, since the contact interface moves with the traffic flow, the velocity has to be continuous over a contact discontinuity.

Expansion waves

Finally, note that the conditions for the occurrence of a *compression shock* can be expressed by the fact that the characteristics on both sides intersect the shock. This means that information carried by the characteristics is propagated towards the discontinuity. Hirsch (1990b) proposes a hypothetical *expansion shock* would lead to a situation where $(V_{(u,j)} + c_{(u,j)})_{Y_1^+} > C_{(u,j)} > (V_{(u,j)} + c_{(u,j)})_{Y^+}$ instead, and to characteristics carrying information *away* from the discontinuity.

E.2 Traffic dynamics and the Riemann problem

Let us consider the aggregate-lane aggregate-class inviscid traffic flow equations[3] cast using the pseudo-primitive variables (see section 7.3):

$$\frac{\partial r}{\partial t} + \frac{\partial m}{\partial x} = 0 \tag{E.29}$$

$$\frac{\partial V}{\partial t} + V\frac{\partial V}{\partial x} = -\frac{\Theta}{r}\frac{\partial r}{\partial x} - \frac{\partial \Theta}{\partial x} + \frac{V^e - V}{\mathrm{T}} \tag{E.30}$$

$$\frac{\partial P}{\partial t} + 3P\frac{\partial V}{\partial x} + V\frac{\partial P}{\partial x} = 2\frac{P^e - P}{\mathrm{T}} \tag{E.31}$$

Let us define the Riemann problem for this traffic flow model by considering a roadway with *homogeneous* and *equilibrium* traffic conditions, i.e. $\partial \mathbf{w}/\partial x = 0$, and $m = m^e$, and $e = e^e$ for all $x \neq 0$ at the initial time $t = 0$. However, at $x = 0$, a discontinuity is present. That is, a jump in the traffic density, velocity, and pressure. Let us assume that the density jump is positive. Since traffic operates under equilibrium conditions, the jump in the velocity is negative. The jump in the traffic pressure can either be positive, zero, or negative, depending on the velocity that occurs due to the discontinuity at $x = 0$.

Let us now discuss the traffic dynamics for $t>0$ in the case that the initial conditions are equal to the situation described in the previous section. To this end, we will distinguish two situations, namely when the shock-wave originating from the discontinuity at $x = 0$ moves upstream or downstream.

In chapter 7 we have established that the shock-wave-velocity V^C equal the ratio between the momentum jump $[rV]$ and the density jump $[r]$ across the discontinuity. This shock-wave is a result from intersecting C^- characteristics. Let us first consider the case where the shock-

[3] The notions discussed here can be applied effortlessly to the MLMC traffic flow equations presented in this dissertation thesis.

wave has a negative velocity V^C. This implies that both the momentum rV and the pressure P are decreased across the discontinuity (see chapter 7).

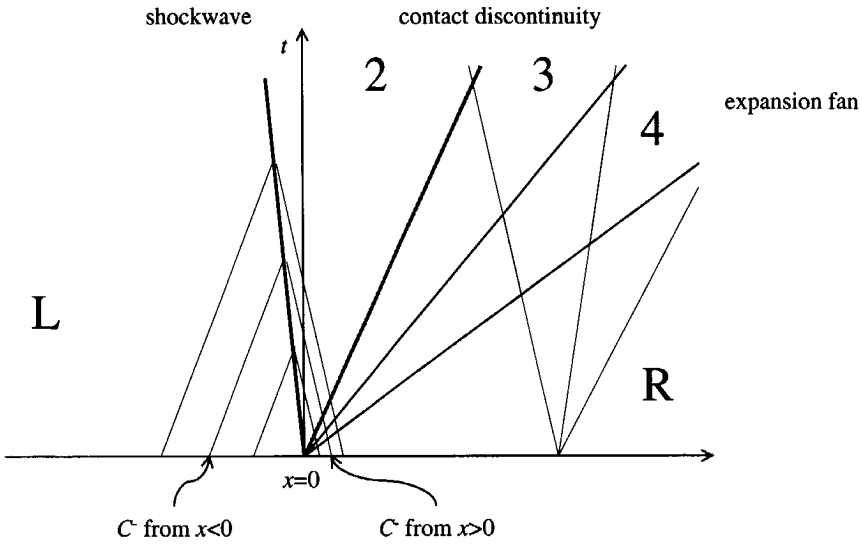

Figure E-2: Characteristics and discontinuities at the interface between two traffic states.

Over time, five regions are formed. The regions L and R indicate the regions where the traffic conditions are unaffected. The region L is defined by the *shock wave* moving upstream into the upstream high pressure region, while the region R defined by the C^+ forming an downstream moving *expansion fan* which is formed by the C^+ characteristics emanating from the low pressure region having slopes $V+c$. This wave also originates from the discontinuity at $x = 0$. Finally, a *contact discontinuity* separating the two traffic regimes propagates downstream. Let us consider the characteristics and discontinuities more closely. Since both the shock and the contact discontinuity move in the regions of uniform traffic conditions, they will have a constant velocity (see Figure E-2).

The shock wave separates the region of undisturbed high traffic pressure L from the region 2 of disturbed high traffic pressure. The contact discontinuity separates this region 2 from the disturbed low traffic pressure region 3, which in turn has been influenced by the expansion fan – region 5 – propagating to the left into the undisturbed low traffic pressure region L.

Shock waves

We have mentioned that a shock wave is generated between the regions L and 2. For the velocity V_2 and the pressure P_2, the Rankine-Hugoniot conditions (E.1)–(E.3) apply. By consideration of these conditions, Hirsch (1990b) shows that the following relations hold:

$$\frac{r_2}{r_R}=\frac{1+2P}{2+P} \qquad \frac{V_2-V_R}{c_R}=\tfrac{1}{3}\sqrt{3}\cdot\frac{P-1}{\sqrt{1+2P}}$$
$$\frac{C-V_R}{c_R}=\frac{(P-1)c_R}{3(V_2-V_R)} \qquad \left|\frac{c_2}{c_R}\right|^2=P\frac{2+P}{1+2P} \tag{E.32}$$

where $P = P_2/P_R$ is the traffic pressure ratio.

Contact discontinuity

The contact surface sustains a discontinuity in the density. The traffic pressures and velocities are however continuous. Therefore, the contact discontinuity propagates at a velocity $V = V_2$. Along this surface, we have:

$$P_3 = P_2 \tag{E.33}$$

$$V_3 = V_2 = V \tag{E.34}$$

Expansion fan

The expansion fan is formed by the right running characteristics with slopes $V+c$ and the information between the regions L and 3 that is transmitted along the C^0 and the C^+ characteristics. Hirsch (1990) shows that along the C^0 characteristic, we have:

$$P_3 / r_3 = P_L / r_L \tag{E.35}$$

Along the C^- characteristic, the Riemann-variable is constant:

$$V_L - c_L = V_3 - c_3 \tag{E.36}$$

By combining these relations, we obtain a relation between P_3 and V:

$$V_L - V_3 = c_L(1-\sqrt[3]{P_3 / P_L}) \tag{E.37}$$

The above relations allow the determination of all constant states in the regions 2, 3 and L. In particular, expressing equation (E.35) in equation (E.32) leads to a relation between $V_2 = V$ and the pressure ratio P. Another relation between V and P is obtained by introducing the condition of pressure continuity across the contact surface (E.33) in equation (E.37). Elimination of V between these two relations leads to an implicit equation for the pressure ratio P:

$$\tfrac{1}{3}\sqrt{3}\frac{P-1}{\sqrt{1+2P}}=\frac{c_L}{c_R}\left[\left(\frac{P_L}{P_R}\right)^{1/3}-P^{1/3}\right]+\frac{V_L-V_R}{c_R} \tag{E.38}$$

This equation can be solved, for example using an iterative method. Using P, all other quantities can be determined from the relations (E.32)-(E.37).

F DATA-AGGREGATION APPROACH

This appendix presents the approach to aggregate observations of individual vehicles described in section 8.2 into aggregate traffic flow observations. Since choosing fixed aggregation intervals can result in a very low number of observations per user-class – or very long aggregation intervals – we have opted for an alternative data aggregation method. That is, rather than choosing fixed interval lengths, we consider fixed sample sizes (e.g. 25 person-cars, or 10 trucks). In addition to being beneficial from the viewpoint of user-class distinction, from a statistical point of view this approach also has its merits, as will be pointed out in the remainder of this appendix.

F.1.1 Data aggregation and analysis approach

Let us consider *temporal aggregation* of individual vehicle observations collected during a period $[t,t+\Delta t)$, aiming to determine statistically significant estimations of expected values of relevant traffic flow variables. By aggregating observations, we aim to delineate stochastic fluctuations inherent to traffic flow observations from dynamic changes in these expected values. For instance, we aim to determine an estimation of the expected velocity $V(x,t)$ that, on the one hand, is statistically significant, while on the other hand, clearly shows dynamic changes in the expected velocity caused by changes in traffic conditions.

Considering the expected velocity $V(x,t)$, it is well known that an unbiased estimate can be determined by considering the *harmonic average* of the (local) velocity measurements:

$$\hat{V}(x,t) = \left(\frac{1}{|\,\mathrm{A}(x,t;\Delta t)\,|} \sum_{\alpha' \in \mathrm{A}(x,t;\Delta t)} \frac{1}{v_{\alpha'}} \right)^{-1} \tag{F.1}$$

where $\mathrm{A}(x,t;\Delta t)$ is the set of vehicles that have passed the observation location x during the interval $[t,t+\Delta t)$, and $|\mathrm{A}|$ is the number of elements in the set A. The statistical significance of

this estimate depends among others on the variance in the velocity observations during the observation period and on the number of observations |A|. The variance in the velocity observations is determined by the variance of the velocity distribution on the one hand, and the dynamic changes of the expected velocity on the other hand.

As has been observed from empirical studies (cf. Helbing (1997)), the *equilibrium velocity variance* is a *decreasing function* of the traffic density. That is, when traffic becomes increasingly congested, the velocity variance decreases accordingly. Conequently, when traffic conditions are dilute, velocitys variance are relatively large. However, for uncongested traffic conditions, the number of observations in the sample (that is, the number of vehicles that have passed the observation location during the interval $[t,t+\Delta t)$) is an *increasing* function of traffic density. That is, when the density increases, the number of observations increases. As a consequence, the statistical significance *reduces* with *decreasing* traffic density, due to both the increase in the velocity variance on the one hand, and a decrease on the number of observations in the sample on the other hand. Moreover, since the number of observations in the sample is not known a priori, we cannot estimate the significance of derived approximations.

With respect to *multiclass multilane data analysis*, the number of observations with respect to each of the distinguished user-classes will also vary significantly. That is, if only 15% of the traffic consists of trucks, the number of observed trucks in a period is likely to be small, implying that the relevant means can only be determined with small accuracy, or using a very long interval length.

F.1.2 Alternative data aggregation approach

In this thesis, we propose a different approach, solving the problems of time-aggregation to a certain extent. Instead of classifying the data according to the different periods, the data is aggregated according to the number of vehicles having passed the observation point. That is, starting at some time instant t_n, the number of observed vehicles from the considered user-class is accumulated until a fixed number N of observations are collected. Then, the averages of the relevant traffic flow variable can be determined. These averages have comparable statistical accuracy.

Let us reconsider the individual traffic measurements. Let $i_{\mathbf{a}}(\alpha)$ denote the passage number of vehicle α. That is, the $i_{\mathbf{a}}(\alpha)$-th vehicle sharing the attribute-set **a** passing the observation point x is vehicle α. The inverse function $\alpha_{\mathbf{a}}(i)$ indicates the vehicle α that is the i-th vehicle of class **a** to pass the observation point x. Using these functions, we will map the observations y_α of vehicles α to observations $y_{\mathbf{a}}(i)$ of the i-vehicle with attribute-set **a** passing the observation point. For instance, the passing time satisfies:

$$t_{\mathbf{a}}(i) \overset{def}{=} t_{\alpha_{\mathbf{a}}(i)} \tag{F.2}$$

F.1.3 Aggregate traffic flow variables

Let us now show how the traffic flow variables of interest can be determined from the individual vehicle measurements using the aggregation approach presented in the previous section. To this end, let $M_{\mathbf{a}}$ denote the sample-size for vehicles **a**. Moreover, let $k = 0,1,2,\ldots$ denote the sample number. The k-th sample is defined by all vehicles sharing attribute-set **a** that

pass the observation point during period $[t_a(kM_a),t_a(k+1)M_a)$. Clearly, the length of this period equals:

$$\Delta t_a[k] \overset{def}{=} t_a[k+1] - t_a[k] = t_a((k+1)M_a) - t_a(kM_a)^4 \tag{F.3}$$

Aggregate traffic flow variables derived from direct observations

The *average passage time* $t_a[k]$ is defined by the time-mean arrival time:

$$t_a[k] = \frac{1}{M_a}\sum_{i=0}^{M_a-1} t_a(i+kM_a) \tag{F.4}$$

The *harmonic average velocity* (*space-mean speed*) $v_a[k]$ is defined by:

$$v_a[k] = \left(\frac{1}{M_a}\sum_{i=0}^{M_a-1} 1/v_a(i+kM_a)\right)^{-1} \tag{F.5}$$

The harmonic average velocity can also be written as a *weighted sum* of the individual velocity measurements, that is:

$$v_a[k] = \frac{1}{M_a}\sum_{i=0}^{M_a-1} \beta_a(i;k)v_a(i+kM_a) \tag{F.6}$$

where the weighting parameters $\beta(i)$ equal:

$$\beta_a(i;k) = \left(\frac{1}{M_a}\sum_{j=0}^{M_a-1} \frac{v_a(i+kM_a)}{v_a(j+kM_a)}\right)^{-1} \tag{F.7}$$

This *harmonic weighting* can be applied when the use of local traffic flow variables yields overestimation of the contribution to the relevant flow variable due to fast vehicles. In this thesis we propose using harmonic weighting on all *spatially orientated traffic flow variables*, e.g. distance headway, the gap, and the spatial velocity variance.

The *harmonic average velocity variance* $\Sigma_a[k]$ is determined by considering the harmonic average of the deviations of the velocity with respect to the harmonic mean velocity. That is:

$$\Sigma_a[k] = \frac{1}{M_a}\sum_{i=0}^{M_a-1} \beta_a(i;k)(v_a(i+kM_a) - v_a[k_a])^2 \tag{F.8}$$

Also the *average vehicle length* $L_a[k]$ is a spatially oriented flow variable that is derived from local measurements. Therefore, $L_a[k]$ can be correctly determined by determining the harmonic mean operator.

The *average traffic momentum* or *flow-rate* $m_a[k]$ is defined by:

$$m_a[k] = M_a / \Delta t_a(k) \tag{F.9}$$

---

[4] The differences between vehicle i and sample k are indicated by using square brackets when referring to samples.

As a consequence, the average spatial density $r_a[k]$ equals:

$$r_a[k] = m_a[k]/V_a[k] \tag{F.10}$$

Aggregate traffic flow variables derived from indirect observations

We can also apply similar data aggregation techniques to the indirect vehicle observations. That is, we can determine the average gross time headway $H_a[k]$ and the average net time headway $h_a[k]$ by application of the time-mean operator. The average gross distance headway $D_a[k]$, and the average distance gap $d_a[k]$ are determined by application of the harmonic operator since these latter variables are *spatially oriented*

Aggregate traffic flow variables derived from derived observations

Finally, the average velocity variance $\Theta_a[k]$, and the average level of constrainedness $\theta_a[k]$ are determined by application of the harmonic operator to the available velocity deviation and the constrainedness-level observations respectively.

F.1.4 Required number of observations

In this section we aim to establish an expression for the number of observation necessary to accomplish a specific statistical accuracy. In illustration, we assume that our objective is to determine an estimate of the *expected local velocity*. An estimation of the variable can be determined using arithmetic mean of the velocity measurements:

$$v_a[k] = \frac{1}{M_a}\sum_{i=0}^{M_a-1} v_a(i + kM_a) \tag{F.11}$$

Let us assume that these velocity measurements are instances of a Gaussian distributed random variate $\underline{V}$, with mean V_a and variance $\sigma_a^2 = \Theta_a$. Assuming that the velocity distributions are *independent* – which is usually not the case in a real-life study – yields that the arithmetic mean $v_a[k]$ is also a Gaussian distributed random variate with mean V_a and variance σ_a^2/M_a.

Let $Z = (v_a[k]-V_a)/(M_a^{1/2}\sigma_a)$ is $N(0,1)$ distributed. If we let $z_{\alpha/2}$ satisfy $\text{Prob}(|Z| > \alpha/2) = \alpha$, then a $100(1-\alpha)\%$ confidence interval for the sample average is given by:

$$\left[V_a - z_{\alpha/2}\frac{\sigma_a}{\sqrt{M_a}}, V_a + z_{\alpha/2}\frac{\sigma_a}{\sqrt{M_a}}\right] \tag{F.12}$$

Assuming that we are able to determine adequately accurate approximations of the mean and the variance, then using (F.12) we can construct a $100(1-\alpha)\%$ confidence interval for the sample mean $v_a[k]$ for which the null-hypothesis $H_0: v_a[k] = V_a$ is falsely rejected with probability α. Let us assume that we allow $\beta\%$ deviation from the mean. That is, we allow the confidence interval to deviate $\beta\%$ from $v_a[k]$. Consequently, the number of observations necessary satisfies:

$$\beta V_a = z_{\alpha/2}\frac{\sigma_a}{\sqrt{M_a}} \quad \rightarrow \quad M_a = \left(z_{\alpha/2}\frac{\sigma_a}{\beta V_a}\right)^2 \tag{F.13}$$

Figure F-1 shows derived values of the ratio between the standard velocity deviation and the velocity $\sigma_a(i)/v_a(i)$ on the respective lanes of the A9 motorway for person-cars and trucks. Clearly, for person-cars, the value decreases with decreasing velocities. For trucks, this decrease is not as profound. Moreover, the ratio $\sigma_a(i)/v_a(i)$ is generally smaller for trucks than for person-cars. This implies that, to attain the same level of confidence, the number of person-cars in the sample should be larger than the number of trucks. From the figure we observe that the ratio $\sigma_a(i)/v_a(i)$ for person-cars seldom exceeds 0.10, while for trucks, this ratio is almost never larger than 0.05 (two times smaller than the ratio for person-cars).

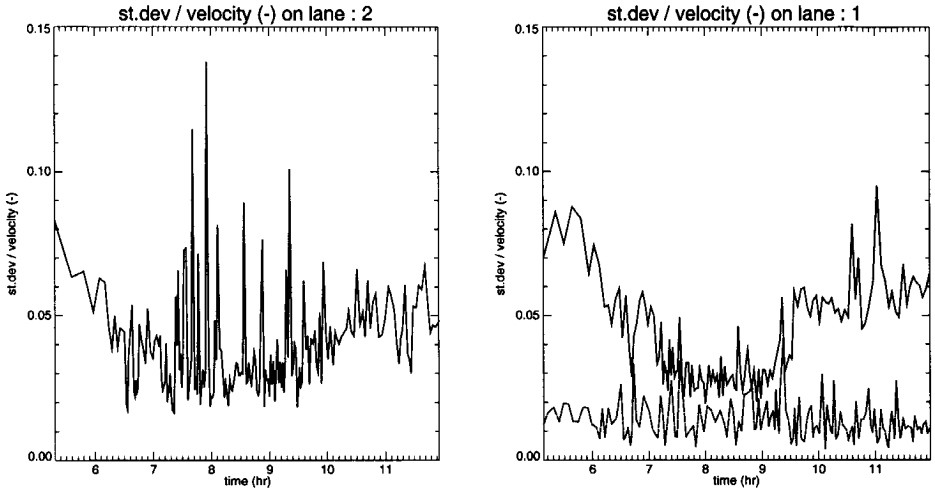

Figure F-1: Ratio between standard velocity deviation and estimation of the expected velocity of person-cars and trucks on the left lane (left picture) and the right lane of the A9 motorway.

Note that, since the $\sigma_a(i)/v_a(i)$-ratio for passenger-cars is *two* times larger than $\sigma_a(i)/v_a(i)$-ratio for trucks, the number of person-car observations needed to determine the mean with a specific accuracy is *four* times the number of truck observations needed for the same accuracy. Table 1 shows the number of person-car observations necessary to obtain approximation of the mean, which at most deviates from the actual mean with percentage β, while retaining a $100(1-\alpha)\%$ level of confidence.

Table 1: The number of observations necessary for each period to find an estimate for the mean velocity within the range of $100\beta\%$ of the expected velocity with confidence α.

confidence α ($z_{\alpha/2}$)	10%	5%	2%	1%
allowed deviation β from expected value	(1.65)	(1.96)	(2.33)	(2.58)
10%	3	4	5	7
5%	11	15	22	27
2%	68	96	135	166
1%	272	384	543	665

G FILTERING TRAFFIC MEASUREMENTS

G.1 Filtering individual traffic measurements

Traffic measurements collected for individual vehicles are apt to both structural dynamic changes on the one hand and stochastic noise on the other hand. In this appendix, we propose a new approach to distinguish between both. Key to the approach is the representation of the measurements in the Fourier domain. That is, rather than considering the measurements using a time-based approach, we will consider the collection of Fourier signals of which the measurements are composed. These Fourier signals reflect periodic signals of different frequencies. The Fourier analysis reveals the composition of the signal into these periodic signals. Assuming that the 'slow' varying structural dynamics are composed of low-frequency signals, while the measurement noise is reflected by high-frequency signals, enables the decomposition of the original signal into structural dynamic changes in the traffic dynamics on the one hand, and noise on the other hand.

The collected measurements are either the passage time $t[i]$, the velocity $v[i]$, the headway $h[i]$, the length of the vehicle $l[i]$, and the lane the vehicle is occupying at the time it passes the observation cross-section $j[i]$. Of these measurements, the $t[i]$, $v[i]$, and $h[i]$ are candidates for our filtering approach. The other observations are used only for classification purposes. Moreover, other derived individual traffic variables (e.g. distance headway, or gap) can serve as input for our filtering approach equally well.

G.1.1 Discrete dynamic signals

Let us assume that the traffic measurement to be smoothed concerns the characteristic $x[i]$ of vehicle i, where $i = 0,\ldots,M-1$. The $x[i]$ can indicate the velocity, the headway, etc. Also, the

user-class and the lane can be used: in this case, $x[i]$ indicates the measurement x of the i-th vehicle of class u on lane j. Note that $x[i]$ is not a conventional signal, since the i does not indicate fixed time instants $i\Delta t$ or periods $[i\Delta t,(i+1)\Delta t)$.

To apply Fourier analysis on the discrete-event signal $x[i]$, we *periodically extend* the aperiodic signal $x[i]$ by defining $y[i+kN] = x[i]$, for $i = 0,\ldots,M-1$, and $N \geq M$, and all integer k. The periodic extension $y[i]$ is periodic with period N, i.e. $y[i] = y[i+N]$. Moreover, y is zero for all i where x is not defined. The *complex exponential*

$$\phi_k[i] \stackrel{\text{def}}{=} e^{ik(2\pi/N)i} = \cos(k(2\pi/N)i) + i \cdot \sin(k(2\pi/N)i) \tag{G.1}$$

where 'i' indicates the imaginary complex number, is also periodic with period N, for each integer k, since they all share the same fundamental frequency (the 'ground' frequency) $2\pi/N$. The Fourier theory states that the periodic signal $y[k]$ can be represented by the sum of these complex exponentials ϕ_k, that is:

$$y[i] = \sum_{k=0}^{N-1} a_k \phi_k[i] \tag{G.2}$$

where the coefficients a_k are equal to:

$$a_k = \frac{1}{N}\sum_{i=0}^{N-1} y[i]e^{-ik(2\pi/N)i} = \frac{1}{N}\sum_{i=-\infty}^{\infty} x[i]e^{-ik(2\pi/N)i} = \frac{1}{N}X(k\omega_0) \tag{G.3}$$

where the *sample spacing* is defined by $\omega_0 = 2\pi/N$, and the *envelope* $X(\omega)$ is defined by:

$$X(\omega) \stackrel{def}{=} \sum_{i=-\infty}^{\infty} x[i]e^{-i\omega i} \tag{G.4}$$

By substitution of $N = 2\pi/\omega_0$ we find:

$$y[i] = \frac{1}{2\pi}\sum_{k=0}^{N-1} X(k\omega_0)\omega_0 e^{ik(2\pi/N)i} \tag{G.5}$$

If we now let $N \to \infty$, then this summation passes to an integral. Then, $x[i] = y[i]$, for all i, and:

$$x[i] = \frac{1}{2\pi}\int_{2\pi} X(\omega)e^{i\omega i}d\omega \quad \Leftrightarrow \quad X(\omega) = \sum_{i=-\infty}^{\infty} x[i]e^{-i\omega i} \tag{G.6}$$

The function $X(\omega)$ is referred to as the *discrete-time Fourier transform* of $x[i]$. The expression of $x[i]$ above (the *synthesis equation*) is in effect a representation of $x[i]$ as a linear combination of complex exponentials that are infinitesimally close in frequency, and which have amplitudes equal to $X(\omega)d\omega/2$. From this perspective, the Fourier transform $X(\omega)$ can be considered as the *spectrum* of $x[i]$, as it provides information on how $x[i]$ is composed of complex exponentials at different frequencies.

The Fourier transform has some very interesting properties that provide further insight into the transform and are often useful in reducing the complexity in the evaluation of transforms and inverse transforms. For an overview of these properties, see Oppenheim *et al.* (1983).

G.1.2 DFT and FFT

Some very powerful tools exist for the analysis and synthesis of signals and systems by Fourier analysis for discrete-time signals. At the heart of these methods is a technique called the *Discrete Fourier Transform* (DFT) for finite duration signals. We briefly describe the DFT.

First, the finite duration signal $x[i]$ (which is zero outside the interval $0 \le i \le M-1$) is periodically extended with a period N, yielding the periodic signal y. Basically, the DFT of $x[i]$ is the discrete-time Fourier transform of the periodic signal y, with coefficients:

$$\tilde{X}(k) \stackrel{\text{def}}{=} a_k = \frac{1}{N}\sum_{i=0}^{N-1} y[i]e^{-ik(2\pi/N)i} = \frac{1}{N}\sum_{i=-\infty}^{\infty} x[i]e^{-ik(2\pi/N)i} \tag{G.7}$$

where the original signal can be reproduced from the DFT as follows:

$$x[i] = \sum_{k=0}^{N-1} X(k)e^{ik(2\pi/N)i} \tag{G.8}$$

An important feature of the DFT is that there is a very efficient algorithm available for the computation of the DFT, namely the *Fast Fourier Transform* (FFT). As a last note, we emphasise that the duration $N > M$ is not fixed. Therefore, we will refer to the DFT with a specific N as the N-point DFT.

Transformations of traffic flow variables

In illustration, let us consider the DFT's of some of the key traffic flow variables. To this end, we consider the morning (5:30AM-10:00AM) of Friday, 20 October 1994. Figure G-1 and Figure G-2 show velocity-observations and headway-observations of person-cars driving on the right-lane of the motorway.

The figures show the original signal (i.e. $v[i]$ and $h[i]$ respectively), and the power-spectrum of the signals. The power-spectrum equals the absolute value of the Fourier-coefficients a_k. These reflect contributions of complex exponentials with frequency $2\pi k/N$ to the original signals.

G.1.3 Low-pass filtering of the traffic measurements

Based on the assumption that 'traffic signals' (e.g. velocity observations, headway observations) consist of low-frequency dynamic (structural) terms on the one hand, and high-frequency noise on the other hand, decomposition of the signal in terms of contributions of complex exponentials can be beneficial. That is, by using the power-spectrum, we can distinguish low-frequency signals from high-frequency noise. This is accomplished by *filtering*.

Ideal frequency selective filters

An *ideal frequency selective filter* is a filter that passes the complex exponentials at one set of frequencies and completely rejects the rest. In the frequency domain, such a filter can be described by the so-called *frequency response function* $H(\omega)$, that is defined by:

$$H(\omega) = \begin{cases} 1, & |\omega| \le \omega_c \\ 0 & |\omega| > \omega_c \end{cases} \tag{G.9}$$

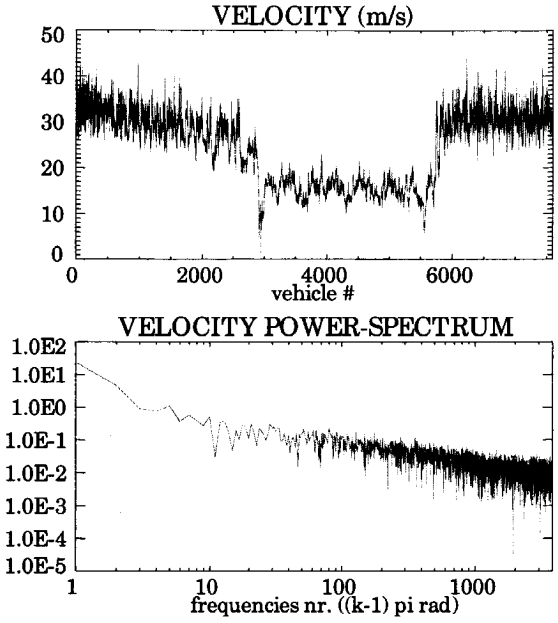

Figure G-1: Person-car velocities and spectrum on the right-lane of the motorway.

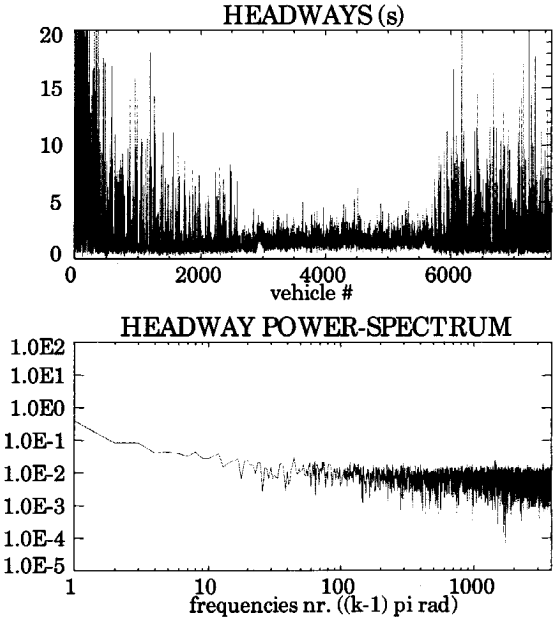

Figure G-2: Person-car time headways on the right-lane of the motorway.

The ideal low-pass filter defined by this frequency response function passes all frequencies smaller than the cut-off frequency ω_c, while it rejects all frequencies larger that the cut-off frequency ω_c. The Fourier-representation of the filtered traffic flow variables can be determined by simple multiplication by the frequency response $H(\omega)$, i.e.:

$$Z(\omega) = H(\omega)X(\omega) \tag{G.10}$$

Then, by applying the inverse discrete time Fourier transform, the filtered signal $z[i]$ results. Figure G-3 shows the results of applying an ideal low-pass filter to the velocity observations. Let us note that the choice of the cut-off frequency determines the smoothness of the resulting filtered signal. That is, when the cut-off frequency is small, the filtered signal will be smooth, and vice-versa. In illustration, see Figure G-4.

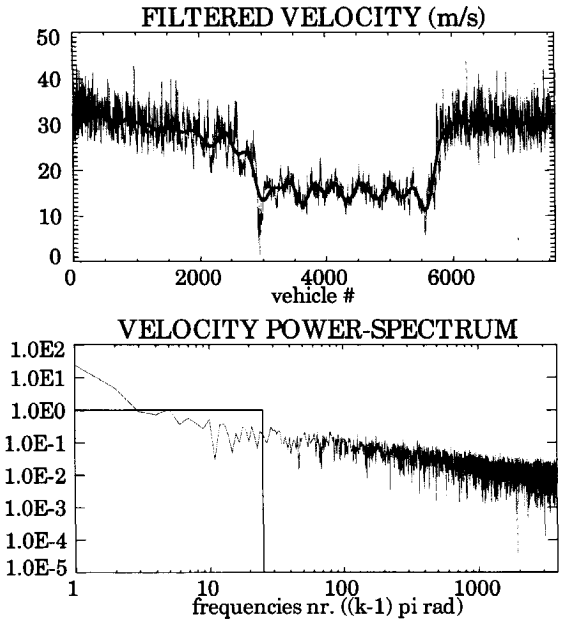

Figure G-3: Application of an ideal low-pass filter to the velocity observations. Spectrum of person-cars and an ideal low-pass filter.

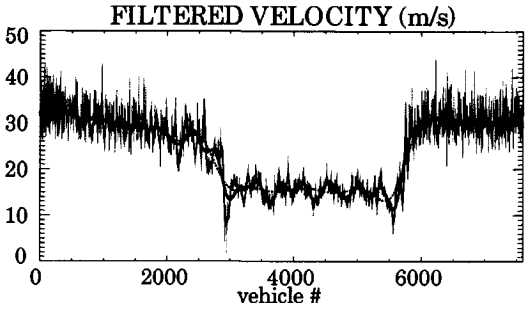

Figure G-4: Filtered velocity, using low-pass filter with different cut-off frequencies with $\omega_c = \omega_0/2$ (thick), $\omega_c = \omega_0$ (thin), and $\omega_c = 10\omega_0$ (dashed) respectively, where $\omega_0 = 8\pi/N$).

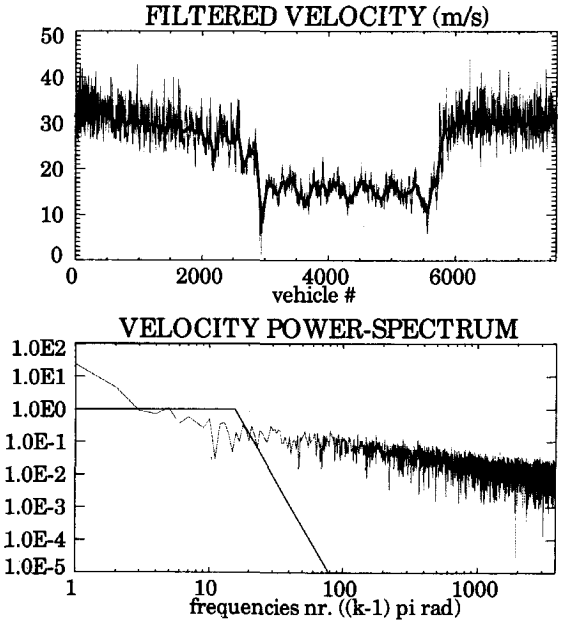

Figure G-5: Filtered velocity using a linear filter.

Linear low-pass filter

It is unlikely that the transition between the structural dynamic signal on the one hand, and the measurement noise on the other hand can be delineated by a single threshold value. Rather, the transition is likely to be gradual. Consequently, we propose using a linear filter, as indicated in Figure G-5.

The Butterworth filter

A *Butterworth filter* of order N is defined by the following frequency response function:

$$H(\omega) = \sqrt{\frac{1}{1+(\omega/\omega_c)^{2N}}} \tag{G.11}$$

where ω_c denotes the cut-off frequency. Figure G-6 shows the frequency response functions for $N = 1,2,4$ and 8.

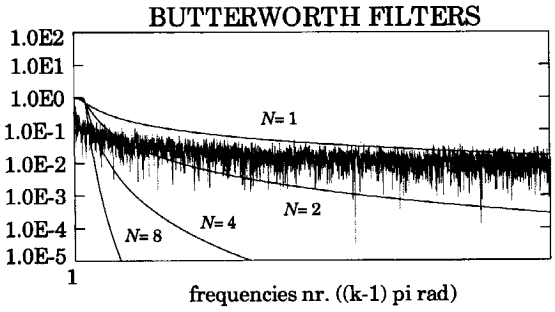

Figure G-6: Butterworth filters of various orders

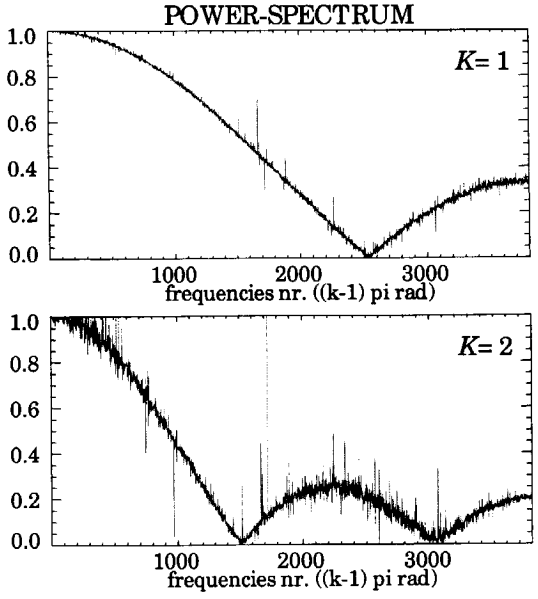

Figure G-7: Approximation of frequency response of moving average filter ($K = 1$, and $K = 2$).

A large number of alternative filters can be employed. Well-known examples are the Butterworth filter, and the Hamming filter.

The moving average

A method that is widely used in the smoothing of traffic flow data is the moving average, which is determined by calculating the mean of the observations in a moving–window:

$$z[i] = \frac{1}{K+1} \sum_{i'=0}^{K} x[i-i'] \tag{G.12}$$

We can easily determine the frequency-response of this filter by considering the ratio between the Fourier transform of the filtered signal z and the original signal x, i.e.:

$$H(\omega) = Z(\omega) / X(\omega) \tag{G.13}$$

Figure G-7 shows the frequency response for two moving average filters with $K = 1$ and $K = 2$ respectively.

H THE DISCRETISED MACROSCOPIC MLMC MODEL

This appendix summarises the numerical approach to macroscopic simulation of MLMC traffic flow using the model established in this thesis. The approximation scheme can be roughly divided into the following five steps:

- Determination of the cell width Δx and the time-step Δt;
- Determination of the initial conditions ($k = 0$);
- Discretised approximation of the source-term:
- effect of diffusion[5], acceleration and deceleration;
- effect of immediate lane-changing;
- effect of postponed and spontaneous lane changing;
- Discretised approximation of the *convective flux* $\mathbf{f}^C$ using Van Leer's flux vector splitting scheme;
- Updating the approximation for the new time step (k: = k+1) and continue (step 2).

[5] The term *diffusion* indicates the higher-order processes in the MLMC flow-model.

H.1 Determination of the initial conditions

We will determine the initial conditions by assuming that the system initially operates under equilibrium conditions. Consequently, given a vector $\mathbf{r} = \{r_{(u,j)}[i,0]\}$ of *average densities* on the cells i ($= [i\Delta x,(i+1)\Delta x)$), the initial momentum and energy, and the lane-distribution of the density, momentum, and energy are determined by assuming the equilibrium conditions and subsequent application of the algorithm presented in chapter 8.

H.2 Discretised approximation of the source-term and the diffusive flux

The source-term $\mathbf{x}$ describes the dynamic influence of the non-continuum acceleration, deceleration, immediate lane-changing, and postponed/spontaneous lane changing processes. The diffusive flux-term $\mathbf{f}^D$ represents the effect of higher-order processes in the MLMC traffic flow dynamics. In this respect, preliminary investigations of the numerical results have shown[6] the need to handle the event-driven and state-driven lane-changing processes consecutively in order to guarantee non-negative densities *irrespective of* Δx *and* Δt.

H.2.1 Acceleration, deceleration, and diffusion

To determine the dynamic influence of acceleration and deceleration, the interaction-rates $\mathcal{I}^1_{(u,j)}$ and $\mathcal{X}^1_{(u,j)}$ are determined. Moreover, we determine the modified densities and use these to determine the fraction of constrained vehicles $\theta_{(u,j)}$, and the equilibrium variance $\Theta^e_{(u,j)}$ on each lane. Finally, the acceleration velocity $W_{(u,j)}$, the acceleration time $T_{(u,j)}$, and the probability $p_{(u,j)}^{(u,j')}$ that interacting vehicles can immediately change lanes to lane j' are determined. Using these quantities, the equilibrium momentum $m^e_{(u,j)}$ and energy $m^e_{(u,j)}$ are determined for each triple (i,u,j) at time t_k. Then, the combined dynamic effect of acceleration and deceleration equals:

$$\{\Delta m_{(u,j)}[i,k]\}_{rel} = (m^e_{(u,j)}[i,j] - m_{(u,j)}[i,j]) / T_{(u,j)}[i,k] \tag{H.1}$$

and:

$$\{\Delta e_{(u,j)}[i,k]\}_{rel} = \tfrac{1}{2}(e^e_{(u,j)}[i,j] - e_{(u,j)}[i,j]) / T_{(u,j)}[i,k] \tag{H.2}$$

The *diffusive flux* $\mathbf{f}^D$ is approximated using a second order central difference scheme (see section 9.6), yielding the term $\{\Delta \mathbf{w}_{(u,j)}\}_{dif}$.

H.2.2 Immediate lane-changing

In combining the interactions rates $\mathcal{I}^l_{(u,j)}$ for $l = 0,1$, and 2 and the probability that vehicles of class u on lane j can immediately change to either adjacent lane j', we can determine the average flow from the current lane j to the adjacent lanes j':

$$\{\Delta r_{(u,j)}[i,k]\}^{j\to j'}_{imm} = -p^{(u,j')}_{(u,j)}[i.k] \cdot r_{(u,j)}[i,j] \cdot \mathcal{I}^0_{(u,j)}[i,k] \tag{H.3}$$

---

[6] We have observed that when these processes are handled non-sequentially, negative values for the density, momentum, and energy may result.

$$\{\Delta n_{(u,j)}[i,k]\}_{imm}^{j\to j'} = -p_{(u,j)}^{(u,j')}[i.k]\cdot m_{(u,j)}[i,j]\cdot \mathcal{I}_{(u,j)}^{1}[i,k] \tag{H.4}$$

and:

$$\{\Delta e_{(u,j)}[i,k]\}_{imm}^{j\to j'} = -p_{(u,j)}^{(u,j')}[i.k]\cdot e_{(u,j)}[i,j]\cdot \mathcal{I}_{(u,j)}^{2}[i,k] \tag{H.5}$$

Similarly, we can approximate the flow from the adjacent lanes j' to the current lane j due to immediate lane changing.

H.2.3 Postponed and spontaneous lane-changing

Preliminary numerical investigations have shown that the non-sequential implementation of immediate lane changing processes on the one hand, and postponed/spontaneous lane changing processes on the other hand, may result in *negatively valued conservative variables* for some choices of Δt. That is, the lateral vehicular density flow due to immediate, postponed and spontaneous lane changing tends to be larger than the total number of vehicles on the lane. The cause for this is the fact that the processes are *non-disjoint* for finite values for the period length Δt. In other words, while for infinitesimal periods dt, the probability that a vehicle can immediately change to an adjacent lane *and* is able to perform a postponed/spontaneous lane change is negligible, this generally does not hold for arbitrarily long periods Δt.

A relatively simple remedy for this problem is to first determine the approximation of the conservative variables on the cells of the roadway, and subsequently determine the between-lane flows due to postponed and spontaneous lane changing. That is, we first determine:

$$\mathbf{w}_{(u,j)}^{*}[i,k] = \mathbf{w}_{(u,j)}[i,k] + (\{\Delta\mathbf{w}_{(u,j)}[i,k]\}_{rel} + \{\Delta\mathbf{w}_{(u,j)}[i,k]\}_{imm})\Delta t \tag{H.6}$$

after which we can approximate the flows between the roadway lanes due to postponed and spontaneous lane changing:

$$\{\Delta\mathbf{w}_{(u,j)}[i,k]\}_{post/spon}^{j\to j'} = -\Delta_{(u,j)}^{(u,j')}[i.k]\cdot \mathbf{w}_{(u,j)}^{*}[i,j] \tag{H.7}$$

By doing so, the combined lane-changing effects show that the flux of the conservative variables *out* of a lane can never be larger than the total amount of the conservative variable in the respective lane. Consequently, the resulting approximations of the conservative variables is non-negative.

H.3 Approximation of the convective flux

We have observed that the Van Leer flux-vector splitting scheme yields the best results most efficiently. Hänels variant of this scheme was applied to the MLMC traffic flow model (see section 9.4.4), yielding the approximation $\mathbf{h}_{i+1/2}[i,k]$ of the flux out of the cell at the cell interface at $x_{i+1/2}$, and of the flux $\mathbf{h}_{i-1/2}[i,k]$ into the cell at the cell interface at $x_{i-1/2}$.

H.4 Updating the approximation for time step k: = k+1

For temporal integration we have used a first order accurate forward difference approach. That is, we determine the approximation of the conservative variables $\mathbf{w}_{(u,j)}[i,k+1]$ by the following explicit equation:

$$\begin{aligned}\mathbf{w}_{(u,j)}[i,k+1] := \mathbf{w}_{(u,j)}[i,k] &+ (\mathbf{h}_{(u,j)}[i-1/2,k] - \mathbf{h}_{(u,j)}[i+1/2,k])\Delta t/\Delta x \\ &+ \{\Delta \mathbf{w}_{(u,j)}[i,k]\}_{rel}\Delta t + \{\Delta \mathbf{w}_{(u,j)}[i,k]\}_{dif} \\ &+ \sum_{j'=j\pm1}(\{\Delta \mathbf{w}_{(u,j)}[i,k]\}_{imm}^{j\to j'} + \{\Delta \mathbf{w}_{(u,j')}[i,k]\}_{imm}^{j'\to j})\Delta t \\ &+ \sum_{j'=j\pm1}(\{\Delta \mathbf{w}_{(u,j)}[i,k]\}_{post/spon}^{j\to j'} + \{\Delta \mathbf{w}_{(u,j')}[i,k]\}_{post/spon}^{j'\to j})\Delta t\end{aligned} \tag{H.8}$$

I MODELLING DISCONTINUITIES

To enable the description of more general situations in traffic flow, we need mechanisms to model traffic operations near on- and off-ramps, merges and diverges, lane-drops, incidents and accidents, etc. In this appendix, we present a modelling approach for discontinuities. The key to the approach is the introduction of an additional user-class, which we will refer to as *phantom-cars*. These are non-moving vehicles without physical length. Using these phantom-cars, we can model discontinuities without needing to modify the class- and lane-specific model parameters, such as the desired speeds, and the overtaking probabilities. Thus, we can predict the traffic operations due to discontinuities without the need to recalibrate the model parameters for each different situation. Moreover, the *invariant driver personality* requirement is satisfied, since we need not modify the class-specific invariant parameters.

I.1 Modelling a lane drop using phantom-cars

To illustrate the approach, we consider the simplest discontinuity imaginable: the lane drop. Although other discontinuities are more complex, a similar approach can be taken in most cases. Let us remark that also the occurrence of an incident or accident can be described as a temporal lane-drop. Let us first consider the traffic operations near a lane drop from a qualitative macroscopic viewpoint.

Vehicles driving at the discontinued lane will try to change lanes before reaching the end of the lane. During their approach, the incentive to change lanes increases. Drivers that are unable to change towards the adjacent lane will need to reduce their velocity, and may even need to come to a complete standstill. If we consider this process, we conclude that the lane-changing mechanism at the lane-drop can be mimicked by an interaction process: on the one hand, vehicles that interact with slower vehicles will try to change to an adjacent lane. On the other hand, they will reduce their velocity if they are unable to do so.

This observation leads to the introduction of the so-called *phantom-cars*. These non-moving infinitesimal vehicles are located on the discontinued lane. Their density increases with increasing x to the extent that at the end of the lane-drop, their presence results in vehicles from other classes coming to a complete stand-still due to interaction.

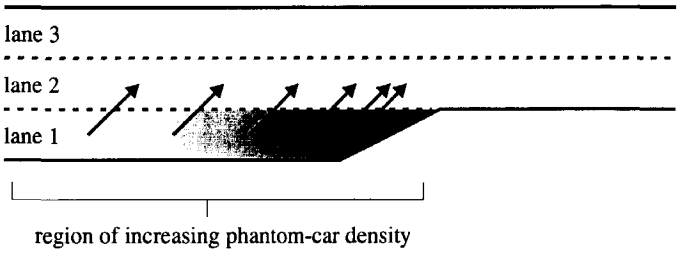

Figure I-1: Modelling a lane drop using phantom-cars.

Figure I-1 shows how a lane-drop can be modelled using phantom-cars. Similarly, we can model an on-ramp, although in this case no vehicles can overtake in the upstream region.

I.2 The effect of phantom-cars on the interaction moments

To quantify the reduction in the respective conservative variables due to interaction on the one hand, and the flows between the roadway lanes of these conservative variables due to immediate lane changing on the other hand, we have introduced the following *interaction moments* (see chapter 6):

$$\mathcal{I}^{k}_{(u,j)} \overset{def}{=} \left\langle \int_{w<v} v^{k}(w-v)\tilde{\rho}_{(*,j,1)}(w)\,\mathrm{d}w \right\rangle_{(u,j)} \tag{I.1}$$

and:

$$\mathcal{X}^{k}_{(u,j)} \overset{def}{=} \left\langle \int_{w<v} w^{k}(v-w)\tilde{\rho}_{(*,j,1)}(w)\,\mathrm{d}w \right\rangle_{(u,j)} \tag{I.2}$$

where the unconstrained aggregate-class reduced phase-space density equals:

$$\tilde{\rho}_{(*,j,1)}(x,v,t) = \sum_{u'} \tilde{\rho}_{(u,j,1)}(x,v,t) \tag{I.3}$$

Since all phantom-cars have zero velocity, we have:

$$\tilde{\rho}_{(phantom,j,1)}(x,v,t) = r_{(phantom,j)}(x,t)\cdot\delta(v) \tag{I.4}$$

Therefore, the contribution of interactions of vehicles of class u on lane j with phantom vehicles equals:

$$\mathcal{I}^{k}_{(u,j)} = r_{(phantom,j)}(x,t)\left\langle \int_{w<v} v^{k}(v-w)\delta(w)\mathrm{d}w \right\rangle_{(u,j)} = r_{(phantom,j)}(x,t)\left\langle v^{k+1}\right\rangle_{(u,j)} \tag{I.5}$$

Evaluating this expression for $k = 0$, 1, and 2 yields:

$$\Delta\mathcal{I}^0_{(u,j)} = r_{(phantom,j)}(x,t)\cdot V_{(u,j)}(x,t) \tag{I.6}$$

$$\Delta\mathcal{I}^1_{(u,j)} = r_{(phantom,j)}(x,t)\cdot (V^2_{(u,j)}(x,t) + \Theta_{(u,j)}(x,t)) \tag{I.7}$$

$$\Delta\mathcal{I}^2_{(u,j)} = r_{(phantom,j)}(x,t)\cdot (2V_{(u,j)}(x,t)H_{(u,j)}(x,t) + \Gamma_{(u,j)}(x,t)) \tag{I.8}$$

Similarly, we have:

$$\Delta\mathcal{X}^k_{(u,j)} = \begin{cases} -r_{(phantom,j)}(x,t)\cdot V_{(u,j)}(x,t), & k=0 \\ 0, & k>0 \end{cases} \tag{I.9}$$

The effect of the phantom-cars is now easily incorporated in the macroscopic MLMC model of chapter 6, by substituting $\mathcal{I}' = \mathcal{I} + \Delta\mathcal{I}$ and $\mathcal{X}' = \mathcal{X} + \Delta\mathcal{X}$ in the model equations presented in section 6.8. If we quantify the modifications in the model equation, we find:

$$\frac{\partial r_{(u,j)}}{\partial t} + \ldots = \ldots - \sum_{j'=j\pm1} (p^{(u,j')}_{(u,j)} r_{(phantom,j)} m_{(u,j)} - p^{(u,j)}_{(u,j')} r_{(phantom,j')} m_{(u,j')}) \tag{I.10}$$

$$\frac{\partial m_{(u,j)}}{\partial t} + \ldots = \ldots - \sum_{j'=j\pm1} (2p^{(u,j')}_{(u,j)} r_{(phantom,j)} e_{(u,j)} - 2p^{(u,j)}_{(u,j')} r_{(phantom,j')} e_{(u,j')}) \tag{I.11}$$

$$\begin{aligned} \frac{\partial e_{(u,j)}}{\partial t} + \ldots = \ldots &- \sum_{j'=j\pm1} (p^{(u,j')}_{(u,j)} r_{(phantom,j)} m_{(u,j)} H_{(u,j)} - p^{(u,j)}_{(u,j')} r_{(phantom,j')} m_{(u,j')} H_{(u,j')}) \\ &- \tfrac{1}{2} \sum_{j'=j\pm1} (p^{(u,j')}_{(u,j)} r_{(phantom,j)} J_{(u,j)} - p^{(u,j)}_{(u,j')} r_{(phantom,j')} J_{(u,j')}) \end{aligned} \tag{I.12}$$

where the equilibrium momentum and energy are respectively modified according to:

$$m^e_{(u,j)} = \ldots - (1 - p^*_{(u,j)})\mathrm{T}_{(u,j)} r_{(phantom,j)} 2e_{(u,j)}(x,t) \tag{13}$$

and:

$$e^e_{(u,j)} = \ldots - (1 - p^*_{(u,j)})\mathrm{T}_{(u,j)} r_{(phantom,j)} (2m_{(u,j)} H_{(u,j)} + J_{(u,j)}) \tag{14}$$

In illustration, in chapter 10 both a lane-drop and an incident scenario are considered by macroscopic simulation.

SUMMARY

The aim of Dynamic Traffic Management on motorway networks is to make optimal use of available infrastructural facilities and roadway space, as well as to improve the quality of travel by providing information to the road-users. With respect to the first objective, Dynamic Traffic Management can provide efficient tools to remedy the negative side effects of congestion. A large number of these contemporary control measures are lane-specific and class-specific. Examples of such measures are (dynamic) overtaking prohibition for specific classes such as trucks, dynamic lane-allocation control, class-specific ramp-metering control, and on-board information provision to and guidance of equiped vehicles. However, the resulting control task of the heterogeneous traffic flow is characterised by the highly complex interplay of the multiple control measures, multiple objectives, multiple target-groups and the significant behavioural differences between user-classes with their asymmetric interactions.

From a traffic control perspective, gaining a clear insight into the response behaviour of the heterogeneous flow to traffic control strategies is of dominant importance since such insights reveal control strategies that can improve the efficiency of the motorway network. To derive such control strategies, the high complexity of the control task requires a model-based control approach. However, for the application of such a model-based control approach a much more elaborate flow theory of motorway traffic flow operations is necessary.

In this dissertation, we have established a new continuum theory and macroscopic model describing heterogeneous traffic flow operations on multilane roadways. This theory provides a genuine extension and generalisation of traditional macroscopic traffic flow theory. The model provides insight into both the interactions between the distinct user-classes and the interaction between the lanes of the motorway.

The work presented in this dissertation has evolved into a fairly broad scope: it contains contributions to the fields of traffic flow theory development, gas-kinetic and macroscopic flow modelling, numerical approximation schemes, data analysis and estimation techniques, and

model applications. In this summary, we present the main achievements and conclusions of this dissertation.

The theories and models developed in this thesis are based on the concept of the generalised Phase-space density (PSD). This generalisation of traffic density represents the joint probability distribution of the velocity-vector and continuous attributes (e.g. desired velocities, acceletion times, reaction times) of general traffic entities characterised by a set of discrete attibutes (e.g. state of the entity, lane, user-class) in the n-dimensional space. In the thesis, generic gas-kinetic equations are presented describing the dynamics of the generalised PSD. It appears that these dynamics are governed by both continuum processes (i.e. convection, acceleration, and smooth adaptation of continuous attributes) as well non-continuum processes, respectively describing smooth changes and non-smooth changes in the generalised PSD. With respect to non-continuum processes, event-driven processes and condition-driven processes are distinguished. Event-driven processes are stimulus-response-like processes, where changes in velocities or continuous attributes are caused by an event (usually interactions between traffic entities). Condition-driven processes reflect non-smooth changes due to the condition of traffic entities.

To correctly describe the correlation between location, velocity and acceleration behaviour of vehicles in the traffic stream, we have chosen a *probabilistic platoon-based* traffic description, in opposition to the traditional approach to describe traffic as a collection of 'independent' particles. The platoons are described by specifying the generalised PSD for one-dimensional multilane multiclass (MLMC) traffic systems. The resulting state-specific MLMC-PSD describes the class-specific lane-specific *expected number* per unit roadway length of both free-flowing platoon-leaders as well as platooning vehicles, driving with velocity v while having desired velocity v^0.

Subsequently, we have specified the generic gas-kinetic equations to describe one-dimensional MLMC traffic flow. The resulting equations describe dynamic changes in the MLMC-PSD governed by phase-space convection (e.g. vehicles flowing from x to $x+dx$, or vehicles accelerating from v to $v+dv$), event-driven transitions (vehicles decelerating after an interaction event, vehicles immediately changing lanes after an interaction), and condition-driven transitions (drivers changing lanes to their preferred lane, platooning drivers changing lanes to improve their driving conditions). The interaction-events are asymmetric in that faster classes are more influenced by other vehicles than slower classes.

The derived model is a MLMC-generalisation of the gas-kinetic equations, and thereby constitutes one of the first theoretical developments in the field of mesoscopic multiclass traffic flow modelling distinguishing lanes of the roadway. With respect to other gas-kinetic models, we have observed that because of the vehicular chaos assumption, the interaction term of these models overestimates the vehicle interaction rate. We show that by considering the flow as a collection of platoons, this is remedied. To further improve the vehicle interaction term, the space requirements of vehicles in the flow are used, yielding an increase in the vehicular interaction rate. In addition, the proposed acceleration term reflects acceleration towards the desired velocity of the platoon-leader. On the contrary, traditional gas-kinetic models assume that either *all* vehicles (free-flowing or platooning) accelerate towards their own desired velocity (cf. Paveri-Fontana (1975)), or do no accelerate at all (cf. Helbing (1996)).

The number of unknown model parameters and dependent variables in the MLMC gas-kinetic equations is large, hampering their practical (on-line) application in for instance

model-based control. Therefore, to arrive at a tractable macroscopic model a method similar to the method of moments has been developed and applied to the gas-kinetic model equations. The approach yields lane-specific dynamic equations for the conservative multiclass traffic flow variables density, momentum and energy, based on the platoon-based multilane multiclass gas-kinetic principles. This conservative model form constitutes a new type of macroscopic traffic flow model, which is excellently suited for efficient numerical solution approaches. On the output side, the developed model describes the dynamics of the lane- and user-class specific conservative traffic flow variables density, momentum and energy, rather than the traditionally used primitive variables density, velocity and velocity variance. On the input side, the model enables specification of class-specific desired velocity, acceleration time, traffic viscosity, kinematic coefficient, immediate lane-changing probability, lane-changing rate, etc.

The density dynamics are described by generalised conservation of vehicles equations. Comparable relations hold for the traffic momentum and traffic energy dynamics. However, traffic momentum and energy also change due to drivers aiming to drive at their user-class dependent desired velocity on the one hand and interactions with other vehicles without lane-changing opportunities on the other hand.

By inspecting these aggregate-state macroscopic MLMC equations, lane-specific and class-specific equilibrium relations for the momentum and the energy were identified. These relations resulting from acceleration and deceleration processes quantify the asymmetric user-class and lane interactions, and. The aggregate-state model also provides insight into the density distribution on the roadway lanes. These densities follow implicitly from the modelling approach. They are dependent on the expected number of vehicular interactions, the resulting number of immediate lane-changes per unit time, and the expected number of spontaneous and postponed lane-changes per unit time on the respective roadway lanes.

The mixed-state conservative macroscopic model has been transformed into two other model formulations, namely the traditional primitive formulation using density, velocity and velocity variance, and the characteristic formulation, using the characteristic or *Riemann* variables. Although the model formulations are equivalent, each has its own merits and drawbacks. For instance, while its use in mathematical and numerical model analysis is limited, the *primitive formulation* is very well suited for comparison with currently available macroscopic models. By doing so, we have tracked the main differences between the developed model and the traditional macroscopic. Moreover, by comparing these models with the MLMC model developed in this thesis, our multiclass formulation reveals that the *behavioural interpretation* of the *pressure term* in traditional macroscopic models in terms of driver's anticipation-behaviour is flawed. Rather, the pressure term is a result of the vehicular flow with a given variability in the velocity.

Using the *characteristic formulation*, we have analysed the propagation of perturbations in the multiclass flow. Similar to the flows in continuous media, small disturbances in vehicular flow move along three so-called *characteristic curves*. Using the insights revealed by these characteristics, the formation of *expansion fans* (reflecting vehicular diffusion due the vehicles accelerating towards different acceleration velocities) and *shock waves* (describing sharp transitions in the (worsening) traffic conditions) has been studied. We have shown that in opposition to fluidic flows, the expansion fan *precedes* the shock wave. In addition, we have observed that when traffic is congested, perturbations are transported in both the downstream

and the upstream direction, while in free-flow conditions, the effects of a perturbation is transported downstream only. These congested traffic conditions are similar to subsonic flows in fluids or gasses, and can be identified by comparing the average vehicular velocity V with the local sonic velocity c which is proportional to the velocity variance Θ ($c = \Theta\sqrt{3}$).

We have shown that insight into the propagation mechanics of disturbances in the vehicular flow is of dominant importance to correctly compute numerical solutions. These insights enable use to develop improved numerical solution approaches. The resulting solution approach consists of an adapted Van Leer scheme, characterised by a sequential consideration of the acceleration, immediate lane-changing, spontaneous lane-changing, and postponed lane-changing. The approach is based on the conservative model formulation. It employs the insights gained by studying the characteristic model form.

In order to prepare empirical calibration and validation, new analysis techniques were developed applying a low-pass filter to the velocity measurements of individual vehicles. The filter yields the correct smoothing of the velocity, while preserving the structural dynamic fluctuations. That is, in traffic conditions-transition periods, the filtered mean velocity follows the dynamics effectively.

Finally, we have presented results of model applications for a number of test-cases, which on the one hand were intended to show the validity of the model in remedying the criticisms on higher-order flow models, while on the other hand aimed at showing the plausibility of the new model by calculating outcomes that are of practical interest.

We conclude that the discrete macroscopic MLMC model remedies both the anisotropy and the unaffected slow vehicle criticism. We have shown that the extent to which the invariant personality condition is resolved depends on the level of class-aggregation. Moreover, the model captures the observed differences between user-classes and lanes plausibly (although more elaborate model calibration and validation is required).

We have also shown by macroscopic simulation that a number of interesting phenomena observed in real-life traffic flow, such as hysteresis and phantom jams, are captured convincingly. Finally, we have shown that traffic management measures have an impact on the occurrence of these phenomena. For example, the model predicts that speed-homogenising control postpones the occurrence of congested flow caused by hysteresis-effects. In opposition, we have also demonstrated the unexpected outcome that an overtaking prohibition for trucks *accelerates* the occurrence of congestion.

SAMENVATTING

De doelstelling van Dynamisch Verkeersmanagement is zowel het optimaal gebruiken van beschikbare infrastructurele faciliteiten en ruimte op autosnelwegen, als het verbeteren van de kwaliteit van verplaatsingen door informatie aan weggebruikers te verschaffen. Met betrekking tot de eerstgenoemde doelstelling kan Dynamisch Verkeersmanagement geschikte middelen verschaffen om de negatieve effecten van congestie op autosnelwegen te verminderen. Een aantal van de hedendaagse beheersingsmaatregelen maken zowel onderscheid tussen voertuigklassen als tussen rijstroken. Voorbeelden van strook- en klassenspecifieke beheersingsmaatregelen zijn selectieve toeritdosering, (dynamisch) inhaalverbod voor specifieke voertuig- of gebruikersklassen (bijvoorbeeld vrachtverkeer), informeren en routering van geïnstrumenteerde voertuigen en dynamische rijstrookgebruiksregelingen. De resulterende regeltaak wordt echter gekenmerkt door onder meer de zeer complexe wisselwerking van beheersingsmaatregelen, de grote variëteit aan doelstellingen, de grote verschillen in gedrag tussen de gebruikersklassen en de asymmetrische interacties tussen deze klassen.

Vanuit het perspectief van de verkeersregeling is inzicht in de response van de heterogene verkeersstroom op de verschillende regelstrategieën van essentieel belang. Hiermee kunnen we immers die strategieën aan het licht brengen welke tot een verhoging van de efficiëntie van het systeem leiden. Voor het bepalen van efficiënte regelstrategieën maakt de genoemde complexiteit van de regeltaak een op modellen gebaseerde aanpak noodzakelijk. Voor de toepassing van een soortgelijke aanpak is echter een strook- en klassenspecifieke verkeersstroomtheorie voor autosnelwegen noodzakelijk. Vanuit dit oogmerk voldoen de huidige macroscopische verkeersstroommodellen niet, daar deze geen onderscheid maken tussen de verschillende rijstroken en gebruikersklassen.

In dit proefschrift zijn een nieuwe macroscopische verkeersstroomtheorie en een nieuw stroommodel ontwikkeld voor het beschrijven van heterogene verkeersstromen op autosnelwegen bestaande uit meerdere rijstroken. De theorie is een uitbreiding van de traditionele

macroscopische stroomtheorie en verschaft inzicht in de wisselwerking tussen de verschillende gebruikersklassen en rijstroken.

Dit proefschrift omvat een breed scala aan onderwerpen: het beschrijft enkele uitbreidingen van de verkeersstroomtheorie, macroscopische stroommodellen en schema's voor het numeriek oplossen van deze modellen. Bovendien behandelt het proefschrift enkele aspecten van de data-analyse en de schattingsproblematiek, en enkele toepassingen van het ontwikkelde macroscopisch verkeersstroommodel. In deze samenvatting geven we een korte beschrijving van de belangrijkste onderzoeksresultaten en conclusies.

De in dit proefschrift ontwikkelde theorie en modellen zijn gebaseerd op de zogenaamde gegeneraliseerde dichtheid in de faseruimte (Phase-Space Density; PSD). Deze generalisatie van de verkeersdichtheid beschrijft de gemeenschappelijke verdelingsfunctie van de snelheid en de continue attributen (bijvoorbeeld de wenssnelheid, de acceleratietijd, de reactietijd) van verkeersdeeltjes die zijn gekarakteriseerd door een verzameling discrete attributen (bijvoorbeeld de strook, de klasse, of de toestand van een verkeersdeeltje) in de n dimensionale ruimte. De dynamica van de gegeneraliseerde dichtheid wordt bepaald door zowel continue processen (convectie, acceleratie, aanpassing van continue attributen), als discontinue processen. Deze processen beschrijven respectievelijk geleidelijke als niet-geleidelijke veranderingen in de gegeneraliseerde dichtheid. Met betrekking tot discontinue processen onderscheiden we processen in reactie op gebeurtenissen (*event-driven processes*) en processen ten gevolge van de toestand van een verkeersdeeltje (*condition-driven processes*). Met een gebeurtenis wordt in het onderhevige geval een interactie tussen verkeersdeeltjes aangeduid.

Om tot een correcte beschrijving van de correlatie tussen de verschillende voertuigen in de voertuigstroom te komen is in deze dissertatie een probabilistische beschrijving ontwikkeld die gebaseerd is op zogenaamde *peletons* bestaande uit één leider en een (niet-negatief) aantal volgers. Deze beschrijving van de verkeersstroom staat in tegenstelling tot de reguliere macroscopische beschrijving, die de voertuigstroom voorstelt als een verzameling van onafhankelijk bewegende deeltjes. De peletons worden beschreven door de gegeneraliseerde dichtheid voor strook- en klassenspecifieke (MLMC) één dimensionale verkeersstromen te specificeren voor zowel vrijrijdende als volgende voertuigen. De hieruit volgende MLMC-PSD beschrijft het strook- en klassenspecifieke *verwachte* aantal vrijrijdende of volgende voertuigen per eenheid weglengte die met snelheid v rijden en wenssnelheid v^0 hebben.

Vervolgens zijn de gegeneraliseerde gas-kinetische vergelijkingen gespecificeerd voor het één dimensionale strook- en klassenspecifieke geval. De dynamica blijkt te worden bepaald door *convectie* in de faseruimte (veroorzaakt door voertuigen die zich van x naar $x+dx$ verplaatsen, of voertuigen die accelereren van v naar $v+dv$), door transities in reactie op *gebeurtenissen* (voertuigen die afremmen of van strook wisselen *na* een interactie met een langzamer voertuig) en door transities veroorzaakt door de *toestand* waarin het voertuig zich bevindt (voertuigen die een *spontane* strookwisseling uitvoeren, òf volgende voertuigen die een *uitgestelde* strookwisseling uitvoeren). De *interacties* blijken asymmetrisch, d.w.z. snelle voertuigen ondervinden meer hinder van langzame voertuigen dan omgekeerd.

Het strook- en klassenspecifieke gas-kinetische model is een generalisatie van traditionele gas-kinetische modellen binnen de mesoscopische verkeersstroomtheorie en is één van de eerste theoretische ontwikkelingen op het gebied van strook- en klassenspecifieke stroommodellen. Met betrekking tot de genoemde gas-kinetische modellen is gebleken dat het aantal interacties tussen voertuigen als resultante van de '*voertuigchaos*' aanname (d.w.z. voertui-

gen bewegen nagenoeg onafhankelijk van elkaar) wordt *overschat*. In dit proefschrift tonen we aan dit probleem op te lossen is door de voertuigstroom als een verzameling van peletons te beschouwen. Bovendien is deze beschrijving zeer nuttig bij het modelleren van het acceleratiegedrag van volgende voertuigen, door te veronderstellen dat voertuigen accelereren naar de wenssnelheid van de vrij-rijdende leider van het peleton. Hiermee worden onrealistische aannames dat òf alle voertuigen kunnen accelereren naar hun eigen wensnelheid (Paveri-Fontana (1975)) òf alle *volgende* voertuigen niet kunnen accelereren, (Helbing (1996)) onnodig. Als laatste merken we op dat het ruimtebeslag van voertuigen expliciet in de modelbeschrijving is verdisconteerd.

Het aantal onbekende parameters en afhankelijke variabelen in het ontwikkelde strook- en klassenspecifieke gas-kinetische model is relatief groot. Dit bemoeilijkt een real-time toepassing van het model. Daarom is de *momentenmethode* toegepast met als doel een strook- en klassenspecifiek *macroscopisch* model af te leiden. Het resulterende model beschrijft de dynamica van de *conservatieve* variabelen (verkeersdichtheid, impuls en energie), in plaats van de bij dit type stroommodel gebruikelijke *primitieve* variabelen (de dichtheid, de snelheid en eventueel de snelheidsvariantie). De invoer van het model bestaat uit diverse strook- en klassenspecifieke parameters, waaronder de gemiddelde wenssnelheid, de acceleratietijd, de gemiddelde voertuiglengte, de reactietijd en de viscositeit.

De dynamica van de dichtheid wordt beschreven door een gegeneraliseerde behoudswet (longitudinale en laterale instroom en uitstroom van voertuigen per gebruikersklasse). De vergelijkingen die de dynamica van impuls en energie beschrijven zijn deels identiek aan die van de dichtheid. De dynamica van impuls en energie worden echter ook beïnvloed door voertuigen die accelereren naar de klassenspecifieke wenssnelheid van de leider van het peleton en voertuigen die moeten afremmen na een interactie met een langzamer voertuig.

Herschrijving van de vergelijkingen leidt tot de formulering van zowel het strook- en klassenspecifieke evenwichtsimpuls en de evenwichtsenergie, als de klassenspecifieke evenwichtsverdeling van voertuigen over de rijstroken. Deze evenwichtsrelaties kwantificeren de asymmetrische wisselwerking tussen de klassen welke resulteert uit de acceleratie en deceleratie van voertuigen en volgen, evenals de verdeling van voertuigen over de rijstroken, impliciet uit de beginselen van de gas-kinetische modelformulering.

Uitgaande van de conservatieve macroscopische modelformulering zijn twee andere formuleringen afgeleid, namelijk de *primitieve formulering* en de *karakteristieke formulering*. Deze beschrijven respectievelijk de dynamica van strook- en klassenspecifieke *primitieve* (dichtheid, snelheid en snelheidsvariantie) en *karakteristieke variabelen*. Ofschoon ze equivalent zijn, hebben de verschillende formuleringen elk hun voor- en nadelen.

Zo is de *primitieve formulering* bij uitstek geschikt voor het vergelijken van het ontwikkelde model met traditionele macroscopische modellen, waarmee de verschillen tussen het strook- en klassenspecifieke model en laatstgenoemde modellen tot uiting komen. Uit de klassenspecifieke formulering volgt de correcte interpretatie voor de verkeersdruk. De interpretatie vanuit het *anticiperend gedrag* van bestuurders, welke in het verleden is toegedicht aan de uitdrukking voor de *verkeersdruk* (d.i. bestuurders anticiperen op ruimtelijke veranderingen van dichtheid en snelheidsvariantie), blijkt niet correct. De ruimtelijke partiële afgeleide van deze druk beschrijft niets anders dan een convectie effect (balans tussen respectievelijk de *instroom* en de *uitstroom* van groepen voertuigen met verschillende snelheidsvariaties).

Door gebruik te maken van de *karakteristieke formulering* is de wijze waarop kleine verstoringen zich in de voertuigstroom verplaatsen geanalyseerd. Deze verstoringen blijken zich te verplaatsen langs de *karakteristieke krommen* vergelijkbaar met de verplaatsing van verstoringen in een continu medium. Door gebruik te maken van deze karakteristieken zijn we in staat om het ontstaan van zowel *schokgolven* (discontinue verandering in verkeerscondities) als '*expansion fans*' (diffusie door accelererende voertuigen met verschillende wenssnelheden) te beschrijven. In tegenstelling tot vloeistofstromen, gaat hier de expansion fan de schokgolf voor. Door gebruik te maken van de analogie met het kinematische model van Lighthill and Whitham (1955), waarin *congestie* wordt gekenmerkt door stroomopwaarts bewegende karakteristieken, kunnen we concluderen dat tijdens *congestie* (vergelijkbaar met de subsone toestand in een continu medium) verstoringen zowel *stroomopwaarts* als *stroomafwaarts* bewegen (langs de karakteristieke krommen). Tijdens *vrije verkeersafwikkeling* (vergelijkbaar met de supersone toestand in een continu medium) planten verstoringen zich alleen stroomafwaarts voort. Kortom, congestie wordt gekenmerkt doordat de gemiddelde snelheid V van het verkeer *lager* is dan de 'geluidssnelheid' c, welke proportioneel is met de snelheidsvariantie Θ (d.i. $c = \Theta\sqrt{3}$).

We concluderen bovendien dat inzicht in de mechanismen die de dynamica van de verstoringen beschrijven van essentieel belang is voor de correcte bepaling van numerieke oplossingen. De opgestelde numerieke benadering bestaat uit een variant op het Van Leer flux-vector splitting schema. Het ontwikkelde schema is gekarakteriseerd door sequentiële beschouwing van de niet-convectieve processen acceleratie en deceleratie, ogenblikkelijk strookwisselen, en spontaan en uitgesteld strookwisselen. Het schema is enerzijds gebaseerd op de conservatieve formulering, terwijl het anderzijds gebruik maakt van de inzichten verkregen uit de karakteristieke modelvorm.

Ten bate van modelcalibratie is een nieuwe dataverwerkingstechniek ontwikkeld, gebaseerd op het toepassen van een korte-band (*low-pass*) filter op een *discrete-event* signaal. Dit signaal bestaat uit waarnemingen $v[k]$ (snelheden) van het k-de voertuig dat het observatiepunt passeert. Het filter vlakt de waargenomen snelheden zo af dat de structurele dynamische verandering behouden blijven. Dit betekent dat in periodes waar de snelheid een scherpe transitie ondergaat (zoals bij de overgang van *vrije* naar *gedwongen* verkeersafwikkeling), het gefilterde signaal de dynamica correct volgt. Dit in tegenstelling tot vele andere filters, zoals de periode-gemiddelde snelheid.

Tot slot is een verscheidenheid aan macroscopische simulaties met het model gedaan, enerzijds met als doel de validiteit van het model met betrekking tot de verschillende punten van kritiek op (hogere-order) stroommodellen te laten zien, terwijl anderzijds de plausibiliteit van het model is aangetoond door praktisch relevante resultaten te bepalen.

We kunnen concluderen dat het discrete strook- en klassenspecifieke macroscopische model voldoet aan zowel *anisotropie* (bestuurders reageren primair op *stroomafwaartse* stimuli), als de 'ongehinderde langzame voertuigen' conditie. Aangaande de invariantie van de persoonlijkheid van bestuurders, zetten we dankzij de scheiding van klassen en de daarmee afnemende snelheidsvarianties, een stap in de goede richting. Bovendien volgt uit de toepassingen de plausibiliteit van de modelaanpak betreffende de verschillen tussen voertuig-klassen en rijstroken. Desondanks is verdere modelcalibratie en -validatie, liefst met op het modelcalibratie toegespitste verkeersgegevens, gewenst.

Ook hebben we middels macroscopische simulatie een aantal interessante fenomenen gesimuleerd, zoals hysteresis en *phantom-jams* (*'Stau-aus-dem-Nichts'*), welke kenmerkend zijn voor verkeersstromen op autosnelwegen. Tot slot hebben we laten zien hoe verkeersbeheersingsmaatregelen in het model kunnen worden geïmplemeteerd, en hoe deze maatregelen effect hebben op het ontstaan van eerder genoemde fenomenen, zoals volgens het model worden voorspeld. Zo voorspelt het model bijvoorbeeld dat snelheidssignalering het spontaan ontstaan van congestie (de zogenaamde *Stau-aus-dem-Nichts*) door hysteresis kan uitstellen (en zelfs voorkomen). In tegenstelling tot wat wordt verwacht, voorspelt het strook- en klassenspecifieke model dat een inhaalverbod voor vrachtverkeer juist het ontstaan van congestie bespoedigd.

CURRICULUM VITAE

Serge Paul Hoogendoorn was born in the Dutch city of Rotterdam, in 1971. In 1994, he received a master's degree (with distinction) in control engineering from the Delft University of Technology, Faculty of Applied Mathematics. His masters thesis concerned an investigation of viscosity solutions of the Hamilton-Jacobi-Bellman equations, which frequently arise in continuous time optimal control problems.

Since 1995, Serge is affiliated with the Transportation and Traffic Engineering section of the Faculty of Civil Engineering and Geosciences, Delft University of Technology, where he has worked on among other things evaluation methodologies for co-ordinated traffic control measures (the DACCORD project) and the assessment of the perspectives of fuzzy logic in traffic engineering.

In addition to research regarding the application of control theory in dynamic traffic management in general, and the dynamic assignment of freeway lanes to specific user-classes in particular (within the PhD. research Project "Dynamic Lane Usage"), Serge has developed a new estimation technique for the parameters in composite headway distribution models. Among his other research interests are macroscopic multiclass traffic flow models and their numerical approximation, pedestrian traffic flow operations, chaos in traffic flow, conflict analysis, genetic algorithms, and Cellular Automata models.

SUBJECT INDEX

J

L

M

N

T

U

V

TRAIL Thesis Series

A series of The Netherlands TRAIL Research School for theses on transport, infrastructure and logistics.

Nat, C.G.J.M., van der, *A knowledge-based concept exploration model for submarine design*, T99/1, March 1999, TRAIL Thesis Series, Delft University Press, The Netherlands

Westrenen, F., van, *The maritime pilot at work; Evaluation and use of a time-to-boundary model of mental workload in human-machine systems*, T99/2, May 1999, TRAIL Thesis Series, Eburon, The Netherlands

Veenstra, A.W., *Quantitative analysis of shipping markets,* T99/3, April 1999, TRAIL Thesis Series, Delft University Press, The Netherlands

Minderhoud, M.M., *Supported Driving: Impacts on Motorway Traffic Flow*, T99/4, July 1999, TRAIL Thesis Series, Delft University Press, The Netherlands

Hoogendoorn, S.P., *Multiclass Continuum Modelling of Multilane Traffic Flow*, T99/5, September 1999, TRAIL Thesis Series, Delft University Press, The Netherlands